NASA CONTRACTOR REPORT

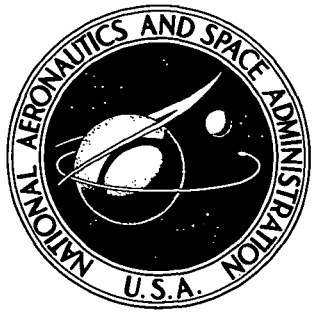

NASA CR-113925

NASA CR-113925

CONCEPTUAL DESIGN STUDY OF A NUCLEAR BRAYTON TURBOALTERNATOR-COMPRESSOR

Prepared by
GENERAL ELECTRIC COMPANY
Cincinnati, Ohio 45215
for Lewis Research Center

NATIONAL AERONAUTICS AND SPACE ADMINISTRATION • WASHINGTON, D. C. • NOVEMBER 1971

1. Report No.	2. Government Accession No.	3. Recipient's Catalog No.
CR-113925		

4. Title and Subtitle	5. Report Date
CONCEPTUAL DESIGN STUDY OF A NUCLEAR BRAYTON TURBOALTERNATOR-COMPRESSOR	November 1971
	6. Performing Organization Code
7. Author(s)	8. Performing Organization Report No. GESP-493
	10. Work Unit No.
9. Performing Organization Name and Address General Electric Company Cincinnati, Ohio 45215	11. Contract or Grant No. NAS 3-13449
	13. Type of Report and Period Covered Contractor Report
12. Sponsoring Agency Name and Address National Aeronautics and Space Administration Washington, D.C. 20546	14. Sponsoring Agency Code

15. Supplementary Notes Work done in conjunction with subcontractors, Mechanical Technology, Incorporated, and Westinghouse Aerospace Electrical Division; report edited by R. D. Brooks, General Electric Company; Project Manager, Joseph P. Joyce, Space Power Systems Division, NASA Lewis Research Center, Cleveland, Ohio

16. Abstract

The NASA is engaged in a research and technology investigation of nuclear powered Brayton cycle space electric power systems. The turboalternator-compressor (TAC) component of the system is one of the most critical. As part of this program, the General Electric Company has performed a comprehensive analysis and conceptual design study of the turboalternator-compressor components using HeXe as the working fluid. The study was conducted in three phases: general configuration analysis (Phase I), design variations (Phase II), and conceptual design study (Phase III). During the Phase I analysis, individual turbine, alternator, compressor, and bearing and seal designs were evaluated. Six turboalternator-compressor (TAC) configurations were completed. Phase II consisted of evaluating one selected Phase I TAC configuration to calculate its performance when operating under new cycle conditions, namely, one higher and one lower turbine inlet temperature and one case with krypton as the working fluid. Based on the Phase I and II results, a TAC configuration that incorporated a radial compressor, a radial turbine, a Lundell alternator, and gas bearings was selected. During Phase III a new layout of the TAC was prepared that reflects the cycle state points necessary to accommodate a zirconium hydride moderated reactor and a 400 Hz alternator. The final TAC design rotates at 24,000 rpm and produces 160 kWe, 480 V, 3-phase, 400 hertz power.

17. Key Words (Suggested by Author(s))	18. Distribution Statement
Turboalternator compressor design Brayton cycle Space electric power	Unclassified - unlimited

19. Security Classif. (of this report)	20. Security Classif. (of this page)	21. No. of Pages	22. Price*
Unclassified	Unclassified	526	$3.00

*For sale by the National Technical Information Service, Springfield, Virginia 22151

TABLE OF CONTENTS

TABLE OF CONTENTS (CONT'D)

I. SUMMARY

The Brayton TAC study was conducted with a number of component designs and lubrication systems as candidates for selection. In Phase I it was concluded that the radial in-flow turbine, centrifugal compressor, and 1200 Hz Rice-Lundell alternator, mounted on gas lubricated bearings, best met the contract requirements. This unit is shown in Figure 1 in the original configuration. In Phase II slight modifications were found to be necessary for the low temperature application and in Phase III the modified contract requirements necessitated additional geometric changes and the 400 Hz Lundell alternator was selected.

The principal features of the TAC, as shown in Figure 1, included a titanium alloy compressor wheel with back-swept blades to obtain maximum efficiency. The alternator rotor is of bimetallic construction with 4340 and Inconel 718 to be bonded by HIP welding. Cooling is provided for the pole face losses by circulation of the working fluid through the gap and stack to a heat exchanger cooled by oil along the periphery of the stator. The reference voltage is 240 (L-N) with reconnectability to 480 volts. The insulation systems considered included high temperature ceramic materials previously developed by NASA and inorganic insulation for lower temperature application. Corona effects at low pressure operation will limit the design voltage but the 240 volt requirement appears attainable. The radial in-flow turbine has been designed of Rene 80 alloy for maximum stress capability. The exit diffuser configuration provides for minimum loss at the low Mach number specified. A comparison of losses with previous work by the Lewis Research Center indicated a well-matched turbine design. Cooling for the gas bearings is provided by flow through the central shaft in the hole through which the tie bolt passes. The thrust bearing is cooled by a liquid heat exchanger mounted on the runners. The pivoted pad journal bearings are coated with chrome oxide for improved starting and stopping capability. The spiral groove thrust bearing is also

NUCLEAR BRAYTON TAC 24000RPM GAS BEARINGS RADIAL COMPRESSOR, RADIAL INFLOW TURBINE

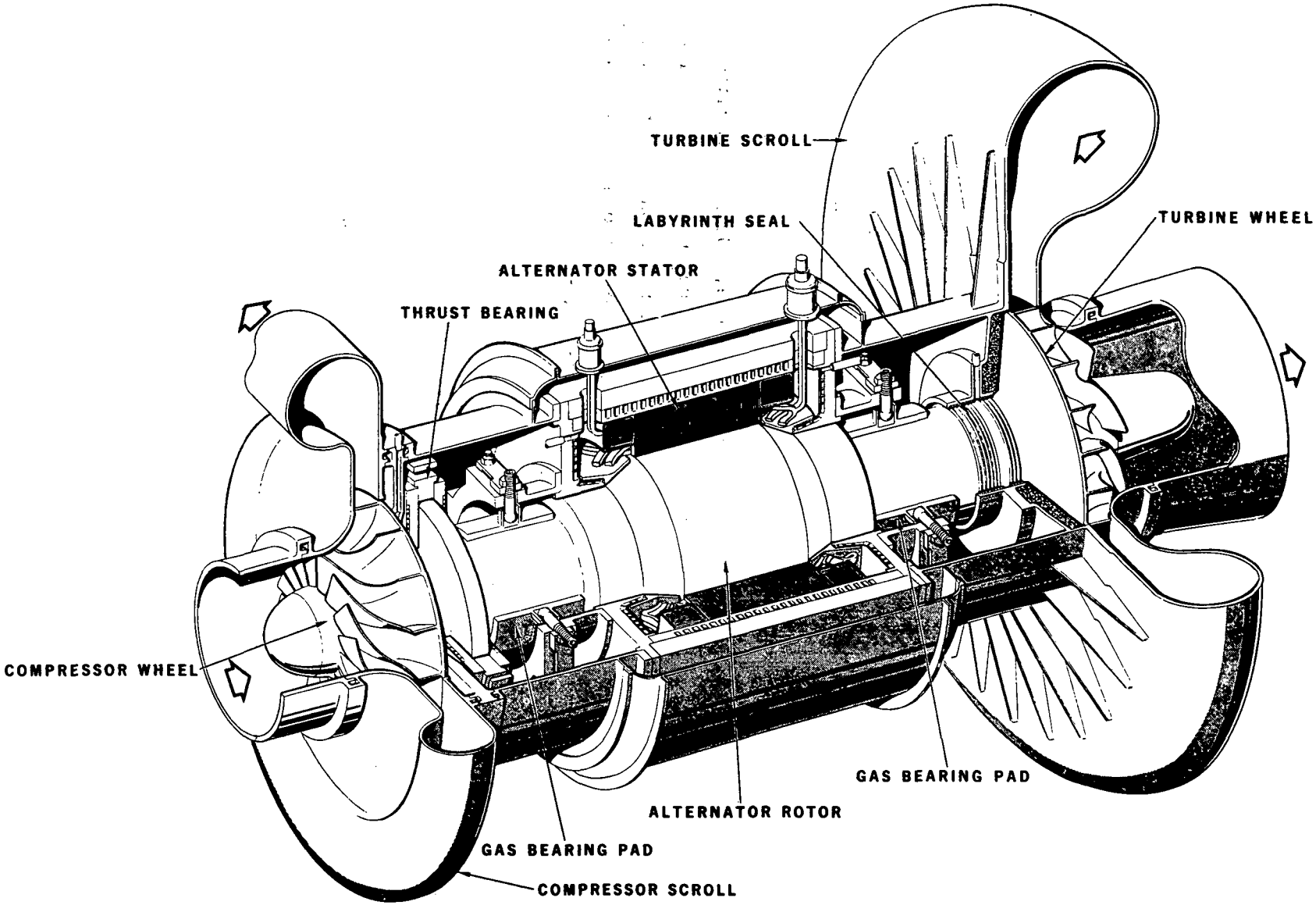

FIGURE 1.

similarly coated. Both designs have been successfully applied in gas lubricated rotating machinery. Thrust balancing of the compressor and turbine will be accomplished by scalloping of the turbine and appropriate selection of seal diameters. Labyrinth seals are used to isolate the high pressure turbine and high pressure compressor regions from the bearing cavities. The dynamic response of the machine indicated a third critical for the Phase III design of over 40,000 rpm.

The performance of this unit is shown in Table I for the Phase I study, Phase II low temperature case, and Phase III. The windage losses of the 2-pole machine are slightly higher than the 6-pole machine due to the longer alternator rotor. The turbine pressure ratio increase specified for Phase III has improved the cycle efficiency obtained significantly. To assist in achieving the low system pressure drop suggested by this change, the compressor discharge Mach number was reduced to .005. The alternator electromagnetic efficiency for the 2-pole machine is shown for the 60 slot design. On the basis of the overall machine performance, the 2-pole, 400 Hz alternator is found to be feasible with no additional major development problems. The magnetic unbalance forces of this machine were estimated on a simplified basis providing what is considered a very high value. The magnetic unbalance did not produce design problems for the gas bearing system. An improved calculational method to account for the rotating flux influence will be necessary for final design purposes but the values are expected to be substantially less than those estimated. If the spacecraft requirement is for 400 Hz power, the development of the TAC to directly produce that power appears feasible and practical. The major alternator problem is the state-of-the-art of rotor bonding that must be solved for any Lundell design, which is the only development problem in this unit.

One of the major critical design problems for the TAC is related to start-up procedures. These procedures will produce transients in temperature, voltage, and pressure which have not been evaluated by the study. The number of such transients and their severity could require modifications to the design or its operating characteristics. Jacking gas provisions have been made for starting and the machine should be compatible with gas injection or motor starting with the alternator.

TABLE I

TAC PERFORMANCE COMPARISON

	Phase I	Phase II	Phase III	
	6 Pole	Low Temp. 6 Pole	6 Pole	2 Pole
Losses, KW	7.36	7.36	7.36	8.61
Leakage, % Flow	3.23	3.23	3.23	3.23
Compressor Efficiency	.859	.859	.859	.859
Turbine Pressure Ratio	1.786	1.786	1.824	1.824
Turbine Efficiency	.91	.91	.91	.91
Alternator Efficiency	.942	.942	.942	.93
Cycle Efficiency	.284	.257	.275	.27
Flow Rate, lb/sec	9.85	14.07	12.81	13.06

In the turbomachinery, matching of the compressor rotor and diffuser and maintenance of operating clearances will be critical design problems. For the turbine, the casing design to obtain acceptable deflections in the maintenance of clearances must also be verified. The pressure balance of the turbomachinery for the TAC at all loads must be similarly determined experimentally. For the alternator, the problems include the magnetic unbalance analysis, the cooling design and the pumping performance obtained with a conical rotor section. The current work at the Lewis Research Center on windage losses and pumping will be important to this program. Corona effects for the high temperature insulation at reduced pressures in helium mixtures must be verified. The use of Anadur as the high temperature insulation appears questionalbe due to flaking problems and a substitute material must be selected. The alternator design also requires a non-conducting baffle to guide the returning cooling flow to the gap region. The selection of this material and method of attachment are at present undefined. The non-uniform strains with the bimetallic rotor construction will require analysis, particularly with respect to start-up transients. The critical design areas for the bearings will include verification of cooling adequacy to minimize distortions, thrust bearing mounting, and verification of the magnetic interaction effects. The dynamic response for the rotor and the characteristics of the principal resonances must also be investigated. Other areas requiring design study are discussed in the body of this report. Research packages for the individual components and a dynamic simulator would be expected to provide results for most of these critical design problems.

The contract requirements for the Phase I study are shown in Table II. These conditions were used for the study of six machines to determine the unit most suitable to the reactor Brayton system. It was found that the 36,000 rpm designs required evacuation of the alternator cavity and that this could be accomplished with external gas pumping. The sealing of the cavity by oil or gas was deemed feasible. The oil bearing machines, however, had excessive parasitic losses and particularly low efficiency resulted at part load operation. All conditions were met by the Phase I unit shown in Figure 1. The system for which this unit was considered is shown in Figure 2 with the operating temperatures indicated. The characteristics of the TAC would appear to integrate well with such a system and to provide high performance for a very wide range of power output with only modest control

TABLE II

CONTRACT REQUIREMENTS

SINGLE SHAFT TURBINE ALTERNATOR COMPRESSOR FOR BRAYTON CYCLE POWER PLANT

160 KWe DESIGN PT. LOAD, 3 PHASE, .75 p.f.

40-160 KW OPERATING RANGE

24,000 OR 36,000 RPM GAS OR OIL BEARINGS

5 YEARS CONTINUOUS OPERATING LIFE

HIGH EFFICIENCY LIGHT WEIGHT FLIGHT PROTOTYPE MACHINE

1.9 COMPRESSOR PRESSURE RATIO

1.786 TURBINE PRESSURE RATIO

700^{o}R COMPRESSOR INLET TEMPERATURE

2060^{o}R TURBINE INLET TEMPERATURE

55 PSI COMPRESSOR INLET PRESSURE AT 24,000 RPM

120 TO 300 PSI AT 36,000 RPM

39.94 GAS MOLECULAR WEIGHT

10^{7} RADS 10^{13} NVT FAST NEUTRON RADIATION LEVEL

SHOCK, VIBRATION, ACCELERATION PER NASA SPECS P2241-1 AND P2242-2

496^{o}F ALT. COOLANT TEMPERATURE

185^{o}F BEARING AND LIQUID SEAL COOLANT TEMPERATURE

120 TO 480 VOLTS

FREQUENCY-MULTIPLE OF 400 Hz

ALTERNATOR DESIGN TO MEET SPEC MIL-G-6099 (A) WITH MODIFIED PHASE BALANCE REQUIREMENTS

- OUTPUT VOLTAGE .5 PERCENT MODULATION
- 320 KVA .9 p.f. OVERLOAD FOR 5 SECONDS AFTER TEMPERATURE EQUILIBRIUM
- SUITABLE FOR PARASITIC LOAD FREQUENCY CONTROL AND PARALLEL OPERATION
- STARTUP BY MOTORING OR GAS INJECTION

TYPICAL NUCLEAR BRAYTON POWER CONVERSION UNIT

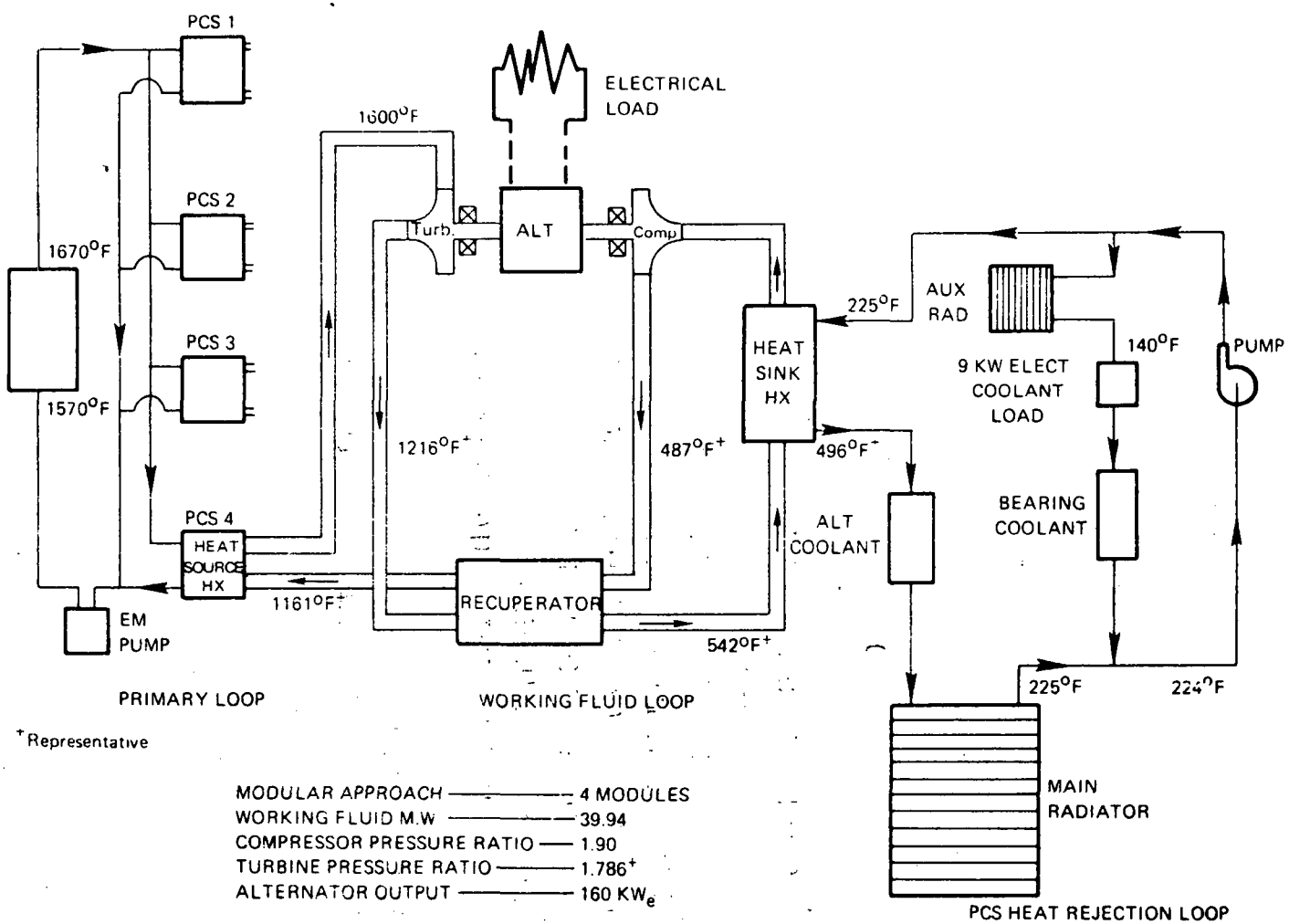

FIGURE 2.

requirements. In Phase II consideration was given to the low temperature application, the use of high molecular weight gas and a high temperature application. The low temperature application was for the SNAP-8 Brayton system as shown in Figure 3. For the Phase III study the contract requirements were modified to include:

Total He-Xe mass flow rate	13.73 lb/sec
Turbine pressure ratio	1.824
Compressor inlet pressure	70 psia
Turbine inlet temperature	1610^{o}R
Compressor inlet temperature	580^{o}R
Test working fluid	Argon
Rated voltage	240 L-N
Alternator coolant temperature	325^{o}F

Direct substitution of organic insulated windings with a coolant temperature of 107^{o}F will be possible. The environmental acceleration was reduced to 1.5 g's during operation. In addition, the capability for operation at a turbine inlet temperature of 2060^{o}R to produce 160 KWe was maintained. The results of the Phase III study demonstrate the versatility of the TAC to operate over a range of power levels and temperatures with only minimum modifications. This flexibility permits it to be used for many module sizes with the appropriate heat source system.

SNAP-8 BRAYTON SCHEMATIC

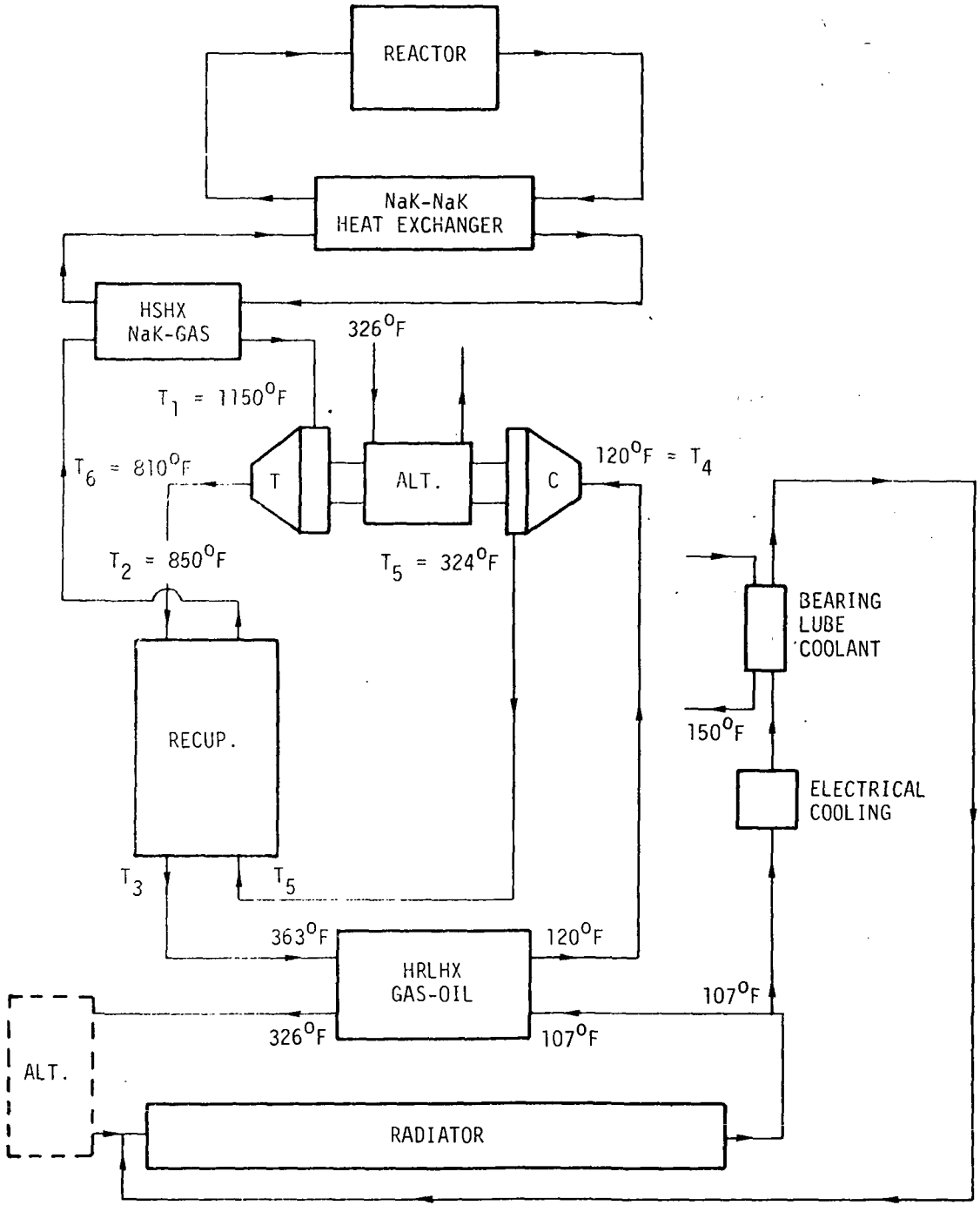

FIGURE 3.

II. INTRODUCTION

This program, which included a preliminary screening analysis of applicable turbomachinery followed by a conceptual design study of one turbo-alternator-compressor, has been conducted by an engineering team from General Electric, Mechanical Technology, Inc., and Westinghouse. The work of the program was planned to utilize the pertinent capabilities of each organization in the design and analysis of the candidate TAC units. The Aircraft Engine Technical Division performed the definitive studies for the turbomachinery and provided key inputs on material selection and rolling element bearing practices. The gas lubricated bearing and oil film bearing and seal work, as well as the bearing rotordynamic evaluations, were conducted by MTI. The alternator studies were provided by the Aerospace Electric Division of Westinghouse. NSP has provided overall management of the program, conceptual integration of components and mechanical and thermal integration of the total package. The extensive resources of each company for analysis and design in each of the major disciplines required by this complex unit have been applied to this program. Individual computer programs are identified in each section of the report. The most recent engineering practices as well as results of operational and development programs have been integrated into the considerations of the study. As the contract requirements have changes, the response by the program team has reflected the new emphasis.

At all times, an attempt has been made to bring realism to the program in terms of providing designs with a high degree of producibility. It was recognized that the best design must still be built with the practical procedures used in modern aircraft engines and aerospace electrical equipment. Of course, it is also evident that special attention must be given to those requirements which cannot be met by existing techniques. A particular case in point is the Lundell bimetallic alternator rotor for which NASA has prudently initiated development in advance of the present program. Where

possible, extra design margin has been provided to improve the reliability of the unit and increase its flexibility for application. One example of this is in the cooling of the alternator which will operate at 100°F below the maximum established by the specification and the dynamic response which indicates an overspeed design margin of over 50% compared to the 20% requirement. Wherever practical, such features have been incorporated and are described in the report.

TABLE III

TURBOMACHINERY SUMMARY

● COMPRESSOR

TYPE	RADIAL		AXIAL	
SPEED, RPM	24000	36000	24000	36000
NUMBER OF STAGES	1	1	7	6
INLET TIP DIAMETER, IN.	7.25	4.84	8.10	5.50
INLET HUB DIAMETER, IN.	2.62	1.75	6.05	4.10
EXIT TIP DIAMETER, IN.	10.36	6.91	7.52	5.09
EXIT BLADE HEIGHT, IN.	0.420	0.280	0.734	0.495
LENGTH, IN.	3.0	2.0	6.67	4.00
TIP SPEED, FPS	1086	1086	849	864
CHORD, IN.	-	-	0.6	0.4
REYNOLDS NUMBER, $\rho VL/\mu$	12.9×10^6	18.7×10^6	3.61×10^5	5.38×10^5
CLEARANCE, MIL	10	10	10	10
FLANGE TO FLANGE TOTAL EFFCY	0.862	0.862	0.866	0.862
ONE QUARTER POWER EFFCY	0.860	0.860	0.837	0.840

● TURBINE

TYPE	RADIAL	
SPEED, RPM	24000	36000
INLET TIP DIAMETER, IN.	11.11	7.40
EXIT TIP DIAMETER, IN.	7.76	5.18
EXIT HUB DIAMETER, IN.	3.12	2.07
INLET BLADE HEIGHT, IN.	0.956	0.692
LENGTH, IN.	3.6	2.4
TIP SPEED, FPS	1163	1162
REYNOLDS NUMBER, $W/\mu R_t$	4.5×10^5	6.8×10^5
CLEARANCE, MILS	10	10
FLANGE TO FLANGE TOTAL EFFCY	0.917	0.916
ONE QUARTER POWER EFFCY	0.902	0.901

cavity to about 2-4 psia and sealing from the working fluid pressures. The rotor stress levels were also sufficiently high to make this design unattractive. The Lundell unit at 1200 Hz was found to meet the electromagnetic requirements at reasonable stress levels and to have acceptable windage losses operating at compressor inlet pressure for the 24,000 rpm unit. The diffusion bonding of the bimetallic rotor is currently under development and requires further work for this application. Corona considerations were found to limit the machine to 120 volts (L-N) for a minimum operating pressure of 16 psia.

Bearing designs were established for both gas and oil lubricated systems. The tilting pad journal and spiral groove thrust bearings are adequate designs for this application. The gas bearings are sized to provide overload capacity margin at all conditions. The 4-G load environmental requirement at the 40 KWe power level does impose severe loading of the thrust bearing which will be further examined in Phase III. The bearing surface material will be CrO_2 to provide start-stop and high speed mmf capability. The gas bearings offer minimum losses and design simplicity without contamination by the lubricant. The oil film journal and thrust bearings are lightly loaded and would have high reliability. The rolling element bearings are relatively highly loaded for the 5-year life requirement and represent an extension of existing practice. The advanced SNAP-8 spiral groove face seal was evaluated for use in isolating the alternator cavity. The oil mist lubrication system from the Brayton "A" engine program was adopted to the TAC requirements. On the basis of the relative simplicity and low parasitic losses, the gas lubricated bearings offer the most favorable design approach.

From a comparison of the mechanical designs it is concluded that the 24,000 rpm centrifugal compressor with the 1200 Hz Lundell alternator, radial in-flow turbine on gas lubricated bearings, as shown in Figure 5 , provides

BRAYTON CYCLE
TURBO-ALTERNATOR-COMPRESSOR
24RG-3a

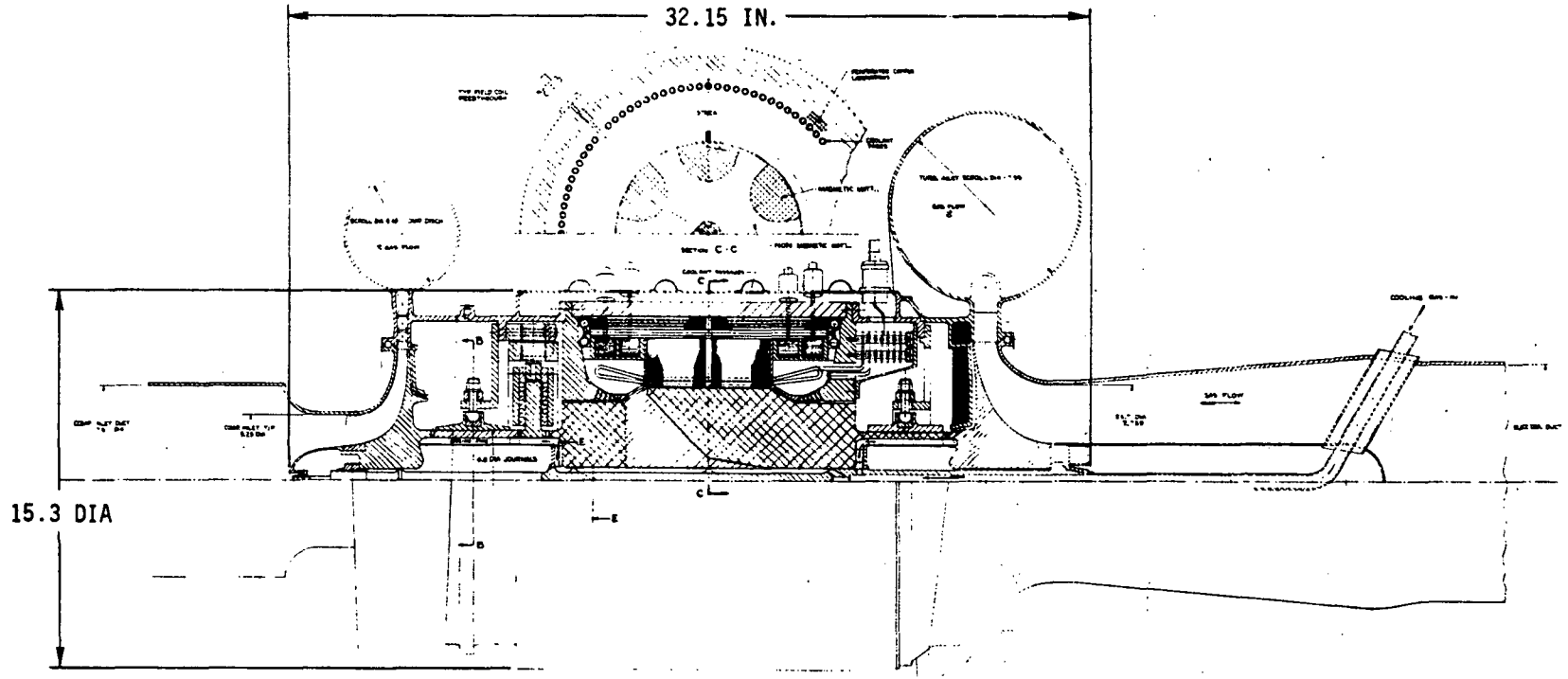

Figure 5

the most suitable unit for the design conditions. The overall performance of this unit offers a cycle efficiency of 28.4% at 160 KWe and 24.7% at 40 KWe. When operated at SNAP-8 conditions it offers a cycle efficiency of 24.2% at 160 KWe due to the lower turbine inlet temperature. The Lundell alternator requires no isolation by seals to meet the windage losses. Further consideration of part-load corona effects and rotor bonding will be required in Phase III. The tilting pad gas bearings provide a high over-capacity and the dynamic response analysis shows a third critical of 48,930 rpm. This unit was recommended for conceptual design in Phase III.

B. MECHANICAL DESIGN

INTRODUCTION

The mechanical design studies can be roughly divided into component design and configuration design. The component mechanical design studies dealt with all the problems which had to be solved in order to make each of the components practical and reliable. In these studies both centrifugal and axial-flow compressors were studied but the study was limited to radial-inflow turbines. The gas bearing sizes and design details had to be determined along with the necessary seals and coolant passages. Both hydrodynamic and ball bearings lubricated with oil were considered and the proper seals and cooling for these systems were designed. Design studies were made of various problem areas associated with the rotor, the casing, the scrolls, and the ducting.

Six different configuration designs were made, with each assigned a designating symbol in order to quickly identify it. The first two digits identify the rotative speed in thousands of revolutions per minute, followed by either an R or an A for radial-flow and axial-flow compressors. The fourth symbol is a G for gas bearings, M for mist-lubricated ball bearings, or L for liquid film bearings.

Three TAC units on gas bearings were selected for study under this program. The 24RG and 24AG are TAC units rotating at 24,000 rpm, the first having a radial-flow compressor, and the second having an axial-flow compressor. Both of these machines had no seal between the alternator and the bearing cavities. At 36,000 rpm a gas bearing machine (36AG) was designed with an axial-flow compressor. Because of the high compressor inlet pressure specified it was necessary to provide a spiral-groove (hydrodynamic) gas face seal between the alternator and bearing cavities.

All of the oil-lubricated bearing machines were designed for a rotative speed of 36,000 rpm. Both axial-flow and radial-flow compressors (36RM and 36AM) were used in the two ball-bearing machines. Only one liquid film bearing machine (36RL) using oil as a lubricant was designed, which had a radial-flow compressor.

Before discussing these mechanical designs, the design specifications will be summarized. The alternator output power range was to be from 40 to 160 KW, electrical, with a power factor of 0.75, lagging. The alternator

was to produce 3-phase power. Mechanical design considerations were to include operating speeds from 0 to 120 percent of the design values. The compressor inlet pressures were to be 55 psia for 24,000 rpm and from 120 to 360 psia for 36,000 rpm. Although the turbine inlet temperature was specified as 1600°F, it was necessary to design the turbine for operation at 1640°F due to the deadband anticipated in the reactor. The compressor inlet temperature was specified as 240°F. Two heat sinks for cooling were specified. The oil coolant for the alternator was to be supplied at 496°F and oil to cool certain seals and the oil absorber was to be supplied at 185°F.

For the gas bearing machines the working fluid was to act both as coolant and lubricant. Argon was specified for development but the final spacepower plant was to use a helium-xenon gas mixture having the same 39.94 molecular weight as argon. Both paraffinic- and napthenic-base oils were to be considered as the liquid coolant and lubricant.

The powerplant was required to operate in a radiation environment having an integrated gamma dose of 10^7 rads and a neutron flux of 10^{13} nvt fast neutrons per square centimeter (> 1 Mev).

Environmental specifications P-2241-1 and P-2241-2 were adhered to for the TAC unit. Although these specifications are quite detailed, the most severe condition is the 3.5G acceleration maneuver load the powerplant is subjected to in space flight. This load sizes the thrust bearings.

The design life of the TAC was specified as 5 years. This puts emphasis on high reliability and encourages simplification of the designs.

For the mechanical design of the compressor and turbine and for the integration of all the components into TAC configurations several programs were utilized.

THERMAL AND STRESS ANALYSIS

The transient heat transfer computer code THTD was used to determine both transient and steady state temperature distributions. This is a finite-node heat-transfer program which has been well developed through years of use in GE-AEG and NSP. The static and rotating parts are divided into three-dimensional elements, with the program able to model blade elements and flowing fluid nodes when required.

Provisions are made for body and boundary radiation, surface heat flux, internal heat generation, variable material properties, variable boundary conditions, and phase changes.

Output may be called for at selected time intervals so that transient temperature plots may be made.

The TAC models utilized about 1000 nodes and output was printed at 1, 10, 100, 1000, and 10,000 sec.

ROTOR is an important new finite-element computer program developed by GE-AEG for the GE-12 engine to determine the stress and deformation of centrifugal compressors. The program permits the efficient and accurate analysis of three-dimensional axisymmetric stress distribution in solids of revolution, with or without radial blades attached, and subject to static, thermal, and centrifugal loads. It calculates the variation of material properties with temperature and the ratio of allowable stress to imposed effective stress. Automatic plotting is available.

The SNAP program analyses structures as systems of cones, disks, cylinders, and toroidal shells with or without rigid ring connectors. Unusual elements such as cutouts can be analyzed provided the equations of compatibility can be written. It is particularly applicable to the TAC casings.

The program allows the imposition of axisymmetric loads, including centrifugal loads, and temperature variations. Elastic stresses and deformations are determined at a number of stations for each structural element. It is widely used in GE-AEG but is limited to relatively thin structures to which small deflection theory is applicable and materials which follow Hooke's Law; it excludes buckling.

MASS is an elemental or lumped-parameter approach for the analysis of redundant structures. Stresses, loads, and deflections are obtained for mechanical loadings, thermal gradients, and sinusoidal forcing functions. This program was used to ascertain critical frequencies and mode shapes of the casing of one typical TAC configuration.

RECAP (Rolling Element Computer Analysis Program) is a well-established computer program used by many organizations throughout the country to analyze rolling-element bearings. Standard AFBMA formulas are used, with the addition of centrifugal loading of the outer races by the balls.

The following two basic bearing systems may be evaluated:

- A rigid system, where all deflections occur in the bearings.
- A flexible system, where shaft and housing deflections are also considered.

The program considers the effect of external radial and axial loads imposed on a set of two bearings as well as the ball centrifugal forces.

Stresses and predicted B_{10} life are calculated, based upon the use of bearing quality 52100 steel. Adequate lubrication at all times is assumed.

In addition, both critical speed and forced (unbalance) response computer programs were used which take into account bearing mass, bearing support stiffness and damping, stiffness and damping of the lubricant film itself, rotor flexibility and gyroscopic effects, and effects of couplings. The programs permit analysis of the effects of casing flexibility on rotor critical speeds and response. A computer program is also available to determine lateral response of rotors supported by rolling-element bearings having non-linear stiffness characteristics.

TAC Material Allowable Stresses

The principal materials considered for use in the TAC machine are listed in Table IV, with the alternator materials discussed later. The compressor material is the titanium alloy Ti-6Al-5V, which is used in aircraft gas turbine engines and airframe parts. The principal range of temperature interest for this material is 250-500°F. At the lower temperatures the short-term 0.2 percent yield stress and ultimate tensile stress can be of more importance when they are less than the long-term properties. This is because the allowable design stresses for the short-term 120 percent speed conditions are reduced by an overspeed corrector below their average properties minus three standard deviations (99.6 percent assurance against receiving material with lower properties). By doing so, the rotor components may be analyzed at design speed only, with conservatively safe assurance that the rotor stresses will not exceed the allowable stresses at overspeed. At about 550°F the five year 0.2 percent creep and rupture properties of Ti-6Al-4V become less than the adjusted short-term properties. No overspeed correction is applied to the

TABLE IV

TAC MATERIAL ALLOWABLE STRESSES

COMPRESSOR MATERIAL

MATERIAL	TEMPERATURE °F	0.2% Y.S. KSI	5-YR 0.2% CREEP KSI	UTS KSI	5-YR RUPTURE KSI
Ti-6Al-4V	250	96.0	-	100.0	-
	500	-	66.3	-	80.3

ROTOR MATERIALS

RENE 80	800	84.0	-	109.0	-
	1470	-	17.2*	-	21.0
H-11	500	124.8	-	137.1	-
	800	-	53.6	-	81.4

*0.1% CREEP

CASING MATERIAL

HASTELLOY X	250	38.4	-	95.7	-
	1640	-	-	-	2.4

five year properties because overspeed will occur for only short periods of time.

The turbine material considered is the nickel-base superalloy Rene' 80 which is used in aircraft gas turbine blades and nozzle vanes. Its principal range of interest is between 800-1470°F. The dominance of the five year properties over the adjusted short-term properties starts about 1100°F.

The iron-base alloy H-11 is considered for use in the stub shafts, bearings, and seal plates because it is one of the materials which might be used in the alternator and is typical of the other materials which could be specified. It is one of the hot-work die steels. The five year properties of H-11 are of primary importance above 700°F.

The casing material considered is Hastelloy X, a nickel-base alloy used in aircraft gas turbine blades, nozzle vanes, and sheet metal components. Its primary range of interest is from 250-1640°F. It possesses more strength than needed for the casing forward end to the aft end of the alternator and a cheaper material could be substituted. At the highest temperature in the turbine inlet scroll, a material of even higher strength will be needed unless the scroll can be effectively cooled.

CONFIGURATION COMPARISONS

The 24RG Configuration

The configuration drawing of the 24,000 rpm, centrifugal compressor TAC on gas bearings is shown by Figure 5. The argon or helium-xenon mixture gas enters the TAC from the left side of the figure at 240°F and 55 psia and passes through the centrifugal compressor, which has eye and tip diameters of 5.25 and 8.8 inches, respectively. The diffuser has three vane rows. The working fluid leaves the compressor at 105 psia and 500°F. It returns from the reactor at 1600°F with a slight decrease in pressure to the turbine inlet scroll at the aft end of the TAC. Passing through the turbine nozzle vanes, the gas enters the turbine rotor at 1400°F and is discharged at 1310°F and 56 psia. The mass flow rate is 11.1 lb/sec. The turbine inlet tip diameter is 11.11 in. and its exit tip diameter is 7.76 in.

BRAYTON CYCLE
TURBO-ALTERNATOR-COMPRESSOR
24RG-3a

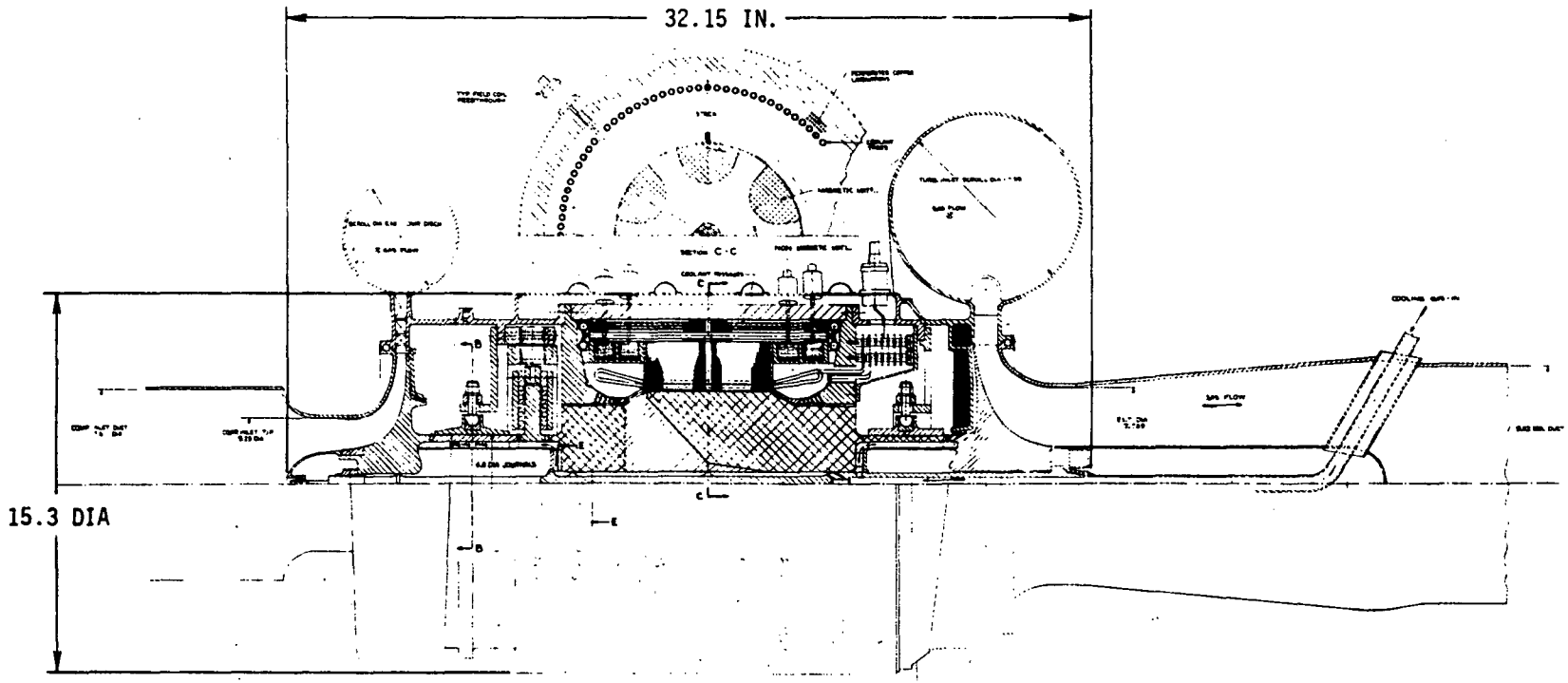

POTENTIAL ADVANTAGES

- GOOD ROTOR DYNAMICS
- NO ALTERNATOR SEAL
- LOW BEARING POWER LOSS

MAJOR PROBLEMS

- ALTERNATOR BONDING
- ALTERNATOR ROTOR COOLING
- TIP CLEARANCES

Figure 5.

The rotor is supported by tilting-pad gas bearings which straddle mount the alternator. The compressor and turbine are overhung. The tilting-pad gas thrust bearing is located between the compressor and alternator. The bearing cavities are vented (by means not shown) to the compressor inlet pressure. The heat generated in the gas journal bearings is removed by a flow of cooling gas ducted from the compressor discharge to the aft end of the hollow tiebolt. The gas flows through fins inside the two journals, discharging along the turbine disc forward face and into the forward bearing housing. The thrust bearing stator is an oil-cooled heat exchanger which removes the heat generated in the bearing.

The rotor is joined by curvic couplings which are clamped by an axial preload provided by the tiebolt.

Because the Lundell alternator has low windage losses, it is possible to minimize the sealing problems by allowing the alternator to operate in an environment of gas at compressor discharge pressure. Simple labyrinth seals are needed only aft of the compressor and forward of the turbine.

The thermal analysis of this machine, typical of the rest of the configurations, used a thermal model of about 1000 volume elements. The assumed temperatures used as boundary conditions are shown in rotor and stator cavities and the alternator, with another number in parentheses which is the surface heat transfer coefficient for all surfaces bounded by the cavities. At lines indicating the contact of two different components the figures in parenthesis indicate contact coefficients. The 10,000 second temperatures are considered the steady-state conditions, which can be verified by plotting the temperatures of selected elements versus time. Such plots also identify areas of high thermal gradients.

A more detailed representation of the isotherms of the 24RG turbine is shown in Figure 6. The maximum turbine temperature of 1470^{o}F occurs at the blade inlet tips, where the stresses are very low. The temperature of the most highly stressed point, the hub bore directly beneath the hub tip, is 1225^{o}F.

The thermal expansion of the 24RG configuration is shown on Figure 7. This is based upon the thermal analysis, the thermal expansion properties of the materials, the original lengths of components, and the combined thermal and dynamic distortions of the rotor components as

STEADY-STATE ISOTHERMS FOR 24RG-1a TAC TURBINE

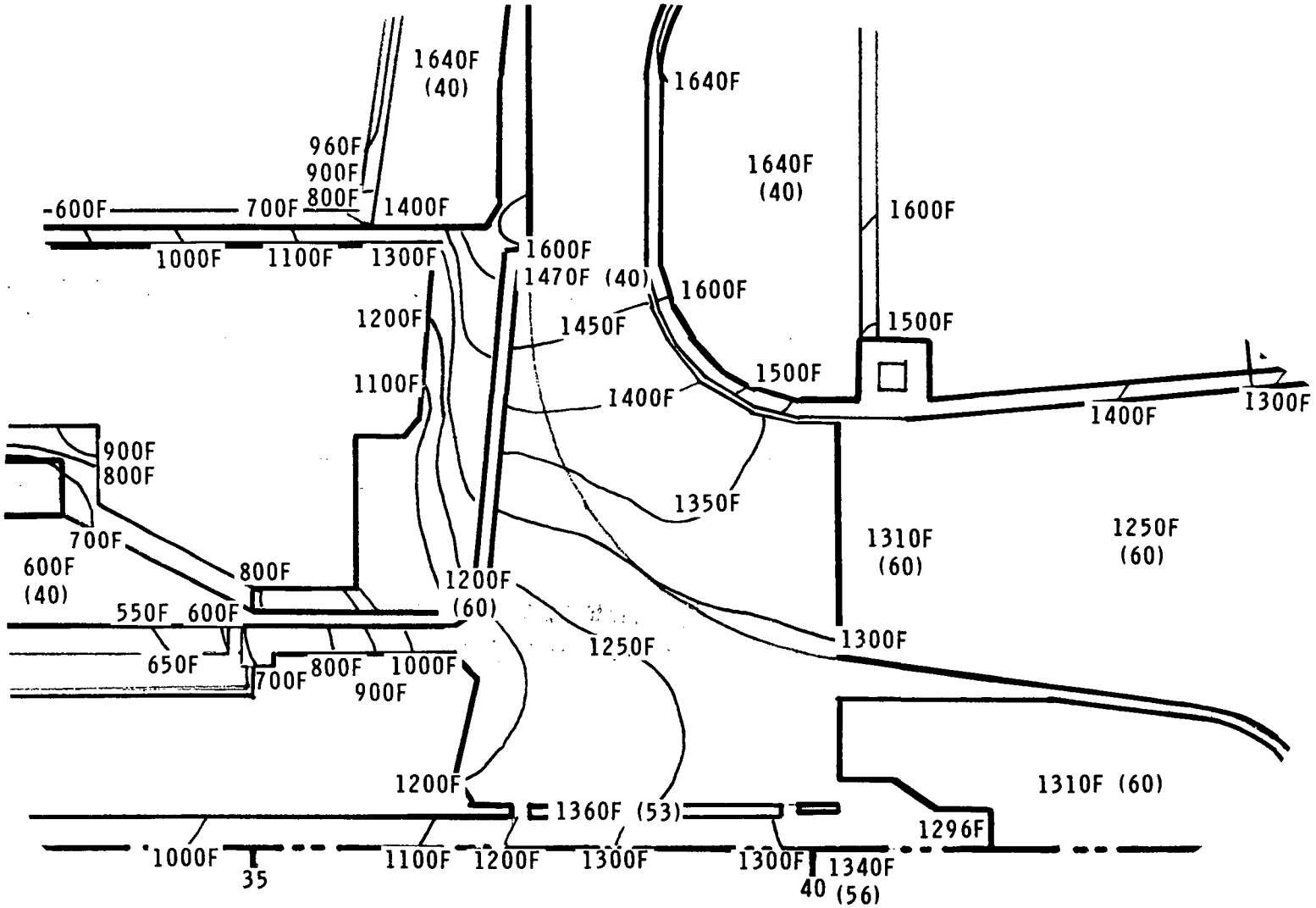

Figure 6.

BRAYTON TAC 24RG
THERMAL EXPANSION, IN.

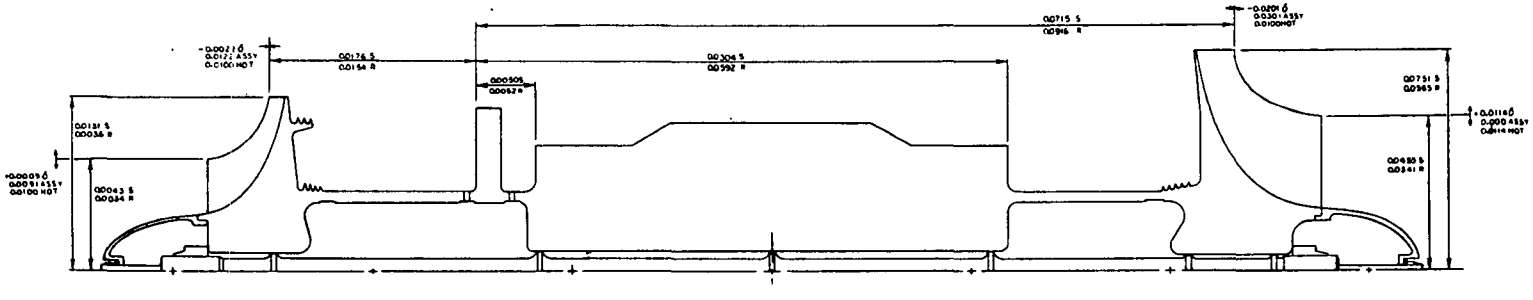

Figure 7.

calculated by the stress analysis computer program. The thrust bearing is considered the fixed point axially. The thermal expansions are shown by the sets of two numbers, the number followed by "S" being the expansion of the stator and that followed by "R" being the expansion of the rotor over the indicated length. The groups of three numbers at points where clearances are critical identify the opening or closing of the gaps due to centrifugal and thermal deformations (δ), the required or allowable assembly clearances (Assy), and the resulting hot running clearances (Hot). These indicate that it might be possible to achieve the desired ten mil hot running clearances. However, there are other clearance considerations.

The steady-state isotherms from the thermal analysis of the 24RG configuration are shown in Figure 9. The figure defines a zone of temperatures less than 500^{o}F which includes the forward end of the rotor to the alternator, and the tiebolt and the forward end of the casing to the aft end of the alternator. The thrust bearing is slightly above 500^{o}F. Temperatures between 500-1000^{o}F exist in the alternator rotor and stator, the aft stub shaft, short lengths of the tiebolt and aft bearing housing (casing), and the insulation around the turbine inlet scroll and exhaust duct.

The other clearance considerations are listed in Table V. A principal one is the practical assembly consideration that the desired dimensions may be missed by 2.5 mils even with the greatest of care. Also, interference between components can be excluded. The assumptions for thrust- and journal-bearing deflections are listed. No casing deflections have been determined. The minimum clearance is set by bearing deflection caused by operation at an acceleration of 4G.

The synopsis of clearances at zero G are shown in Table VI. The opening or closing of the critical gaps is the first item listed for each clearance, and comes from Figure 7. The next is the zero bearing deformation with its 4G limit. The third is the desired assembly gap clearance with its tolerance. The last two figures in each group are the minimum and maximum hot running clearances, with the maximum being of most importance because of its adverse effects on efficiency. The table shows that it will probably be impossible to guarantee ten-mil clearance at the turbine inlet blade tip axial gap, the turbine exit blade tip radial gap, and the compressor exit blade tip axial gap.

STEADY-STATE ISOTHERMS FOR 24AG-1b TAC

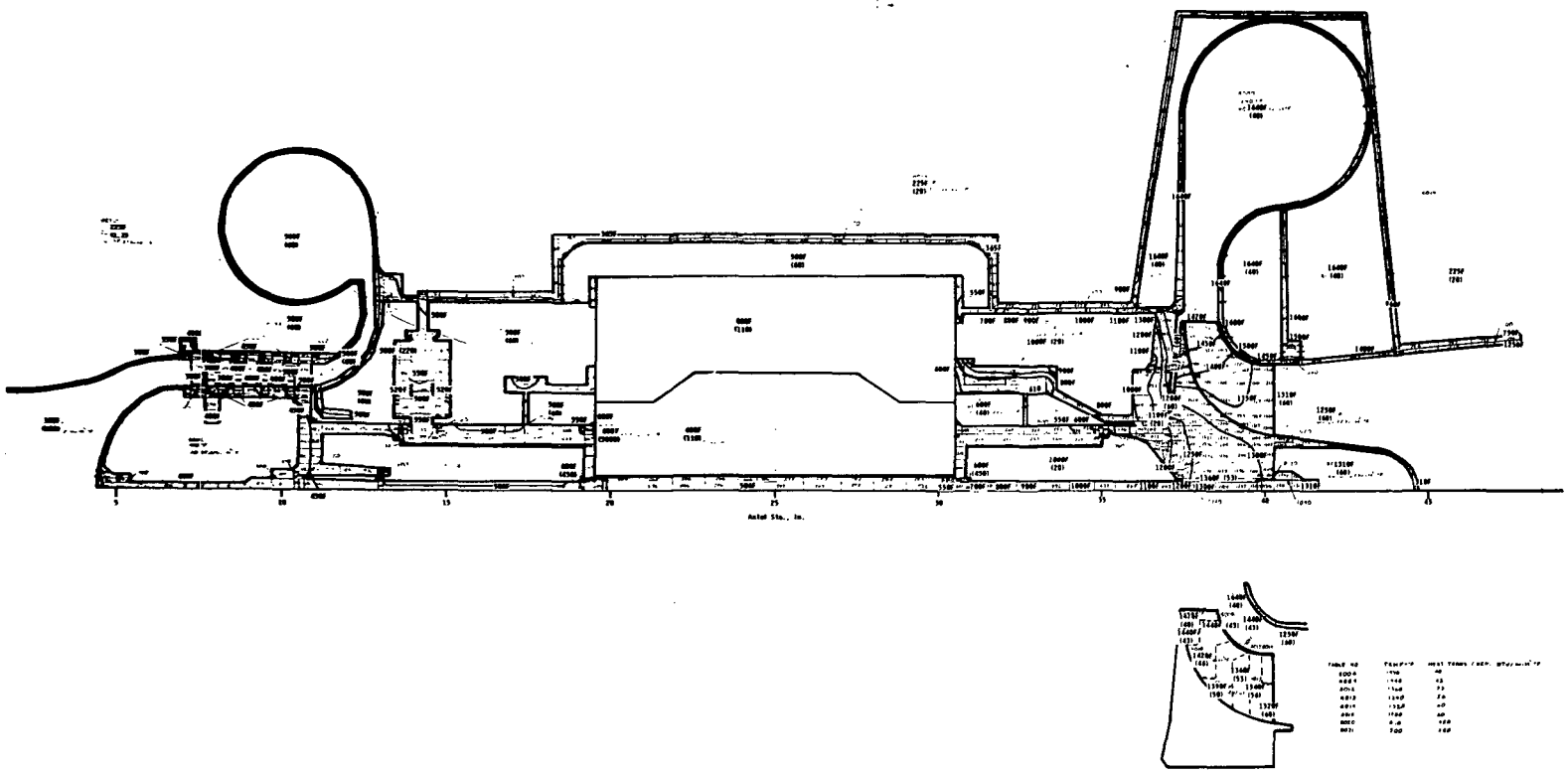

TABLE V

DIFFERENTIAL THERMAL EXPANSION AND TAC TURBOMACHINERY CLEARANCES

- MINIMUM ASSEMBLY CLEARANCE $\pm$ 2.5 MILS
- TOTAL THRUST BEARING DEFLECTION AND DISPLACEMENT (4G), MILS
  - GAS BEARINGS 13.2
  - BALL BEARINGS 1.0
  - LIQUID FILM BEARINGS 4.0
- TOTAL RADIAL BEARING DEFLECTION AND DISPLACEMENT (4G), MILS
  - GAS BEARINGS 7.1
  - BALL BEARINGS 4.2
  - LIQUID FILM BEARINGS 4.0
- NO CASING DEFLECTION ASSUMED
- TARGET TIP CLEARANCE (ZERO G) 10 MILS
- TARGET AXIAL CLEARANCE (AXIAL COMPRESSORS) 40 MILS
- MINIMUM CLEARANCES SET BY OPERATION AT 4G

TABLE VI

24 RG CLEARANCE AT 0g

Mils

		(1)
TURBINE AXIAL CLEARANCE	THERMAL	-20.1
	BEARING	0 ± 3.6
	ASSEMBLY	+29.2 ± 2.5
	HOT	15.2
		3.0
TURBINE RADIAL CLEARANCE	THERMAL	+ 11.4
	BEARING	0 ± 0.3
	ASSEMBLY	+ 2.5 ± 2.5
	HOT	16.7
		11.1
COMPRESSOR AXIAL CLEARANCE	THERMAL	- 2.2
	BEARING	0 ± 3.6
	ASSEMBLY	+ 11.3 ± 2.5
	HOT	15.2
		3.0
COMPRESSOR RADIAL CLEARANCE	THERMAL	+ 0.9
	BEARING	0 ± 0.3
	ASSEMBLY	+ 5.1 ± 2.5
	HOT	8.8
		3.2

NOTES: (1) - MEANS GAP CLOSES

(2) CASING DEFORMATION NOT INCLUDED

The effective stresses calculated for the 24RG configuration, based upon centrifugal and thermal stresses and external loads, are shown in Figures 10 and 11. The external loads include the tiebolt preload of 5000 pounds and the journal- and thrust-bearing loads distributed as indicated. The most critical compressor stress is 26 ksi at its aft bore, which gives a factor of safety of 2.1 with respect to the material allowable stress. The 60 ksi thrust bearing bore stress gives a factor of safety of 1.8. The alternator stresses are explained in more detail later, but its maximum indicated bore stress of 55 ksi gives a factor of safety of 2. The critical turbine bore stress of 40 ksi uses all of the material strength, giving a unity factor of safety.

The potential advantages of this arrangement are that it has good rotor dynamic characteristics, requires no alternator seal, has low bearing power losses, and higher system efficiency than the similar TAC with a radial compressor.

Major problems of the design to be overcome include the alternator bonding problems, alternator rotor cooling problems, and the maintainance of tip clearances.

The 24AG Configuration

The configuration drawing of the 24,000 rpm, axial compressor TAC on gas bearings is shown by Figure 12. The major details of this machine differ from those of the previously described 24RG TAC only in the compressor details. The 7-stage compressor has a maximum diameter of 8 in. The compressor blading is followed by an outlet guide vane and a diffusion scroll.

For best clearance control the thrust bearing has been placed forward of the turbine, since the axial compressor can tolerate axial displacement better than the turbine.

Other details shown are the compressor blade locking method and the scalloped turbine hub required to decrease the stresses in the turbine bore.

The steady-state isotherms of the 24AG TAC shown by Figure 13 are very similar to those of 24RG. Its thermal expansions are shown by Figure 14 and its critical clearances are summarized in Table VII. The turbine inlet blade tip axial gap, turbine exit blade tip radial gap,

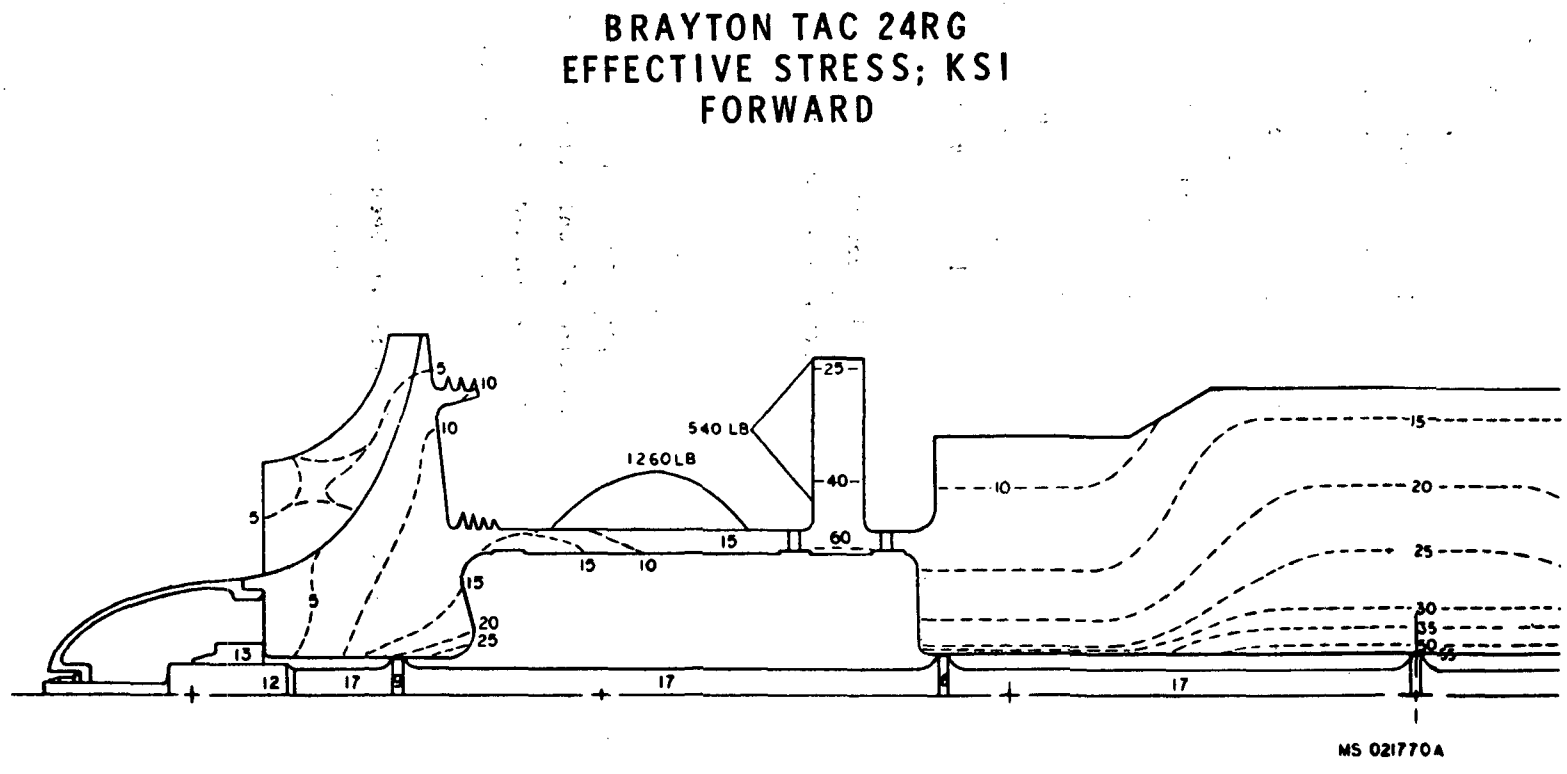
BRAYTON TAC 24RG
EFFECTIVE STRESS; KSI
FORWARD
540 LB
1260LB
MS 021770A

Figure 10.

BRAYTON TAC 24RG
EFFECTIVE STRESS; KSI
AFT

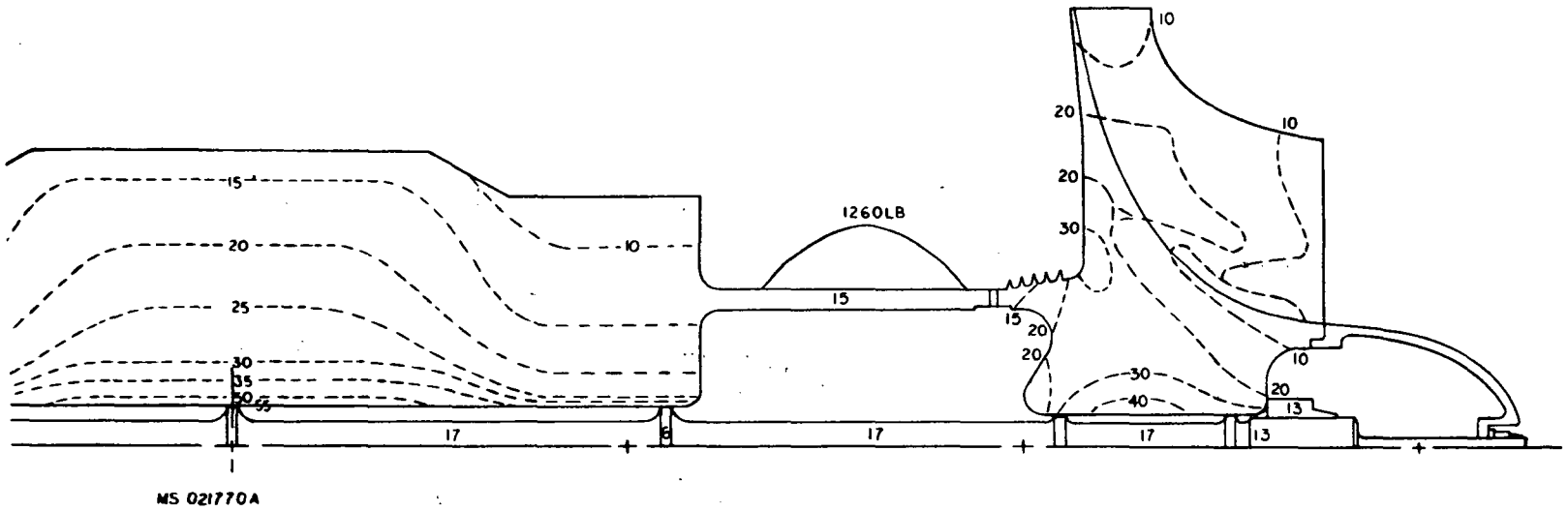

Figure 11.

BRAYTON CYCLE
TURBO-ALTERNATOR-COMPRESSOR
24AG-2a

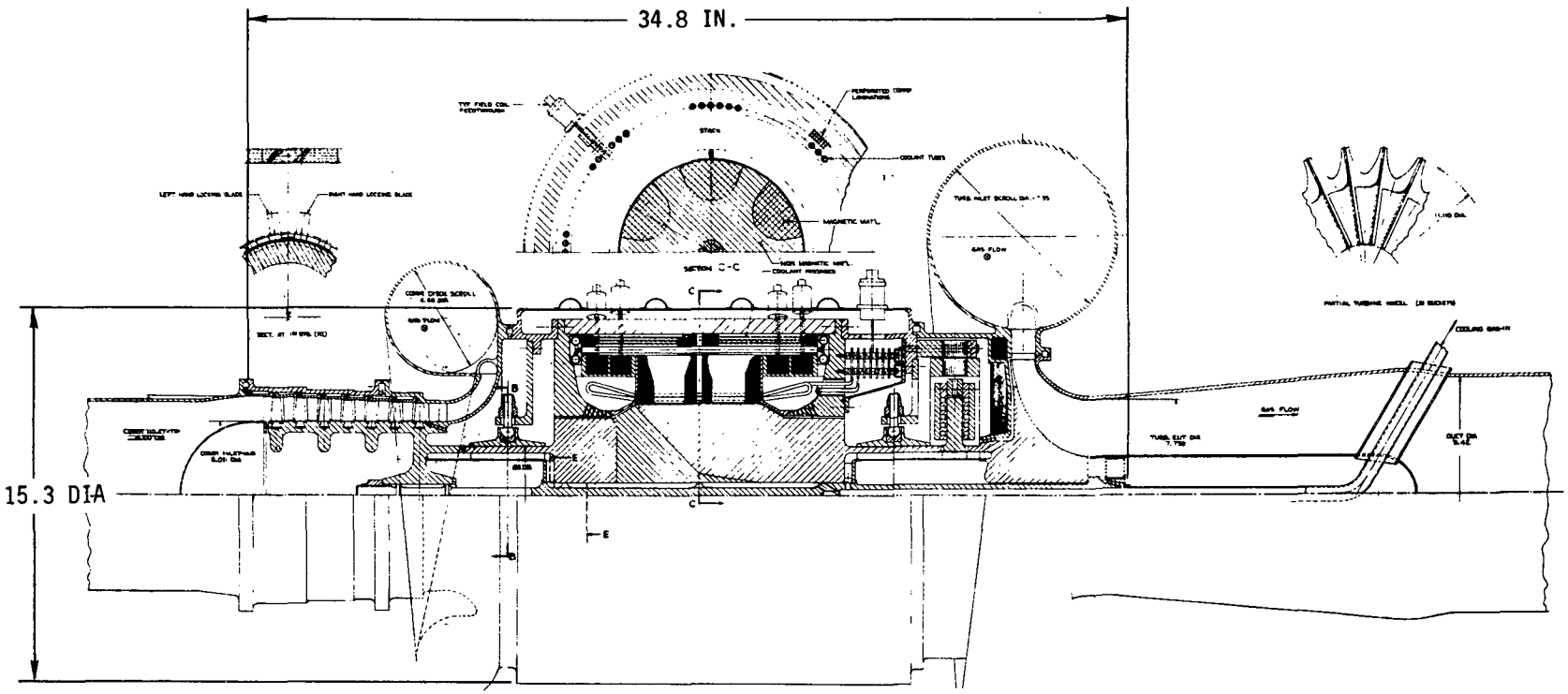

POTENTIAL ADVANTAGES

- GOOD ROTOR DYNAMICS
- NO ALTERNATOR SEAL
- LOW BEARING POWER LOSS
- HIGHER SYSTEM EFFICIENCY

MAJOR PROBLEMS

- ALTERNATOR BONDING
- ALTERNATOR ROTOR COOLING
- TIP CLEARANCES
- COMPLEXITY OF AXIAL COMPRESSOR

Figure 12.

STEADY-STATE ISOTHERMS FOR 24RG-1a TAC

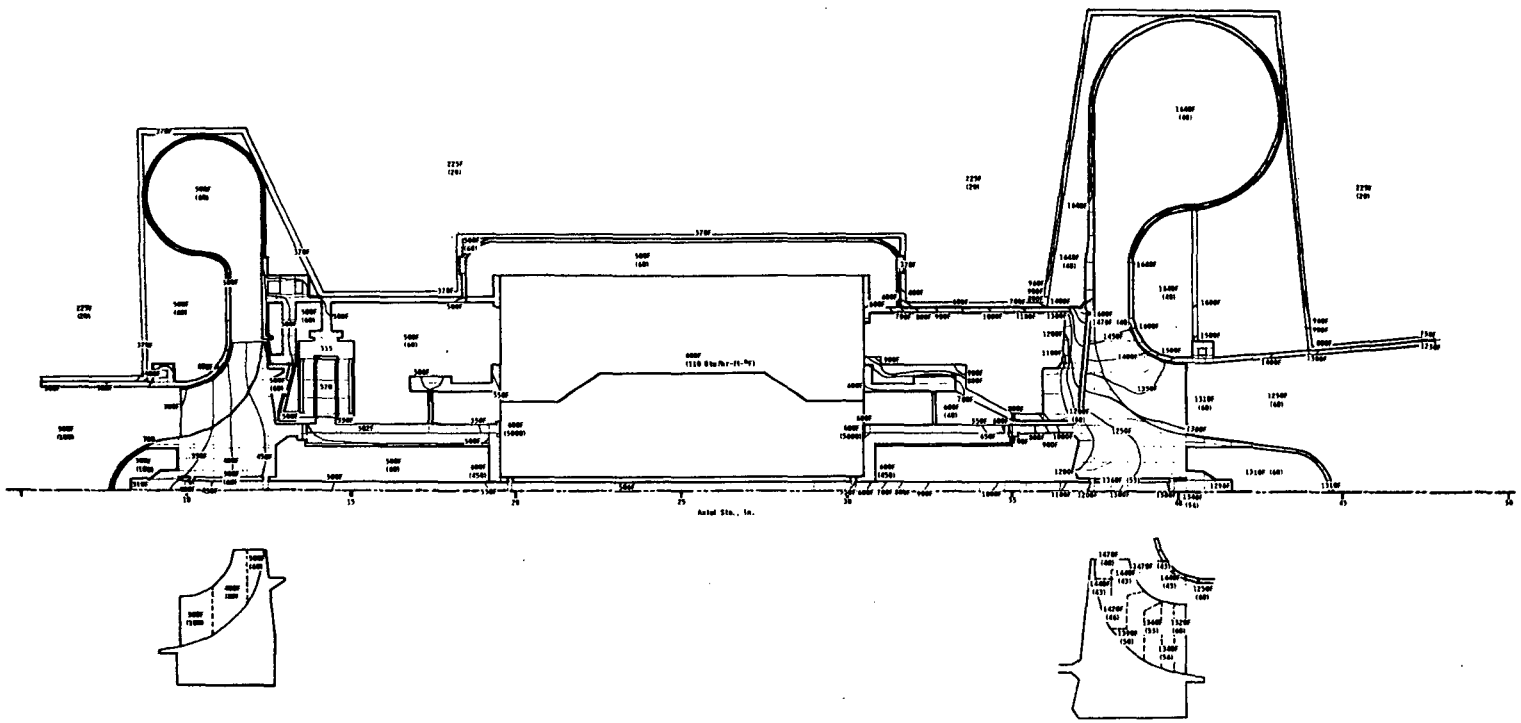

Figure 13.

BRAYTON TAC 24AG
THERMAL EXPANSION, IN.

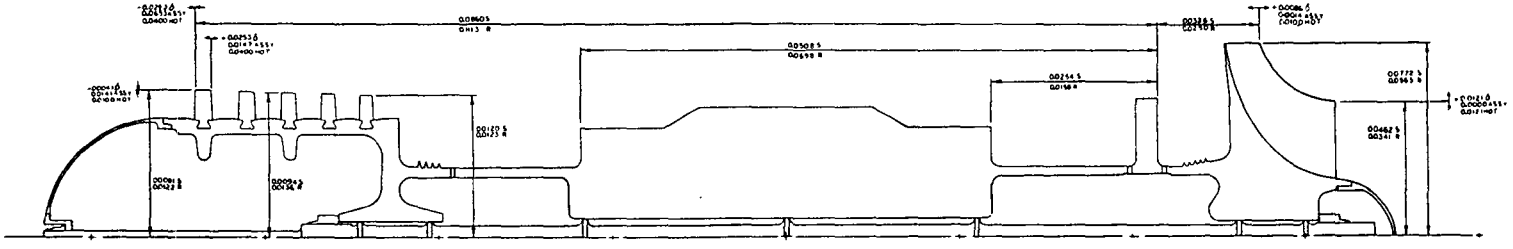

Figure 14.

TABLE VII

24 AG CLEARANCE AT 0g

Mils

TURBINE AXIAL CLEARANCE	THERMAL	+ 8.6 (1)
	BEARING	0 ± 3.0
	ASSEMBLY	+ 2.5 ± 2.5
	HOT	17.2
		5.0
TURBINE RADIAL CLEARANCE	THERMAL	+ 12.1
	BEARING	0 ± 0.3
	ASSEMBLY	+ 2.5 ± 2.5
	HOT	17.4
		11.8
COMPRESSOR AXIAL CLEARANCE	THERMAL	+ 25.3 / - 25.3
	BEARING	0 ± 3.6 / 0 ± 3.6
	ASSEMBLY	+ 14.7 ± 2.5 / + 65.3 ± 2.5
	HOT	46.1 / 46.1
		33.9 / 33.9
COMPRESSOR RADIAL CLEARANCE	THERMAL	- 4.1
	BEARING	0 ± 0.3
	ASSEMBLY	+10.1 ± 2.5
	HOT	8.8
		3.2

NOTES: (1) + MEANS GAP OPENS

(2) CASING DEFORMATION NOT INCLUDED

and compressor blade axial gap maximum hot running clearances all exceed the target values. The desired axial clearance between the axial compressor blades and vanes is 40 mils or slightly greater.

The effective stresses of the 24AG TAC are shown in Figures 15 and 16. The maximum compressor effective stress of 45 ksi at the center support ring gives a factor of safety of 1.23. The critical stresses and factors of safety in the other rotor components are the same as for 24RG. Figure 17 shows representative compressor blade principal stresses for both 24,000 and 36,000 rpm axial compressors. The factors of safety for all locations and speed conditions are quite generous.

Blade vibration calculations made using theoretical and empirical formulas from the literature[1-4] are summarized in Table VIII. The ratios of exitation frequency to critical frequency f_{ex}/f are closer than desirable for the third critical frequencies of the initial stages of both 24 and 36 krpm axial compressors, for the second and third critical frequencies of the 24 krpm axial compressor final stage, and for the third critical frequency of the 36 krpm axial compressor final stage. The problems can be minimized by shifting half of the nozzle vanes circumferentially[5] and by changing the number of nozzle vanes per stage.

The potential advantages of this arrangement are that it also has good rotor dynamic characteristics, requires no alternator seal, and has low bearing power losses.

The major problems to be overcome include those of rotor bonding, alternator rotor cooling, and maintenance of tip clearances.

BRAYTON TAC 24AG
EFFECTIVE STRESS, KSI
FORWARD

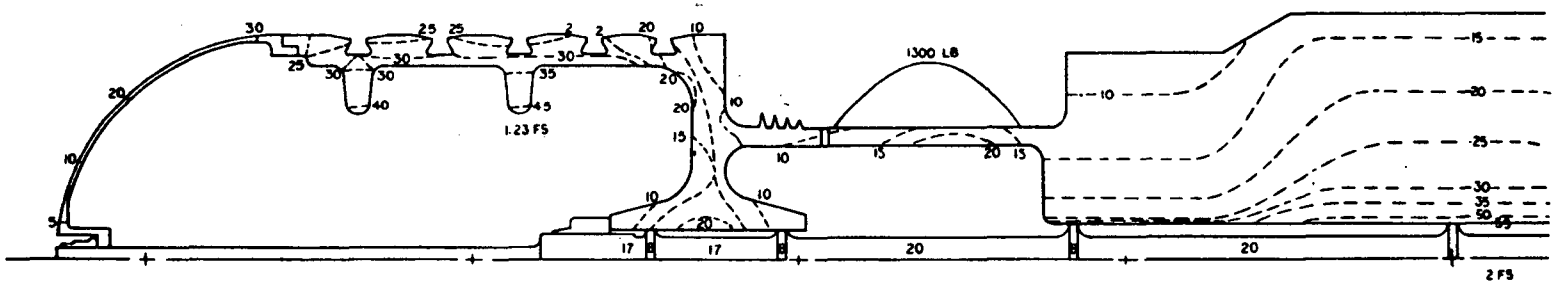

Figure 15.

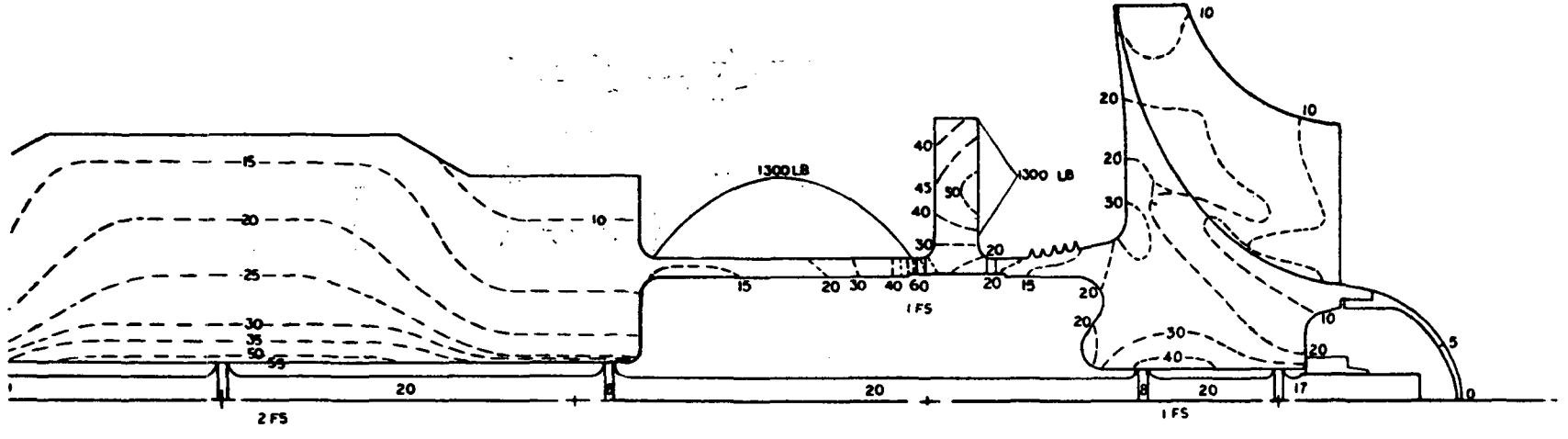
BRAYTON TAC 24AG
EFFECTIVE STRESS, KSI
AFT
1300 LB
1300 LB
1 FS
2 FS
1 FS

Figure 16.

REPRESENTATIVE AXIAL COMPRESSOR BLADE AND DOVETAIL STRESSES AND FACTORS OF SAFETY FOR Ti-6Al-4V MATERIAL

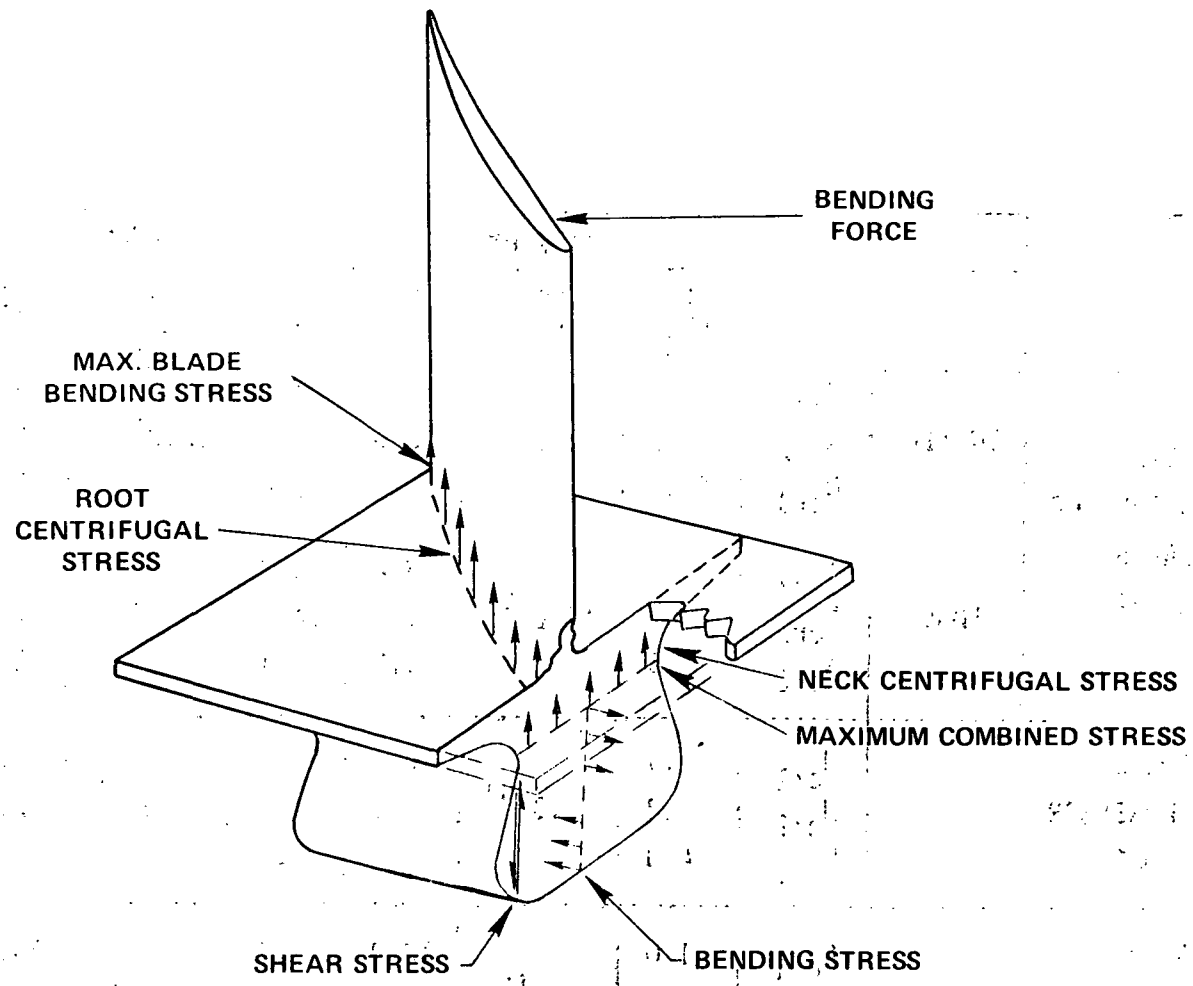

	100% SPEED (CREEP)		120% SPEED (YIELD)	
COMPRESSOR	24 AG	36 AG	24 AG	36 AG
STAGE	1	5	1	5
TEMPERATURE, °F	350	450	350	450
ALLOWABLE STRESS, KSI	75.0	72.0	87.7	79.0
ROOT CENTR. STRESS, KSI	8.8	8.3	12.7	11.9
FACTOR OF SAFETY	8.5	8.7	6.9	6.6
COMBINED STRESS, KSI	10.6	7.2	15.2	10.3
FACTOR OF SAFETY	7.1	10.1	5.8	7.7

Figure 17.

TABLE VIII

TAC BLADE VIBRATION SUMMARY

			24 KRPM			36 KRPM		
	STG.	CRIT.	f KH_Z	fex KH_Z	$\frac{fex}{f}$	f KH_Z	fex KH_Z	$\frac{fex}{f}$
AXIAL COMPRESSOR BLADES AND VANES	INITIAL	N_{cr1}	1.3	18.8(1)	14.5	1.5	28.2(1)	18.8
		N_{cr2}	9.3		2.0	8.8		3.2
		N_{cr3}	24.8		0.8	25.0		1.1
	FINAL	N_{cr1}	2.1	17.2(2)	8.2	2.3	25.8(2)	11.2
		N_{cr2}	13.4		1.3	14.5		1.8
		N_{cr3}	37.6		0.5	40.1		0.6
RADIAL COMPRESSOR BLADES		N_{cr1}	1.5	8.0(3)	5.2	2.4	12.0(3)	5.0
		N_{cr2}	3.2		2.5	4.8		2.4
		N_{cr3}	4.0		2.0	6.2		1.9
RADIAL TURBINE BLADES		N_{cr1}	1.0	12.0(4)	12.0	1.2	18.0(4)	15.0
		N_{cr2}	2.1		5.6	2.6		7.0
		N_{cr3}	2.6		4.6	3.2		5.7

NOTES: (1) 47 BLADES OR VANES
(2) 43 BLADES OR VANES
(3) 20 INLET STRUTS
(4) 30 INLET NOZZLES

The 36AG Configuration

The configuration drawing of the 36,000 rpm, axial-flow compressor TAC on gas bearings is shown in Figure 18.

The arrangement of the major components is very similar to that of the 24AG TAC previously described, the primary differences being in the areas of gas properties, component sizes, and the need for alternator seals. While the rotor cooling system is shown as being different from that of the previous machines, it could actually be the same.

The argon or helium-xenon gas mixture enters the TAC compressor at 240°F and 120 psia and passes aft through the axial compressor, which has a maximum tip diameter of 5.3 in. Turning ninety degrees through a diffuser, the gas enters the compressor discharge scroll at 228 psia and 500°F. It returns from the reactor at 1600°F with negligible decrease in pressure to the turbine inlet scroll. Passing through the turbine inlet guide vanes, the gas enters the turbine rotor at 1400°F and is discharged at 1310°F and 125 psia. The mass flow rate is 11.7 lb/sec. The turbine inlet tip diameter is 7.27 in. and its exit tip diameter is 5.18 in.

The thermal expansions and clearances of the 36AG TAC are summarized by Figure 19 and Table IX. Only the turbine inlet blade tip axial clearance and the compressor axial gap exceed the target values slightly.

The rotor effective stresses are shown on Figures 20 and 21. The minimum compressor factor of safety is 1.2, alternator minimum factor of safety is 1, thrust bearing minimum factor of safety is 1.8, and the turbine minimum factor of safety is unity.

The alternator seals (described later) are items of considerable complexity and are required because of high windage losses which would occur if the alternator were operated at the compressor inlet pressure, even though the smooth outer surface of the Lundell alternator rotor minimizes windage losses.

The major potential advantages of this arrangement include low bearing losses, good rotor dynamics, and good tip clearance control.

BRAYTON CYCLE
TURBO-ALTERNATOR-COMPRESSOR
36AG-1b

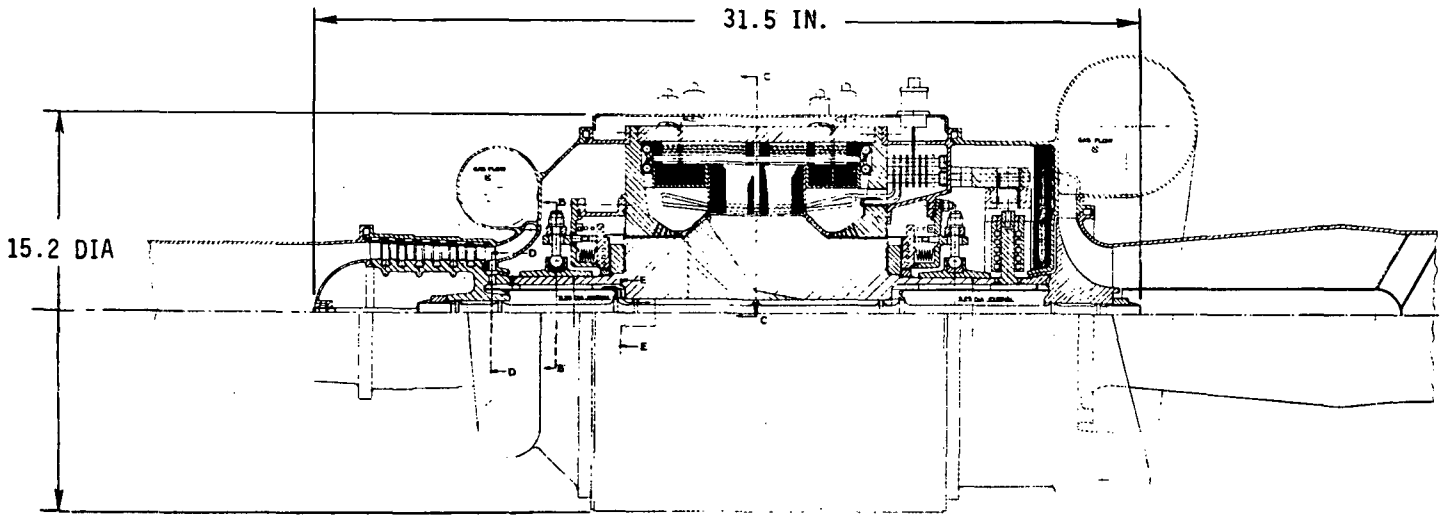

POTENTIAL ADVANTAGES

- LOW BEARING LOSSES
- GOOD ROTOR DYNAMICS
- GOOD TIP CLEARANCE CONTROL

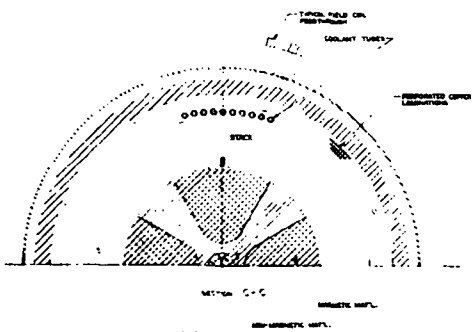

MAJOR PROBLEMS

- ALTERNATOR BONDING
- SPIRAL GROOVE ALTERNATOR SEALS
- EXCESSIVE ALTERNATOR ROTOR STRESSES
- COMPLEXITY OF AXIAL COMPRESSOR

Figure 18.

BRAYTON TAC 36AG
THERMAL EXPANSION, IN.

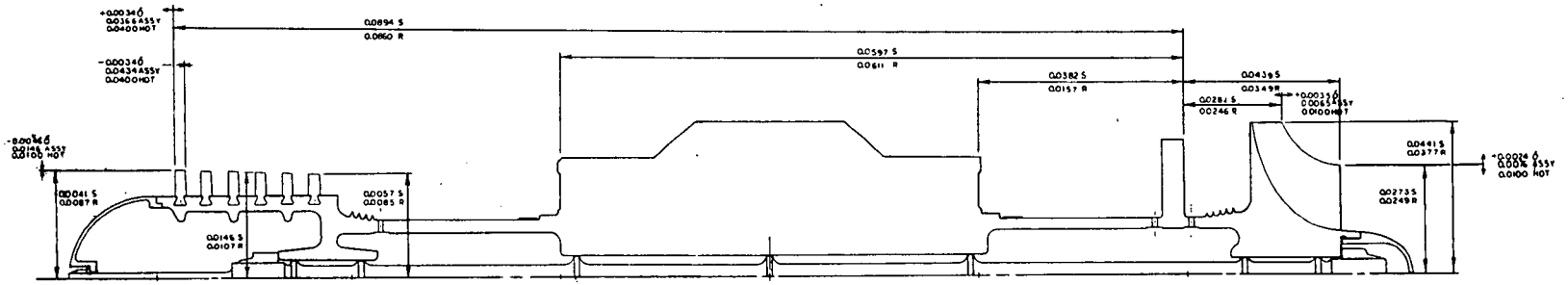

Figure 19.

TABLE IX

36 AG CLEARANCE AT 0g

Mils

TURBINE AXIAL CLEARANCE	THERMAL	(1) + 3.5	
	BEARING	0 ± 3.6	
	ASSEMBLY	+ 5.6 ± 2.5	
	HOT	15.2	
		3.0	
TURBINE RADIAL CLEARANCE	THERMAL	+ 2.4	
	BEARING	0 ± 0.3	
	ASSEMBLY	+ 3.6 ± 2.5	
	HOT	8.8	
		3.2	
COMPRESSOR AXIAL CLEARANCE	THERMAL	+ 3.4	+ 3.4
	BEARING	0 ± 3.6	0 ± 3.6
	ASSEMBLY	+36.6 ± 2.5	+43.4 ± 2.5
	HOT	46.1	46.1
		33.9	33.9
COMPRESSOR RADIAL CLEARANCE	THERMAL	- 4.6	
	BEARING	0 ± 0.3	
	ASSEMBLY	+10.6 ± 2.5	
	HOT	8.8	
		3.2	

NOTES: (1) + MEANS GAP OPENS

(2) CASING DEFORMATION NOT INCLUDED

BRAYTON TAC 36AG
EFFECTIVE STRESS; KSI
FORWARD

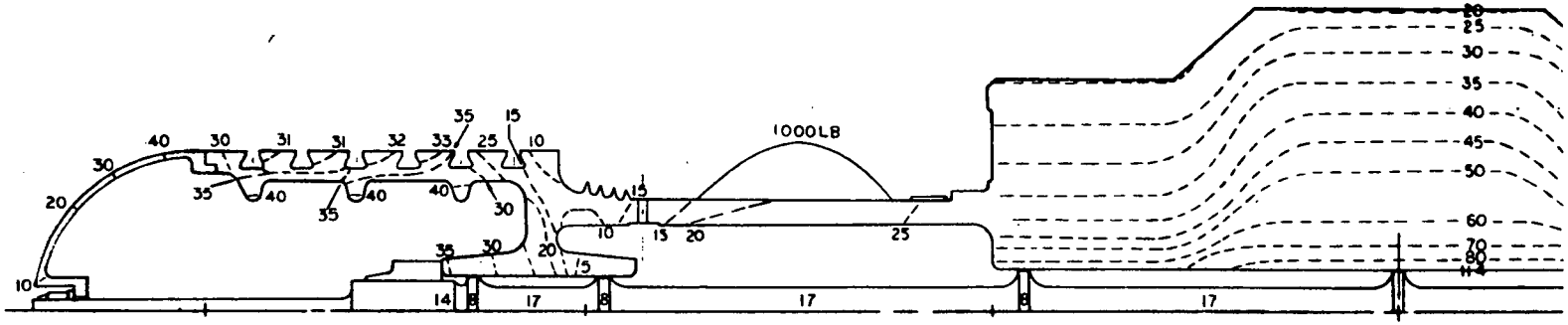

Figure 20.

BRAYTON TAC 36AG
EFFECTIVE STRESS; KSI
AFT

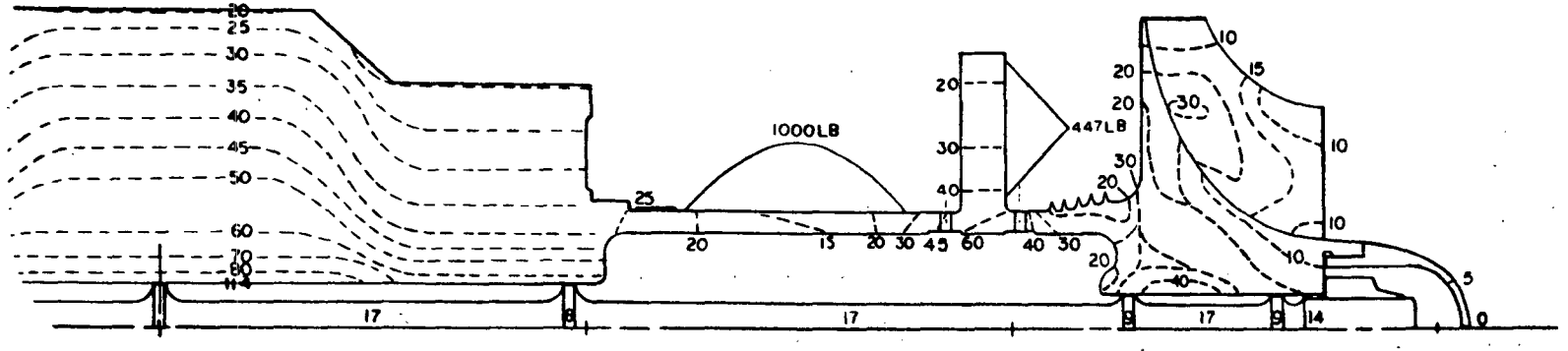

Figure 21.

Major problems include those of alternator bonding, the necessity of the spiral-groove alternator seals, excessive alternator rotor stresses, and the complexity of the axial-flow compressor.

The 36AM Configuration

The configuration drawing of the 36,000 rpm, axial compressor TAC on oil-mist lubricated rolling-element bearings is shown by Figure 22 . It is quite different in many respects from the machines previously discussed, but the gas properties are the same as for the 36AG TAC and the compressor and turbine sizes are similar.

The rotor is supported by 35 mm 18° angular contact bearings at each end which are opposed and preloaded, with the forward bearing/ floating and the aft bearing/fixed. The bearings are both mounted inside housings in the inlet and exhaust gas streams, which exposes the aft bearing to a high temperature environment. Contained within the bearing housings are the necessary lubrication system components: labyrinth seals, liftoff face seals, impellers, oil vapor separators, lubricant passages, springs, and flexible bearing mounts. Two oil heat exchangers, an accumulator, and a chemical absorber are required outside the TAC.

The alternator is a homopolar inductor which has poor windage losses because of its protruding poles. For its most efficient operation the alternator cavity must be evacuated. Therefore, complex spiral groove seals and molecular pumps are required forward and aft of the alternator rotor.

The 36AM TAC thermal analysis results are deduced from those of the 36RM TAC. The difference in compressor types does not alter the thermal analysis significantly. The thermal expansions and clearances are shown by Figure 23 and Table X. The maximum hot running clearances all meet the ten mil aim and the 40 mil goal for axial compressor blade axial clearance is only missed by 2.6 mils.

The effective stresses are shown by Figure 24. The minimum factors of safety are; compressor - 1.2, alternator - 1.1, and turbine - unity.

The potential advantages of this machine are that the ball bearing technology is well established in that even special bearings are relatively minor variants of proved designs, no separate thrust bearing

BRAYTON CYCLE
TURBO-ALTERNATOR-COMPRESSOR
36AM-2a

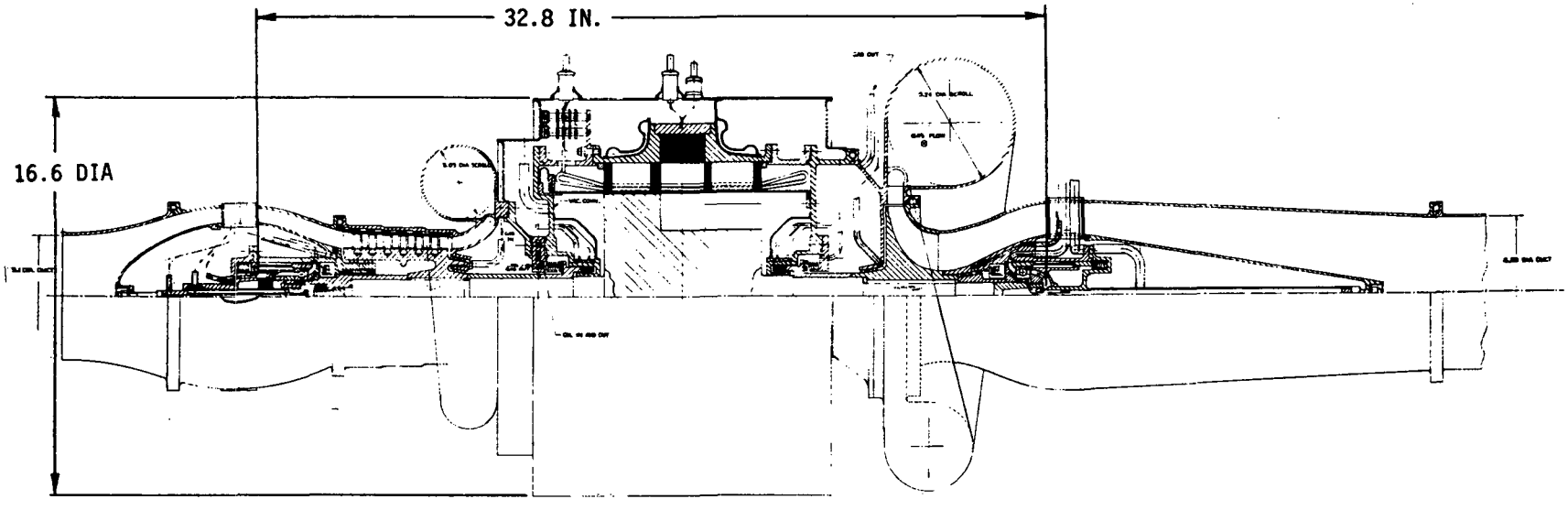

POTENTIAL ADVANTAGES

- BALL BEARING TECHNOLOGY WELL ESTABLISHED
- NO SEPARATE THRUST BEARING
- LOW FRICTION LOSSES
- BEST CONTROL OF TIP AND SEAL CLEARANCES
- HIGHER SYSTEM EFFICIENCY

MAJOR PROBLEMS

- BEARING LIFE
- NO OVERLOAD CAPACITY
- AUSFORMED M-50 STEEL DEVELOPMENT
- POOR ROTOR DYNAMICS
- COMPLEX LUBRICATION SYSTEM
- OIL CONTAMINATION OF SYSTEM
- DETERIORATION OF LUBRICANT
- ALTERNATOR BORE SEAL REQUIRED
- AXIAL COMPRESSOR COMPLEXITY

Figure 22.

BRAYTON TAC 36AM
THERMAL EXPANSION, IN.

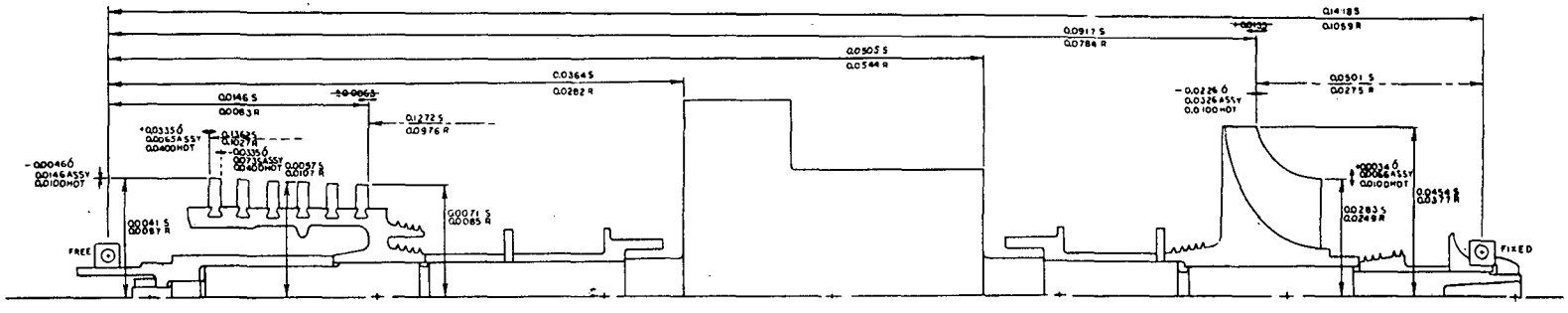

Figure 23.

TABLE X

36 AM CLEARANCE AT 0g

Mils

		(1)
TURBINE AXIAL CLEARANCE	THERMAL	- 22.6
	BEARING	0 ± 0.1
	ASSEMBLY	+ 25.6 ± 2.5
	HOT	5.6
		0.4
TURBINE RADIAL CLEARANCE	THERMAL	+ 3.4
	BEARING	0 ± 2.0
	ASSEMBLY	+ 2.5 ± 2.5
	HOT	10.4
		1.4
COMPRESSOR AXIAL CLEARANCE	THERMAL	+ 33.5 / - 33.5
	BEARING	0 ± 0.1 / 0 ± 0.1
	ASSEMBLY	+ 6.5 ± 2.5 / + 73.5 ± 2.5
	HOT	42.6 / 42.6
		37.4 / 37.4
COMPRESSOR RADIAL CLEARANCE	THERMAL	- 4.6
	BEARING	0 ± 2.0
	ASSEMBLY	+ 9.2 ± 2.5
	HOT	9.1
		0.1

NOTES: (1) -MEANS GAP CLOSES

(2) CASING DEFORMATION NOT INCLUDED

(3) TURBINE BEARING FIXED

BRAYTON TAC 36AM
EFFECTIVE STRESS, KSI

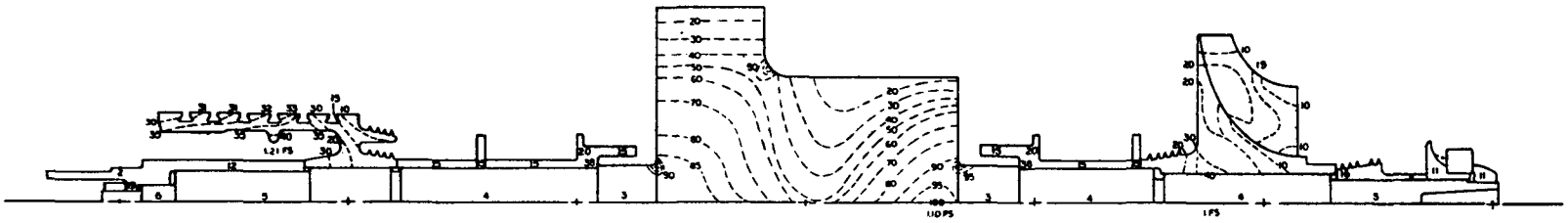

Figure 24.

is required when angular contact ball bearings are used, the bearings and seals have low friction losses, the best control of tip and seal clearances is provided because of the small bearing clearances, and the axial compressor offers higher system efficiency than the comparable machine with a radial compressor.

Major problems are that the bearings have no overload capacity since five-year life cannot be guaranteed at the expected normal operating conditions, the bearings require the use of ausformed M-50 steel which is still a development item, the small diameter shafts dictated to achieve best bearing life and the long bearing span give poor rotor dynamic performance, the complex oil lubrication system which is very likely to contaminate the system power fluid, the probable deterioration of the lubricant in the high temperature and radiation environment for five years, the complicated alternator bore seal required, and the complexity of the axial compressor.

The 36RM Configuration

The configuration drawing of the 36,000 rpm radial compressor TAC on oil mist lubricated rolling-element bearings is shown by Figure It is similar in all major respects to the 36AM TAC except for the substitution of the compressor.

The results of the thermal analysis of the 36RM TAC are shown by Figure 25a. The temperature distribution is similar to previous ones, with the forward end of the stator and rotor less than 500°F, the alternator stator rotor, aft seals, and aft shaft between 500-1000°F, and the turbine, its inlet scroll, and exhaust duct, including the aft bearing housing, between 1000-1640°F.

The 36RM thermal expansions are shown by Figure 26 and Table XI synopsizes the clearances, all of which meet the 10 mil goal or exceed it insignificantly. The forward bearing is fixed in this machine.

The minimum factors of safety in the 36RM TAC are: compressor - 2.2, alternator - 1.1, and turbine - unity. The effective stresses are shown on Figure 27.

Although the centrifugal compressor reduces the complexity of the configuration, the shorter length permissible does not improve the rotor

BRAYTON CYCLE
TURBO-ALTERNATOR-COMPRESSOR
36RM-2a

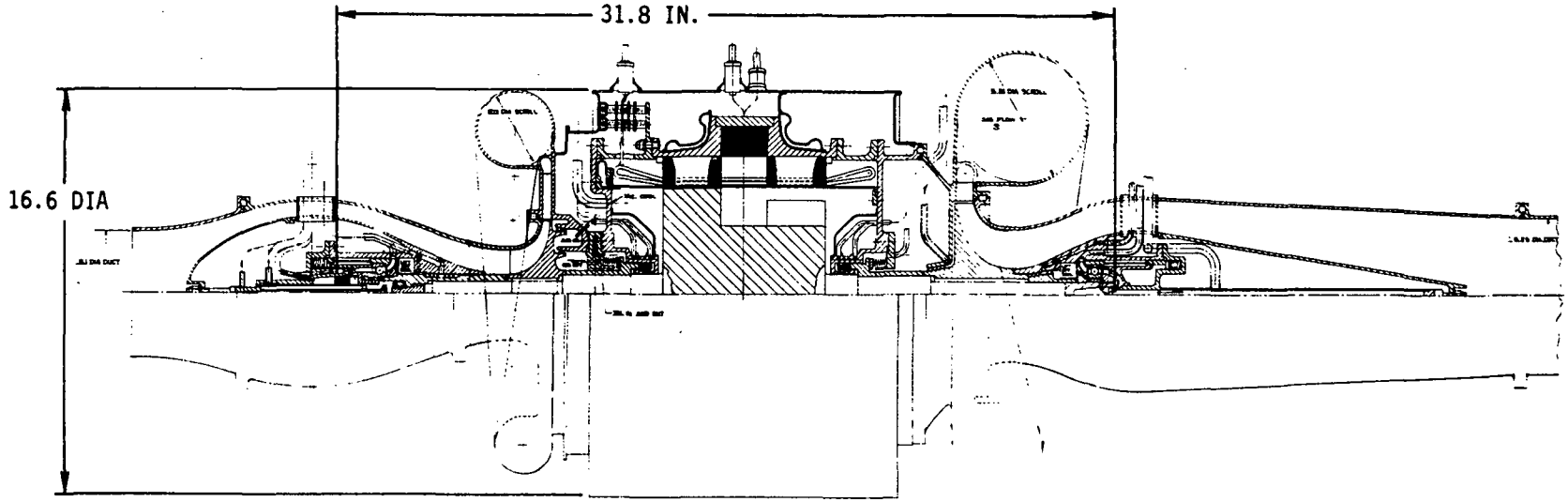

POTENTIAL ADVANTAGES

- BALL BEARING TECHNOLOGY WELL ESTABLISHED
- NO SEPARATE THRUST BEARINGS
- LOW FRICTION LOSSES
- BEST CONTROL OF TIP AND SEAL CLEARANCES

MAJOR PROBLEMS

- BEARING LIFE
- NO OVERLOAD CAPACITY
- AUSFORMED M-50 STEEL DEVELOPMENT
- POOR ROTOR DYNAMICS
- COMPLEX LUBRICATION SYSTEM
- OIL CONTAMINATION OF SYSTEM
- DETERIORATION OF LUBRICANT
- ALTERNATOR BORE SEAL REQUIRED

Figure 25.

STEADY-STATE ISOTHERMS FOR 36RM-1a TAC

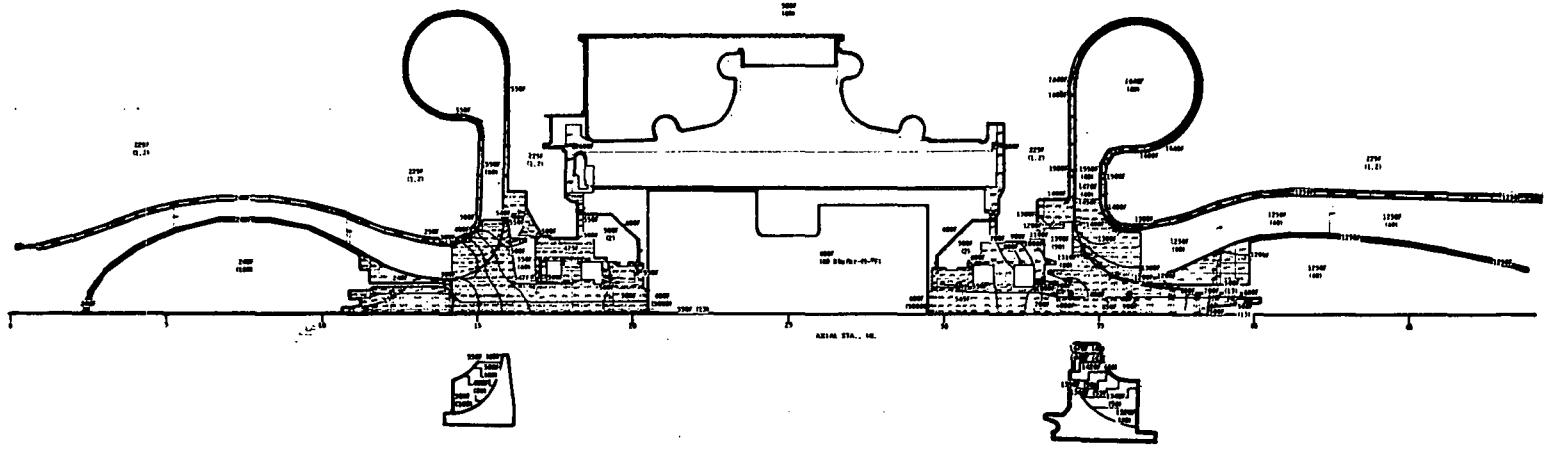

Figure 25a

BRAYTON TAC 36RM
THERMAL EXPANSION, IN.

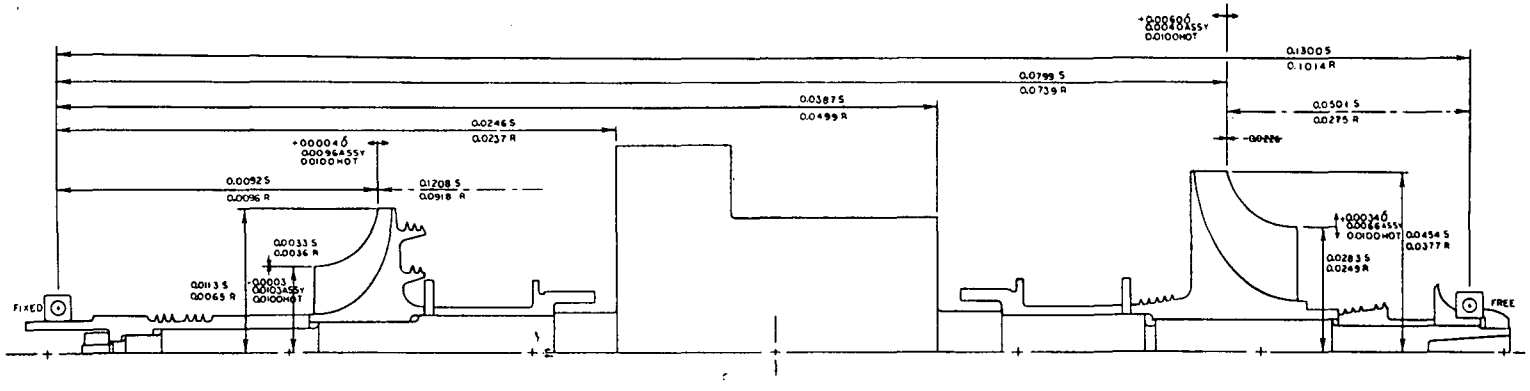

Figure 26.

TABLE XI

36 RM CLEARANCE AT Og

Mils

		(1)
TURBINE AXIAL CLEARANCE	THERMAL	+ 6.0
	BEARING	0 ± 0.1
	ASSEMBLY	+ 2.5 ± 2.5
	HOT	11.1
		5.9
TURBINE RADIAL CLEARANCE	THERMAL	+ 3.4
	BEARING	0 ± 2.0
	ASSEMBLY	+ 2.5 ± 2.5
	HOT	10.4
		1.4
COMPRESSOR AXIAL CLEARANCE	THERMAL	+ 0.4
	BEARING	0 ± 0.1
	ASSEMBLY	+ 2.6 ± 2.5
	HOT	5.6
		0.4
COMPRESSOR RADIAL CLEARANCE	THERMAL	- 0.3
	BEARING	0 ± 2.0
	ASSEMBLY	+ 4.9 ± 2.5
	HOT	9.1
		0.1

NOTES: (1) + MEANS GAP OPENS

(2) CASING DEFORMATION NOT INCLUDED

(3) COMPRESSOR BEARING FIXED

BRAYTON TAC 36RM
EFFECTIVE STRESS, KSI

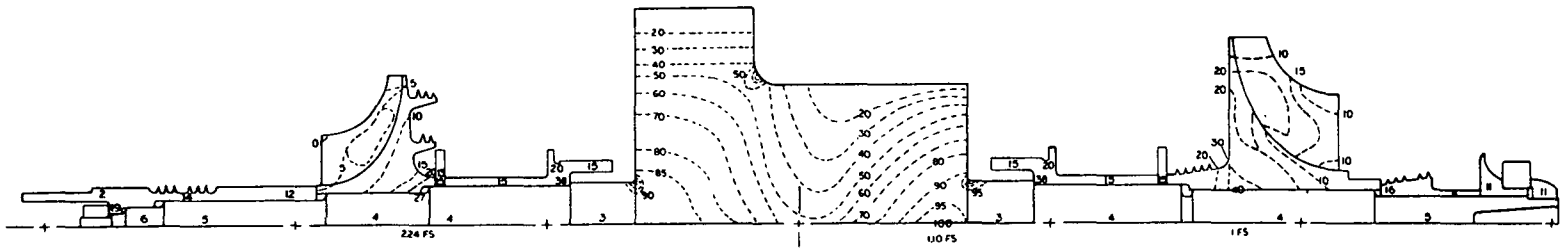

Figure 27.

dynamics substantially over that obtained in a 36AM configuration.

The potential advantages and disadvantages of this machine are the same as for the previous one except that some loss of efficiency is associated with the more simple radial compressor.

The 36RL Configuration

Shown in Figure 28 is a 36RL configuration which is completely different from any of the five configurations shown previously. A major difference is that both the compressor and turbine are overhung together from one side of the homopolar inductor, alternator which is straddle-mounted on the oil film bearings. The compressor and alternator are overhung considerably aft of the aft bearing, a combined journal and thrust oil-film bearing. The primary reason for the large overhang is the space requirement for the compressor inlet scroll. All of the previous machines were able to use compressor inlet ducts. Combined molecular pumps and recirculating seals giving minimum leakage of oil vapor into the alternator cavity are required.

The temperature distribution in the 36RL TAC is shown by Figure 29, which shows a pattern quite different from the other machines because the compressor and turbine are mounted back-to-back. In this machine the region of temperatures below 500°F includes not only the stator and rotor forward of the alternator but also the stator and rotor from the aft bearing to the center of the compressor. The rest of the compressor, most of the compressor exit scroll, the aft end of the shaft, and the alternator stator and rotor are between 500-1000°F. The turbine, turbine scroll, and exhaust duct are 1000-1640°F. This design produces high thermal gradients in the vicinity of the compressor and turbine.

The 36RL thermal expansions are shown by Figure 30 and the clearances are summarized in Table XII. Despite the adverse thermal patterns, the 10 mil clearance goal is met at all critical gaps except the turbine inlet blade tip axial gap of 15.4 mils maximum.

At this point all of the TAC clearances have been described and are summarized by Table XIII. It should be remembered that the casing deformations are not included and that for all of the machines with axial compressors the axial compressor gap goal might be slightly greater than 40 mils. The 36AM TAC had its aft ball bearing fixed while the opposite

BRAYTON CYCLE
TURBO-ALTERNATOR-COMPRESSOR
36RL-2a

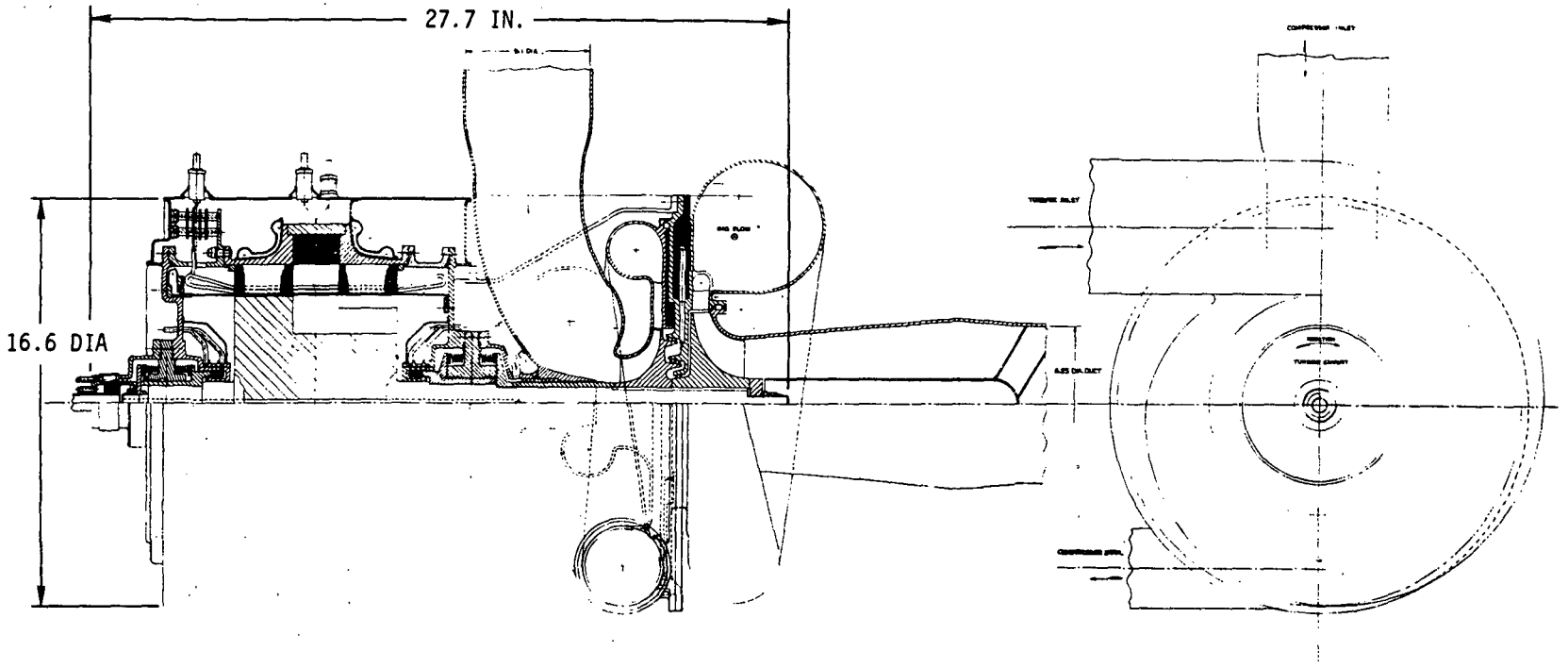

POTENTIAL ADVANTAGES

- HIGH BEARING OVERLOAD CAPACITY
- GOOD TIP CLEARANCE CONTROL
- OIL SEALS REDUCE ALTERNATOR WINDAGE

MAJOR PROBLEMS

- ROTOR DYNAMICS POOR
- BEARING AND SEAL POWER LOSSES EXCESSIVE
- COMPLEX LUBRICATION SYSTEM
- OIL CONTAMINATION OF SYSTEM
- ALTERNATOR BORE SEAL REQUIRED

Figure 28.

STEADY STATE TEMPERATURE DISTRIBUTION FOR 36 RL TAC

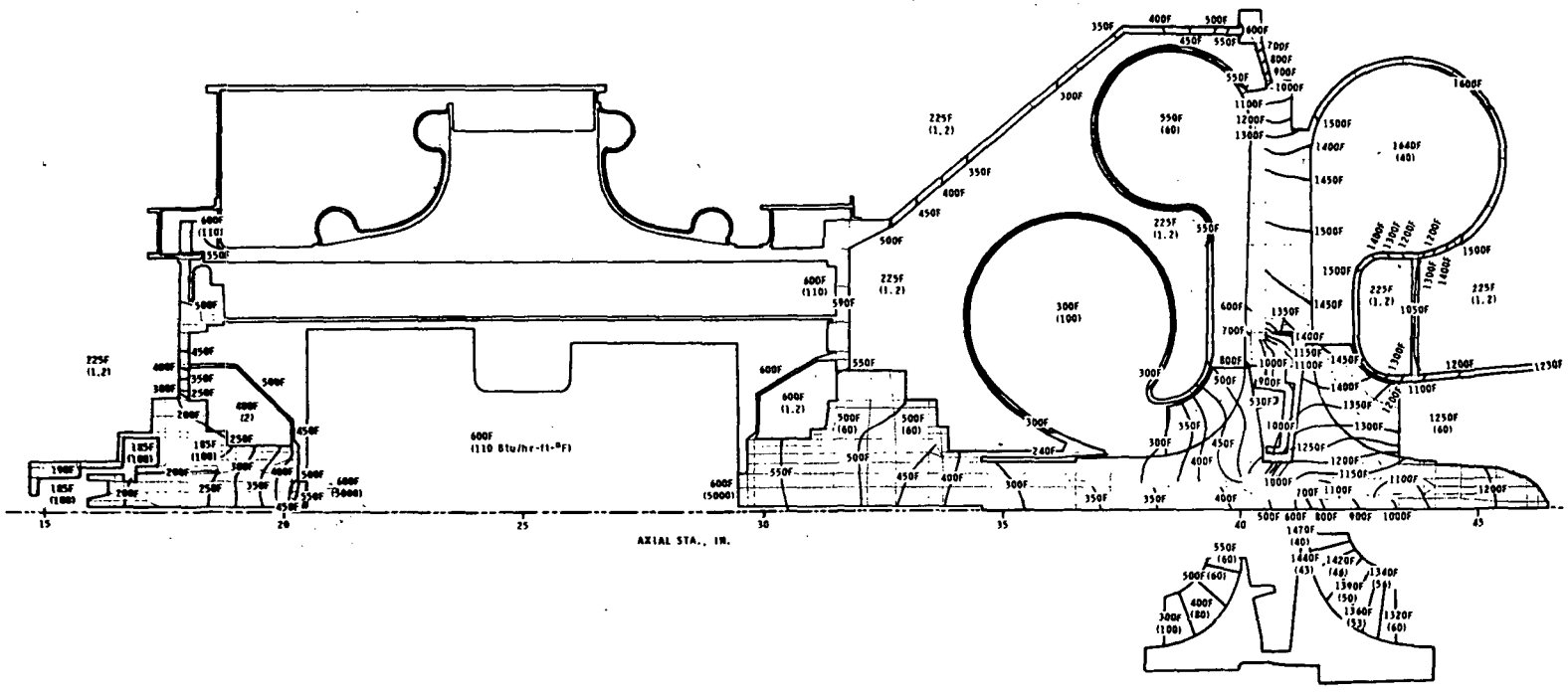

Figure 29.

BRAYTON TAC 36RL
THERMAL EXPANSION, IN.

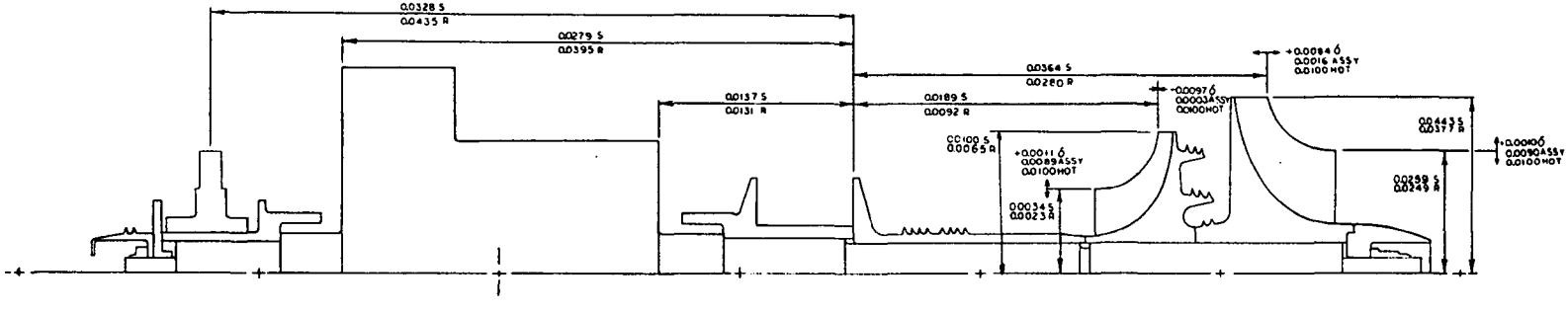

Figure 30.

TABLE XII

36 RL CLEARANCE AT 0g

Mils

		(1)
TURBINE AXIAL CLEARANCE	THERMAL	+ 8.4
	BEARING	0 ± 2.0
	ASSEMBLY	+ 2.5 ± 2.5
	HOT	15.4
		6.4
TURBINE RADIAL CLEARANCE	THERMAL	+ 1.0
	BEARING	0 ± 0.4
	ASSEMBLY	+ 3.5 ± 2.5
	HOT	7.4
		1.6
COMPRESSOR AXIAL CLEARANCE	THERMAL	- 9.7
	BEARING	0 ± 2.0
	ASSEMBLY	+ 14.2 ± 2.5
	HOT	9.0
		0
COMPRESSOR RADIAL CLEARANCE	THERMAL	+ 1.1
	BEARING	0 ± 0.4
	ASSEMBLY	+ 3.4 ± 2.5
	HOT	7.4
		1.6

NOTES: (1) + MEANS GAP OPENS

(2) CASING DEFORMATION NOT INCLUDED

TABLE XIII

MAXIMUM TAC HOT RUNNING CLEARANCE SUMMARY - OG
MILS

	36AG	36RL	36AM(1)	36RM(2)	24AG	24RG
TURBINE AXIAL CLEARANCE	15.2	15.4	5.6	11.1	17.2	15.2
TURBINE RADIAL CLEARANCE	8.8	7.4	10.4	10.4	17.4	16.7
COMPRESSOR AXIAL CLEARANCE	46.1 33.9	9.0	42.6 37.4	5.6	46.1 33.9	15.2
COMPRESSOR RADIAL CLEARANCE	8.8	7.4	9.1	9.1	8.8	8.8

was true for the 36RM TAC. The 36AM and 36RM machines meet all hot running clearance goals because of the superior clearance and deformation control inherent in the angular contact ball bearings. The 36AG and 36RL machines meet the clearance goals at all the critical gaps except the turbine inlet blade tip axial gaps, which are slightly greater than 15 mils. The 24AG TAC exceeds the 10 mil goals at the turbine inlet blade tip axial gap and turbine exit blade tip radial gap by 7.2 and 7.4 mils. The 24RG TAC misses the goals by slightly less at the same two locations, but also misses the goal at the compressor exit blade tip axial gap by 5.2 mils. The effect of the greater gap clearances is discussed later

The effective stresses in the 36RL TAC are shown in Figure 31. The minimum factors of safety are 2.3 for the compressor and unity for the alternator and turbine, assuming the use of Rene' 80 for this compressor because of its higher temperature than any other compressor considered.

The advantages of this machine are that there is high bearing overload capacity, good tip clearance control, and the oil seals reduce the alternator windage to a palatable value. However, the reduction in windage loss is overridden by a large bearing and seal loss. As was the case for the other oil lubricated configurations, a complex lubrication system is required to prevent oil contamination of the entire Brayton system. And, as before, an alternator bore barrier is required to prevent carburization of the oil on the windings. In spite of reducing the number of seals required for this configuration to reduce losses by overhanging the compressor and turbine on the same side, the bearing and seal power losses are excessive. In addition, because of the overhang of the compressor and turbine on one side, the rotor-bearing response is very poor.

TAC Weight Summary

The weight summary for all the machines which were investigated is shown by Table XIII. It is seen that the 24 krpm compressors and turbines weigh about three times as much as the 36 krpm components because of the difference in sizes. The axial compressors weigh about twice as much as the comparable radial compressors (36RL has the only Rene' 80 compressor). There is little variation in the stubshafts and tiebolt weights. The

BRAYTON TAC 36RL
EFFECTIVE STRESS, KSI

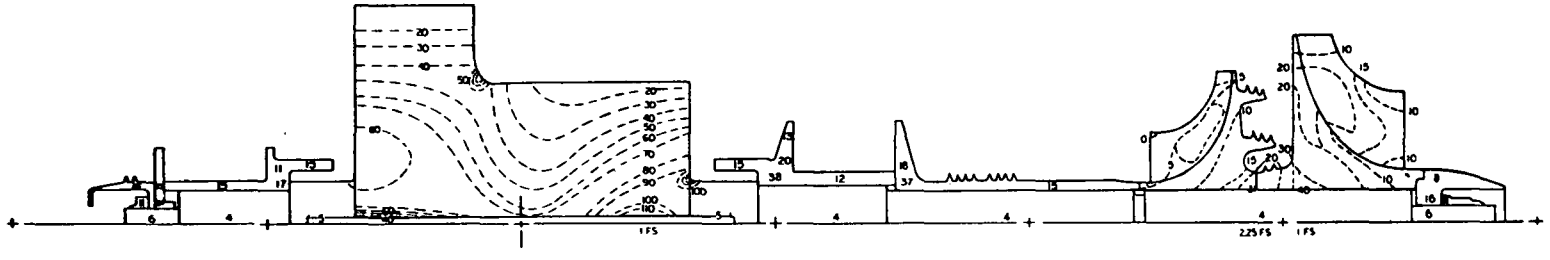

Figure 31.

TABLE XIII

TAC WEIGHT SUMMARY
(POUNDS)

	24RG	24AG	36AG	36AM	36RM	36RL	24RG*
COMPRESSOR	10	20	6	6	2	5	8
ALTERNATOR-ROTOR	98	98	92	83	83	83	135
TURBINE	25	25	8	8	8	8	22
STUBSHAFTS/TIEBOLT	19	22	17	22	19	22	22
TOTAL ROTOR	152	165	123	119	112	118	187
ALTERNATOR-STATOR	181	181	180	155	155	155	331
CASING	265	259	160	170	167	153	351
TOTAL STATOR	446	440	340	325	322	308	682
TOTAL WEIGHT	598	605	463	444	434	426	869

* PHASE III

alternator rotor weights are 60-75 percent of the total rotor weights, with the Phase I Lundell stators weighing about 18 percent more than the homopolar inductor stators.

The Lundell alternator stators weigh about 16 percent more than the homopolar inductor stators and are 41-53 percent of the total rotor weights. The 24 krpm casings weigh about 60 percent more than those of the 36 krpm machines because of the size differences.

The net result is that the Phase I 24 krpm TACs weigh about 600 pounds, about 37 percent more than the 426-463 pound weights of the 36 krpm machines.

Mechanical Design Comparison

Now that the details of the design studies in the mechanical design area have been presented, the configurations will be compared and the mechanical designs will be evaluated.

Shown in Table XIV is a mechanical design comparison of the six configurations. The first line shows the designation of the various configurations previously explained and the second line distinguishes between the radial- and axial-flow compressors. The number following the letter A designating an axial flow compressor specifies the number of stages. The table indicates that all of the axial-flow compressors have peak stresses of 46,000 to 47,000 psi. Since all the radial-flow turbine designs are similar, a peak stress of 40,000 psi is encountered in the bore of these turbines, and is considered to be barely acceptable

The peak alternator stresses in all of the 36,000 rpm designs are almost 100,000 psi. However, the Lundell alternator at 24,000 rpm has a peak stress of only 56,000 psi at 100 percent speed.

The significant comparative bearing values are the bearing lives. All configurations meet the 5-year life with the exception of the two ball bearing configurations, whose life is predicted to be less than 3 years. Therefore, they have no overload capability.

The comparison of the configurations in terms of rotor dynamics is clearly in favor of the 24RG configuration, which has a third critical rotative speed 68 percent beyond the 20 percent overspeed point. The two axial configurations at 24,000 and 36,000 rpm have third critical

TABLE XIV

TAC PHASE I
CONFIGURATION COMPARISON

ARRANGEMENT	24 RG	24 AG	36 AG	36 AM	36 RM	36 RL
COMPRESSOR	R	A-7	A-6	A-6	R	R
DIA., INCH	8.8	8.6	5.3	5.3	5.92	5.92
*PEAK STRESS, PSI	26,000	46,000	47,000	47,000	27,000	31,000
TURBINE	RADIAL INFLOW					
DIA., INCH	11.1		7.27			
*PEAK STRESS, PSI	40,000					
ALTERNATOR	LUNDELL			INDUCTOR		
ROTOR DIA., INCH	7.500		7.125	9.155		
*PEAK STRESS, PSI	56,000		91,000	99,000		
BEARINGS	GAS			OIL MIST	LI. OIL	
JOURNAL DIA., INCH	4.0		3.25	1.38 (=3.5 MM)	2.0	1.63
LENGTH, INCH	3.0		2.6		0.5	0.4
THRUST OD, IN.	8.0		7.0	NONE	2.89	
ID, IN.	4.25		3.5		2.13	
BEARING.LIFE, YRS.	5.0		5.0	<3	5.0	
ROTOR DYNAMICS						
THRID CRITICAL, RPM	48,930	38,010	56,500	25,494	43,239	
THIRD CRIT./OVERSPEED	1.68	1.32	1.31	.57	.96	

*PEAK STRESS AT 100% SPEED

speeds around 30 percent greater than the 100 percent overspeed condition. The rotor-bearing response of the oil-lubricated configurations is very poor.

Shown in Table XV is a mechanical design evaluation of the six configuration studies. For the 24,000 rpm configurations, the stress levels are safe for all three components, the compressor, turbine and alternator. The clearance control on these two configurations is rated poorer than for all the 36,000 rpm configurations. The bearing life is good for all configurations except for those having ball bearings. The rotor bearing response is best for the 24RG configuration and only fair for the axial compressor configurations designated 24AG and 36AG. Poor response is indicated for all of the oil lubricated bearing configurations.

For both of the 24,000 rpm configurations, the three developments needed are the alternator rotor bonding, alternator stator cooling, and thrust bearing development. The thrust bearing development can be removed if a lower maneuver load is specified, which would make the thrust bearing a size within present developments. The 36AG configuration has two serious development problems. The bonding of the 36,000 rpm Lundell rotor is serious because of the high stresses. The helical-groove face seal needed to reduce the pressure in the alternator cavity is considered a difficult development because of small running clearances and large probable distortions of the runner and stator. The helical groove face seals for the oil-lubricated film bearings are considered to be a development of a lesser magnitude than the gas helical groove face seal for the 36,000 rpm gas bearing configuration. No risk items are listed for the 24,000 rpm configurations and the only other drawback is the complexity of the axial-flow compressor. As a result, the 24RG configuration was considered to be the best choice from a mechanical standpoint for the TAC unit based on the specifications provided in this study.

TABLE XV

TAC PHASE I

MECHANICAL DESIGN EVALUATION

ARRANGEMENT	24 RG	24 AG	36 AG	36 AM	36 RM	36 RL
STRESS SAFETY FACT.						
COMPRESSOR	VERY SAFE					
TURBINE	SAFE					
ALTERNATOR	SAFE		UNSAFE			
CLEARANCE CONTROL	FAIR	FAIR	GOOD	GOOD	GOOD	GOOD
BEARING LIFE	GOOD			POOR		GOOD
BEARING-ROTOR RESPONSE	GOOD	FAIR	FAIR	POOR		
DEVELOPMENTS						
ALTERNATOR						
BONDED ROTOR	X	X	XX			
STATOR COOLING	X	X	X			
BORE SEAL				X	X	X
HELICAL GROOVE FACE SEAL			XX	X	X	X
THRUST BEARING	X	X	X			
RISK						
ROTOR STRESS			X	X	X	X
OIL-GAS MIXING				X	X	X
BEARING LIFE				X	X	
COMPLEXITY						
OIL HANDLING SYSTEM				X	X	X
AXIAL COMPRESSOR		X	X	X		
BEST MECHANICAL	X					

ROTOR DYNAMIC STUDIES

The primary purpose of the rotor dynamic studies was to establish the vibrational behavior of the rotor-bearing system when subjected to rotating unbalance. Several analyses were made during the course of the Phase I study on several different rotor configurations for each machine concept. These analyses led to a specification of the rotor geometry, size, and arrangement which resulted in acceptable vibrational behavior. Rotor-bearing resonances were defined, and the rotor vibration amplitudes as a function of speed driven by rotor unbalance, were calculated.

Included in the studies were the rotor flexibility and the support compliance where significant. The influence of bearing film stiffness and damping as a function of operating conditions was also included. Furthermore, the location of the exciting force (mechanical unbalance) was evaluated and worst case situations are presented.

The following sections summarize the results of the final Phase I machine configuration dynamic studies. Oil lubricated and gas lubricated machines are discussed separately since their dynamic behavior and approaches taken to achieve a solution are somewhat different.

Gas Bearing Machines

The component arrangement for the gas bearing machines studied in Phase I typically had the alternator mounted between journal bearings with the turbine and compressor overhung from opposite shaft ends. This arrangement leads to the most straightforward entrance and exit ducting, minimizes seal problems, and generally leads to the simplest machine assembly.

With this type of arrangement and particular mass distribution the third critical speed has a mode shape with the nodes typically near the bearings as shown pictorially in Figure 33 . Such a situation leads to little or no relative shaft-bearing displacement near the third critical, thus little potential for squeeze film damping. Without significant damping in the rotor bearing system, operation near such a bending critical would result in excessive vibration amplitudes possibly leading to failure.

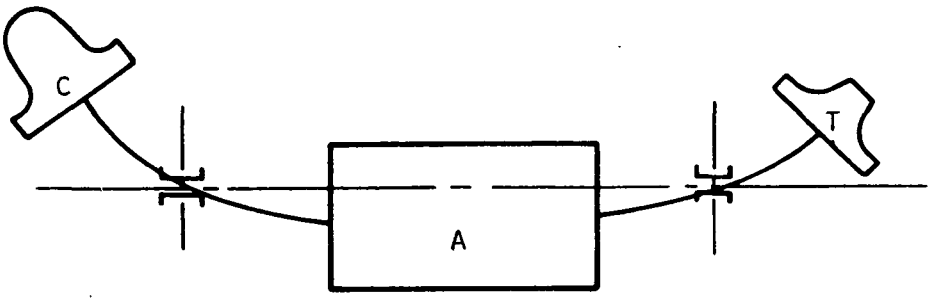

TYPICAL 3rd CRITICAL MODE SHAPE

Figure 33

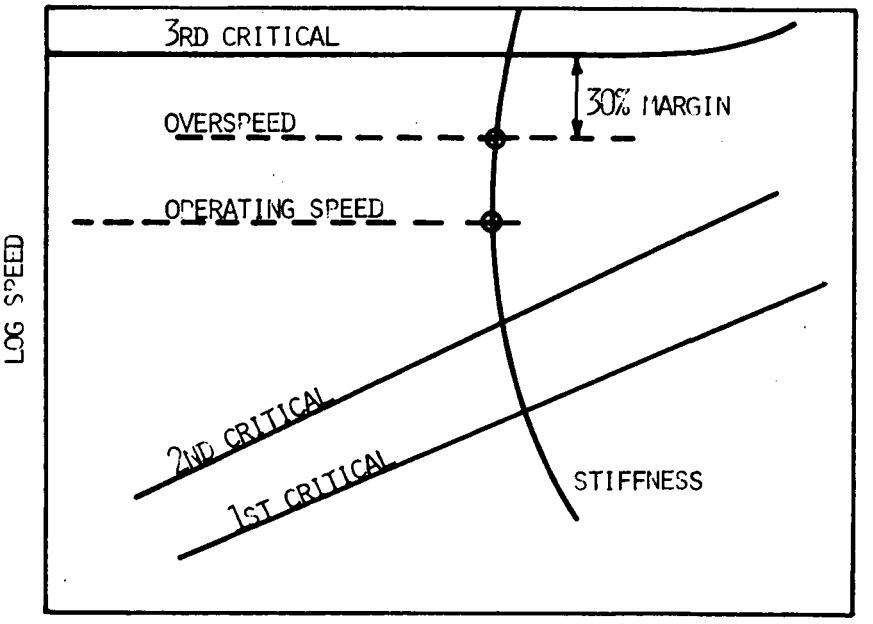

CRITERIA FOR 3rd CRITICAL SPEED

Figure 34

For this reason, all the gas bearing machines have been designed to operate below the third critical speed and have at least a 30% margin between the 20% over speed condition and the third critical (see Figure 34). The 30% minimum margin (ω/ω_n = .78) is a standard MTI design criteria which usually results in acceptably small amplification factors (typically less than 3) at the upper speed limit. This can be seen on Figure 35 which shows the amplifications as a function of critical speed for a simple mass-spring system.

The critical speed maps for the three gas bearing machines (36AG, 24AG, and 24RG) along with mode shape diagrams are shown on Figures 36, 37 and 38 . As can be seen from these figures, the rotors are extremely stiff and the first two critical speeds are rigid body modes as is evidenced by the mode shape plots and the straight line critical speed-bearing stiffness characteristics. The third critical, which of course is bending, is in all cases well above the 20% overspeed case as is summarized below.

Configuration	3rd N_{cr} (at K = 10^5 $\frac{lb}{in}$)	$N_{cr}/1.2 \times N_{des}$
24 AG	38010	1.32
24 RG	48930	1.68
36 AG	56500	1.31

Typical bearing stiffness versus speed characteristics for 1g (horizontal) operation are plotted on Figures 37 and 38 for the 24,000 rpm machines. In addition to the stiffness-speed characteristics, damping-speed characteristics were also calculated and used in the rotor response analyses for the 24,000 rpm machines shown on Figures 39 and 40 . For the purpose of calculating the bearing dynamic characteristics the following significant assumptions regarding the journal bearings were made:

Number of Pads:	4
Diameter:	4.0 inches
Length:	3.0 inches
$R_{pad}-R_{shaft}$:	.004 inches*
Radial Clearance:	.002 inches*

*Clearance at 24,000 rpm. At other speeds, clearance changes due to (.25 inch thick) rotor centrifugal growth variation and pad load variation causing pad flexure displacement. These variations are computed at each speed.

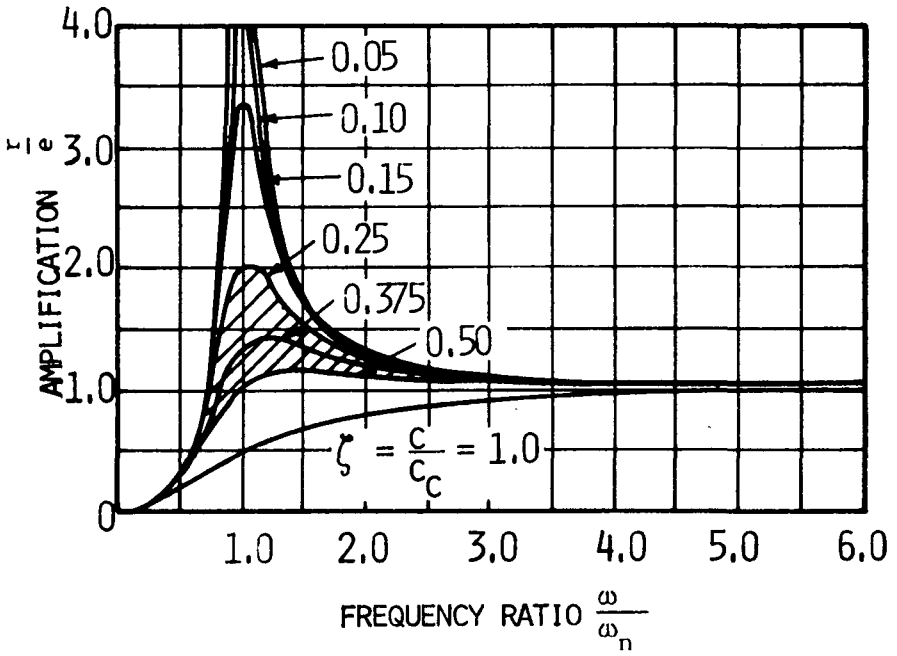

TYPICAL RESPONSE CURVE INCLUDING DAMPING

Figure 35

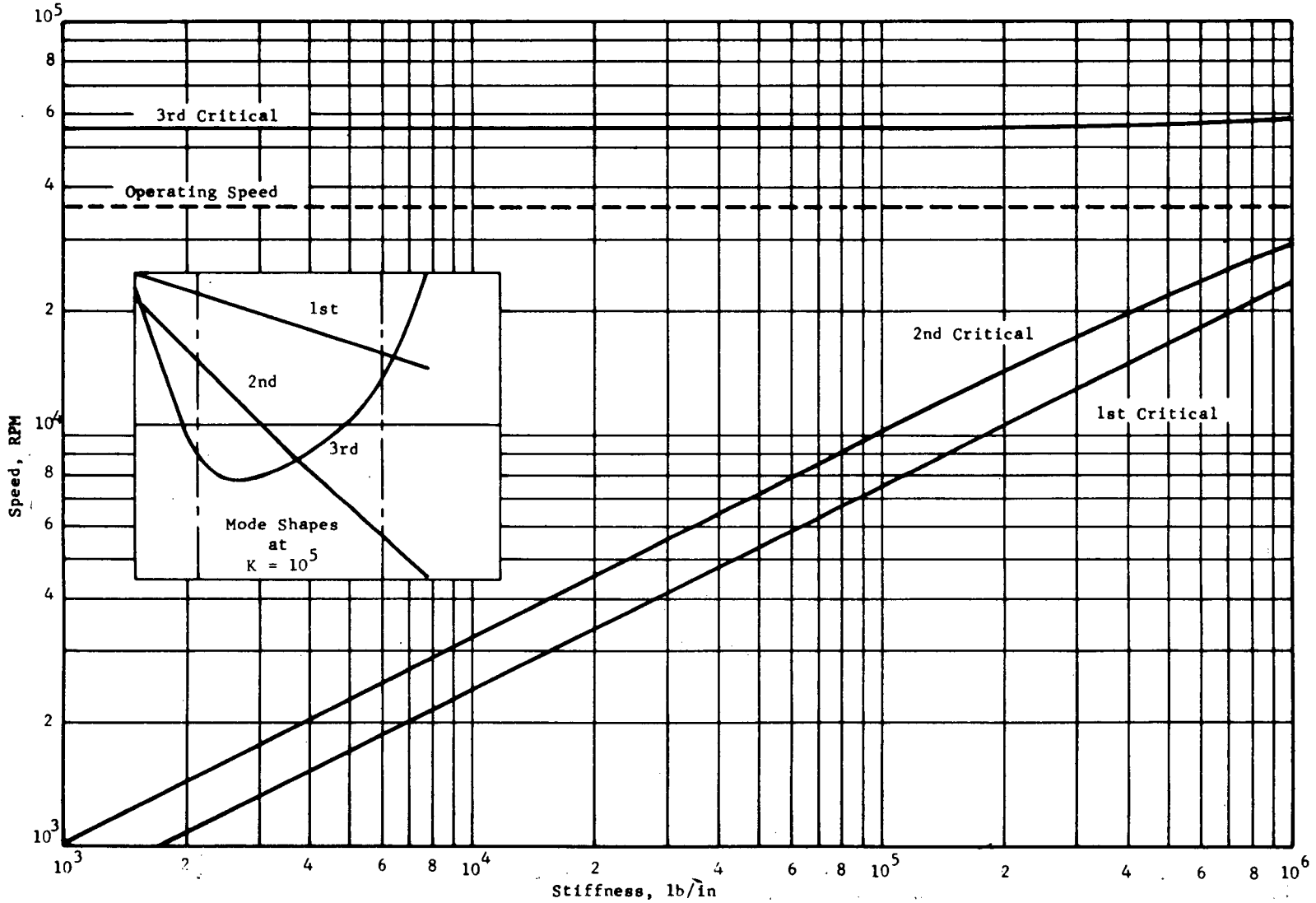
UNDAMPED CRITICAL SPEED
36 AG
3rd Critical
Operating Speed
1st
2nd
3rd
Mode Shapes
at
K = 10^5
2nd Critical
1st Critical
Speed, RPM
Stiffness, lb/in
10^5
8
6
4
2
10^4
8
6
4
2
10^3
10^3
2
4
6
8
10^4
2
4
6
8
10^5
2
4
6
8
10^6

Figure 36

UNDAMPED CRITICAL SPEEDS
24 AG TAC

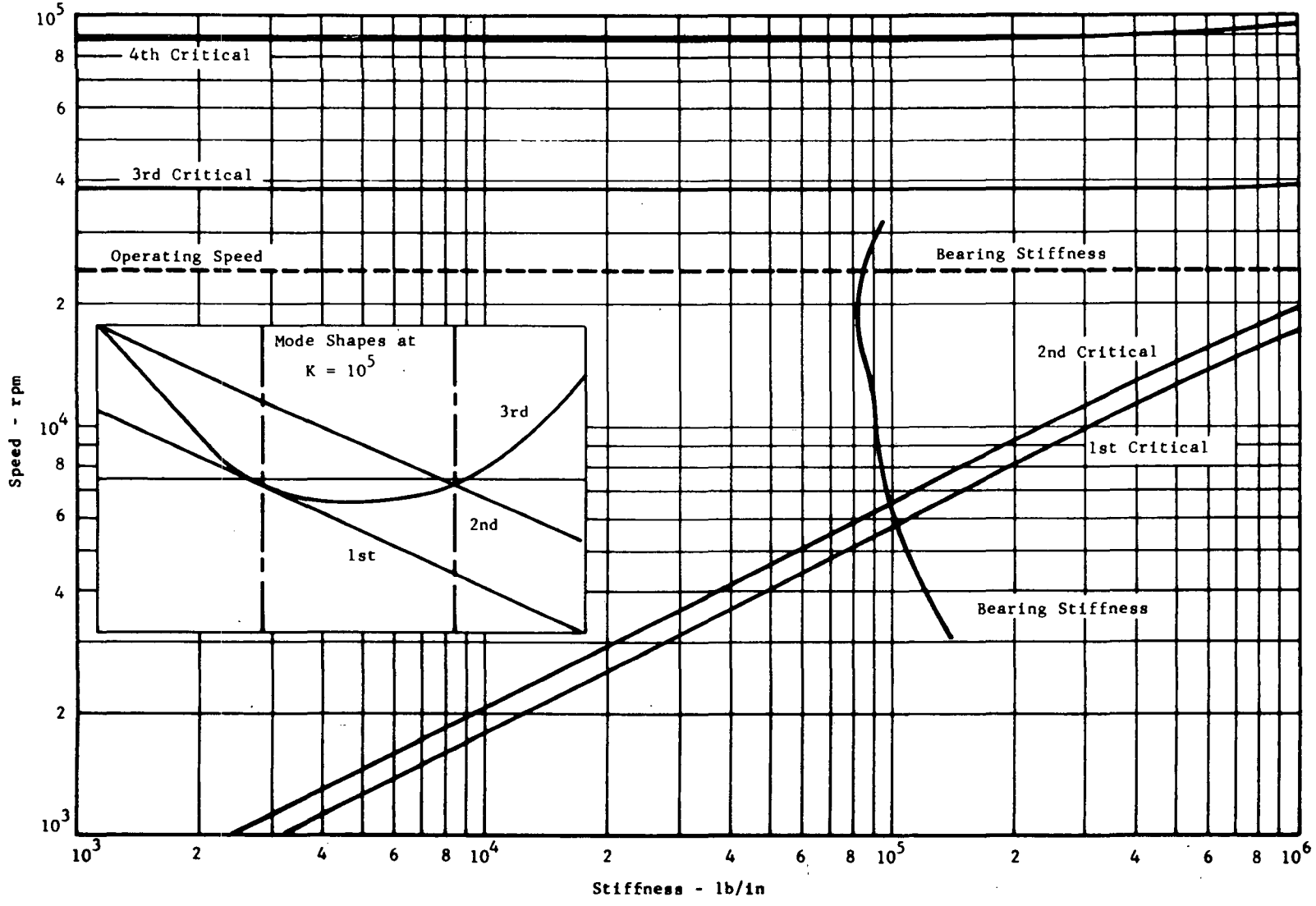

Figure 37

UNDAMPED CRITICAL SPEEDS
24 RG TAC

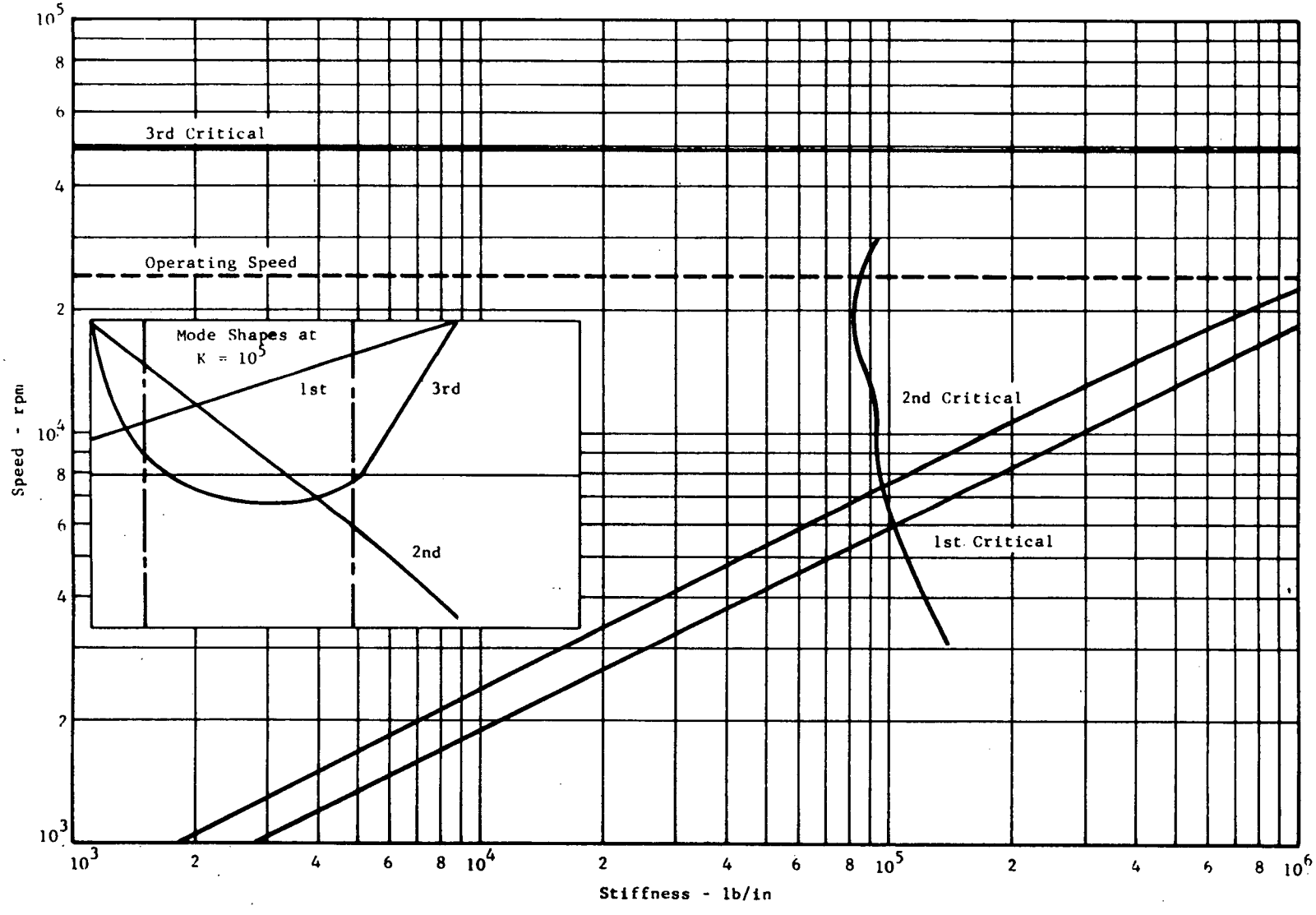

Figure 38

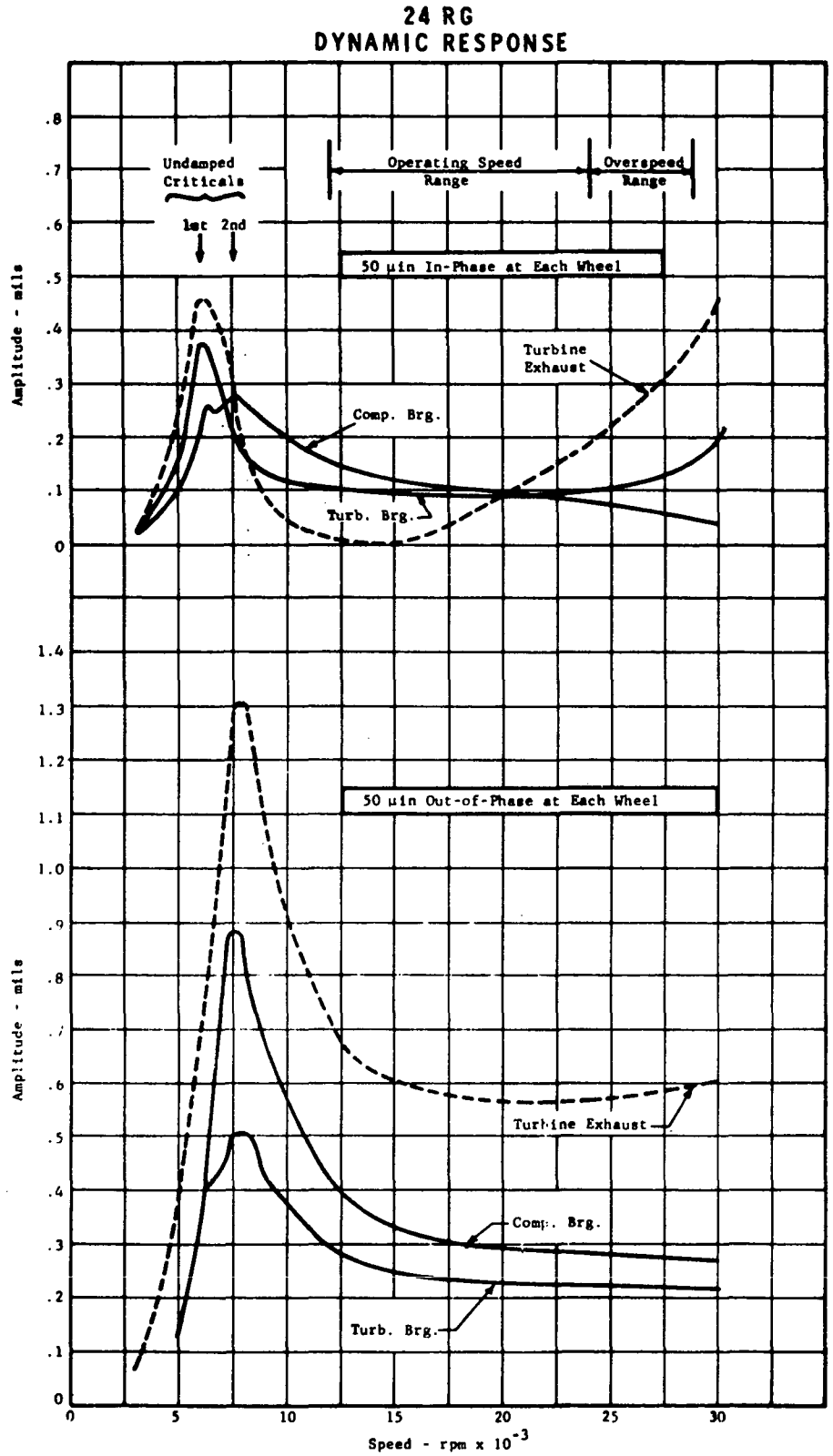
24 RG
DYNAMIC RESPONSE
Undamped Criticals
1st 2nd
Operating Speed Range
Overspeed Range
50 µin In-Phase at Each Wheel
Turbine Exhaust
Comp. Brg.
Turb. Brg.
50 µin Out-of-Phase at Each Wheel
Turbine Exhaust
Comp. Brg.
Turb. Brg.
Amplitude - mils
Speed - rpm x 10^-3

Figure 39

24 AG
DYNAMIC RESPONSE

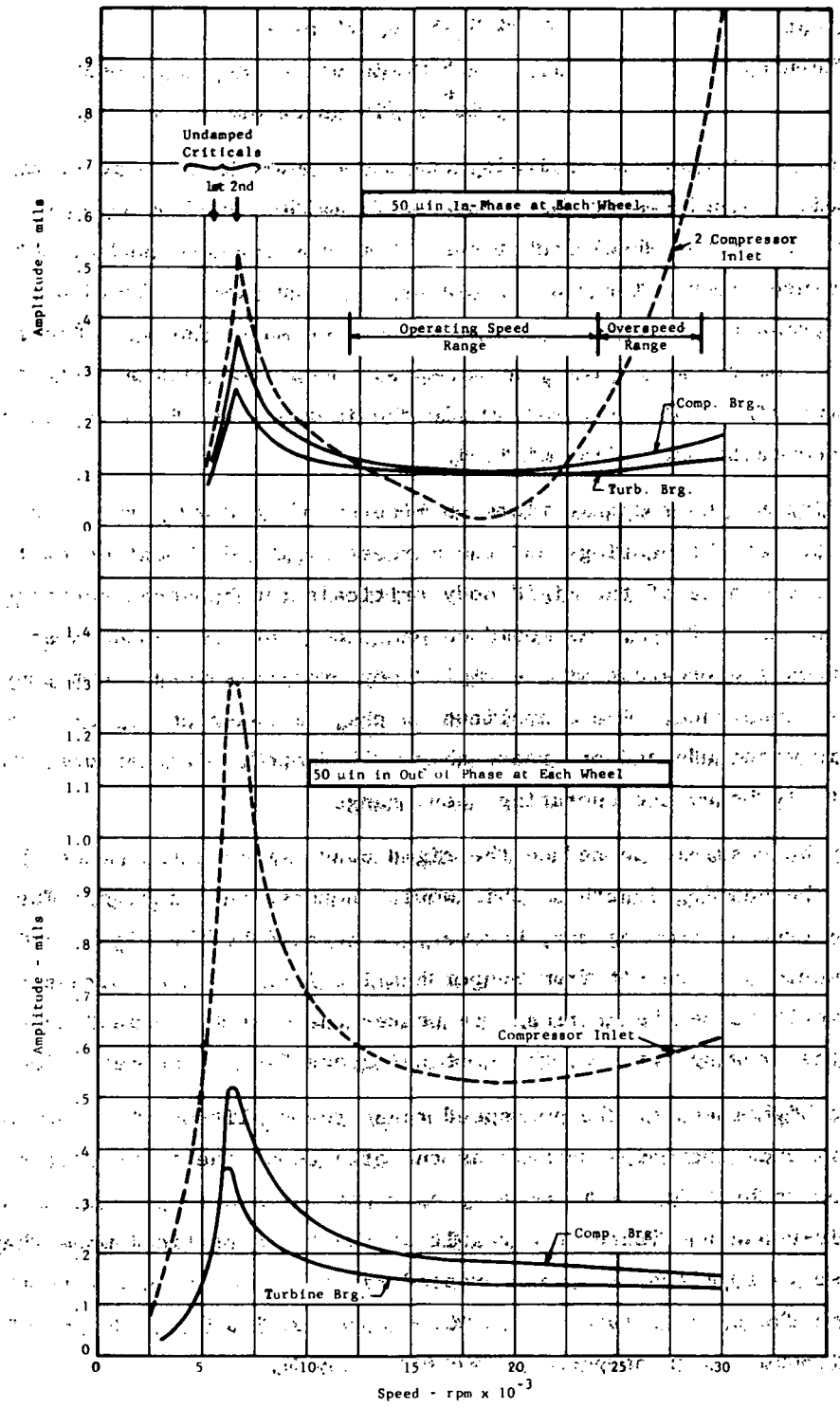

24 AG
Dynamic Response

Figure 40

Lubricant:	29.94 H_e-X_e at 60 psia
Pad Flexure:	1.5×10^4 lb/in on two adjacent pads
	1.0×10^6 lb/in on opposite two pads

For the rotor response analysis, unbalance equivalent to 100 μ inches of rotor weight displacement was assumed and divided equally between the compressor and turbine wheel back faces. Both the in-phase and out-of-phase unbalance orientation was calculated. The unbalance placed at each wheel produces the worst case situation (see mode plots). Also as can be seen from the mode plots, out-of-phase unbalance will accentuate the first two rigid body criticals while the in-phase unbalance at each end will accentuate the third critical.

Referring to the response plots on Figures 39 and 40 , which show the amplitudes at the bearings and the largest amplitude location on the rotor, clear evidence of the rigid body criticals can be seen occurring between 5000 and 8000 rpm. As would be expected from their mode shapes, the amplitudes are greatest at the rigid body criticals when excited by out-of-phase unbalance. These amplitude peaks, although sharp, are not excessive in magnitude and are reasonably well damped. Furthermore, they lie comfortably below the operating speed range.

It may be possible to reduce the rigid body critical amplitudes by increasing the bearing length as this would increase the damping. The effect of increased damping may, however, be negated by the higher stiffness that would also result from longer bearing length since increased stiffness would raise the criticals to nearer the operating speed range and raise the driving force at the critical speed (speed squared effect).

At the higher end of the overspeed range the amplitude of vibration at the shaft ends increases sharply as the effects of the third critical speed begins to be felt. This effect, as would be expected, is accentuated with in-phase unbalance as a result of the third critical mode shape. The increase in amplitude in the overspeed range is more severe with the machine with the axial compressor (24AG) because of its lower third critical speed (38010 rpm as compared to 48930 for 24RG).

The sharp increase in amplitude above 25,000 rpm experienced with the 24AG machine could be significantly reduced by increasing the compressor and journal bearing diameter. This would stiffen the shaft with a resulting

increase in the third critical speed such that its effect within the overspeed range would be minimal.

In summary, the results of the Phase I rotor dynamics studies indicate that the three gas bearing machine concepts presented have acceptable dynamic characteristics. All have a margin between the 20% overspeed and third critical speed of at least 30%. In the case of the 24AG machine, a greater margin is required but this can be accomplished by stiffening the shaft with a larger diameter journal at the compressor end.

Both the 24,000 rpm machines experience resonances at the rigid body critical speeds but it may be possible to reduce these amplitudes by increasing bearing length. The maximum amplitudes with the bearing sizes used for these studies are less than 1.3 mils at the shaft ends which is acceptable. Over this operating speed range (11,000 to 24,000 rpm) maximum rotor vibration amplitudes never exceed 0.6 mils with the assumed 100 μ inch balance.

Oil Lubricated Machines

With the oil lubricated machines one is motivated to minimize shaft diameters in the bearing and seal areas so as to achieve an acceptable level of parasitic power loss and, in the case of ball bearings, maintain low DN values. Small shaft diameters leads to a situation where operation through or near bending criticals may be required and where the introduction of damping is mandatory.

In the case of the oil film lubricated machine (36RL), two approaches were considered. One was a machine arrangement similar to the gas bearing machines with the turbine and compressor overhung from opposite shaft ends and the alternator straddled between bearings. The other approach was to have both the turbine and compressor overhung from the same end. These two approaches are pictorially shown on Figure 41 .

The first approach (Configuration 1 in Figure 41) requires the same third critical speed criteria as for the gas bearing machines because of the potential for poorly damped resonances resulting from the proximity of the nodes to the bearings. In the case of Configuration 2, it is possible to operate near or on a bending critical, because the bearings

BEARING AND SEAL LOSSES FOR 36 RL TAC

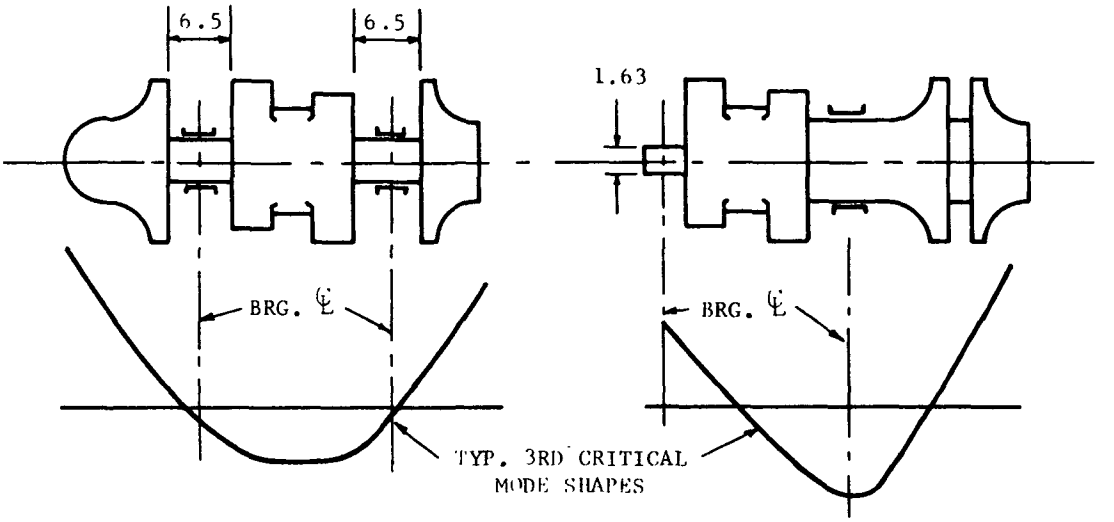

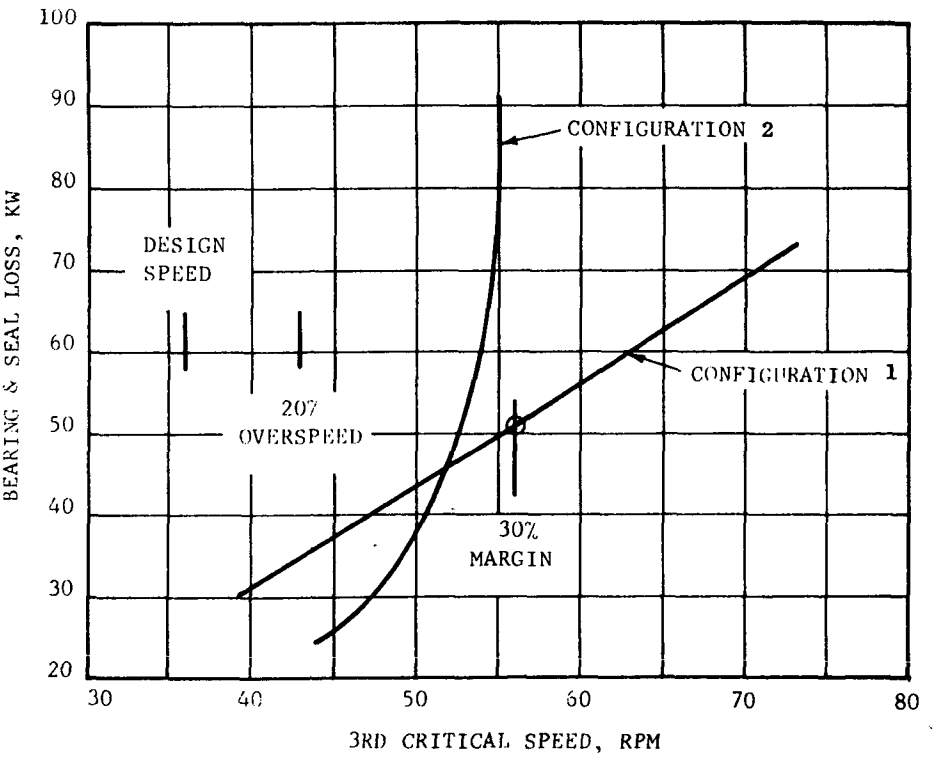

Figure 41

are far displaced from the nodes and the full fluid film damping effect can be realized.

To achieve a 30% margin between the 25% overspeed condition and the third critical speed with Configuration 1 the bearing becomes so large that 50 kw in combined bearing and seal losses result as is shown in Figure 41*.

This is obviously an intolerable situation for a unit designed for 40 to 160 kw of useful output. To achieve the same margin with Configuration 2, even larger bearing power loss results (see Figure 41).

However, if the full damping potential of the bearings is utilized, design speed operation near the third critical is no penalty. For this reason the major emphasis has been on the second approach (Configuration 2) where small diameter bearings resulting in about 24 kw of power loss could be utilized. (Although 24 kw is still a sizable loss, smaller sizes are impractical as the seal becomes prohibitively small to support the required pressure difference).

The critical speed map of the 36RL (Configuration 2) along with the normalized mode plot is shown in Figure 42 . As can be seen from Figure 42 the bearing stiffness curves intersect the undamped third critical speed curve at approximately 40,000 rpm. However, the response plot shown on Figure 43 which includes the bearing fluid film stiffness and damping reveals no amplitude peaks in the speed range to 55,000 rpm. This indicates that the bearing-rotor dynamic system is, for all practical purposes, critically damped.

The ball bearing supported rotors have all components (turbine, alternator, and compressor) straddle mounted between the bearing located at each end of the shaft. This arrangement was necessary to keep the ball bearings at a size small enough (35 mm max.) to assure a reasonable life expectancy. Such an arrangement obviously results in an extremely limber rotor as is evidenced by the 36RM critical speed map shown on Figure 44 . Here it can be seen that, unlike the rotors discussed previously, the 36RM has first and second critical speeds that are bending in

*The reader is referred to BEARING AND SEAL DESIGNS for a detailed discussion on bearing and seal design and loss breakdown.

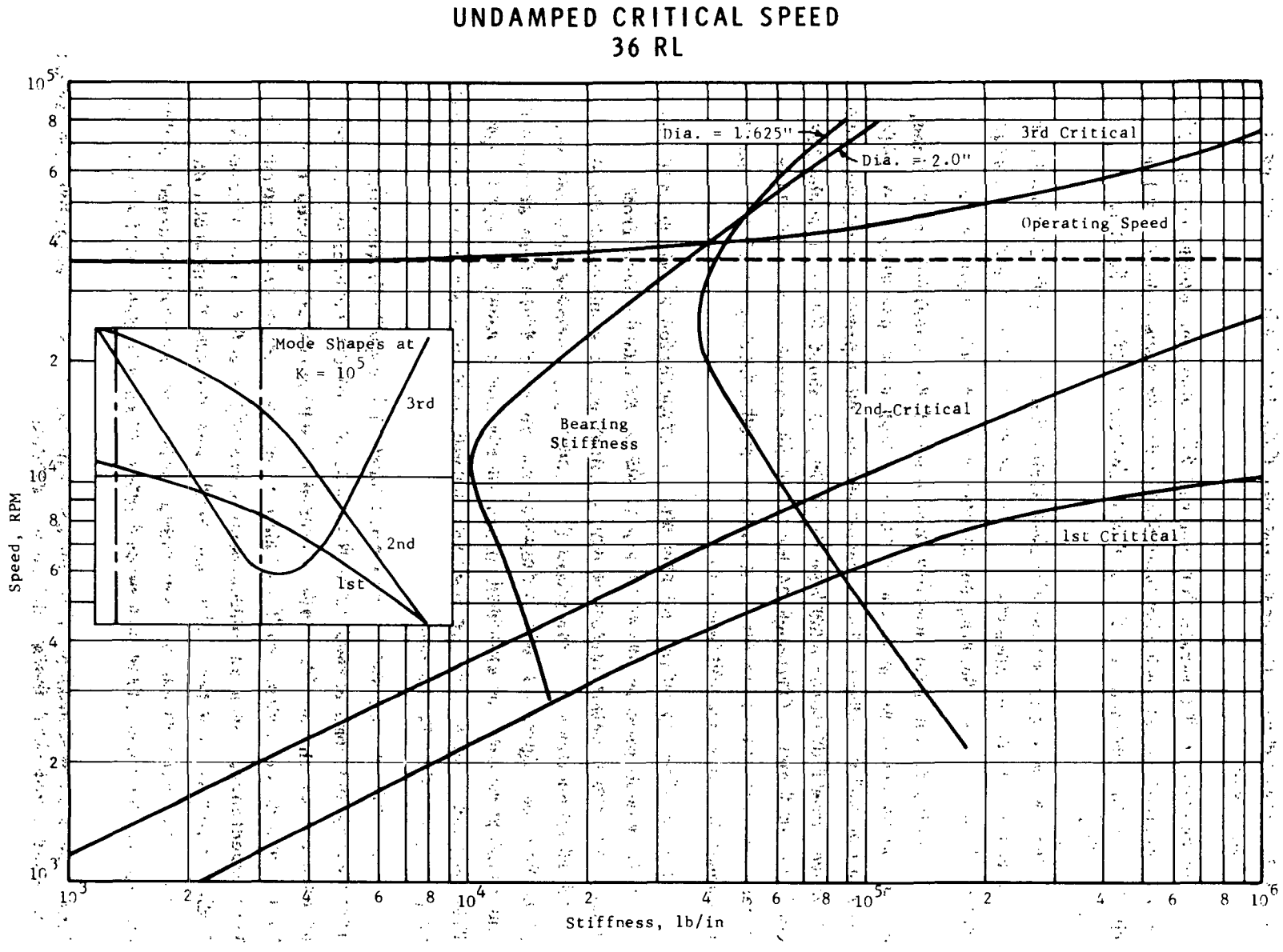

Undamped Critical Speed
36 RL

Figure 42

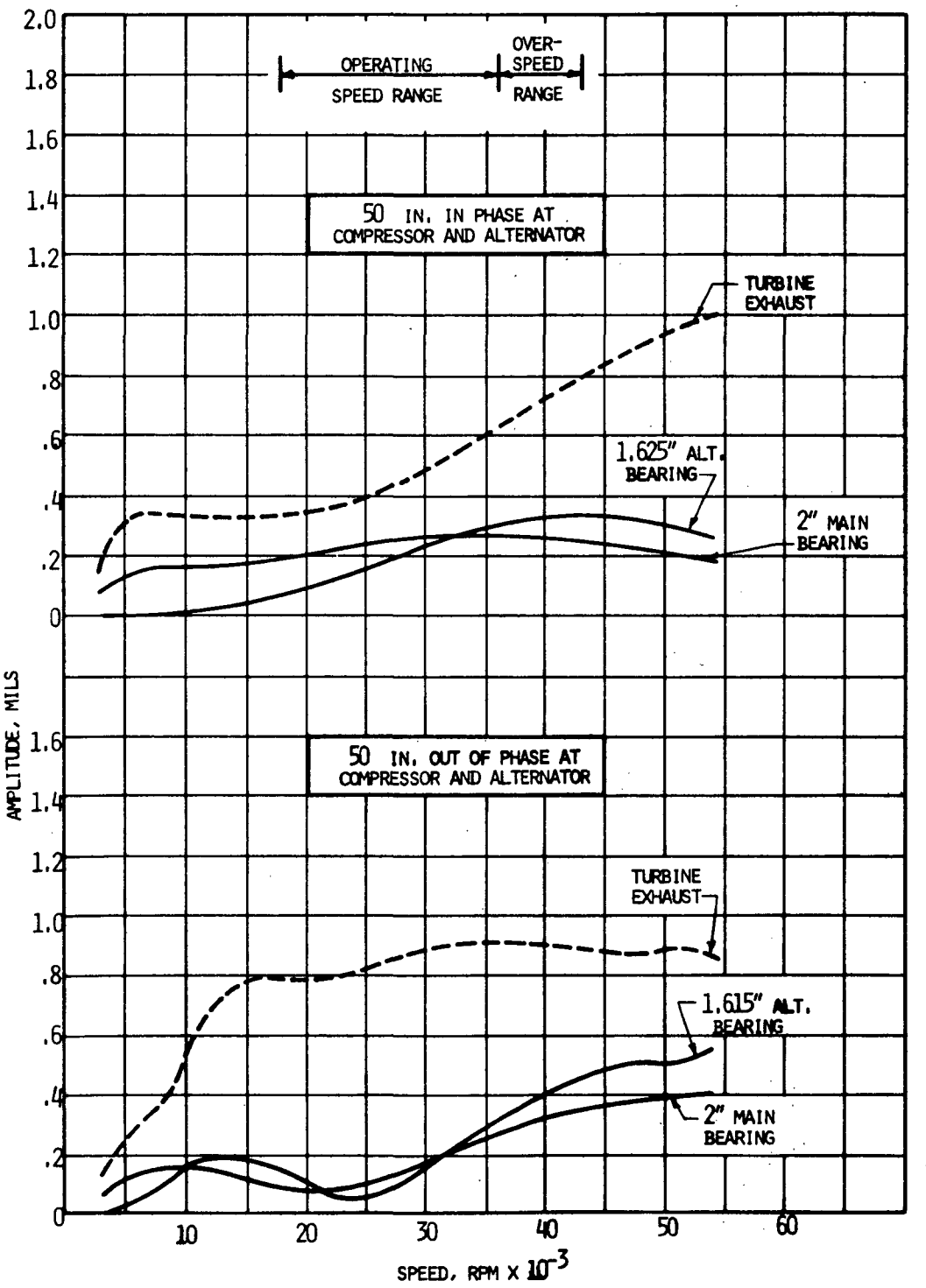
36 RL
DYNAMIC RESPONSE
OPERATING SPEED RANGE
OVER-SPEED RANGE
50 IN. IN PHASE AT COMPRESSOR AND ALTERNATOR
TURBINE EXHAUST
1.625" ALT. BEARING
2" MAIN BEARING
50 IN. OUT OF PHASE AT COMPRESSOR AND ALTERNATOR
TURBINE EXHAUST
1.615" ALT. BEARING
2" MAIN BEARING
AMPLITUDE, MILS
SPEED, RPM X 10^-3
2.0
1.8
1.6
1.4
1.2
1.0
.8
.6
.4
.2
0
10
20
30
40
50
60

Figure 43

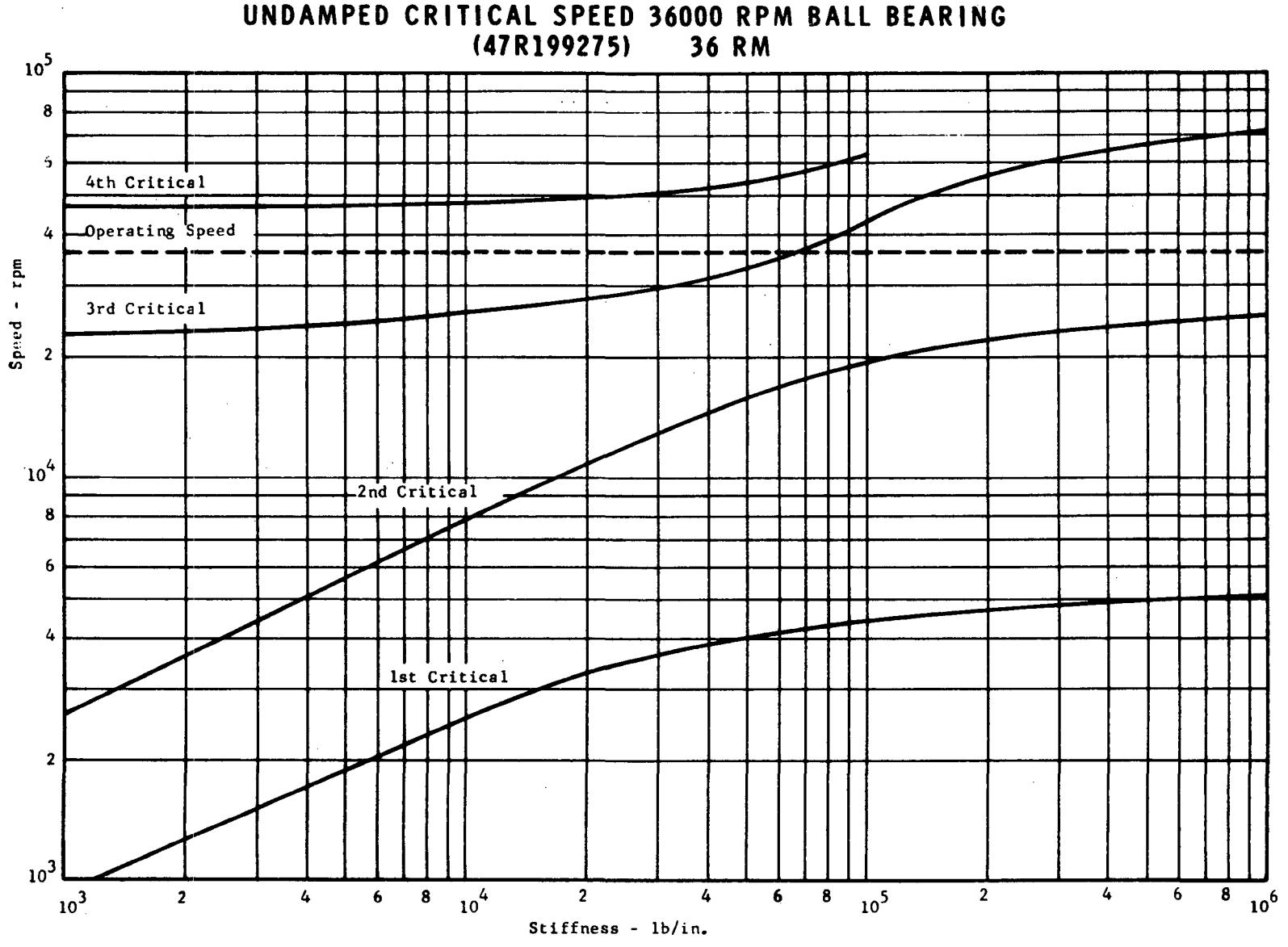
UNDAMPED CRITICAL SPEED 36000 RPM BALL BEARING
(47R199275) 36 RM
4th Critical
Operating Speed
3rd Critical
2nd Critical
1st Critical
Speed - rpm
Stiffness - lb/in.

Figure 44

nature with support stiffnesses greater than 10^4 lb/in as is evidenced by the deviation from a straight line characteristic. It should be noted that the model used for the analysis is a shortened version of that shown on Figure 25 . The model assumed a two inch shorter shaft connection between the alternator and each of the aerodynamic components. This was done in an effort to achieve the potentially stiffest shaft configuration.

The ball bearings have stiffnesses of the order 10^5 lb/in or greater and their stiffness is, for all practical purposes, independent of speed. With the bearings mounted rigidly to the frame, the first three critical speeds would be experienced at about 4,000 to 5,000 rpm, 20,000 to 22,000 rpm, and 42,000 to 50,000 rpm. Because the ball bearings by themselves do not offer any damping, the critical speeds are violent in nature and an intolerable situation results with the operating speed range between the second and third bending criticals.

To improve the 36RM dynamic situation the ball bearings have been mounted on compliant structures as shown in Figure 45 . The purpose of this structure is twofold. First it softens the rotor mounting system such that the critical speeds are reduced and radial motion occurs in the mount. Secondly, it provides a means of introducing damping into the system by utilizing the thin (a few mils) oil filled space in the snubber area (see Figure 45) as a squeeze film damper.

The results of the rotor response analyses utilizing the compliant mounting approach are shown in Figure 44 . The motions of the components with critical clearances (turbine and compressor) are seen to have reasonably well controlled amplitudes with no sharp resonance peaks. The load transmitted to the bearings display the same characteristic and are relatively large in magnitude - approaching 90 pounds.

Both the turbine maximum amplitude and turbine end bearing dynamic load are a maximum near the 36,000 rpm design speed. Although minor variations in support stiffness, damping, and rotor stiffness can be introduced, it is doubtful that the dynamic response characteristics can be significantly altered from that shown on Figure 44 .

In summary, the oil lubricated machines tend toward having flexible rotors dictated by bearing and seal considerations. This situation leads to the necessity to introduce damping into the rotor bearing system to attentuate the bending critical speeds.

EXAMPLE OF RADIALLY COMPLIANT, AXIALLY STIFF, SNUBBED SUPPORT FOR BALL BEARING

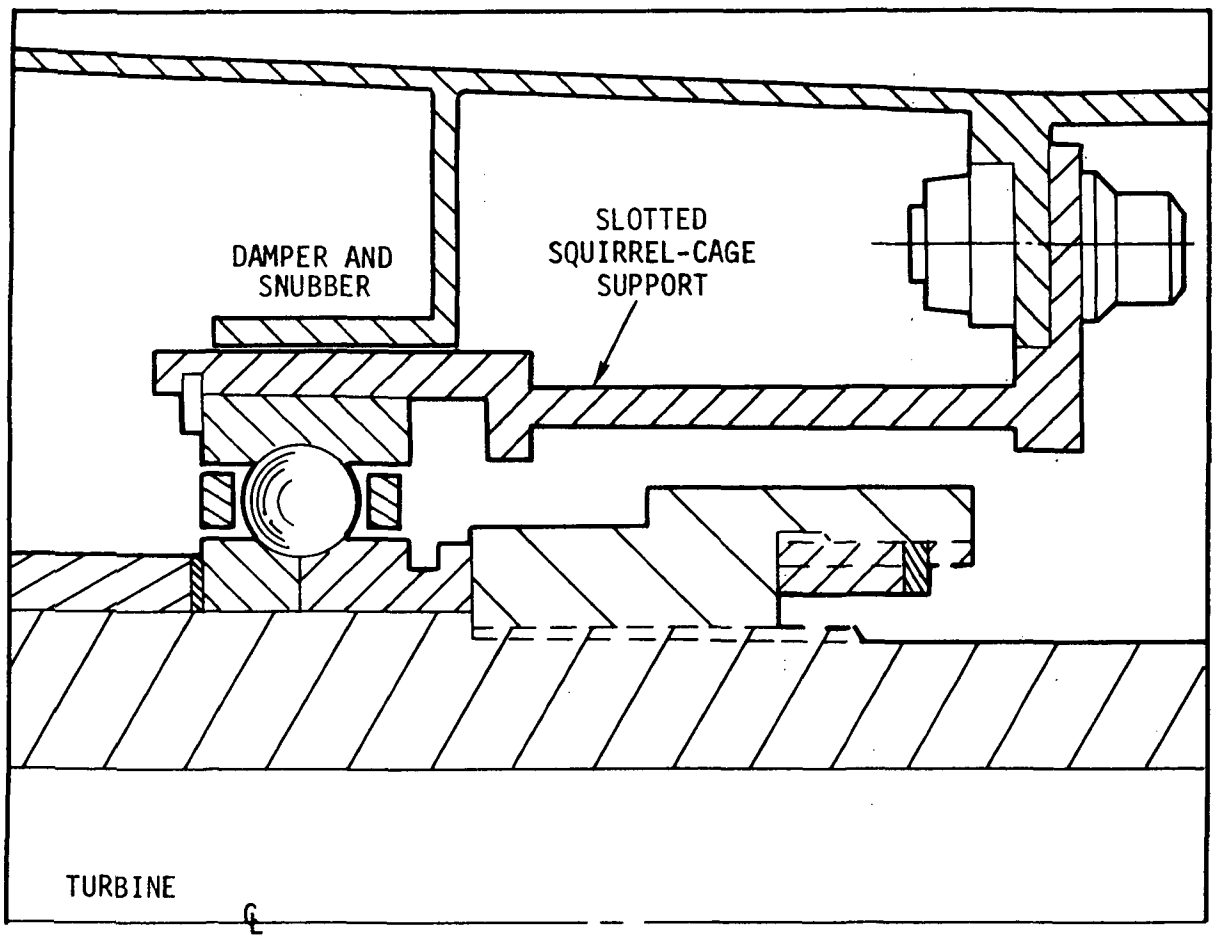

Figure 45

Both the oil lubricated machine approaches, with proper damping included show no evidence of critical speed problems and vibration amplitudes can be maintained at less than 1 mil with a total rotor unbalance of 100 μ inches. The dynamic loads transmitted to the ball bearings are high - approaching 90 pounds - and are a maximum near design speed.

C. AERODYNAMIC DESIGN

INTRODUCTION

The turbomachinery design studies include conceptual designs of axial-flow compressors, centrifugal compressors, and radial-flow turbines. Six configurations in all were requested; two at a rotating speed of 24,000 rpm with a compressor inlet pressure of 55 psi and four configurations at 36,000 rpm with a compressor inlet pressure varying between 120 and 360 psia. The design requirements for these studies are presented in Table XVI.

The prime objective of these studies is to obtain the highest possible component efficiencies consistent with the best TAC performance but within mechanical, vibrational and material constraints.

APPROACH

The approach to the axial-flow compressor design studies was to use a computerized pitchline computer code called the Compressor Unification Study. This computer code was developed by the Aircraft Engine group of the General Electric Company and is based on a large amount of compressor test data. Through the use of this computer code, the stall potential of a new compressor is obtained from that observed in the test of a base compressor by making rational adjustments for blade speed, axial velocity, swirl level, blade solidity, aspect ratio, tip clearance and Reynolds number. It is assumed in the design of the compressor that adjustments will be made in the blading to assure the radial flow balance of the working fluid and that the Mach number effects will be accounted for by adjustments in blade thickness. These variations can then be removed from consideration in a pitchline design model. The design calculation is based on the static pressure rise achievable in a blade row divided by the inlet dynamic pressure. Basically, the method of calculation takes the measured differential pressure over dynamic

TABLE XVI.

● DESIGN REQUIREMENTS

TURBINE INLET TEMPERATURE,	1600°F
COMPRESSOR INLET TEMPERATURE,	240°F
COMPRESSOR PRESSURE RATIO	1.9
DESIGN POWER OUTPUT (40 KWe AT REDUCED PRESSURE)	160 KWe
WORKING FLUID (HELIUM-KRYPTON) MOLECULAR WEIGHT	39.94
TURBINE DIFFUSER EXIT MACH NO.	$\leq$0.1

head from each state in the base compressor at design speed stall, adjusted in a rational way for solidity, aspect ratio, clearance, and Reynolds number and applies it to the corresponding stage in a new compressor. The blade speed, axial velocity, and swirl level of the new compressor lead to values for the dynamic pressure and these are used with the new values of static pressure rise divided by dynamic pressure to obtain the stall pressure rise.

Compressor stall experience has been unified by demonstrating that the measured loading parameters of a large number of compressor stages are mutually consistent within the framework of the method. The details of the method are considered to be proprietary to the General Electric Company.

The efficiency level was calculated using a loss model based on the compressor test experience of the Aircraft Engine group. The effect of diffusion parameter and Mach number were taken into account in determination of the profile loss. Corrections to the total pressure loss coefficient are made for the effects of secondary flow and annulus drag. For small machines where the tip clearance is important, a correction is also made for this loss. Finally, the calculated efficiency is corrected for the Reynolds number.

The prime aerodynamic variables investigated in the axial-flow compressor design studies included the number of stages, the blade chord, the axial-velocity level, swirl level, inlet radius ratio, and solidity. Since the compressor length affects the rotor-bearing response and in turn is affected by the number of stages, blade chord and swirl level, the parametric data was plotted against length. The final selection and recommendation of a design were tempered by considerations of the exit system which has a significant effect on axial-flow compressor performance.

With regard to the centrifugal compressor design studies, a meridional analysis was made in an attempt to optimize the main geometric features of the compressor utilizing realistic loss data and taking into account the important flow problems. The prime variables in this meridional

analysis were the inlet radius ratio, the hub radius, the exit blade height, the slip factor, the radial extent of the vaneless space, the vaned diffuser chord and the flare of the vaned diffuser section. The consideration of a large range of slip factor value brought into the study a range of values of the blade exit angle. The object of the meridional analysis was to optimize the configuration of the centrifugal compressor overall efficiency. Several configurations were laid out under selected optimized conditions.

Special flow problems in the centrifugal compressor included three dimensional effects in the impeller and problems associated with the exit system. With regard to the impeller, a computerized design technique was utilized to determine the flow characteristics of a given impeller on axisymmetric stream surfaces and then the blade-surface velocity distributions were calculated on the surfaces. With regard to the exit system, a three vane-row diffuser was designed with a matching scroll giving an exit Mach number less than 0.1.

With regard to the radial turbine, a meridional analysis was carried out to optimize the turbine configuration including an exit diffuser for highest efficiency. The prime variables investigated were the stator exit velocity, stator exit angle, tip speed, ratio of the rotor exit to inlet relative velocity, the rotor exit mean-to-inlet diameter ratio, and diffuser included angle.

Special flow problems included the three dimensional effects in the runner. These were explored using the same computerized technique as described for the radial flow compressor. Special studies were made of the exit diffuser to assure high performance and a good margin between operating point and stall at an exit Mach number of 0.1.

It was not possible to divorce entirely the aerodynamic studies of the turbomachinery from the complete TAC unit itself. For example, because the adverse effect of tip clearance on turbomachinery components, it was considered important to minimize the operating tip clearance. However, the minimum tip clearance which is practical is heavily influenced by the differential thermal expansion of the rotor and stator

parts, as well as the deflection of the rotor and stator parts under load. Since the means for making the TAC operate over a 4 to 1 power range was to reduce the compressor inlet pressure at low values of power, reducing the Reynolds number, the effect of the reduced Reynolds number on the turbomachinery performance was considered. The rotor dynamic response of the TAC unit is sensitive to the mass and overhang of the compressor and turbine wheels. Thus the design of the turbomachinery is influenced by the effect that certain configurations would have on rotor-dynamic response. The temperatures experienced in a turbomachine affect the allowable stress and the tip speeds of a turbomachine and certain dimensions affect the actual stresses which in turn are limited by the allowable stresses. Because of the large life or power loss penalty of thrust bearings, the aerodynamic thrust loads on the compressor and turbine must be balanced. Compressor-turbine thrust balancing usually requires the use of labyrinth seals, sometimes at large diameters, resulting in costly leakage losses. The use of the working fluid as coolant means that a larger flow rate will pass through the compressor than through the turbine, resulting in a reduction in the performance of the TAC unit itself which is significant. In addition, the returning of the coolant gas to the flowing system often causes additional losses due to the disturbance of the main flow. Since rotor-bearing dynamic response is affected by component weight, length and overhang, the aerodynamic design of the components influences rotor-bearing response and may be constrained by it.

AXIAL COMPRESSOR

Axial flow compressor designs were carried out for two rotating speeds. At 24,000 rpm the compressor inlet pressure set by contract was 55 psia; at 36,000 rpm the compressor inlet pressure of 120 psia was chosen as the value giving the highest component efficiencies for the radial flow components.

Basis for Comparison

As indicated previously, the highest efficiency axial flow compressor configurations were sought as a function of the axial length of these machines. The axial lengths were selected as a parameter of

merit because of a significant influence axial length has upon rotor dynamic response of the entire unit. The design specifications shown in Table XVII were utilized in the axial-flow compressor studies. The design parameters which had the most influence on the design were as follows: number of stages, blade chord (which means Reynolds number effects and aspect ratio), axial velocity level, swirl level, radius ratio (which means mean blade speed), and solidity. Early in the study it was established by parametric analysis that a pitchline solidity of 1.25 was a level which would avoid excessive choking at the hub and excessive loading at the tip of the blades. For 7 stages a radius ratio of about 0.75 gave close to the optimum efficiency and was used throughout the remainder of the study.

The designs were constrained by using a constant axial velocity throughout the compressor and having the same pitchline velocity diagrams for all stages.

The analytical model which was used as a basis of comparison of the various compressor configurations was developed for Aircraft Engine use. The stall prediction capabilities of this computer code discussed above are based fairly well upon experimental data. The efficiency prediction method is still under development but it was felt this method was far enough along to give consistent trends of compressor performance over the ranges of the prime design parameters of this study. The analytical model used to compare the various configurations evaluates the effects of the blade loading, Reynolds number, clearance, stator angle and the reaction on the compressor performance. From the calculated variation of efficiency with compressor length a compressor configuration was selected. Then the efficiency level of the selected blading design was adjusted to the level of efficiency demonstrated in the T-58 compressor which is approximately the right physical size and was adjusted for collection system losses.

There were some additional constraints and evaluation criteria which were applied to the design studies. A chord of 0.4-inch was selected as the minimum value for accurately machined blades to the usual tolerances. As indicated earlier, the length of the axial compressor was considered

TABLE XVII.

AXIAL FLOW COMPRESSOR DESIGN SPECIFICATIONS

RPM	24000	36000
Inlet Temperature	700°R	700°R
Inlet Pressure*-psia	55 (13.7)	120 (30)
Pressure Ratio	1.9	1.9
Gas Molecular Weight	39.94	39.94
Corrected Mass Flow	3.41	1.56

*Modulation to 1/4 power by inlet pressure level

to be a significant output since it had a noticeable effect on rotor dynamics. Most of the compressor design studies were carried out without consideration of the collection system. The collection system of the axial compressor was found to have a significant effect on the efficiency. Therefore, the collection system was studied in some detail and certain constraints were placed upon the axial compressor design to favor the collection system. The actual parametric data, however, was computed without regard to the losses in the collection system. The final assessment of the recommended compressor configuration efficiency was adjusted to take into account the effect of collection system on efficiency.

THE COLLECTION SYSTEM

Because of the relatively low compressor pressure ratio, 1.9, the energy tied up in the collection system of the compressor is large compared to the total energy added to the gas in the compressor itself. In order to determine quantitatively the effect of the collection system on the compressor performance the number of points in adiabatic efficiency associated with the collection system was determined for several exit absolute Mach numbers. At an exit absolute Mach number of 0.33, 15.7 points in adiabatic efficiency are tied up with the collection system; at an exit absolute Mach number of 0.26, 9 points in efficiency are tied up with the collection system.

Reneau, Johnston and Kline (Ref. 6) have shown that for a two dimensional diffuser design the absolute maximum pressure recovery occurs in long diffusers with high length to width ratios. The value and location of this maximum recovery depend largely on the inlet boundary layer thickness. The bulk recovery obtained by them was 85% at a value of nondimensional boundary layer thickness which is highly optimistic considering that the diffuser follows a turbomachine.

The results of Sprenger (Ref. 7) show that at an area ratio of 4, the best diffuser at all boundary thicknesses investigated by them was a straight circular one with a total cone angle of 8°. The best recovery obtained by Sprenger for such a diffuser was 86%. These

results indicate that even at the best values of boundary layer thickness it has not been possible to obtain greater than 86% recovery.

The boundary layer condition at the exit of the compressor will not be as favorable as the best ones obtained under the experimental conditions of Reneau, et al. and Sprenger. Hence, assuming only 80% recovery from the exit of the last compressor rotor, it is possible to obtain an overall compressor efficiency based on the inlet total and collector exit total conditions.

A schematic diagram of a typical collection system is shown in Figure 46. For such a collection system the last compressor stator would be designed for static pressure rise which was 55% of the dynamic head leaving the rotor. This corresponds to a total pressure loss of 0.1 dynamic head for the last stator. The recovery of 50% of the kinetic energy remaining in the outlet guide vane, diffuser and scroll was estimated. This results in static pressure rise of 72% of the dynamic head at the last rotor exit or an overall total pressure loss of 0.18 dynamic head. Later, when overall compressor performance is presented the above values of pressure recovery will be used to characterize the collection system. As a result of the study of the collection system, the exit axial Mach number in all of the compressors studied was 0.18 which results in a 0.26 absolute exit Mach number for a swirl level of 45°.

PARAMETRIC STUDIES

As mentioned earlier in the section, a systematic variation of the different parameters was carried out using the Compressor Unification Study model in order to arrive at the final choice of the design. The final choice depended not only on the overall adiabatic efficiency and the compressor length but also on the pitch line vector diagrams, rotor and stator camber and stagger angles, blade loadings and stall margin. Designs with highly loaded blade rows, very low stall margin, and camber and stagger angles outside the realm of past experience were eliminated from comparisons. The designs found acceptable after meeting the above criteria were then compared in order to optimize efficiency with respect to the length at full and one quarter power.

TYPICAL COLLECTION SYSTEM

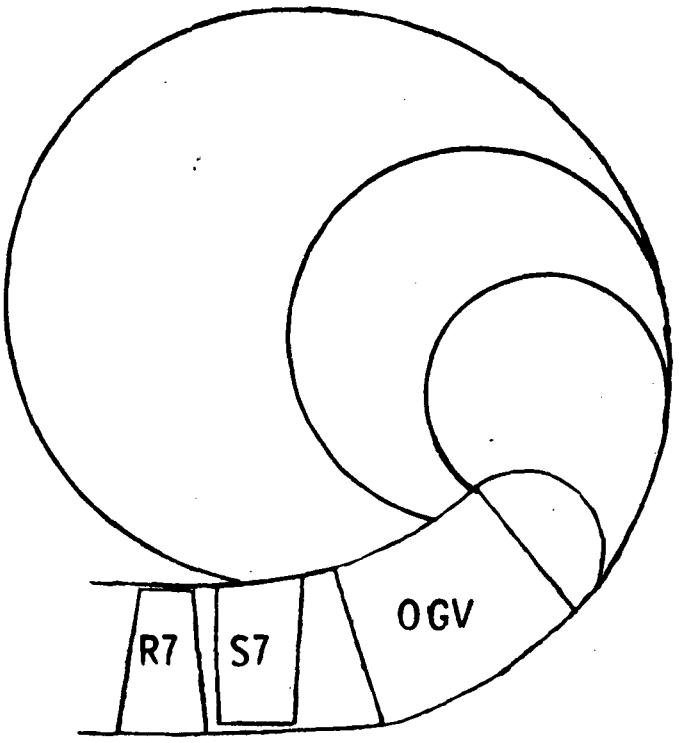

For recovery of Kinetic Energy after rotor 7, design S7 for $\frac{\Delta p_s}{q} = .55$, $\frac{\Delta p_t}{q} = .1$

OGV - diffuser and scroll recovery 50% of remaining Kinetic Energy, while dissipating 22%.

Overall $\frac{\Delta p_s}{q} = .72$; Overall $\frac{\Delta p_t}{q} = .18$

FIGURE 46.

Having chosen a pitch line solidity value of 1.25, the effects of the variation of radius ratio and number of stages on efficiency were studied. The efficiencies were obtained for full and one quarter power and for five- and seven-stage machines at a pitch line chord value of 0.75 inches. The swirl entering all rotors was 45°, thus making each stator remove just the additional swirl introduced by the previous rotor. The swirl leaving the last stator was assumed to be 45°. The results show clearly that a radius ratio of 0.75 for seven stage compressors has the best full power and one quarter power efficiencies. It was also found that at a radius ratio of 0.8 for seven stage compressors and 0.85 for five stage compressors very low flow coefficients resulted giving rotor cambers and staggers outside the realm of past experience. The efficiency gain for more than seven stages is more than offset by the increase in length beyond mechanically accepted limits.

Shown in Figure 47 is the variation in adiabatic efficiency with compressor length for different numbers of stages and different values of blade chord. The blade chord values are at the pitch line and are held constant for all rotors and stators, causing a very small variation in pitch line aspect ratio due to the slight convergence of the flow path. The radius ratio chosen for Figure 47 is 0.75. It is noted that there is a progressive improvement in adiabatic efficiency with increasing number of stages, due to lighter loadings of the blade rows. The trend appears to indicate that considerably higher efficiencies can be obtained by increasing the stages to 8 or 9. A careful study shows that the gain in efficiency from increasing the number of stages drops progressively and that the overall compressor length increases considerably with the higher number of stages for the same value of mean chord. It was found that an 8-stage compressor gave a very small increase in full power adiabatic efficiency and a much higher length, beyond the length limits set by mechanical considerations, for the same chord value as compared to a 7 stage compressor.

The effect of blade chord (and consequently aspect ratio) on length and efficiency is seen in Figure 47. At the higher chord values, the effect of low aspect ratio dominates the behavior of the full power

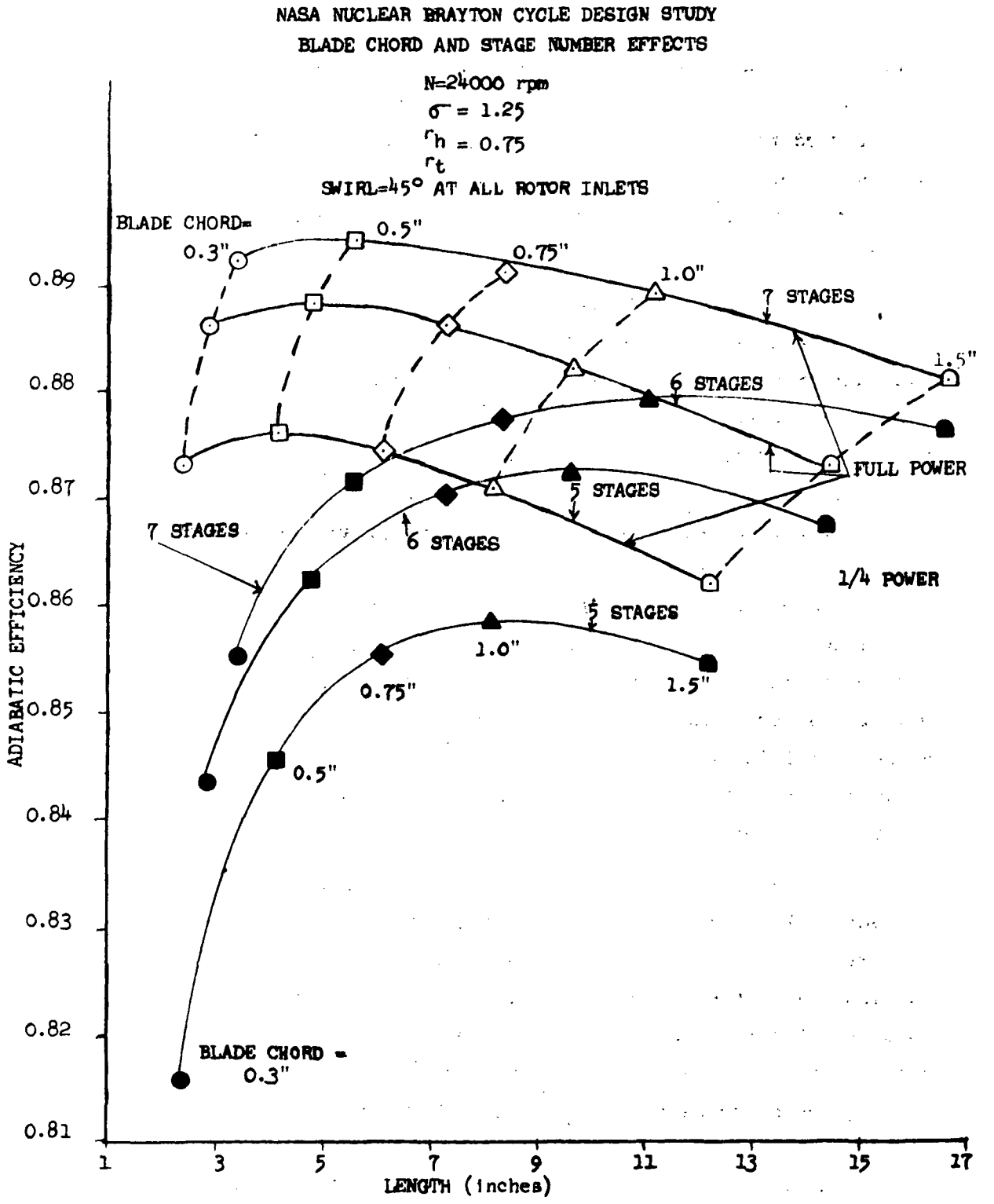
NASA NUCLEAR BRAYTON CYCLE DESIGN STUDY
BLADE CHORD AND STAGE NUMBER EFFECTS
N=24000 rpm
σ = 1.25
r_h = 0.75
r_t
SWIRL=45° AT ALL ROTOR INLETS
BLADE CHORD=
0.3"
0.5"
0.75"
1.0"
1.5"
7 STAGES
6 STAGES
5 STAGES
FULL POWER
1/4 POWER
ADIABATIC EFFICIENCY
0.89
0.88
0.87
0.86
0.85
0.84
0.83
0.82
0.81
1
3
5
7
9
11
13
15
17
LENGTH (inches)

FIGURE 47.

efficiency in spite of the favorable effect of the Reynolds number on efficiency. On the other hand, at the one-quarter power condition superimposed in Figure 47 the Reynolds number are low enough that the increase in Reynolds number at high chord makes a significant contribution toward the efficiency outweighing the adverse effect of the decreasing aspect ratio. It is seen from Figure 47 that a chord of 0.6 inch will give the best compromise between full and one-quarter power efficiencies and yet keep the overall length of the compressor within 6.67 inches.

After the number of stages, pitch-line chord, radius ratio, and solidity were selected the effects of the variation of swirl and exit Mach number were re-examined. Shown in Figure 48 is a plot of the variation of efficiency with compressor length at different exit axial Mach numbers and swirl levels. For any particular case, the pitch line swirl at all rotor inlets and the compressor exit were held constant at a given value. Three values of swirl, namely, 25, 35 and 45° were considered. At each of these values of swirl the exit Mach number was varied. The absolute Mach number desired at the exit of the collector flange is 0.1. The higher the Mach number at the compressor exit, the higher will be the losses through the collection system diffusing to a Mach number of 0.1, but at the same time, the higher is the efficiency of the compressor alone (total inlet to total exit). Hence it is necessary to pick an optimum Mach number at the compressor exit to optimize the overall compressor inlet to collector exit efficiency.

For a given swirl level, the compressor exit absolute Mach number was varied by increasing the flow path area by 10 and 20% from the minimum area required to pass the given mass flow at an exit axial Mach number of 0.18. The inlet to exit area ratio was maintained in all cases at a value which permitted a nearly constant axial velocity through the compressor. For example, the line marked "swirl, 45°" is obtained by varying the areas as mentioned above. The line marked "axial Mach number, 0.181" is obtained by varying the swirl angle and keeping a certain flow path with exit area adjusted to pass a given weight flow at axial Mach number of 0.181. It is noticed that keeping a higher swirl level through the compressor at a constant axial exit Mach number results in higher

NASA NUCLEAR BRAYTON CYCLE DESIGN STUDY
EXIT AXIAL MACH NUMBER AND ROTOR INLET SWIRL EFFECTS

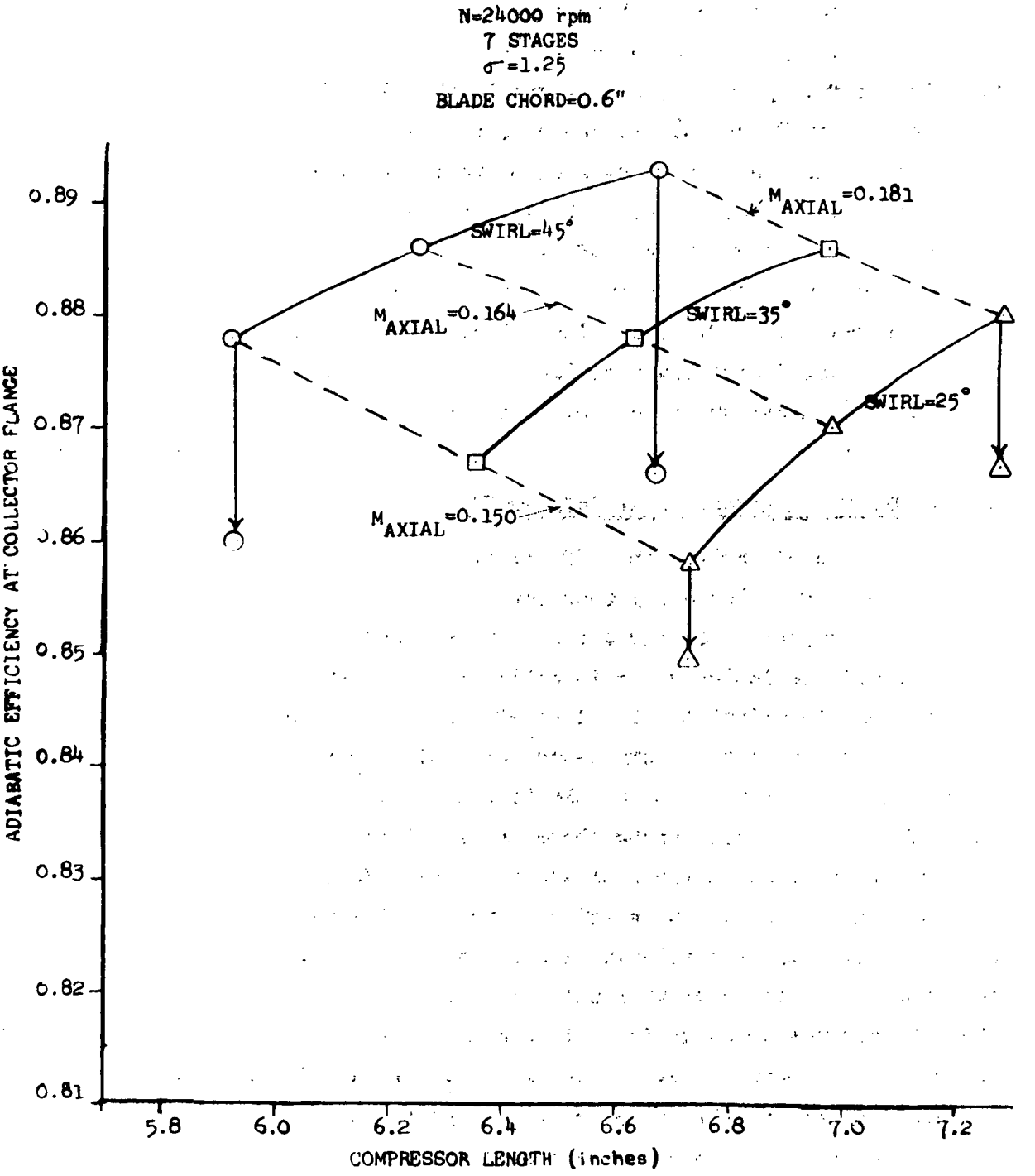

FIGURE 48.

efficiencies at shorter lengths. This is partly due to the higher absolute Mach numbers at a higher swirl for a given axial Mach number. It can be seen from Figure 48 that at a constant swirl angle of 45° a flow path designed to give an exit axial Mach number of 0.181 gives the highest full power efficiency within the allowable length. The efficiencies in Figure 48 are the result of applying the collector losses mentioned in a previous section to the parametric data presented in Figure 48. From the figure it is seen that there is no compelling reason to depart from the 45° of swirl and the axial Mach number of 0.181. The low swirl angle and high axial Mach number result in a very slight increase in efficiency with a large increase in compressor length. As a result the design characterized by the highest swirl angle and highest axial Mach number was selected for the TAC compressor operating at 24,000 rpm.

AXIAL COMPRESSOR EXPERIMENTAL BACKGROUND

As indicated earlier the efficiency prediction feature of the Compressor Unification Study computer code is still undergoing development. The computer code gives the correct trends of compressor efficiency with the main variables under investigation. However, at present it is necessary to adjust the level of efficiency calculated by reference to background experience on compressors of a similar type. The T-58 compressor has features which make it comparable in many ways to the TAC axial-flow compressor. Among these are small size, including chords of 0.4 inches and blade heights of approximately 1/2-inch in the latter stages. Unlike the TAC axial-flow compressor the T-58 compressor is designed for transonic relative Mach numbers in the front stages. In addition, as is the case with all gas turbine compressors for aircraft, the T-58 compressor is designed to operate over a range of flow and pressure ratio conditions. In contrast the TAC axial-flow compressor operates at essentially one operating point on the compressor map. And, as such compromises are not necessary in the TAC axial compressor for off design operation. Another significant difference between the T-58 and the TAC axial-flow compressor is that the former has a large number of stages and generates a rather large pressure ratio compared to the

1.9 pressure ratio of the TAC compressor. Because of the differences in the number of stages and pressure ratio of the two compressors the most logical way to compare them is on the basis of small stage or polytropic efficiency.

Shown in Figure 49 for the T-58 engine along its operating line is the variation of compressor efficiency with gas generator corrected speed as percents of design-speed values. It is apparent from the curve that at design operating conditions the compressor efficiency is somewhat lower than the peak value. However, at design conditions the T-58 compressor is operating transonically in the front stages and the stages are not fully matched. Therefore, it is reasonable to compare the TAC compressor and the T-58 compressor where the T-58 stages are well matched. This is at the T-58 compressor maximum efficiency point which occurs at approximately 89% of corrected design speed. At this point the T-58 polytropic efficiency is .886. When the Compressor Unification Study computer code is used to predict the T-58 performance at this condition of 89% corrected speed the polytropic efficiency is .909. This amounts to 2.3 percentage points in efficiency difference between the actual measured performance of the compressor and the value calculated by the computer model.

For the TAC axial flow compressor having 7 stages and a chord length of 0.6 inch the Compressor Unification Study computer code yields 0.928 as the TAC polytropic efficiency. When this is decreased by the 2.3 points compressor efficiency difference between the T-58 model and measured data, the TAC axial-flow compressor polytropic efficiency is 0.905. For the TAC compressor at a pressure ratio of 1.9 when the polytropic efficiency of 0.905 is converted to adiabatic efficiency the value is 0.893. Finally, when the overall efficiency is calculated including the exit system loss, the efficiency becomes .866. This efficiency is based on a radial tip clearance of 10 mils.

There are a number of reasons why the Compressor Unification Study code gives a higher polytropic efficiency to the TAC axial flow compressor than for the T-58 compressor. The TAC axial-flow compressor has a

GENERAL ELECTRIC T58-10
GAS TURBINE ENGINE
ENGINE 297-002
TEST DATE MARCH-APRIL, 1966

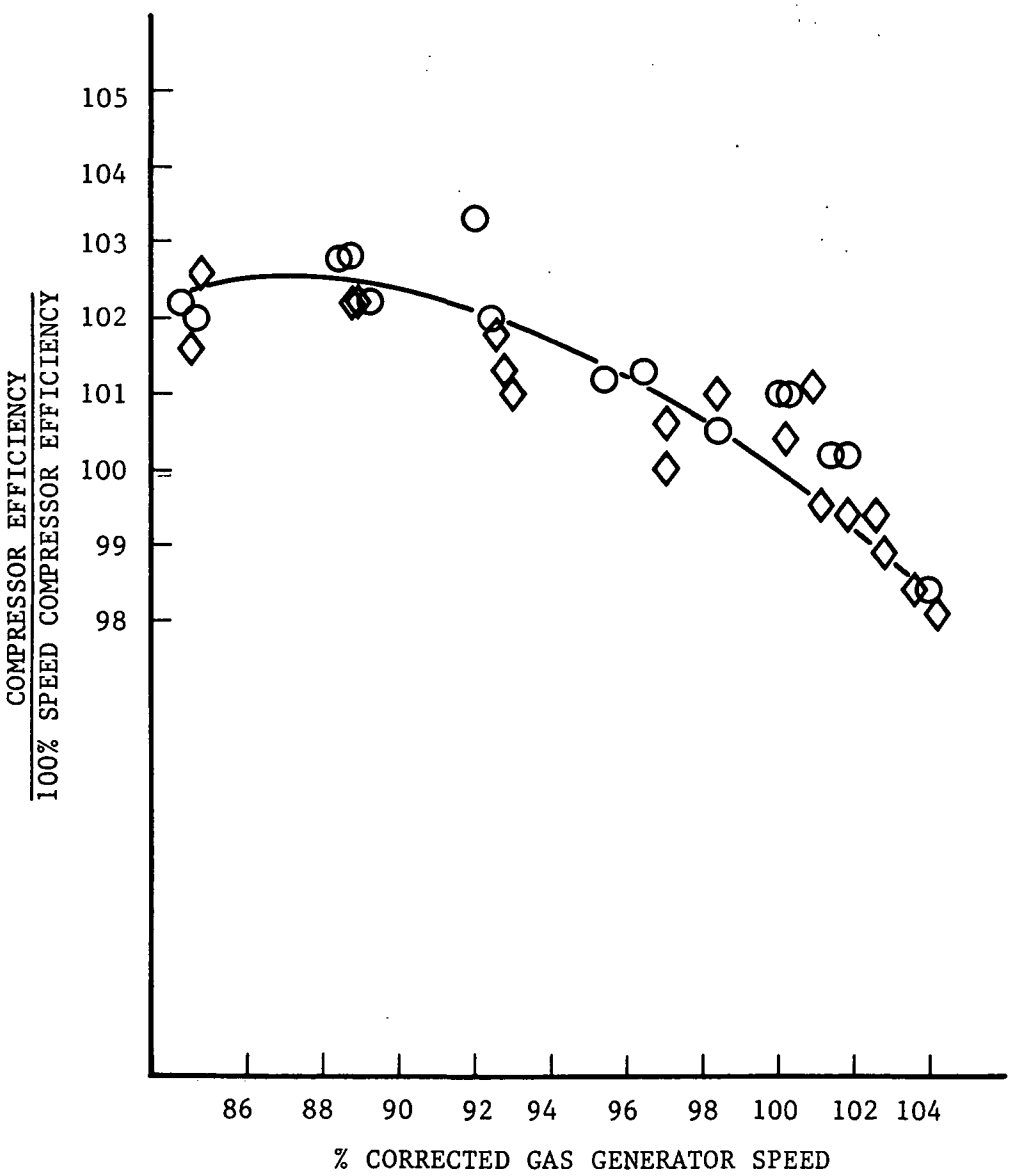

Figure 49

higher Reynolds number due to the high inlet pressure and it has lighter blade loading and a more favorable tip clearance.

AXIAL FLOW COMPRESSOR DESIGN RECOMMENDATIONS

Shown in Table XVIII is the design recommendation for the TAC axial flow compressor at 24,000 rpm. The compressor has 7 stages with an inlet radius ratio of 0.75. The blade chord length is 0.6 inch. The swirl level entering the rotors is 45°. The overall length of the turbomachine, exclusive of the exit system, is 6.67 inches. For a clearance of 10 mils the adiabatic efficiency is 0.866 including the collection system.

Shown in Figure 50 is a schematic diagram to scale which depicts the recommended TAC axial-flow compressor for 24,000 rpm. The hub radius is slightly in excess of 3 inches. The tip radius varies from slightly in excess of 4 inches at the inlet to about 3.8 inches at the exit. The axial length of the blading exclusive of the collection system and inlet guide vanes is 6.67 inches.

A study similar to the one reported in detail in previous sections was also carried out at 36,000 rpm. For these compressor parametric studies the inlet pressure was specified as 120 psia instead of 55 psia specified for the 24,000 rpm case. The Reynolds number for the 36,000-rpm compressors were high enough that a smaller penalty was paid for off design performance, namely at one-quarter power, than for the 24,000 rpm compressors primarily due to the higher compressor inlet pressure at 36,000 rpm. This made it possible to obtain a efficiency comparable to the selected 24,000 rpm compressor with the use of six stages. The recommended design for the 36,000 rpm compressor is shown in Table XIX. Like the 24,000 rpm compressor it has an inlet radius ratio of 0.75 and a swirl level entering the rotors of 45°. However, it was possible to use a chord length of only 0.4, resulting in an overall turbomachine length of 3.81 inches. The adiabatic efficiency of this machine is 0.862 including the collection system.

Shown in Figure 51 is a schematic diagram to scale which depicts the recommended axial-flow compressor for 36,000 rpm. The hub radius is

TABLE XVIII

DESIGN RECOMMENDATION

At 24,000 rpm	Number of Stages 7	Radius Ratio 0.75
Swirl level entering rotors, degrees,		45
Axial velocity level, ft/sec		215
Chord Length, inches		0.6
Overall Turbomachine Length,		6.67
Radial Clearance, mils		10
Adiabatic Efficiency (incl. collection system)		0.866

NASA NUCLEAR BRAYTON CYCLE DESIGN STUDY

24000 RPM

0.6 inch chords, 7 stage

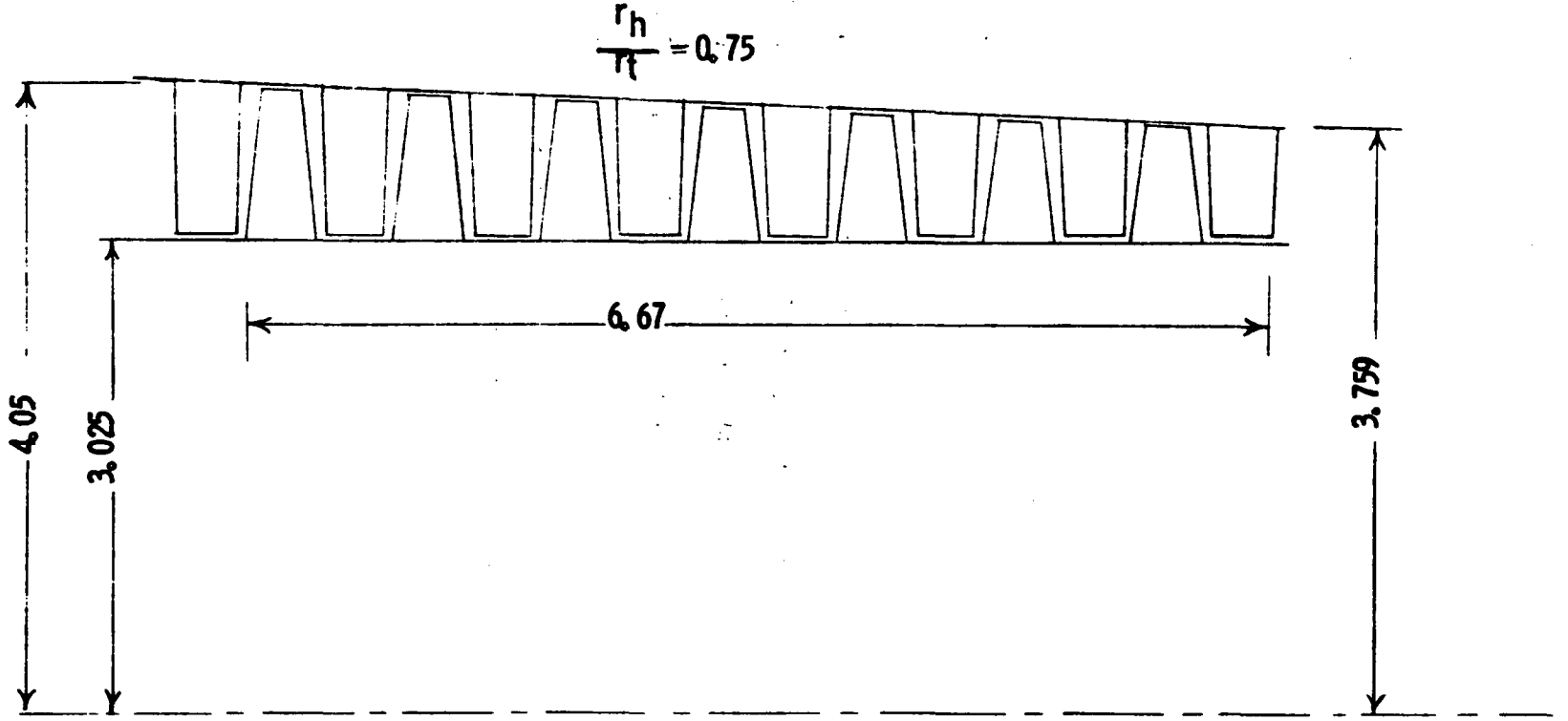

FIGURE 50.

TABLE XIX

DESIGN RECOMMENDATION

At 36,000 rpm

Number of stages	6
Radius ratio	0.75
Swirl level entering rotors, °	45
Axial velocity level, ft/sec	215
Chord length, inches	0.4
Overall turbomachine length, in.	3.81
Radial clearance, mils	10
Adiabatic efficiency (including collection system)	0.862

NASA NUCLEAR BRAYTON CYCLE DESIGN STUDY

36000 RPM

6 stage, 0.4 inch chords

$$\frac{r_h}{r_t} = 0.75$$

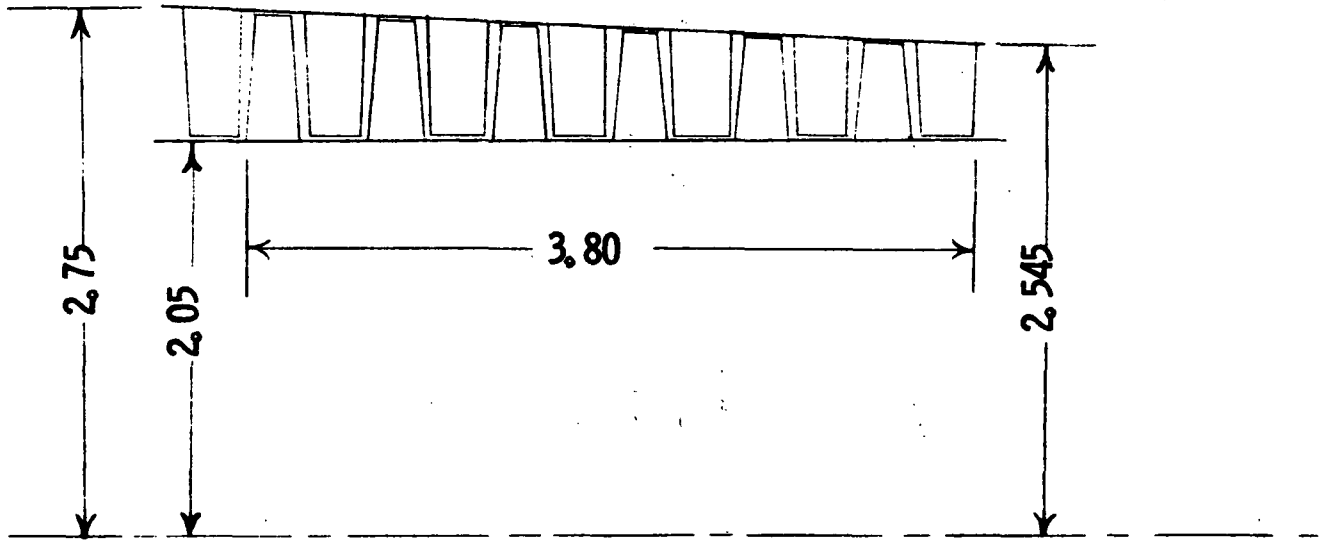

FIGURE 51.

slightly in excess of 2 inches and the tip radius varies from about 2.75 to 2.45 inches front to rear. The overall length of the blading from the exit of the inlet guide vane to the exit of the last stator is 3.81 inches.

CONCLUDING REMARKS

A very careful study was made of the axial flow compressor, both for 24,000 and 36,000 rpm as components for the TAC. Because of the low pressure ratio required by the recuperated Brayton system for the TAC the energy leaving the axial-flow compressor is a large portion of the energy put into the gas. This emphasizes heavily the careful design required for the exit system. Since the axial-flow compressor does not, by definition, impart a radial component to the flow of any significant value, the collection system must be added to the compressor in the axial direction. As a result the overhang of the compressor for the bearing becomes an important input to the rotor-bearing response of the TAC unit. Thus, although an efficiency can be substantiated at a competitive level for the axial-flow compressor it is not recommended for use in the TAC where the pressure ratio is so low that the advantages of the axial flow compressor cannot be fully utilized.

CENTRIFUGAL COMPRESSOR

A preliminary design study was carried out for a centrifugal compressor with a maximum efficiency stage of 1.90:1 total pressure ratio. Weight or size were not a major factor because of other system characteristics.

The results of this study consist of a parametric study for the 24RG and 36RL compressors, performance estimates for radial and backward-curved impellers with vaned diffusers, and a comparison of the objective performance with experimental data. A rather detailed aerodynamic analysis is carried out for the rotor and diffuser in order to substantiate the expected performance.

Parametric Study For Impeller Geometry

A parametric study was carried out for each compressor to analyze the inducer and overall impeller performance at a nominal level of diffuser loss. The analytic model considered the losses associated with the impeller blade loading, skin friction, clearance, mixing, and disc windage. The basic parameters which were varied were:

1. Inducer hub diameter
2. Inducer hub/tip ratio
3. Impeller tip width
4. Impeller work coefficient ($\Delta H/Ut^2$)

The model iterated for the impeller tip diameter using the above losses to satisfy the required overall pressure ratio of 1.90:1. The parametric analysis examined the general trends of geometry on performance level in order to locate the design in an efficient area, but it should be pointed out that it is basically a one-dimensional analysis and some judgment is required to interpret the results. The empirical factors for the loss estimate are limited to current design practice and any results for extreme departures from the norm cannot at this present time be considered completely valid.

The general procedure for the parametric study is first to analyze the inducer in order to locate a region of low relative Mach number and flow angle, and second to analyze the impeller tip holding the inducer geometry constant. This method typically reduces the number of configurations from 1050 to only 64, since any design with a poor inducer would be ruled out.

There was no inlet pre-whirl because the level of inducer tip Mach number was not excessive. A combination of low inducer relative Mach number and turning occurred for the 24RG at a hub radius of 1.3125 inches and a hub/tip ratio of .50. The 36RL inducer design point was at a hub radius of .788 and a hub/tip ratio of .4375.

The impeller tip width and work coefficient was varied using the above inducer designs. The range of impeller work coefficient was from .63 to .98, which would include designs from backward-curved to forward-curved impeller blade designs. The calculated impeller efficiency is shown in figures 52 and 53. The peak impeller efficiency varied from 92.5% for the .98 work coefficient to 91.8% for the .63 work coefficient.

The .98 work coefficient has a high exit Mach number and the overall performance calculated from a diffuser total pressure loss coefficient (ΔP_t) of .16 shows this somewhat higher impeller efficiency offset by increased diffuser loss (See Figures 54 and 55). Note that the exit blade height for peak overall efficiency does not necessarily correspond to the blade height for peak impeller efficiency because of the effect of inlet Mach number on the actual diffuser loss. The estimated overall diffuser loss of .16 was reasonable since the actual Task I designs were .153 and .140 for the 24RG diffuser and .148 for the 36RL diffuser.

To carry out the preliminary design study, a work coefficient of .88 and .63 was selected for the 24RG and .88 for the 36RL compressors. These levels would cover the range of radial and backward-curved blades. The backward-curved blades were considered because analytic and experimental results have shown performance improvements with backward-curved blades. Because of the amount of work involved for an axisymetric flow analysis of each design, the alternative design at the lower work coefficient could not be considered.

Overall Performance For Turboalternator-Compressor

A performance assessment was made for the 24RG with a .63 and .88 work coefficients and for the 36RL with a .88 work coefficient. The resultant flow paths are shown in Figures 56 and 57 for the 24RG design. An alternative 36RL design at a lower work coefficient was not made because the concurrent design studies indicated the 24,000 RPM machine

EFFECT OF BLADE TIP HEIGHT AND SLIP FACTOR ON IMPELLER ADIABATIC EFFICIENCY

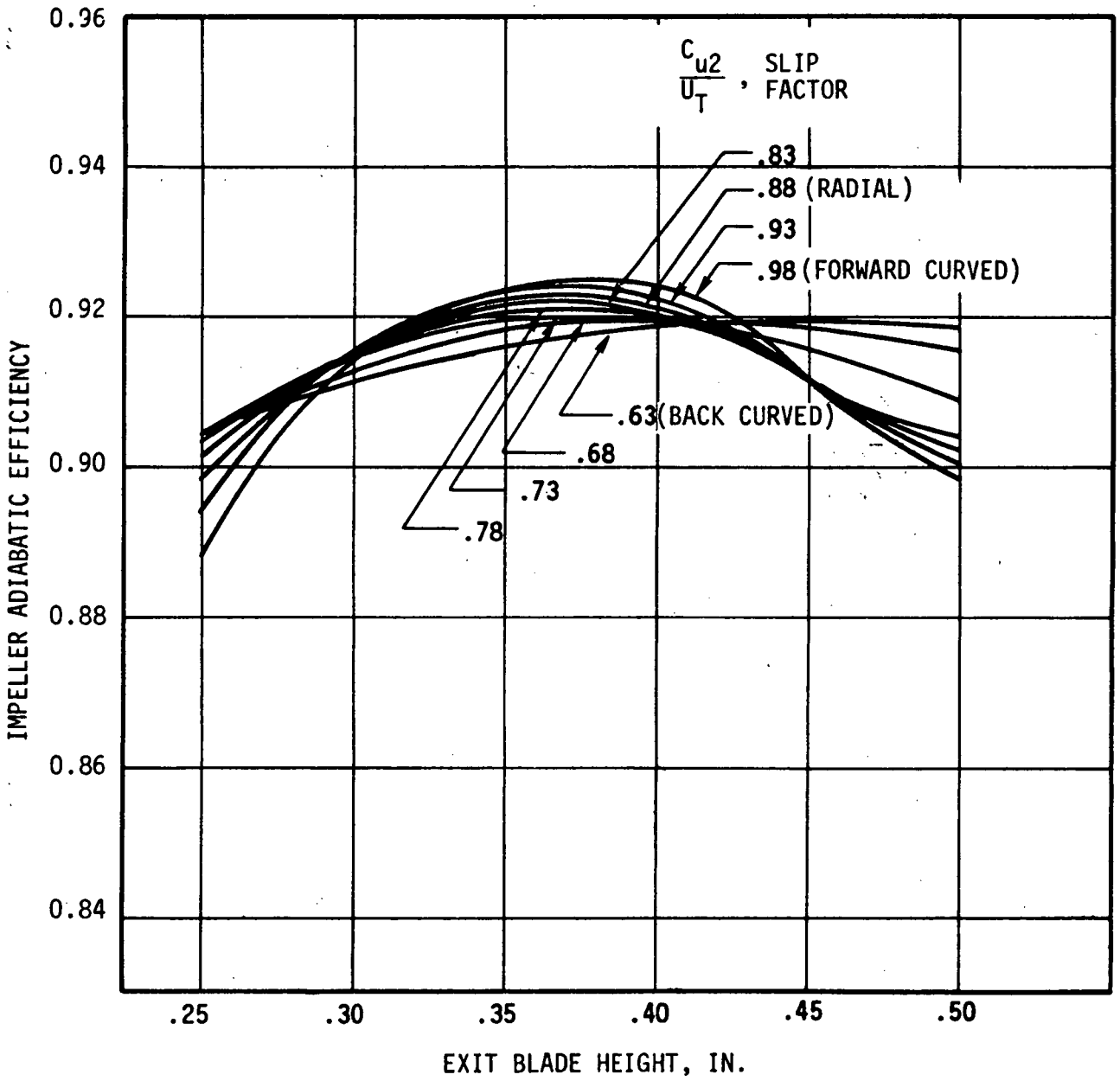

Figure 52.

EFFECT OF BLADE TIP HEIGHT AND SLIP FACTOR ON OVERALL EFFICIENCY

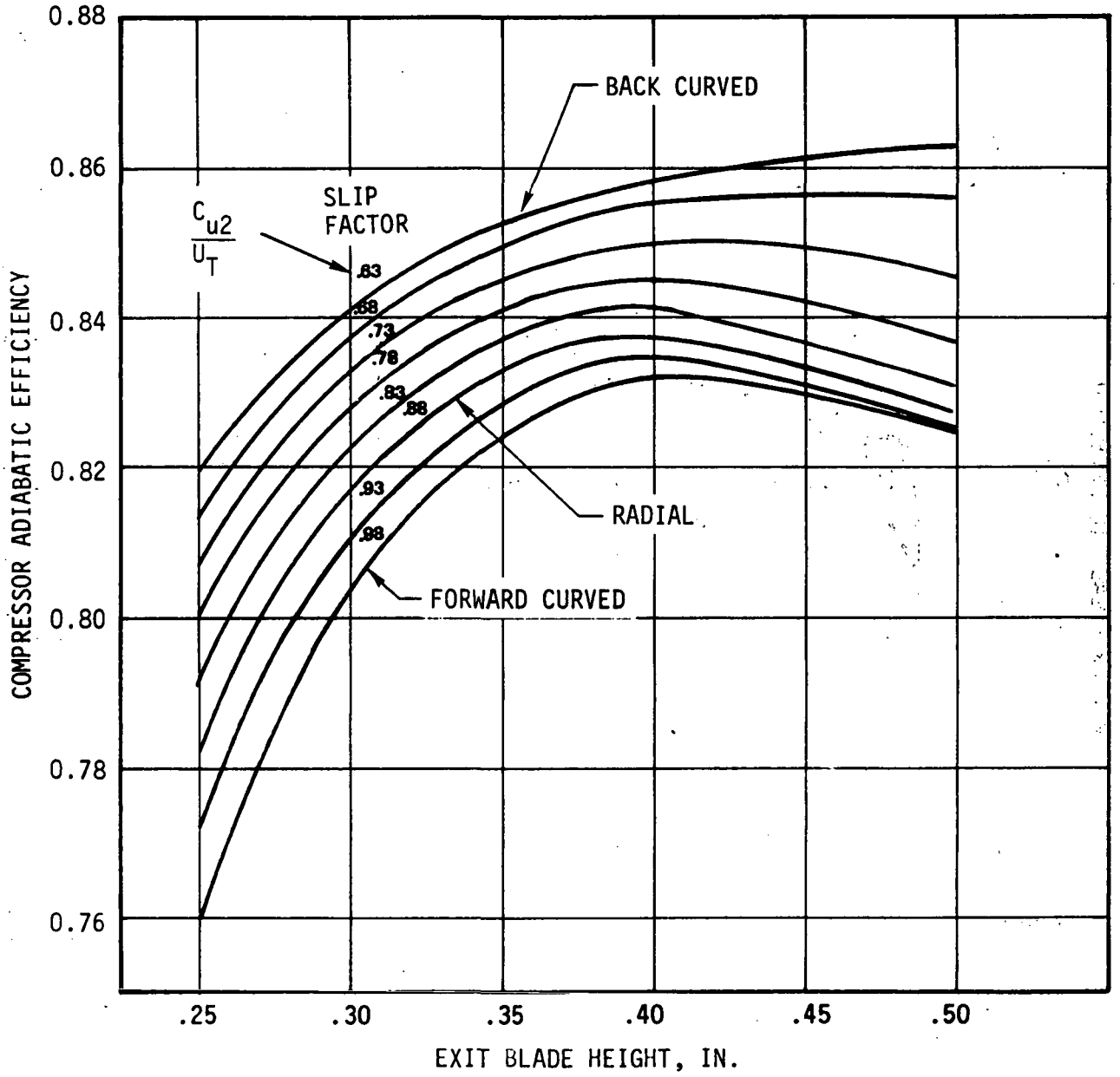

Figure 53.

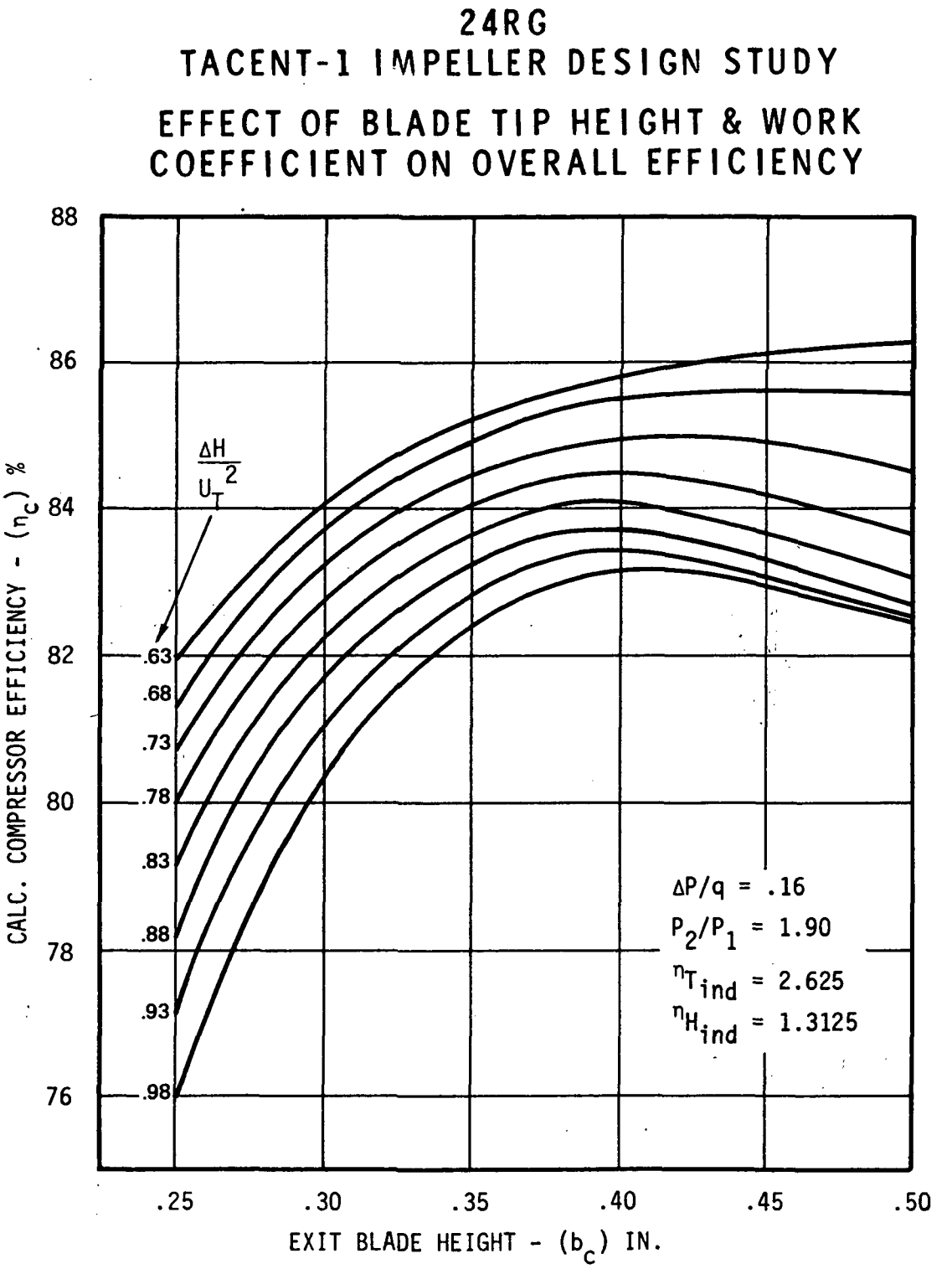
24RG
TACENT-1 IMPELLER DESIGN STUDY
EFFECT OF BLADE TIP HEIGHT & WORK COEFFICIENT ON OVERALL EFFICIENCY
CALC. COMPRESSOR EFFICIENCY - (η_c) %
88
86
84
82
80
78
76
$\frac{\Delta H}{U_T^2}$
.63
.68
.73
.78
.83
.88
.93
.98
$\Delta P/q$ = .16
P_2/P_1 = 1.90
$\eta_{T_{ind}}$ = 2.625
$\eta_{H_{ind}}$ = 1.3125
.25
.30
.35
.40
.45
.50
EXIT BLADE HEIGHT - (b_c) IN.

Figure 54.

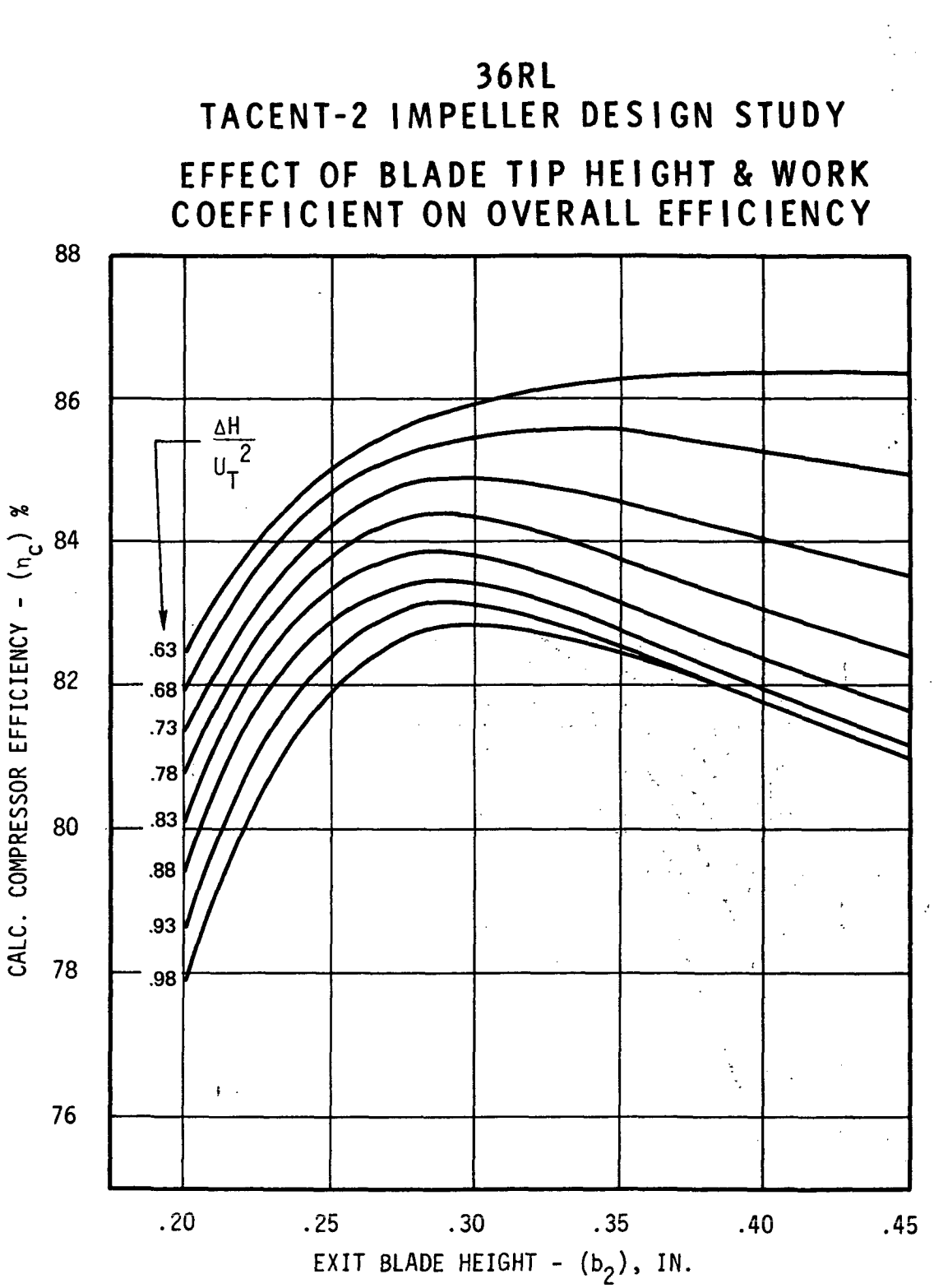
36RL
TACENT-2 IMPELLER DESIGN STUDY
EFFECT OF BLADE TIP HEIGHT & WORK COEFFICIENT ON OVERALL EFFICIENCY
CALC. COMPRESSOR EFFICIENCY - (η_c) %
88
86
84
82
80
78
76
$\frac{\Delta H}{U_T^2}$
.63
.68
.73
.78
.83
.88
.93
.98
.20
.25
.30
.35
.40
.45
EXIT BLADE HEIGHT - (b_2), IN.

Figure 55.

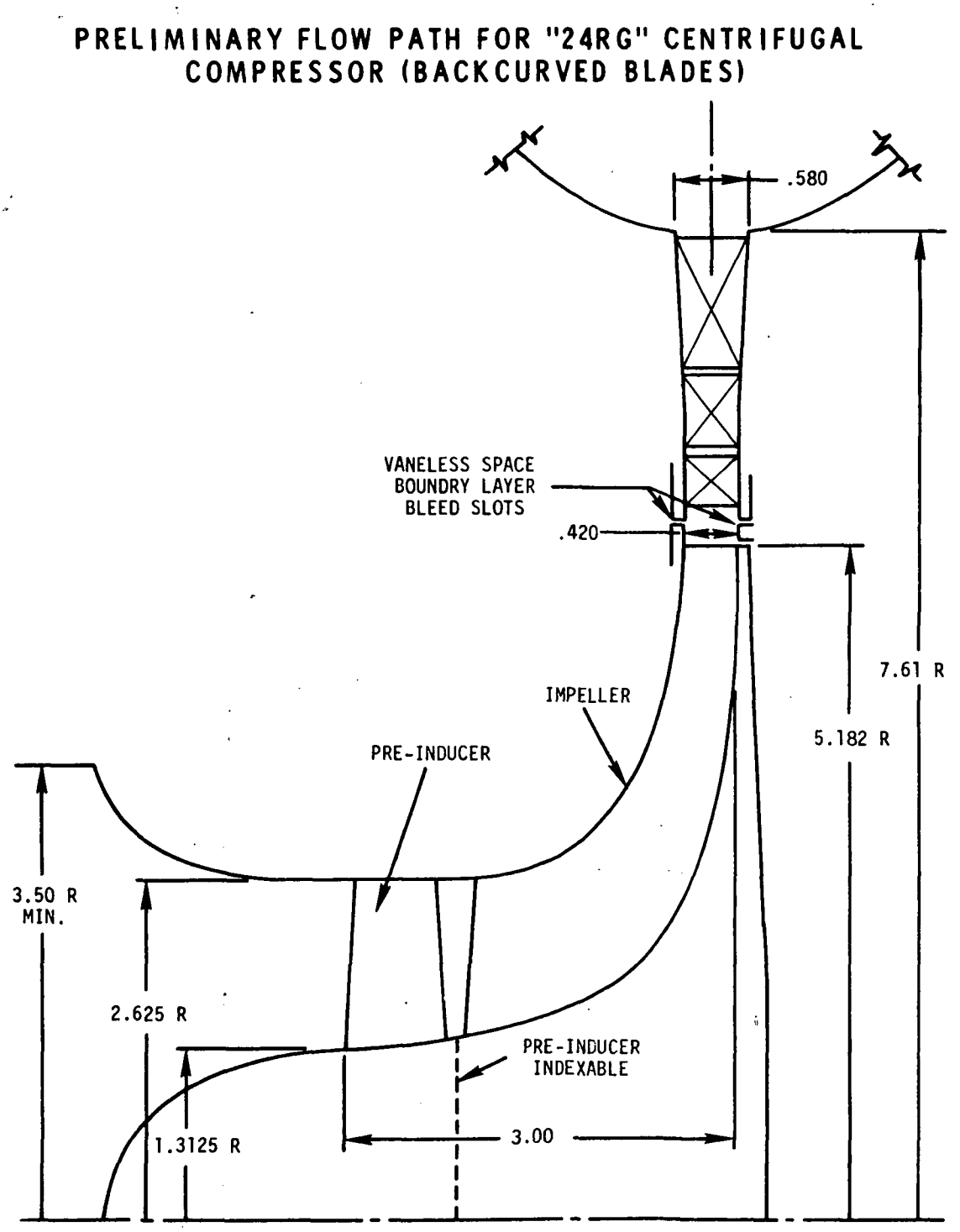
PRELIMINARY FLOW PATH FOR "24RG" CENTRIFUGAL COMPRESSOR (BACKCURVED BLADES)
.580
VANELESS SPACE
BOUNDRY LAYER
BLEED SLOTS
.420
7.61 R
IMPELLER
5.182 R
PRE-INDUCER
3.50 R
MIN.
2.625 R
PRE-INDUCER
INDEXABLE
1.3125 R
3.00

Figure 56.

PRELIMINARY FLOW PATH FOR "24RG" CENTRIFUGAL COMPRESSOR (RADIAL BLADES)

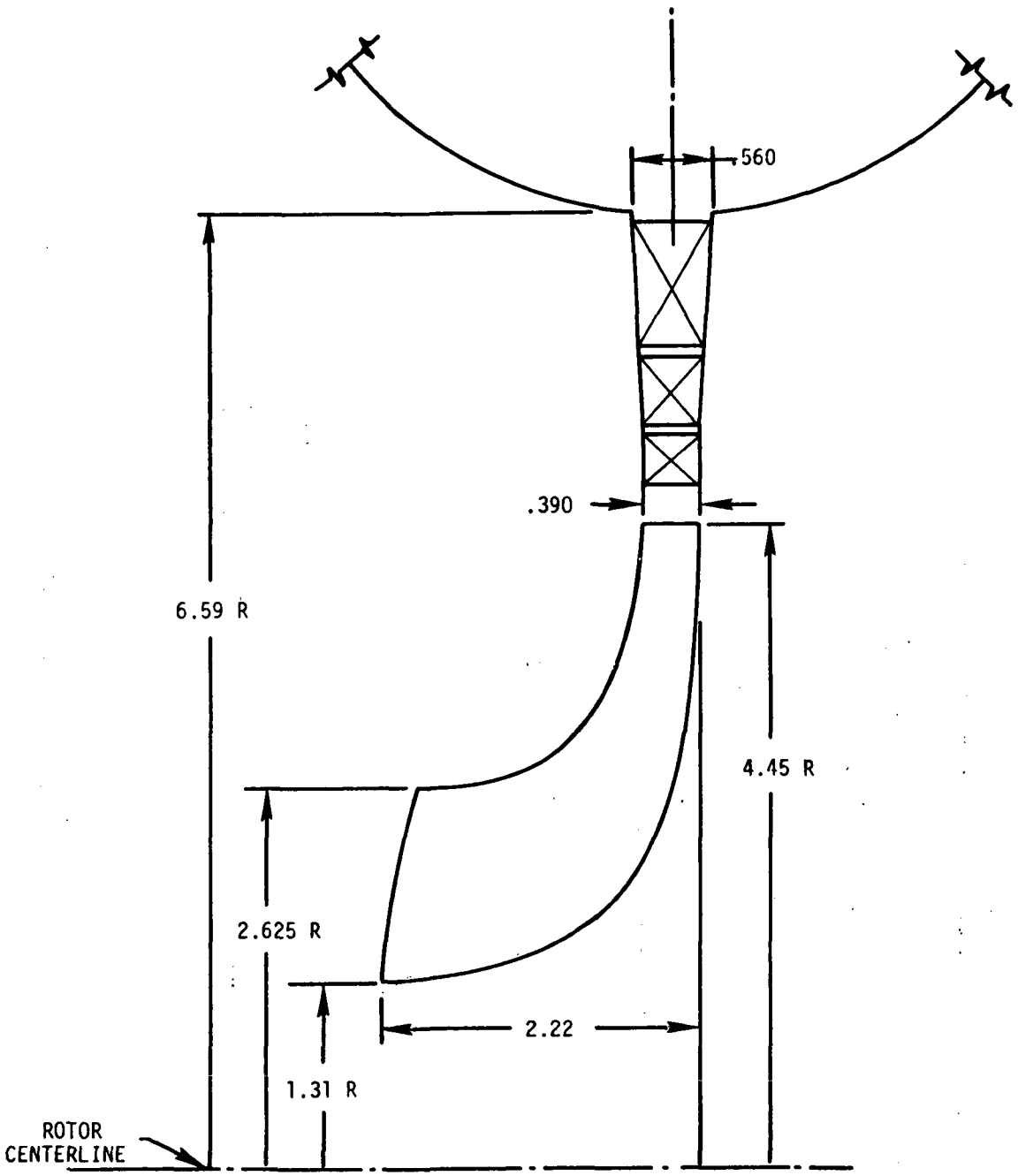

Figure 57.

would most likely be selected for the final study, and the performance for the two design speeds is nearly identical owing to the near constant specific speed. This closed cycle compressor operates at a constant mechanical speed, volume flow, and inlet temperature so that changes in output power are accomplished by changing the inlet pressure. This mode of operation resulted in Reynolds number changes proportional to power changes; therefore potential deterioration of performance down to 1/4 power was important.

This compressor system consisted of a centrifugal impeller followed by a three-vane row cascade diffuser which delivered the flow into a difusing scroll. The overall performance estimate is "flange-to-flange" and a breakdown is also presented for the individual components. A summary of the design input data is presented in Table XX.

The general level of Mach numbers in the machine are low because of the high critical velocity and low overall pressure ratio. The tip speeds for the stage are higher than with air for the same pressure ratio because of the high specific heat ratio of 5/3.

The performance of the .88 work coefficient designs are presented in Tables XXI and XXII, for the 24RG and 36RL compressors, respectively. The design point efficiency was 84.4% for each design. No deterioration in performance is expected down to 1/4 power since the Reynolds numbers do not go below $2x10^6$ where the effects of Reynolds number becomes measureable.

Recent test data at various Reynolds numbers on the compressor using reference 8 is plotted in Figure 58. Earlier results, reference 9, show for low Reynolds numbers below $2x10^6$ the Reynolds number various to the 1/5 power.

This characteristic line is also shown in Figure 58 for the NASA 6-inch compressor and agrees well with the test data. The Reynolds number losses of the NASA 6-inch compressor level off about $1.5x10^6$. Analytic computations using the design computer program at 1/4 power for the 24RG and 36RL compressors showed negligible effects. The first vane row inlet flow angle decreased only $.1^o$ and overall efficiency was .2% lower. The match of the diffuser-to-impeller should not be adversely affected by Reynolds number because the inlet flow angle is constant.

TABLE XX

DESIGN CONDITIONS FOR TAC

1. DESIGN SPEED 24,000 & 36,000 RPM
2. DESIGN WEIGHT FLOW
   - 24 RG 11.10 LB/SEC
   - 36 RL 11.73 LB/SEC
3. COMPRESSOR INLET TEMP. 700°R
4. COMPRESSOR INLET PRESSURE
   - 24 RG 55 PSIA
   - 36 RL 120 PSIA
5. WORKING FLUID: HELIUM-XENON MIXTURE
   - SPECIFIC HEAT RATIO 5/3
   - MOLECULAR WEIGHT 39.94
6. STAGE PRESSURE RATIO 1.90
7. EXIT MACH NO. .10
8. FLUID VISCOSITY EQUATION

TABLE XXI

SUMMARY OF COMPRESSOR PARAMETERS

24 RG DESIGN $\frac{\Delta H}{U_T^2} = .88$

COMPRESSOR DESIGN PARAMETER	BASED ON DESIGN INLET PRES. & TEMP.
OVERALL (INLET-TO-FLANGE EXIT)	
1. PRESSURE RATIO (TOTAL-TO-TOTAL)	1.9127
2. EFFICIENCY (TOTAL-TO-TOTAL)	.844
3. ROTATIVE SPEED, RPM	24000.
4. WEIGHT FLOW, LB/SEC	11.1
5. SPECIFIC SPEED	87.76
6. REYNOLDS NO.	9.35×10^6
IMPELLER	
1. PRESSURE RATIO (TOTAL-TO-TOTAL)	2.0177
2. ADIABATIC EFFICIENCY (TOTAL-TO-TOTAL)	.924
3. POLYTROPIC EFFICIENCY	.934
4. IMPELLER TIP SPEED, FPS	932.
5. IMPELLER SLIP FACTOR	.88
6. IMPELLER ENTHALPY RISE, BTU/LB	30.53
7. RELATIVE INDUCER TIP MACH NO.	.56
8. RELATIVE INDUCER INLET FLOW ANGLE	56.5
9. ABSOLUTE IMPELLER EXIT MACH NO.	.74
10. ABSOLUTE IMPELLER EXIT FLOW ANGLE	59.7
DIFFUSER	
1. STATIC PRESSURE RECOVERY, $\Delta P_s/q_c$	.834
2. STATIC EFFICIENCY - OVERALL	.862
3. TOTAL PRESSURE LOSS, $\Delta P_T/q_c$	
- OVERALL	.153
- VANELESS + VANED	.087
4. SCROLL INLET MACH NO.	.180
5. SCROLL INLET FLOW ANGLE	40.9
6. SCROLL EXIT MACH NO.	.075

$\gamma = 5/3$

TABLE XXII

SUMMARY OF COMPRESSOR PARAMETERS

36 RL DESIGN

COMPRESSOR DESIGN PARAMETER	BASED ON DESIGN INLET PRES. & TEMP.
OVERALL (INLET-TO-FLANGE EXIT)	
1. PRESSURE RATIO (TOTAL-TO-TOTAL)	1.9086
2. ADIABATIC EFFICIENCY (TOTAL-TO-TOTAL)	.844
3. ROTATIVE SPEED, RPM	36000.
4. WEIGHT FLOW, LB/SEC	11.73
5. SPECIFIC SPEED	91.83
6. REYNOLDS NO.	13.8×10^6
IMPELLER	
1. PRESSURE RATIO (TOTAL-TO-TOTAL)	2.0085
2. ADIABATIC EFFICIENCY (TOTAL-TO-TOTAL)	.920
3. POLYTROPIC EFFICIENCY (TOTAL-TO-TOTAL)	.930
4. IMPELLER TIP SPEED, FPS	930.5
5. IMPELLER SLIP FACTOR	.88
6. IMPELLER ENTHALPY RISE, BTU/LB	30.43
7. RELATIVE INDUCER TIP MACH NO.	.56
8. RELATIVE INDUCER INLET FLOW ANGLE	58.6
9. ABSOLUTE IMPELLER EXIT MACH NO.	.73
10. ABSOLUTE IMPELLER EXIT FLOW ANGLE	60.2
DIFFUSER	
1. STATIC PRESSURE RECOVERY, $\Delta P_s/q_c$	.840
2. STATIC EFFICIENCY - OVERALL	.867
3. TOTAL PRESSURE LOSS, $\Delta P_T/q_c$	
- OVERALL	.148
- VANELESS + VANED	.093
4. SCROLL INLET MACH NO.	.177
5. SCROLL INLET FLOW ANGLE	40.9
6. SCROLL EXIT MACH NO.	.073

$\gamma = 5/3$

6-INCH NASA CENTRIFUGAL COMPRESSOR LOSS VARIATION WITH REYNOLDS NUMBER

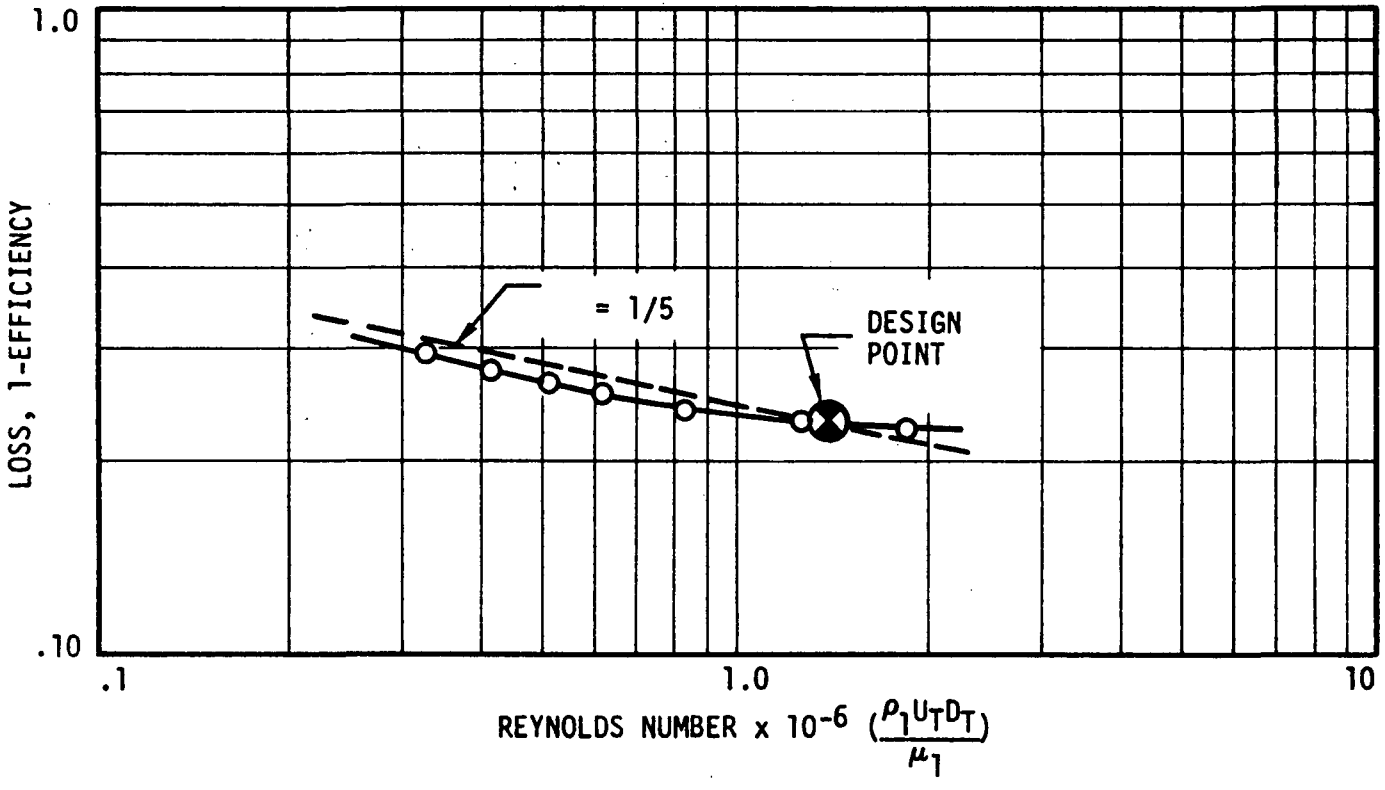

Figure 58.

The performance level for the TAC impeller is nominally 92% at design speed in order to achieve the objective performance. This performance level is considered equivalent to the performance level (10) measured for the GE 2.2 lb/sec compressor. The efficiency for the 2.2 lb/sec compressor is plotted in Figure 59, where 91% efficiency was recorded versus its design objective of 90%. The specific speed for the 2.2 lb/sec stage was 70 versus about 90 for the TAC. Considering the lower Mach number level, the higher specific speed, and the more lightly loaded compressor it would seem reasonable to expect a 92% level for the TAC rotor efficiency.

The parametric studies indicated superior overall efficiency for the lower work coefficients. The lower work coefficient resulted in backward-curved blades, higher reaction, and lower diffuser inlet Mach numbers; hence lower diffuser losses. The backward-curved blades have more conservative blade surface velocities when compared to radial blades. For the above reasons a .63 work coefficient stage was considered for the 24RG requirement. The nominal blade tip exit angle of 45^{o} for the .63 work coefficient was considered a good compromise between lower blade surface velocities and higher blade skin friction. Stress was not a factor because of the low mechanical tip speed.

The performance results for the 24RG and 36RL conditions are summarized in Table XXIII. The estimated adiabatic efficiency is .844 from the parametric studies for both cases.

Balje (11) has shown the effect of the degree of reaction (R_x) on the overall efficiency by the following expression:

$$\eta = \eta_R - (1 - R_x) \quad (1 - \eta d)$$

The degree of reaction is increased from .415 for the 24RG radial blades to .599 for the 24RG backward-swept blades. The above expression estimated the overall efficiency at 86.8% for a 91.9% rotor and an 86% diffuser. The efficiency level appears reasonable from the parameter comparison in Table XXIV and GE's 2.2 lb/sec data.

The parametric studies for the 24RG and 36RL rotors established the inducer and impeller tip dimensions as well as the expected performance level. This phase of the effort investigated the impeller blade surface

GE 2.2 LB/SEC CENTRIFUGAL COMPRESSOR IMPELLER ADIABATIC EFFICIENCY VERSUS INDUCER FLOW COEFFICIENT

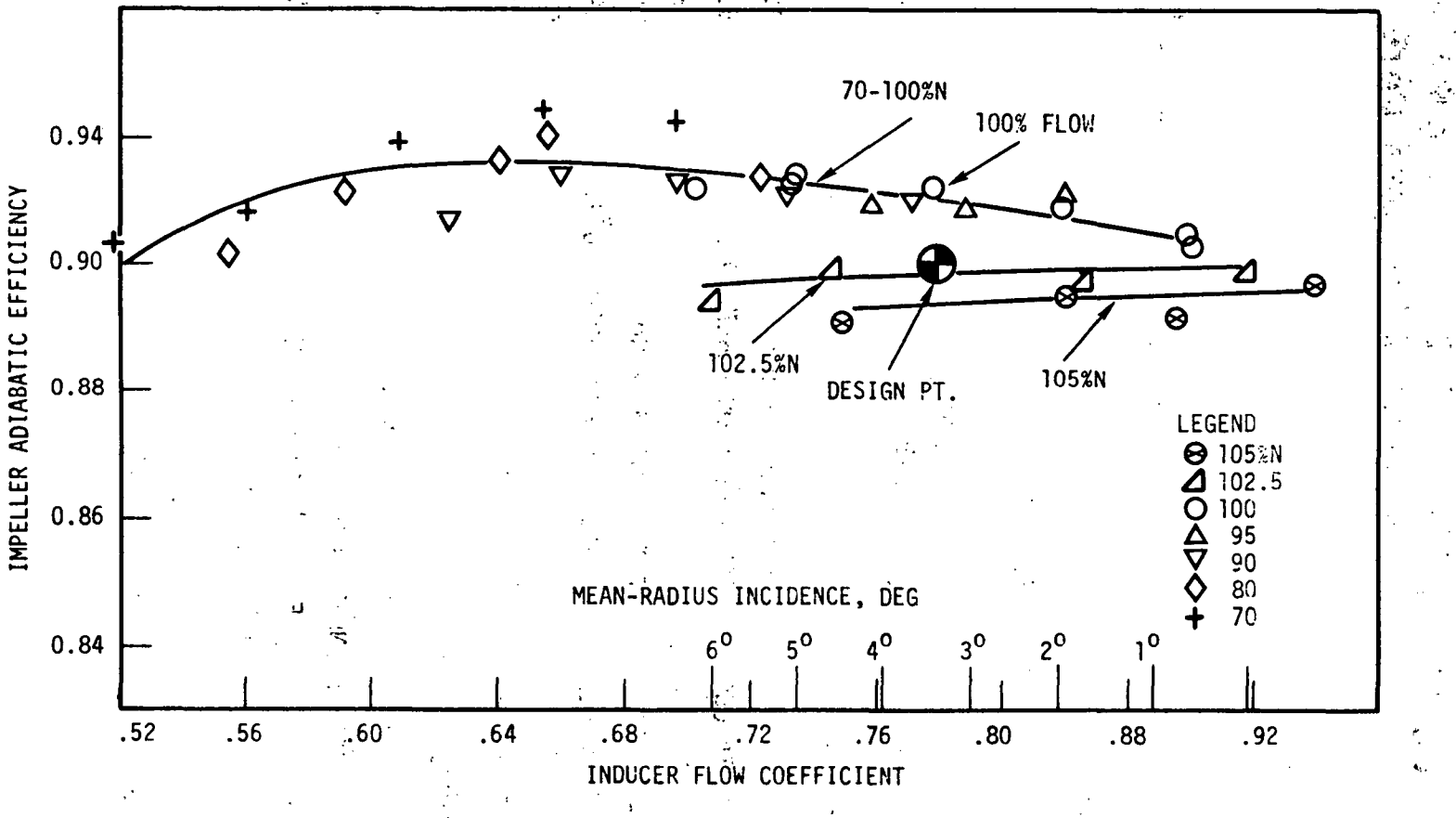

Figure 59.

TABLE XXIII

COMPARISON OF TAC RADIAL COMPRESSORS FOR 24000 AND 36000 RPM

DESIGNATION	24 RG	36 RL
● GENERAL		
- ROTATIVE SPEED, RPM	24000	36000
- FLOW RATE, PPS	11.1	11.7
- SPECIFIC SPEED, CFM, RPM, FT	88	92
- REYNOLDS NUMBER X 10^{-6}	9.4	13.8
● IMPELLER		
- INDUCER TIP RELATIVE MACH NO.	0.56	0.56
- INDUCER TIP RELATIVE FLOW ANGLE, DEG.	56.5	58.6
- TIP SPEED, FPS	932	930
- IMPELLER EXIT ABSOLUTE MACH NO.	0.74	0.73
- IMPELLER EXIT ABSOLUTE FLOW ANGLE, DEG.	59.7	60.2
- SLIP FACTOR	0.88	0.88
- ADIABATIC EFFICIENCY	.924	.920
● DIFFUSER AND SCROLL		
- TOTAL PRESSURE LOSS COEF.	.153	.148
- SCROLL INLET MACH NO.	.180	.177
- SCROLL INLET FLOW ANGLE, DEG.	40.9	40.9
- SCROLL EXIT MACH NO.	.075	.073
● OVERALL		
- ADIABATIC EFFICIENCY	.844	.844

TABLE XXIV

TAC RADIAL COMPRESSORS WITH RADIAL AND BACK CURVED BLADES, 24000 RPM

	RADIAL	BACK CURVED
● IMPELLER		
INDUCER TIP RELATIVE MACH NO.	0.56	0.56
INDUCER TIP RELATIVE FLOW ANGEL, DEG.	56.5	56.5
TIP SPEED, FPS	932	1085
IMPELLER EXIT ABSOLUTE MACH NO.	0.74	0.58
IMPELLER EXIT ABSOLUTE FLOW ANGLE, DEG.	59.7	62.6
SLIP FACTOR	0.88	0.63
TIP CLEARANCE, MILS	5	5
ADIABATIC EFFICIENCY	0.924	0.919
● DIFFUSER AND SCROLL		
TOTAL PRESSURE LOSS COEF.	.153	.140
SCROLL INLET MACH NO.	0.180	0.150
SCROLL INLET FLOW ANGLE, DEG.	40.9	40.4
SCROLL EXIT MACH NO.	0.075	0.062
● OVERALL		
ADIABATIC EFFICIENCY	0.844	0.868

velocity diagrams to substantiate the performance estimate and to provide approximate hub, shroud, and blade shapes for the preliminary design. The velocity diagrams were obtained from the "Marsha" axisymetric flow program using an arbitrary blade definition.

The blade coordinates for the axisymetric flow analysis are generated from a program entitled, "RACOMP - Radial Compressor Coordinate Generator". The hub and shroud coordinates are needed as well as sub-routines to generate the partial derivatives,

$$\left.\frac{\delta\Theta}{\delta Z}\right|_r \quad \text{and} \quad \left.\frac{\delta\Theta}{\delta r}\right|_Z, \quad \text{as a function of r and Z:}$$

$$\left.\frac{\delta\Theta}{\delta Z}\right|_r = f(r, Z)$$

$$\left.\frac{\delta\Theta}{\delta r}\right|_Z = f(r, Z)$$

The hub/shroud envelope is divided into "n" equal area elements which are spline curve-fitted to generate the slope angle, A, so that the blade angle (β) can be determined from:

$$\text{TAN } \beta = r\frac{d\Theta}{dm}$$

where,

$$\frac{d\Theta}{dm} = \left.\frac{\delta\Theta}{\delta r}\right|_Z \text{SIN A} + \left.\frac{\delta\Theta}{\delta Z}\right|_r \text{COS A}$$

The blade angle (β) is determined by numerical integration of the $\left(\frac{d\Theta}{dm}\right)$ function by the Runge - Kutta - Gill technique along each element. This program permits great flexibility in arbitrary blade shapes as well as very "smooth" input data for the "Marsha" program. A thickness distribution similar to the GE2.2 compressor was used.

The 24RG rotor analysis for the .88 work coefficient considered six modifications to determine the final velocity diagrams. The hub stream-tube is plotted in Figure 60. The modifications included various leading edge cutbacks to control incidence and two inducer lengths.

TAC 24RG BLADE SURFACE VELOCITY DISTRIBUTION - HUB STREAMTUBE

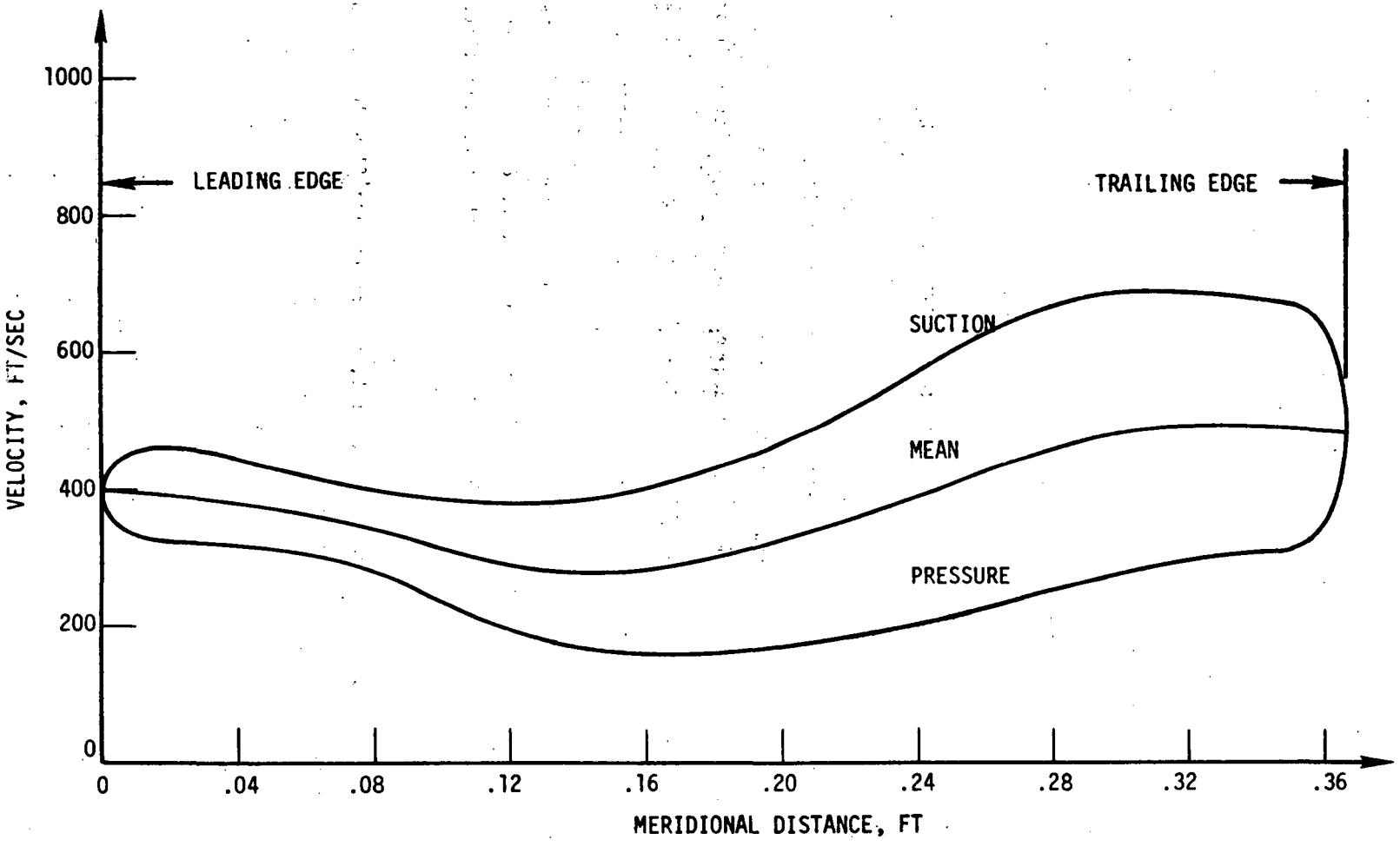

Figure 60.

The amount of the leading-edge cutback is dependent on the inlet shape and the 24RG rotor used a spinner. The resultant flow angle blade angle, and relative inlet Mach number is plotted in Figure 61 . The amount of the cutback was larger than anticipated and in a 24,000 RPM, Task III design, the impeller axial length would be increased about 10%. The 24RG velocity diagrams were obtained using 19 blades and are only nominally loaded. A comparison of these velocity diagrams to the GE 2.2 lb/sec rotor is shown in Table XXV.

The 36RL rotor was designed using the same procedure and the resultant velocity diagrams obtained . The inducer cutback was somewhat different than the 24RG design since an annular duct preceded the impeller (See Figure 62).

The performance level estimated for these impellers is summarized in Table XXIII. The polytropic efficiency of .934 and .930 for the 24RG and 36RL impeller designs compares favorably with the .933 polytropic efficiency achieved in the radially-bladed, GE 2.2 lb/sec impeller.

The velocity diagrams for the backward-curved rotor would be more conservatively loaded than for the equivalent radially-bladed rotor.

Preliminary Diffuser Design Study

The preliminary vaned diffuser design study investigated the effects of vaneless space size, vane loading level, and scroll inlet swirl in order to arrive at the proposed design. The diffusing system consisted of a vaneless diffuser followed by a vaned diffuser which dumps into a collecting scroll. The losses for each section of the diffuser are calculated in the same fashion as the GE 2.2 lb/sec diffuser since good correlation with experimental data had been achieved. The vaned diffuser losses include profile, wall, and secondary flow losses; hence preliminary diffuser blading was designed for each case to arrive at these losses. A second method was also used to estimate the performance by computing a diffuser overall effectiveness to determine the diffuser recovery.

Experience with vaned diffusers with supersonic inlet Mach numbers has indicated vaneless space widths in the 1.1 to 1.2 $r/_{rt}$ as optimum. Small vaneless spaces have lower vaneless losses but larger vaned losses from the higher vane inlet mach numbers. The

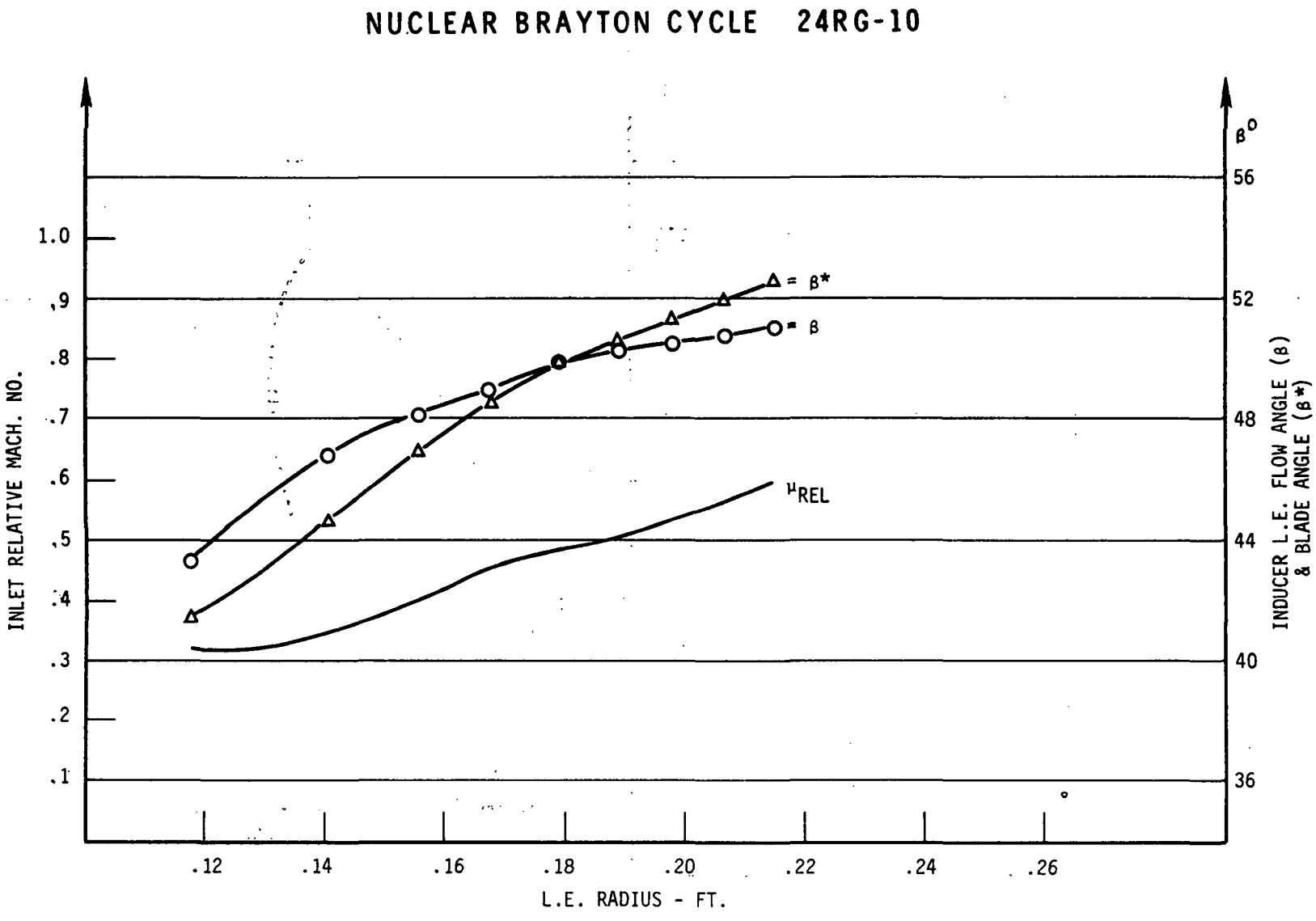
NUCLEAR BRAYTON CYCLE 24RG-10
INLET RELATIVE MACH. NO.
1.0
.9
.8
.7
.6
.5
.4
.3
.2
.1
β°
56
52
48
44
40
36
INDUCER L.E. FLOW ANGLE (β)
& BLADE ANGLE (β*)
= β*
= β
μREL
.12
.14
.16
.18
.20
.22
.24
.26
L.E. RADIUS - FT.

Figure 61.

TABLE XXV

COMPARISON OF ROTOR VELOCITY DIAGRAMS

ITEM	GE 2.2#/SEC COMPRESSOR ROTOR	24 RG ROTOR	36 RL ROTOR
1. $V_{max,\ s}/V_1$			
- SHROUD	1.253	1.213	1.229
- HUB	1.227	1.723	1.624
2. V_1/V_2			
- SHROUD	1.356	1.409	1.495
- HUB	.935	.825	.961
3. $V_{max,\ s}/V_2$			
- SHROUD	1.699	1.710	1.839
- HUB	1.147	1.412	1.561

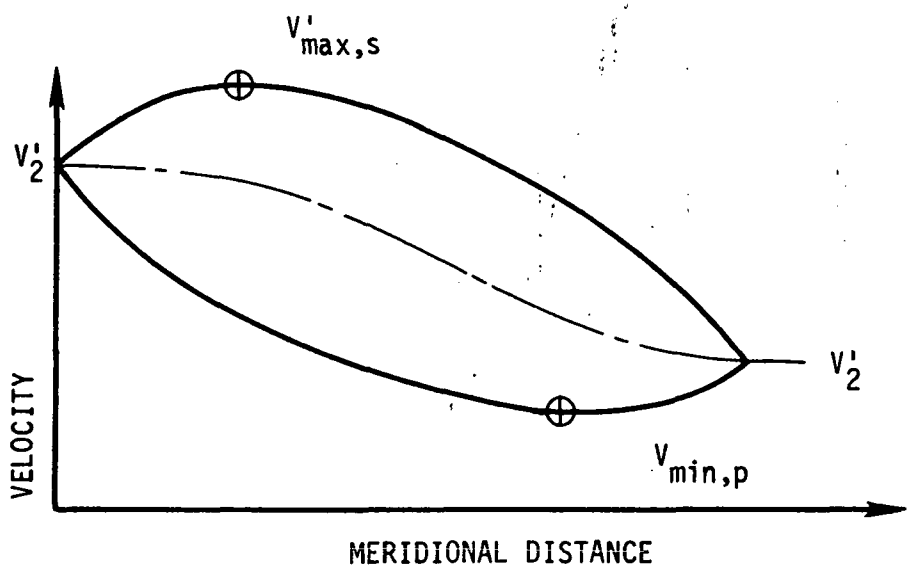

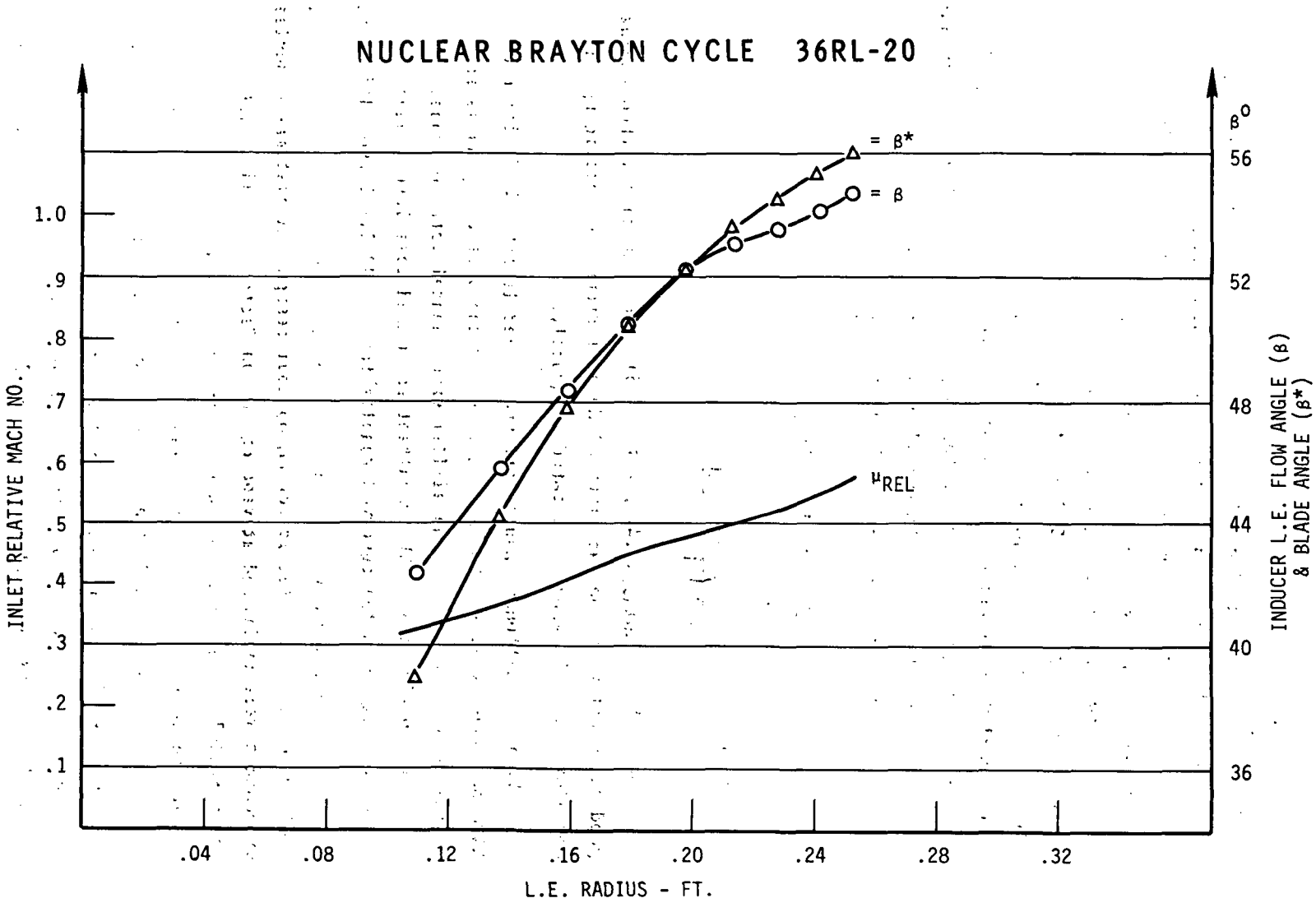
NUCLEAR BRAYTON CYCLE 36RL-20
INLET RELATIVE MACH NO.
1.0
.9
.8
.7
.6
.5
.4
.3
.2
.1
= β*
= β
μREL
β°
56
52
48
44
40
36
INDUCER L.E. FLOW ANGLE (β)
& BLADE ANGLE (β*)
.04
.08
.12
.16
.20
.24
.28
.32
L.E. RADIUS - FT.

Figure 62.

initial design was carried out for a 1.15 vaneless radius ratio, but it was not as efficient as the 1.06 vaneless radius ratio. A 1/2 point higher efficiency was calculated for the smaller vaneless space deisgn, while holding vane diffusion factors and solidities constant. The reason for this improved performance is the lower subsonic Mach numbers encountered in the TAC machine. The vaneless space anslysis followed the method of Stanitz (12) which consideres the flow as one-dimensional with friction. The impeller exit mixing loss is handled in the impeller analysis so the vaneless losses only account for the turbulent flow with friction. The turbulent skin friction factor (c_f) is related to the passage Reynolds number as defined by Goldstein (13):

$$\frac{1}{\sqrt{C_f}} = 4.00 \, LOG_{10} \, (R_E \sqrt{C_f}) + .80$$

where,

$$R_E = \left(\frac{2 \, Af}{L}\right) \frac{\rho U}{\mu}$$

The work of Faulders (14) and Dean (15) show that this method yields good agreement with the experimental data of Brown (16) providing the impeller mixing lossses are treated separately.

The vaned diffuser results are summarized in Table XXVI for the 24RG and 36RL designs. The loss levels for the vaneless plus vaned diffusers are compared to the similar experimental data for vaned diffusers in Figure 63. The resultant estimated loss levels have agreed closely with the observed results for the GE 2.2 lb/sec diffuser.

Since the vaned diffuser delivers the flow into a diffusing scroll, a diffusion to zero swirl is not an optimum design. A systematic series of designs were evaluated at vane diffusion factors of .35 to .50 and parallel to diverging walls to arrive at the designs shown in Figures 56 and 57. The analysis considered the scroll losses for each case and the final design was based on "flange-to-flange" efficiency.

The scroll analysis for the preliminary design followed the method of Eckert (17) where the skin friction losses are considered. The computed area distribution, was for a uniform exit static pressure which would be required for stable operation. This area distribution is

TABLE XXVI

COMPARISON OF GE12 AND 24RG DIFFUSERS (RADIAL BLADED IMPELLERS)

	GE12 (G10) VANED DIFFUSER	TAC 24RG DIFFUSER
● DIFFUSION PARAMETER		
- FIRST VANE ROW	.518	.399
- SECOND VANE ROW	.539	.449
- THIRD VANE ROW	.603	.452
● STATIC PRESSURE RISE COEFFICIENT		
- FIRST VANE ROW	.484	.415
- SECOND VANE ROW	.526	.488
- THIRD VANE ROW	.557	.542

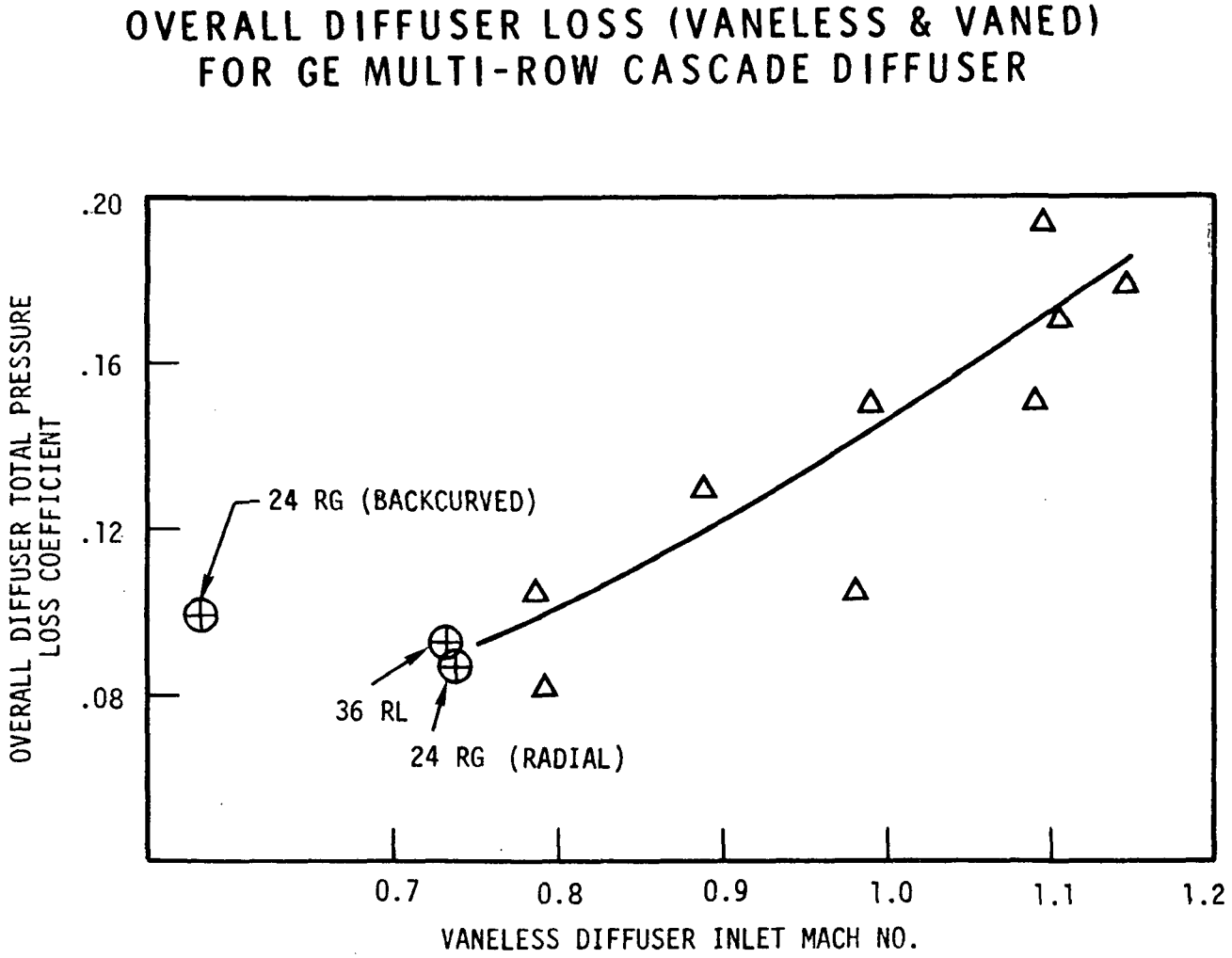
OVERALL DIFFUSER LOSS (VANELESS & VANED)
FOR GE MULTI-ROW CASCADE DIFFUSER
OVERALL DIFFUSER TOTAL PRESSURE
LOSS COEFFICIENT
.20
.16
.12
.08
24 RG (BACKCURVED)
36 RL
24 RG (RADIAL)
0.7
0.8
0.9
1.0
1.1
1.2
VANELESS DIFFUSER INLET MACH NO.

Figure 63.

sufficiently accurate for a preliminary design study. A more rigorous analysis should be carried out in Task III where the effects of finite recirculation and local skin friction would be considered. This method would be used to more accurately design the tongue area of the scroll but is not expected to have a major change in other regions.

A second method of estimating the diffuser performance employed the method of Sovran and Klomp where the effects of blockage and loss are included in an expression for the overall diffuser effectiveness ($\bar{\varepsilon}_o$). The diffuser overall effectiveness as defined by Sovran and Klomp (18) is:

$$\bar{\varepsilon}_o = \frac{\bar{C}_p}{C_p^*}$$

where, $\bar{C}_p$, is the actual static pressure recovery and C_p^* is the one-dimensional ideal static pressure recovery factor.

$$\bar{C}_p = \frac{P_{S2} - P_{S1}}{P_{T1} - P_{S1}}$$

As indicated by Runstadler and Dean (19) the $\bar{C}_p^*$ for compressible flow is somewhat higher owing to compressibility effects. Sovran and Klomp related the diffuser overall effectiveness ($\bar{\varepsilon}_o$) to the diffuser blockage, geometry, and core total pressure loss ($\bar{\omega}_m$):

$$\bar{\varepsilon}_o = \frac{1}{E_1^2} \left\{ \frac{1 - \frac{(E_1/E_2)^2}{AR^2}}{1 - \frac{1}{AR^2}} \right\} - \frac{\bar{\omega}_m}{1 - \frac{1}{AR^2}}$$

For the GE 2.2 lb/sec vaned diffuser, the overall effectiveness was .7508 for a loss .16 at an inlet Mach number of 1.05. The ideal compressible pressure recovery is .965 so the computed recovery with loss and blockage is .725. This computed recovery can be compared to the observed recoveries of .695 to .771 for this diffuser at this level of loss and Mach number. This method was applied to the 24RG vaned diffuser in order to account for the change in loss, exit blockage, and Mach number level expected for this design. The exit blockage resulting from decreased vane wake thickness is estimated at .55 versus .48 for the GE12 (Note: Blockage defined by Sovran and Klomp is based on core velocity). The overall diffuser effectiveness for the 24RG, .88 work coefficient, is computed to be .9041 for the loss level of .087. The ideal compressible

recovery is .914 so the computed static pressure recovery is .827. The static pressure recovery determined from the other design for the vaneless plus vaned diffuser is .813 for the 24RG diffuser.

The development of the vaned diffuser for the TAC would require a minimum of two diffuser flow sizes to properly match with the impeller. Previous experience has indicated that this matching is most critical to the achievement of the design objectives and it would be folly to attempt this sensitive match using a single diffuser design. Another area in question is the required stall margin for this machine since a large stall flow range would necessarily compromise the design point performance. The stall margin reflected in these design estimates would be about 8%, based on flow at design speed. Additional margin beyond this limit would need serious study in Task III. The indicated mode of operation is at a constant corrected flow and speed so a large stall margin requirement would seem unlikely at this time.

Concluding Remarks

Preliminary radial-bladed compressor designs were carried out for both the 24,000 and 36,000 rpm centrifugal compressors. The estimated performance of these designs was substantiated by the experimental performance of GE 2.2 lb/sec compressor performance. However, one dimensional parametric design studies indicated that even at the low value of Mach number encountered at the entrance to the vaned diffuser, an improvement in efficiency could be made by using 45-degree back-curved blades. A preliminary design of such a compressor was carried out for the 24RG TAC configuration. This compressor had a three-vane-row diffuser and scroll. The design-point efficiency at a radial tip clearance of 5 mils was 0.868.

GLOSSARY OF TERMS

Symbol	Description
A	Flow angle to axis - degree
A_f	Vaneless Diffuser Flow Area - Ft^2
AR	Diffuser Area Ratio
C_f	Skin friction coefficient
C_p	Diffuser static pressure recovery
C_p*	Ideal static pressure recovery
E_1	Diffuser inlet blockage based on core flow
E_2	Diffuser exit blockage based on core flow
H	Enthalpy, BTU/LB
L	Vaneless diffuser passage width, feet
M	Mach number
m	Meridional distance, feet
P_T	Total Pressure, PSF
P_s	Static Pressure, PSF
q_c	Compressible dynamic head, PSF
R_e	Reynolds Number
R_x	Degree of Reaction
r	Radius, feet
U	Velocity, FPS
Z	Axial distance, feet
β	Blade angle, degree
δ	Specific heat ratio
$\bar{\epsilon}_o$	Diffuser Effectiveness
η	Efficiency
Θ	Angular coordinate, radians
μ	Viscosity, $lb_m/sec\text{-}ft$
ρ	Density, lb/ft^2
$\bar{\omega}$	Total pressure loss coefficient based on compressible inlet head

RADIAL INFLOW TURBINE

Introduction

Design Requirements

Design requirements for the turbo-alternator compressor (TAC) drive turbine discussed in this report (24EG) are as follows:

Turbine Inlet Temperature	2060 deg R
Pressure Ratio	1.786
Molecular Weight of Working Fluid	39.94
Ratio of Specific Heats	5/3
Rotational Speed	24,000 rpm
Turbine Inlet Pressure	101.4 psia
Mass Flow	11.1 lb/sec
Diffuser Exit Mach Number	0.1
Specific Speed	83 rpm $ft^{3/4}/sec^{1/2}$

A second machine of approximately equal specific speed was also investigated. Design requirements for this turbine (36RL) were identical to those given above except for the following three quantities:

Rotational Speed	36,000 rpm
Turbine Inlet Pressure	221.1 psia
Mass Flow	11.73 lb/sec

Because of the equivalence in specific speed, the two machines are essentially scaled versions of each other. As a result, the optimization procedure described in the next section resulted in very similar aerodynamic designs for the two stages. To avoid repetition, only the 24,000 rpm design is described in detail. However, the final overall dimensions of both turbines have been included in the design summary. The slightly different mass flows projected for the TAC configurations utilizing axial-flow compressors (24AG, 36AM, 36AL, 36RM) have not been treated in detail, since the general trade-offs underlying the preliminary turbine design would not have been affected.

Design Limitations

Three constraints were imposed to define the range of mechanically and aerodynamically acceptable design variations. Rotor exit absolute swirl was limited to ±15 degrees to eliminate the possibility of unsteady

or recirculatory flows in the diffuser. Rotor exit hub/tip ratio was limited to a minimum of 0.4 since blade attachment problems and excessive trailing edge blockages would be encountered below this value. Finally, the ratio of exit shroud diameter to inlet tip diameter was limited to a maximum of 0.7 so that flow separation would not occur at the shroud. There is little incentive for using values of hub/tip ratio lower than 0.4, since only 16% of the maximum possible annulus area remains unused at this limit. The choice of 0.7 for the shroud curvature index is somewhat more arbitrary, being based primarily on good design practice.

The use of radial element rotor blading in the final design was anticipated. However, this limitation was not imposed during the preliminary meanline optimization in an effort to discover whether non-radial blades offered any significant performance advantages.

Parametric Meanline Design Optimization

Values of six parameters in addition to the design requirements are required to define the meanline velocity triangles completely. These are the following:

1. Ratio of rotor-exit to rotor-inlet relative velocity.
2. Absolute stator exit angle.
3. Absolute stator exit velocity.
4. Ratio of exit mean to inlet tip diameter.
5. Blade speed.
6. Efficiency.

For each set of values of the first five parameters, a value of efficiency was calculated iteratively using standard aerodynamic relations and the loss equations given by Rohlik in Reference 20. In this formulation, stator and rotor losses are based on a simplified form of the Stewart correlation (Reference 21). Clearance loss is assumed to be proportional to the average value of the ratio of clearance to blade height. (Fixed axial and radial clearances of 0.010 inch were assumed for this study.) Windage loss is calculated from a relation given by Shepherd in Reference 22. In computing static efficiency, the dynamic head corresponding to the absolute exit velocity is assumed to be lost. (The diffuser exit loss in addition includes the tangential component of the rotor exit head.) Finally, the conical diffuser performance correlation given by Henry in Reference 23 was employed to estimate diffuser losses.

Clearance and windage losses were treated as "external" losses, Δh_{ext}, which act to reduce the useful work output below the value, Δh, implied by the velocity triangles; the remaining losses constituted "internal" losses, Δh_{int}, which act to increase the pressure ratio required to obtain a given set of velocity diagrams. The efficiency is then defined as

$$h \equiv (\Delta h - \Delta h_{ext})/(\Delta h + \Delta h_{int}).$$

Total-to-static efficiency based on diffuser exit conditions was chosen as the performance index which was to be optimized. The effects on this efficiency of each of the five independent stage design parameters are described in the following paragraphs.

Relative Velocity Ratio

The exit-to-inlet relative velocity ratio fixes the overall acceleration of the flow relative to the rotor blades. Large values of this ratio lead to high rotor exit relative velocities and therefore to increased losses. On the other hand, low values of acceleration require high solidities to avoid excessive blade surface diffusion, and thus again to large kinetic energy loss.

Details of this trade-off are presented in Figure 64 for three levels of stator exit velocity. In generating these curves, stator angle and exit-to-inlet diameter ratio were held constant at 74 deg and 0.49, respectively. Blade speed was varied to obtain the best efficiency at each point. The trends of efficiency with velocity ratio were found to be essentially independent of stator exit velocity level; in each case a velocity ratio of 1.6 proved to be optimal. However, the effects of blade speed and flowpath curvature are to decrease the acceleration near the hub section. In anticipation of this situation, a velocity ratio of 1.8 was considered more desirable than the absolute peak point. This choice entailed a performance penalty of less than one-tenth point, and was in feet required to satisfy the 15 degree exit swirl limitation.

Stator Angle

The effect of varying the stator exit angle at a fixed exit Mach number is to vary the rotor tip axial width. Ths loss correlation employed in the parametric study assumed that the stator chordal aspect ratio was a constant. Hence low stator angles correspond to small tip

VARIATION OF EFFICIENCY WITH ACCELERATION (OPTIMUM EFFICIENCY POINTS)

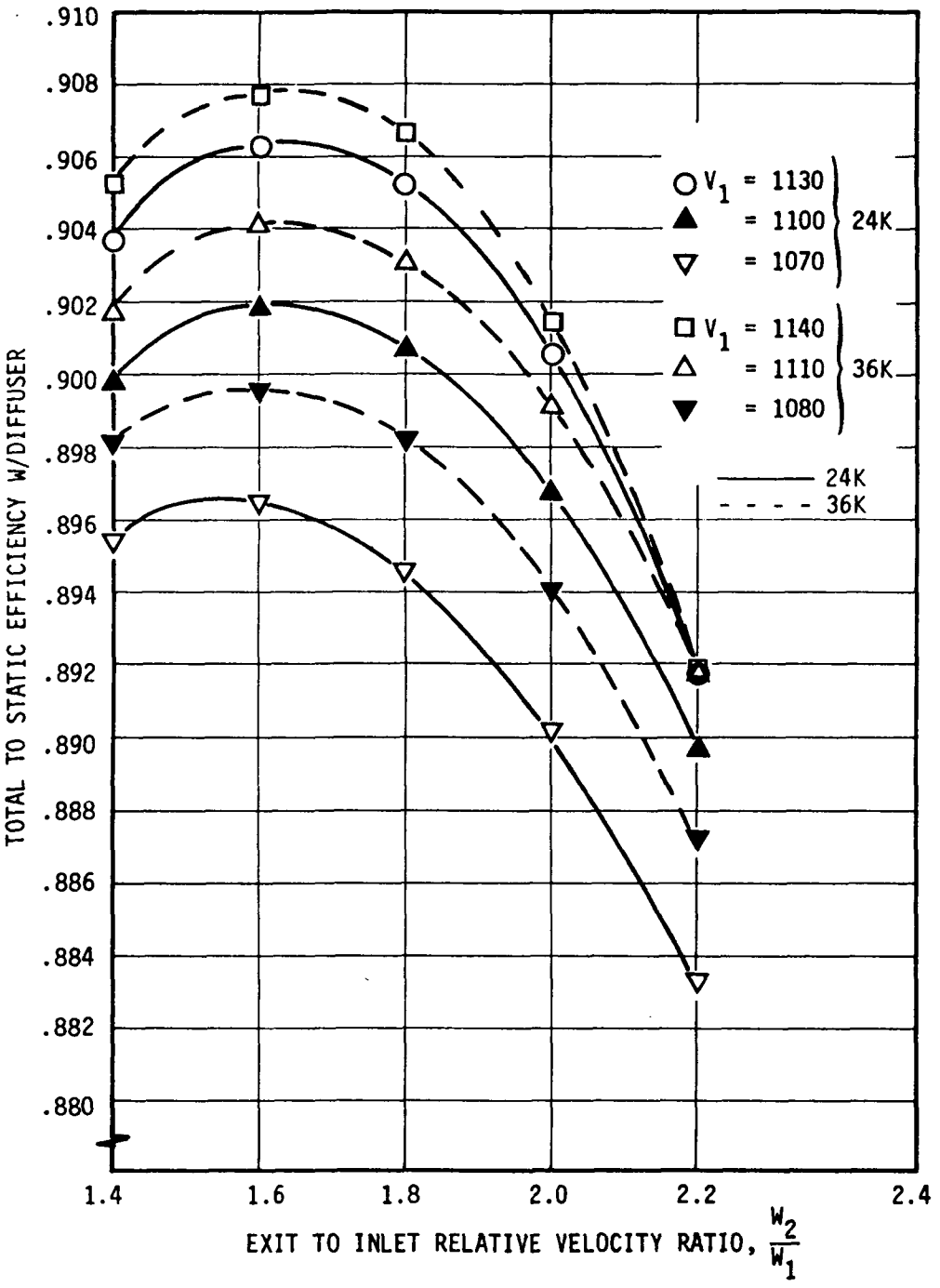

FIGURE 64

widths, short chords, and high blade loadings. Conversely, high nozzle angles imply long blades with large frictional losses.

The effect of these factors on stage efficiency has been plotted in Figure 65 . Rotor velocity ratio was set at its most desirable value as determined from Figure 64; the level of stator exit velocity which yielded the highest efficiency in that study was also employed. Predicted efficiency was found to vary substantially with moderate stator angle changes. Optimum efficiency of approximately 90.5% occurred at a nozzle setting of 74 degrees.

Stator Exit Velocity

The tangential velocity upstream of the rotor is determined by the stator exit absolute flow angle and velocity. Efficiency variation with the second of these parameters is shown in Figure 66. Stator angle, rotor velocity ratio, and blade speed were held at their optimum values. The results showed that the 1130 fps value used in Figures 64 and 65 were close to, but slightly below, the absolute peak value of 1160 fps. However, when the constraint of 0.4 hub/tip ratio is imposed, the predicted performance benefit of the higher stator velocity amounts to only 0.1%; that is, the curve of Figure 66 is flattened in the region of the optimum. In addition, the higher velocity would require considerably larger rotor incidence if radial rotor blades were used. It was therefore decided to avoid excessive blade loading near the leading edge by employing the slightly smaller exit velocity in the final design.

Exit-to-Inlet Diameter Ratio

The ratio of exit geometric mean diameter to tip diameter was used to relate inlet and exit blade speeds. A value of 0.49 was employed for this parameter in the three previous studies, so that the constraints on hub/tip ratio and shroud curvature would be reached simultaneously as exit annulus height increased. To investigate the possible advantages of departing from this procedure, the diameter ratio was varied from 0.45 to 0.52 with the other parameters set to optimum values. Results are given in Figure 67. No significant effect on performance was predicted. Since designs near the hub and shroud constraints were required to obtain the best efficiency, the 0.49 diameter ratio was retained for the final study.

VARIATION OF EFFICIENCY W/NOZZLE ANGLE

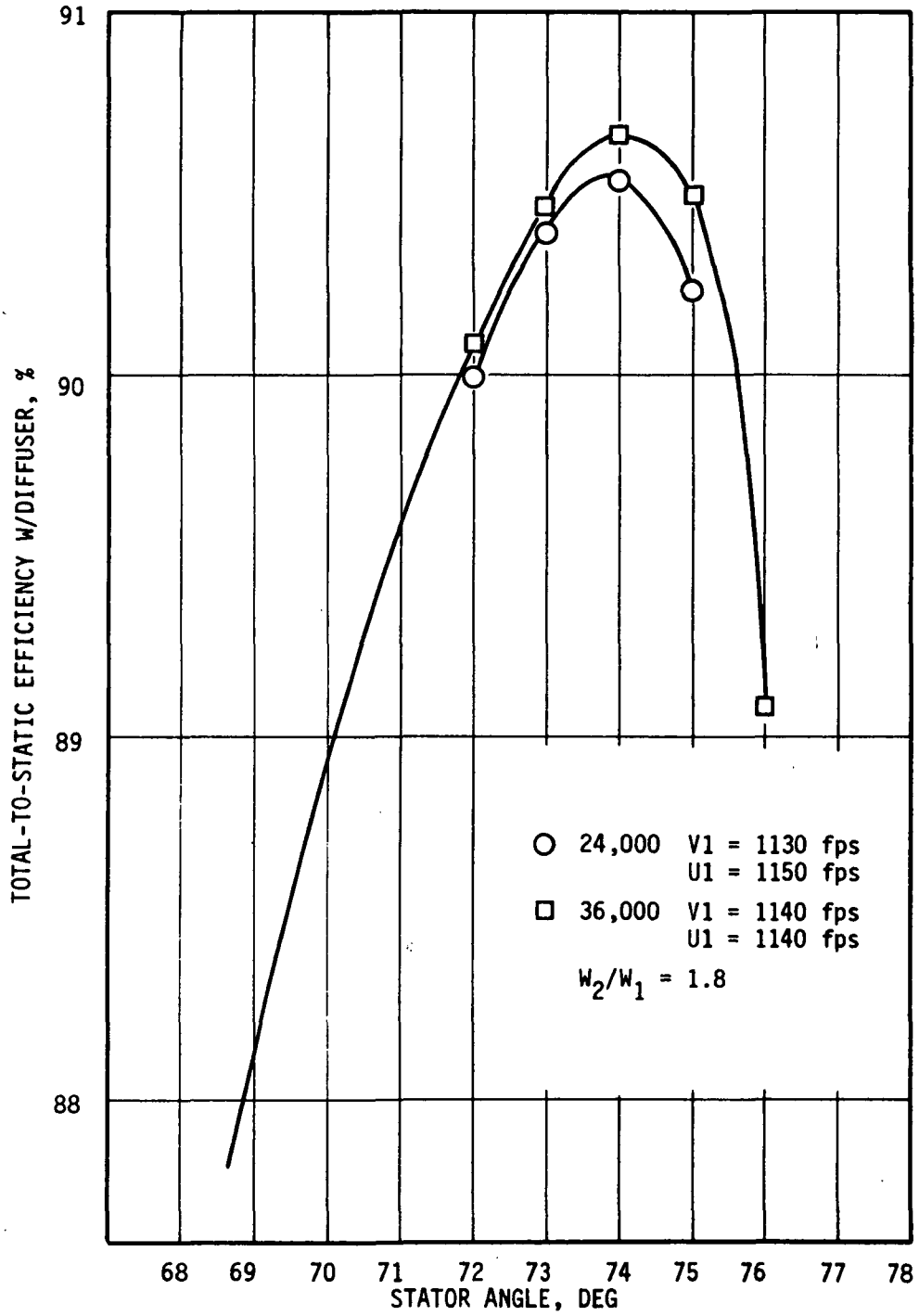

FIGURE 65

VARIATION OF EFFICIENCY WITH STATOR VELOCITY

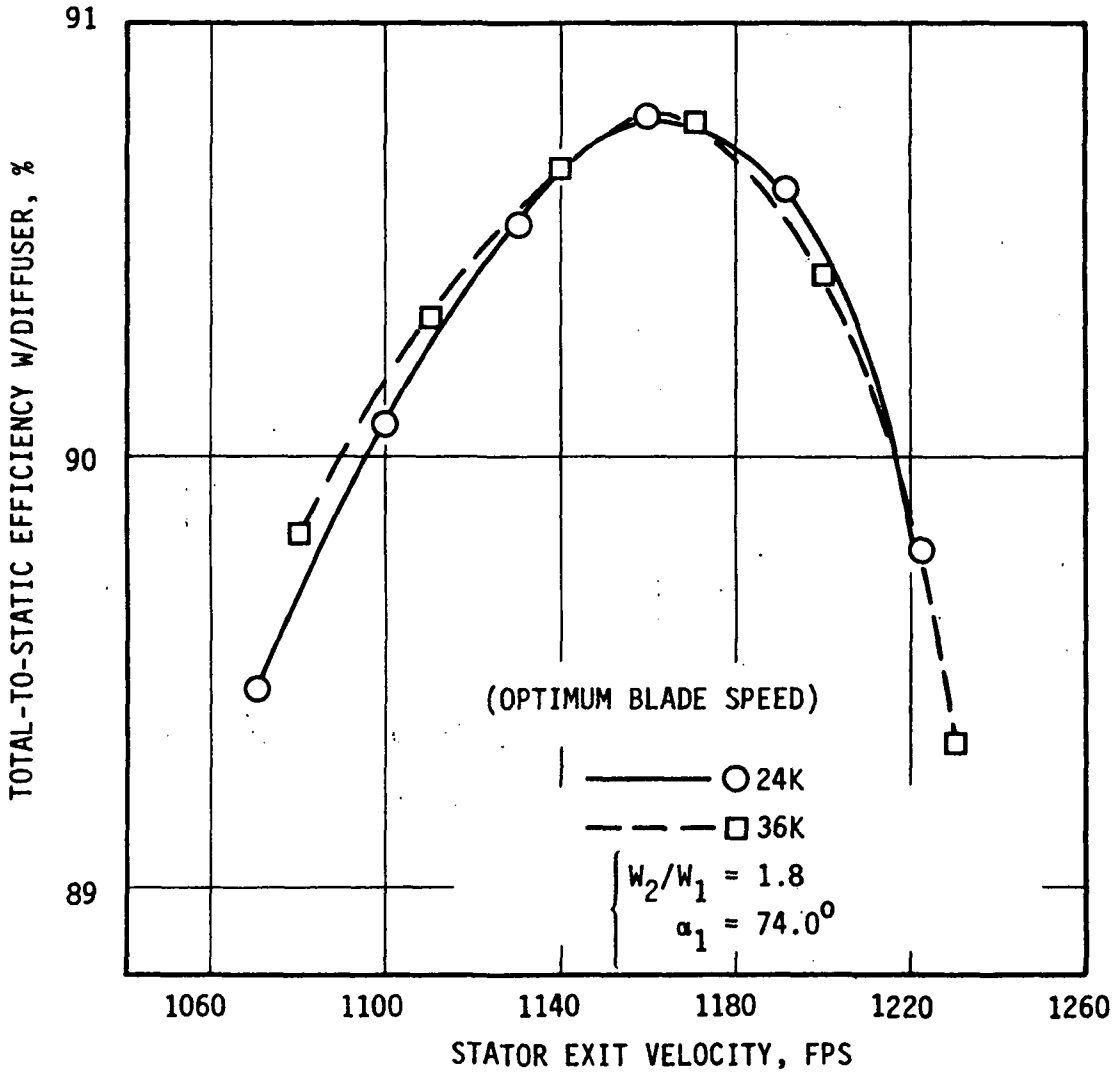

FIGURE 66

VARIATION OF EFFICIENCY WITH DIAMETER RATIO

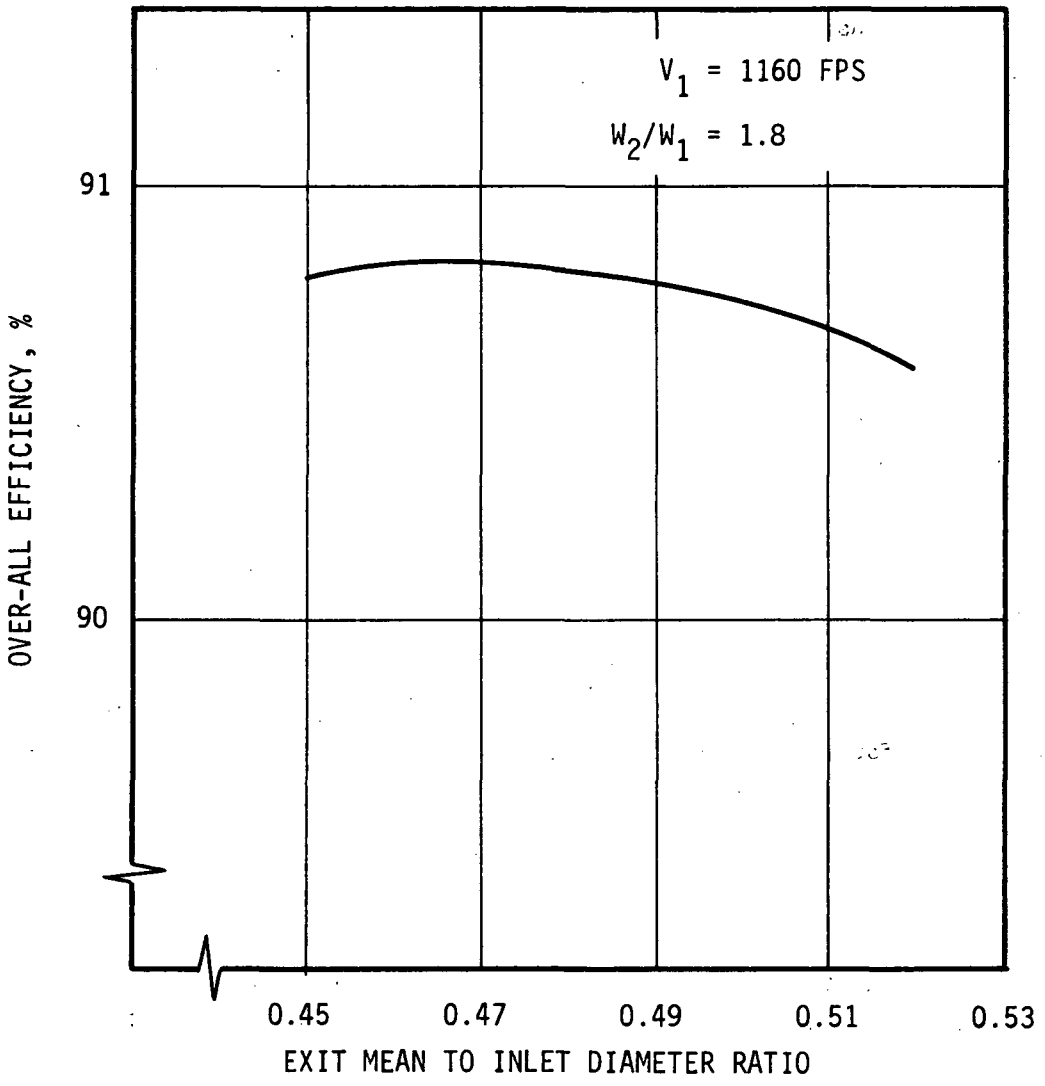

FIGURE 67

Tip Diameter

Calculated efficiency is presented in Figure 68 as a function of blade speed, using the optimum values derived in the previous studies for the four remaining parameters. For purposes of comparison, curves representing rotor velocity ratios of 1.6, 2.0 and 2.2 have been included. To illustrate the influence of the constraints, calculated exit swirl angles and hub/tip ratios are also shown. It will be observed that no 1.6 velocity ratio design satisfies the 15 degree exit swirl limitation. Secondly, whereas hub/tip ratio at the optimum efficiency point decreases as velocity ratio is reduced, efficiency at the 0.4 hub/tip ratio point increases, reaching a peak at a velocity ratio of 1.8. Predicted efficiency (excluding scroll losses) at this constrained optimum is 90.4%; the corresponding value of blade speed is 1163 fps. Exit swirl at this point is only a fraction of a degree beyond the nominal limit. Hence this point was chosen as the final Task I design point.

Optimized Designs

A parametric study very similar to that described above was also conducted for the 36,000 rpm turbine. The optimized values of the independent parameters for the two designs, subject to the constraints on hub/tip ratio and exit swirl, were as follows:

	24,000 rpm	36,000 rpm
Rotor Relative Velocity Ratio	1.8	1.8
Stator Angle	74.0 deg	74.0 deg
Stator Exit Velocity	1130 fps	1140 fps
Exit Mean-to-Inlet Diameter Ratio	0.49	0.49
Inlet Blade Speed	1163 fps	1162 fps

The implied values of the dependent variables are as follows:

Inlet Diameter	11.106 in.	7.398 in.
Exit Shroud Diameter	7.759 in.	5.182 in.
Exit Hub Diameter	3.124 in.	2.068 in.
Hub/Tip Ratio	0.4	0.4
Inlet Relative Flow Angle	-13.8 deg.	-11.9 deg.
Exit Relative Flow Angle	-56.4 deg.	-53.1 deg.
Exit Absolute Flow Angle	15.6 deg.	17.1 deg.
Blade-to-Jet Speed Ratio	0.704	0.702
Predicted Overall Total-to-Static Eff.	90.4%	90.2%

SELECTION OF 24,000 RPM TAC TURBINE DESIGN POINT

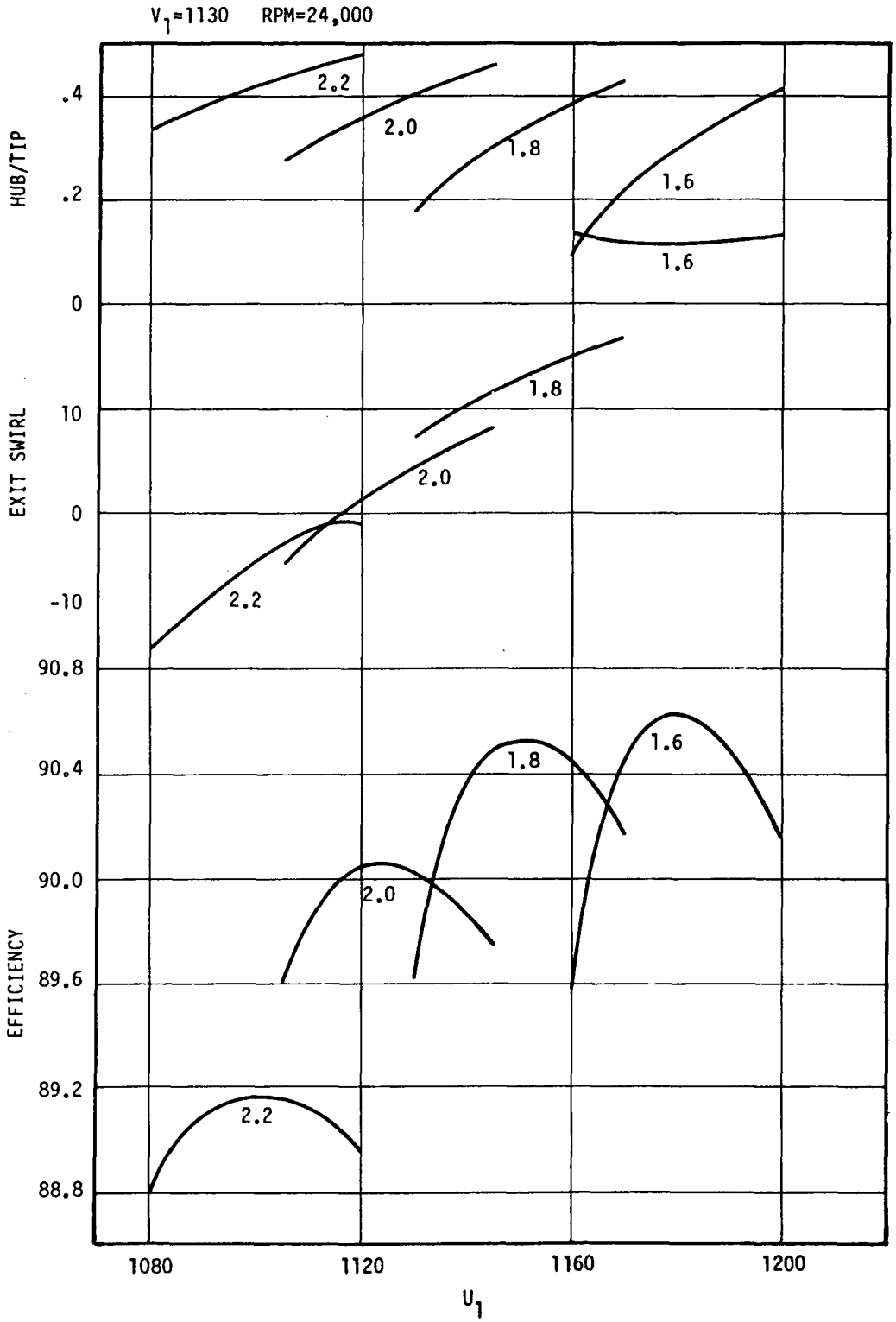

FIGURE 68

Intra-stage values of total and static pressures and temperatures for the 24,000 rpm design have been listed in Table XXVII. Corresponding pitchline velocity triangles are shown in Figure 69 .

Verification of Efficiency Prediction

In view of the relatively high efficiency which was predicted, an assessment of the accuracy of the loss formulation was undertaken. Performance of the 4.97 inch turbine reported in Reference 24 was calculated from the design velocity triangles. The computed efficiency of 88.2% compared favorably with the test value of 88.8%. It was concluded that the performance predicted for the subject turbine represented a realistic goal. A comparison of the efficiency loss breakdown for the two turbines is given in Figure 70. The bulk of the performance gain predicted for the subject turbine resulted from reduced rotor and clearance losses. Rotor losses were lowered by reducing the ratio of rotor exit kinetic energy to stage work output; clearance losses declined due to increased blade heights.

Since achievable rotor clearance depends, among other things, on the chosen bearing design, it may prove impractical to maintain the relatively tight clearances assumed in the parametric study. The influence of deviations in radial or axial clearance from the nominal 0.010 inch values is illustrated in Figure 71 . Alternative predictions are given, based on both the loss formula used for the parametric study and the more recent empirical data of Reference 25.

Effect of Reynolds Number

The Reynolds number customarily used to correlate turbine performance is based on stator span and exit velocity:

$$R_e = w/(\mu\ r_t)$$

where w = mass flow, lbm/sec

μ = viscosity, lbm/ft. sec.

r_t = rotor tip radius, ft.

Since only a relatively small range of tip diameters were considered in the parametric study, the corresponding Reynolds number effects on turbine efficiency could be disregarded. During part-power operation, however, the larger Reynolds number variation may be expected to influence performance significantly.

TABLE XXVII

INTRA-STAGE PRESSURES AND TEMPERATURES

	PRESSURE, psi		TEMPERATURE, deg. R	
	Total	Static	Total	Static
SCROLL INLET	101.40	100.56	2060.0	2053.2
SCROLL EXIT	101.13	98.18	2060.0	2035.7
NOZZLE EXIT	99.84	76.47	2060.0	1851.6
ROTOR EXIT	57.34	55.80	1664.6	1646.6
DIFFUSER EXIT	56.65	56.18	1664.6	1659.1

$P_o/P_o = 1.790$ $P_o/P_o = 1.805$

PITCHLINE VELOCITY TRIANGLES

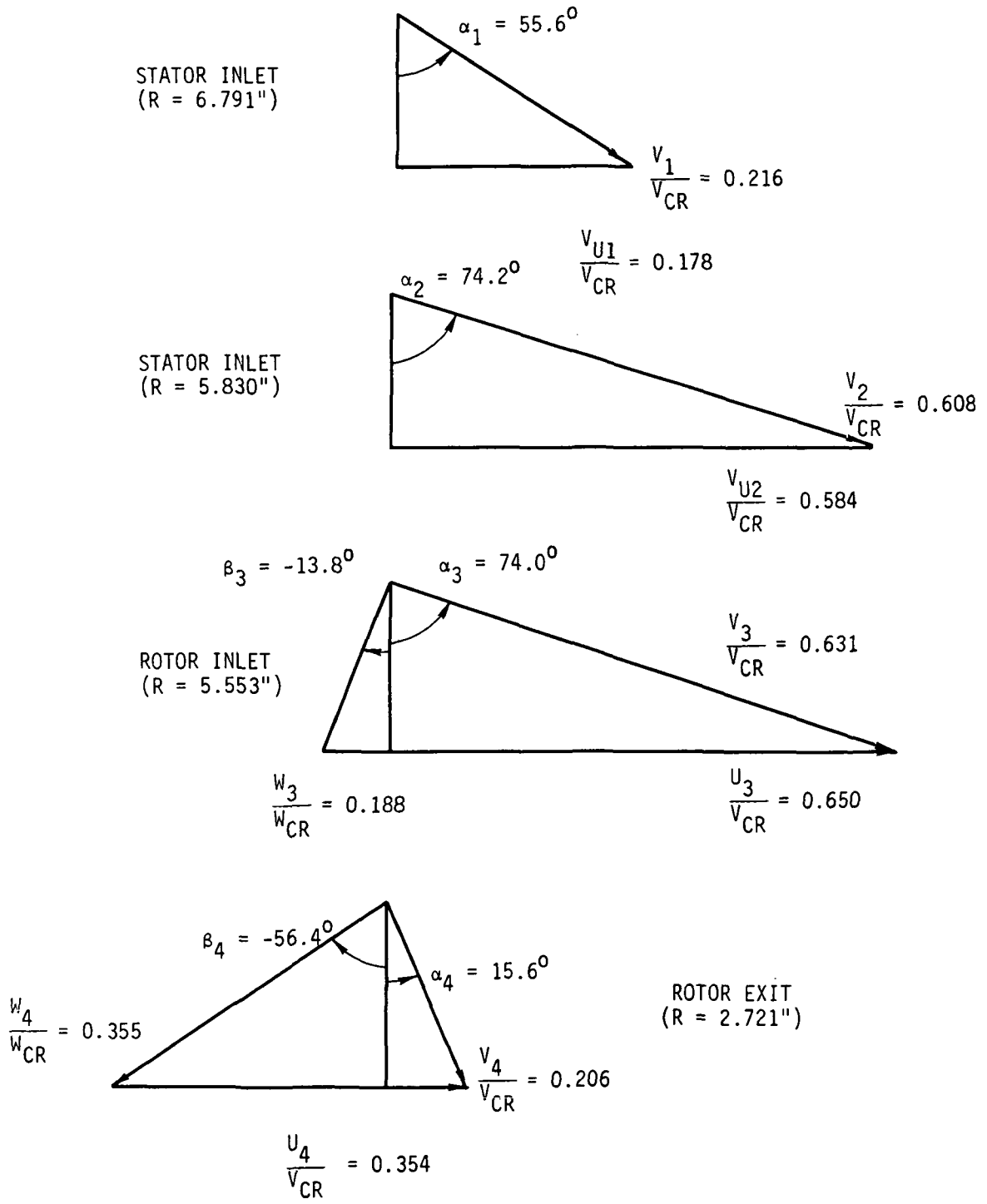

FIGURE 69

COMPARISON OF PREDICTED PERFORMANCE NASA AND 24RG TURBINES

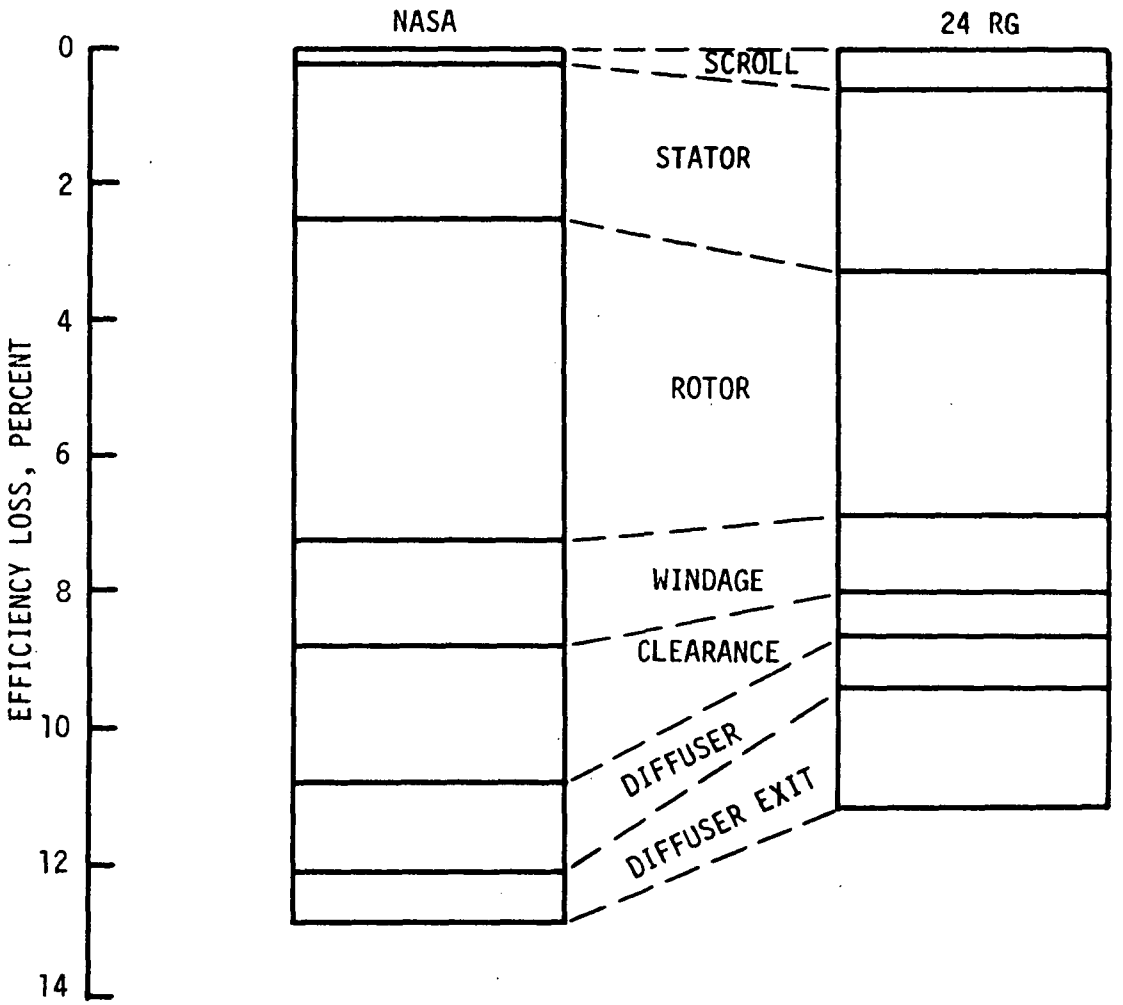

TIP DIAMETER, IN.	4.97	11.11
PREDICTED EFFICIENCY, TOTAL-TO-STATIC	.882	.903
TEST RESULT	.888*	
SPECIFIC SPEED	76	72.5
CLEARANCE, MILS	10	10
SPECIFIC WORK, BTU/LB	20	49

*NASA TD D-5090

FIGURE 70

EFFECT OF CLEARANCE ON TURBINE EFFICIENCY

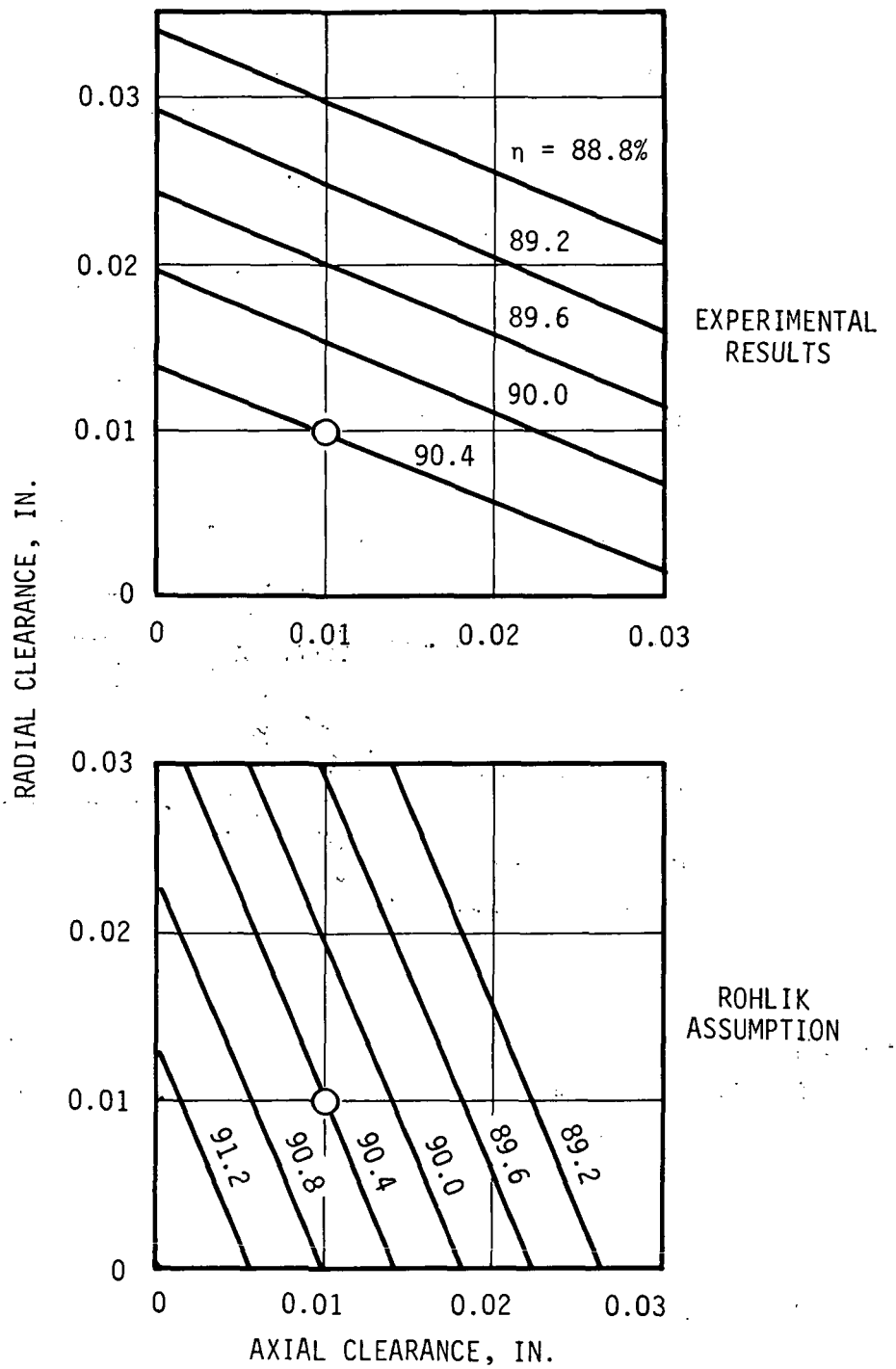

FIGURE 71

Experimental tests reported in Reference 26 showed that the efficiency variation could be approximated by a formula of the form:

$$\frac{1 - \eta_t}{1 - \eta_{t,ref}} = A + B \left(\frac{R_e}{R_{e_{ref}}} \right)^{-1/5}$$

where A = 0.4 and B = 0.6, indicating the relative magnitudes of the non-viscous and viscous losses, respectively, and $\eta_{t,ref}$ is the efficiency at a reference Reynolds number of 225,000.

The major difficulty in applying this equation is to determine the Reynolds number to be associated with the efficiency calculated in the parametric study. The efficiency obtained in the performance comparison shown above was approximately correct for a machine with R_e = 76,200. Thus it would not be unreasonable to expect the subject turbine, with a design Reynolds number of 535,000, to exhibit performance superior to that predicted over the entire power range. Nevertheless, a more conservative approach of accepting the correlated design point efficiency without modification is adopted here. The resulting part-power efficiency characteristic is shown in Figure 72. The predicted efficiency decrement at the quarter-power point amounted to 1.3%.

Detailed Aerodynamic Design

Inlet System

The inlet system consists of a scroll, a radial nozzle, and a vaneless space. A radius ratio of 1.05 was selected for the latter to insure adequate mixing of the stator wakes. The effect of viscous friction in the vaneless space was approximated by assuming that the tangential velocity varied inversely with 0.8 power of radius. Hence, if the passage axial width does not vary with radius, a flow angle of 74.2 degrees is required at nozzle exit to obtain design rotor inlet conditions.

The nozzle exit radius of 5.830 in. is of course determined by the radius ratio of the vaneless space. The nozzle inlet radius was fixed by employing uncambered vanes of constant height, operating at zero incidence. Assuming that the inlet duct Mach number is 0.1, a nozzle inlet angle of 55.6 degrees and an inlet radius of 6.791 in. may be derived from continuity. Tangential shear losses in the low velocity

EFFECT OF REYNOLDS NUMBER ON TURBINE TOTAL EFFICIENCY

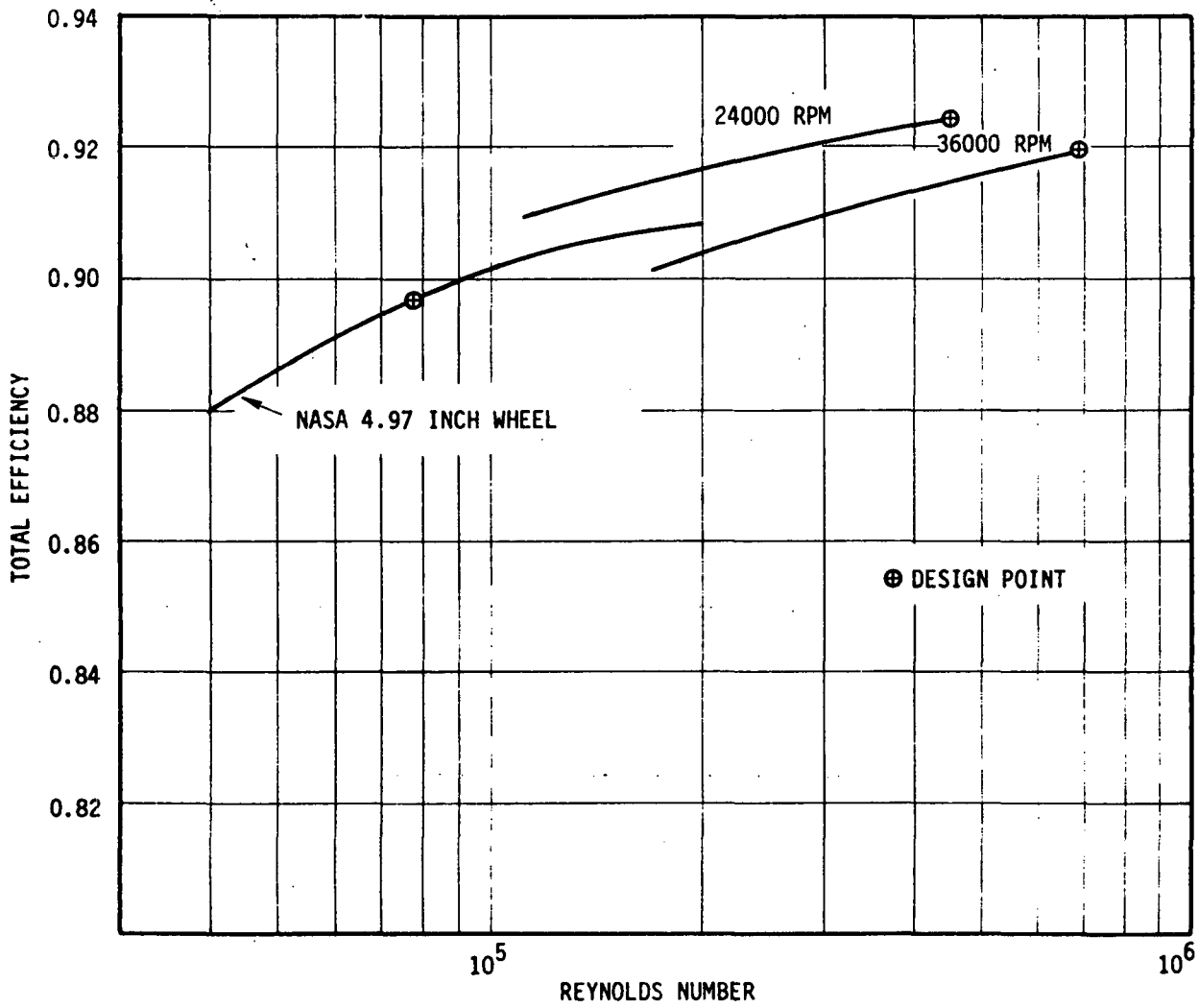

FIGURE 72

scroll flow were neglected in this calculation. Two blades from the resulting cascade are shown in Figure 73. Allowance has been made for 2.3 degrees deviation between the camber line blade angle at the trailing edge and the absolute flow angle just downstream of the blades, as computed from the equation given in Reference 27.

Approximate blade surface velocities, based on an assumption of incompressible flow, were calculated using the same equations employed for the rotor analysis (see below). Results are presented in Figure 74 from which it will be seen that 25 vanes were sufficient to prevent excessive diffusion on either surface. Chordal Reynolds number based on exit conditions was 780,000.

Cross-sectional scroll radii were calculated by the method described by Eckert in Reference 28. Assuming a free-vortex distribution of tangential velocity across the scroll, this procedure calculates the scroll area distribution which yields circumferentially uniform nozzle inlet static pressures. Allowance is made for the variation of scroll centerline radius about the periphery and for the total pressure losses in the flow direction. Results have been tabulated in Table XXVI. The apparent overlay of the scroll tongue and the inlet duct does not in fact occur if the near surface of the scroll is placed tangent to the rotor disc. If a symmetrical scroll is chosen in the final design phase, a small amount of inlet duct blockage or recirculation will be unavoidable.

Rotor Design

The rotor flowpath and blading was designed using the Marsha computer program described in Reference 27. This program calculates conditions on the surface of the blades in two stages. The locations of the stream surfaces in the meridional plane are first obtained by solving the axisymmetric equations of motion. Streamline slopes and curvatures are determined iteratively. Velocity variations in the tangential direction are then calculated assuming zero absolute circulation within the blade passage and linear velocity variation across the channel. The effects of total pressure loss are simulated by specifying a polytropic efficiency for the expansion process.

Empirical verifications of such a calculation tool are of course exceedingly difficult to obtain. However, static pressure measurements

NOZZLE DESIGN - 25 VANES

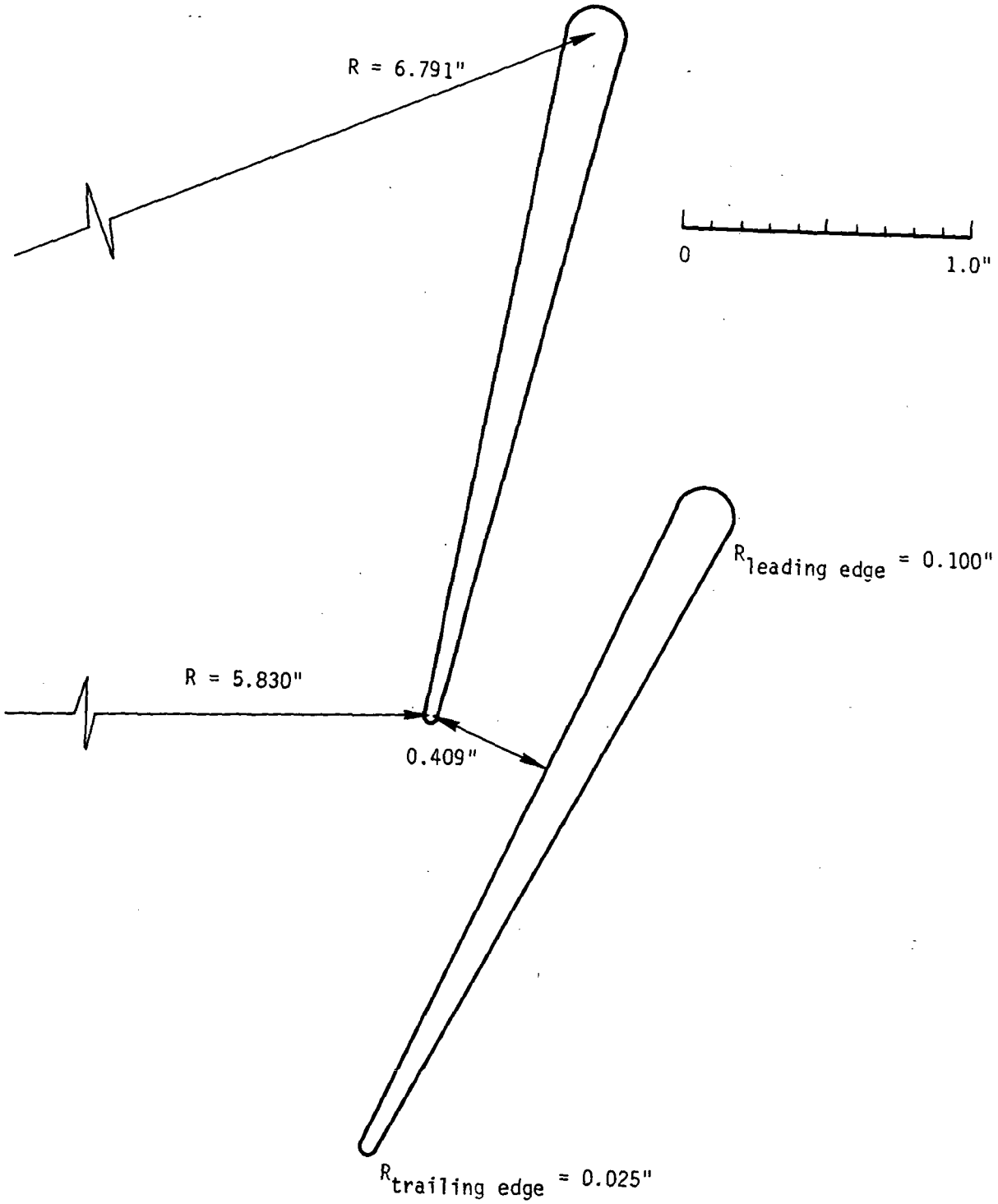

FIGURE 73

STATOR BLADE SURFACE VELOCITY DISTRIBUTION

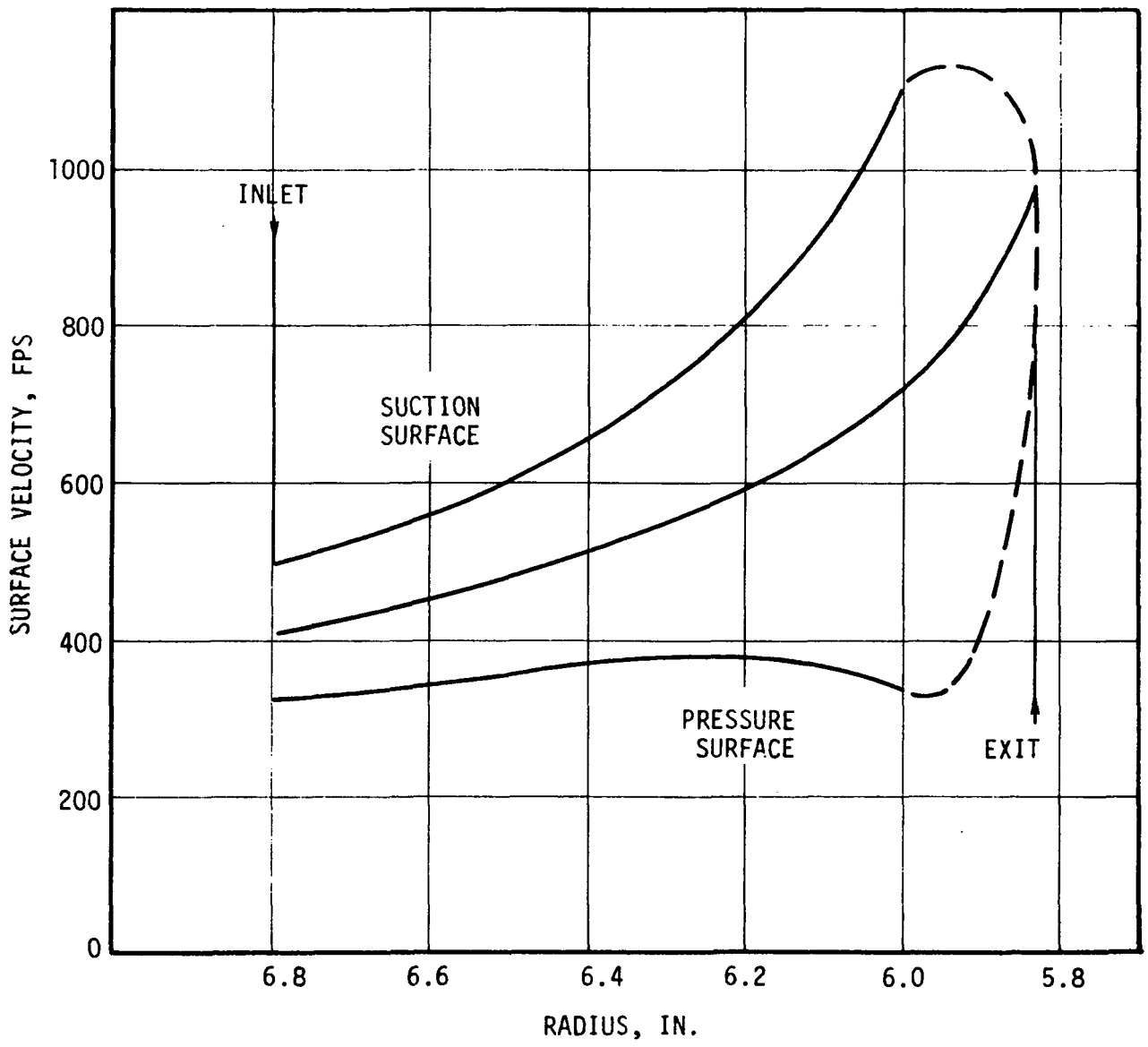

FIGURE 74

along the shroud of machines designed by this technique have generally shown good agreement with the numerical predictions, in cases where gross flow separation is avoided. In addition, indirect evidence for the accuracy of the solution may be obtained by comparison with the results of wholly independent calculation schemes. In one published comparison, for example (Reference 29), the method of Katsanis computed significantly different velocities only near the blade trailing edge at the shroud.

Radial and axial flowpath coordinates of hub and shroud are given in Table XXVII. A total of 22 blades (whole plus splitter blades) were specified for the design, based on the correlation given in Reference 30. Both the hub and shroud contours are defined by circular arcs, thereby minimizing the meridional curvatures. The hub blade angle distribution was chosen to satisfy the following requirements:

1. Zero blade angle at tip.
2. Acceptable hub suction surface diffusion.
3. Minimal upguided turning downstream of the throat.

Meridional mid-stream tube locations calculated for the design are shown in Figure 75. The distributions of meridional velocity along these streamlines are presented on Figure 76 . Apart from the unavoidable discontinuity due to blockage at the trailing edge, the meridional velocity distributions are smooth and show no abrupt decelerations. Corresponding relative velocity distributions are given in Figure 77 for the preliminary case of 22 whole blades and Figure 78 for the recommended configuration with 11 whole blades and 11 splitters. It can be seen that the flow generally accelerates along the entire blade, except over the initial portion of the hub suction surface and the latter portion of shroud suction surface. In both these latter cases only moderate diffusions which should not cause flow separation are encountered. Flow reversals are entirely absent. The light loadings on the downstream third of the blade are a result of the attempt to minimize upguided turning. The substantial loading predicted at the leading edge is a consequence of the effective positive incidence required by the design velocity triangles.

Blade exit conditions were calculated at both the trailing edge plane and at diffuser inlet, 0.1 foot downstream. It was assumed that mass, energy, and momentum were conserved in the blade-free space. Use of

TABLE XXVII

COORDINATES OF ROTOR HUB AND SHROUD CONTOURS

HUB		SHROUD	
Radial Distance, ft.	Axial Distance, ft.	Radial Distance, ft.	Axial Distance, ft.
0.4625	0.0000	0.4625	0.0797
.4230	.0000	.4380	.0814
.3850	.0050	.4150	.0876
.3460	.0160	.3928	.0980
.3060	.0320	.3731	.1118
.2670	.0550	.3558	.1288
.2300	.0840	.3419	.1486
.2130	.1020	.3360	.1600
.1970	.1210	.3316	.1708
.1810	.1430	.3278	.1824
.1680	.1660	.3250	.1943
.1550	.1920	.3236	.2068
.1450	.2190	.3233	.2189
.1390	.2400	.3233	.2400
.1350	.2600	.3233	.2600
.1320	.2800	.3233	.2800
.1300	.3000	.3233	.3000

ROTOR STEAMTUBE LOCATIONS

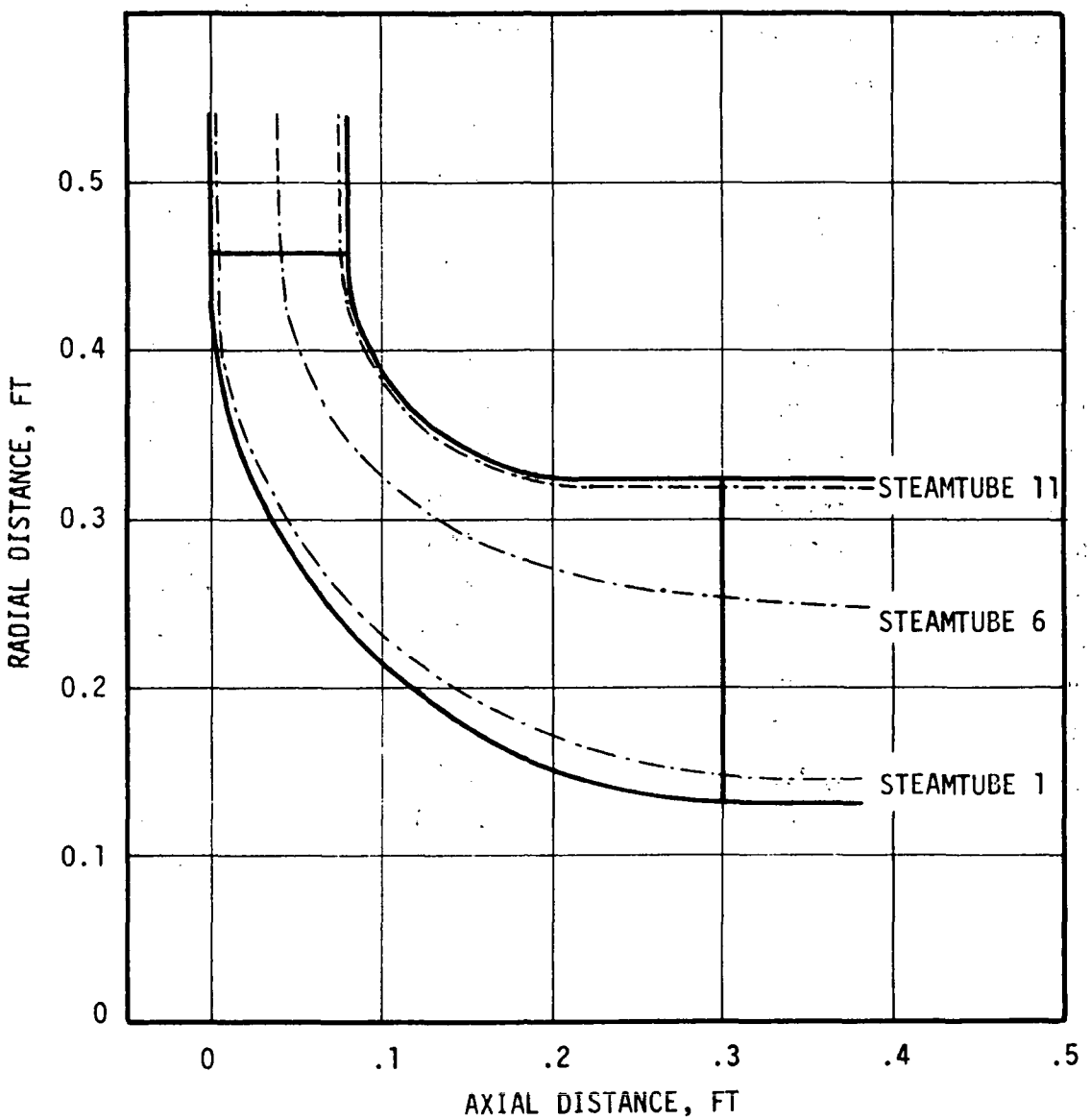

FIGURE 75

MERIDIONAL VELOCITY DISTRIBUTIONS

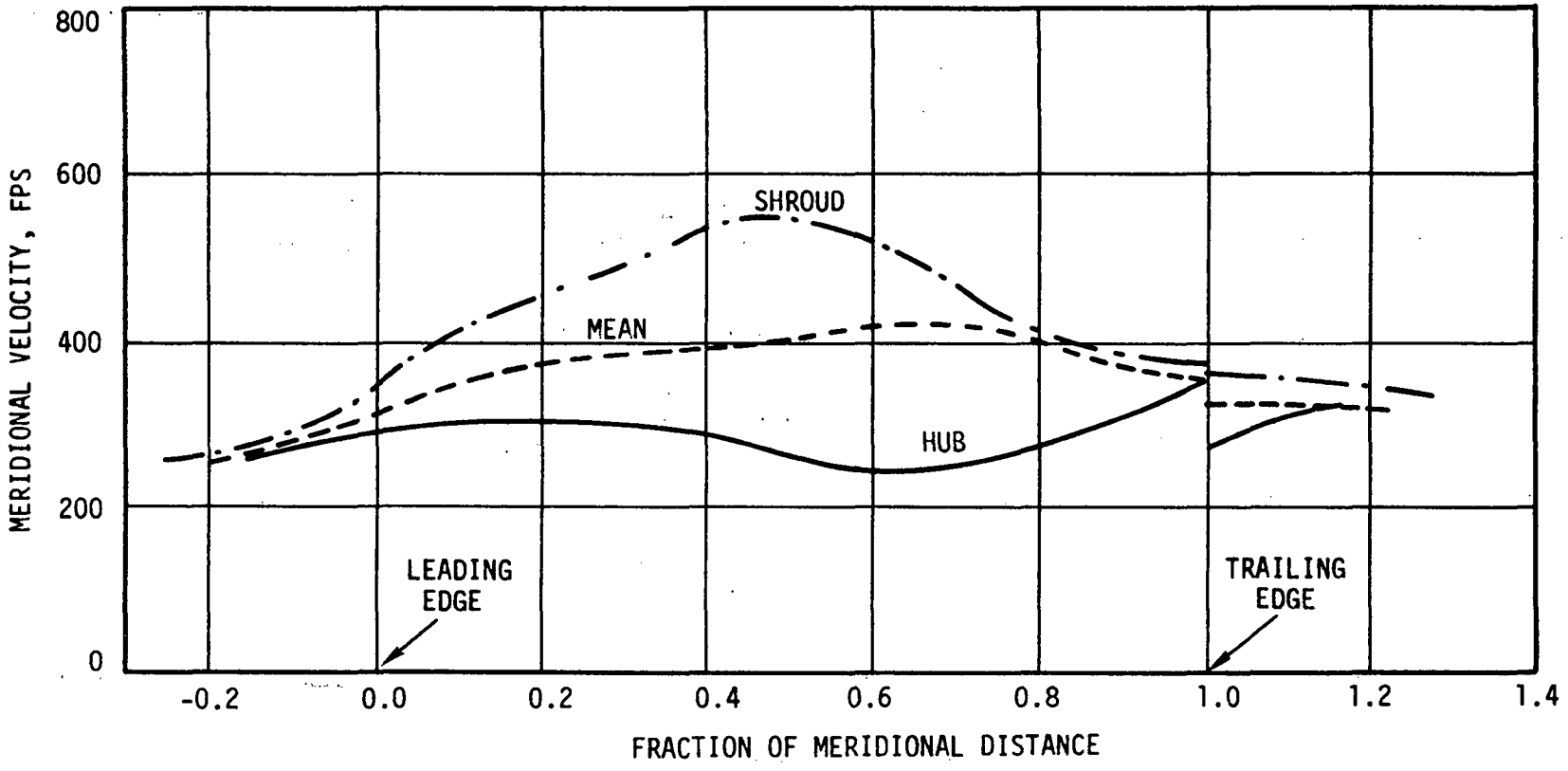

FIGURE 76

BLADE SURFACE RELATIVE VELOCITY DISTRIBUTIONS

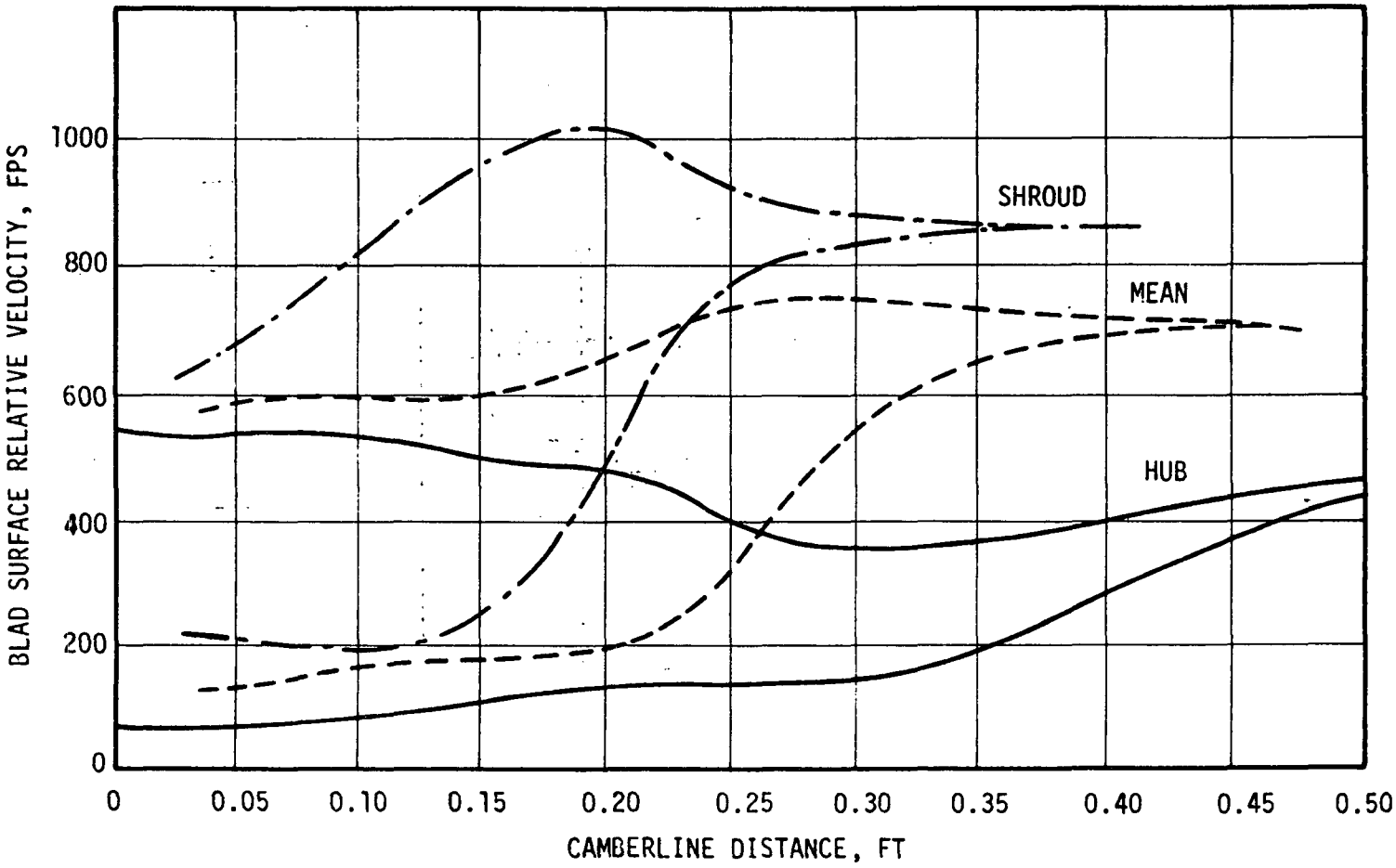

FIGURE 77

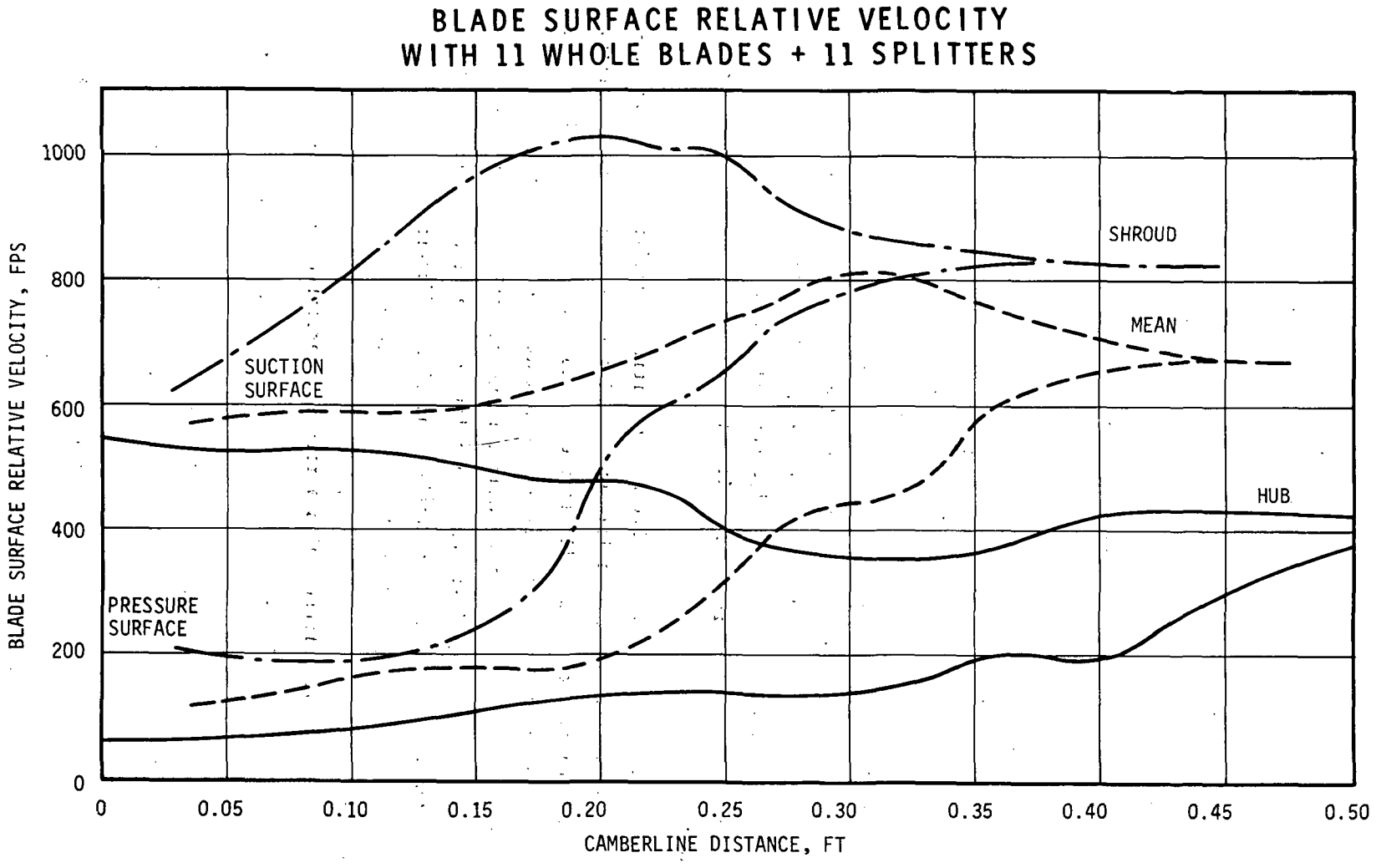
BLADE SURFACE RELATIVE VELOCITY
WITH 11 WHOLE BLADES + 11 SPLITTERS
BLADE SURFACE RELATIVE VELOCITY, FPS
1000
800
600
400
200
0
SHROUD
MEAN
HUB
SUCTION
SURFACE
PRESSURE
SURFACE
0
0.05
0.10
0.15
0.20
0.25
0.30
0.35
0.40
0.45
0.50
CAMBERLINE DISTANCE, FT

FIGURE 78

splitters shorter than those indicated in Figure 78 would be desirable in that blade wetted area could be reduced. However, the calculated surface velocity distributions show that any significant reduction would lead to greatly increased diffusion at the exducer shroud. Since this is normally the portion of the flowpath most susceptible to separation, the splitter trailing edges have been conservatively located at an axial position of Z = 0.2 feet.

Exhaust System

The dynamic head at rotor exit represents the equivalent of nearly four points in turbine efficiency. Hence the design of a highly effective exit diffuser is of considerable importance to overall stage performance. Unfortunately, the performance obtained in practice has traditionally been quite low. However, it is difficult to determine the extent to which this behavior has resulted from poor rotor (or diffuser) design practice. Therefore, the preliminary diffuser design has been based on the diffuser data published in References 23 and 31 without applying any arbitrary correction factors.

The performance of three alternative diffuser configurations was investigated as a function of axial length. The first design was an annular diffuser with constant inner diameter equal to that of the rotor hub, and exit outer diameter equal to that of the exhaust duct. The second design, also annular, had the same inner diameter but slightly increased exit diameter so that the diffuser exit velocity equalled the velocity in the exhaust duct. The centerbodies of both annular diffusers were supported by tilted struts fastened near the discharge flange. Strut loss data were taken from Reference 32 . The final configuration which was studied consisted of a conical diffuser with a rotating centerbody at rotor exit.

The calculated variation of overall stage total-to-static efficiency with diffuser axial length is shown in Figure 79 . Stall lines based on correlation of empirical data given in Reference 31 have been included. The larger annular diffuser was found to offer a potential performance improvement of approximately one percent over the conical design. There was little advantage in increasing diffuser length beyond that required to avoid stall, which was 8.2 inches at an area ratio of 1.76. However, in view of the nonuniform velocity profiles which may be expected at

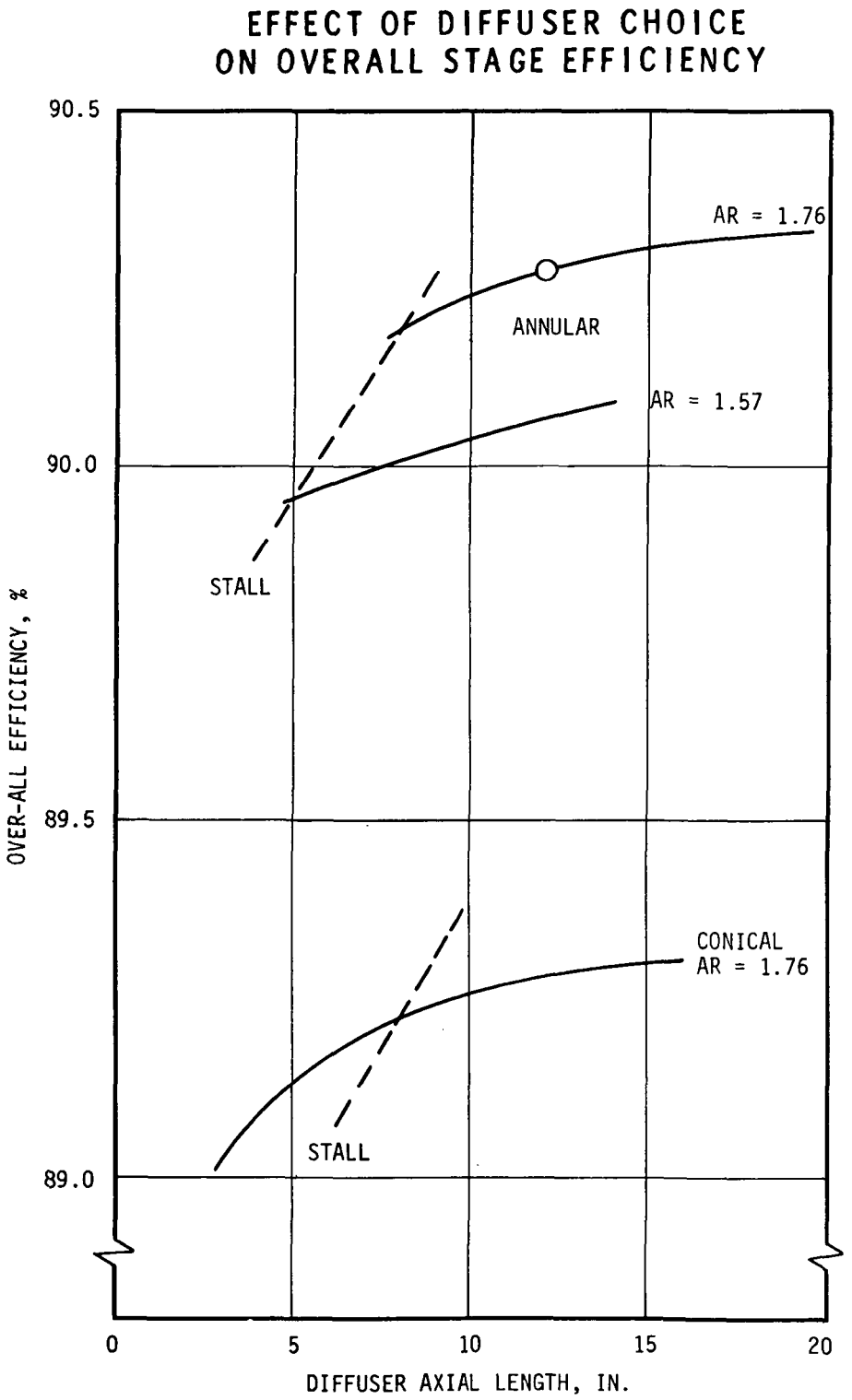
EFFECT OF DIFFUSER CHOICE
ON OVERALL STAGE EFFICIENCY
90.5
90.0
89.5
89.0
OVER-ALL EFFICIENCY, %
AR = 1.76
ANNULAR
AR = 1.57
STALL
CONICAL
AR = 1.76
STALL
0
5
10
15
20
DIFFUSER AXIAL LENGTH, IN.

FIGURE 79

diffuser inlet, a conservative length of 12 inches was selected for both the conical and annular designs. The resulting configurations are shown schematically in Figure 80. Since a short transition region is required downstream of the annular design, its actual overall length will be approximately 14 inches. The final calculated efficiency of this design was 90.25% including inlet scroll losses.

If the predicted performance can be achieved, it is clear that the annular design should be used. However, it must be admitted that a recent test of a similar configuration (Reference 24) demonstrated an effectiveness of only 47% as against the 80% implied for the present design by the data of Reference 31. A possible explanation of this situation is illustrated in Figure 81 where stall is indicated at the diffuser design point employed in Reference 24. However, since no detailed diffuser exit traverses were reported, it is unfortunately not possible to verify this prediction. It would therefore be desirable to test both alternative diffuser configurations to determine whether the increased mechanical complexity of the annular design is justified by its performance.

A schematic view of the overall design, showing the relation of inlet scroll, radial nozzle, rotor disk, and exit diffuser is given in Figure 82.

ALTERNATIVE DIFFUSER CONFIGURATIONS

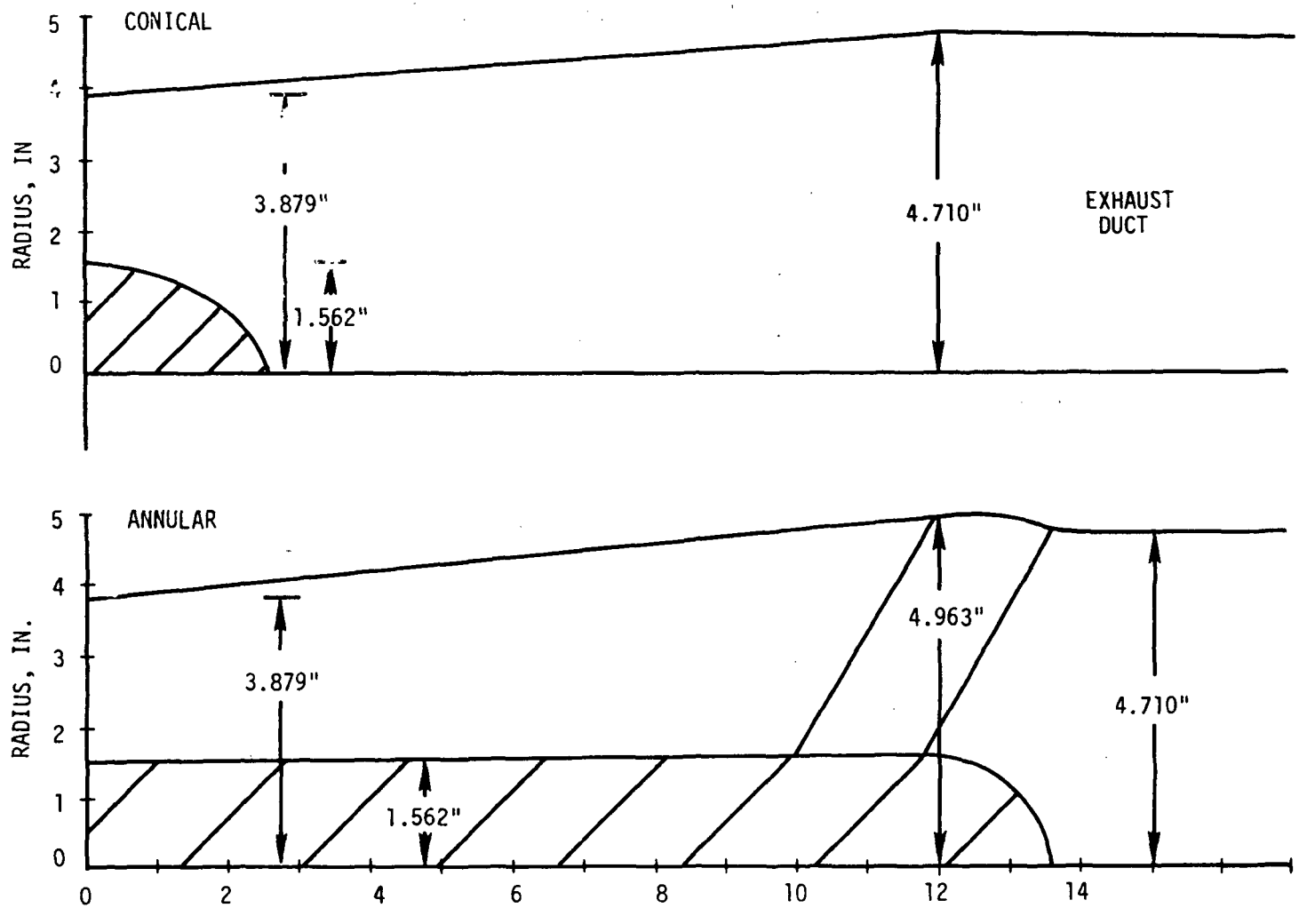

FIGURE 80

DIFFUSER PERFORMANCE

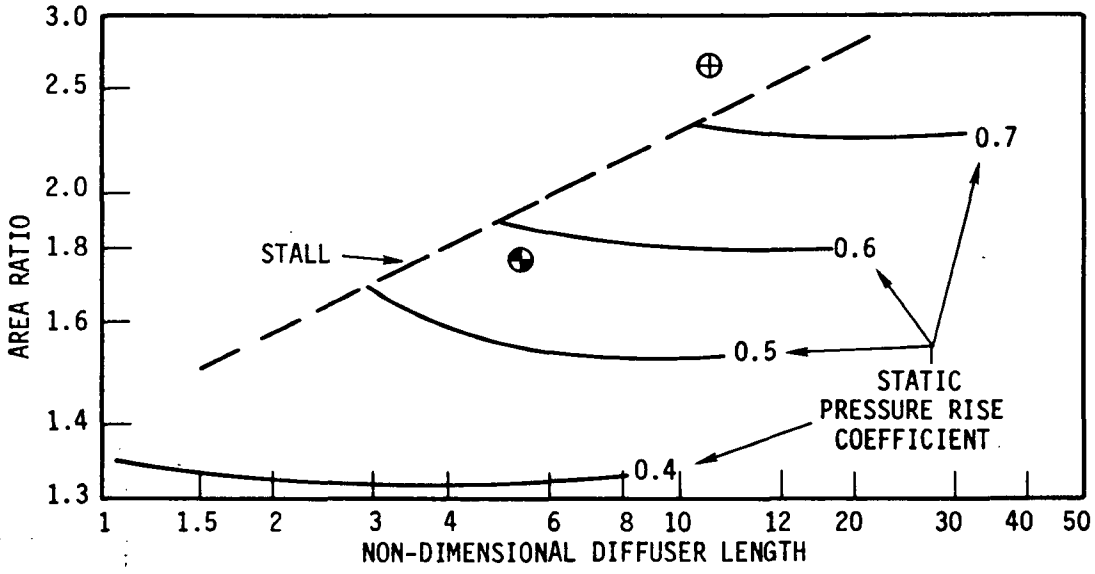

REF.: A.D. COCANOWER ET. AL.: REPORT P.D. 10, STANFORD UNIV., MAY 1965.

FIGURE 81

MERIDIONAL VIEW OF OVERALL DESIGN

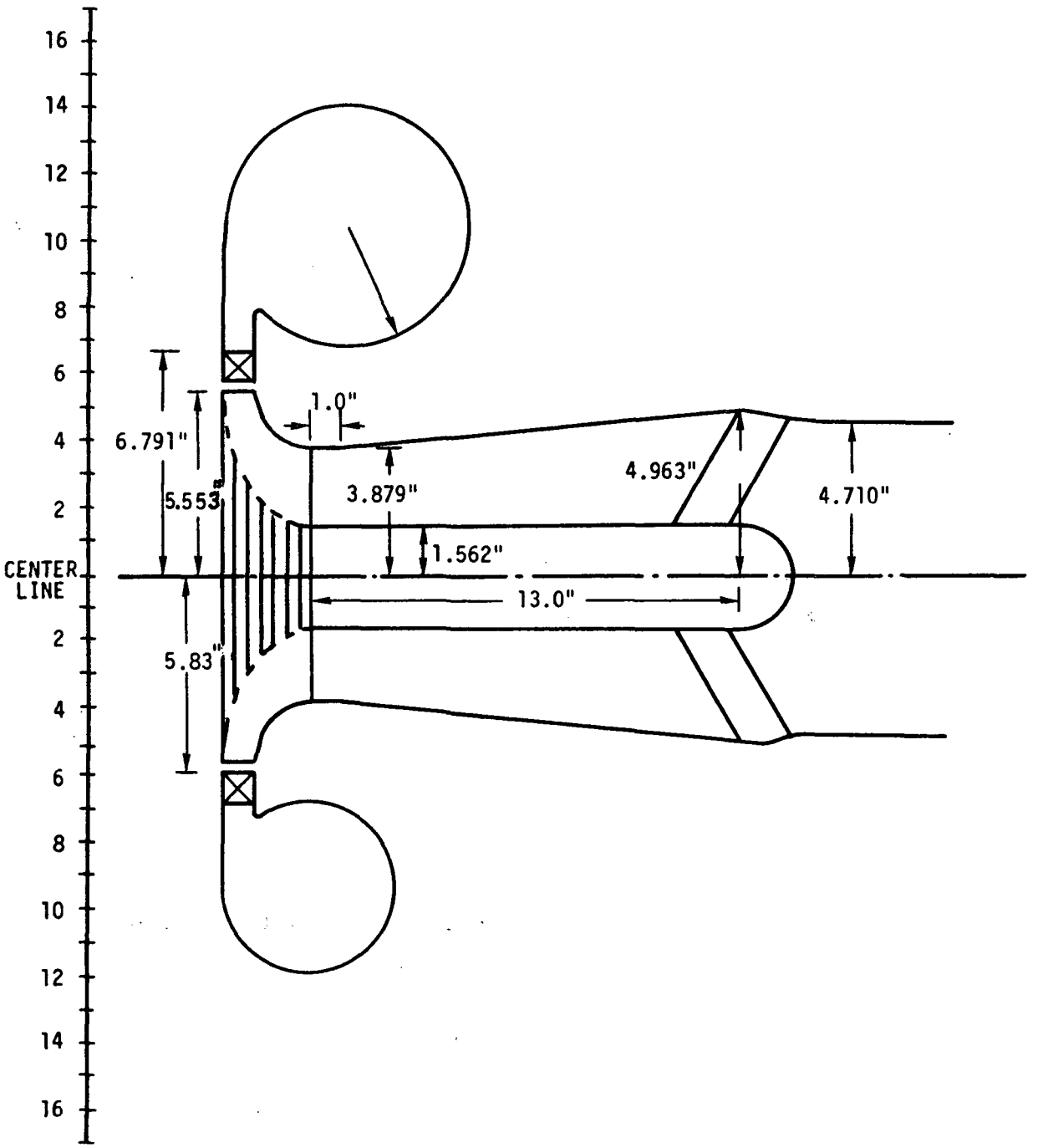

FIGURE 82

PERFORMANCE COMPARISON

The performance of the six TAC configurations was estimated to assist in the selection of a configuration for design in Phase III. To do this it was necessary to estimate the various losses, which are summarized in Table XXIX. The bearing and seal losses of Configurations 4, 5 and 6 are high because of the alternator cavity oil seals, and Configuration 6 has the additional loss of the liquid film bearings. The alternator windage is less for these configurations because the seals permit a lower pressure in the alternator cavity. However the reduced alternator windage does not compensate for the greater losses of the oil seals. The 24,000 rpm machines have lower total losses, with Configuration 1 having a slight advantage over Configuration 2.

Shown in Figure 83 are the effects of losses and component efficiencies on cycle efficiency. It can be seen that bleed has a major effect, almost 3% change in cycle efficiency for 1% bleed. Each kilowatt of parasitic loss reduces cycle efficiency about 1/2%. A 1% change in alternator efficiency reduces the cycle efficiency about 1%, while 1% changes in compressor and turbine efficiencies reduce the cycle efficiency by 1.6 and 1.9%, respectively.

Shown in Table XXX is a performance comparison of the six TAC configurations studied. The first three configurations, with gas bearings, have better cycle efficiency than the other three configurations, which have oil bearings, primarily because the parasitic losses and leakage are less.

Shown in Table XXXI is a loss summary for the TAC designs operating at one-fourth power. The only change from the full load losses in Table XXIX is that the alternator windage is reduced for the gas bearing machines because of the lower pressure levels in the system at part load. The performance comparison of the several configurations at one-fourth power is shown in Table XXXII. Again the gas bearing designs have the better cycle efficiency, and by a greater margin due to decreased windage losses. The TAC Configuration 1 has the best cycle efficiency at part load, primarily because the radial compressor has less decrease in compressor efficiency at the lower Reynolds numbers associated with reduced pressure levels. Since the radial and axial compressor configurations had almost identical performance at full load, the better

TABLE XXIX

SUMMARY OF TAC CONFIGURATION LOSSES - FULLPOWER

● TAC	1 24 RG	2 24 AG	3 36 AG	4 36 AM	5 36 RM	6 36 RL
BEARING & SEAL	2.1	2.1	5.75	12.35	12.35	22.5
ALTERNATOR WINDAGE	4.25	4.25	4.52	2.08	2.08	2.08
PARASITIC	1.01	1.62	0.86	2.55	2.00	1.71
● TOTAL LOSSES	7.36	7.97	11.13	16.98	16.43	26.29
● BLEED, % FLOW						
LEAKAGE	1.23	1.41	0.63	8.97	8.10	4.12
GAS COOLANT	2.00	2.00	2.00	0.50	0.50	0.50
● TOTAL	3.23	3.41	2.63	9.47	8.60	4.62

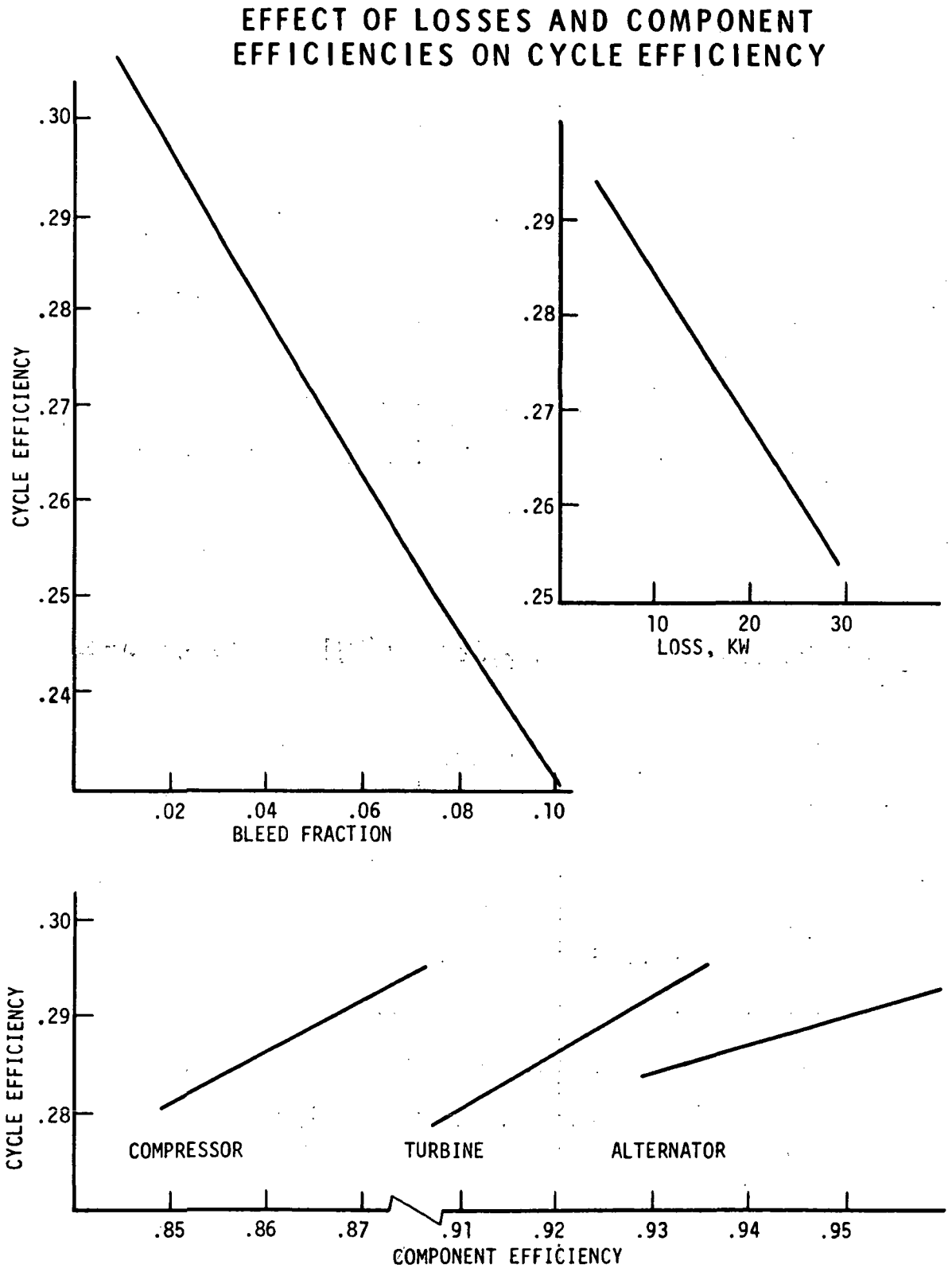
EFFECT OF LOSSES AND COMPONENT EFFICIENCIES ON CYCLE EFFICIENCY
CYCLE EFFICIENCY
.30
.29
.28
.27
.26
.25
.24
.02
.04
.06
.08
.10
BLEED FRACTION
.29
.28
.27
.26
.25
10
20
30
LOSS, KW
CYCLE EFFICIENCY
.30
.29
.28
COMPRESSOR
TURBINE
ALTERNATOR
.85
.86
.87
.91
.92
.93
.94
.95
COMPONENT EFFICIENCY

Figure 83.

TABLE XXX

TAC PERFORMANCE COMPARISON - FULLPOWER

TAC	1 24 RG	2 24 AG	3 36 AG	4 36 AM	5 36 RM	6 36 RL
LOSSES, KW	7.36	7.97	11.13	16.96	16.43	26.29
LEAKAGE, % FLOW	3.23	3.41	2.63	9.47	8.60	4.62
COMPRESSOR CLEARANCE, MIL	12	10	10	10	10	10
TURBINE CLEARANCE, MIL	16.0	17.3	12	10	11	11.4
COMPRESSOR TOTAL TO TOTAL EFFICIENCY	0.859	0.866	0.862	0.862	0.862	0.862
TURBINE TOTAL TO TOTAL EFFICIENCY	0.910	0.908	0.915	0.916	0.916	0.915
ALTERNATOR EFFICIENCY	0.942	0.942	0.943	0.931	0.931	0.931
CYCLE EFFICIENCY	0.284	0.285	0.287	0.242	0.243	0.251
FLOW RATE, LB/SEC	9.85	9.85	9.68	12.80	12.01	11.22

TABLE XXXI

SUMMARY OF TAC CONFIGURATION LOSSES AT 1/4 POWER

● TAC	1 24 RG	2 24 AG	3 36 AG	4 36 AM	5 36 RM	6 36 RL
BEARING & SEAL	2.1	2.1	5.75	12.35	12.35	22.5
ALTERNATOR WINDAGE	1.06	1.06	1.13	2.08	2.08	2.08
PARASITIC	1.01	1.62	0.86	2.55	2.00	1.71
● TOTAL LOSSES	4.17	4.78	7.74	16.98	16.43	26.29
● BLEED, % FLOW						
LEAKAGE	1.23	1.41	0.63	8.97	8.10	4.12
GAS COOLANT	2.00	2.00	2.00	0.50	0.50	0.50
● TOTAL	3.23	3.41	2.63	9.47	8.60	4.62

TABLE XXXII

TAC PERFORMANCE COMPARISON - 1/4 POWER

TAC	1 24 RG	2 24 AG	3 36 AG	4 36 AM	5 36 RM	6 36 RL
LOSSES, KW	4.17	4.78	7.74	16.98	16.43	26.29
LEAKAGE, % FLOW	3.23	3.41	2.63	9.47	8.60	4.62
COMPRESSOR CLEARANCE, MIL	12	10	10	10	10	10
TURBINE CLEARANCE, MIL	16.0	17.3	12	10	11	11.4
COMPRESSOR TOTAL TO TOTAL EFFICIENCY	0.857	0.837	0.840	0.840	0.860	0.860
TURBINE TOTAL TO TOTAL EFFICIENCY	0.895	0.893	0.900	0.901	0.901	0.900
ALTERNATOR EFFICIENCY	0.890	0.890	0.884	0.862	0.862	0.862
CYCLE EFFICIENCY	0.247	0.231	0.226	0.164	0.175	0.165
FLOW RATE, LB/SEC	2.86	3.08	3.11	4.64	4.23	4.33

performance of the centrifugal compressor at part load is a significant factor in the selection of a TAC design.

Phase II activity consisted of three off design calculations for the 24,000 rpm configurations, one at low turbine inlet temperature, one at high turbine inlet temperature and one for a high molecular weight gas. The off design calculation consists of matching the compressor and turbine speed, pressure ratios and flow rates at the specified conditions. For the 24 RG unit a typical compressor map was selected from Figure 13 of Reference 33. Turbine performance was taken from Figures 7 and 8 of Reference 34. These references were used because the turbomachinery had specific speeds close to those of the TAC designs; 85 for the compressor and 76 for the turbine compared with 83 and 73 for the 24 RG TAC components. Multipliers were applied to corrected flow, corrected speed and efficiency to convert the referenced maps to the TAC design values. The compressor design point was selected at a pressure ratio of 1.9 and a corrected flow of 3.06 (1.15 on the map). The corresponding turbine corrected flow was 2.755 (0.503 on the map) at a pressure ratio of 1.786.

For the low temperature application the compressor corrected speed is increased by $\sqrt{700/580}$ or about 10%, and the turbine corrected speed is increaded by $\sqrt{2060/1610}$ or 13%. An attempt to operate the compressor at a pressure ratio of 1.9 was unsuccessful because the compressor flow was to large for the turbine. The two components were matched at a compressor pressure ratio of 2.08. A cycle calculation at the low temperature gave a cycle efficiency of 0.242, which means that the system could produce 145 kw_e with 600 kw thermal input. The compressor inlet pressure required to satisfy the power requirement and the compressor flow function is 56 psia, and the flow rate is 12.46 lb/sec.

An axial flow compressor map was converted to the TAC design values by multipliers on corrected flow, corrected speed and efficiency. The results of the off design calculation were similar to those for the 24 RG unit and are shown in Table XXXIII.

For the high temperature off design case the compressor corrected speed is practically unchanged as the compressor inlet temperature is 691°R compared with the design value of 700°R. The turbine corrected

TABLE XXXIII

COMPARISON OF 24000 RPM TAC AT SNAP-8 CONDITIONS

	24 RG		24 AG	
	TAC	SNAP-8	TAC	SNAP-8
COMPRESSOR PRESSURE RATIO	1.9	2.08	1.9	2.1
COMPRESSOR CORR. SPEED, %	100.	110.	100.	110.
COMPRESSOR EFFICIENCY	.859	.852	.866	.852
COMPRESSOR INLET PRESSURE, PSIA	55	56.	55.	54.
TURBINE EFFICIENCY	.9105	.901	.9085	.897
ALTERNATOR EFFICIENCY	.942	.942	.942	.942
BLEED, %	3.23	3.23	3.41	3.41
LOSSES, KW	7.36	7.36	7.97	7.97
OUTPUT, KWe	160	145	160.	142
INPUT, KWth	564	600	562	600
FLOW RATE, PPS	9.85	12.46	9.85	12.4
CYCLE EFFICIENCY	.284	.242	.285	.237

speed is reduced by $\sqrt{2060/2560}$ or 10%. The two components were matched at a compressor pressure ratio of 1.91. A cycle calculation at the high temperature condition gave a cycle efficiency of 0.353. The compressor inlet pressure required to satisfy the flow function is 37 psia, and the flow rate is 6 lb/sec. for 160 kw_e output. Similar results were obtained for the axial flow compressor and are shown in Table XXXIV.

For the high molecular weight case, the corrected speeds are increased by $\sqrt{83.3/39.94}$ or 44.5%. In order to carry out the matching for this off design condition it was necessary to extrapolate the compressor and turbine maps to such a large extent that the validity of the results is questionable. The components were matched at a compressor pressure ratio of 3.04. A cycle calculation gave an efficiency of 0.135, which means that 1185 kw thermal input are required for 160 kw_e. The flow rate was 30.27 lb/sec. and a compressor inlet pressure of 130 psia is required to satisfy the compressor flow function. If the thermal power input is limited to 600 kw, the output, flow rate and pressure level are sealed down by the ratio of 600 to 1185. A similar extrapolation was made for the axial compressor map and the results of the off design calculations are shown in Table XXXV. The increase in parasitic losses is due to greater alternator windage at the higher pressure levels.

TABLE XXXIV

COMPARISON OF 24,000 RPM TAC AT 2100°F TURBINE INLET TEMPERATURE

	24 RG		24 AG	
	1600°F	2100°F	1600°F	2100°F
Compressor Press. Ratio	1.9	1.91	1.9	1.95
Compressor Corr. Speed %	100	101	100	101
Compressor Efficiency	.859	.864	.866	.87
Compressor Inlet Press. Psia	55	37	55	36
Turbine Efficiency	.9105	.8905	.9085	.8885
Alternator Efficiency	.942	.942	.942	.942
Bleed, %	3.23	3.23	3.41	3.41
Losses, kw	7.36	7.36	7.97	7.97
Output, kw_e	160	160	160	160
Input, kw_{th}	564	440	562	439
Flow Rate, PPS	9.85	6.02	9.85	5.90
Cycle Efficiency	.284	.364	.285	.365

TABLE XXXV

COMPARISON OF 24000 RPM TAC FOR HIGH MOLECULAR WEIGHT GAS

	24 RG		24 AG	
	TAC	HIGH M.W	TAC	HIGH M.W
COMPRESSOR PRESSURE RATIO	1.9	3.04	1.9	2.98
COMPRESSOR CORR. SPEED, %	100	144.	100.	144.
COMPRESSOR EFFICIENCY	.859	.774	.866	.792
COMPRESSOR INLET PRESSURE, PSIA	55.	130.	55.	127.
TURBINE EFFICIENCY	.9105	.881	.9085	.879
ALTERNATOR EFFICIENCY	.942	.942	.942	.942
BLEED, %	3.23	3.23	3.41	3.41
LOSSES, KW	7.36	13.01	7.97	13.62
OUTPUT, KWe	160.	160.	160	160
INPUT, KWth	564.	1185	562	1060
FLOW RATE, PPS	9.85	30.27	9.85	27.46
CYCLE EFFICIENCY	.284	.135	.285	.151

D. ALTERNATOR DESIGN

INTRODUCTION

The majority of the Phase I study effort was directed toward preliminary screening studies and concluding performance analyses of selected alternators. The screening analyses concentrated upon (1) analysis of the influential design tradeoffs associated with Lundell alternators and Inductor alternators, (2) the choice of rotor materials and construction for each, and (3) the losses and cooling of each type alternator. Special attention was also given to determining methods that predicted their windage losses accurately.

The ultimate choice of a Lundell over an Inductor alternator depends heavily upon the decision to either rely on a multipiece bonded rotor (Lundell) or rely upon a scavenge system to evacuate the rotor cavity (Inductor), the latter alternator having a solid, single-piece rotor but requiring a "bore-barrier" separator. Between these two extremes exist a multitude of secondary influences which sway the decision and which represent the bulk of the content of the Phase I screening studies.

In relation to one of the main influences, the Lundell rotor fabrication, recent developments indicate there exist rotor bonding techniques that are amenable to the TAC requirements of high reliability. This lends more credence to the Lundell alternator choice and because of it, concentrated evaluations were carried out to determine how the bonded rotor construction approach could be improved by either (1) making better use of the present concepts utilizing a 4340/Inconel 718 combination or (2) by selecting better material combinations and/or processes. The conclusion reached was that the combinations showing the best possible design improvements were not sufficiently better to warrant the development costs required to reach the same level of technology as the 4340/Inconel 718 combination. Furthermore, since even the known 4340/Inconel 718 technology must be expanded to meet the more stringent TAC strength requirements, the efforts are better spent there.

The initial screening analyses showed that from a purely electromagnetic alternator design standpoint, an 800 Hz Lundell and a 1600 or 2400 Hz Inductor appeared to give the best designs; however, from a combined alternator,

system-utilization standpoint, a compromise of 1200 Hz for both was concluded to be more desirable. Also, from an electromagnetic design standpoint, there appeared to be no distinctive differences among the voltage choices of 120, 240, or 480 volts (L-N). From a corona breakdown standpoint, however, the selection appears limited to 120 volts. Even at that low voltage, the TAC alternator voltage can possibly put restrictions on the minimum load the TAC can ever be operated at. For example, at 1/4 P.U. load, the compressor inlet pressure may be as low as 14 psia which, according to corona calculations, is too low to guarantee prevention of corona breakdown. This is distinctly different from the previous NASA BRU alternator and is a characteristic of the insulation systems required for the higher temperature alternators.

The first reaction to the cooling design selection was to minimize the amount of cooling ducts and penetrations used because of the specified redundancy requirement. However, in the final analysis, a conservative design utilizing several coolant sinks appeared as the most practical approach.

Of the alternators screened, the 24,000 rpm Lundell appears as the most desirable and practical. The 36,000 rpm Lundell shows little promise and must be classified as a borderline design, relative to rotor stress, that requires more background technology development before one can commit to actual alternator fabrication. Substitution, however, of the 4-pole solid rotor inductor for the 36,000 rpm Lundell design does not result in a significantly more reliable rotor since the Inductor rotor stresses are sufficiently large to obviate the gains associated with the greater, single-piece material strengths; this is in addition to the disadvantages of the scavenge system and bore-barrier requirements.

As a result of the studies, it was concluded that the Inductor alternator should not be considered as a prime choice and the choice should be made between the 24,000 rpm/Lundell TAC system and the 36,000 rpm/Lundell TAC system. It must be recognized that the latter has an alternator with little design conservatism which must be traded against any other system benefits which might occur as a result of using the higher speed system. The alternator data provided in the following pages is presented to aid the NASA in reaching that decision. Westinghouse strongly recommends that the 24,000 rpm/Lundell system be selected but acknowledges that, without the central rotor hole, the 36,000 rpm Lundell could be made to look both as feasible and practical.

ELECTROMAGNETIC DESIGN

A. Introduction

Alternator design screening studies were performed to obtain three conceptual configurations to be utilized for interface studies with the various turbine-compressor configurations selected by the prime contractor for the Brayton Cycle Turboalternator-Compressor space electrical power system. The output rating of the conceptual alternators is 214 KVA at 0.75 lagging power factor. Alternator design speeds studied were 24,000 rpm and 36,000 rpm with 120 percent overspeed capability. The alternator rotor cavity environments considered are the gas bearing lubricant at the compressor inlet pressure for the lower speed, and either bearing lubricant oil vapor at lower than subsystem pressures or bearing lubricant gas at compressor inlet pressure (or lower) for the higher speed. Cooling fluid inlet temperature to the alternator is 496^{o}F.

The possible requirement for rotor cavity operating pressures greater than 1 atmosphere and maximum windage losses of 6% of the alternator rated power output dictated that prime consideration be given to minimization of rotor diameter and to the rotor configuration. These same considerations are related to rotor stress and dynamic response and for these reasons two different types of stationary winding radial gap alternators were included in the studies. These types are the inductor alternator and the bonded-rotor Lundell alternator. The inductor alternator rotor is machined from a single forging and requires no joining of magnetic to non-magnetic metals. The rotor contains salient poles on each end which act to create high windage loss. For the 36,000 rpm speed case, however, the rotor cavity can be scavenged to less than subsystem pressures and the windage loss can be greatly reduced. The Lundell rotor requires bonding of dissimilar metals but the resulting smooth surface acts to provide low windage losses. By performing comparative studies of both alternator types, the trade-offs between inherent design advantages and/or disadvantages for the two alternator types could be determined and evaluated in arriving at the optimum alternator conceptual configurations.

Frequency screening studies were performed for each alternator type at each speed. The frequencies considered for the 24,000 rpm speed ranged from 400 Hz to 2400 Hz with parametric points occurring in increments of 400 Hz. Consequently, the number of alternator poles considered ranged from 2 to 12 poles in increments of 2 poles. The specification requirement that the frequency be multiples of 400 Hz limited the frequencies considered for the 36,000 rpm speed case to 1200 Hz and 2400 Hz corresponding to 4-pole and 8-pole alternators, respectively.

The inductor alternator studies included all of the specified frequencies except 400 Hz with the purpose of establishing full range parametric trends. To limit the number of parametric combinations in the screening studies task, the frequencies considered for the Lundell type generator were confined initially to 400 Hz and 800 Hz for the 24,000 rpm speed, and 1200 Hz for the 36,000 rpm speed. A direct comparison between the Lundell and inductor alternator configurations would be available for the common 36,000 rpm, 1200 Hz and 24,000 rpm, 800 Hz four-pole parametric points. During the course of the study, it became apparent that the bonded rotor Lundell configuration had some definite advantages in the high pressure rotor cavity applications, and therefore, a six pole, 1200 Hz 24,000 rpm Lundell design point was added to the study. The speeds and pole configurations are summarized as follows:

Alternator Type	No. of Poles	Frequency (Hz)	No. of Poles	Frequency (Hz)
Lundell	2	400		
Lundell	4	800	4	1200
Lundell	6	1200		
Inductor	4	800	4	1200
Inductor	6	1200		
Inductor	8	1600	8	2400
Inductor	10	2000		
Inductor	12	2400		

The parameters considered in the voltage screening study were 120, 240, and 480 volts, line to neutral. For all other screening studies the line to neutral voltage was assumed to be 240 volts.

Prior to performing the frequency and voltage screening studies, a series of trial designs were made at 24,000 rpm, 1600 Hz and 36,000 rpm, 2400 Hz to determine the approximate values of the internal design factors to meet the specification requirements and evaluate preliminary design tradeoffs. As a minimum, synchronous reactance and radial gap length were investigated. Initial studies were performed at the continuous duty rating of 214 KVA, 0.75 lagging power factor and 240 volts L-N (line-to-neutral). The materials selected for the screening studies are given below:

ELECTROMAGNETIC COMPONENT	MATERIAL
Stator Frame	Hiperco 27
Stator Laminations	Hiperco 27
Rotor	Hiperco 27
Slot Liners	Alumina
Conductor Insulation	"Anadur S"
AC Conductor	Nickel Clad Silver
Field Coil Conductor	"Cube" Alloy

Alternate materials evaluations were performed for several of the electromagnetic components after completion of the screening studies. Primary emphasis was placed on materials for the critical rotor component, especially for the Lundell alternator where bonding of magnetic to non-magnetic alloys is required.

Finally, parametric optimization studies and performance analyses were performed for the three alternator configurations selected for the turbo-alternator-compressor conceptual designs.

Because of the unavoidable complexity in fully screening designs relative to the complete alternator specifications, the specifications were divided into two groups. The first group, listed below, contains those directly considered in the screening analyses.

(a) The alternators shall have a maximum continuous rating of 160 KWe with a 3 phase output at a 0.75 lagging load power factor for 5 seconds after temperature equilibrium has been reached. Speed regulation shall be assumed to be $\pm$1% of design speed.

(b) The alternator designs shall be capable of operating at 120% of design speed without a catastrophic failure under all loads up to and including rated TAC load conditions (160 KWe, 0.75 lagging power factor) for a limited time.

(c) The design life criteria for the alternators shall be 5 years operating time under the specified conditions for the TAC assembly.

(d) The alternators shall be in accordance with MIL-G-6099A (ASG) in accordance with the latest revision in effect on the date of contract for the following:

(1) Short-Circuit Capacity. Paragraph 4.5.12 for a minimum time of 5 seconds for each occurrence.

(2) Phase Balance. Paragraphs 4.5.10, 4.5.10.1 and 4.5.10.2 except that paragraph 4.5.10.1 is amended to read "... the individual phase voltages shall not deviate from the average by more than 2.25, 4.5, and 9 percent*, respectively."

(e) The alternators shall be designed to the maximum extent possible so as to reduce to a minimum windage losses. The 6 percent windage specified for a pressurized rotor cavity shall be considered a design goal.

(f) Temperature Level. For systems radiator size and weight considerations, it is desired to operate the alternator stator at elevated temperatures. The contractor shall select the high-temperature magnetic, electrical and insulation materials and employ the design techniques as described in NASA Reports SP 3043-Magnetic Materials, CR 54090 - Summary of High Temperature Materials, CR 54092 - Electrical Conductors & Insulation which are incorporated herein by reference and made a part hereof. These materials include

- - - - - - - - - -

* The individual phase voltages shall be 2.25, 4.5, and 9 percent in the Phase I studies but 1.5, 3 and 6 percent figures shall be a goal for the later Phase III studies.

the use of Inconel-clad silver for the conductors, Anadur "S" for the insulation between conductors, and high-purity ceramic, 99.5 percent alumina for the slot insulators. However, a maximum of 300°F temperature increase shall be permitted between the coolant supply temperature and the alternator hot spots at the 160 KWe power level.

The second group of specifications listed below, though not considered directly in the screening analyses, are applicable to all selected designs.

(a) The stator cooling configuration shall be such that it does not permit adverse heating in the rotor or rotor stub shafts due to the higher stator temperatures (i.e., higher than the cooler rotor temperatures.)

(b) Specification MIL-G-6099(A) (ASG).

(1) Waveform. Paragraph 4.5.16* - In addition, the total rms harmonic content of the line-to-neutral voltage wave, when the alternator is operating into a purely resistive load, shall be less than 5 percent from 10 percent to 100 percent maximum design load of 160 KWe.

(2) Output Voltage Modulation*. Paragraph 4.5.13, except that modulation shall not exceed 0.5 percent.

(c) Shock, Vibration, and Acceleration. Alternators shall be in accordance with the environmental specifications NASA Nos. P1224-1 and P1224-2.

(d) Radiation Environment. The design radiation environment shall be 10^7 rads, 10^{13} nvt fast neutrons per square centimeter (> 1 Mev) unless otherwise specified.

- - - - - - - - - -

* This shall be a design goal without analytical verification.

(e) Position Sensitivity. The alternator shall be designed to operate in any position in both zero "G" and one "G" environments.

(f) Voltage-Regulator-Exciter and Speed Control. While the VRE, speed control, and power conditioning equipment are not a part of the study, their effects on the alternator shall be considered in the design study. The speed control for transient load changes shall be of the phase-controlled parasitic load type. Frequency regulations shall be assumed to be within $\pm$1 percent of design frequency for a change in external load of from 10 percent to full design output power. Some form of system gas pressure modulation is contemplated for long term or scheduled control of power level.

(g) Parallel Operation. It is anticipated that the TAC units described herein shall be employed in multiple units thus they may be required to be electrically paralleled. The contractor shall consider this requirement in his alternator design.

B. Inductor Screening Studies

Results of the inductor alternator frequency study are presented in Figure 84 . Efficiency curves are presented with and without windage losses included. Windage losses were calculated assuming a rotor cavity pressure of 55 psia and without smoothing of the rotor. Nonmagnetic pieces can be joined to the inductor alternator rotor between the salient poles to provide a smooth rotor surface for reduction of windage losses. This rotor required bonding such as that required for the Lundell alternator. Such an inductor probably would never be built because the smooth rotor would no longer have the high reliability of the single piece construction. The 1600 Hz alternator design provided the best combination of weight, efficiency, and performance regarding the specification requirements.

Only two frequencies were considered for the 36,000 rpm speed condition and, therefore, a graphical plot of the data is not meaningful. The data is summarized below for comparison.

FREQUENCY STUDY
INDUCTOR ALTERNATOR - 36,000 rpm - EVACUATED ROTOR CAVITY

FREQ HZ	ELECTROMAGNETIC WEIGHT, LBS	EFFICIENCY,%	ROTOR WEIGHT, LBS	% VOLTAGE UNBALANCE	AC WINDING HOT SPOT TEMP °F
1200	231	92.8**	83	10.7	885
2400	161	92.4**	61	6.8	763

From the data above, it is apparent that the 2400 Hz alternator provides the best electromagnetic design of the two frequencies considered at 36,000 rpm. A voltage study was not performed for the inductor alternator selected in the screening studies because the three specified voltages could be obtained for many of the designs by simply reconnecting the alternator parallel circuits internally. Therefore, the voltage study was deferred until the final alternator designs were selected.

---

*See Table XXXVI for tabulation of data

**Without Windage. Windage loss is small for the evacuated rotor cavity and would not significantly affect the relative efficiency.

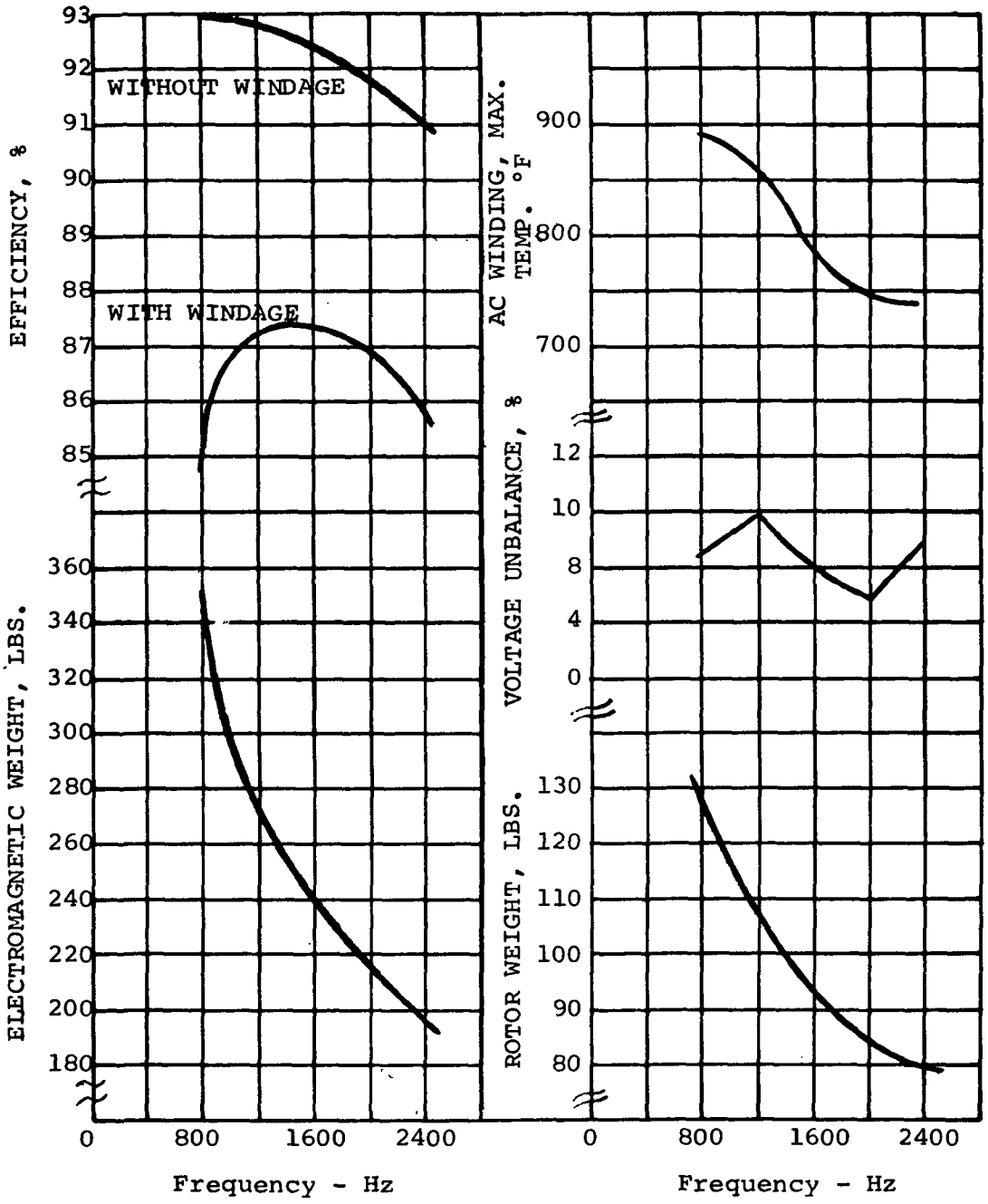

FREQUENCY STUDY
INDUCTOR ALTERNATOR - 24000 RPM

Figure 84.

TABLE XXXVI

Design Reference Number	Speed (rpm)	Poles	Frequency (Hz)	Volts per Phase	Rotor Steel	X_d Synchronous Reactance Per Unit[a]	Turns per Phase	Slots	Machine Dimensions (inches)			
									Stack Length	Frame Diameter	Overall Length	Rotor Diameter
A-1	24,000	2	400	240	Hiperco 27	1.3	8	48	4.95	17.2	14.2	8.
B-1	24,000	4	800	240	Hiperco 27	0.95	12	72	3.45	13.3	8.0	7.
C-1	24,000	6	1200	240	4340 R_c 49	0.55	10	90	3.4	14.9	10.8	9.25
C-2	24,000	6	1200	240	4340 R_c 49	0.85	15	90	2.5	14.0	9.3	8.0
C-3	24,000	6	1200	240	4340 R_c 49	1.33	21	63	1.91	14.1	8.15	7.45
C-4	24,000	6	1200	240	4340 R_c 33	0.87	15	90	2.7	13.6	9.5	7.5
C-5	24,000	6	1200	120	4340 R_c 33	0.76	7	63	2.7	13.3	9.5	7.5
D-1	36,000	4	1200	120	H-11 *		8	96	3.56	13.3	9.56	7.5
D-2	36,000	4	1200	240	H-11 *	0.86	10	60	3.12	12.73	9.22	7.125
D-3	36,000	4	1200	240	4340 R_c 33	1.04	12	72	2.9	12.07	8.7	6.35

(a) Main Gap = 0.07 inches, auxiliary gap = 0.05 inches, except design (*) or 4340 @ 49 R_C

214 KVA Lundell Generator Design Summaries
.75 P.F. Lag

Sheet 1 of 2

TABLE XXXVI (Continued)

Design Reference Number	Densities			Losses (watts)				Efficiency (%)		Electric Weight (lbs)	Phase Balance, % 2/3 1ø, 1.pF	Estimate Temperature °C (°F)
	Armature Amp/in^2	Field Amp/in^2	Rotor KL/in^2	Pole Face	Windage[b]	Field	Total	Electro-magnetic	Overall			
A-1	4700	2560	82	2207	5454	2138	16,919	93.31	90.43	618	8.0	517 (963)
B-1	4721	2465	97	586	2643	1392	11,251	94.89	93.45	295	8.0	406 (763)
C-1	5000	2099	70	3228	6567	1191	17,649	93.52	90.06	388	5.1	378 (712)
C-2	4760	2110	72	1906	3312	1312	13,204	94.18	92.38	285	9.7	406 (763)
C-3	4329	2074	72	3214	2420	1474	16,282	92.03	90.76	270	14.31	487 (909)
C-4	5072	2014	84	1551	2884	1158	12,736	94.20	92.63	279	8.9	418 (784)
C-5	4783	2078	88	2581	2884	1200	13,049	94.03	92.46	280	7.8	409 (768)
D-1	6750	2000	67	1185		792				293	6.0	429 (804)
D-2	5625	2180	75	2524	13,065	1165	22,767	94.28	87.55	272	7.4	447 (837)
D-3	4980	2358	89	2185	9524	1312	19,125	94.34	89.32	221	9.25	421 (790)

(b) Windage based on 55 psia at 24,000 rpm and 120 psia at 36,000 rpm.

214 KVA Lundell Generator Design Summaries

.75 P.F. Lag

Sheet 2 of 2

Additional design study details are reported in a subsequent section the reader is referred to that section for additional details on the inductor alternator design procedures and assumptions.

C. Lundell Screening Studies

1. Study Variables and Assumptions

Variables

The following variables were considered in this study.

Phase Voltage: 120, 240.

Rotor Steels: Hiperco 27, H-11, 4340 @ R_c33 and 4340 @ R_c49.

Main Radial Gap: 0.04 to 0.16 inch.

Synchronous Reactance (X_d): 0.55 to 1.3 (Turns per phase: 10 to 21 for 240 L-N Volts);

Frequency: 400,800,1200 Hz.

Poles	Speed (rpm)	Frequency (Hz)	Design Ref. Letter
2	24,000	400	A
4	24,000	800	B
6	24,000	1200	C
4	36,000	1200	D

Assumptions and Constants

Stator Steels: Hiperco 27 for frame and punchings (0.004 in. thick). Hiperco 27 steel was chosen for its good magnetic characteristics at high temperatures.

Auxiliary Gap: 0.05 inches.

Gap at Conical Section: Rotor dia/100, (used for windage).

Flux Densities:

Main Gap: 52 Kilolines/inch^2.

Auxiliary Gap: 55 Kilolines/inch^2.

Rotor: 67 to 97 Kilolines/inch^2. Flus densities were chosen depending on the steel to give approximately 60 amp-turns/inch. Higher flux densities could have been chosen but increased field loss and/or field weight would have resulted.

Teeth: (Hiperco 27): 130 Kilolines/in^2, approximately.

Back Iron (Or Depth Below Slot): 66 Kilolines/in^2, approximately. At this density the differential iron weight versus core loss in the back iron is in the order of 30 lbs per KW loss.

Frame and End Bell Frame: 115 Kilolines/in^2.

Current Densities:

A-C Armature: 4300 to 6700 amps/in^2. The current density was chosen to give approximately 795°F A-C winding temperature determined by a computer calculation which assumed conduction of heat to the stator punching O.D. and assumed radiation of heat from the winding end turns with an emissivity factor of 0.4.

Field Wire Current Density: 2000 to 2600 amps/in^2. The field winding was sized and determined to match the total field amp-turn requirements of the generator. Thus, more and more field turns were added to the field until the increase in weight of the field and resulting decrease in field losses gave a figure of approximately 30 pounds per KW loss.

Armature Stacking Factor: 0.9.

Slot and Wire Insulation: Wire insulation assumed 0.0055 inches per side. Slot cell liner = 0.018 inch. Slot phase separator = .021 inches.

Total accumulated clearance in slot: 0.018 inch (width) and 0.02 inch (depth).

Winding: 60° phase belt and 2/3 coil pitch. No skew.

Rotor Bore Dia: 1.0 inch.

Pole Embrace: 0.667.

Per Cent Rotor Steel: 55% magnetic. That is, a cross section of the rotor at any point under the stator stack is 55% magnetic steel.

Gas in Cavity (for windage): 0.1764 lbs/ft^3 (He-Xe at 55 psia) at 24,000 rpm, full-load and 0.384 lbs/ft^3 (He-Xe at 120 psia) at 36,000 rpm, full load. Gas pressure was assumed to vary linearly with generator input power requirements. The kinematic viscosity assumed was 0.0000792 ft^2/sec.

Stray Loss Factor: Based on experience with actual machines, it was assumed that the ratio of actual core loss to the Epstein core loss is 2.5.

2. Frequency Study

For the frequency study, consider designs A-1, B-1, and C-4 (Table XXXVI) as extracted below:

Design Ref.	Poles	Speed, rpm	Freq., Hz	Xd P.U.	Turns Per Ph.	Elec.	Windage	lbs	Phase Volt Unbal. (2/3, single phase)
A-1	2	24,000	400	1.3	8	93.3	90.43	618.	8.0
B-1	4	24,000	800	0.95	12	94.9	93.4	295.	8.0
C-4	6	24,000	1200	0.87	15	94.2	92.6	279.	8.9

In general, there is little electrical difference in the designs. The large weight difference between the 2 and 4 pole generators results from the large back iron and flux requirements for the 8 turns in the 2 pole machine.

The 1200 Hz machine was selected because a potential application for the generator would be with a cycloconverter. The cycloconverter would require frequencies of 1200 Hz, or higher. For frequencies higher than 1200 Hz (6 poles), problems could result from excessive rotor leakage flux in the Lundell machines and excessive eddy current factors in the A-C armature winding (skin effects at higher frequencies).

3. Voltage

Changing the voltage rating of the machines did not effect the designs to any great extent (with the exception of the effect on corona, as discussed below). In most cases, to change the rated voltage, it was only necessary to change connections in the A-C winding. In some cases, however, this was not possible. For example, design C-4 was rated 240 volts, L-N. It had 6 poles and 2 parallel paths in the A-C armature winding. To change to 120 volts, L-N, would require 4 parallel paths which is not possible in a 6 pole machine. To accomplish the 120 volts, design C-4 was changes to design C-5 by decreasing the slots from 90 to 63 and increasing the parallel paths from 2 to 3. As can be seen in Table XXXVI , the efficiency and weight were hardly affected. The synchronous reactance, Xd, and voltage unbalance were reduced.

4. Synchronous Reactance, Xd, Study

To study the effect of synchronous reactance on the alternator design and performance, three designs (C-1, C-2 and C-3) were considered. These were 6 pole, 24,000 rpm, 1200 Hz machines with 10, 15, and 21 turns per phase. Figure 85 summarizes the results of this study. A loss breakdown is as follows:

Design	C-1	C-2	C-3
X_d, Per Unit	0.55	0.85	1.33
Losses, watts			
A-C Winding	1,683	2,761	5,448
Field Winding	1,191	1,312	1,474
Pole Face	3,228	1,906	1,890
Teeth	1,309	1,577	2,200
Back Iron	3,667	2,336	2,227
Total Electro-magnetic	11,078	9,892	13,239
Windage	6,567	3,312	2,420
Total with windage	17,649	13,204	15,660
Efficiency			
Electromagnetic	93.52%	94.18%	92.36%
Overall	90.06%	92.38%	91.09%

Maximum efficiency occurs for the C-2 design with an X_d of 0.85 per unit. At higher values of X_d, the pole face loss decreased at the rotor diameter was reduced. But at these higher values of X_d, copper losses increased because of increased armature turns and increased eddy current factors.

Voltage unbalance met the specification requirements of 9% at X_d values of 0.85 and lower.

The conclusions of this study were to select a value of X_d of about 0.85 per unit.

5. Main Gap Study

In this study, design C-4 was chosen as the base design. It had a main gap of 0.07 inches. For the study this gap was varied

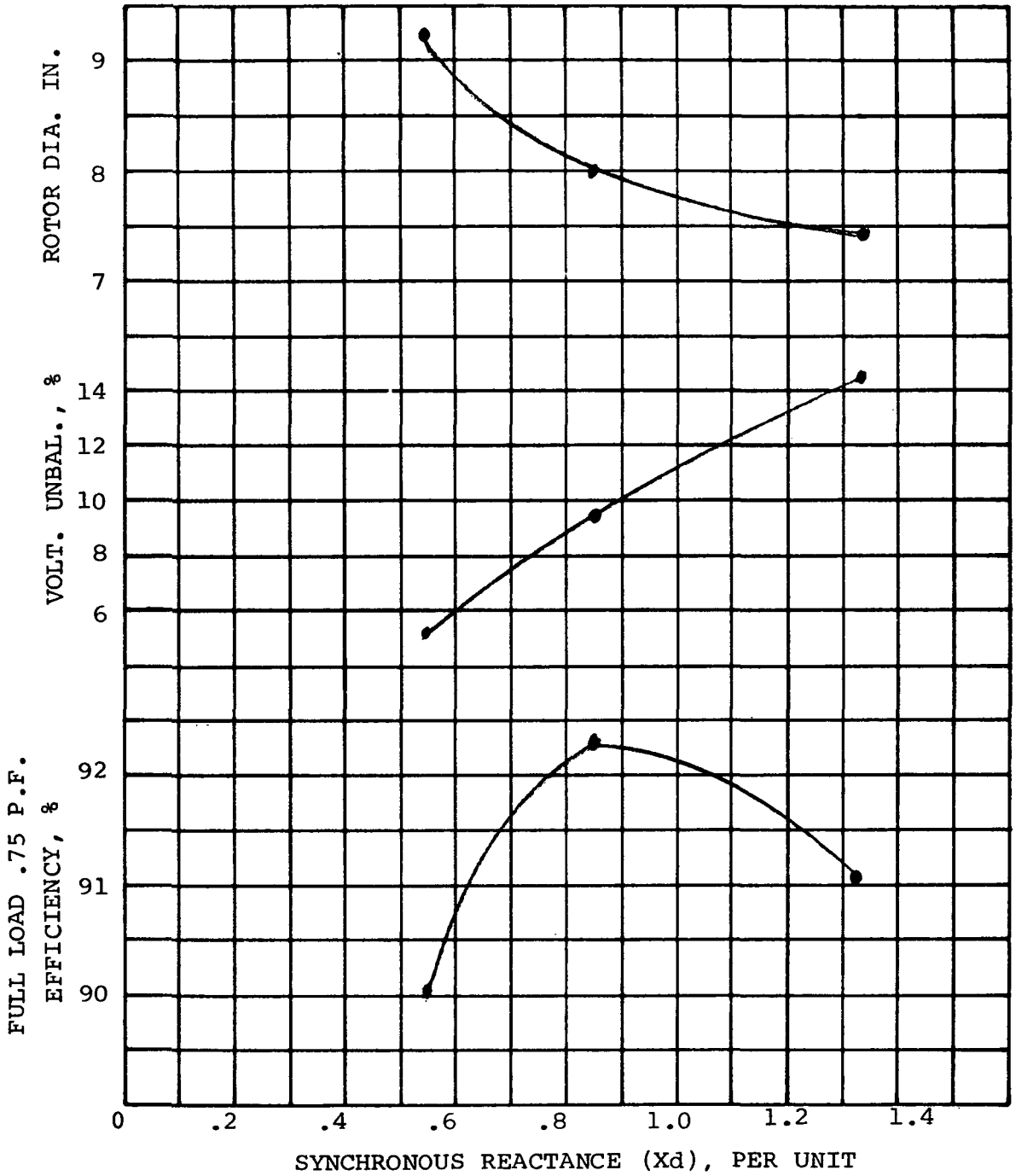

LUNDELL ALTERNATOR 24,000 RPM, 1200 Hz (C1, C2, C3)
MAIN GAP 0.07, AUXILIARY GAP 0.05
(ROTOR STEEL SAE 4340 700°F R_C48-50)

SYNCHRONOUS REACTANCE STUDY

Figure 85

from 0.04 to 0.16 inches with no other design changes. Figure 86 summarizes these results. A loss breakdown is shown below:

Main Gap, Inches	0.04	0.07	0.10	0.13
Losses, watts				
A-C Winding	3,248	3,247	3,245	3,243
Field Winding	813	1,158	1,704	2,979
Pole Face	5,642	1,551	677	400
Teeth	1,692	1,683	1,676	1,669
Back Iron	2,116	2,213	2,288	2,355
Total Electro-magnetic	13,511	9,852	9,590	10,646
Windage	2,915	2,884	2,864	2,850
Total with Windage	16,426	12,736	12,454	13,495
Efficiency				
Electromagnetic	92.21%	94.20%	94.35%	93.76%
Overall	90.69%	92.63%	92.78%	92.22%

It is seen that as the gap increases, the pole face losses decrease, while the field losses increase. The conclusion of this study is that the main gap should be 0.07 to 0.10 inches for best efficiency. The smaller gap should probably be favored since this gap would induce less rotor leakage flux.

6. Rotor Magnetic Materials and Diameters

Various rotor magnetic materials were considered in this study. In general, the better the magnetic material, the higher the flux density at which it can be operated, and the smaller the required rotor diameter. Design C-2 used SAE 4340 steel at a hardness of R_C 49. The rotor diameter was 8.0 inches. If better magnetic materials were used in the rotor, the rotor diameter could theoretically be reduced as indicated by the chart below:

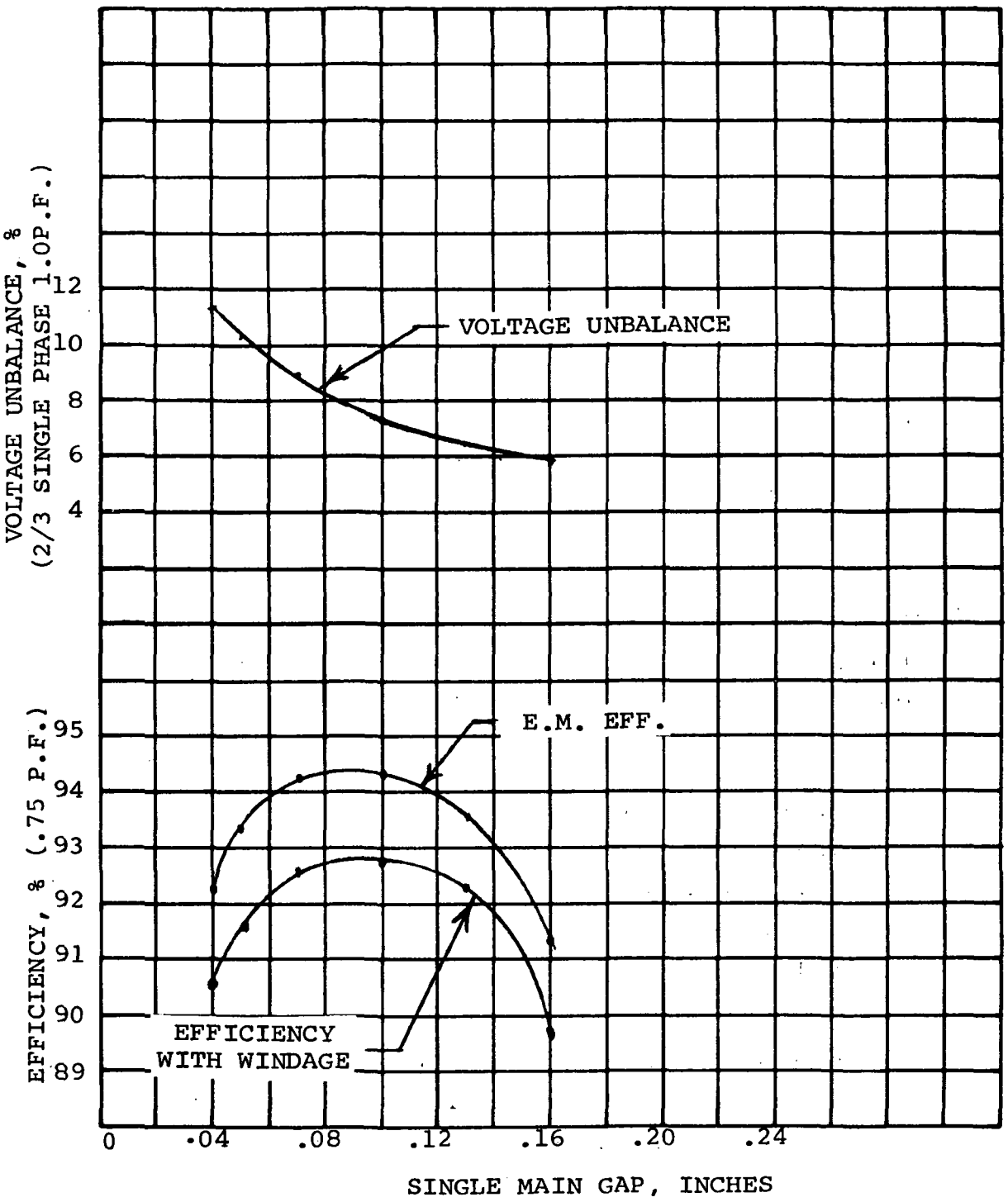

LUNDELL ALTERNATOR 24,000 RPM, 1200 Hz (C4)
AUXILIARY GAP 0.05
(ROTOR STEEL SAE 4340 700°F R_C33)
LUNDELL GAP STUDY

Figure 86

STEEL	TEMP Rc	FLUX DENSITY, B, AT 80 AMP-TURN/INCH	THEORETICAL ROTOR DIAMETER*
HIP 27	700F -	115 KL/IN^2	6.3 "
4340	700F 33	96	7.0
H11	700F 45	78	7.7
4340	700F 49	72	8.0 (C-2)

* Based on:

$$\frac{\text{Rotor Dia. \#2}}{\text{Rotor Dia. \#1}} = \sqrt{\frac{B1}{B2}}$$ (where B = rotor flux density)

to keep excitation constant for a given machine.

Whether this theoretical diameter may acutally be realized will depend on other effects. For example, the lower diameter machine may have narrow, deep slots that might cause a large eddy current factor. Generator designs C-2 and C-4, at 24,000 rpm, had the same electrical designs but different rotor steels. A comparison follows:

Design	Rotor Dia.	Rotor Steel	Rotor Wt. lbs	Electromagnetic WT.	Electromagnetic #KVA	Electromagnetic EFF.	Eff'y Incl. Wind.	X_d	Volt Unbal. %	Rotor Flux Density
C-2	8.0 (8.0)	4340 R_C49	102	285.0	1.33	94.2	92.4	.85	9.7	72
C-4	7.5 (7.4)	4340 R_C33	98	279.4	1.30	94.2	92.6	.87	8.9	84

Note: Values in parenthesis are theoretical diameters.

The electrical efficiency for C-2 and C-4 were approximately the same. In reducing the diameter, the pole face losses were reduced but the A-C armature losses increased primarily due to an increased eddy current factor resulting from a deep narrow slot. The improvement in efficiency when windage is included would, of course, have been greater for 36,000 rpm machines.

D. Selection of Three Representative Designs

The final selection of three alternator configurations was coordinated with the prime contractor and the NASA in order that pertinent turbine and system considerations could be factored into the selection.

All of the 24,000 rpm inductor alternator designs had high windage losses. The high windage losses were caused by the dynamic effect of the rotor salients at the compressor inlet pressure of 55 psia. The 24,000 rpm bonded rotor Lundell alternators have smooth rotor surfaces and were characterized by relatively low windage losses at the high cavity pressure.

At the 36,000 rpm speed, the pressure of the rotor cavity was scavenged to less than the system compressor inlet pressure and windage losses for the inductor alternator were reduced to secondary significance. At this high speed, rotor stress became a predominant consideration. The alternator designs considered in the selection process are presented in Tables XXXVI & XXXVII, the latter being limited to designs A-1, B-1 & C-4.

An evaluation of all the designs was made based on an adaptation of the U.S. Army, Modified Improvement Coefficient procedure (reference 35) which utilizes weighting factors for the various generator design parameters considered. A top ranking was obtained for the 24,000 rpm, 800 Hz Lundell alternator with the ranking for all other alternators falling lower but very close to each other. Based on electric power utilization considerations, however, the 800 Hz frequency does not appear attractive because the use of cycloconverters for frequency conversion to 400 Hz require at least a three to one frequency conversion ratio. Based on this consideration, the minimum alternator frequency is 1200 Hz unless the direct generation of 400 Hz total power is required for the system.

The Lundell alternator type proved to have definite design advantages over the inductor type for the 24,000 rpm pressurized rotor cavity study condition, primarily due to the lower windage losses. The 1200 Hz 6 pole, 24,000 rpm Lundell alternator configuration was selected as one of the candidates for final consideration.

TABLE XXXVII

DESIGN REFERENCE NUMBER	ALTERNATOR TYPE	RPM	ROTOR MATERIAL	POLES	FREQUENCY Hz	E.M.(1) EFFICIENCY %	WINDAGE(2) LOSS-KW	OVERALL EFFICIENCY %	E.M.(1) WEIGHT LBS	ROTOR WEIGHT LBS	ROTOR O.D. INCH	ROTOR LENGTH INCH	RADIAL GAP LENGTH INCH	POLE FACE LOSSES KW	% VOLT. UNBALANCE 2/3-SINGLE PHASE	STATOR HOT SPOT TEMP °F
I-1	INDUCTOR	24000	HIP-27	4	800	92.9	15.9	85.0	348	127	9.101	11.0	.07	.99	8.4	898
I-2	INDUCTOR	24000	HIP-27	6	1200	92.6	10.3	87.4	265	100	8.275	10.56	.07	1.35	9.9	862
I-3	INDUCTOR	24000	HIP-27	8	1600	92.8	10.6	87.5	238	98	8.335	10.23	.07	1.15	8.0	784
I-4	INDUCTOR	24000	HIP-27	10	2000	91.9	12.3	85.8	237	103	8.422	10.38	.07	0.96	6.0	738
I-5	INDUCTOR	24000	HIP-27	12	2400	91.1	9.7	86.3	192	79	8.070	9.02	.07	1.31	8.9	743
I-6	INDUCTOR	36000	H-11	4	1200	92.8	>30.	<79.	231	83	8.848	7.87	.08	1.19	10.7	885
I-7	INDUCTOR	36000	H-11	8	2400	92.4	>30.	<79.	161	61	8.575	6.55	.08	0.93	6.8	763

(1) E.M. = electromagnetic components only.

(2) Preliminary estimates, assume 55 psia pressure for 24,000 rpm speed, 120 psia for 36,000 rpm.

214 KVA INDUCTOR ALTERNATOR DESIGN SUMMARIES

Of the three alternators screened for the 36,000 rpm speed, the 4 pole, 1200 Hz Lundell alternator and the 4 pole, 1200 Hz inductor alternator were selected for further consideration. The 2400 Hz frequency of the 8 pole inductor alternator was considered higher than desirable for the electrical power distribution system.

E. Detailed Electromagnetic Design Performance Analyses

A preliminary optimization of design and performance parameters of the recommended alternator configurations was performed and electrical performance was determined at design power output and 0.75 lagging power factor.

1. 24,000 RPM Lundell

Design C-4 was the final 24,000 rpm Lundell design. The layout of this design is shown in Figure 87 and the layout of the slot is shown in Figure 88. Table XXXVIII presents a summary of the design details. The saturation curves are shown in Figure 89 . This design has an electrical efficiency of 94.2%, decreasing to 92.6% when windage is included. Figure 90 shows the efficiency variation with load. A breakdown of losses versus load (0.75 P.F.) is shown below:

Power Output, KWe	40	80	120	160
Losses, watts				
AC Winding	180	732	1,732	3,247
Field Winding	473	634	854	1,158
Pole Face	521	735	1,086	1,552
Teeth	1,560	1,600	1,642	1,683
DBS	2,051	2,104	2,158	2,213
Electromagnetic	4,785	5,805	7,472	9,853
Windage	768	1,471	2,158	2,884
Total Loss	5,553	7,276	9,630	12,737
Efficiency				
Electromagnetic	89.32%	93.24%	94.14%	94.20%
Overall	87.8 %	91.7 %	92.6 %	92.6 %

The efficiency is relatively constant from full load to half load but begins to fall off at 1/4 load. The efficiency at 1/4 load could be improved by reducing the iron losses. For example, if the back iron were increased 30%, changes would result as follows:

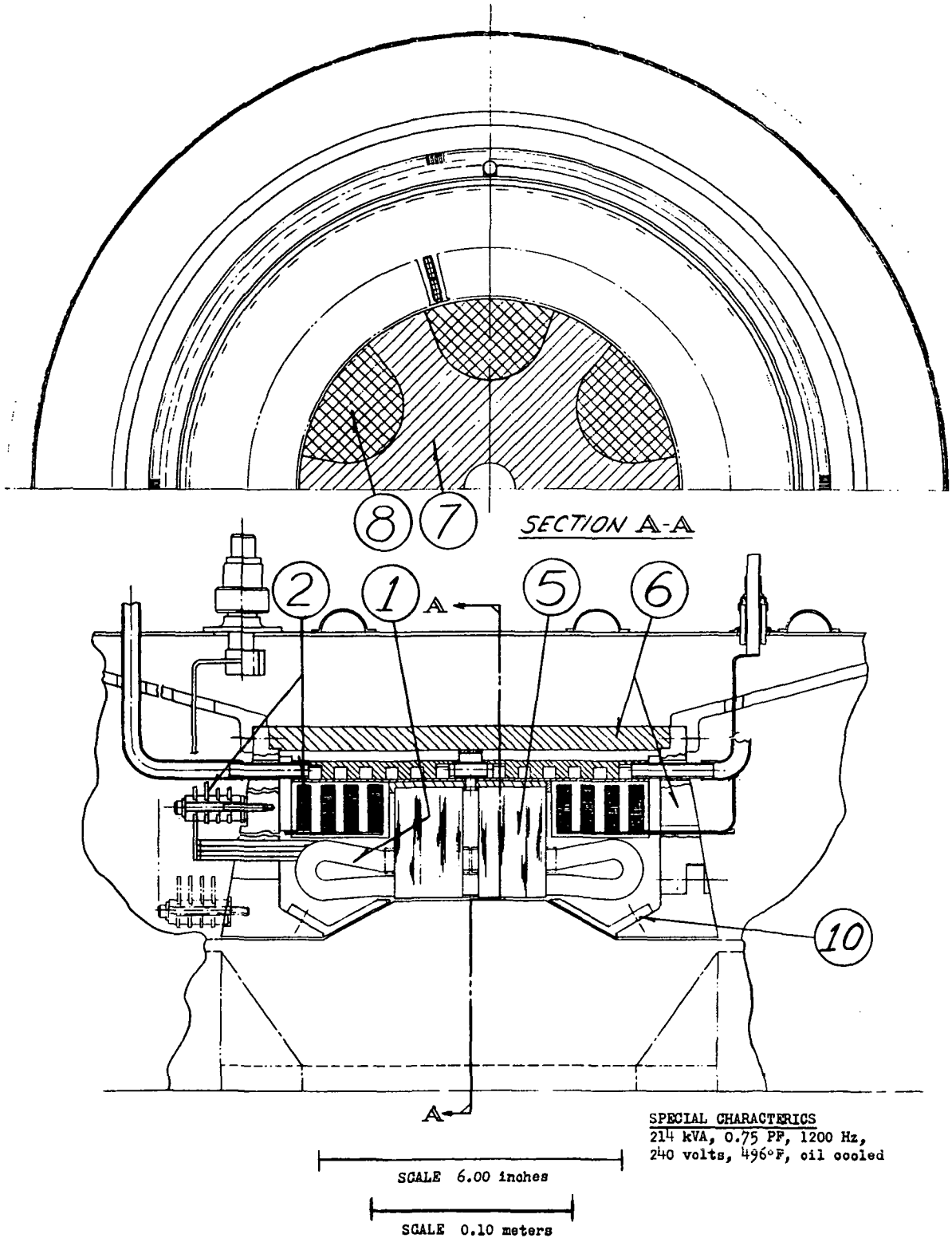

LUNDELL ALTERNATOR, 24,000 RPM

Figure 87

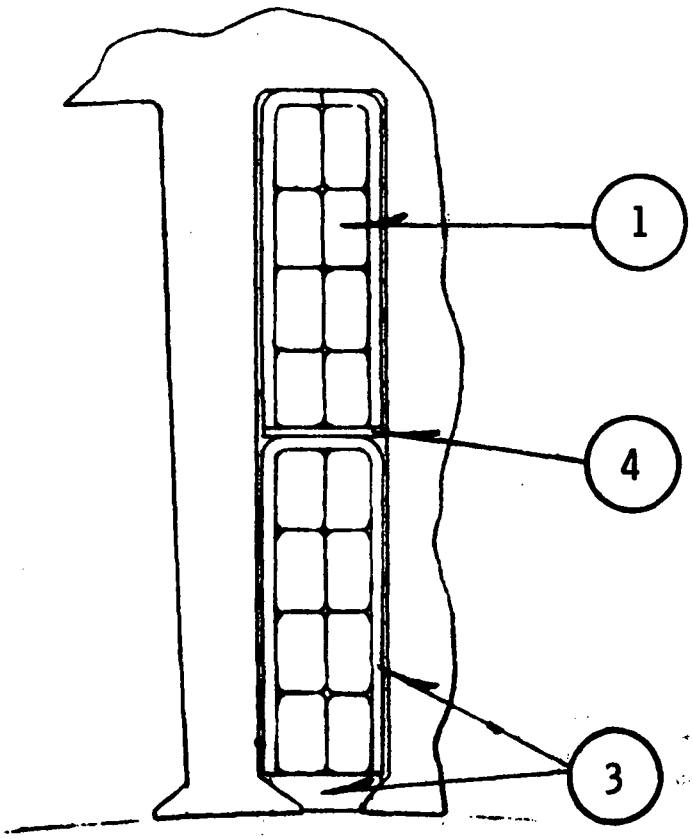

ENLARGED DETAIL OF
STATOR SLOT

SCALE = 4:1

LUNDELL ALTERNATOR
24,000 RPM

Figure 88

TABLE XXXVIII

INTERNAL DESIGN DETAILS SUMMARY:

60° Phase Belts, 2/3 Pitch; 90% Stacking Factor:

		6-POLE LUNDELL (C-4) 24,000 RPM	4-POLE LUNDELL (D-2) 36,000 RPM	4-POLE INDUCTOR 36,000 RPM
Current Densities ($amps/in^2$)	- Armature	5071	5625	4788
	- Field	2014	1165	3885
Flux Densities (kl/in^2)	- Back Iron	64	65	59
	- Teeth	129	124	135
	- Main Air Gap	52	46	56
	- Pole	84	75	80
	- Frame	110	115	112
	- Aux. Air Gap	57	57	N.A.
Rotor & Magnetic Steel -		55	55	N.A.
% Harmonics	- Third	0	0	0
	- Fifth	3.3	3.3	1.3
	- Seventh	2.0	2.0	1.7
F.L. Losses (watts)	- Pole Face	1552	2538	1089
	- Back Iron	2213	2935	4771
	- Teeth	1683	841	798
	- Armature	3247	2236	3218
	- Field	1158	1165	1990
	- Windage	2884	13065	2080
	(@ psia)	(55)	(120)	(1)
	- Total	12.73%	22780	13.946
Overall Efficiency-		92.6%	87.6%	92.0%
No Load Loss -		5200	6000	----
Electrical Weights (pounds)	- Armature	13	9	16
	- Field	49	42	22
	- Frame	85	88	36
	- Stacks	35	41	81
	- Rotor	98	92	83
	- Total	280	272	238

TABLE XXXVIII (Continued)

INTERNAL DESIGN DETAILS SUMMARY:

60° Phase Belts, 2/3 Pitch; 90% Stacking Factor:

		6-POLE LUNDELL (C-4) 24,000 RPM	4-POLE LUNDELL (D-2) 36,000 RPM	4-POLE INDUCTOR 36,000 RPM
Dimensions (inches)	- Rotor O.D.	7.5	7.125	9.155
	- Rotor Length	9.5	9.22	7.59
	- Stack Length	2.7	3.12	2.856
	- Stack O.D.	12.016	11.305	13.000
	- Overall O.D.	13.56	12.73	15.23
	- Overall Length	9.5	9.22	12.97
Rotor Steel -		4340 R_C 33	4340 R_C 48	H-11
Number of Slots -		90	60	108
Conductors per Slot -		2	2	2
Series Turns -		15	10	9
Parallel Paths -		2	2	4
Parallel Strands -		8	6	2
Resistances, Hot (ohms)	- Armature (Per Phase)	0.0125	0.0084	0.0126
	- Field Coil	0.152	0.159	0.327
Main Gap, inch -		0.07	0.07	0.09
Auxiliary Gap, inch -		0.05	0.05	--
Reactances (P.U.)	- Xd (Unsat.)	0.867	0.86	1.216
	- X'd (Sat.)	0.462	0.33	0.341
	- X"d	0.462	0.33	0.341
	- Xq	0.434	0.41	0.594
	- X"q	0.434	0.41	0.594
	- X2	0.448	0.37	0.467
	- X0	0.0177	0.01	0.0119
Time Constants, Hot (seconds)	- T'D1[a]	0.403	0.37	0.156
	- T'D0	--	--	2.09
	- TA	0.004	0.005	0.0061
	- T_d"	0.0017	0.0017	--

(a) T'D1 is T'D0 except it does not assume a solid steel flux circuit.

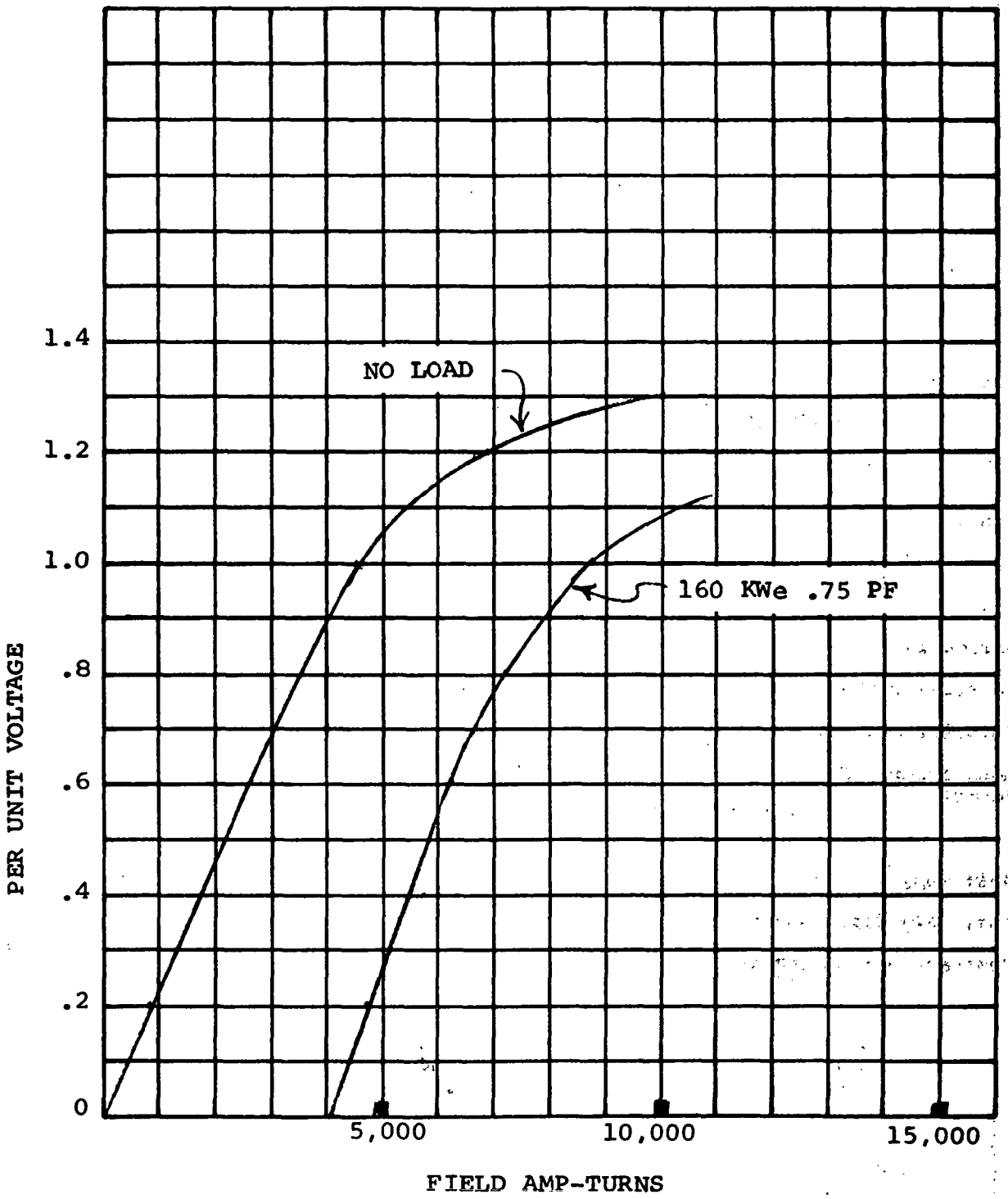

LUNDELL ALTERNATOR 24,000 RPM, 1200 Hz (C4)

SATURATION CURVES

Figure 89

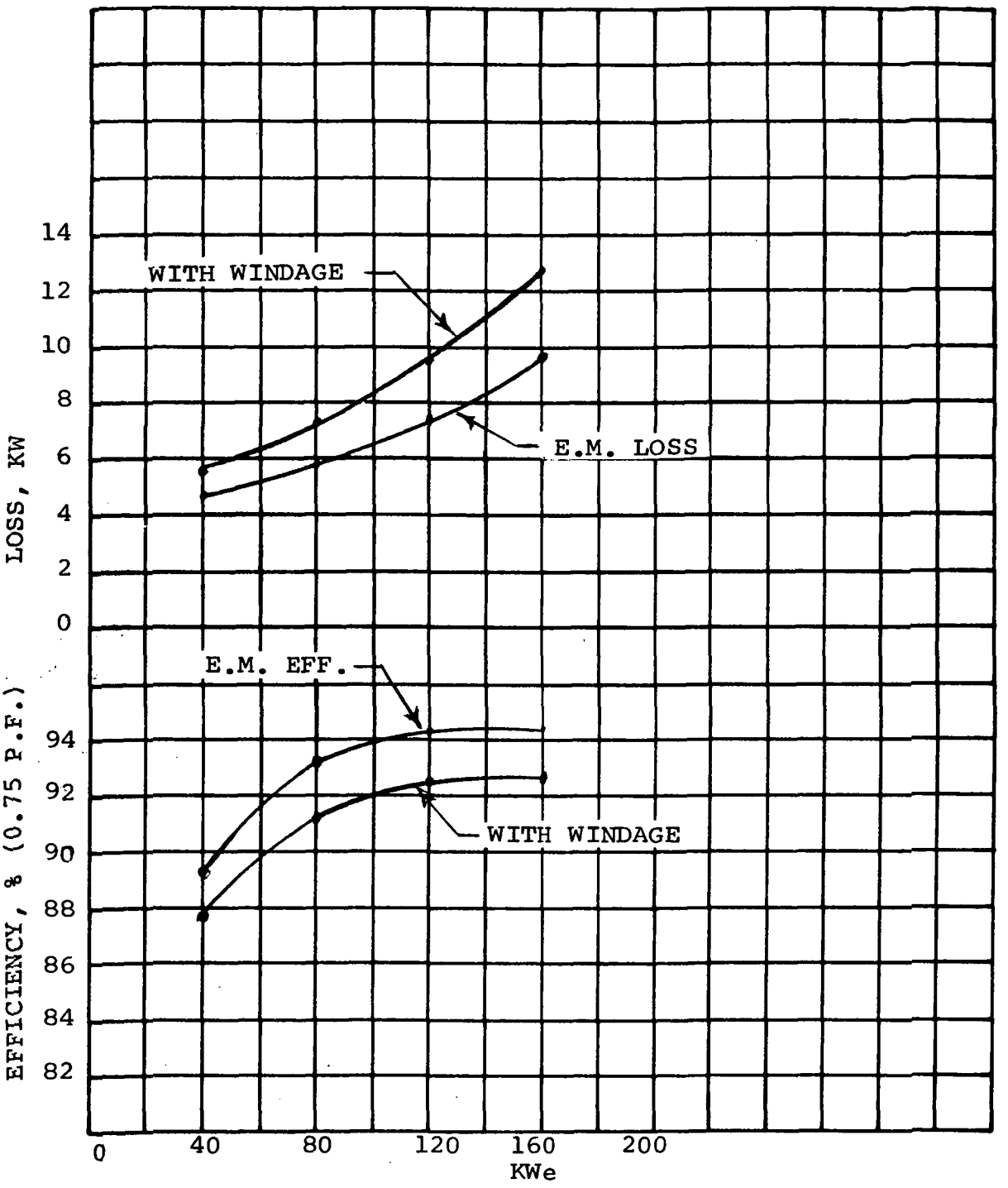

LUNDELL ALTERNATOR 24,000 RPM, 1200 Hz (C-4)

EFFICIENCY

Figure 90

Design:	C-4	Back Iron Modified
Back Iron Thickness, in.	1.245	1.62
Frame, O.D., in	13.56	14.31
Back Iron Losses, watts		
Full Load	2,213	1,883
1/4 Load	2,051	1,745
Total Electromagnetic Losses, watts		
Full Load	9,853	9,523
1/4 Load	4,785	4,479
Electromagnetic Efficiency		
Full Load	94.20%	94.38%
1/4 Load	89.32%	89.93%
Electromagnetic Weight, lbs.	279	290

2. 36,000 RPM Lundell

Design D-2 was the final electromagnetic 36,000 rpm Lundell design. The layouts of this design and slot punching are shown in Figure 91 and 92. Table XXXVIII presents a summary of the design details. Saturation curves are shown in Figure 93 . Efficiency curves are shown in Figure 94 . A breakdown of generator losses versus load (0.75 P.F.) is shown below:

Power Output, KWe	40	80	120	160
Losses, watts				
AC Winding	117	484	1,157	2,236
Field Winding	468	631	853	1,165
Pole Face	915	1,246	1,784	2,524
Teeth	804	816	829	841
DBS	2,804	2,847	2,890	2,935
Total Elec.	5,108	6,025	7,512	9,702
Windage	3,529	6,787	9,842	13,065
Total Loss	8,637	12,812	17,354	22,767
Efficiency				
Electromagnetic	88.68%	93.00%	94.11%	94.28%
Overall	82.24%	86.20%	87.36%	87.56%

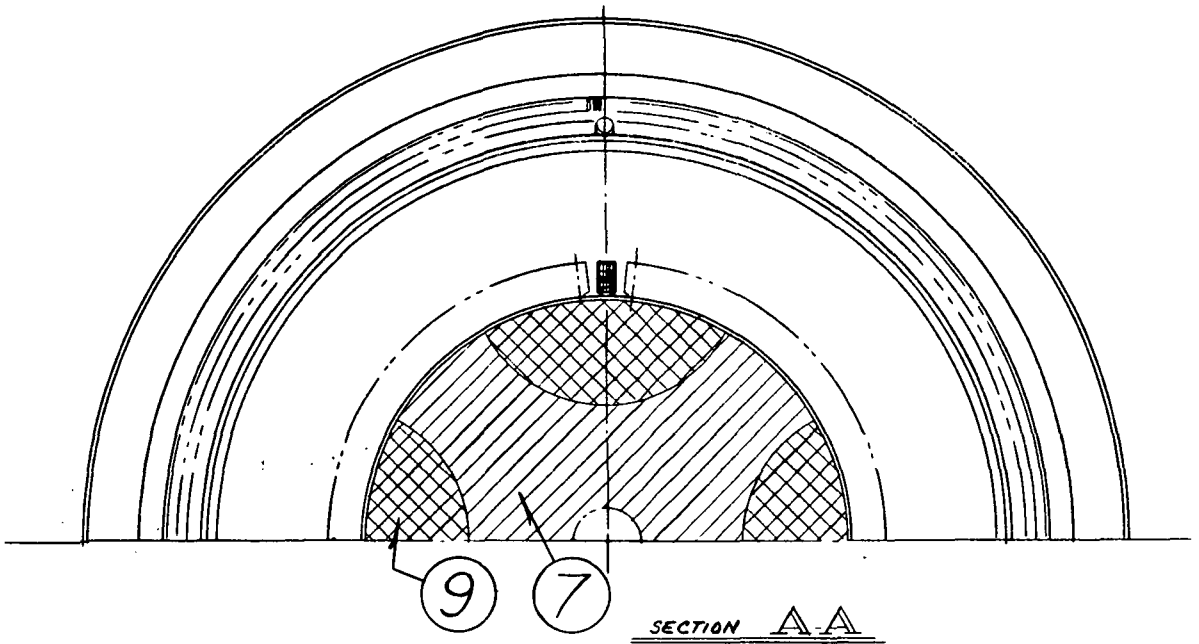

SECTION A-A

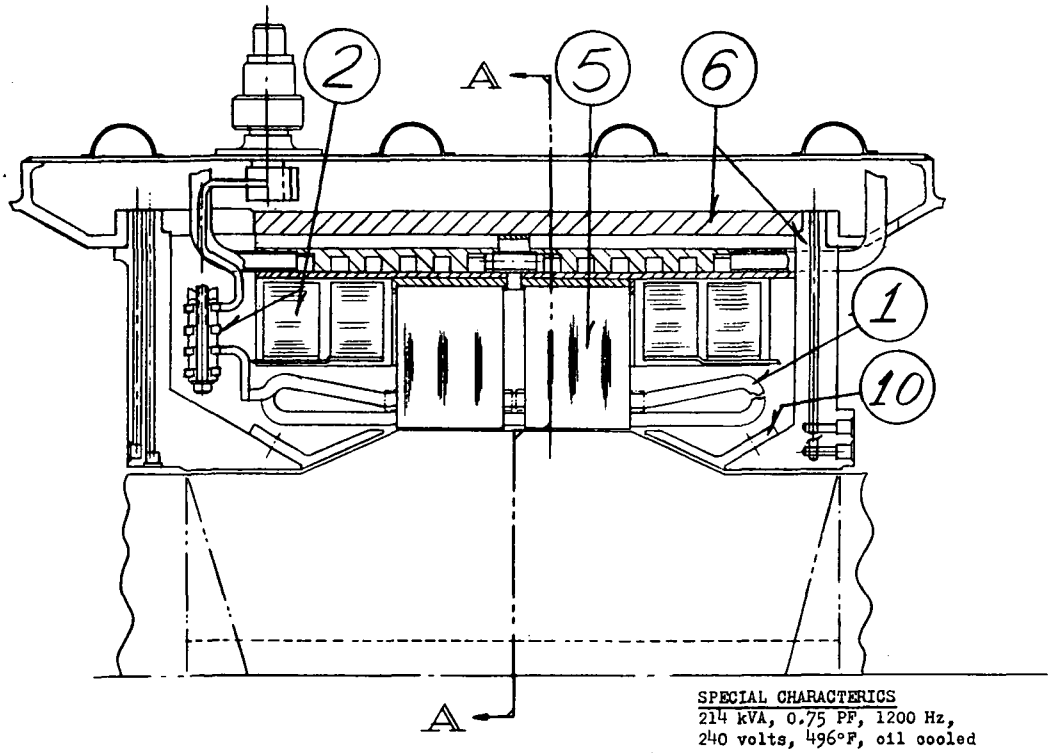

SPECIAL CHARACTERICS
214 kVA, 0.75 PF, 1200 Hz,
240 volts, 496°F, oil cooled

SCALE 0.10 meters

SCALE 6.00 inches

LUNDELL ALTERNATOR, 36,000 RPM

Figure 91

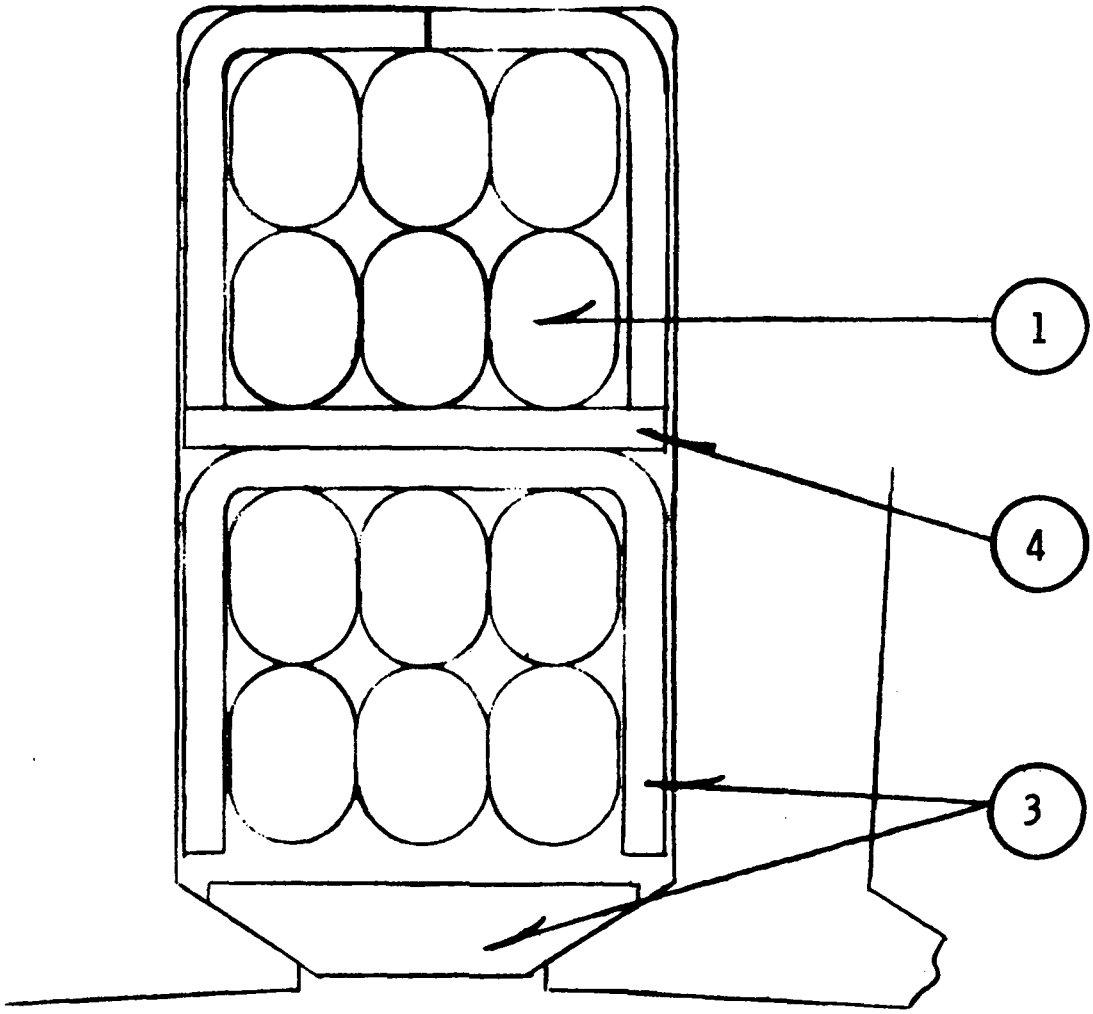

ENLARGED DETAIL OF
STATOR SLOTS - 60 SLOTS

SCALE 10/1

LUNDELL ALTERNATOR

36,000 RPM

Figure 92

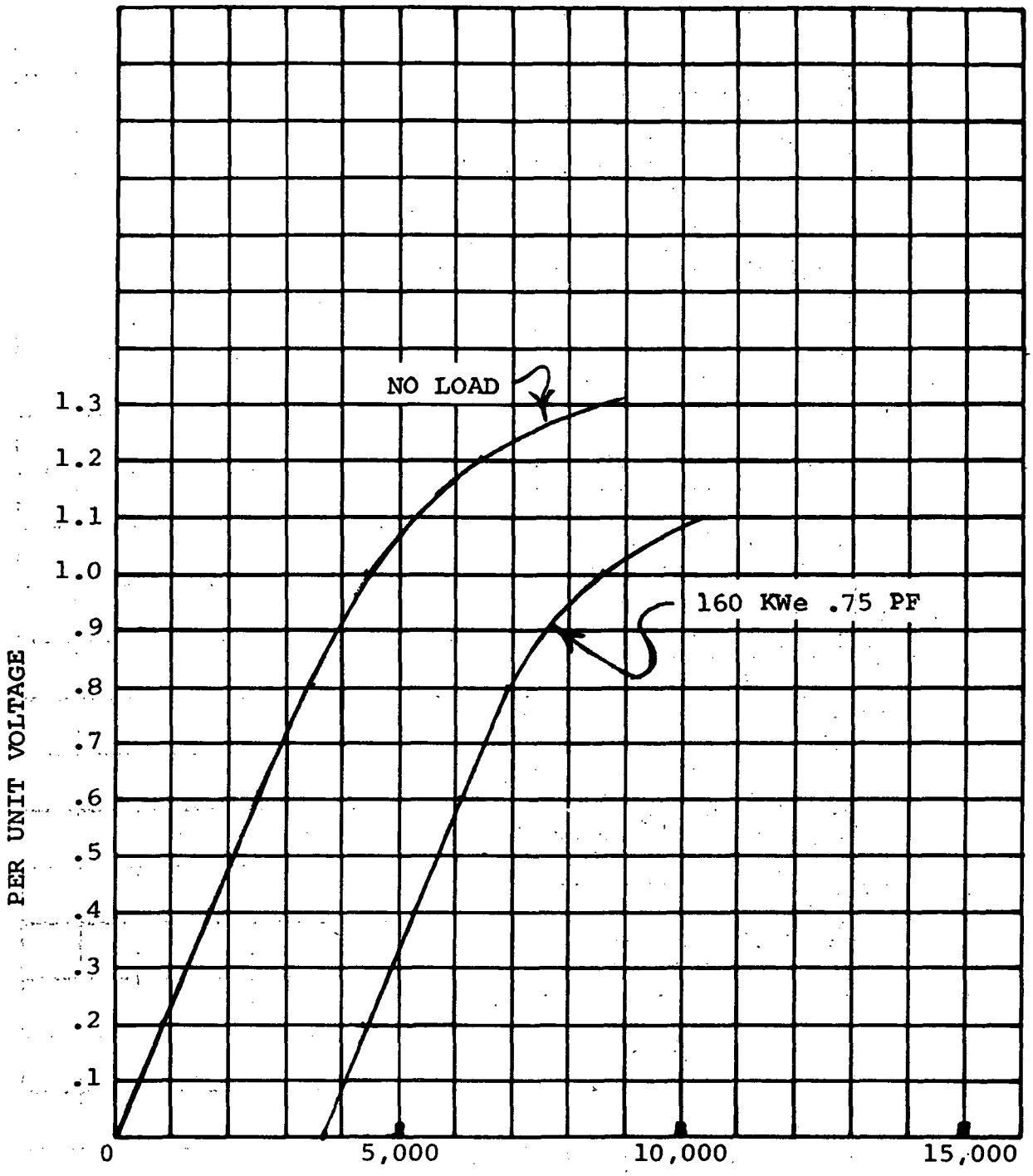

LUNDELL ALTERNATOR - 36,000 RPM, 1200 Hz (D2)

SATURATION CURVES

Figure 93

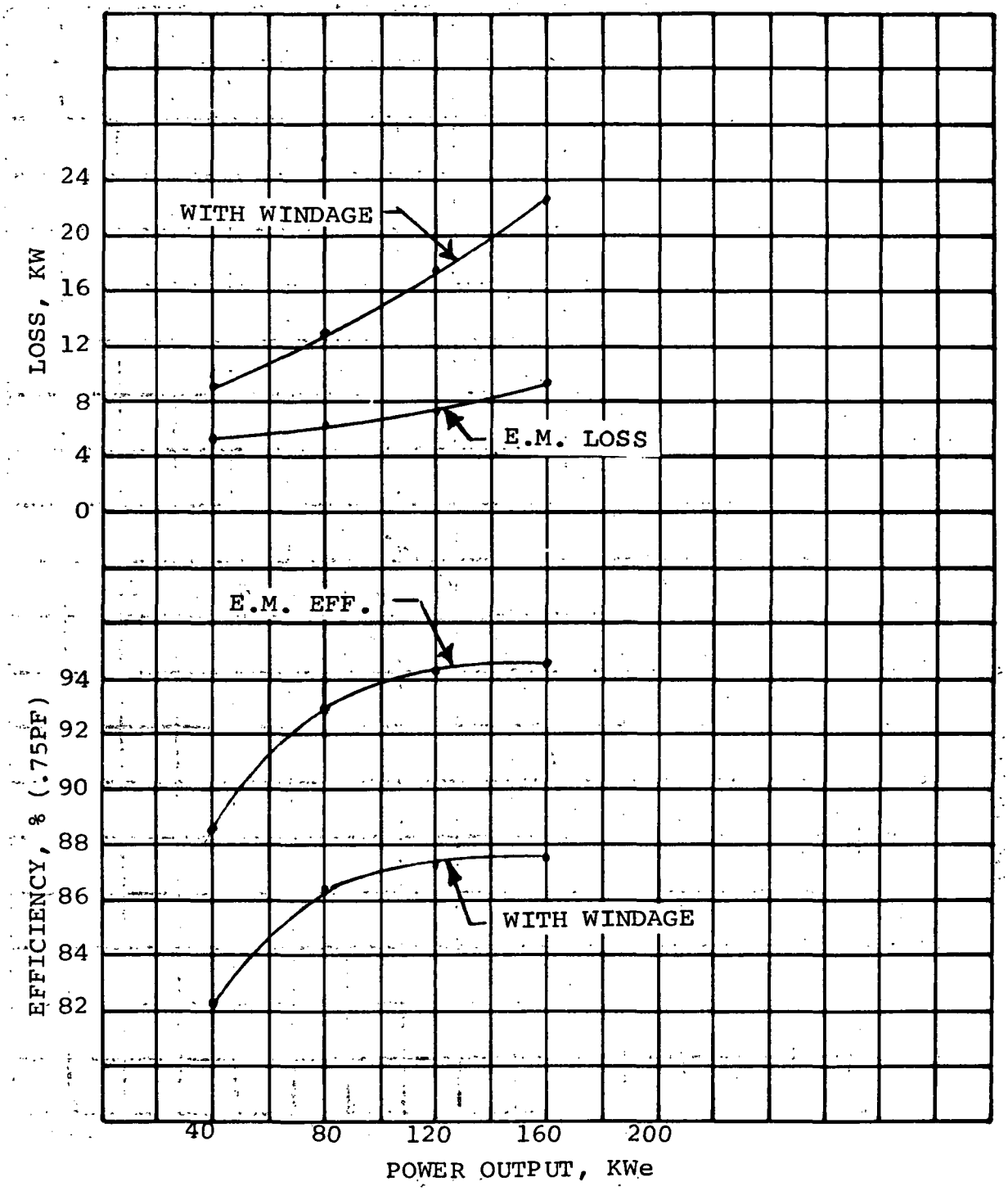

LUNDELL ALTERNATOR - 36,000 RPM, 1200 Hz (D2)

EFFICIENCY

Figure 94

3. 36,000 RPM Inductor

Figure 95 presents the parametric trends established as the air gap was varied for the selected 36,000 rpm, 4 pole, 1200 Hz inductor alternator. The minimum allowable gap, considering inclusion of a bore barrier (solid separator between the stator and rotor cavities), is 0.090-inch. A 0.090-inch gap also provides approximately the best combination of parameters if the inclusion of a bore barrier is not allowed; therefore, this value was selected for the remaining studies.

An a.c. winding current density of approximately 5000 amperes per square inch was selected from results of the current density study shown in Figure 96 . The reasons for the selection are evident from the established trends.

Figure 97 presents the trends established for variations in a.c. flux density in the armature depth behind the slot (DBS). Efficiency increased slightly with decreasing flux density and alternator weight increased rapidly for flux densities less than 60 kiloline per square inch. A flux density of 60 kl/in^2 was selected for the final designs.

The trends established for the tooth flux density sutdy, shown in Figure 98, clearly indicates that a high value of tooth flux is desired for optimum performance. A flux density of approximately 135 kl in^2 was selected for the final designs.

A study of per unit direct axis synchronous reactance X_d was performed to verify the previously selected value (1.2) established for the preliminary trial designs. Study trends are presented in Figure 99 . The voltage unbalance of 9% was slightly exceeded for the value of X_d.

The final study performed was the voltage study. Results are presented in Figure 100 . Unfortunately, the selected 4-pole machine does not allow the parallel circuits to be reconnected to decrease the voltage from 240 volts to 120

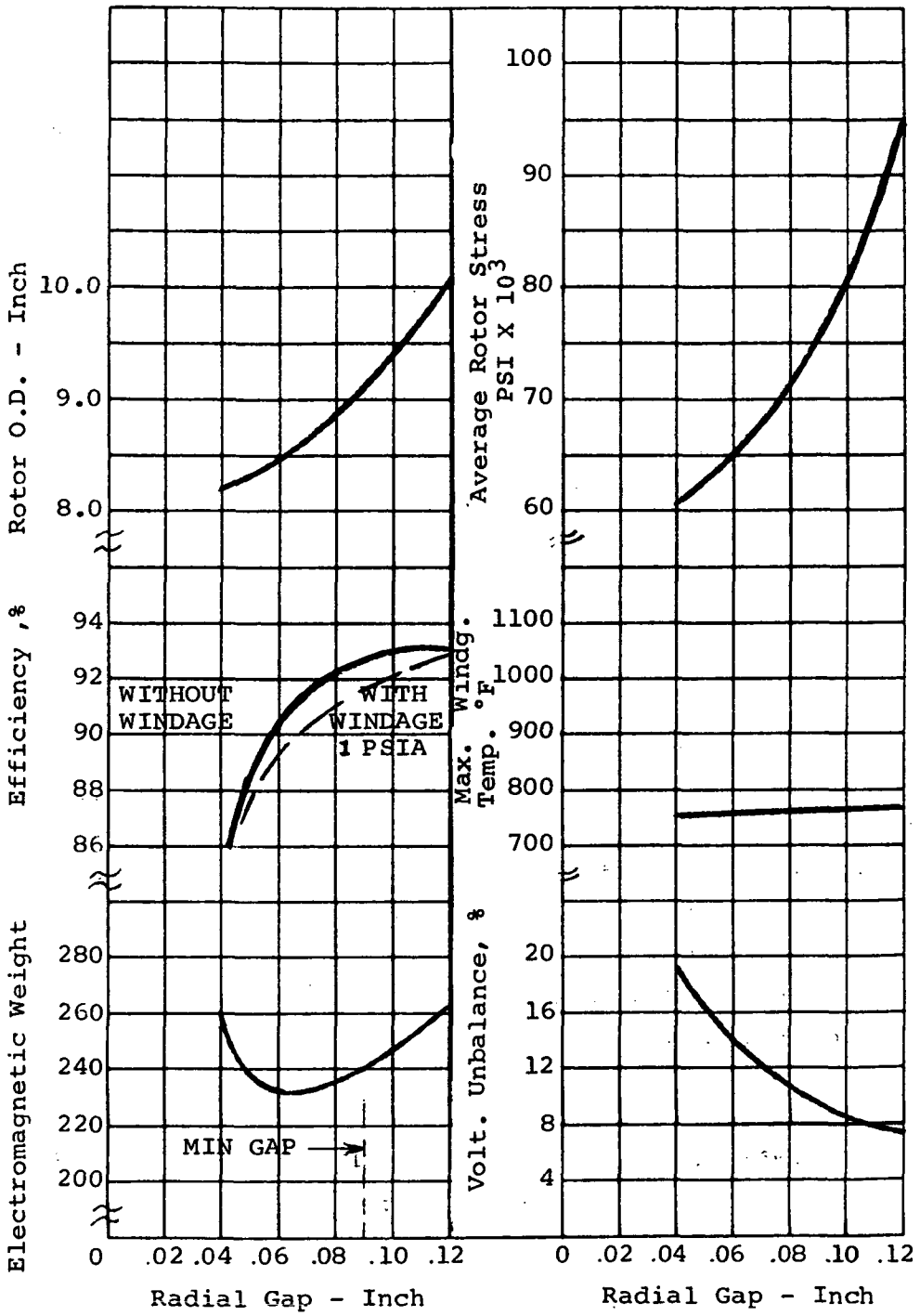

RADIAL GAP STUDY
INDUCTOR ALTERNATOR - 36000 RPM - 4 POLE

Figure 95

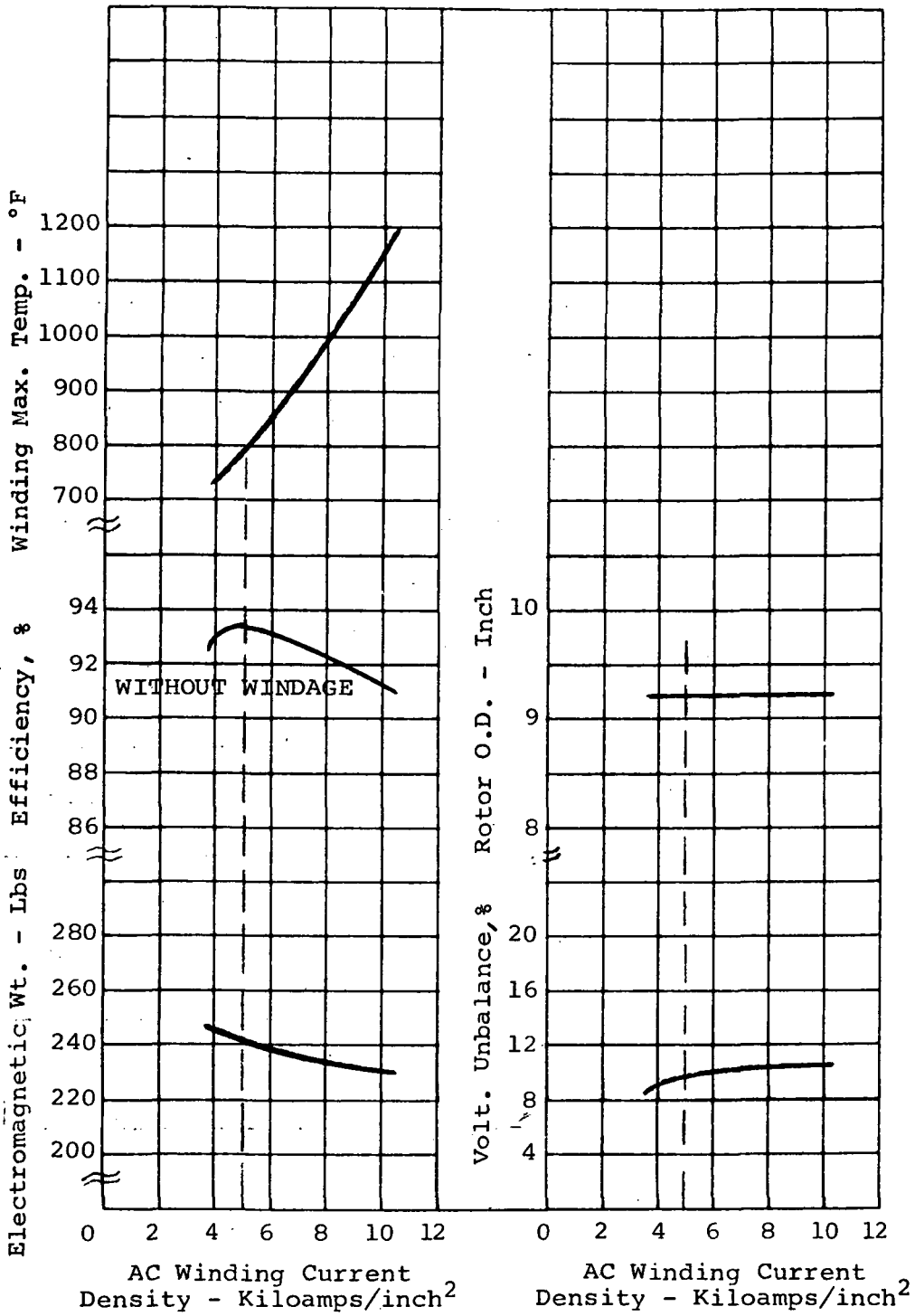

AC WINDING CURRENT DENSITY STUDY
INDUCTOR ALTERNATOR - 36000 RPM - 4 POLE

Figure 96

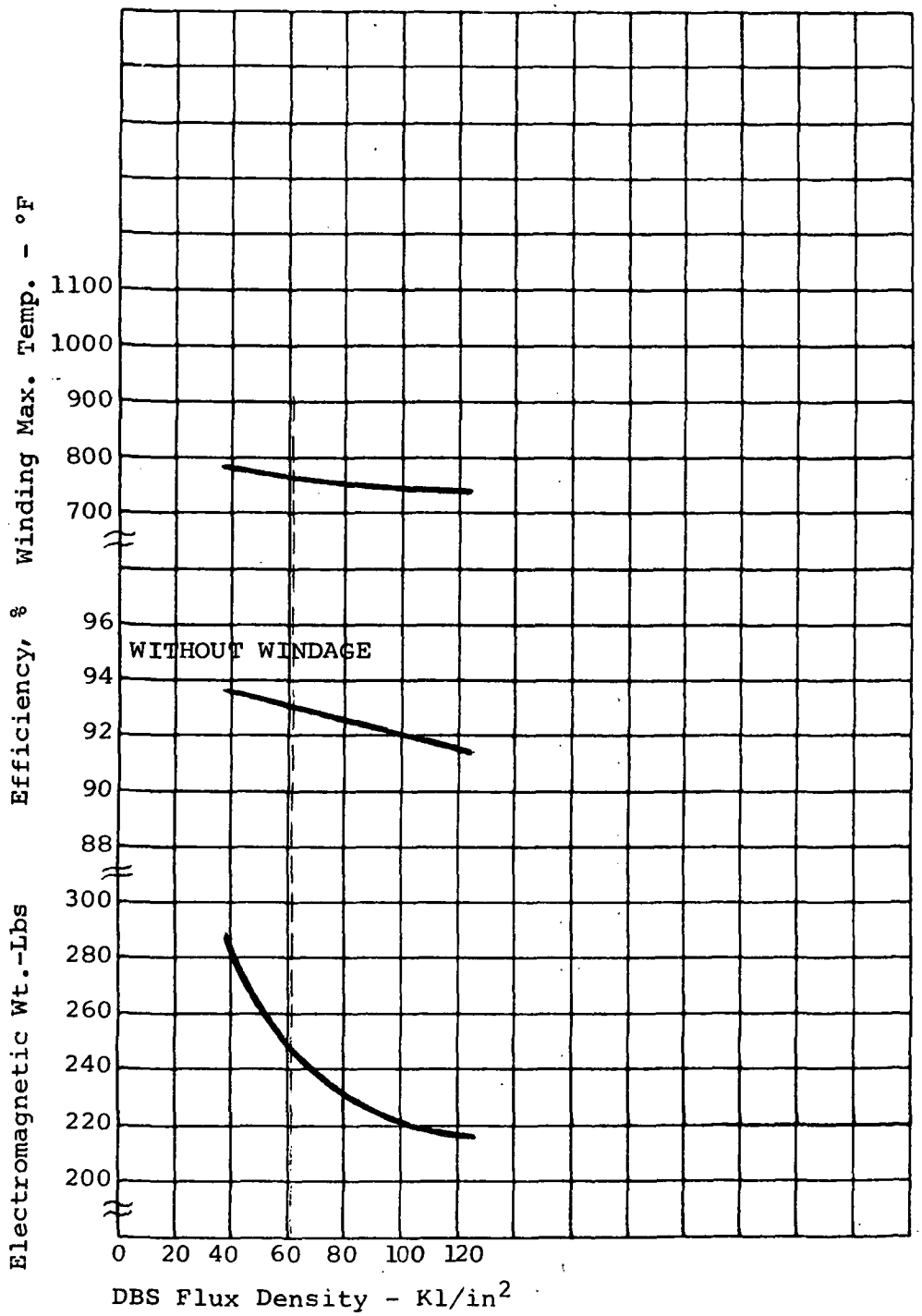

ARMATURE CORE FLUX DENSITY STUDY
INDUCTOR ALTERNATOR - 36000 RPM - 4 POLE

Figure 97

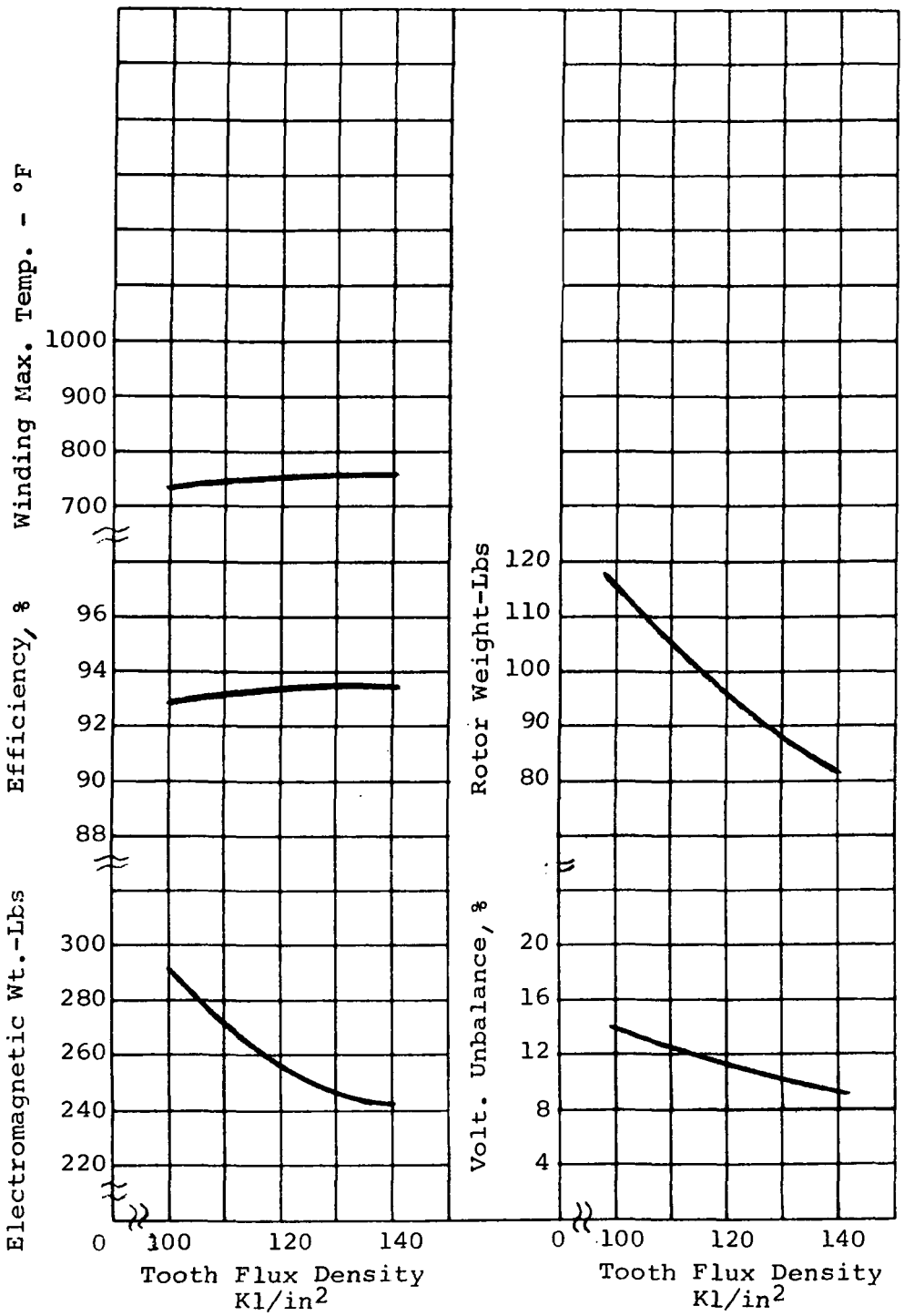

TOOTH FLUX DENSITY STUDY
INDUCTOR ALTERNATOR - 36000 RPM - 4 POLE

Figure 98

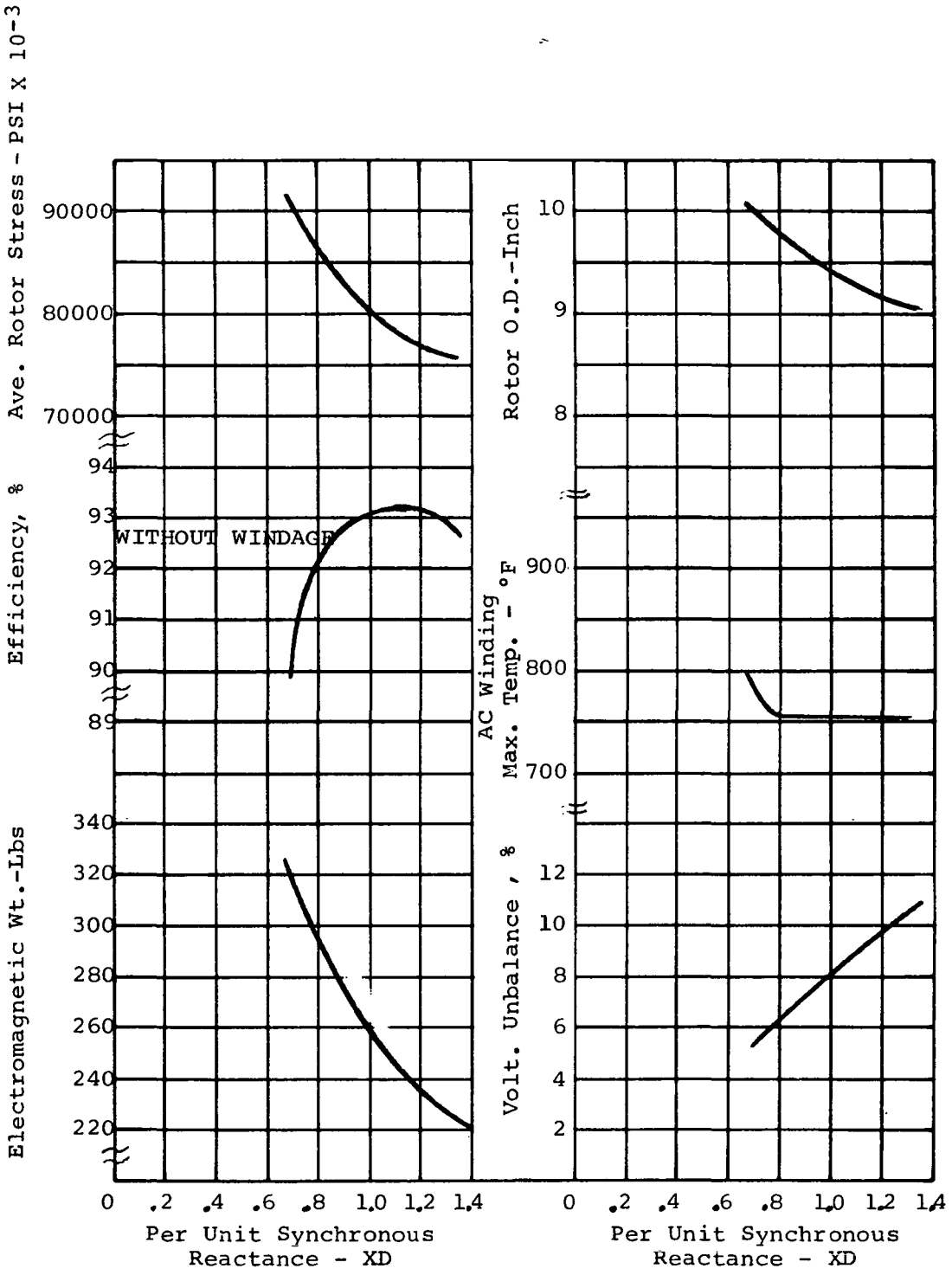

SYNCHRONOUS REACTANCE STUDY
INDUCTOR ALTERNATOR - 34000 RPM - 4 POLE

Figure 99

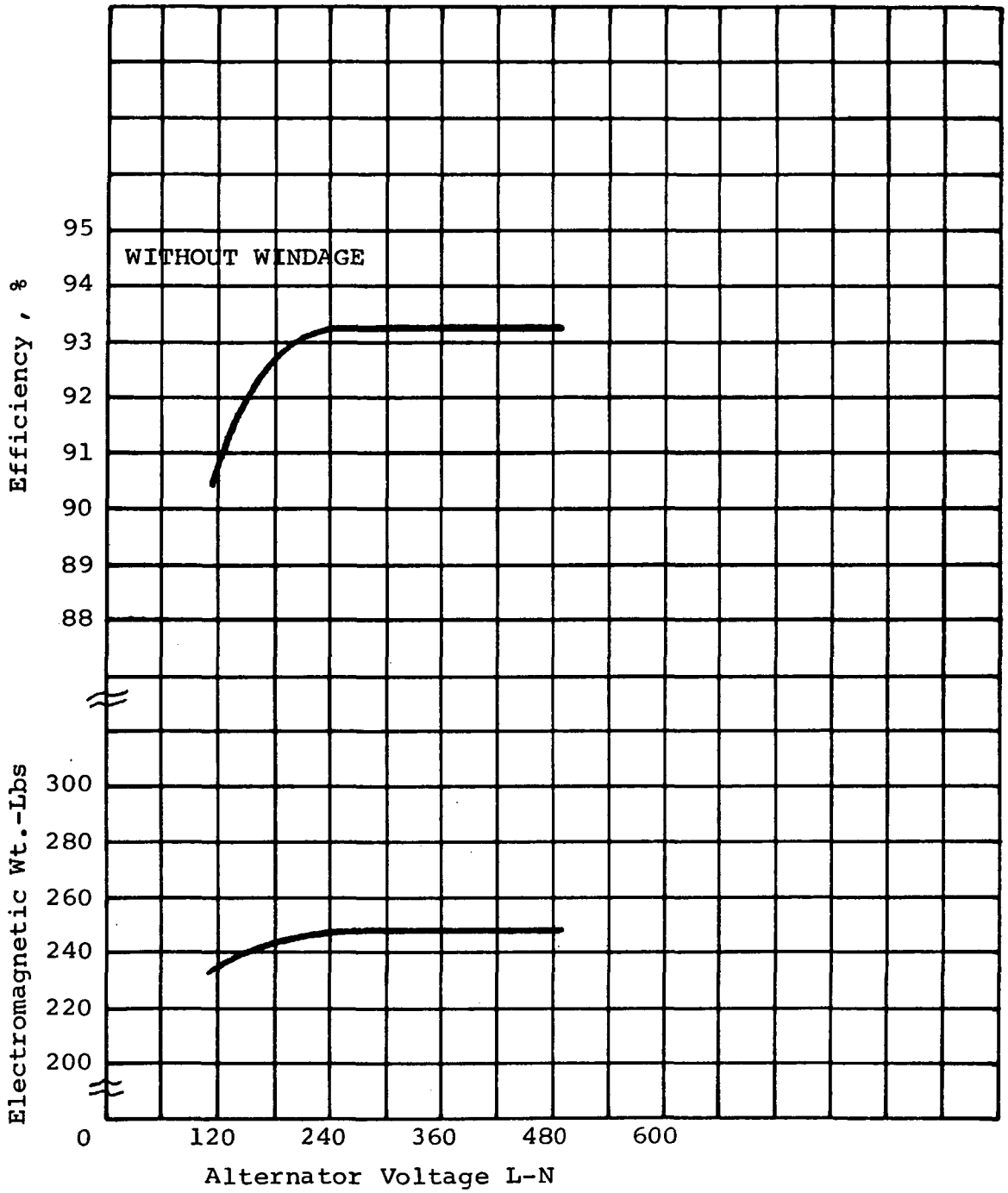

VOLTAGE STUDY
INDUCTOR ALTERNATOR - 36000 RPM - 1200 Hz - 4 POLE

Figure 100

volts as the maximum number of parallel circuits was utilized in the initial design. Therefore, the number of stator slots had to be reduced to obtain 120 volts line to neutral and this resulted in reduced efficiency for the alternator.

The layout of the 36,000 rpm inductor alternator design is shown in Figures 101 and 102. Table XXXVII presents a summary of the design and performance details. Saturation curves are shown in Figure 103 .

4. Alternate Stator Material Analysis

Alternator stator materials were evaluated as a part of the electromagnetic design analyses task to determine if any significant design advantages could be obtained by their use. Specifically, an alternator conductor for the a.c. winding was required to replace the nickel clad silver conductor because of the possibility of the conductor operating temperatures being lower than the 680°F curie temperature of the nickel cladding. Operation below the curie temperature of the nickel cladding would create high magnetic losses in the nickel. Nickel clad silver conductors were initially selected because of the better coil forming characteristics of this clad conductor. A 321 stainless steel clad silver conductor was selected to replace the nickel clad conductor as the 321 stainless steel cladding is non-magnetic and the conductor has better coil forming characteristics than Inconel clad silver conductors (which were also considered).

The use of mica mat slot liners to replace the alumina slot liners and the use of bare dispersion strengthened copper "Cube" alloy conductors were also evaluated. The effects of the use of these materials on alternator efficiency and weight, together with notations regarding evaluation of the materials is presented in Table XXXIX .

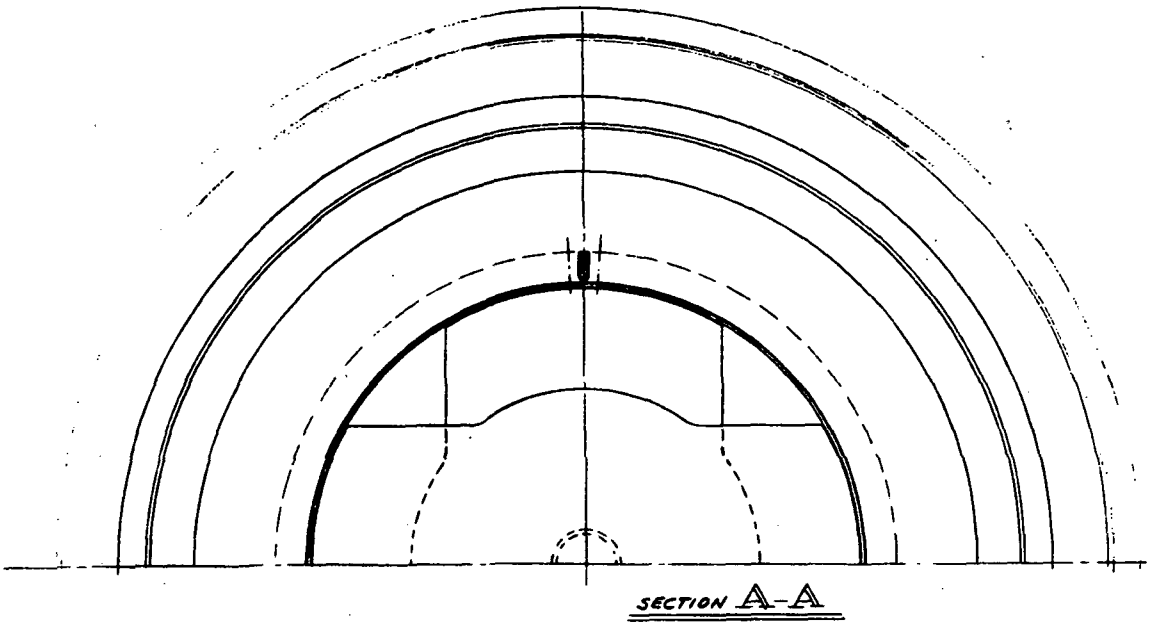

SECTION A-A

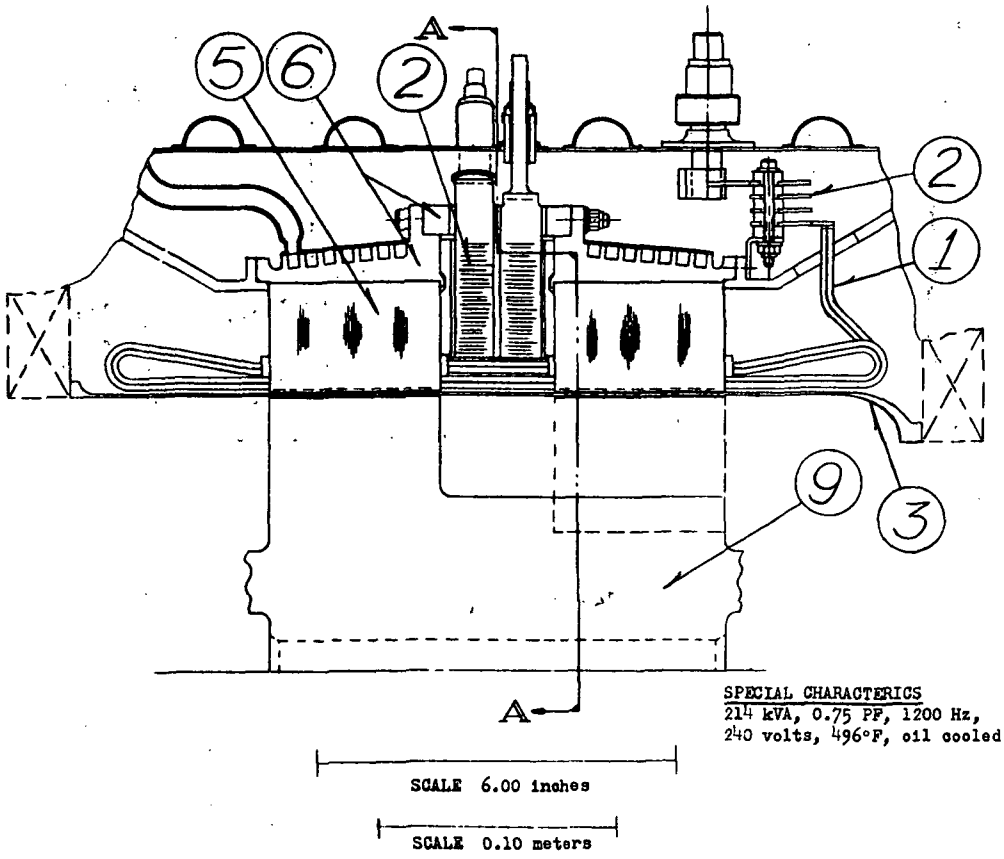

INDUCTOR ALTERNATOR, 36,000 RPM

Figure 101

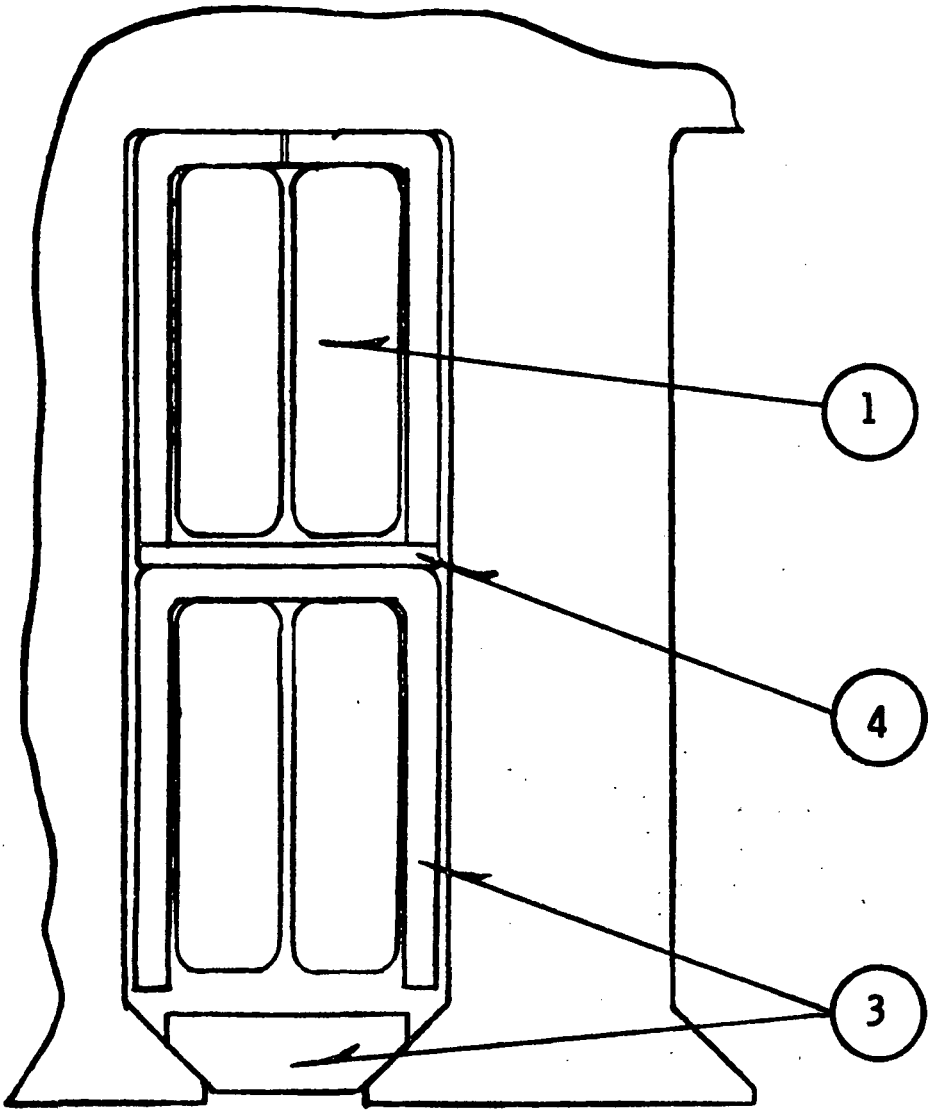

ENLARGED VIEW
OF STATOR SLOT

SCALE 10/1

INDUCTOR ALTERNATOR
36,000 RPM

Figure 102

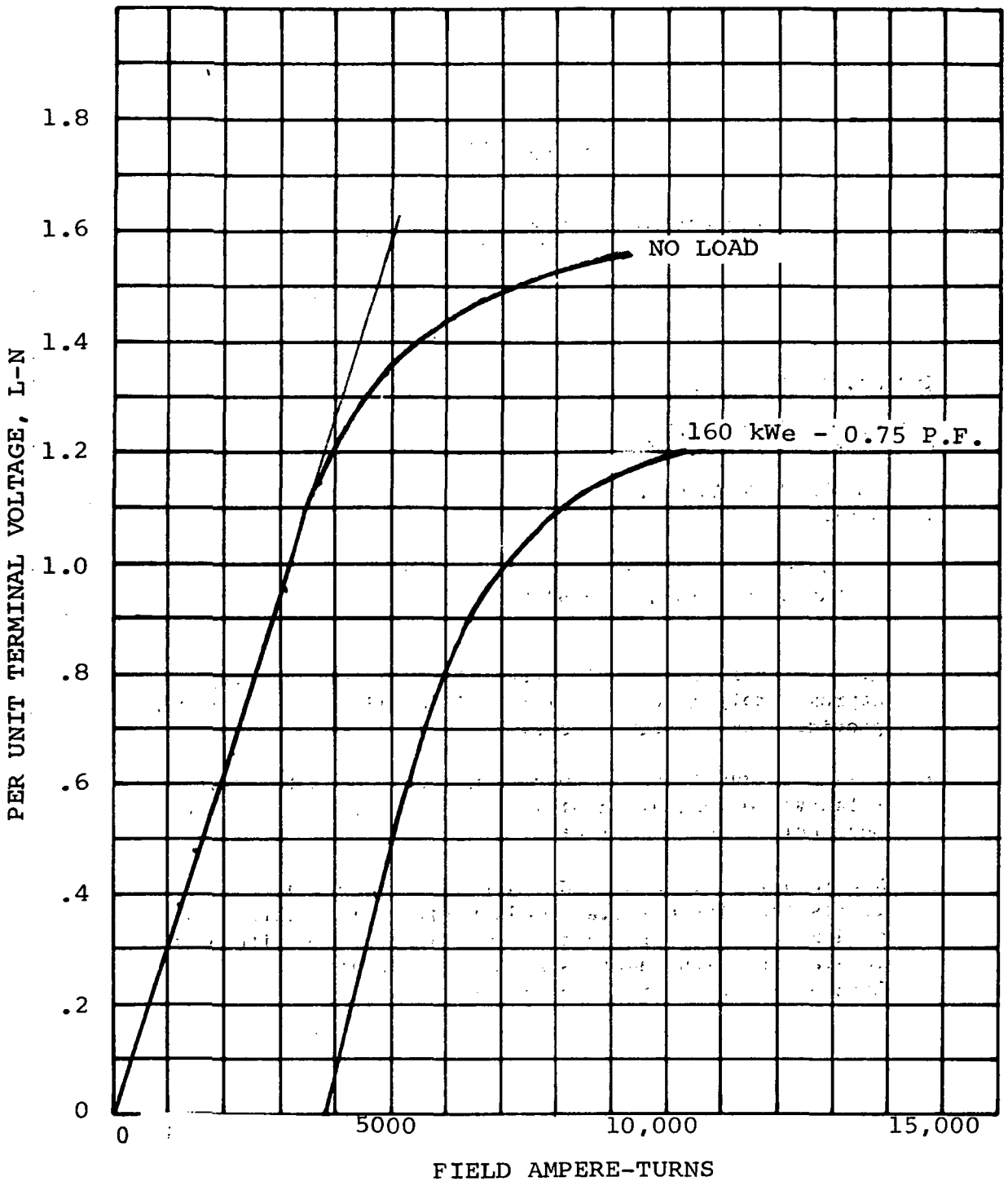

INDUCTOR ALTERNATOR-36000 RPM, 1200HZ
SATURATION CURVES

Figure 103

TABLE XXXIX

EVALUATION OF OTHER STATOR MATERIALS

MATERIALS	APPROXIMATE PERCENT CHANGE* EFFICIENCY	WEIGHT	NOTE
MICA MAT SLOT LINERS	nil	-2.5	1
BARE CUBE WIRE IN AL_2O_3 SLOT CELLS	nil	-10.5	2
321 STAINLESS STEEL CLAD SILVER WIRE	nil	nil	3

* Based on inductor alternator designs. Base configuration has Anadur insulated nickel clad silver conductors.

1) Mica mat has some flexibility. Thermal conductivity approximately 1% of that for 99.5% alumina, but probably provides lower thermal contact resistance.

2) This configuration has poor insulation characteristics relative to ionization of gas. Cube alloy has extremely poor coil forming characteristics.

3) Non-magnetic cladding. Has better coil forming characteristics than Inconel clad conductors. 304 stainless steel clad zirconium copper not recommended for use with Anadur insulation which requires 1200°F cure temperature. Zirconium copper over-ages at approximately 900°F.

F. Corona Considerations for Voltage Selection

The ambient atmosphere in which the stator winding of the TAC alternator will be operating is composed of a mixture of helium and xenon gases approximating 72% helium and 28% xenon by volume. Dr. T. Dakin of Westinghouse Research and Development Laboratories was consulted for information regarding the properties of the helium-xenon gas mixture in the stator cavity. Accor ing to Dr. Dakin, helium will have a predominant influence on the gas mixtures' electrical characteristics. Therefore, the properties given by Paschen's curve for helium are used to determine the maximum premissible voltage of the armature winding to preclude corona.

The minimum spacing between phase conductors is 0.029-inch (equal to the thickness of the slot liner and conductor double insulation thickness). An a.c. winding voltage of 415 volts rms or 587 crest volts line to line is assumed for this analysis. The corresponding crest voltage is 881 volts when allowance is made for a 50% voltage transient. The minimum pressure for voltage breakdown at 881 volts and 0.029-inch gap is 25 psia according to the Paschen's curve for helium, which would be the case for a break in the insulation.

The case of a helium gap in series with solid insulation between conductors must also be considered. A basic law of electrostatics states that the total voltage "E_T" across series dielectrics is divided in proportion to the ratio of the thichnesses "t_n" of the individual dielectrics to the respective dielectric constants "K_n" as indicated by Equation 1.

$$E_T = \frac{D}{\epsilon_o}\left(\frac{t_1}{K_1} + \frac{t_2}{K_2} + \frac{t_3}{K_3} \cdot \cdot \cdot \cdot \cdot\right)$$

D = electrostatic flux density

ϵ_o = permittivity of free space

A result of this relation is the concentration of voltage across the low dielectric constant media, such as a gas, when it appears in series with high dielectric constant solid materials. Ceramic insulations are particularly poor in this respect because of their relatively high dielectric constant.

For the TAC alternator, there are two insulating materials (Anadur and alumina) of known thicknesses in series with a gas filled gap of unknown thickness. The dielectric constant of alumina is approximately 10 while the dielectric constant of Anadur is estimated as equal to that of Borosilicate glass at 350°C (662°F), which is about 5.6. The dielectric constant of helium is assumed equal to that of free space, that is 1.0. Thickness of the alumina is 18 mils and the double thickness of Anadur is 11 mils for phase to phase voltage in the slot (See Figure 104).

The thickness of the gas filled gap cannot be determined as it is a variable quantity throughout the winding. However, it is not necessary to establish an exact value for the gap in order to determine the minimun pressure below which ionization of the gas will occur. The percent voltage, "$\%V_{HE}$ across any helium gap length can be determined by solution of Equation 2 for various values of gap length "t_1".

$$\%V_{HE} = \frac{100}{1 + \left(\frac{t_2}{K_2} + \frac{t_3}{K_3}\right)\frac{K_1}{t_1}}$$

where:

t_1 = gap length

K_1 = dielectric constant of gas in gap

t_2, t_3 = thickness of solid insulations in series with gap

K_2, K_3 = dielectric constants of solid insulations

Solution of Equation 2 for the case under consideration results in the curve given in Figure 105 . The maximum voltage across the various gap lengths can now be determined from the product of $\%V_{HE}$ and the maximum expected winding voltage as previously determined. The pressure (p) times spacing (d) value, "pd",is determined from Paschen's curve for the gas in question and corresponding to the voltages calculated above. The minimum pressure below which ionization of the gas will occur is determined by dividing Paschen's pd value by the gap length used in determining the gap voltage. A plot of minimum pressure versus length of gap for the TAC alternator, assuming helium gas in the gap, is presented in Figure 106 . This curve shows that ionization of the helium gas in the stator cavity will not occur for pressures greater than 66 psia regardless

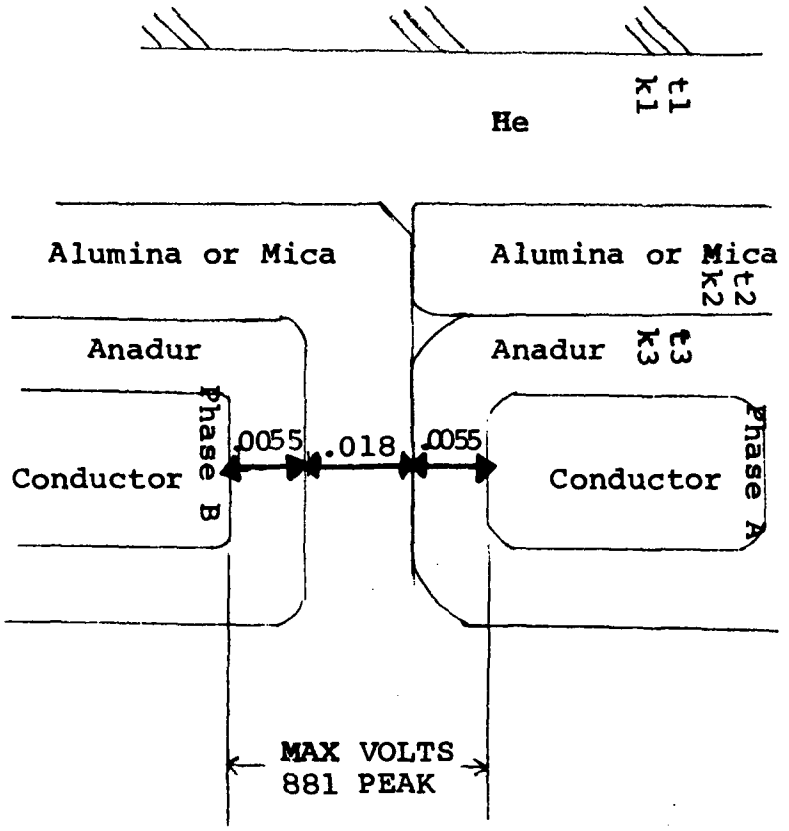
t1
k1
He
Alumina or Mica
Alumina or Mica
t2
k2
Anadur
Anadur
t3
k3
Phase B
.0055
.018
.0055
Phase A
Conductor
Conductor
MAX VOLTS
881 PEAK

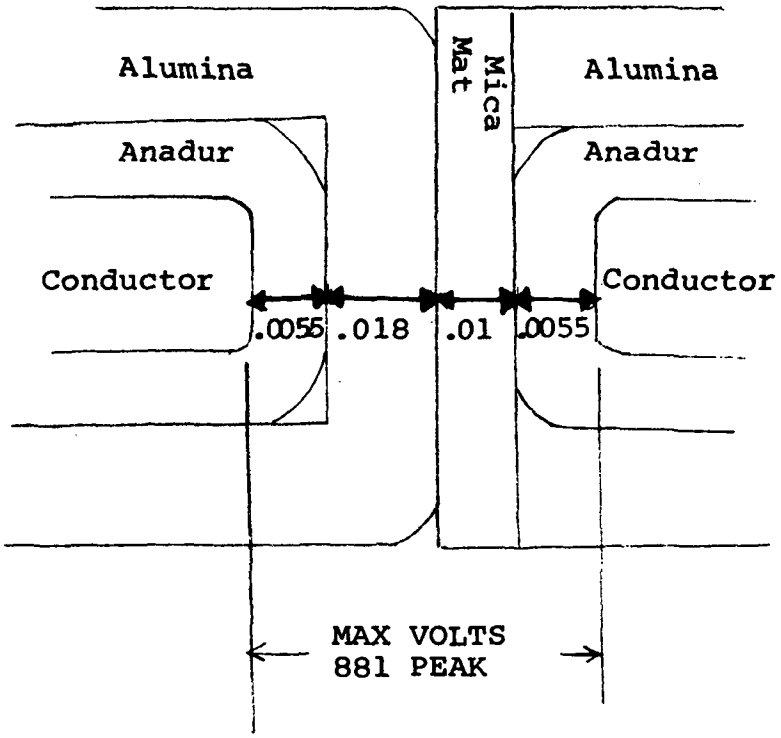
Alumina
Mica
Mat
Alumina
Anadur
Anadur
Conductor
Conductor
.0055
.018
.01
.0055
MAX VOLTS
881 PEAK

Figure 104

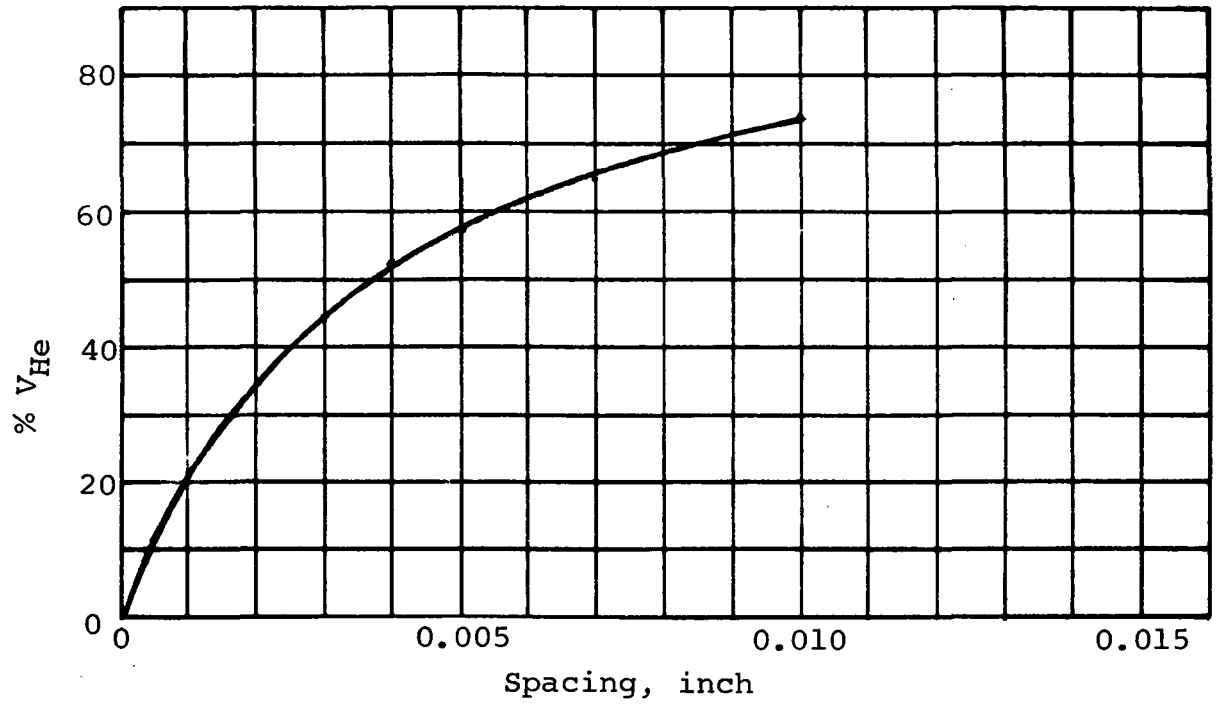

Figure 105

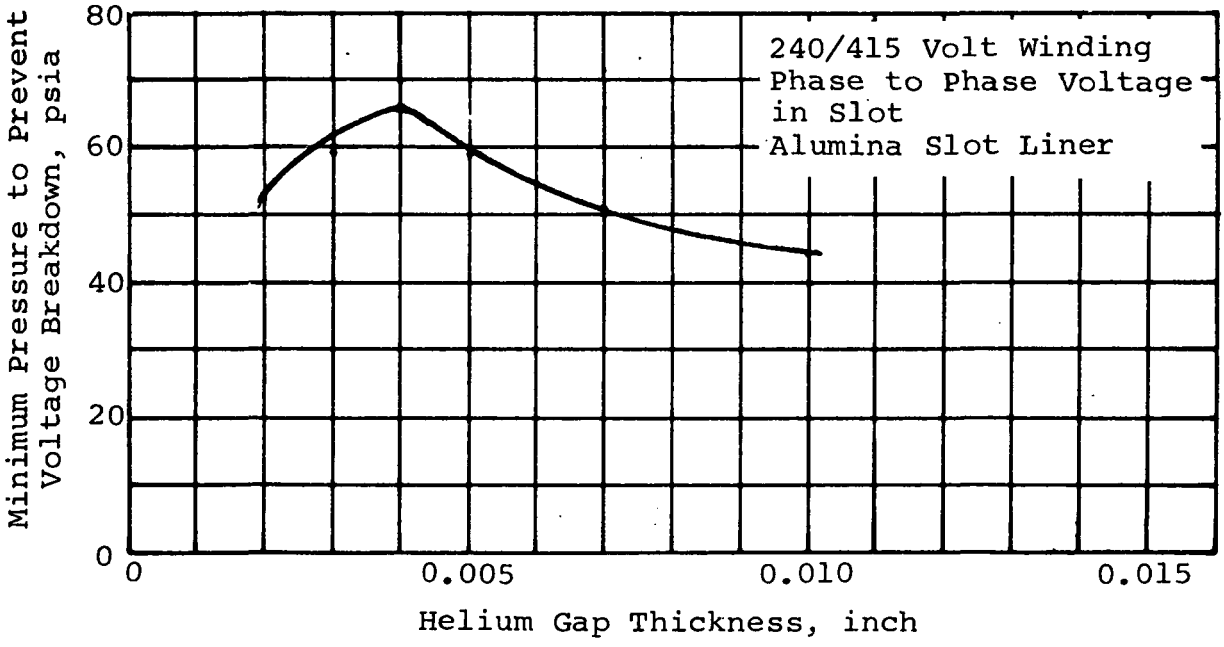

Figure 106

of the length of the gap (containing helium) in series with the Anadur and alumina insulation, assuming, of course, that the maximum expected winding voltage is not exceeded. The gap length at which ionization would occur is 0.004-inch from Figure 106 . The probability of this gap length occurring in the alternator is very high and therefore it can be concluded that stator cavity pressure must exceed 66 psia to prevent ionization of the gas mixture in the stator cavity for the insulation configuration and voltage described in Figure 104 .

Other conditions investigated are conductor to stack voltage in the slot, Figure 107 , phase to phase voltage in the slot with mica slot liners, Figure 104 , phase to phase voltage in the slot with alumina slot liner and 10 mil mica mat phase separator, Figure 104 , and 120/208 volt connected winding. Results are presented in Figure 108 .

The pressure in the stator cavity will decrease when system load is decreased. For this reason, it is recommended that the 120/208 alternator voltage be selected.

A voltage transient of 50% was assumed in the corona analysis. If actual systems voltage transients are less or if a gas with a better Paschen's characteristic is selected, the minimum pressure values given in Figure 98 would be lower. In any case, the minimum allowable stator cavity pressure should be determined by test under conditions selected for the final configuration. At present, however, a minimum cavity pressure of 16 psia is recommended.

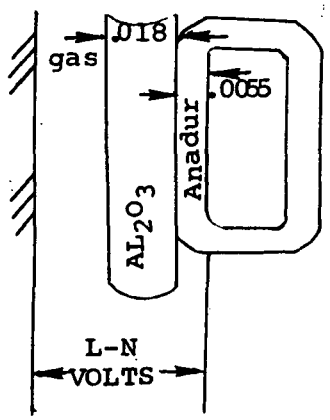

FIGURE 107

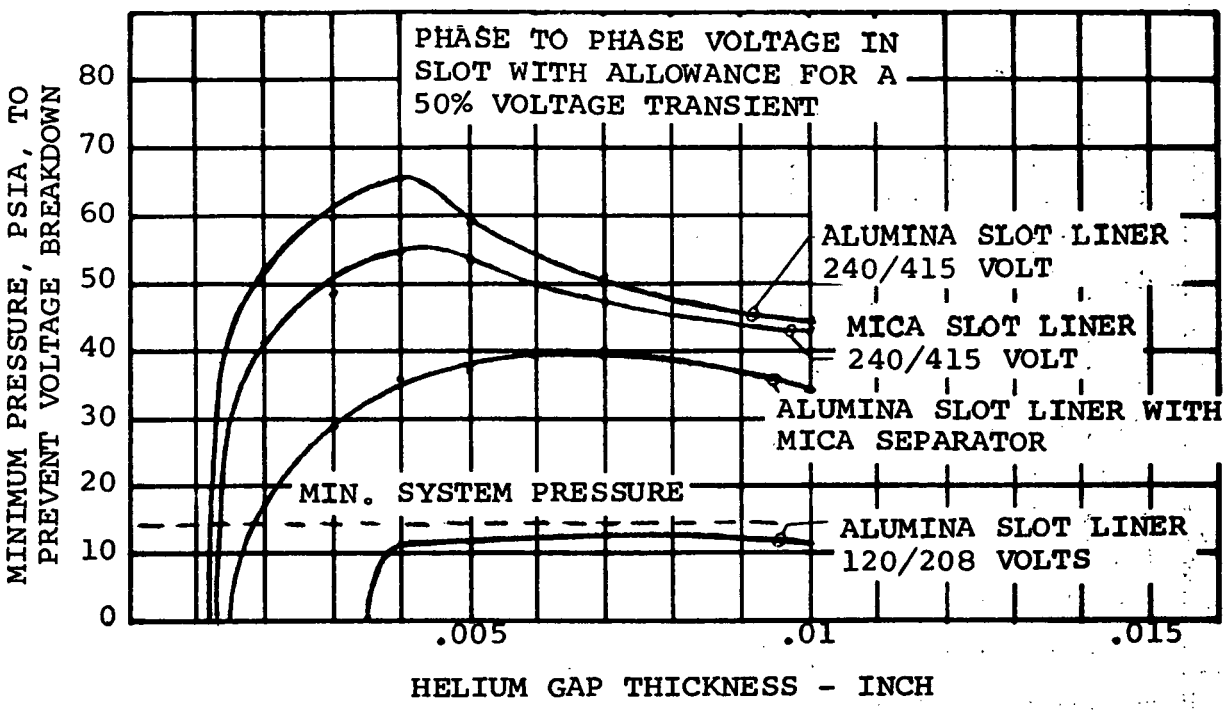

ALTERNATOR VOLTAGE WYE CONNECTED	MINIMUM ALLOWABLE PRESSURE TO PREVENT IONIZATION OF GAS, PSIA		
	PHASE TO PHASE IN SLOT	PHASE TO STACK IN SLOT	HELIUM GAP OF 29 MILS, NO INSULATION
240/415	40 (with Mica separator)	26	25
120/208	13	2	8
240 DELTA CONNECTED	13 (with Mica separator)	26	10

IONIZATION OF HELIUM IN TAC ALTERNATOR

Figure 108

G. Conclusions

Three alternator configurations were selected from results of the electromagnetic screening studies for consideration in the turbine-compressor-alternator final performance analyses. These are, the 24,000 rpm, 1200 Hz, 6 pole Lundell alternator (design C-4 of Table XXXVI), the 36,000 rpm, 1200 Hz, 4 pole Lundell alternator (design D-2 of Table XXXVI), and the 36,000 rpm, 1200 Hz, 4 pole inductor alternator (design I-6 of Table XXXVII) with evacuated stator cavity.

As a result of the corona considerations study for voltage selection, the recommended alternator voltage is 120 volts per phase with a minimum stator cavity pressure of 16 psia. It is recommended that corona testing be performed before the final stator configuration is selected. The effects of changing the alternator voltage from 240 volts per phase to 120 volts per phase for the 24,000 rpm Lundell alternator were insignificant as shown by comparing designs C-4 and C-5 of Table XXXVI; thus the subsequent analyses carried out on C-4 (see following sections) for example are applicable to the design eventually recommended for Phase III consideration, e.g., design C-5.

Relative to the 36,000 rpm Lundell design (D-2), the original concept utilized a central hole in the rotor, thereby requiring a high strength steel, e.g., H-11 or 4340 @ 49R_c. Late in the Phase I study it was recognized that it is also possible to assemble the TAC unit without a central hole in the alternator rotor, and a lower strength alloy could be used, e.g., 4340 @ 33 R_c. In that case, the D-3 design (Table XXXVII) is recommended over the D-2 design for subsequent Phase III consideration.

ROTOR DESIGN

A. Introduction

A distinct advantage offered by the Lundell alternator configuration is that it is feasible to construct a rotor which has smooth exterior surfaces. This feature produces acceptable windage losses even when the rotor is operated in the working fluid at compressor inlet pressure. Techniques for construction of a rotor with smooth exterior surfaces for the inductor alternator were considered also. However, this was considered a technically unsound solution to the windage problem associated with this type of rotor. A less sophisticated solution for the inductor alternator is offered by reduction of the pressure within the rotor cavity.

The solid Lundell rotor is formed by bonding a non-magnetic material to the magnetic material. Development effort has been focused upon various techniques for bonding of Inconel Alloy 718 to SAE 4340 steel. The preferred process consists of subjecting the materials to heat and pressure in an autoclave. A loose-fitting assembly of the magnetic parts and the non-magnetic filler alloy is hermetically canned to exclude the autoclave pressure from the interfaces. Compaction of the container and assembly is produced by gas pressure at an elevated temperature. The surfaces are forced into intimate micro-contact whereby thermally activated diffusion bonds are produced.

The time-temperature-pressure cycle is controlled to accelerate diffusion and to produce the proper heat treatment of the alloys. The diffusion bonding technique within an autoclave can be used to fabricate a rotor with a magnetic material other than SAE 4340.

The results of a magnetic material screening study for the Lundell alternator are summarized here.

B. Magnetic Material for Lundell Rotor

Table XL gives four magnetic materials, including 4340 steel, which are candidate for high speed rotors which operate at or below 700°F. The materials are listed in order of magnetic preference.

The smallest rotor and the highest efficiency are provided by the Hiperco 27 alloy. Smaller rotor diameters are obtained by virtue of the superior magnetic properties of this material; efficiency is higher by

TABLE XL

ROTOR MATERIALS

ALLOY	HEAT TREATMENT (NORMAL)	STRENGTH @ 700°F .2% Y.S.,	U.S.,	CONDITION
INCONEL 718 NON-MAGNETIC	Anneal @ 1925±25°F plus aging @1400°F/10hr,F.C. to 1200°F, Age @1200°F/10hr,A.C. OR Anneal @ 1825±25°F plus aging @1325°F/8 hr,F.C.to 1150°F, age @ 1150°/10 hr, A.C.	46.0 KSI, 154.0 KSI, SAME AS ABOVE	104.KSI, 181.KSI,	ANNEALED AGED
HIPERCO-27 T=700°F H=100 Oersteds B=22 Kilog	Cannot be strengthened by heat treatment	37.0	70.0	ANNEALED
4340 T=700°F RC=11 H=100 Oer. B=16 Kilog.	Anneal @ 1450-1550°F Hardening temperature 1500-1550°F Oil quench and temper to desired hardness	50.5 115.5	70.5 131.5	RC 11 RC 32
RC=32 H=100 Oer. B=16.3 Kilog.	RC=50 H=100 Oer. B=14.4 Kilog.			
H-11 RC45,T=700°F H=100 Oer. B=15 Kilog.	Heat to 1850±25°F, hold for 1 to 6 hr, follow by force air quench to R.T., two to three 1.5 hr tempers @ 1050 to 1150°F are used to bring hardness to RC 45	104. 150.	121 187	ANNEALED,RC33 RC 45
18%Ni Maraging T=700°F H=100 Oer. B=12.2 Kilog	Solution anneal @ 1500°F, Air cool to R.T., Age @ 900°F for 3 to 6 hrs	160.	172.	AGED TYPE(200)

virtue of lower excitation, pole face, and windage losses. In general, a Hiperco 27 Lundell alternator rotor has approximately 1.5 kw less loss than a design with an SAE 4340 rotor. Hiperco 27 alloy can only be strengthened during the forming process (work-hardening). Thus, a Hiperco 27 rotor which is fabricated in an autoclave at an elevated temperature can be expected to have a strength equal to that of the annealed alloy. Annealed investment castings of Hiperco 27 have a 0.2% yield strength of approximately 37,000 psi at 700°F.

From the standpoint of strength, these limitations and requirements are imposed upon a Hiperco rotor for a Lundell alternator:

(a) The strength of Hiperco 27 alloy is not adequate for a 36,000 rpm rotor.

(b) The strength of Hiperco 27 alloy is adequate for a 24,000 rpm rotor provided the rotor does not have a central hole.

(c) The diameter of the rotor is limited to 7.0 inches (stress intensity equals 35,200 psi at 20% over speed); electro-magnetic requirements of the alternator require a 6.9 inch diameter for the rotor.

(d) A high joint efficiency between the Hiperco 27 alloy and alloy 718 is required since the strength of one of the parent materials has imposed design limitations.

Since a Hiperco 27/Inconel 718 rotor offered only a small performance and weight advantage over a 4340/718 rotor, it would be economically and technologically unsound to recommend a Hiperco 27 rotor for the 24,000 rpm Lundell alternator.* This conclusion is supported by the fact that a rotor without a central hole requires a sophisticated turbine-alternator-compressor arrangement.

SAE 4340 steel offers good magnetic properties for the rotor. Direct current magnetization tests at 700°F for annealed material (R_c 11) and for normalized material (R_c 32) show the magnetic properties are not sensitive

---

* Or any higher strength material having magnetic properties as good since there is no apparent system advantage.

to the two hardnesses of the steel at the level of induction of interest for the TAC alternator.

Compaction and bonding of SAE 4340 and alloy 718 have been performed by subjecting this assembly to 29,000 psi for four hours at a temperature above 1650°F plus 10 hours at 29,000 psi and 1200°F. The pressure was then decreased and the assembly cooled simultaneously. This time-temperature cycle produced a Rockwell C hardness of 11 by virtue of the isothermal transformation from austenite to pearlite at 1200°F. With this hardness for SAE 4340 steel, the 0.2% Y.S. at 700°F becomes 60,000 psi, reference Figure 109 . The actual stress intensity around a one-inch central hole in a rotor (7-1/2 diameter at 28,800 rpm) is 81,000 psi. Thus, the strength of SAE 4340 at 700°F/R_c 11 is not adequate and the hardness must be increased to R_c 25 or greater.

The time-temperature cycle in the autoclave for the previous experiment was selected to produce annealed SAE 4340 steel and aged Inconel Alloy 718 - a 10-hour age was performed at 1200°F. A modification of the time-temperature cycle will prevent a transformation from austenite to pearlite during the aging period for the 718 alloy. A 10-hour age at 1375°F will produce adequate strength for the 718 alloy and allows the assembly to be cooled before transformation of SAE 4340 steel occurs. An isothermal transformation diagram for the SAE 4340 steel, Figure 110, indicates a transformation below 1000°F will produce an adequate hardness for the magnetic steel.

In general, a heat treatment cycle for a composite 4340/718 rotor for a 24,000 rpm alternator appears to be compatible for both materials. A greater hardness is required to strengthen the rotor for a 36,000 rpm alternator. The feasibility of heat treating the SAE 4340 steel in an autoclave for the 36,000 rpm alternator is questionable since a hardness of at least R_c 41 is required for designs having a central hole in the rotor.

From a magnetic standpoint, H-11 steel is an acceptable material for the rotor. However, it does not appear to be feasible to diffusion bond H-11 steel to alloy 718 in an autoclave and simultaneously heat treat the composite structure to an adequate strength for the 36,000 rpm

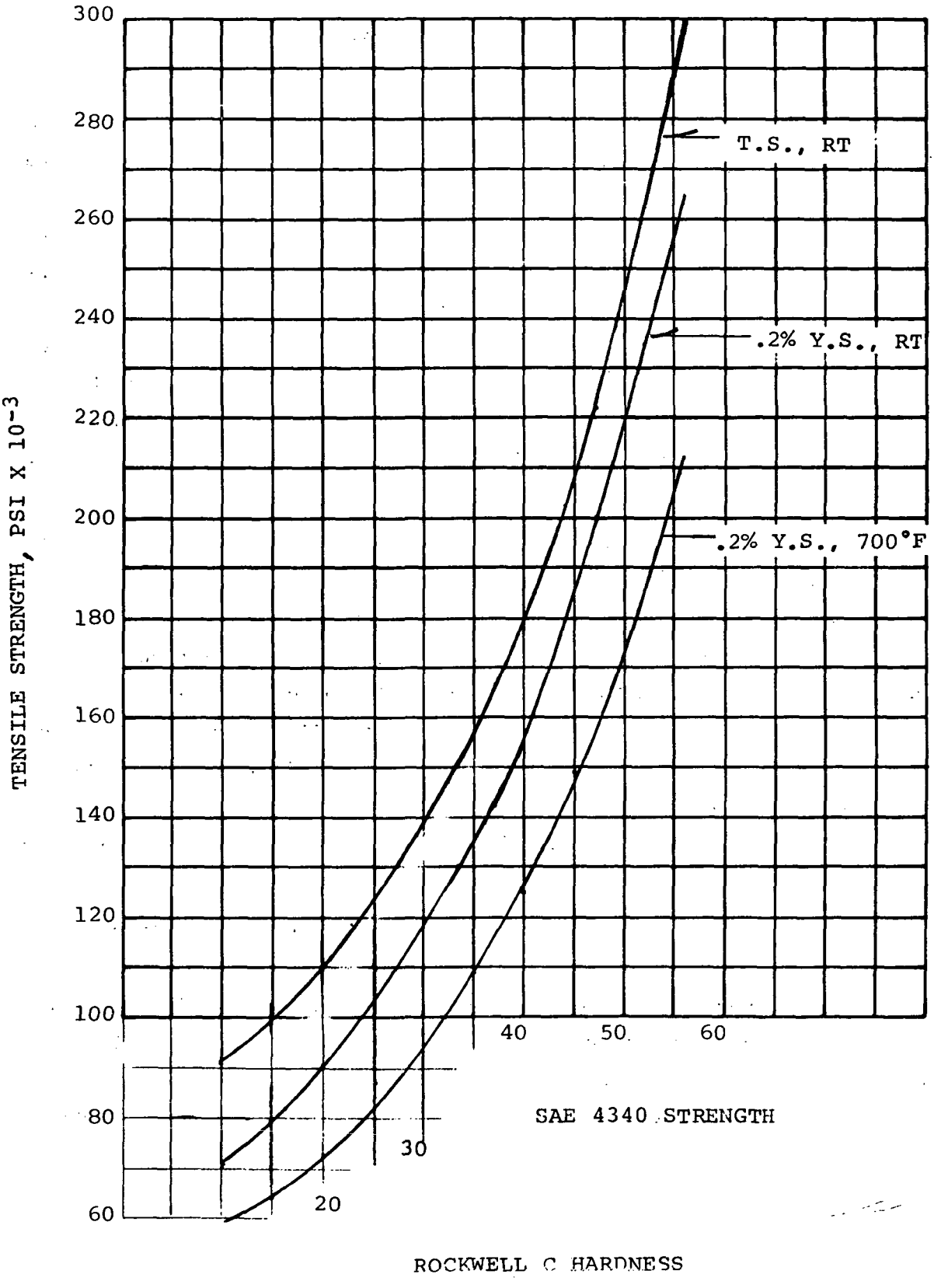
TENSILE STRENGTH, PSI X 10⁻³
300
280
260
240
220
200
180
160
140
120
100
80
60
T.S., RT
.2% Y.S., RT
.2% Y.S., 700°F
40
50
60
SAE 4340 STRENGTH
30
20
ROCKWELL C HARDNESS

Figure 109

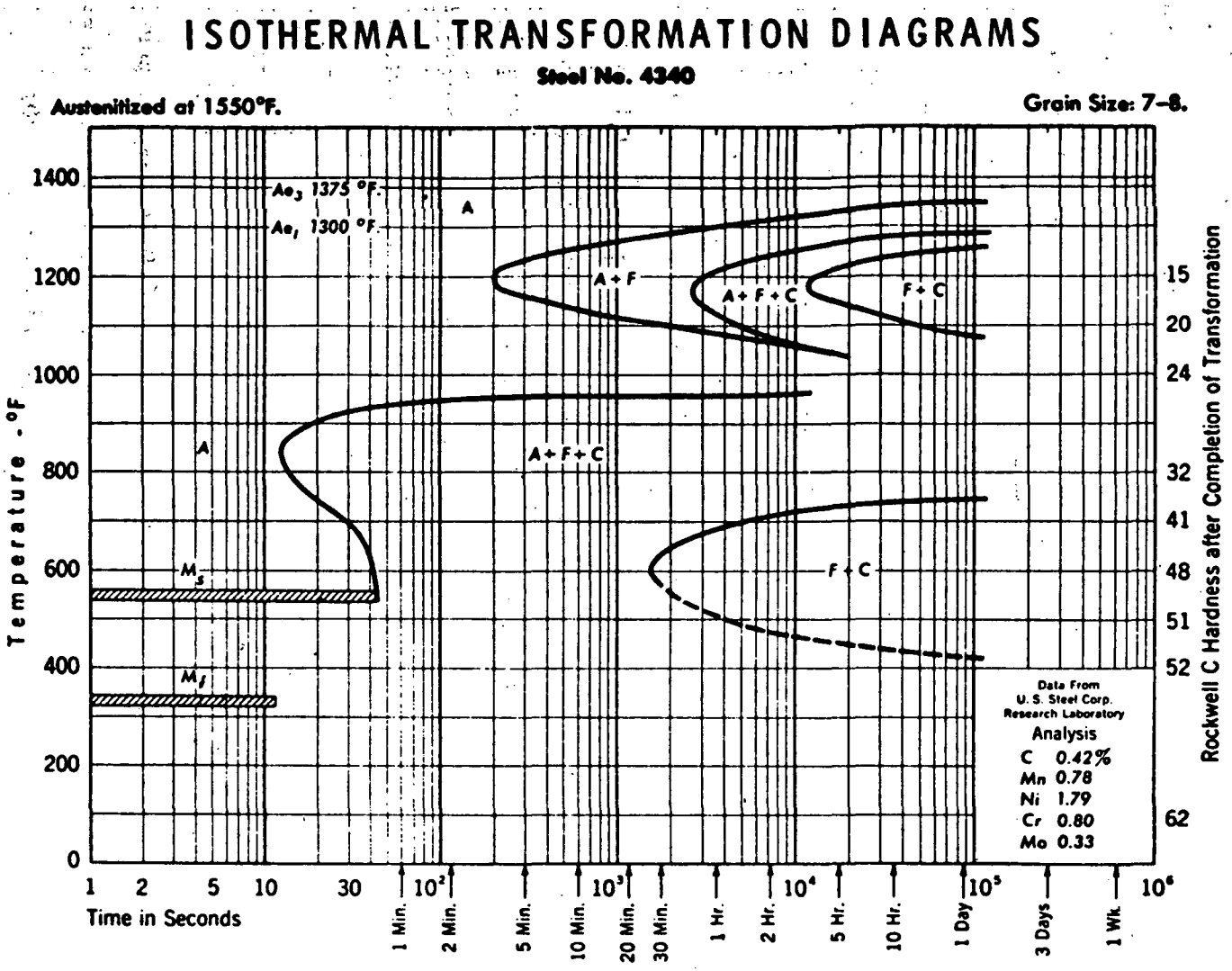
ISOTHERMAL TRANSFORMATION DIAGRAMS
Steel No. 4340
Austenitized at 1550°F.
Grain Size: 7–8.
Ae3 1375 °F.
Ae1 1300 °F.
A
A + F
A + F + C
F + C
A
A + F + C
F + C
Ms
Mf
Temperature - °F
1400
1200
1000
800
600
400
200
0
1 2 5 10 30 10² 10³ 10⁴ 10⁵ 10⁶
Time in Seconds
1 Min. 2 Min. 5 Min. 10 Min. 20 Min. 30 Min. 1 Hr. 2 Hr. 5 Hr. 10 Hr. 1 Day 3 Days 1 Wk.
15 20 24 32 41 48 51 52 62
Rockwell C Hardness after Completion of Transformation
Data From
U. S. Steel Corp.
Research Laboratory
Analysis
C 0.42%
Mn 0.78
Ni 1.79
Cr 0.80
Mo 0.33

Figure 110

alternator. The isothermal transformation diagram for H-11 steel, Figure 111, an aging diagram for alloy 718, Figure 112, show that transformation of the H-11 steel occurs when alloy 718 is aged for strengthening. Since full strengthening of both materials is required for the 36,000 rpm Lundell alternator, it becomes technologically unsound to use H-11 steel for that alternator.

Additional studies also showed that the annealed strength of H-11 steel, Figure 113, for an H-11/718 rotor (8.0 inch diameter) would not be adequate for even the 24,000 rpm Lundell alternator.

Further evaluations showed that 18 percent Ni maraging steel and alloy 718 have a compatible heat treatment cycle. For this case, alloy 718 would be aged at 1375°F where the 18 percent Ni maraging steel is in an austenite phase. On cooling, the steel changes to martensite at about 310°F. The assembly would then be reheated to 900°F for aging of the 18 percent Ni maraging steel. During the maraging treatment, the martensite would be strengthened by precipitation and an ordering reaction and alloy 718 would not be altered.

The magnetic properties of 18 percent Ni maraging steel in the range of interest are inferior to hardened SAE 4340 steel and H-11 steel. The relative diameters of rotors using these materials are 8.9 inches (18 percent Ni) and 8.0 inches (fully hardened 4340) for the 24,000 rpm alternator and 8.22 inches (18 percent Ni) and 7.12 inches (fully hardened 4340) for the 36,000 rpm alternator. The strength of the composite rotor is adequate for the 24,000 rpm Lundell alternator. However, the strength of alloy 718 in the composite rotor for the 36,000 rpm alternator is not adequate. Thus, the use of 18 percent Ni maraging steel offers no

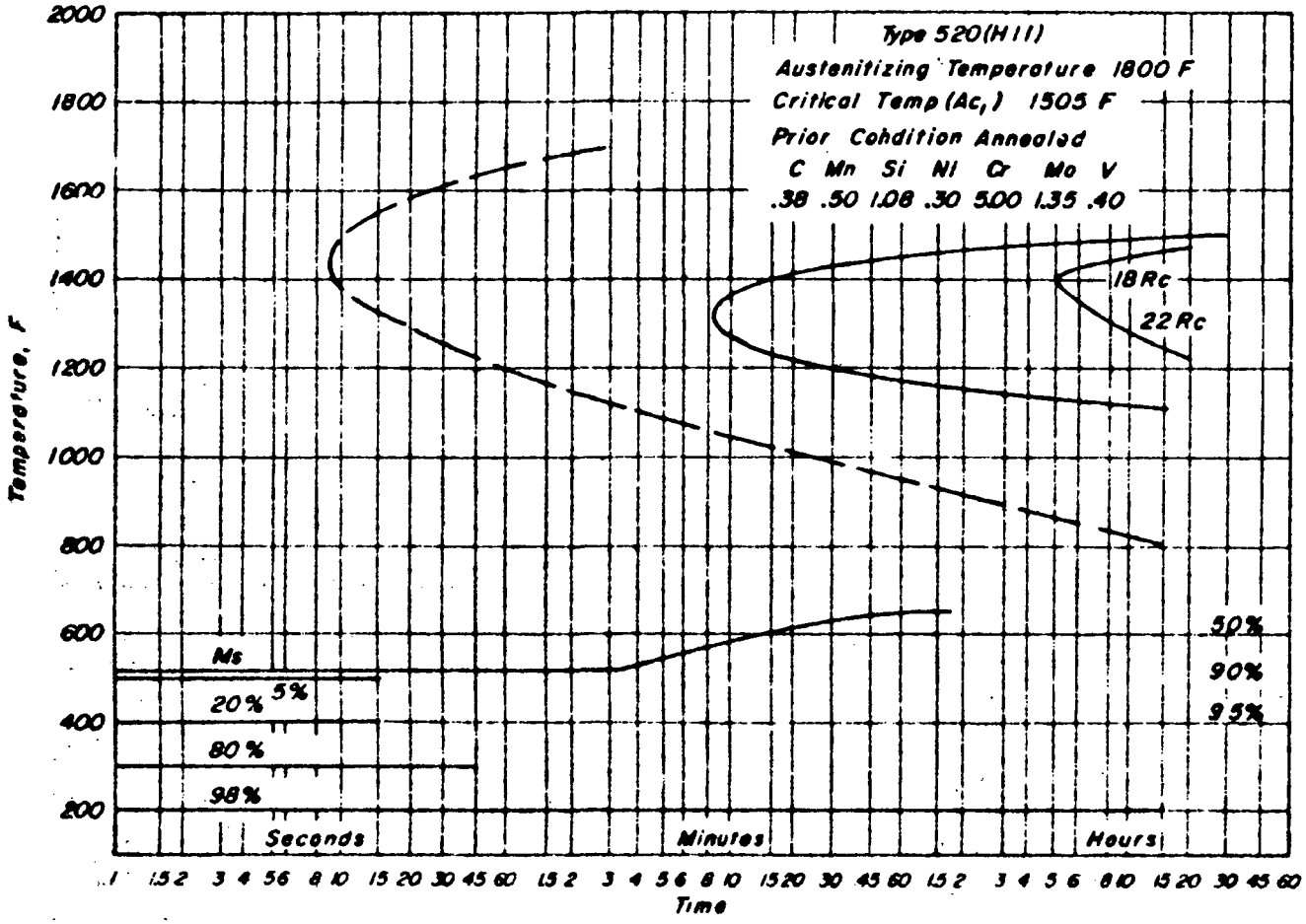

ISOTHERMAL TRANSFORMATION DIAGRAM H-11 STEEL

Figure 111

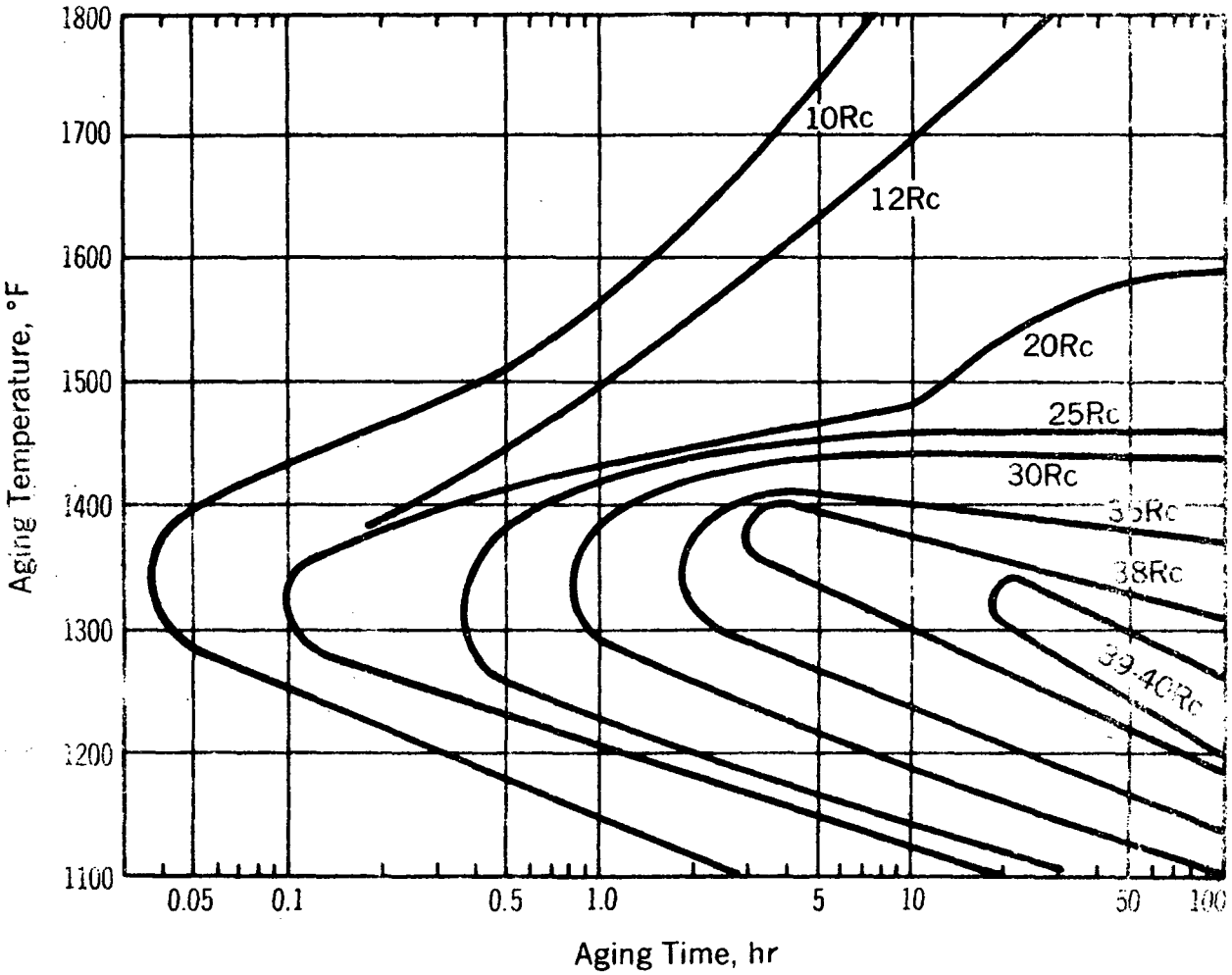

HARDNESS OF ANNEALED ALLOY 718
FOR VARIOUS AGING CONDITIONS

Figure 112

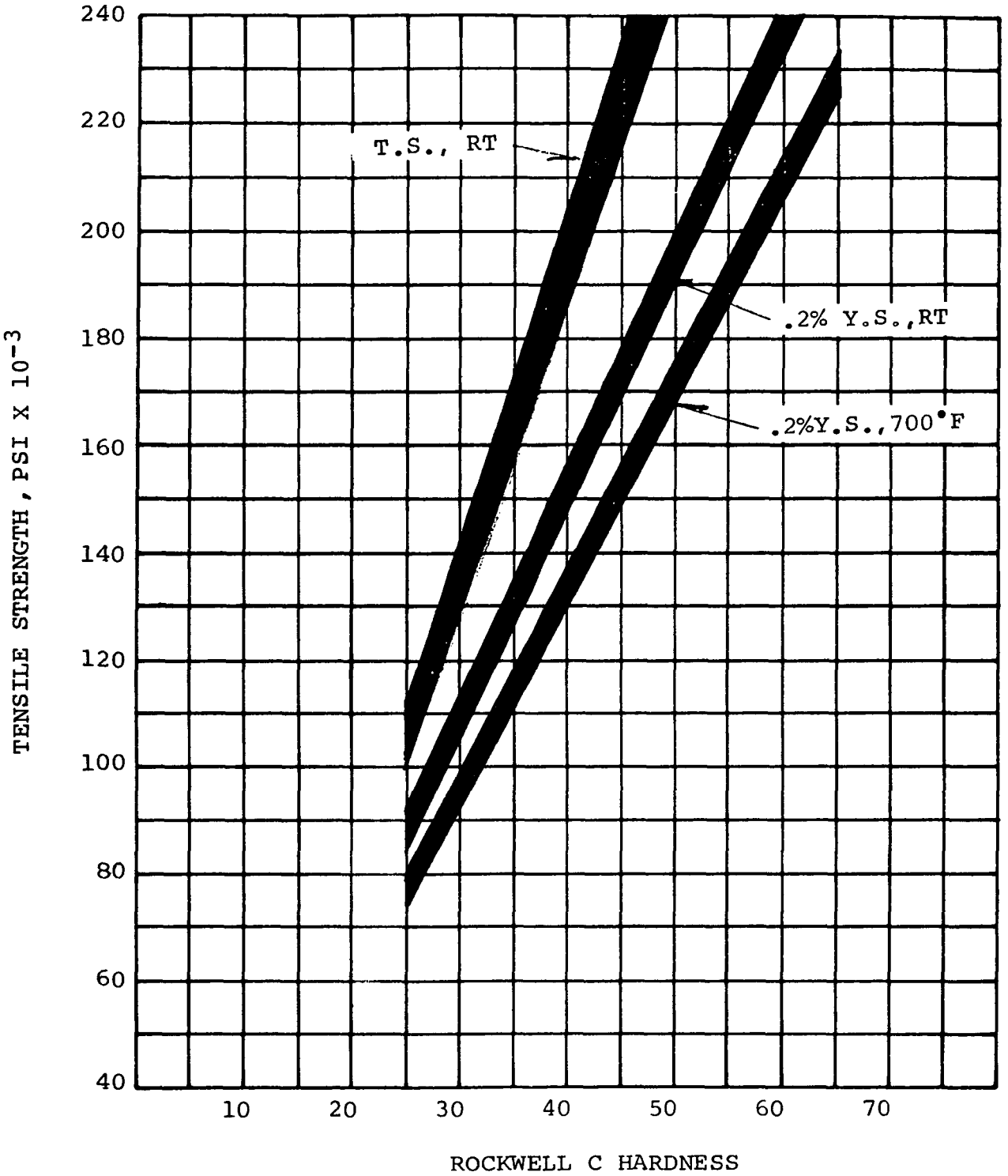

H-11 STEEL STRENGTH

Figure 113

advantages for the 36,000 rpm Lundell alternator. The only advantage 18 percent Ni maraging steel offers over SAE 4340 steel for the 24,000 rpm Lundell alternator is a less sophisticated heat treatment cycle of the alloys in the autoclave.

The preferred composite construction for the Lundell rotors is SAE 4340 steel pressure diffusion bonded to alloy 718 in an autoclave cycle. Both of these alloys must be strengthened during the bonding process to satisfy the specific requirements for the TAC alternators. To accomplish this, alloy 718 must be age-hardened at a temperature which prevents the SAE 4340 steel from transforming from the austenite phase to the pearlite phase. A transformation temperature of approximately 1000°F is required to strengthen the steel for the 24,000 rpm alternator. The strength of alloy 718 as a function of hardness is given in Figure 119.

The feasibility of heat treating the SAE 4340 steel in an autoclave for the 36,000 rpm rotor can probably only be clarified by experiments since a hardness of at least R_c 41 is required for this alternator.

The critical crack size at the bore of the rotors was investigated using fracture toughness data corresponding to R_c 48. The calculated minimum critical defect size (0.1 x 0.5 inches) can be readily detected by non-destructive inspection techniques. Thus, fracture of the rotors due to defects does not appear to be a problem.

C. Rotor Design Summaries

The maximum stress intensity within a Lundell rotor occurs around the central hole at the center of the rotor. Judgement of the integrity of the rotor was based upon the criterion that the maximum stress intensity must be less than the 0.2 percent yield strength of the materials. A safety factor is introduced by using the stress associated with a 20 percent overspeed condition provided the tensile strength of the joint between the magnetic and non-magnetic material is greater than the yield strength of the parent materials. Tensile tests of diffusion-bonded SAE 4340 and alloy 718 demonstrate that the strength of the joint approaches the ultimate strength of the 4340 steel. If this characteristic continues when the 4340 steel is strengthened for the specific requirements of TAC, the criterion for judgement of the integrity of the rotors will have been

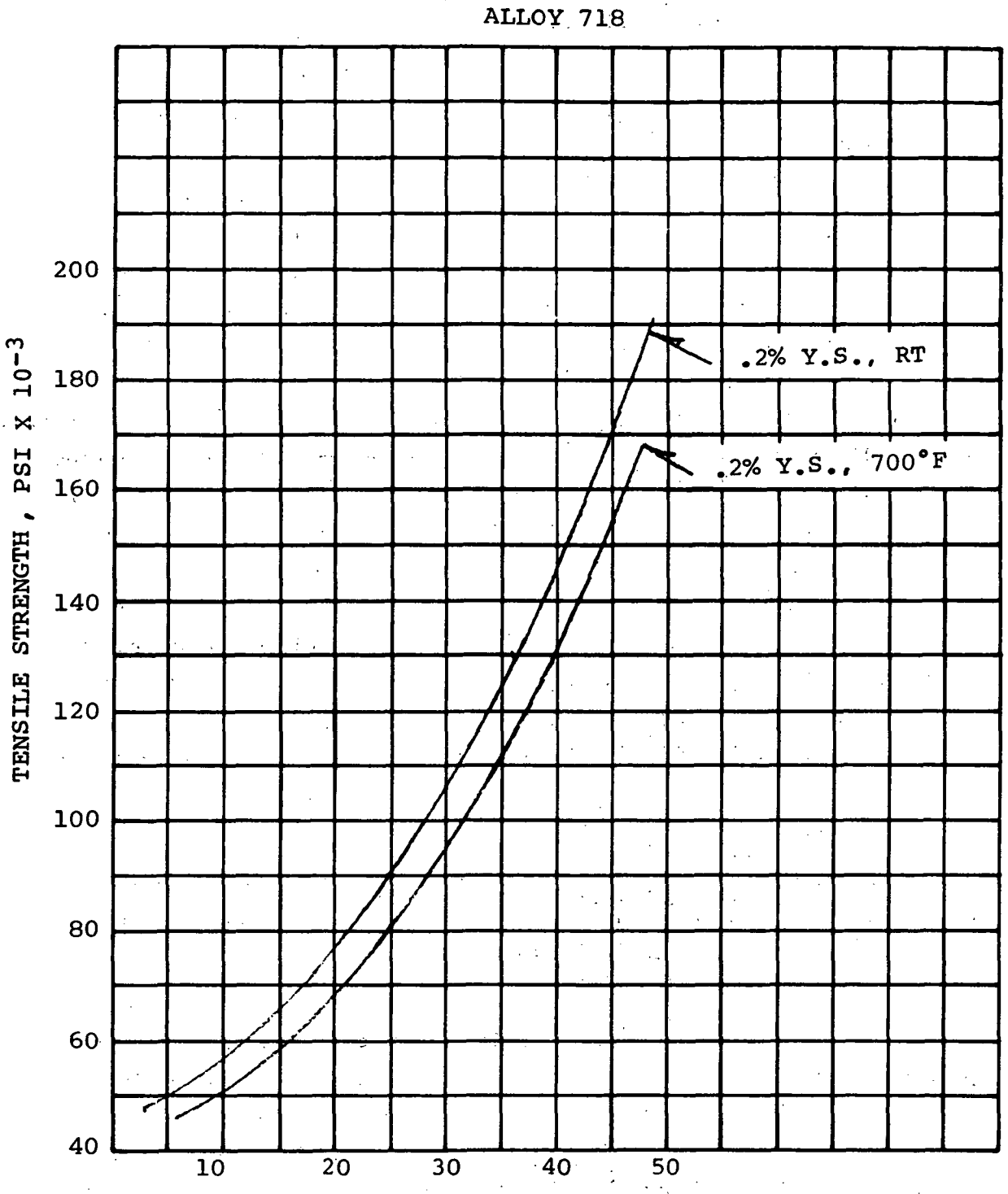

ALLOY 718 STRENGTH

Figure 114

conservative. If the strength of the joint does not increase when the strength of the 4340 steel is increased, the criterion for judgement of the integrity of the rotor will have been incorrect. This point can only be clarified by tests.

Table XLI gives a summary of the stresses within the 24,000 rpm Lundell alternator. The 0.2 percent yield strength for SAE 4340 steel at a hardness of R_c 32 was used for judgement of this design. The maximum stress intensity (81,000 psi) in the rotor(at 20 percent overspeed) is 73.5 percent of the yield strength of SAE 4340 at this hardness. Therefore, a lower hardness, approximately R_c 25, would be acceptable for this design. However, the latter design would have little design conservatism. Figure 115 shows the tangential stress profile for the 7.500 inch diameter cylinder. The high stress intensities are concentrated around the central hole and attenuation of the stress is rapid. This stress profile will change if the rotor is operated at 24,000 rpm plus 20 percent by virtue of the plastic strain (creep) which will occur around the central hole. Figure 116 gives the creep strain of the SAE 4340 steel as a function of time, temperature, and stress. Very little creep strain occurs in the rotor at the normal operating speed of 24,000 ± 1% rpm. For this case, the maximum stress intensity at the bore is 57,500 psi and the temperature of the material is about 700°F. Thus, the creep strain will be less than 0.001 percent.

Table XLII gives a summary of the stresses within a 36,000 rpm, 6.35 diameter, Lundell rotor. Similarly, Table XLIII gives a summary of the stresses within a 7.125 diameter rotor. The tangential stress profiles for these rotors are given in Figure 117 and Figure 118, respectively.

The rotor dimensions for the smaller rotor were based upon magnetic properties for R_c 32 steel. However, a hardness of at least R_c 41 is required for this rotor, but the magnetic properties at this hardness and at 700°F are not available. Therefore, the magnetic properties for R_c 32 were used, based upon the assumption that the magnetic performance of the steel is not significantly altered when the hardness is increased to R_c 41. This point can only be clarified by magnetic tests. Table XLII gives the dimensions and stresses for the 36,000 rpm alternator based upon magnetic properties for R_c 48 at 700°F. The inferior magnetic

TABLE XLI

24000 RPM LUNDELL ROTOR

MATERIALS	HARDNESS	700°F .2%Y.S.	700°F T.S.
SAE 4340	RC 32	110,000 psi	130,000 psi
INCONEL 718	RC 38	125,000 psi	150,000 psi

STRESS INTENSITIES	STRESS @ $\frac{\sigma}{\text{Y.S.}}$ 24000 RPM, Y.S.	STRESS @ $\frac{\sigma}{\text{Y.S.}}$ 24000 + 20% RPM, Y.S.
7.500" DIA. CYLINDER		
CENTRAL HOLE	56,350 psi, 51%	81,000, 73.5%
AVERAGE	26,110 psi, 24%	37,600, 34%
6.000" DIA CYLINDER		
CENTRAL HOLE	34,552 psi, 31.3%	49,750 psi, 45%
AVERAGE	16,577 psi, 15%	23,850 psi, 21%

MAX JOINT STRESS = 81,000 psi

REQUIRED JOINT EFFICIENCY= 63% (BASED UPON THE TENSILE STRENGTH OF PARENT MATERIALS)

CREEP STRAIN AT BORE 0.001% IN FIVE YEARS.

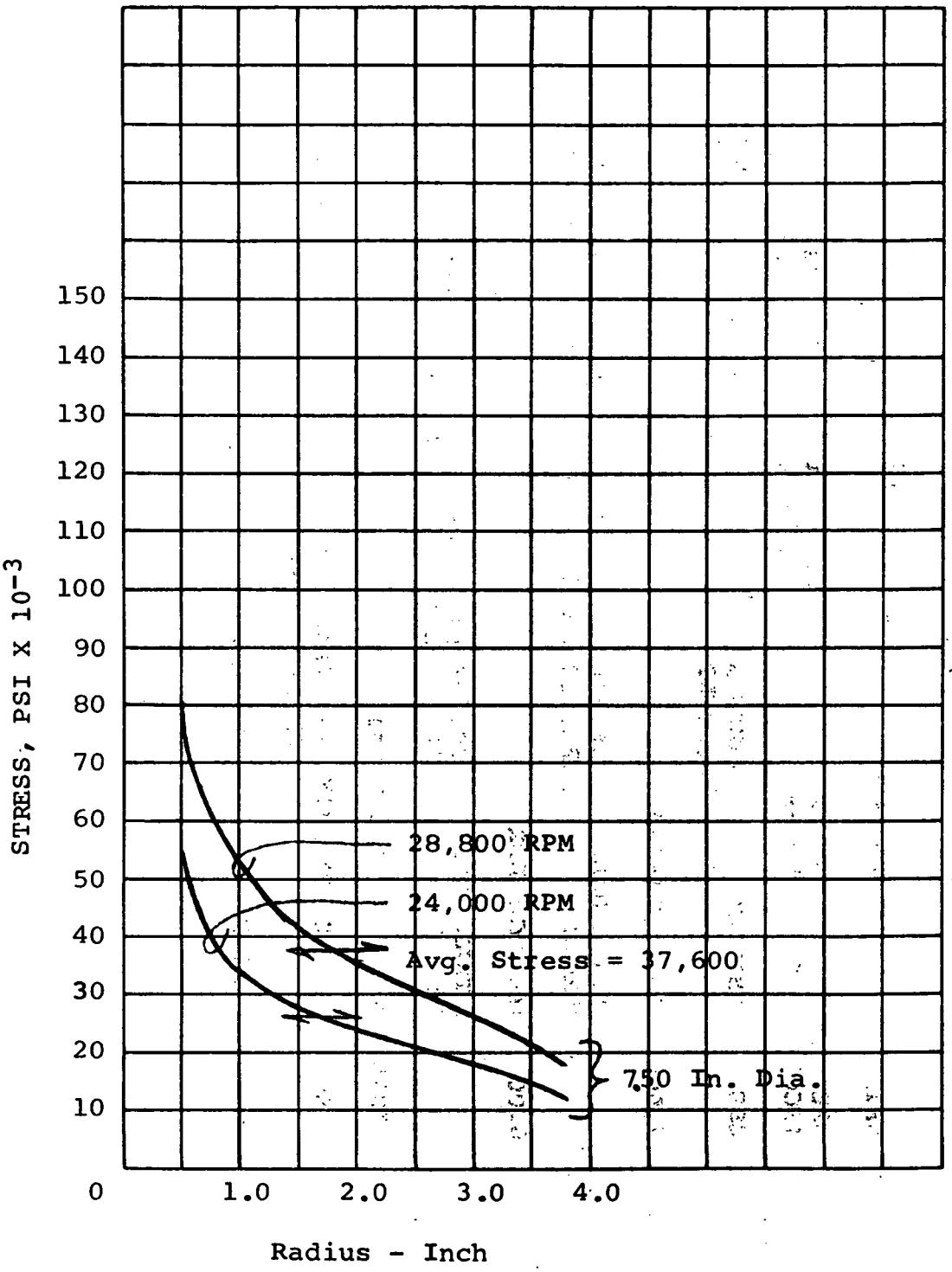

24,000 RPM LUNDELL STRESS

Figure 115

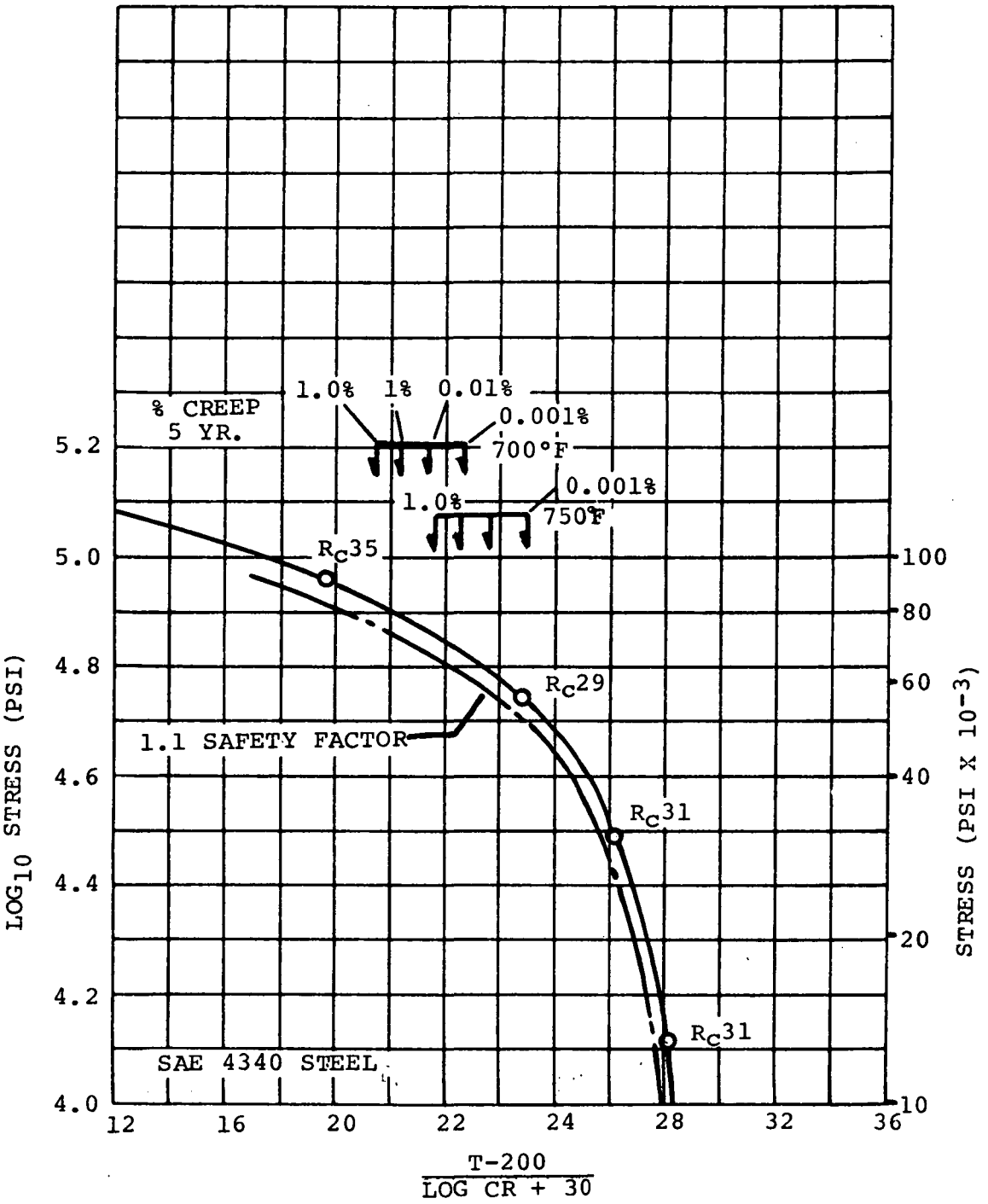

MANSON-HAFERD PARAMETER PLOT OF CREEP RATE VERSUS STRESS
CR = CREEP RATE, ΔL/L/HR., T = TEMP., °F

Figure 116

TABLE XLII

36000 RPM LUNDELL ROTOR

MATERIALS	HARDNESS	700°F .2% Y.S.	700°F T.S.
SAE 4340	Rc41	130,000 psi	150,000 psi
INCONEL 718	Rc40	130,000 psi	170,000 psi

STRESS INTENSITIES	STRESS @ 36000 RPM,	$\frac{\sigma}{\text{Y.S.}}$	STRESS @ 36000 + 20%,	$\frac{\sigma}{\text{Y.S.}}$
6.35" DIA. CYLINDER CENTRAL HOLE	91020	70.0%	131,000	101.%
AVERAGE	43252	33.7%	62,300	48.0%
6.000" DIA CYLINDER CENTRAL HOLE	78292	60.1%	112,600	86.6%
AVERAGE	37563	28.8%	54,250	41.6%

MAX. JOINT STRESS = 131,000

REQUIRED JOINT EFFICIENCY = 87.2% (BASED UPON THE TENSILE STRENGTH OF THE PARENT MATERIALS)

CREEP STRAIN AT BORE = 4.4% to 0.5% IN 10,000 HR AT 700°F.

TABLE XLIII

36000 RPM LUNDELL ROTOR

MATERIALS	HARDNESS	700°F .2% Y.S.	700°F T.S.
SAE 4340	Rc48	165,000 psi	180,000 psi
INCONEL 718	Rc42 (FULLY AGED)	140,000 psi	180,000 psi

STRESS INTENSITIES	STRESS @ 36,000RPM	σ Y.S.	STRESS @ 36,000 + 20%,	σ Y.S.
7.125" DIA. CYLINDER				
CENTRAL HOLE	114,470,	81.5%	165,000	117%
AVERAGE	53,429,	38.1%	77,000	49.6%
6.000" DIA. CYLINDER				
CENTRAL HOLE	78,567,	55.3%	113,100	84.5%
AVERAGE	37,694,	26.9%	54,250	36.0%

MAX. JOINT STRESS = 165,000 psi

REQUIRED JOINT EFFICIENCY = 91.5%(BASED UPON THE TENSILE STRENGTH OF THE PARENT MATERIALS)

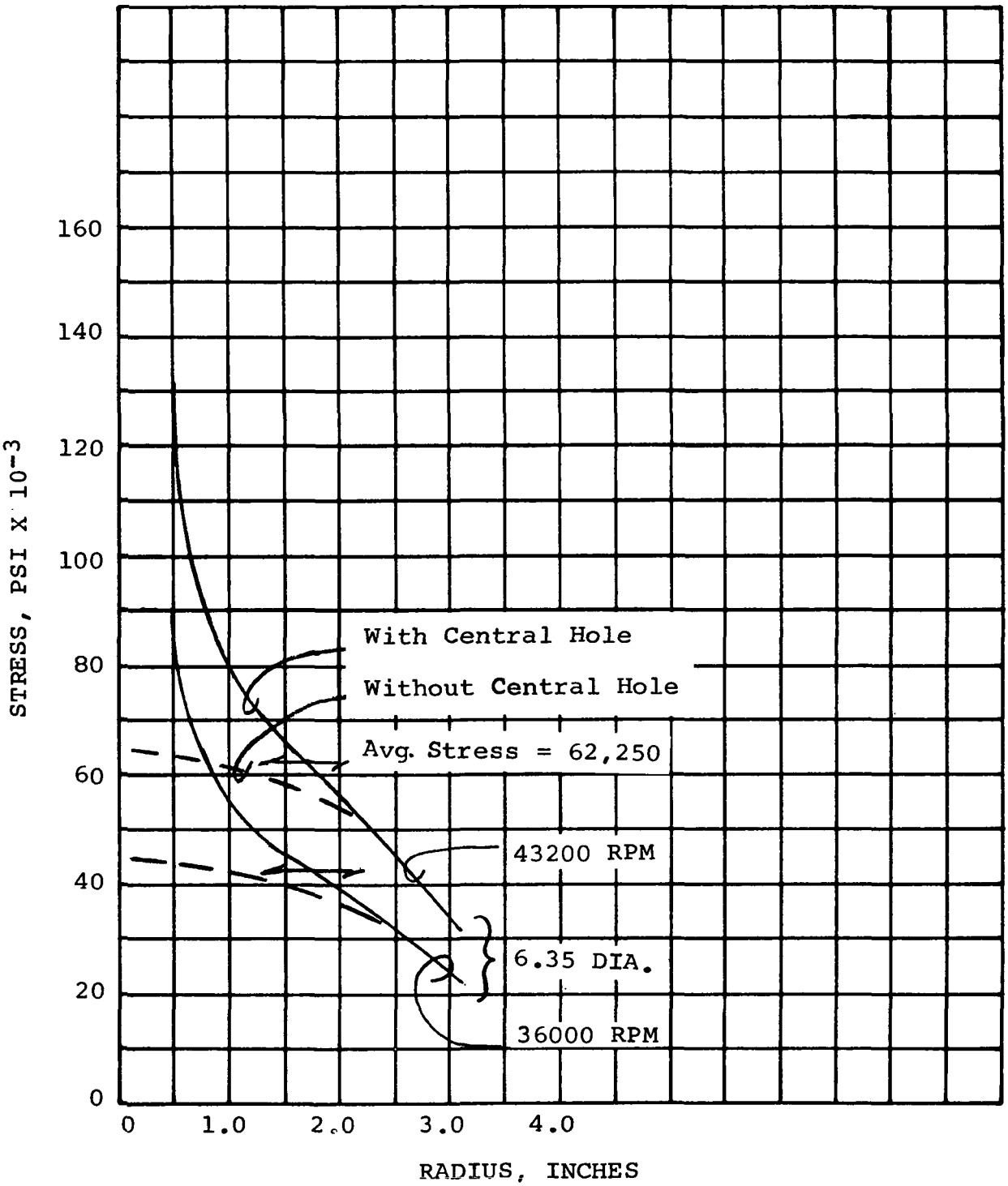

36000 RPM LUNDELL ROTOR

Figure 117

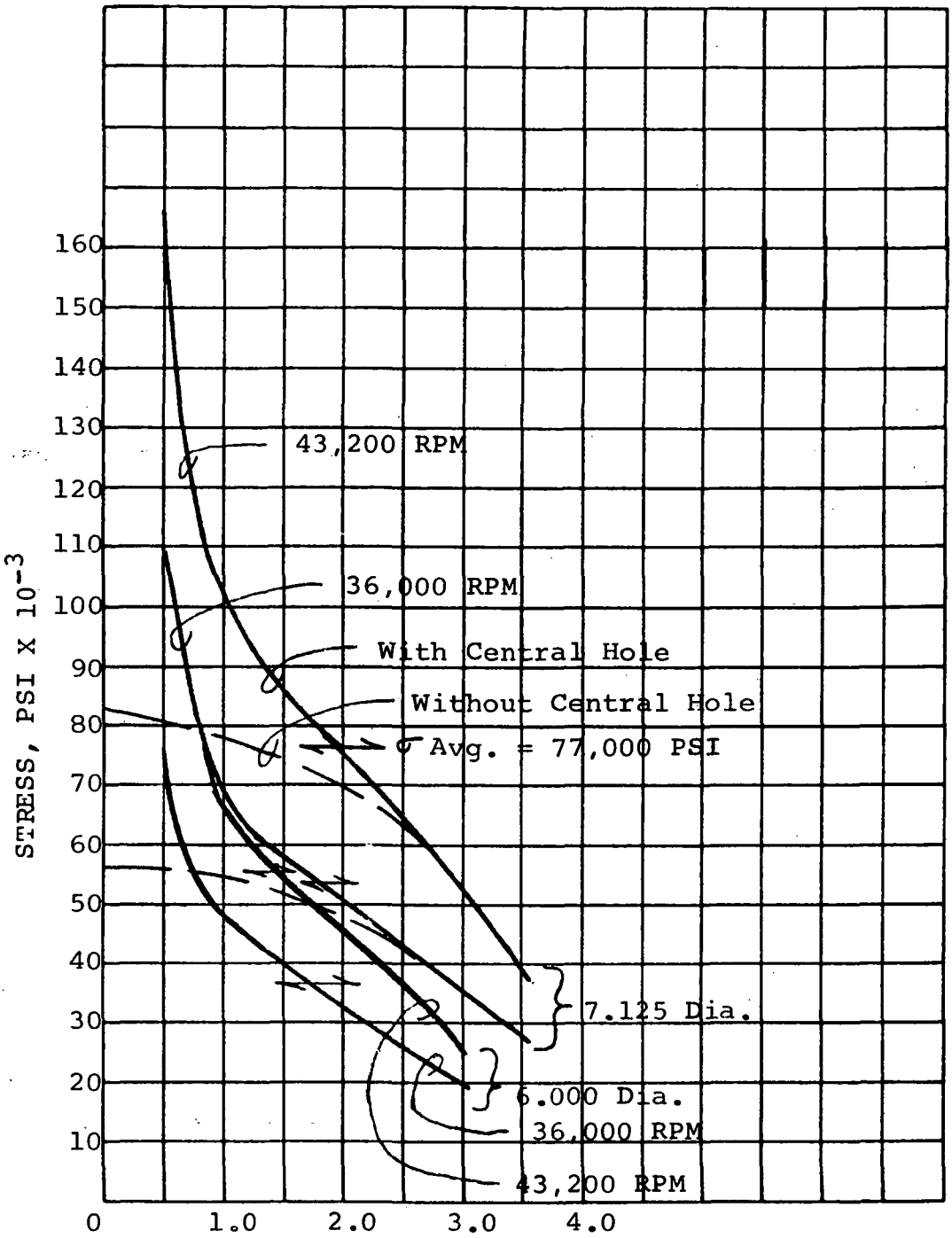

36,000 RPM LUNDELL ROTOR

Figure 118

properties at this hardness, relative to a hardness of R_C 32, increased the rotor diameter from 6.35 inches to 7.125 inches. With this diameter, the strength of alloy 718 is not adequate for the design since the stress factor for the central hole is 117 percent at 20 percent overspeed. Therefore, this design must be considered unacceptable. This conclusion is supported by the fact that a hardness of R_C 48 for SAE 4340 steel cannot be maintained for long term operation in a 700°F environment.

The integrity of the 6.35 inch diameter rotor is open to question since the magnetic property data at the required hardness is not available. However, it is logical to conclude that the magnetic properties at the required hardness will not be as good as the data which was used for the design calculations. Therefore, it is concluded that the design is marginal since the bore stress at 20 percent overspeed is approximately equal to the 0.2 percent yield strength of the materials.

In general, it appears the 36,000 rpm Lundell rotors are unsatisfactory unless the rotor can be constructed without a central hole. If the central hole is eliminated, a conservative 36,000 rpm rotor can be designed for the TAC alternator. Table XLIV gives a summary of the stresses for the 36,000 rpm, 6.35 inch diameter rotor without a central hole. Without the central hole, the hardness required for the 4340 steel decreases from R_C 41 to R_C 32. The maximum stress becomes 65,500 psi which is approximately 60 percent of the 0.2 percent yield strength of the SAE 4340 steel.

Table XLV gives a summary of important stress intensities and Figure 119 is an isostress plot of the equivalent stress for the 36,000 rpm inductor alternator. With a central hole, the stress intensities within the rotor are excessive. Without a central hole, the stress intensities are acceptable for 3-year operation. The maximum stress, 133,500 psi, occurs at the center at 20 percent overspeed. At this point, the stress is 92.4 percent of the 0.2 percent yield strength of the material. The creep strain for 3 years operation, at 96,300 psi (stress at center of rotor at 36,000 rpm) and 700°F is 0.1 percent. Thus, five years of operation, as required for the TAC alternator, at 96,300 psi/700°F will produce a creep strain in excess of 0.1 percent.

TABEL XLIV

36000 RPM LUNDELL ROTOR WITHOUT CENTRAL HOLE

MATERIALS	HARDNESS	700°F 0.2% Y.S.	700°F T.S.
SAE 4340	RC32	110,000 psi	130,000 psi
INCONEL 718	RC38	125,000 psi	150,000 psi

STRESS INTENSITIES	STRESS @ 36000 RPM,	$\frac{\sigma}{\text{Y.S.}}$	STRESS @ 48200 RPM,	$\frac{\sigma}{\text{Y.S.}}$
6.350" DIA. CYLINDER				
MAX STRESS	45500	41.3%	65500	59.5%
AVERAGE STRESS	36500	33.2%	52500	47.7%
6.000" DIA. CYLINDER				
MAX STRESS	39150	35.6%	56400	51.2%
AVERAGE STRESS	31200	28.4%	45000	40.9%

MAX. JOINT STRESS = 65500 psi

REQUIRED JOINT EFFICIENCY = 50.5% (BASED UPON TENSILE STRENGTH OF PARENT MATERIALS)

CREEP STRAIN AT CENTER OF ROTOR = 0.001% IN 5 YEARS @ 36000 RPM, 700°F

TABLE XLV

36000 RPM INDUCTOR STRESS INTENSITIES

Material:	Hardness:	.2% Y.S. @700°F	T.S. @700°F
H-11 Steel	Rc45	150,000 psi	187,000

	36000 RPM	36000 + 20%	36000 + 20% WITHOUT HOLE	$\frac{\sigma}{\text{Y.S.}}$
Pole Root Stress	58075 psi	83500 psi	83500 psi	
Average Stress Mid Way Between Poles	90591	130300	120600,	80.5%
Average Stress Around Central Hole	142920	206000	N.A.	
Stress at Center Hole Mid Way Between Poles, Elastic Solution	283890	409000	138500,	92.4%
Total Equivalent Elastic Strain	1.37%	1.98%		

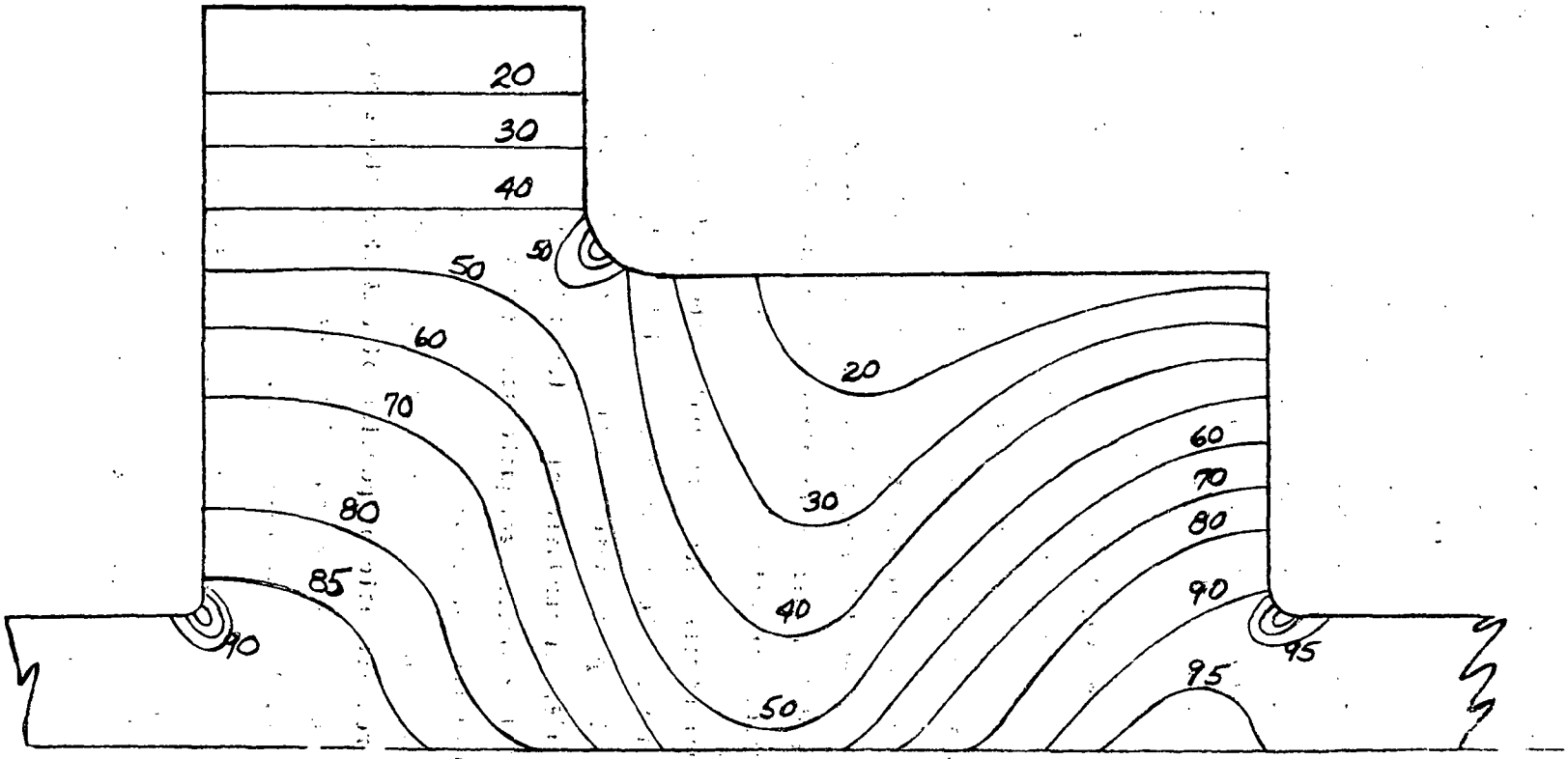

BRAYTON TAC 36,000 RPM

NO CENTRAL HOLE

Figure 119

D. Conclusions

1. The preferred materials for the Lundell rotor are SAE 4340 and alloy 718. This combination of materials can be bonded in an autoclave. Compaction of a loose-fitting assembly is produced by gas pressure at an elevated temperature and thermally activated diffusion bonds are produced.

2. The time-temperature-pressure cycle in the autoclave, which has been developed for bonding rotors with lesser strength requirements, should be modified to produce a higher strength SAE 4340 alloy. (See items 3, 4, and 6 below.) This can be accomplished by aging alloy 718 at a temperature which prevents transformation of the 4340 steel from Austenite to pearlite. The assembly should then be cooled from the aging temperature before transformation occurs to obtain an adequate hardness and strength for the TAC application.

3. The maximum stress intensity within the 24,000 rpm Lundell rotor will be 81,000 psi at 20% overspeed. A hardness between R_c 25 and R_c 32 in the SAE 4340 steel is required to obtain adequate strength for the overspeed condition.

4. The maximum stress intensity within the 36,000 rpm Lundel rotor with a central hole at 20% overspeed is 131,000 psi. This stress intensity is approximately equal to the 0.2% field strength of alloy 718 at 700°F. A hardness of at least R_c 41 in the SAE 4340 steel is required to obtain adequate strength for this overspeed condition. Experiments are necessary to determine whether a hardness of R_c 41 can be produced by a time-temperature cycle within an autoclave. Furthermore, magnetic properties of SAE 4340 steel at R_c 41 and 700°F are needed before positive conclusions can be made relative to the feasibility of this design.

5. A conservative 36,000 rpm Lundell rotor design is obtained by elimination of the central hole. It must be recognized that this design requires a sophisticated turbine-generator-compressor coupling arrangement.

6. The strength of the joint between the SAE 4340 steel and alloy 718 must be greater than the 0.2% yield strength of the parent materials.

7. The stress intensities within the 36,000 rpm inductor rotor with a central hole are excessive. A rotor without a central hole is marginal from the standpoint of strength.

WINDAGE LOSS

A. Introduction

Windage losses are a significant portion of the combined losses within the alternator. Obviously, accurate calculation methods are needed since the magnitude of the windage loss influences the selection of the cooling scheme and the selection of the best alternator for TAC. A comparison of four calculation methods was made to determine their applicability to the Lundell alternators. The relative magnitudes of the windage loss for one rotor configuration and one set of operating conditions are presented in Table XLVI.

In general, the formulation of Vrancik given in NASA TND-4849 gave much higher losses than the other methods. The lowest losses were obtained by using a skin-friction coefficient from Gazley's experiments with concentric, rotating cylinders (Trans ASME, Volume 80, No. 1, Jan. 1958). Vrancik's correlation was also based upon Gazley's skin-friction coefficient. However, there appears to be an error of a factor of four introduced when the skin-friction coefficient was substituted intro Vrancik formulation of the power loss equation.

Gazley defined

$$C_f = \tau/(1/2\ \rho u^2)$$

where $(C_f)^{-1/2} = 2.04 + 1.768\ \ln\ Re\ \sqrt{C_f}$

τ = fluid shearing stress

ρ = fluid density

$u = u_r/2$ = one-half of the peripheral velocity of the rotor surface.

Re = Reynolds number based on the peripheral velocity and the radial clearance between rotor and stator

Vrancik used the same equations except that $\mu = \mu_r$ was used in place of $\mu = \mu_r/2$ as defined by Gazley. This difference produced a factor of four difference in the power loss equations as shown below.

Power loss (cylinder) = (shearing stress)(area of cylinder)
(radius)(speed)

TABLE XLVI

WINDAGE LOSS ANALYSES

Lundell - Evaluated various published methods for comparison, accuracy and applicability to the TAC alternator.

	Typical P.U. Comparison
Vrancik, NASA TND-4849.	3.5
Vohr (or MTI, or Wendt), NASA CR 54320	1.0
Schlichting, Boundary Layer Theory	-
Gazley, ASME, Vol. 80, No. 1	0.9
Friction losses based on Moody type friction factors and shearing	1.20
Et. al. per references in the above	-

- Selected Wendt and Schlichting combination, modified slightly.

  Main Air Gap - use Wendt times 1.1 factor for non-smooth bore
  Auxiliary Air Gap - use Wendt
  Cone Surfaces - use Schlichting, disk loss, slightly modified

- Anticipate recorrelating when NASA/LeRC data becomes available.

Inductor - Used model theory and results from a similar model.

- Data used was the O.G. Smith (Westinghouse) 8 pole rotor. Also compared it with data from a 10 pole 200 kW, 39000 rpm inductor belonging to U.S. Army.

- We cannot guarantee the predicted windage to be closer than 20% of actual because we do not know the effect on windage when rotor has only 4 poles.

$$\text{Power loss (cylinder)} = \frac{C_f}{4} \quad \pi \quad \rho R^4 \omega^3 L \text{ (Gazley)}$$

$$\text{Power loss (cylinder)} = C_f \quad \pi \quad \rho R^4 \omega^3 L \text{ (Vrancik)}$$

If flow within the radial gap is assumed to be symmetrical about the mid-point of the gap as assumed by Gazley, the Moody friction factor (f) for turbulent flow through channels can be used to calculate the windage power loss around a cylinder. For this case

$$\tau = \frac{f}{4}(1/2\rho u^2) \text{ where}$$

$$(f)^{-1/2} = 3.47 \ln (Re\sqrt{f}) + 1.6168$$

and the power loss equation becomes

$$\text{Power loss} = \frac{f}{16} \quad \pi \rho R^4 \omega^3 L$$

The windage loss based upon Moody's friction factor are approximately 35% higher than the losses calculated using Gazley's friction coefficient.

A rotor friction analysis was published by Dr. J. H. Vohr in Volume I, Section C of NASA-C2-54320, "Brushless Rotating Generators for Space Auxiliary Power Systems," in April 1965. The recommended relationships for calculating the friction factor between cylinders with a small radial gap are presented in Figure 120.

The windage power loss for a rotating cylinder obtained with these equations is greater than the loss obtained with Gazley's friction factor and is less than the loss obtained with Moody's friction factor.

B. Lundell Alternators

It was decided that windage power loss on the major diameter and in the auxiliary radial gap would be calculated by using C. Vohr's equations with an allowance for the roughness of the stator in the main radial gap. Ten percent was added to the loss in the main gap to account for the roughness of the slotted stator.

The windage losses on the conical sections was calculated by using the Schlichting closed disk equation adjusted for the increased area of the cone relative to a flat disk.

WINDAGE CALCULATION METHOD, LUNDELL

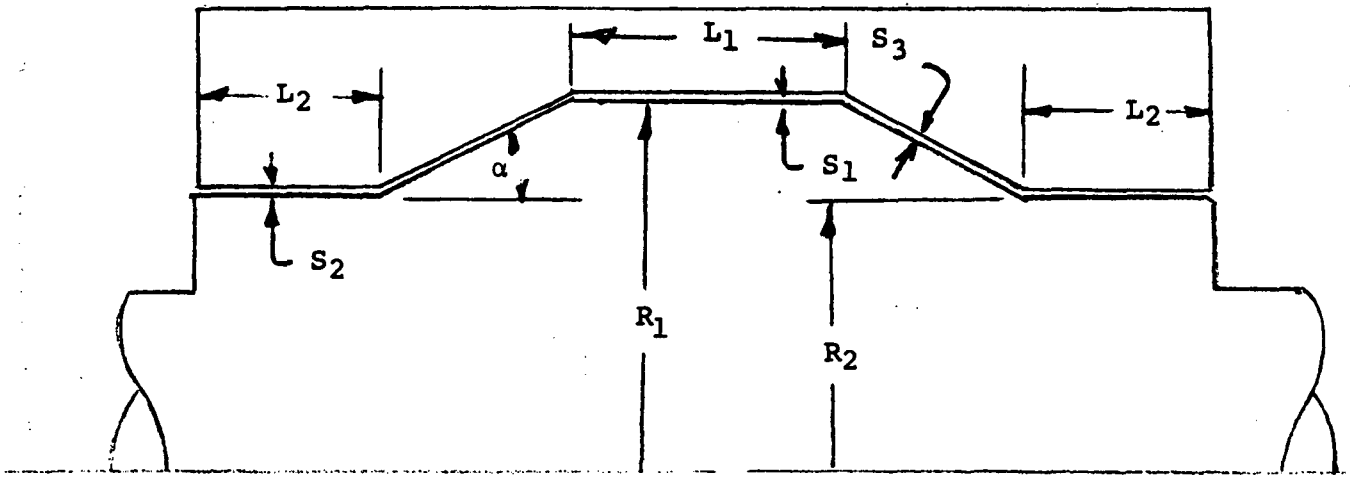

CYLINDERS

$$\text{POWER} = C_d K \frac{\pi \rho}{g_c} \omega^3 R^4 L$$

$$C_d = 0.073 \left(\frac{S}{R}\right)^{.25} (Re)^{-.3} \quad ; Re > 10^4$$

$$C_d = C_{d_1} = 0.46 \left(\frac{S}{R}\right)^{.25} (Re)^{-.5} \quad ; Re < 10^4$$

or

$$C_d = C_{d_2} = 2/Re \quad \text{IF } C_{d_2} > C_{d_1}$$

$$Re = \frac{\rho R \omega S}{\mu}$$

K = 1.0 For Smooth Cylinders
K = 1.1 For Slotted Stator

CONES

$$\text{POWER} = C_M \frac{K}{2} \frac{\rho R_1^5 \omega^3}{g_c} \text{, two sides}$$

$$C_M = .073/Re^{.2} \quad ; \quad Re > 1.58 \times 10^5$$

$$C_M = C_{M_1} = 2.67/Re^{.5} \quad ; \quad Re < 1.58 \times 10^5$$

$$C_M = C_{M_2} = \frac{2\pi}{Re} \frac{R_1}{S_3} \quad \text{IF } C_{M_2} > C_{M_1}$$

$$Re = \frac{\rho R_1^2 \omega}{\mu}$$

$$K = \left[1 - \left(\frac{R_2}{R_1}\right)^5\right] \frac{1}{\sin \alpha}$$

Figure 120.

A summary of equations used to calculate the windage power loss for the Lundell rotor are given in Figure 120.

C. Inductor Alternators

The windage losses for the inductor rotors were obtained using model theory and experimental results from a similar rotor. Experimental results for O. G. Smith's eight-pole rotor, which is published in NASA TND-4849, was used for the model data. The test data for this rotor showed the windage power varied as

$$\text{power loss} = \frac{1.272}{Re^{.14}} \; K \; \frac{\rho R^5 \; \omega^3}{g_c}$$

where $Re = \frac{\rho R^2 \omega}{\mu}$ = Reynolds number based on the peripheral velocity of the pole faces

$K = 1.0$ for unshrouded rotor

$K = .244$ for a shrouded rotor

ρ = fluid density

R = radius of rotor

ω = rotational speed

μ = fluid viscosity

This rotor had a length (L) to radius ratio of 1.33 and a linear relationship of windage loss with L/R was assumed for the rotors in the inductor alternators. Thus, the windage loss equation for these cases becomes:

$$\text{Power loss} = \frac{0.956}{Re^{.14}} \left(\frac{L}{R}\right) \; K \; \frac{\rho R^5 \; \omega^3}{g_c}$$

The inductor rotors had pole depth to radius ratio approximately equal to that of the model rotor. Therefore, the effect of this variable was not included in the windage power equation. It should be noted that the model rotor had eight poles with a 2/3 pole embrace and the equation above will only be reliable for these conditions. The rotors for the TAC study also had a 2/3 pole embrace. However, the 36,000 rpm alternator for TAC has only four poles. Because the effects of the number of poles are not known, the accuracy of the

windage power equation when applied to a four pole rotor can only be clarified by obtaining further experimental data.

COOLING DESIGN

A. Introduction

The purposes of the alternator cooling studies were (1) to determine the techniques required to limit the rotor and stator hot-spot temperatures to 796° F, and (2) to provide preliminary alternator thermal maps. The emphasis of these studies was placed on the Lundell alternators because the thermal aspects of Inductor alternators had been fully studied for the Potassium Turboalternator (KTA) Preliminary Design Study (ref. 36).

Computer programs were utilized to perform all analyses, excepting liquid coolant and gas flow and the pumping requirements. Initial estimates of the stator stack and winding temperatures, including the effects of windage and pole face losses passing through the stack, indicated that excessive winding temperatures would occur. During subsequent detailed analyses, gas flow over the rotor surface was found to limit hot-spot temperatures to the specified level. These analyses excluded only the alternator field coil, which was considered separately because its thermal performance would be nearly independent of other alternator temperatures.

B. Stack Heat/Temperature Influences

The major portion of the alternator losses are to be removed by a liquid coolant flowing through non-rotating parts of the machine. However, some additional thermal paths will be provided by the rotor shaft extensions, the frame mounts and through radiation and convection to the structure surrounding the alternator. The use of a coolant flowing through the rotor has not been considered because it does not appear to be necessary for the TAC alternators.

For the Lundell alternators, the losses are generated in the following areas:

(1) Field coil windings

(2) Armature windings

(3) Stator laminations (both teeth and back iron)

(4) Rotor pole faces

(5) Rotor-to-stator "air"-gaps.

The "air"-gap area is subdivided into the main gap under the stack, the auxiliary gap at the end bells, and the conical gap which connects the main and auxiliary gaps. The windage loss determination methods for these gaps are discussed above in this report. The losses in the other areas are determined in the electromagnetic design section.

The inductor alternator losses occur in the same basic areas. The major difference is that there are no auxiliary or conical gaps. The windage losses are generated in the pole to stack gaps of the salient poles, and on the pole end faces. A complete understanding of inductor alternator thermal considerations can be obtained from reference 36, although much of the following is generally applicable to this machine.

Within the Lundell machine, field coil losses and temperatures will be nearly independent of other alternator losses and temperatures. This results from the intimate contact of the field coil outer surfaces with the liquid cooled heat sink. Losses from the stack, armature windings, rotor and "air" gap will not pass through the field coil unless extreme temperature differentials occur. Within the coil, spiral windings with thin interlaminar insulation and high thermal conductivity ceramic plates potted to the ends of the coil winding sections will be used to reduce the radial thermal gradients. The field coil temperatures, even with cavity gas at about 800°F, can be maintained below the limiting hot-spot temperature of 796°F. The calculated (650°F) temperatures indicated on the thermal maps presented later in this section are considerably below this level.

The armature winding temperatures and losses are interrelated in that increasing losses result in increasing temperatures and further increases in the losses. Directly influencing the temperature distribution in the windings are the slot insulation system, the end turn lengths and the end turn surroundings, while the stack and liquid coolant temperature levels, and the thermal path for windage and rotor pole face losses have indirect effects. Because convective and radiant cooling of the end turns will generally be inadequate for

the losses in these areas, increased end turn lengths will magnify this deficit. Thus, the hot spot temperature would occur in the end turn and could be decreased by decreasing the end turn lengths. Within the slot, the thermal path from the conductor to the iron tooth is through a solid or flexible insulating slot liner and unavoidable, gas filled clearances. While some thermal contact (no clearance) will be normal, its magnitude and effect are uncertain. In addition, as discussed below, corona effects and operating gas pressure levels must be considered in the selection of the slot insulation system. Generally, the gas will present the greatest resistance to the thermal path, therefore minimum tolerances of the conductor, slot liner, tooth dimensions and stack slot alignment are necessary to obtain a low temperature rise from the tooth to the conductor. The indirect effects of the stack and coolant temperature levels on conductor temperature are generally set by the basic design. The rotor pole face and windage losses, if transmitted to the heat sink through the stack iron, will also increase the temperature levels of the teeth and the conductors. Therefore, an alternate thermal path for these losses is desirable. In the TAC Lundell designs this is accomplished by providing a path for the gas in the air gap to flow through the frame-to-stack separator which also provides the flow path for the liquid coolant. This gas circulates through the air gap and the separator, transporting windage losses and rotor pole face losses to the heat sink.

C. Preliminary Thermal Analyses

For the TAC alternators, it was assumed that the effective heat sink temperature would be 525°F, except for the case using a coolant at SNAP-8 temperatures where the heat sink is assumed to be at 345°F. These temperatures are based upon a redundant coolant path system, where the two coolant paths have reversed flows (or counterflow). For the system shown in Figure 121, the 24,000 rpm Lundell alternator, a total flow of about 6,000 lbs/hr would require a temperature rise of 11°F and 1230 watts pumping power (within the alternator envelope). Should one of the paths fail, the flow remaining constant in the other path, the flow of 3,000 lbs/hr would require 615 watts pumping power, but the temperature rise would increase to 22°F. This would result in

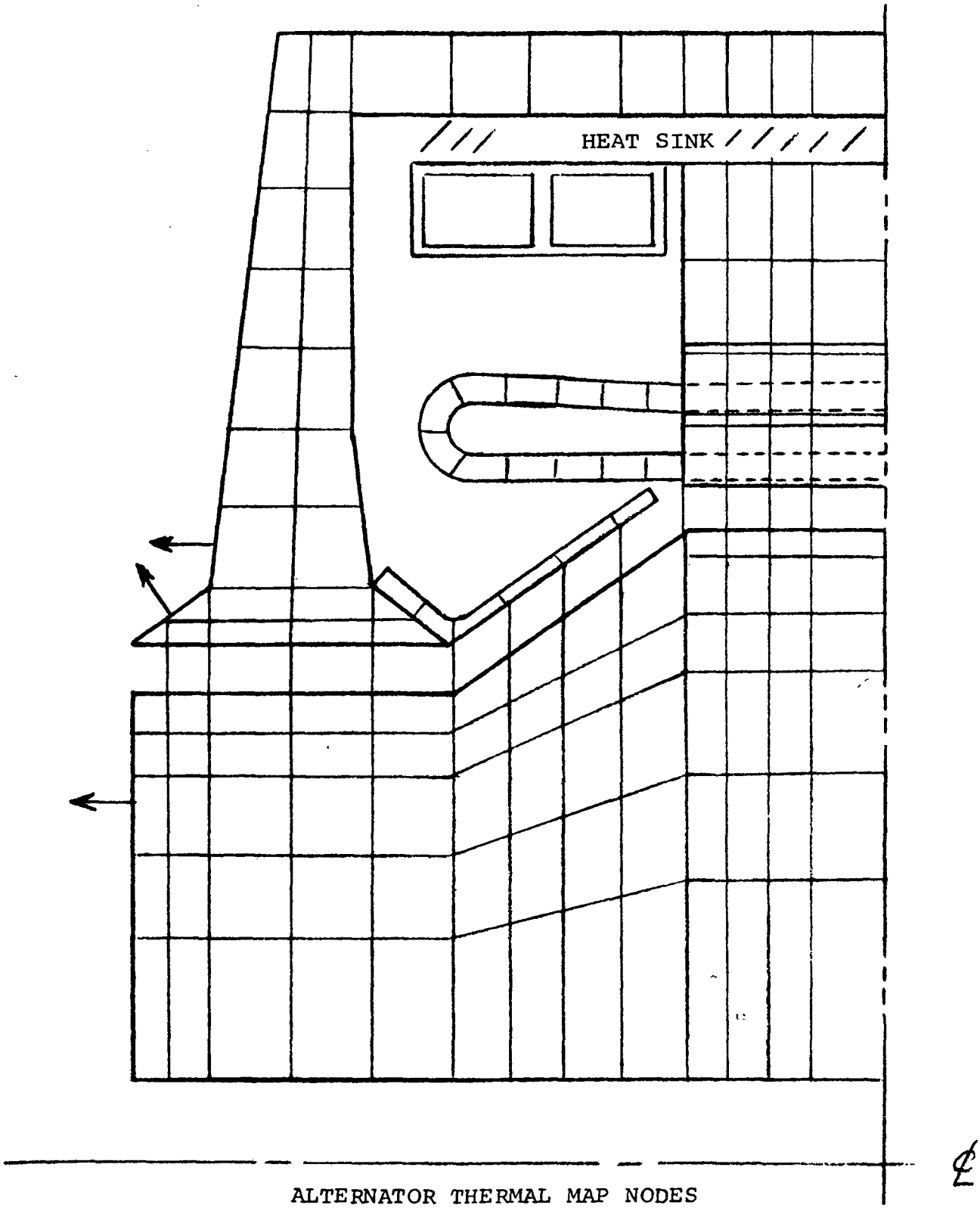

Figure 121.

an alternator axial temperature gradient approximately equal to the coolant temperature rise (there is no gradient in the full flow case). Reduction of the coolant flow rate would result in significant power savings, but more serious temperature gradients, as shown by the relationships of pumping power to coolant temperature rise, Power $\propto (\Delta t \text{ coolant})^{2.75}$.

Preliminary estimates of the stator armature and stack temperatures are obtained in the electrical design and performance programs. However, these programs do not include the effect of heat transfer to the stator teeth from the rotor or "air" gap. A brief analysis was made of these effects, revealing that excessive winding temperatures would be incurred if windage and pole face losses were removed solely through the stack. Since direct rotor cooling by passage of a fluid through the rotor is difficult and results in considerable complexity, cooling by means of a fluid flowing over the rotor surface was deemed necessary.

Preliminary estimates of the feasibility of pumping the cavity gas indicate that a pressure head of approximately 1.0 psi can be developed in the conical gap. Using the 100°F temperature rise assumed for the gas in the thermal map study, the specific heat of the helium xenon mixture, and the energy removed at the "gap heat sinks", the flow rate would be about 860 pounds per hour. Assuming the gas to divide and flow through 205 slots, 0.05 inch wide by 0.2 inch deep over each stack, the pressure drop would be less than 0.1 psi. Similarly, the estimated drop in the "air" gaps, and radially between the stack sections, would bring the total pressure drop to about 0.25 psi. Thus, the flow rate will be greater than was assumed for the thermal maps, and the gas temperature rise in flowing through the gap will decrease. Thus, the assumed temperature rise leads to conservative results in the thermal mapping.

D. Thermal Map Study

The thermal map studies for the Lundell alternator were performed in two segments - (1), the complete alternator except the field coil, and (2) the field coil alone. This was feasible because the thermal performance of the field coil is nearly independent of other alterna-

tor losses or temperatures, field coil losses being conducted directly to the heat sink liquid.

Surfaces of the field coil which "see" other alternator areas will absorb or transmit little thermal energy unless temperature differences exceed about 200°F. In that case, the higher temperature would be more than 300°F above the liquid coolant temperature, violating the specified hot spot limitation for the TAC alternators.

1. Alternator Model for Thermal Maps

The Lundell alternator thermal analyses were performed using a steady state version of the TOSS program (ref. 37). The nodal map is illustrated in figure 121. Approximately 200 nodes, 380 internal conduction paths, 45 connection paths and 11 radiation paths were utilized. In the stack back iron, the nodes are two deep, while in the slots the nodes are four deep (insulated wire, slot liner, clearance and tooth). In all other areas (frame, end bell, rotor, baffle and end turns), the map is only one node deep. The indicated thermal path at the left end of the rotor represents a thermal path to the shaft. The similar paths on the end bell represent redundant coolant loops that may be provided in the end bells.

The nodes in the air gap were required to provide heat sources (windage losses) in this region. Fluid flow was simulated by attaching each "solid" gas node to a heat sink whose temperature was adjusted to proportion the fluid temperature rise to the relative rate of windage loss generation. Heat transfer through the "solid" node is by conduction, the convective heat transfer coefficient being used to establish an equivalent thermal conductivity (e.g., $K = h \Delta x$). The heat transfer coefficients are based upon the empirical equations developed by Becker and Kaye (ref. 38) and supported by the work of Bjorkland and Kays (ref. 39).

2. Alternator Thermal Maps

The first thermal analyses were performed assuming little, or no, gas flow in the air gap, but providing coolant for the end bell. Figure 122 presents the thermal map for one such case in which

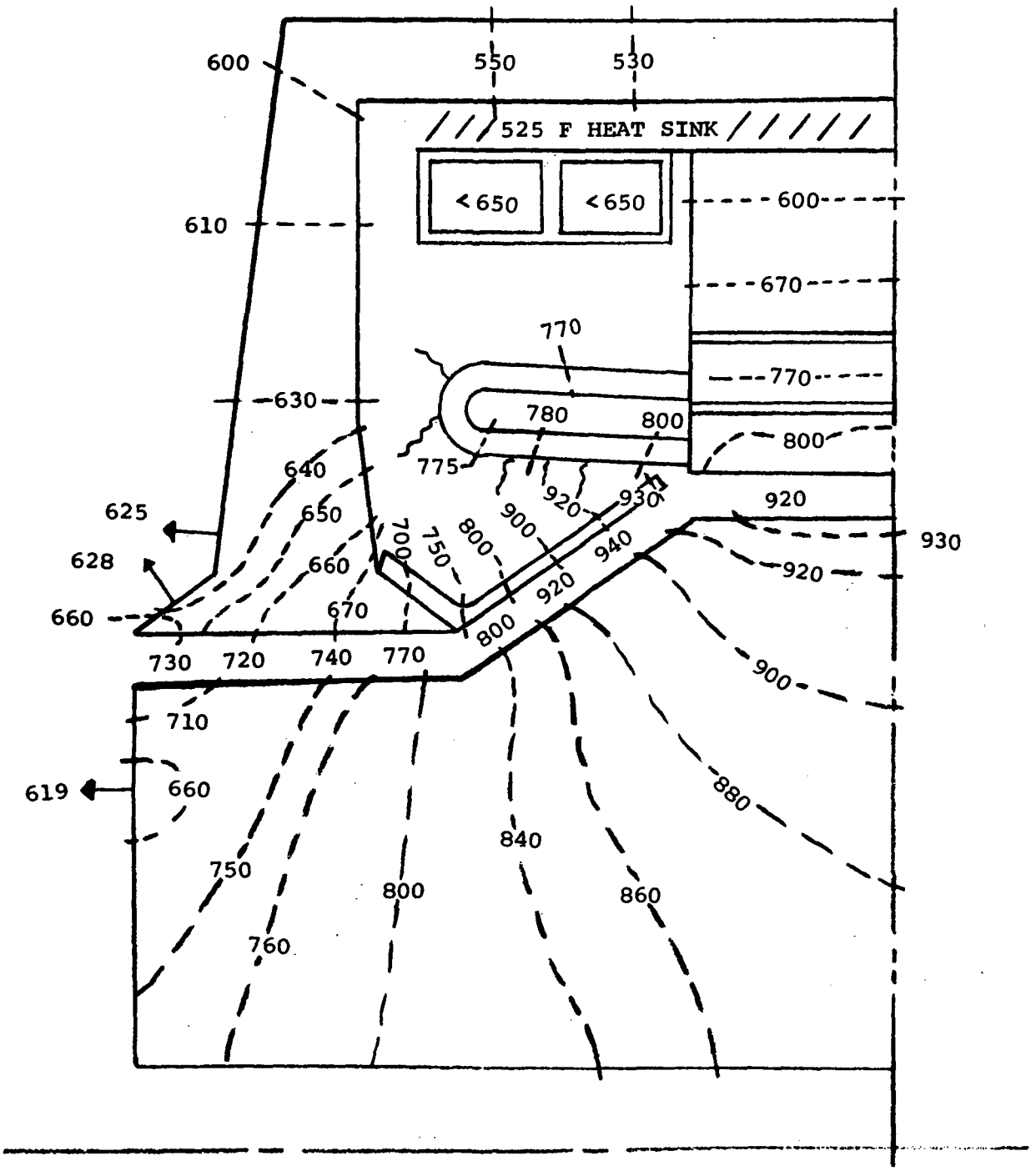

REPRESENTATIVE THERMAL MAP 24,000 rpm LUNDELL
COOLED END BELL, NO GAS FLOW

Figure 122.

about 700 watts (15%) of the windage and pole face losses were carried out by the gas. This thermal map illustrates that with no gas flow, and nearly all windage and pole face losses passing through the gap to the stack or the end bell, the maximum rotor temperature will exceed 900°F. In the highly stressed center hole regions, the temperature would reach 870°F. For the proposed materials, the temperature would be excessive. In addition, the armature winding temperatures are slightly in excess of the specified hot-spot limitation of 796°F.

To reduce the rotor and winding temperatures, gas was permitted to flow through the gap, using the conical section of the rotor as a pump. Assuming a gas temperature rise of 100°F as it flows through the auxiliary, conical, and main gaps to the center of the stack, the maps of figures 123 and 124 are obtained. As these maps show, it is desirable to assure a coolant temperature of not more than 625°F at the entry to the auxiliary gap. If this condition is met, the maximum rotor temperature at the central hole would be about 705°F. Calculations of the heat transfer in the heat sink area indicate that the gas will leave the finned passage at about 30°F above the heat sink temperature, or about 555°F. Assuming some heating before entering the auxiliary gap, it is probable that the gas temperature at this point will be in the range between 580 and 625°F as shown in the figures.

The inclusion of end bell cooling ducts adds considerable complexity to the end bell, and with a failure of one flow path, a circumferential or diametral temperature gradient would be created in the end bell. To evaluate the necessity for end bell colling, the map of figure 125 was obtained. This map can be compared directly with figure 124. The comparison indicates that only the end bell and baffle temperatures are significantly effected by elimination of the end bell cooling ducts. However, this cooling method should be retained for consideration in the next phase of study in that it may prove of greater merit at that time.

During the final stages of the phase I TAC effort, it became

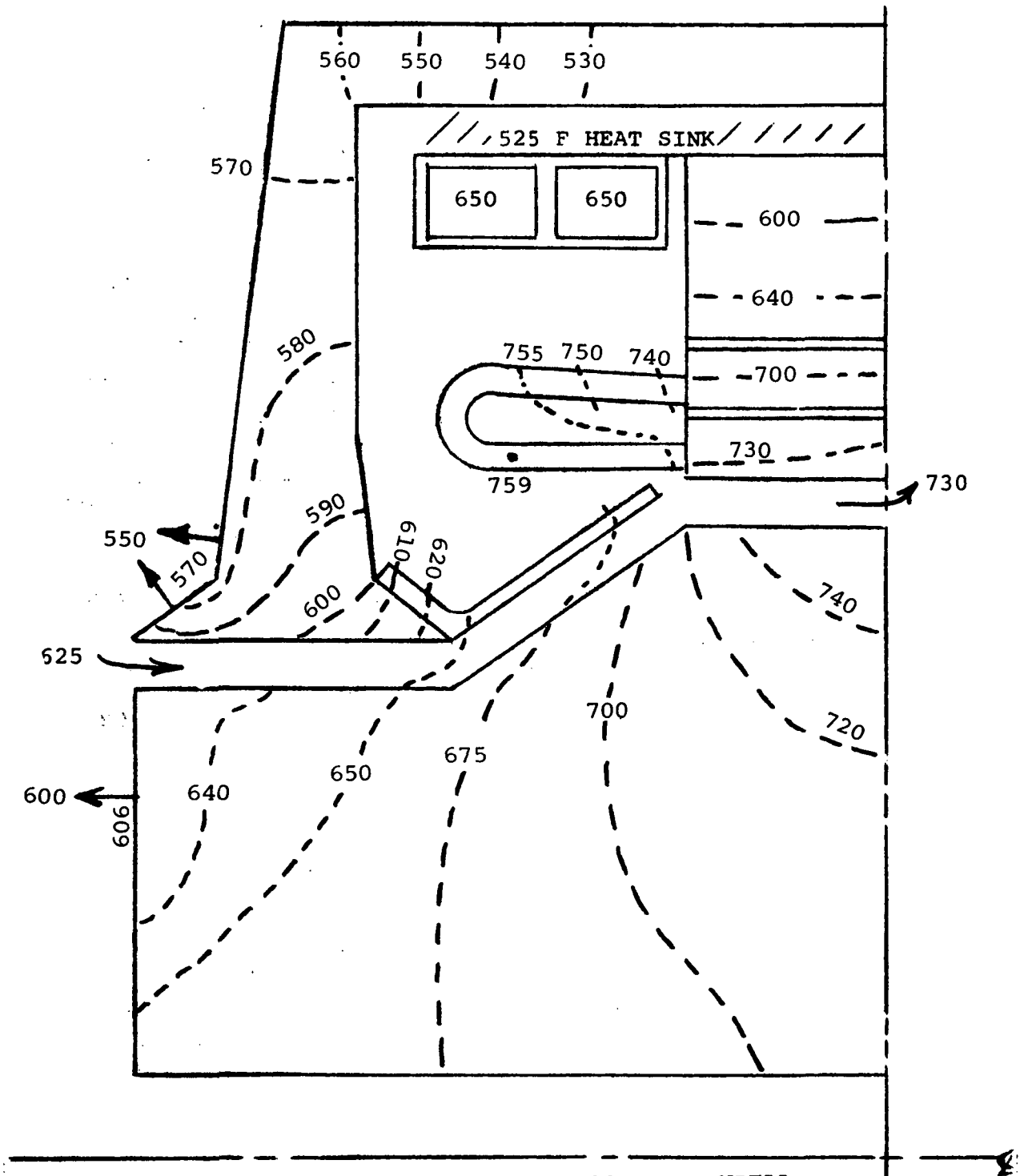

REPRESENTATIVE THERMAL MAP 24,000 rpm LUNDELL COOLED END BELL, GAS FLOW IN GAP

Figure 123.

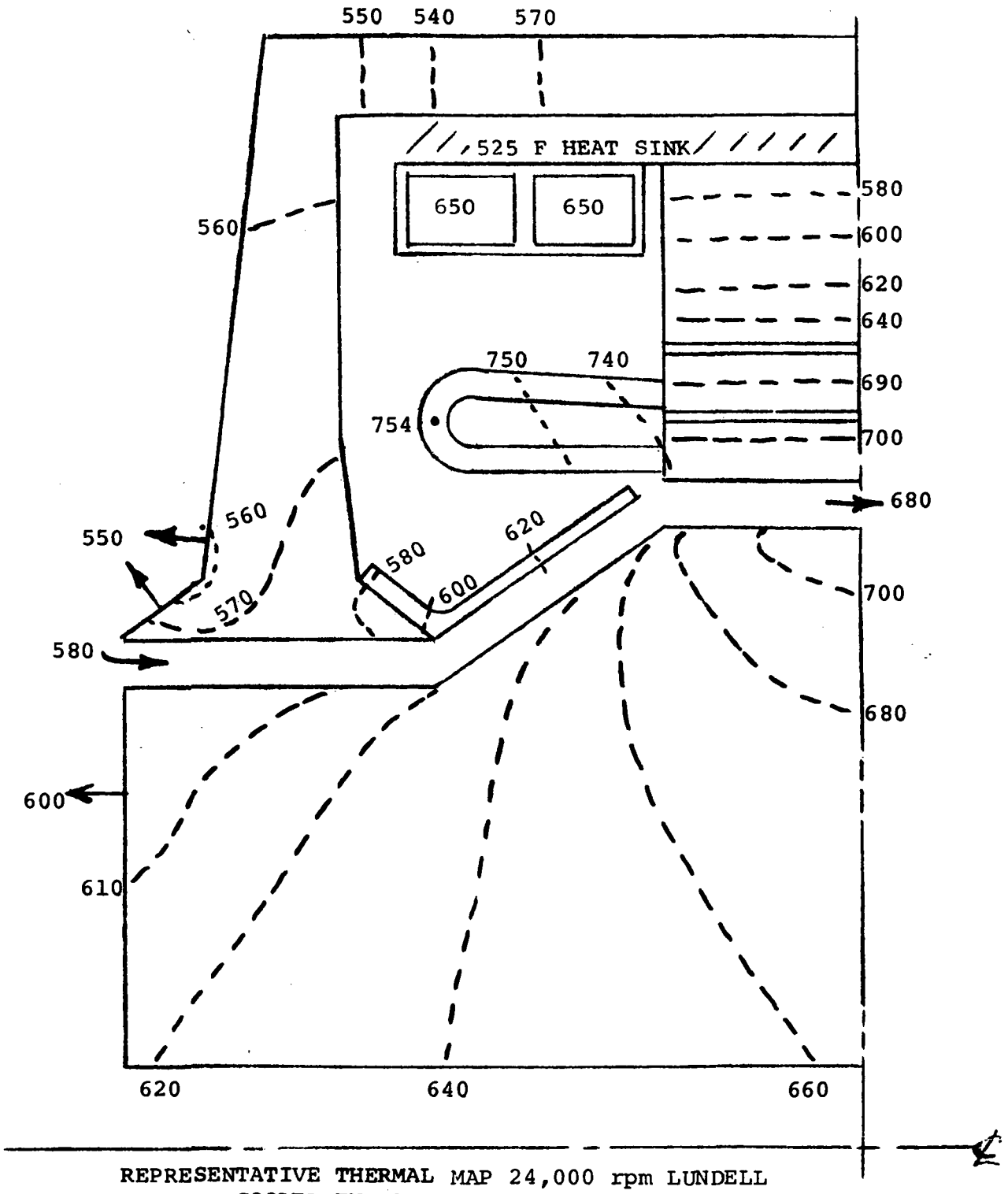

REPRESENTATIVE THERMAL MAP 24,000 rpm LUNDELL
COOLED END BELL, GAS FLOW IN GAP

Figure 124.

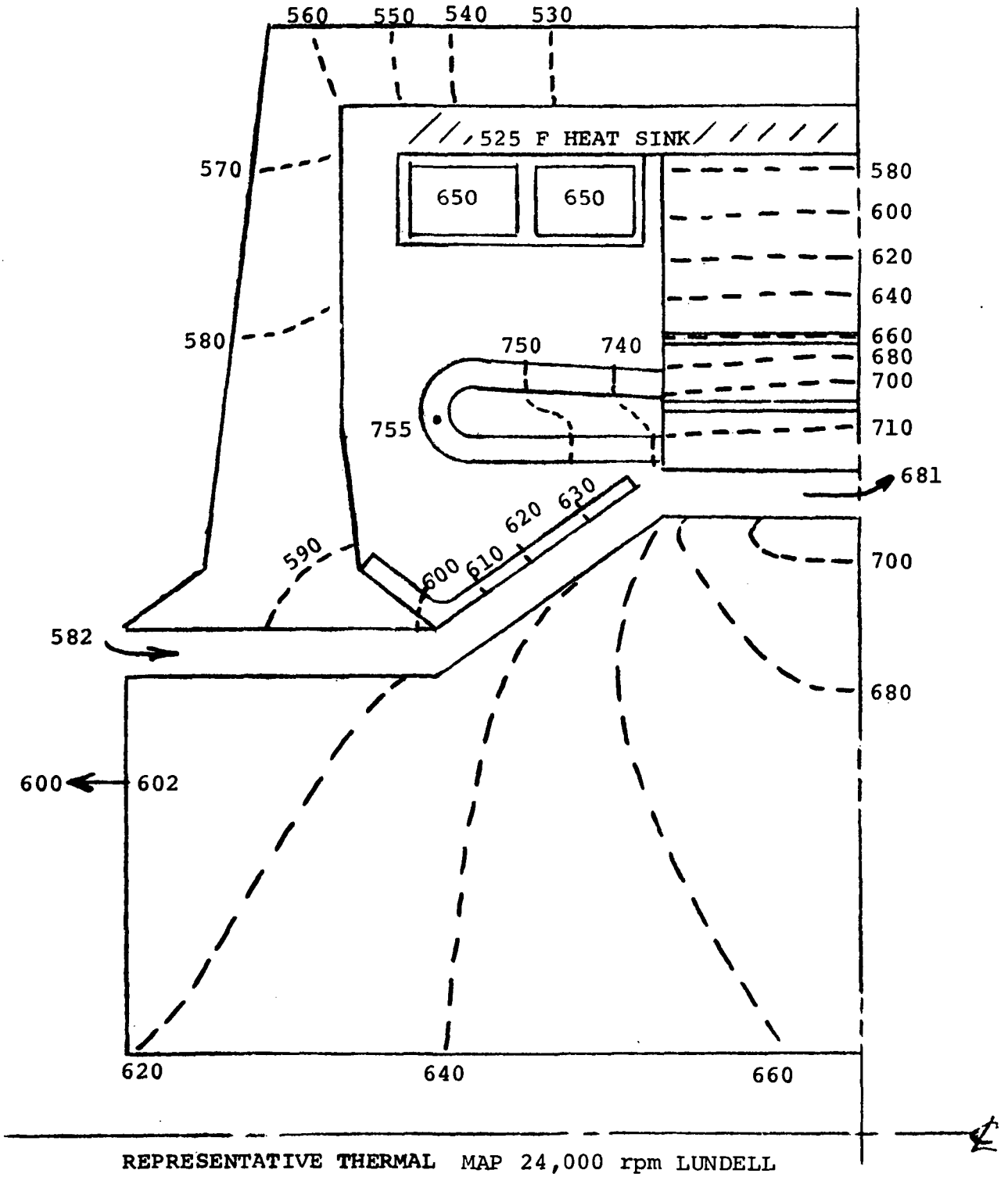

REPRESENTATIVE THERMAL MAP 24,000 rpm LUNDELL
GAS FLOW IN GAP

Figure 125.

apparent that the provision of a flow path for the gas from the heat sink to the outside of the end bell could be difficult. Therefore, a study was made of the thermal performance obtained when the gas was constrained to enter the auxiliary gap near the conical section. The thermal map, figure 126 shows that while the rotor and end bell temperatures near the gap are increased (as compared to figure 124), they are still well within acceptable limits.

The thermal map of figure 128 shows the effect of using a liquid coolant at SNAP-8 temperatures. All temperatures within the alternator are well within the 300°F hot spot temperature limitation of the TAC program.

3, Field Coil Thermal Analyses

The TAC 24,000 rpm Lundell alternator field coil was analyzed utilizing the same program as for the basic alternator. A total of up to 155 nodes were considered. These studies indicated that with the proposed spiral-wound strap conductors, the maximum temperature can be within about 150°F of the liquid coolant temperature. This will require the use of thin insulations between turns, and high thermal conductivity ceramic plates at the ends of each section to assure low radial temperature drops. In addition, it may be feasible to reduce the proposed field coil dimensions, since the electrical resistance will be decreased at the indicated temperatures, resulting in decreased losses.

E. Conclusions

The detailed preliminary analyses discussed above demonstrate that Lundell alternators can be cooled to meet the TAC program hot-spot limitations. Significant findings are enumerated below:

1. To limit the axial temperature gradient of the alternator to about 15°F, a liquid flow rate (nominal) of about 6,000 pounds per hour is required. Pumping power for the coolant, from alternator inlet to outlet, will be about 1230 watts, dropping to 615 watts when the gradient exists due to blockage of one coolant path.

2. Gas flow through the rotor to stator gap must be provided to

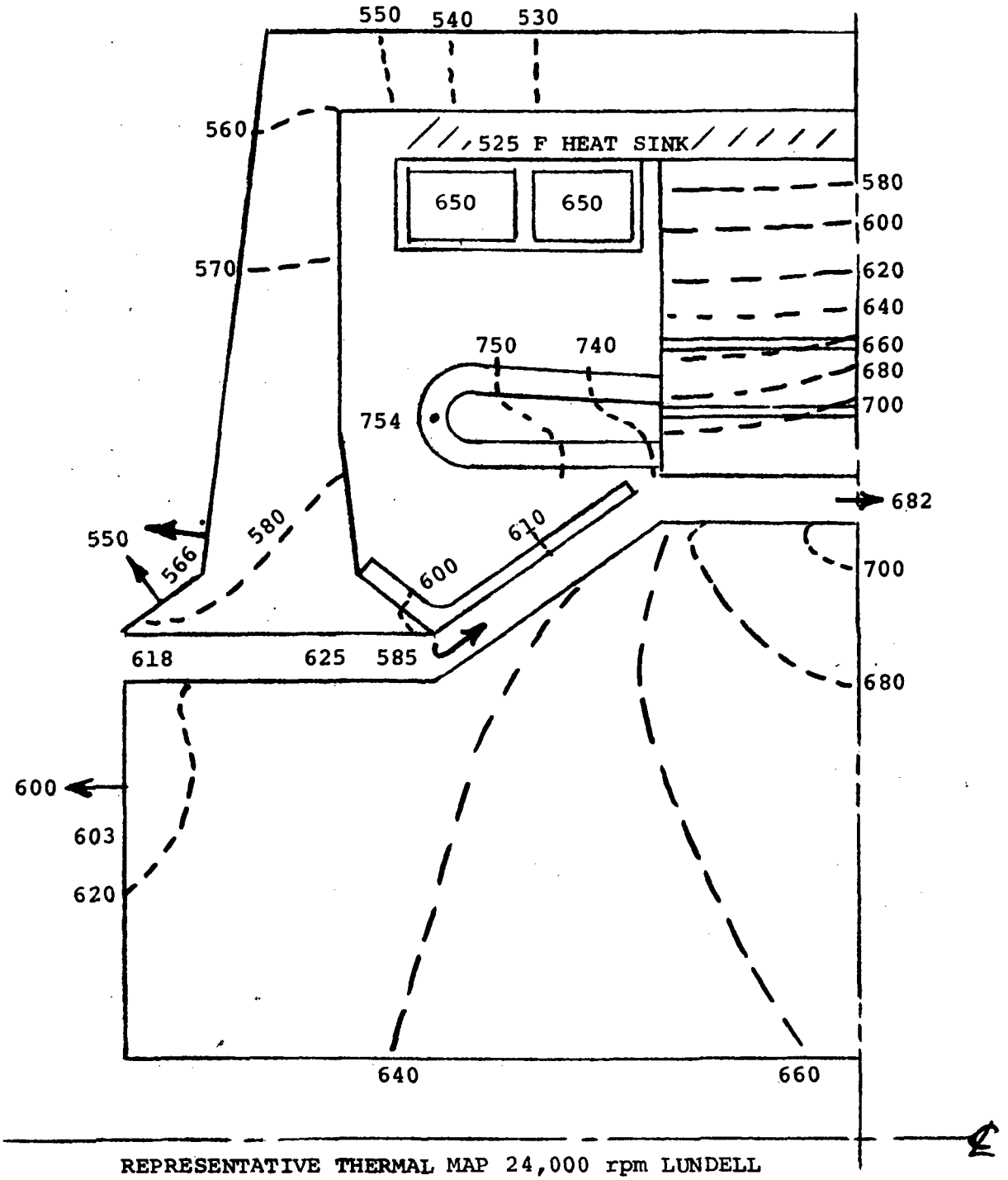

REPRESENTATIVE THERMAL MAP 24,000 rpm LUNDELL COOLED END BELL, GAS FLOW IN CONICAL AND MAIN GAPS

Figure 126.

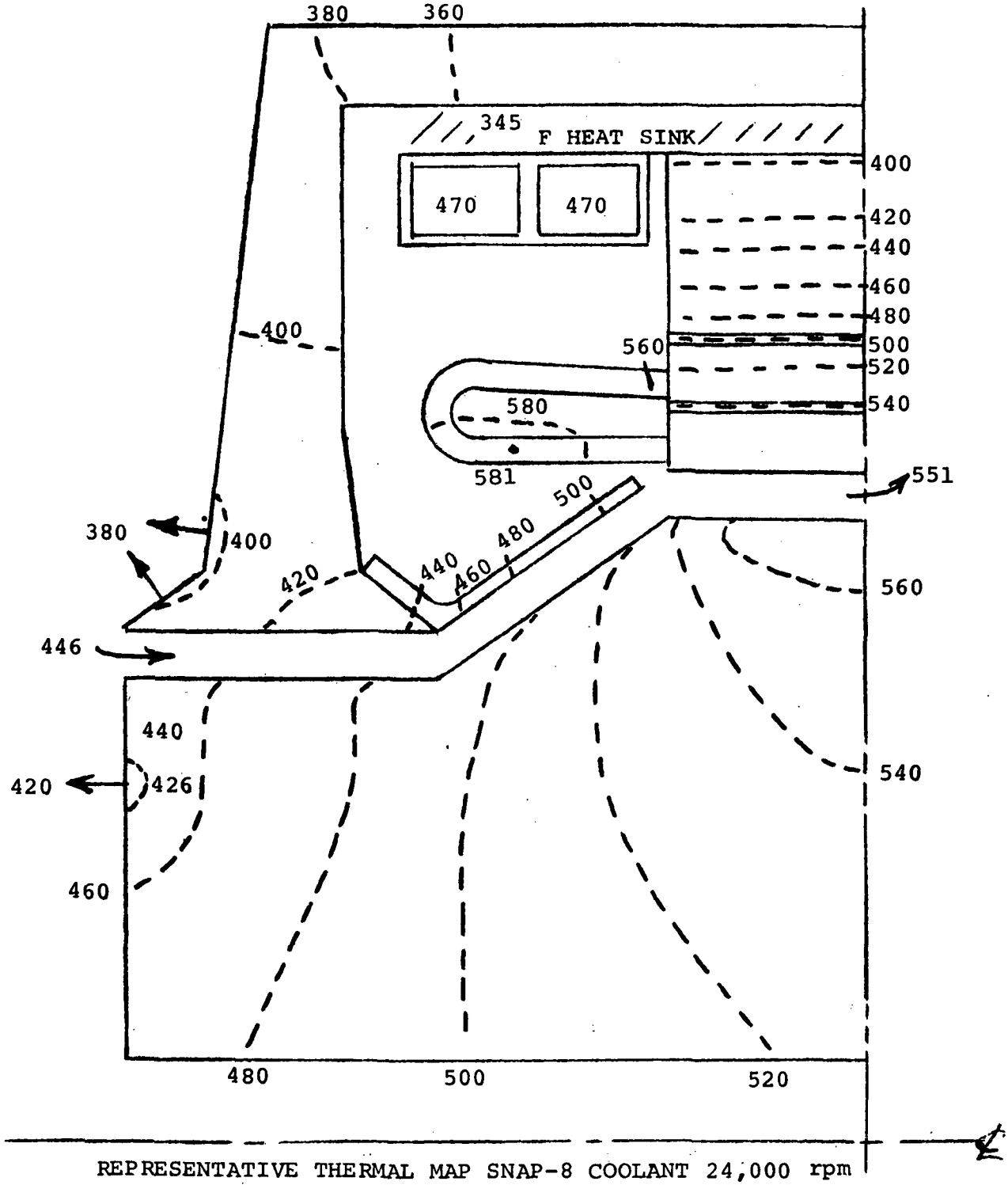
380
360
345
F HEAT SINK
400
420
440
460
480
500
520
540
470
470
400
560
580
581
551
380
400
420
440
460
480
500
560
446
440
420
426
460
540
480
500
520
REPRESENTATIVE THERMAL MAP SNAP-8 COOLANT 24,000 rpm
LUNDELL COOLED END BELL GAS FLOW IN
GAP

Figure 128.

limit the rotor temperature to 700°F. Pumping for this flow can be obtained by placing a conical baffle over the conical portion of the rotor.

3. The "air" gap gas flow can be restricted to the conical and main gap regions with little effect upon the rotor temperature.

4. Addition of liquid coolant passages in the end bells has no significant effect on rotor cooling. However, such coolant passages could reduce the axial temperature gradient caused by loss of one of the redundant cooling flows.

5. Hot spot temperatures, occuring in the armature winding end turns, will be less than 300°F above the liquid coolant temperature.

6. Field coil temperatures will not exceed the hot spot temperature specified for the TAC alternator.

7. If the coolant temperature is changed (e.g., SNAP-8 coolant), all alternator temperatures will change by approximately the same magnitude. However, some deviation from the patterns will result from changes in the losses due to temperature level.

REPRESENTATIVE DESIGNS

This section summarizes details of the two final Lundell alternator designs and the final inductor alternator design to facilitate direct comparisons. The design performance and machine details are presented in Table XXXVIII. Figures 87, 91 and 101 are the configuration layouts for the three designs. The ballooned numbers in these figures relate to the materials used for the indicated areas, the materials list being provided in Table XLVII. As seen on the figures, the basic alternator is made up of the rotor, the magnetic frame, the Hiperco-27 stacks, the armature coils, and the field coils. The rest of the configuration around these fundamental components are to transfer the coolant in and out, transfer the power out and support the stator and rotor. The mounting of the bearing housings to the stator frame is a part of the total TAC configuration (not shown) and is done by mechanically fastening directly to the magnetic frame to utilize the structural rigidity associated with the relatively large magnetic frame.

TABLE XLVII

TAC ALTERNATOR MATERIALS LIST

1. Nickel Clad (20-28%) Silver - AC Windings
   (to be changed to AlSl-321 Clad Silver for Phase III)

2. CuBe Alloy (Dispersion Strengthened Copper Beryllium Alloy) - Field Coil and AC Bus Ring

3. Alumina (Al_2O_3) - Slot Liner, Slot Wedge, Bore Seal

4. Mica mat - Slot Cell Separator for Corona

5. Hiperco 27 Alloy, 0.004 inch Laminations, Magnetic-Stator Stack

6. Hiperco 27 Alloy, Forgings, Magnetic-Stator Frame, End Bells

7. Inconel 718, Non-Magnetic - Rotor

8. AlSl 4340 Steel, Magnetic - Rotor

9. AlSl H-11 Steel Forging, Magnetic - Rotor

10. To be selected, Non-Magnetic, Non-Conducting (Electrical)-Conical Baffle

The armature coil leads pass through end bell (or not at all) to the bus rings. In passing through the end bell, one-half inch spacing is required around each lead. This is to minimize eddy current heating due to the high frequency alternating flux surrounding the lead. This half-inch spacing is adhered to as a general rule for all the electrical leads of the ac armature coil.

The stators are hermetically sealed by the can mounting the terminals. This hermetic shroud is a thin wall reinforced can whose thickness is 30 to 40 mils. There are reinforcing rings around the can.

The stator punchings are 0.004 inch thick Hiperco-27 magnetic alloy, have a semi-closed slot to reduce pole face losses, and are assembled into an unwelded stack to reduce iron losses. A 0.0004 inch thick layer of plasma-arc sprayed alumina constitutes the interlaminar insulation. The small block of material shown dotted on the ends of the stacks are small tabs on the ends of the slot liners. Those hold and align the unwelded stacks preventing the thin teeth from flaring excessively. The bottom slot liner must be slit into an "L" shape in order for the slot liner to be assembled into the semi-closed slot. The upper slot liners are "U" shaped and can be assembled from the ends of the stack at the time of winding.

The field coil is wound into series connected toroids of flat straps. They are electrically insulated from each other and the cooling ducts. There is a flat-to-round transition section between each coil bundle and terminal.

There are four bus rings in each generator. The parallel phase groups of the armature are connected to each bus ring in such a manner that the bus ring I^2R losses are held to a minimum which in turn permits the rings to be cooled by radiation to the stator cavity walls. The maximum bus ring temperature can be expected to be less and 800°F with a 500°F sink temperature. The bus rings are supported by ceramic insulation and a mechanical mount as illustrated in the various views. The rings are not continuous rings, but are partial arcs to permit thermal expansion without diametral growth. The insulation pieces are spaced quite widely on the rings to permit a good field of view for radiation cooling. The leads come directly off

the armature coil into bus rings as seen in the figures and the exposed lead ends are bonded into the bus rings. This is important to the design of the alternator since it simplifies making a sound electrical joint at the time of final assembly. This is even more important should it be necessary to bake out the Anadur and fire it prior to assembly of the windings. This pre-bake will obtain a better slot fit-up at assembly by accounting for the 35 percent Anadur shrinkage prior to winding. Thus, by attaching the wire ends to the bus rings in readily accessable areas, bonding problems are minimized.

There is one terminal per bus ring, centrally located about the armature connections. Because of the temperatures brought on by the high current density and because of the limited space, special terminal studs are required. They are sized rather large to have sufficient cross sectional area to permit them to be self cooled by radiation. Nickel plating is used to obtain an emmisivity of 0.4 on the outer surfaces. They can be cooled by radiation alone to less than 800°F in a 500°F ambient.

The features of the rotor design are found in the bonded construction and slotted pole faces. The slotted pole faces have 0.006 wide by 0.100 inch deep slots, approximately 30 per inch, that are cut with gangs of carbide cut-off wheels. The process for doing this has previously been developed by Westinghouse.

The central hole shown dotted in the rotor core serves an assembly function. It is not used for cooling and may not be necessary for the heat treatment to obtain the desired hardnesses. The angled lines, also dotted, on the two Lundells illustrate the minimum volume needed for magnetic flux carrying purposes.

The cooling system for the Lundell alternators (figures 87 and 91 utilizes the non-magnetic separation between the stacks and the frames. For each machine, this member would be constructed in two sections, one for each half of the stack. Liquid coolant flows through helical grooves near the inner surfaces, parallel grooves in each part being provided to meet the redundant cooling system requirement. The finned outer portion of this separator provides cooling passages for gas pumped by the rotor's conical sections from the end

bell to the center of the stack. The gas will transport pole face and windage losses from the "air"-gap to the separator, providing rotor cooling without overheating of the stator armature windings. The baffles (item 10) are required to assure and direct the pumping action noted above.

The stator can be assembled as a unit separate from the rotor and stub shaft assemblies. This is an important feature for assembly into the TAC or for separate assembly for TAX pre-assembly tests. The alternator is mounted to the TAC through conical frames that mechanically attach the magnetic frame.

Most of the tubing for coolant flows, leads, etc., are not shown precisely due to the lack of definition at this stage of the design. The few tubes shown will actually be parallel tubes spaced 180 degrees apart to equalize the disturbances due to the penetrations. This equalizing rule will be adhered to for all penetrations in general.

The summary data for the three representative designs shown are listed on Table XXXVIII. The losses of the bearings and seals and the weights for the stub shafts, bearings, bearing housings, etc., are not included herein.

OVERALL CONCLUSIONS

The recommended alternator design is the 24,000 rpm, 6-pole Lundell at 120 volts (L-N), the latter being limited by corona considerations which in turn limits the minimum stator cavity pressure (and minimum system pressures indirectly) to 16 psia. Testing is recommended to verify this prior to "freezing" the minimum specified pressure. The rotor for this configuration is constructed of SAE 4340 and Inconel 718, diffusion bonded and hardened to 33 R_C and 38 R_C respectively in an autoclave. The hardness requirements are dictated by the strength requirement and are within the realm of practicality for hardening as a bonded unit within the autoclave. No significant gains could be identified utilizing other magnetic materials having superior magnetic properties or more compatable "heat-treat-as-a-unit" characteristics.

The impact of designing without a central hole in the rotor was

found to be significant to the design choice. With the hole, the 36,000 rpm designs are overstressed and impractical; the 24,000 rpm designs require the magnetic steel to be hardened to 33 R_c. Without the hole, the 36,000 rpm Lundell only requires hardening the 4340 to 33 R_c to make it strong enough; the 24,000 rpm Lundell 4340 may be left in a fully annealed state (R_c11) for adequate strength.

Windage losses are well below the 9.6 kW limit but are very significant to the choice of cooling configuration. A circulating gas, completely within the alternator, is required to limit hot spot and rotor temperatures below safe levels. This gas flow is generated by the dynamic head created in the conical sections of the rotor and the flow need not pass through the auxiliary air-gap sections for adequate cooling. Preliminary calculations indicate the inherent gas flow to be two times the minimum requirement.

End-bell cooling appears to be unnecessary but is being retained for further study in Phase III relative to redundancy requirement in case only one of the two parallel cooling paths is operative.

The alternator meets electrical specifications but we expect to see further improvements in the Phase III design. In particular, the 8.9 percent calculated voltage unbalance appears to be conservatively high and, with improved calculation techniques, should drop below the 6 percent goal. Also, the efficiency at 1/4 P.U. load will be improved low-load performance.

The location of electrical leads, bus rings, terminals and cooling tubes are significant to the TAC assembly configuration. Preliminary agreement on basic configurations must be reached early in Phase III prior to initiating the detailed design analyses as their location can affect all components with the TAC unit.

E. BEARING AND SEAL DESIGNS

INTRODUCTION AND SUMMARY

This chapter of the report describes and provides the results of the preliminary analysis that was conducted under Phase I of Contract NAS3-13449, to select journal and thrust bearings for the 24,000 rpm TAC. Table XLVIII itemizes the principal factors that were included in this analysis.

Primary emphasis in the selection of both the journal and thrust bearings was placed on achieving ample load capacity margin against transient and dynamic loads. In particular, the bearings were sized to support a 4 G load while still maintaining a conservatively high value of the film thickness both at design speed and in the overspeed range. The calculations of bearing performance were made both for the full power, 160 KW(e), and the one-quarter power, 40 KW(e), TAC output levels. To permit optimum,overall design of the TAC, all bearing cavities were maintained at compressore inlet pressure, i.e.,55 psia at 160 KW(e) and 15 psia at 40 KW(e).

The bearing types and sizes selected, based on the performance calculations over the full range of operating conditions of the TAC were as follows:

Journal Bearings: Type - tilting pad

TABLE XLVIII

TAC - PHASE I
PRELIMINARY GAS BEARINGS DESIGN
24000 RPM TAC

1. JOURNAL BEARINGS

- CONDITIONS OF OPERATION
- COMPARISON OF TILTING PAD AND FOIL BEARINGS
- SIZING AND STEADY-STATE PERFORMANCE
- TOLERANCE OF THERMAL GRADIENTS (RADIAL AND AXIAL)
- PIVOT SELECTION

2. THRUST BEARINGS

- CONDITIONS OF OPERATION
- COMPARISON OF BEARING TYPES
- SIZING AND STEADY-STATE PERFORMANCE
- TOLERANCE OF THERMAL DISTORTION

3. SURFACE MATERIALS

- SELECTION AND PAST EXPERIENCE

Size - 4" diameter x 3" long*

Thrust Bearing : Type - double acting (equal forward and reverse faces), helical grooved

Size - 8" O.D. x 4 1/4" I.D.

The preliminary bearing analysis reported herein, which is based on existing and well proven gas bearing theory, did not reveal any serious problems and showed that reliable, conservatively sized gas bearings can be designed and built for the TAC. It should be observed, however, that the 4 G load requirement imposed to meet the orbital requirements described in NASA Specification No. P2241-1, results in loads of 320 lbs. on the journal bearings and 640 lbs. on the thrust bearing. These loads are greater, by about a factor of four, than those carried under steady state conditions on self-acting gas bearings in earlier turbomachinery. In this sense, the TAC bearings represent an extension over past laboratory-test and field experience. Later this year, tests are to be conducted at MTI with gas lubricated bearings carrying loads comparable to those of the TAC, in connection with the development of gas bearings for an advanced air breathing engine (Army Contract DAA 302-69-C-0062). These tests should serve to assess whether any currently unanticipated problem areas will result from the high bearing loads.

Consideration was also given in this preliminary study to the selection of surface materials capable of withstanding, without damage, dry starts and

---

* Under 4 G load at 15 psia ambient pressure this bearing is marginal and may have to be increased in size. All other bearings satisfy the criterion established for load capacity that $h_{min} > 10^{-4} D$ under 4 G load, where h_{min} is the minimum film thickness and D is the bearing diameter (the outer diameter in the case of the thrust bearings).

stops as well as incidental, short duration impacts at design speed. Self-mated chrome oxide is the preferred materials combination for the TAC bearings, based on the earlier experimental studies of gas bearing materials conducted for the NASA and its excellent performance in the NASA's "A" Engine turbocompressor simulator and turboalternator, as well as several other gas bearing turbomachines.

Operating Conditions

The conditions of operation of the gas lubricated journal bearings are shown in Table XLIX for the 160 KW(2) and the 40 KW(e) power levels. The design point speed is 24,000 rpm, however, the bearings must be capable of stable operation and support of the applied loads over the speed range from 50 percent to 120 percent of design speed.

The bearing cavities will be maintained at compressor inlet pressure, i.e., the ambient pressure of the bearings will be 55 psia at 160 KW(e) and 15 psia at 40 KW(e).

The bearings are subjected to a number of load components as follows:

a. Gravity Load

The rotor weight is approximately 160 lbs., with the center of gravity of the rotor at about the mid point of the span between journals. Thus, when the TAC operates horizontally in a 1 G field, the gravity load will be about 80 lbs. per bearing. When TAC operates vertically in a 1 G field or in any orientation in a 0 G field, there is no gravity load component on the journal bearings.

b. Alternator Load

An estimate of the force gradient due to displacement of the center of rotation and the magnetic center of the alternator was requested from Westinghouse. Mr. A. King of Westinghouse estimated that this gradient will be about 34 lbs/mil at full power [160 KW(e)] and 8.5 lbs/mil at

TABLE XLIX

TAC - PHASE I
GAS LUBRICATED JOURNAL BEARINGS FOR 24000 RPM MACHINE

1. CONDITIONS OF OPERATION

160 KW(e)

	LOAD lbs.	SPEED rpm	AMBIENT PRESSURE psia
DESIGN POINTS			
0G OR 1G VERTICAL	0	24000	55
1G HORIZONTAL	80	24000	55
OPERATING RANGE	0 to 165*	12000 to 28800	55

40 KW(e)

	LOAD lbs.	SPEED rpm	AMBIENT PRESSURE psia
DESIGN POINTS			
0G OR 1G VERTICAL	0	24000	15
1G HORIZONTAL	80	24000	15
OPERATING RANGE	0 to 102*	12000 to 28800	15

ORBITAL LOAD: 320 lbs. (MAXIMUM) IN PREFERRED DIRECTION
120 lbs. (MAXIMUM) ALONG OTHER AXES

LUBRICANT : He - Xe MIXTURE, MW = 39.94

* INCLUDED ALTERNATOR LOAD CORRESPONDING TO 5 mils MAXIMUM DISPLACEMENT OF MAGNETIC CENTER. ALTERNATOR GRADIENT = 34 lbs/mil AT 160 KW(e) AND 8.5 lbs/mil AT 40 KW(e).

quarter power [40 KW(e)].

The displacement of the center of rotation relative to the magnetic center of the alternator will be a function of several factors including:

- Manufacturing and assembly tolerances of the alternator stator and rotor.
- Manufacturing and assembly tolerances of the bearings.
- Assembly tolerance of bearing center relative to alternator center.
- Static deflection of the rotor between the alternator center and the bearing centers.
- Eccentricity of the journal in the bearing clearance.
- Deflection of the bearing supports.
- Additional eccentricity due to differential radial thermal growths between the alternator housing and the bearing housing.

In the preliminary design analysis conducted under Phase I, it has been assumed that the total eccentricity between the center of rotation and the magnetic center due to the above causes can be limited to about 5 mils leading to a maximum additional load of 85 lbs/bearing at 160 KW(e) and 22 lbs/bearing at 40 KW(e) power levels.

c. Aerodynamic Unbalance Load

If the gas pressures are not uniform circumferentially around the turbine, compressor and seals, there will be a corresponding radial load component in the journal bearings. Such non-uniformity of the pressures should be

very small so that the bearing load component from this source is not expected to be significant, when compared with the gravity and magnetic load components.

d. Orbital Loads

A requirement of specification P2241-1 is that subsystems and components shall be capable of operating under acceleration loads of 3.5 G in one direction along the lift-off axis and $\pm$ 1 G in all directions in the plane normal to the lift-off axis, for short durations up to 5 minutes. In addition, short duration vibration loads of 0.25 G peak-to-peak must be supported in each of three mutually perpendicular axes. The subsystems and components must also be capable of withstanding a continuous, unidirectional acceleration arising from a 4 rpm spin rate of the spacecraft, the corresponding G loading being a function of the radial location of each subsystem or component with respect to the spin axis.

In view of these requirements and since the location and orientation of the Tac in the space vehicle are not yet defined, the bearings should be designed to support a 4 G load along the axis of the TAC as well as in one radial direction, and 1.5 G in the other radial directions. This operating condition is noted in Table XLIX.

e. Mechanical Unbalance Loads

Dynamic loads will be imposed on the radial bearings of the TAC due to any mechanical unbalance in the rotor. These loads will be a function of the magnitude and location of the unbalance, as well as of attenua-

tion or amplification factors that depend on the proximity of critical speeds. These dynamic loads are computed in the rotor response calculations.

Alternate Journal Bearing Types

The Work Statement specifies that the TAC units requiring gas lubrication shall employ hydrodynamic gas journal and thrust bearings. In the case of the journal bearings, foil type bearings (of the type that Ampex Corporation is currently studying under a separate NASA contract) and tilting pad bearings are to be studied. Gas bearing designs that do not require hydrostatic jacking are preferred.

Figure 129 illustrates schematically the two types of journal bearings. The foil bearing (left hand side of Figure 129) consists of a thin strip of metallic foil that is wound around the pins to form three support pads. After the desired tension is achieved, the pins are used to clamp the ends of each pad of the foil bearing. Parallelism between the pins is important to maintain constant tension axially along the foil.

The tilting pad bearing (right hand side of Figure 129), consists of a number (generally 3 or 4) of individually pivoted pads. Spherical pivots (or flexure pivots as described later in this section of the report) are used to provide self-alignment capability in addition to allowing the pads to incline circumferentially. The pivots are attached to the housing, generally by means of beam type flexures. In order to allow for relative thermal growths between the housing and the rotor, one or more pads are supported on rela-

TAC - PHASE I
JOURNAL BEARING TYPES

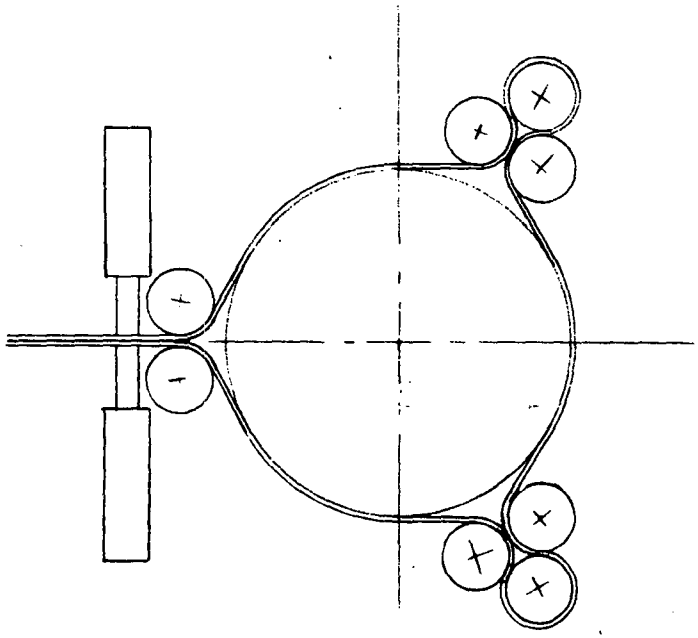

FOIL BEARING

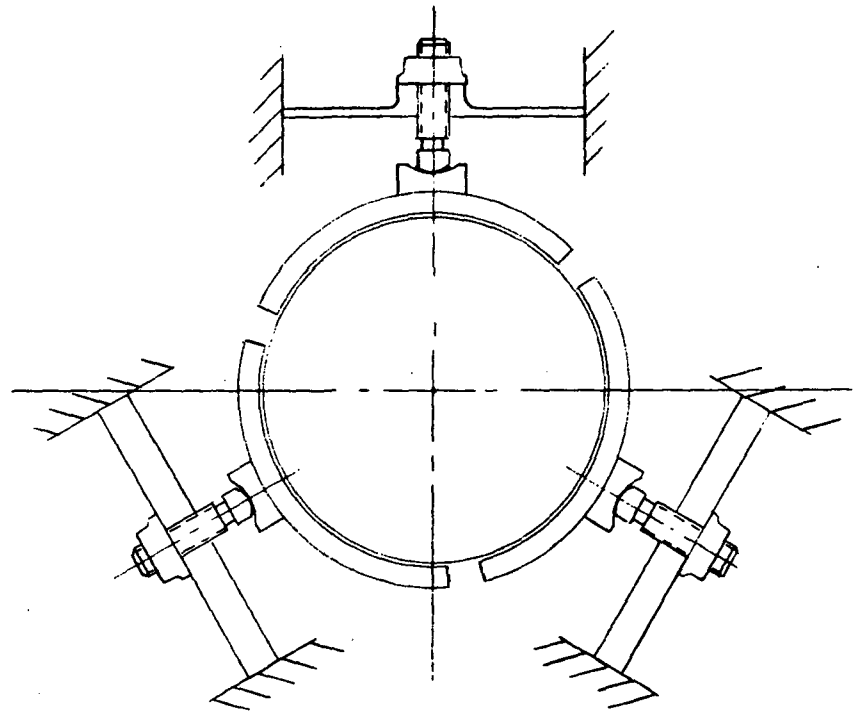

TILTING PAD BEARING

Figure 129

tively soft flexure beams.

Both bearing types have very high thresholds of instability, as required in high speed turbomachinery and, particularly, for space operation where stable operation is necessary even under zero applied load.

Both bearing types also afford good tolerance of relative thermal growths between the rotor and the bearing housing. In the case of the tilting pad bearing, this is achieved by the flexure mounting of one or more pads, so that the relative growth is taken up principally by the deflection of the pad support. In the case of the foil bearing, the relative thermal growth is taken up largely by extension of the foils.

The comparison between the two bearing types was made on the basis of:

a. The current status of the two bearing types and the extent of development required in each case for the TAC application and,

b. The calculated steady state performance at design point and under 4 G load, in each case.

The first of these is illustrated in Table L. The principal point of the comparison is that the tilting pad bearing is, presently, a well developed bearing that has been extensively used in prior gas bearing turbomachinery, while the foil bearing is still a relatively new, although very promising concept for such applications. The areas of technology development that need to be pursued in the near future in order to develop the foil bearing for space power turbomachinery are listed in Table L.

TABLE L

TAC - PRELIMINARY JOURNAL BEARINGS DESIGN COMPARISON OF TILTING PAD AND FOIL BEARINGS

A. CURRENT STATUS AND REQUIRED DEVELOPMENT

	TILTING-PAD BEARING	FOIL BEARING
STATUS	DEVELOPED BEARING CONCEPT, WIDELY USED IN HIGH-SPEED, GAS LUBRICATED TURBOMACHINERY	IN EXPERIMENTAL DEVELOPMENT STAGE
TURBOMACHINERY APPLICATIONS TO DATE	FOR NASA, L.R.C.: "A" ENGINE RADIAL TURBOCOMPRESSOR "A" ENGINE TURBOALTERNATOR "A" ENGINE AXIAL TURBOCOMPRESSOR "B" ENGINE - BRU OTHER: 24000 RPM, 1100 F, N_2 TURBOCOMPRESSOR 120 LBS. ROTOR, 24000 RPM ATR COMPRESSOR VARIOUS MOTOR-DRIVEN, NUCLEAR LOOP COMPRESSORS	FOR NASA, L.R.C.: SMALL, HIGH-SPEED ROTOR TESTS OTHER: SMALL (< 20 LBS.) ROTORS
TECHNOLOGY DEVELOPMENT AREAS	1. MATERIALS RELIABILITY	1. REDUCED BEARING DEFLECTIONS AND DYNAMIC ROTOR ORBITS 2. COATED FOIL MATERIALS 3. REDUCED START-UP PRELOAD 4. SELF-ALIGNMENT 5. JACKING THROUGH STATIONARY MEMBERS 6. GENERALIZED ANALYSIS

POTENTIAL OF FOIL BEARING: VERY HIGH TOLERANCE OF OFF-DESIGN CONDITIONS DUE TO "CONFORMABLE" BEARING SURFACE.

The second comparison required calculation of the performance of the two bearing types. This was done utilizing our computer programs for tilting pad and foil bearings. The computer program for tilting pad bearings has been used extensively during the design of the NASA's "A" Engine bearings (Refs. 40 and 41) and the back-up bearings of the "B" Engine, as well as other gas bearing turbomachinery. It provides accurate data that has correlated very well with laboratory tests and field experience obtained with pivoted-pad gas bearings. The foil bearing program was used during an analytical study of foil bearings for very high operating temperatures (up to 1400 F) and in the presence of large thermal gradients (up to 400 F between shaft and housing) that was conducted for the NASA (Ref. 42). First, however, the foil bearing program was revised and up-dated to incorporate the more recent analysis developed at Ampex Corporation under their study and test of this bearing type for the NASA (Ref. 43). The accuracy of the up-dated foil-bearing program was then tested against the experimental results of Ref. 43.

Figure 130 is a plot of this comparison and it shows that the calculated film thickness is generally smaller than the measured one. The experimental data, however, shows significant differences between the film thicknesses measured in the three pads that support the vertical rotor, so that there may have been some differences in tension between the three pads during the test. At the bottom of Figure 130 the comparisons between measured and calculated critical speed and amplitude amplification factors are given. Since the test rotor was completely rigid over the test speeds, the critical speed comparison is a good assessment of the calculated foil bearing stiffness. As noted, the measured and calculated critical speeds (and, hence, foil bearing stiffnesses) correlate very well.

COMPARISON OF MEASURED AND CALCULATED FOIL BEARING PERFORMANCE
TAC - PRELIMINARY JOURNAL BEARINGS DESIGN

(MEASURED DATA FROM: AMPEX REPORT RR 68-2, FINAL REPORT CONTRACT NASW-1456)

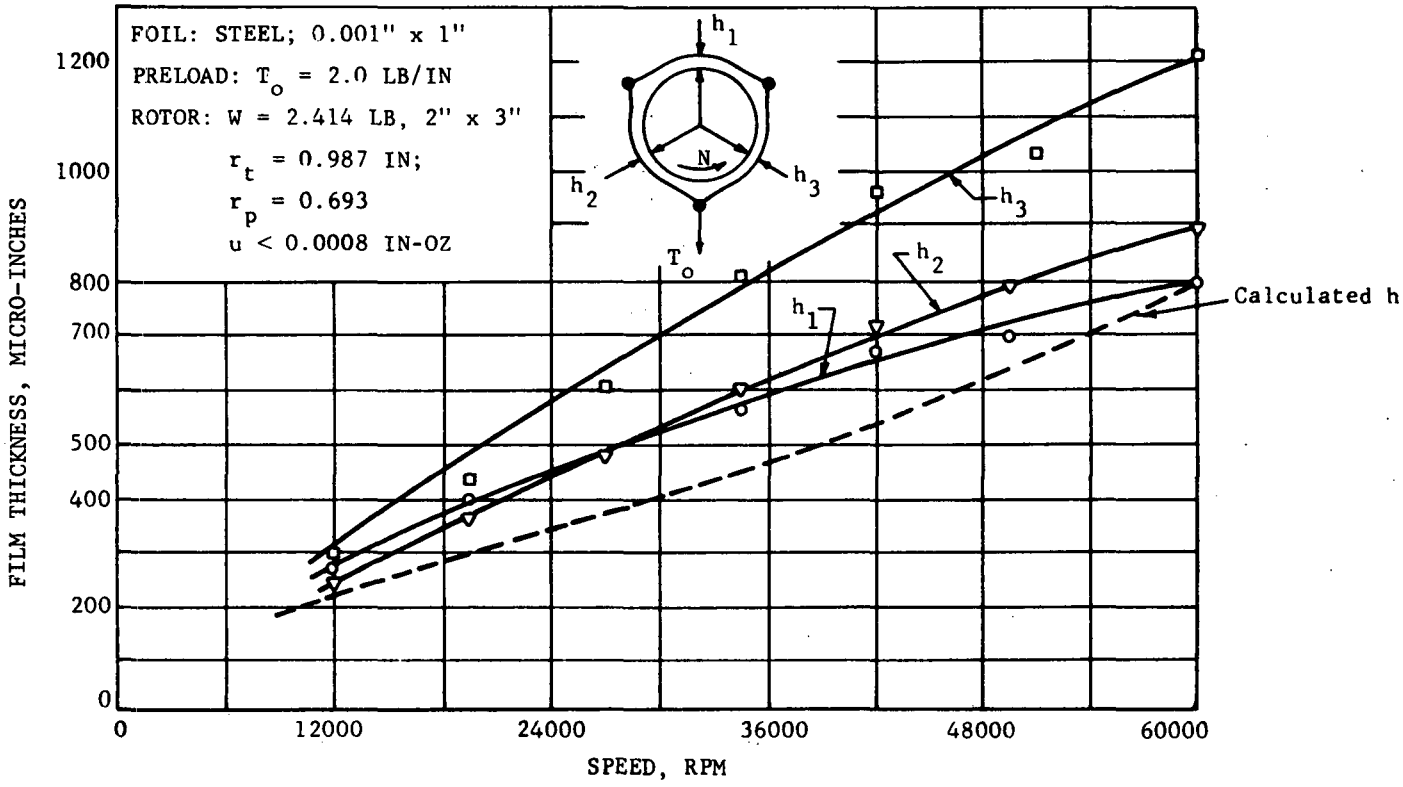

CRITICAL SPEED

CALCULATED: N_c = 8315 RPM
MEASURED : N_c = 8100 RPM

AMPLIFICATION FACTOR

CALCULATED: Q = 13.8
MEASURED: Q > 6.5 (FOR u < 0.0008 IN-OZ)

Figure 130

Similarly, the comparison of measured and calculated amplification factors is a good comparison of measured and calculated foil bearing damping. As noted in Figure 130, the calculated amplitude magnification factor (Q) was 13.8. The test data of Ref. 43, did not provide an exact, measured value of this factor since the residual unbalance in the tests was extremely small and could only be ascertained as being less than 0.8×10^{-3} oz-in. Thus, the test data could be used only to set a lower bound on the amplification factor. On this basis, the test data shows only that the experimental factor was equal to or greater than 6.5. This does not contradict the calculated value of 13.8.

Based on the above described comparison with the test data of Ref. 43, the foil bearing computer program appears to provide reasonable and conservative estimates of steady state performance so that it can be used to estimate foil bearing performance.

The comparison of the calculated performance of tilting pad and foil bearings for the TAC application is given in Table LI. This comparison was based on a 3 pad tilting pad bearing, 4" diameter x 3" long with a radial clearance of 1.4 mils at 24,000 rpm and zero applied load. The foil bearing was a 3 pad, 4" diameter x 4" long bearing using 3.5 mils thick steel foil with an initial tension of 30 lbs. In general, the comparison shows that the foil bearing has somewhat smaller calculated film thickness and higher power loss*. However, the calculated data on stiffness and damping of both bearings appears to be of satisfactory magnitude for good rotor dynamic performance.

---

* This can be improved by using thinner foils and lower initial tension. An analytical and experimental study would probably be required to select optimum foil bearing geometry, foil thickness, material, and initial tension for the TAC application.

TABLE LI

TAC - PRELIMINARY JOURNAL BEARING DESIGN COMPARISON OF CALCULATED TILTING-PAD AND FOIL BEARING PERFORMANCE

N = 24,000 RPM; Pa = 60 PSIA; $\mu = 0.66 \times 10^{-8}$ LB-SEC/IN^2

	4" D. x 3" L. TILTING-PAD LOAD BETWEEN PADS	4" D. x 4" L. FOIL BEARING, 3.5 MILS THICK FOIL	
		LOAD THROUGH PADS	LOAD BETWEEN PADS
1. SHAFT CENTER DISPLACEMENT, MILS			
0 LBS.	0	0	0
80 LBS.	0.3	1.1	1.3
320 LBS.	2.7	4.3	7.2
2. FILM THICKNESS, MILS			
0 LBS.	1.40	0.70	0.70
80 LBS.	0.94	0.46	0.54
320 LBS.	0.45	0.22	0.25
3. POWER LOSS, H.P.			
0 LBS.	0.58	1.24	1.24
80 LBS.	0.69	1.27	1.29
320 LBS.	1.01	1.66	≈ 1.7
4. STIFFNESS, LBS/IN			
0 LBS.	45,000 to 135,000	111,000	111,000
80 LBS.	84,000 to 250,000	132,000 to 86,000	85,000 to 138,000
320 LBS.	168,000 to 503,000	149,000 to 36,000	71,000 to 200,000
5. DAMPING X SPEED, ωB, LBS/IN			
0 LBS.	23,000 to 69,000	42,000	42,000
80 LBS.	25,000 to 74,000	31,000 to 58,000	59,000 to 26,000
320 LBS.	14,000 to 4,300	28,000 to 80,000	5,500 to 3,000

NOTES: 1. FOIL BEARING HAS LARGE DEFLECTIONS.
2. FOIL BEARING HAS LOWER FILM THICKNESS AND HIGHER POWER LOSS.
3. BOTH BEARING HAS LOWER STIFFNESS, BUT SATISFACTORY DAMPING TO STIFFNESS RATIO.

For the present, we recommend that the tilting pad bearing be used as the primary journal bearing for the TAC, based principally on the fact that it satisfies the required criteria on load capacity and stability and is much further advanced than the foil bearing. The latter, however, should be retained as a retro-fittable alternate bearing, pending the results of the future development efforts. Table LII summarizes the conclusions drawn from the comparative study of the two bearing types.

Calculated Bearing Performance

Table LIII shows the design targets established for the tilting pad journal bearings. The objective of these design targets was to provide a bearing system that can tolerate the specified conditions of operation safely and without marginal performance. The requirement for zero preload at start-up was imposed in order to minimize or altogether eliminate the need for hydrostatic jacking.

Table LIV lists the important performance characteristics of the journal bearings that need to be satisfied or optimized during the final design of the bearings. The principal design variables that have to be selected to satisfy or optimize the various performance characteristics are also listed in Table LIV. Pending detailed optimization studies, the following values of the design variables were selected:

Diameter	:	4" - selected based on rotor-dynamic studies
Length	:	3" - minimum required for adequate load capacity under 4 G condition
Number of Pads	:	3 or 4 - see comparison in Table LV.
Machined Clearance Ratio	:	0.0025 in/in at design point - nominal value used in prior turbomachinery

TABLE LII

TAC - PRELIMINARY JOURNAL BEARINGS DESIGN CONCLUSIONS ON SELECTION OF BEARING TYPE

1. THE TILTING-PAD TYPE JOURNAL BEARING IS SELECTED AS THE PRIMARY BEARING FOR THE TAC, FOR THE FOLLOWING REASONS:
    1. MUCH FURTHER ADVANCED FROM STANDPOINTS OF DEVELOPMENT AND PAST EXPERIENCE
    2. SUPERIOR FILM THICKNESS AND LOWER POWER LOSS
    3. SMALL ROTOR DEFLECTIONS AND DYNAMIC ORBITS

2. 4" DIAMETER x 4" LONG FOIL BEARING HAS SATISFACTORY LOAD CAPACITY BUT SUFFERS FROM:
    - HIGH PRELOAD AT START-UP
    - LARGE BEARING DEFLECTION
    - POOR MATERIALS COMPATIBILITY

    THIS BEARING SHOULD BE CONTINUED AS RETRO-FITTABLE, ALTERNATE BEARING, PENDING THE RESULTS OF FUTURE FOIL BEARING DEVELOPMENT EFFORTS.

TABLE LIII

TAC - PRELIMINARY JOURNAL BEARING DESIGN DESIGN TARGETS

1. STABLE, THICK-FILM PERFORMANCE OVER THE FULL OPERATING RANGES FOR 40 KW(e) AND 160 KW(e) POWER LEVELS, INCLUDING FOLLOWING OFF-DESIGN CONDITIONS:
   - 4G LOAD AT DESIGN SPEED AND OVERSPEED
   - 12000 RPM TO 28800 RPM
   - OFF-DESIGN SHAFT-TO-HOUSING TEMPERATURE GRADIENTS RANGING FROM - 100 F TO + 200 F

2. MINIMUM PIVOT POINT FILM THICKNESS > 10^{-4} D AT ALL OPERATING CONDITIONS.

3. ZERO PRELOAD AT START-UP TO ELIMINATE NEED FOR HYDROSTATIC JACKING.

4. MINIMUM PARASITIC LOSSES CONSISTENT WITH ITEMS 1, 2, AND 3.

TABLE LIV

TAC - PRELIMINARY JOURNAL BEARINGS DESIGN TILTING PAD BEARINGS OPTIMIZATION ANALYSIS

PERFORMANCE CHARACTERISTICS

STABILITY

LOAD CAPACITY (PIVOT POINT FILM THICKNESS)

FRICTION LOSS

STIFFNESS AND DAMPING

TOLERANCE OF RADIAL THERMAL GRADIENTS

TOLERANCE OF AXIAL THERMAL GRADIENTS INDUCING CROWNED SHAPE

BEARING SET-UP CHARACTERISTICS (START-UP LOAD AND CLEARANCE)

PAD-FILM-FLEXURE NATURAL FREQUENCIES

DESIGN VARIABLES

DIAMETER

LENGTH

NUMBER OF PADS

MACHINED CLEARANCE

ASSEMBLED CLEARANCE (PRELOAD)

FLEXURE STIFFNESS

PAD MASS

PAD MOMENTS OF INERTIA

TABLE LV

TAC - PRELIMINARY JOURNAL BEARING DESIGN

COMPARISON OF 3 AND 4 PAD BEARINGS

AT 24000 RPM, 1.4 MILS DESIGN POINT RADIAL CLEARANCE

	3 PAD BEARING	4 PAD BEARING
FILM THICKNESS, MILS		
320 LBS., 60 PSIA	0.45	0.46
320 LBS., 15 PSIA	0.27	0.22
POWER LOSS, H.P.		
0 LBS., 60 PSIA	0.575	0.587
320 LBS., 60 PSIA	1.006	0.930
320 LBS., 15 PSIA	1.245	1.350
RADIAL STIFFNESS, LBS/IN		
0 LBS., 60 PSIA, X	45,400	76,000
, Y	135,300	76,000
320 LBS., 60 PSIA, X	168,300	304,000
, Y	502,600	304,000
320 LBS., 15 PSIA, X	176,600	345,000
, Y	527,500	345,000
RADIAL DAMPING, ωB, LBS/IN		
0 LBS., 60 PSIA, X	23,300	38,500
, Y	69,500	38,500
320 LBS., 60 PSIA, X	14,300	33,700
, Y	43,200	33,700
320 LBS., 15 PSIA, X	3,400	13,800
, Y	11,800	13,800
PAD NATURAL FREQUENCIES, CPM		
0 LBS., 60 PSIA, RADIAL	197,400	215,000
PITCH	63,700	62,300
ROLL	57,800	70,900
YAW	15,700	14,500

NOTES:
1. STEADY-STATE PERFORMANCE OF THE TWO BEARINGS IS QUITE SIMILAR.
2. AT 160 KW(e) POWER LEVEL, BOTH BEARINGS MEET THE DESIGN TARGETS OVER THE FULL RANGES OF OPERATING CONDITIONS, INCLUDING THE 4G LOAD POINT.
3. AT 40 KW(e) POWER LEVEL, BOTH BEARINGS HAVE MARGINAL FILM THICKNESS UNDER 4G LOAD.
4. UNDER PHASE III, THE L/D = 1 BEARING SHOULD BE EXAMINED TO IMPROVE LOAD CAPACITY UNDER 4G LOAD AT THE 40 KW(e) POWER LEVEL.
5. UNDER PHASE III, FURHTER COMPARISON OF THE 3 PAD AND 4 PAD BEARINGS SHOULD BE MADE, BASED ON ROTOR-BEARING DYNAMICS PERFORMANCE.

Assembled Clearance Ratio:		0.0007 in/in at 0 G design point - selected to insure stable operation, based on prior experience with NASA's A and B engines
Flexure Stiffness	:	"Lower" pads - rigidly mounted "Upper" pads - 15,000 lbs/in - selected to provide margin for off design temperature gradients, but without requiring preload at start-up
Pad Mass and Moment of Inertia	:	Corresponding to 0.15" thick steel pads

With the above values of the design variables, calculations were made to compare the performance of 3 pad and 4 pad bearings, based on steady state operation both at 0 G and with a 4 G load acting along a line midway between pivots of adjacent pads. The results are tabulated in Table LV for 24,000 rpm operation. As is shown in this table (and as noted at the bottom of the table), there is no appreciable difference between the two designs under steady state conditions. Both bearings have adequate and nearly equal film thicknesses at the high ambient pressure condition. At the low ambient pressure condition (15 psi corresponding to 40 KW(e) power level), both bearings are marginal under 4 G load. Thus, if there are no changes in the dynamic load requirements of the bearings, an improvement in load capacity will be needed and can be achieved, e.g., by increasing the length of the bearings.

Figures 131 and 132 show the calculated performance of the 4-pad bearing over the full speed range (12,000 to 28,800 rpm at 60 psia ambient). Parallel data was calculated for the 3 pad bearing and showed similar performance values.

Table LVI lists the calculated natural frequencies of the pads of the 4-pad bear-

TAC - PRELIMINARY JOURNAL BEARING DESIGN
OPERATION AT DESIGN CONDITIONS

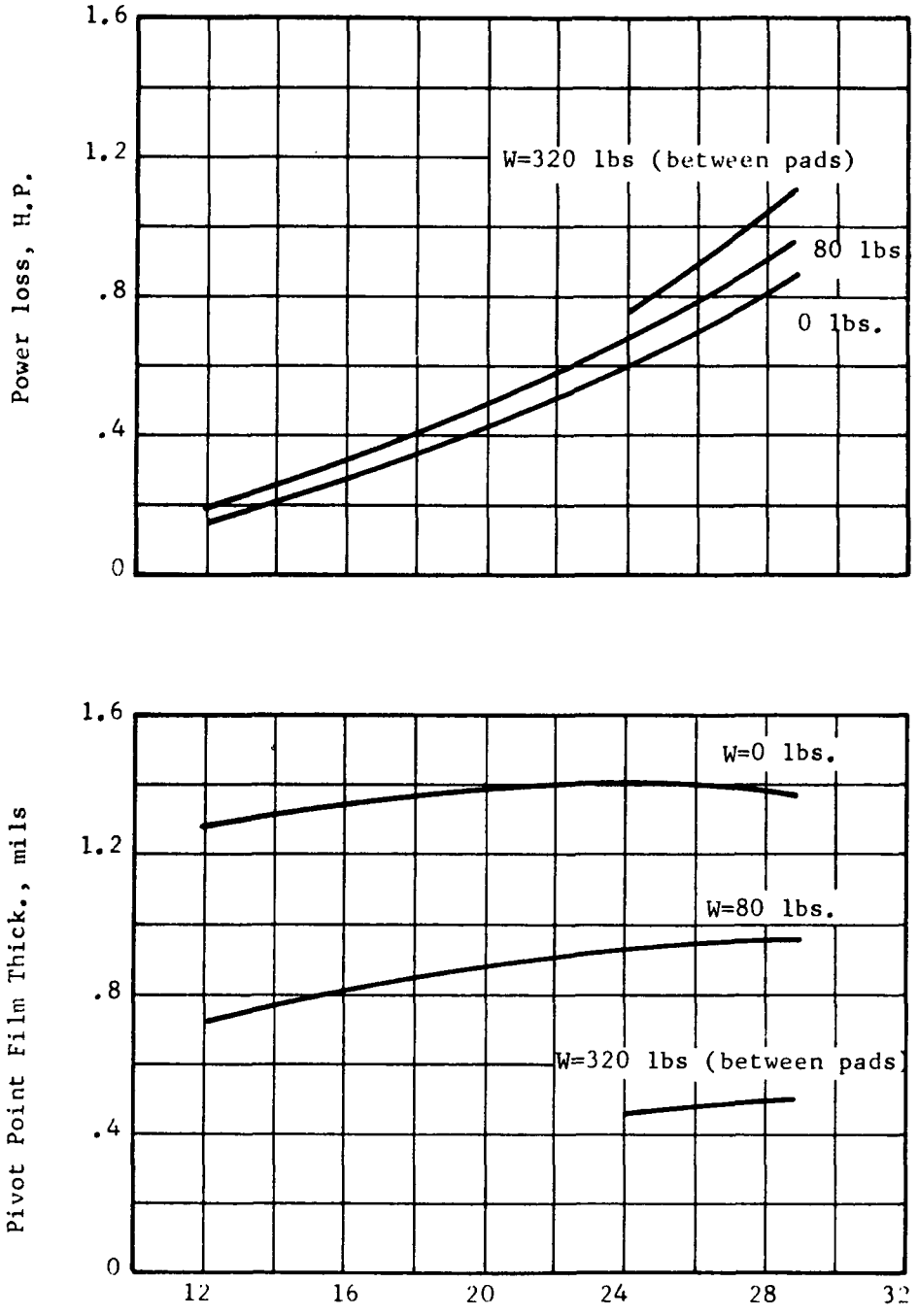

Figure 131

TAC - PRELIMINARY JOURNAL BEARING DESIGN
OPERATION AT DESIGN CONDITIONS

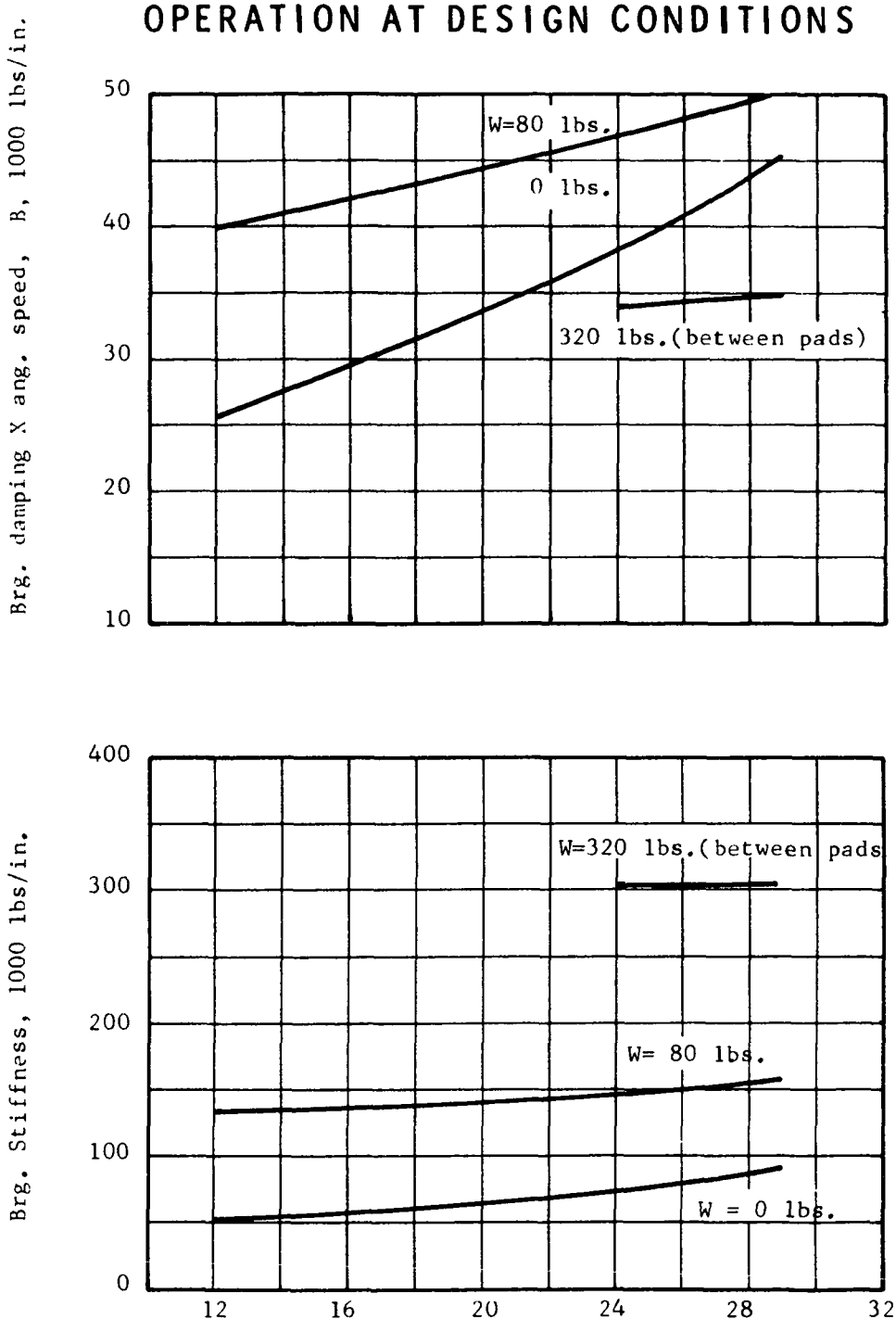

Figure 132

TABLE LVI

TAC - PRELIMINARY JOURNAL BEARING DESIGN OPERATION AT DESIGN CONDITIONS NATURAL FREQUENCIES OF BEARING PADS

		Natural Frequencies, rpm					
		Upper Pads			Lower Pads		
Load lbs.	Speed rpm	Radial	Pitch	Roll	Radial	Pitch	Roll
0	12000	95,900	43,400	55,700	195,000	51,500	55,700
	24000	117,800	54,100	70,900	215,000	62,300	70,900
	28800	128,900	60,100	78,600	224,000	67,900	78,600
80	12000	83,700	37,500	47,200	249,000	87,700	109,500
	24000	109,300	49,800	65,000	256,000	91,200	110,300
	28800	121,300	56,100	72,900	262,000	94,900	114,100
320	24000	96,900	43,600	56,100	369,000	154,000	268,000
	28800	119,980	50,200	64,600	367,000	157,000	280,000

Thus, over the range of design conditions,

$$\frac{N_{crit}}{N} > 1.7 \text{ for the upper pads,}$$

and $$\frac{N_{crit}}{N} > 2.3 \text{ for the lower pads.}$$

ing in the radial direction and in pitch and roll. As noted in this table, the operation is always substantially subcritical, so that the pads should track rotor orbits quite closely and without significant amplitude magnification.

Figure 133 shows the calculated decrease in pivot point film thickness (and the corresponding increase in power loss) as the ambient pressure is reduced. It shows again (as was noted earlier in Table LV) that the film thickness under 4 G load is satisfactory at 55 psia ($h > 0.4 \times 10^{-3}$ inch) but becomes marginal at 15 psia ($h \approx 0.2 \times 10^{-3}$ inches).

Effect of Thermal Gradients

Tolerance of large thermal gradients between the rotor and the bearing housing is necessary for successful application of gas bearings in high speed turbomachinery. Because of the very low mass flow of the lubricant gas in self-acting gas bearings (and its correspondingly small thermal capacity), the bulk of the heat generated in the bearings has to be removed by conduction through the stator and rotor. Thermal gradients are thereby set up in the bearing region which can produce severe distortions of the bearing surfaces and consequent loss of load capacity. Also, before reaching steady state conditions, significant, transient thermal gradients can be set up in the bearing region due to heat flow from other parts of the turbomachinery.

To prevent large clearance changes due to transient or steady state thermal conditions, one or more of the pads of the tilting pad journal bearings are mounted on relatively soft flexures, as described earlier. Figure 134 shows the calculated film thickness and power loss of the journal bearing as a function of off-design thermal gradients between the housing and shaft. These calculations were made assuming a three pad bearing with one of the pads supported on a 15,000 lbs/in flexure.

TAC - PRELIMINARY JOURNAL BEARING DESIGN
EFFECT OF AMBIENT PRESSURE (N=24,000 RPM)

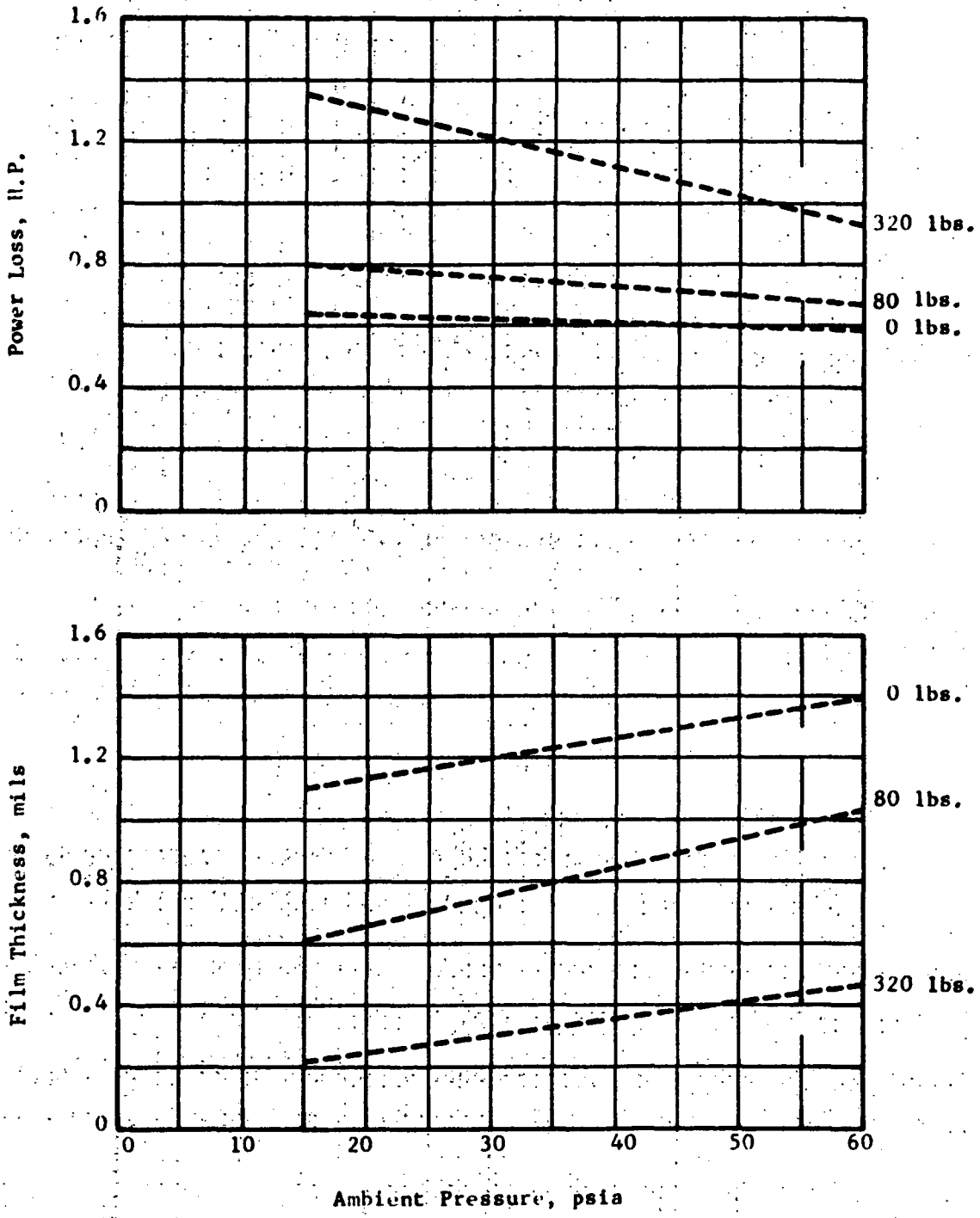

Figure 133

TAC-PRELIMINARY JOURNAL BEARING DESIGN
EFFECT OF RADIAL TEMPERATURE GRADIENT

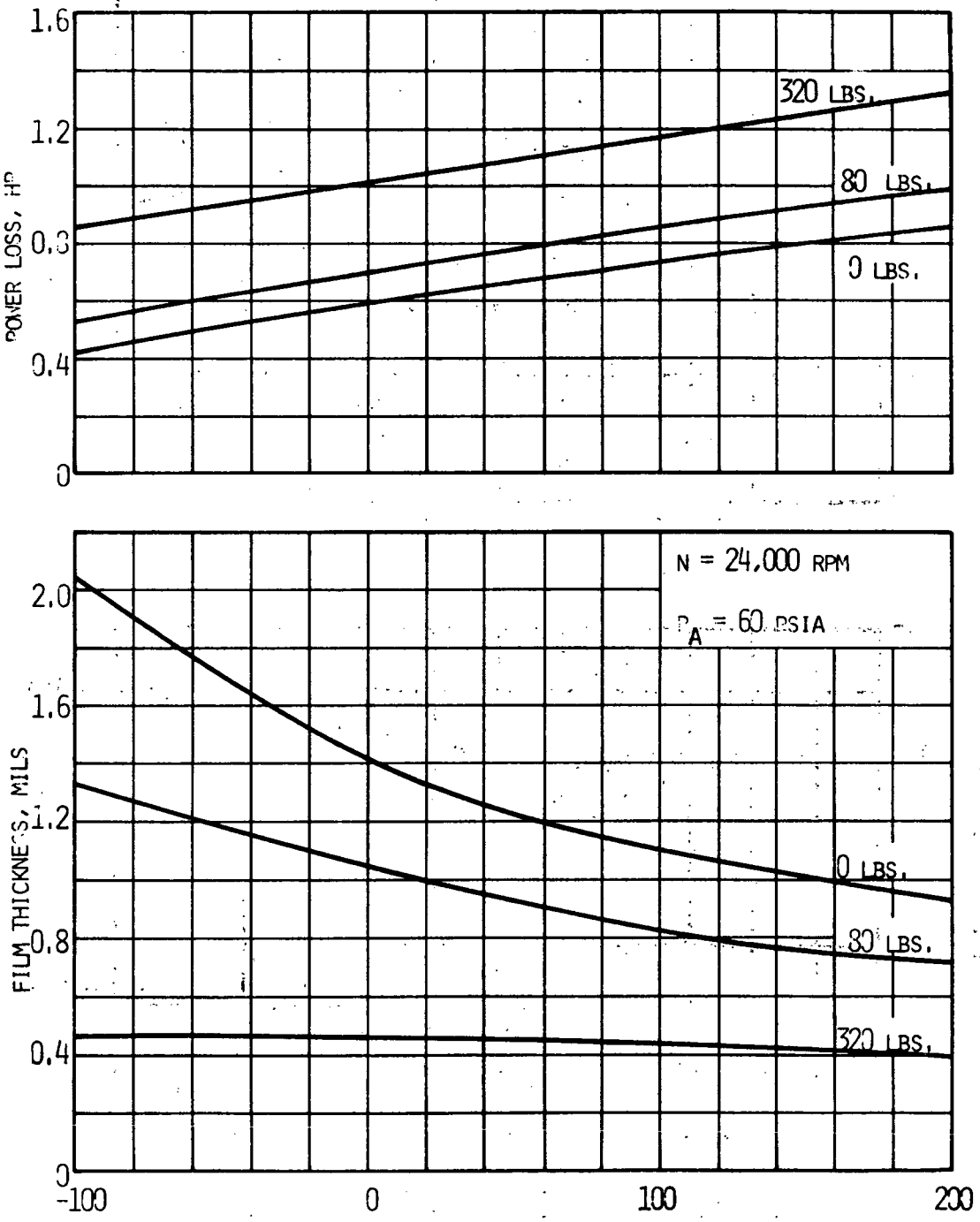

Figure 134

Figure 134 shows that large, positive* values of off-design thermal gradients between the shaft and housing can be tolerated without severely affecting the film thickness and, hence, reliability of the bearing. For example, when the shaft and bearing are at their design value temperatures (i.e. the off-design temperature gradient is zero), the minimum pivot point film thickness is 0.45 mils under a 4 G load. This film thickness stays almost constant, dropping by only 50 μ inches to 0.4 mils, under a 200 F off-design thermal gradient.

Figure 134 also shows that negative* values of off-design thermal gradients will result in an increase in minimum film thickness. This is due to the fact that, when the housing temperature rises relative to the shaft temperature, there is a corresponding increase in radial clearance and reduction of preload. The bearing film thickness is thereby improved, but unstable operation can result at zero or low bearing loads. In view of the large thermal mass of the housing, it is unlikely that the housing temperature can show large temperature rises relative to the rotor, so that the presence of large negative, off-design thermal gradients appears to be remote. Nevertheless, detailed thermal analysis of the system under transient as well as steady state conditions should be made later in the design of the TAC to ascertain the complete, anticipated ranges of housing and shaft temperatures. If these future thermal studies show that bearing instability is a potential problem area due to off-design increases in bearing clearance, the bearing design would have to be adjusted, e.g. by increasing the preload.

Tilting pad bearings have a very high tolerance to axial thermal gradients, provided that these gradients are monotonic, i.e. provided that the temperature difference between the journal and pads is highest at one end and lowest at the other (Ref. 42). Under this condition a "coning" type distortion of

---

* "Positive" value is used here to define off-design thermal gradients where the shaft temperature rises relative to the housing temperature. Conversely, a "negative" value denotes that the housing temperature increases relative to the shaft temperature.

the film shape occurs, which is automatically corrected by the self-alignment capability of the pads. The bearings are, however, less tolerant of thermal gradients that give rise to a "crowning" type of distortion, i.e. where the highest temperature is achieved near the center-line of the bearing and decreases towards each end. This happens when large, axial thermal gradients are set up in the rotor to conduct away the heat generated in the film. To minimize such axial gradients, copper shunts or axial, finned heat exchangers are attached to the bore of the rotor. Figure 135 illustrates the calculated pad distortions for three cases:

a. Heat removed without use of a high thermal conductivity shunt or heat exchanger.
b. Heat removed with 1/4" thick copper shunt in rotor bore.
c. Heat removed with axial heat exchanger in rotor bore.

The magnitudes of pad distortion in this figure are the arc heights. In the absence of either a shunt or a bore heat exchanger, Figure 135 shows that the distortion of the pads is about 2 mils. This amount of distortion is clearly excessive since the bearings are designed to operate at minimum film thicknesses ranging from 1.4 mils at 0 load to about 0.4 mils at 4 G load.

With a copper shunt, the distortion is reduced to about 0.3 mils, while with a bore heat exchanger the distortion becomes extremely small, about 0.1 mils. Thus, provisions for minimizing axial thermal distortions, by use of either a copper shunt or a bore heat exchanger are necessary to insure satisfactory tilting pad bearing performance.

Pivot Design

Table LVII shows the pivot design criteria formulated for the TAC application and

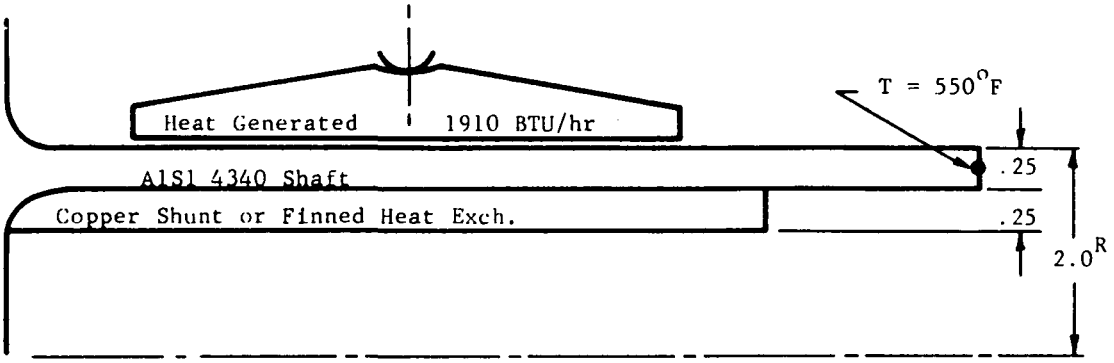
Heat Generated 1910 BTU/hr
T = 550°F
AISI 4340 Shaft
Copper Shunt or Finned Heat Exch.
.25
.25
2.0R

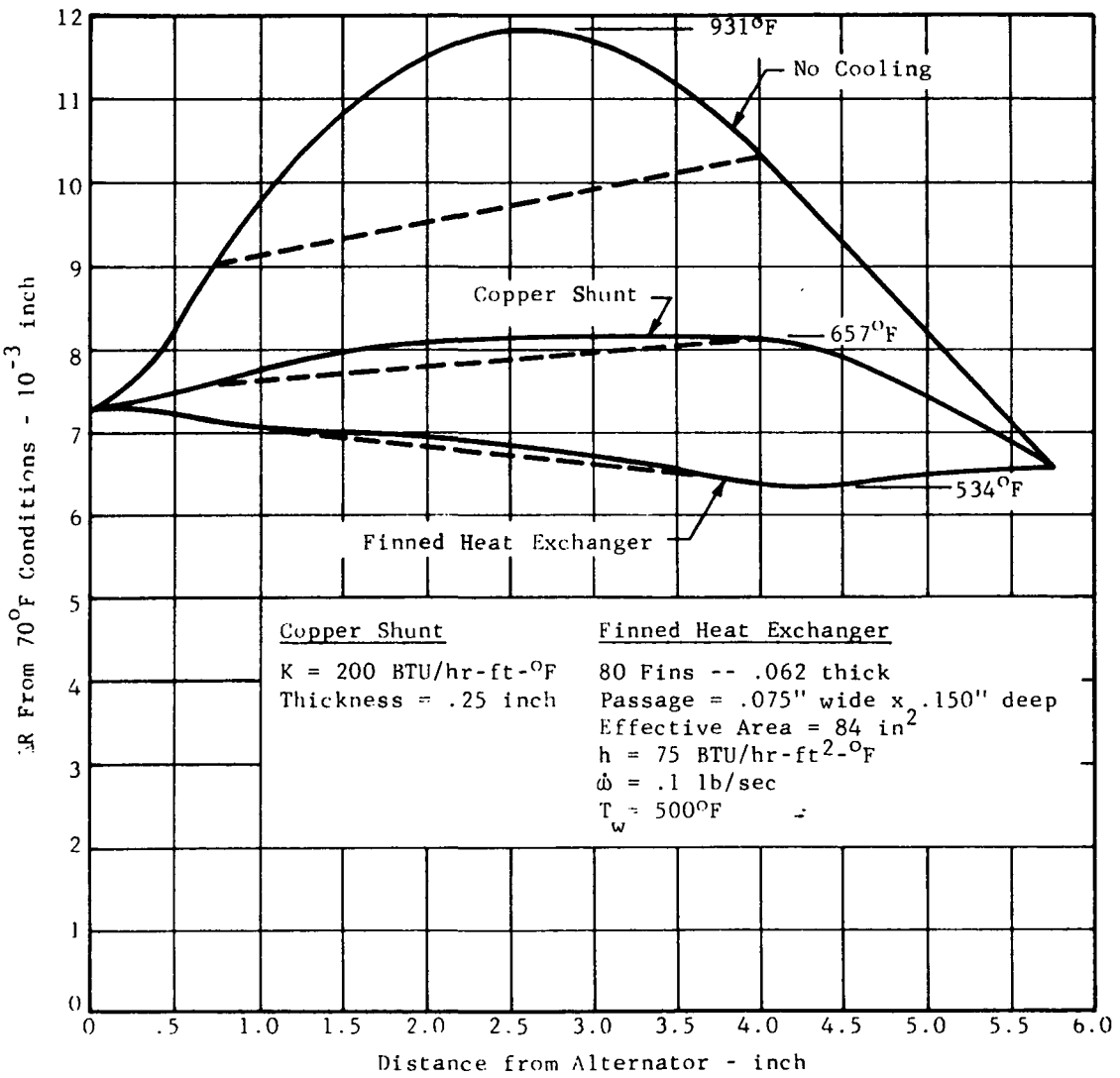
931°F
No Cooling
Copper Shunt
657°F
534°F
Finned Heat Exchanger
ΔR From 70°F Conditions - 10-3 inch
Distance from Alternator - inch
Copper Shunt
K = 200 BTU/hr-ft-°F
Thickness = .25 inch
Finned Heat Exchanger
80 Fins -- .062 thick
Passage = .075" wide x .150" deep
Effective Area = 84 in2
h = 75 BTU/hr-ft2-°F
ẇ = .1 lb/sec
Tw = 500°F

Figure 135

TABLE LVII

TAC - PRELIMINARY JOURNAL BEARING DESIGN PIVOT DESIGN

DESIGN CRITERIA

1. OPERATIONAL CAPACITY TO 700 F
2. NON-CONFORMING SPHERICAL PIVOT
3. PIVOT HERTZIAN STRESS < 120,000 PSI AT DESIGN CONDITIONS
4. PIVOT CONFORMITY (I.E., RATIO OF RADIUS OF CURVATURE OF SOCKET TO RADIUS OF CURVATURE OF BALL) TO BE SELECTED TO GIVE MAXIMUM ROLLING AND MINIMUM SLIDING CHARACTERISTICS, CONSISTENT WITH ACCEPTABLE STRESS LEVEL
5. NO FATIGUE LIMITED MEMBERS

PIVOT DIMENSIONS AND MATERIALS

RADIUS OF CURVATURE OF BALL = 0.35"

RADIUS OF CURVATURE OF SOCKET = 0.42"

MATERIAL: M-2 TOOL STEEL, R_c 50 HARDNESS

MAXIMUM STRESS: AT 0G: 78,000 PSI

AT 1G: 113,000 PSI

AT 4G: 156,000 PSI

ALTERNATE PIVOT DESIGN

"CRUCIFORM" TYPE FLEXURE CURRENTLY UNDER TEST FOR "B" ENGINE BACK-UP BEARINGS

the pivot dimensions and materials selected to meet these criteria. A non-conforming ball-in-spherical socket geometry with a radius ratio (i.e. ratio of socket radius to ball radius) of 1.2 provides for free rolling motions and minimum sliding in the pivots. The geometry and materials noted in this table were successfully tested in Ref. 44 at stress levels up to 200,000 psi and temperatures up to 1000 F. This type of pivot was used successfully in the turboalternator of the NASA's "A" Engine (Ref. 41) and other gas-bearing machinery.

An alternative pivot design that uses, basically, a dual flexural gimbal in place of the Hertzian contact ball-socket arrangement is illustrated in Figure 136. This is the "Cruciform" type of flexural pivot that was developed as the alternate flexure for the back-up bearing system of the NASA's "B" Engine. The "Cruciform" pivot arrangement is designed to have angular stiffnesses in the pitch, roll and yaw directions that are at least two orders of magnitude smaller than the corresponding, calculated angular stiffnesses of the fluid film at its design point operating condition. Under Contract NAS3-10951 tests have been conducted with a bearing pad supported first on a standard ball-socket pivot and then on a "Cruciform" pivot. The test data indicated that the load capacity and threshold of instability were about the same with both pivot types.

The "Cruciform" pivot eliminates unlubricated sliding and allows easy introduction of hydrostatic jacking gas through a capillary tube at the center of the "Cruciform". It also avoids the problem of brinelling of the Hertzian contact members under repeated, high shock loads. However, the "Cruciform" pivot has not yet been fully evaluated and tested in an actual machine, and in particular, it has not yet been subjected to high G vibration and impact tests.

Figure 136. "CRUCIFORM" TYPE FLEXURE PIVOT

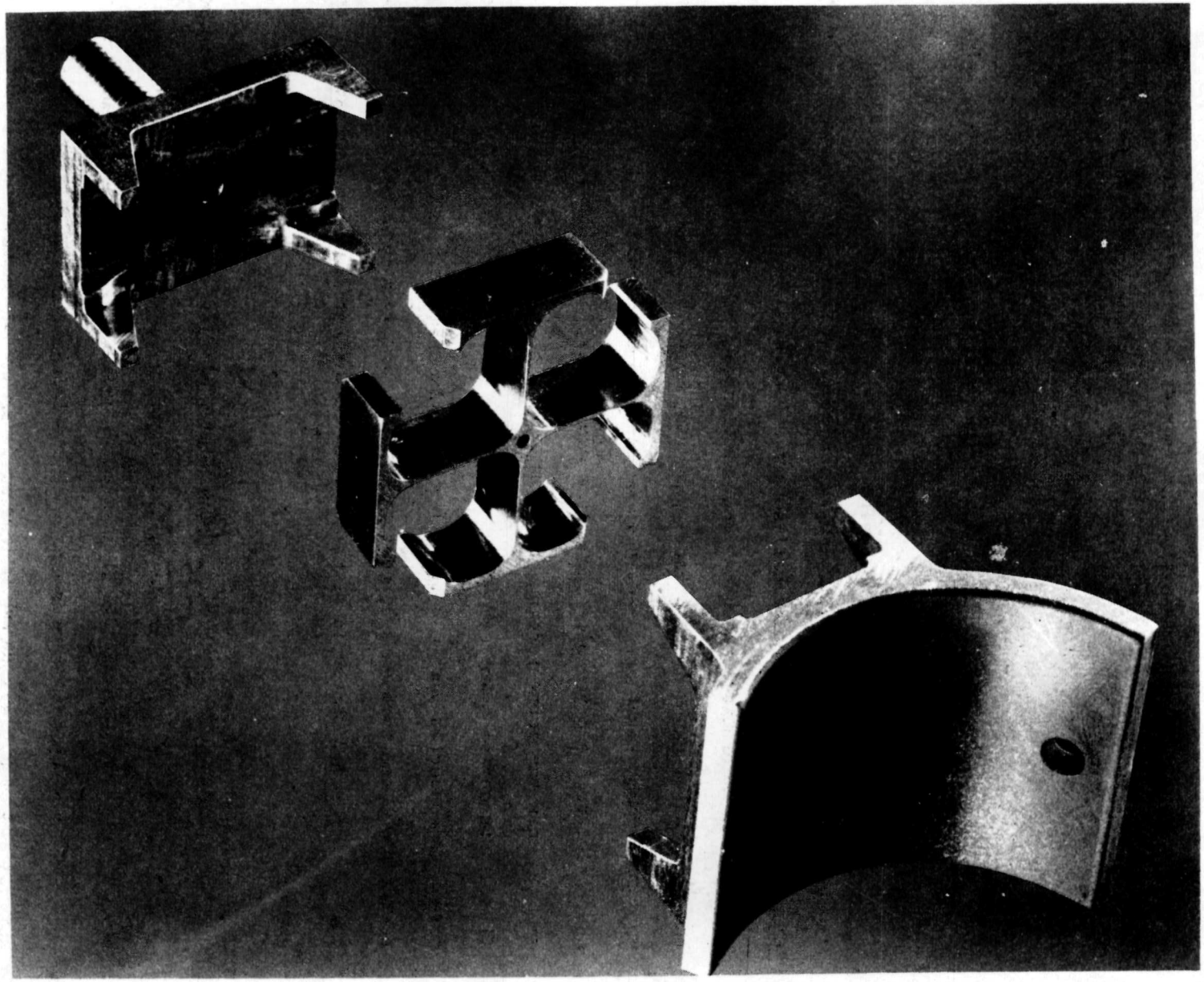

At the present time, therefore, the non-conforming ball-socket pivot is selected for the TAC, with the "Cruciform" pivot retained as a retro-fittable alternate.

Summary of Conclusions

The conclusions of the preliminary design study of the journal bearings conducted as part of Phase I of the TAC Design Study are summarized in Table LVIII. From all aspects of the mechanical design and hydrodynamic performance, including:

- Load Capacity
- Stability
- Tolerance of Thermal Gradients
- Pivot Design

it appears that a conservatively designed, self-acting, gas lubricated journal bearing system can be readily achieved for the TAC.

With regard to hydrostatic jacking, the bearing is designed so that there is no preload (i.e. the pads are free of the shaft) at start-up. Thus, both in 0 G field and in vertical operation in a 1 G field, hydrostatic jacking is not required. In horizontal operation in a 1 G field, each bearing will support an 80 lb. load (i.e. 6.7 psi on a 4" x 3" bearing) plus any alternator load that may be present at start-up. The feasibility of ommitting hydrostatic jacking under this condition of operation will depend on the torque available at start up, as well as on the capability of the materials to withstand low speed rubs under a bout 7 psi pressure.

TABLE LVIII

TAC - PRELIMINARY JOURNAL BEARING DESIGN SUMMARY

1. A 4" DIAMETER x 3" LONG BEARING IS SELECTED. DIAMETER IS SET BY CRITICAL SPEED AND ROTOR-DYNAMICS REQUIREMENTS. LENGTH IS SELECTED TO PROVIDE NECESSARY LOAD CAPACITY WITH MINIMUM PARASITIC LOSS.

2. THIS BEARING MEETS ALL DESIGN TARGETS ESTABLISHED FOR RUGGED, CONSERVATIVE DESIGN, EXCEPT THAT MINIMUM PIVOT POINT FILM THICKNESS IS MARGINAL AT 40 KW(e) POWER LEVEL WITH 4G LOAD.

3. UNDER PHASE III, INCREASE OF BEARING LENGTH TO 4" WILL BE CONSIDERED, TO INCREASE MINIMUM PIVOT POINT FILM THICKNESS TO 0.0004".

4. TILTING PADS ARE DESIGNED WITH 10,000 TO 15,000 LBS/INCH UPPER PAD FLEXURES TO PERMIT:

   - NO PRELOAD AT START-UP
   - TOLERANCE OF OFF-DESIGN, SHAFT-TO-HOUSING THERMAL GRADIENTS RANGING FROM - 100 F TO + 200 F

5. FURTHER OPTIMIZATION RELATIVE TO FLEXURE STIFFNESS AND DESIGN POINT CLEARANCE SHOULD BE CONDUCTED IN PHASE III.

6. DETAILED STABILITY ANALYSIS OF ROTOR-BEARING SYSTEM INCLUDING ALTERNATOR DYNAMIC FORCES SHOULD BE CONDUCTED WHEN ELECTRICAL INPUT IS PROVIDED.

7. NON-CONFORMING PIVOTS ARE SELECTED TO MINIMIZE SLIDING AND RETAIN MAXIMUM PIVOT STRESS BELOW 120,000 PSI AT DESIGN POINT AND LESS THAN 160,000 PSI AT 4G LOAD.

8. JOURNAL BEARINGS DESIGN DOES NOT APPEAR TO POSE MAJOR PROBLEM AREAS OR REQUIRE MAJOR EXTENSIONS OF THE STATE-OF-THE-ART.

THRUST BEARINGS

Operating Conditions

These are summarized in Table LIX. As in the case of the journal bearings discussed earlier, the self-acting thrust bearing must support the applied load over a speed range from 50 percent to 120 percent of design speed. The bearing cavity is maintained at compressor inlet pressure, i.e. at 55 and 15 psia respectively for the 160 KW(e) and the 40 KW(e) power levels. A double-acting thrust bearing, both faces having the same geometry and load capacity, is used.

The operating load of the bearing comprises:

a. Gravity Load

The thrust bearing must support the full weight of the rotor (160 lbs.) when the unit operates vertically in 1 G environment. There is no gravity load when the unit operates horizontally or in 0 G environment.

b. Aerodynamic Thrust Load

The design of the aerodynamic components will be such as to achieve very close balance of the thrust load, within about 100 lbs. This residual unbalance will be supported by the thrust bearing.

c. Alternator Loading

Axial displacements of the alternator rotor will give rise to small magnetic and electrical loads. These, however, are expected to be small in comparison with the gravity and aerodynamic unbalance loading.

TABLE LIX

TAC - PHASE I
GAS LUBRICATED THRUST BEARING FOR 24000 RPM MACHINE

1. CONDITIONS OF OPERATION

160 KW(e)

	LOAD lbs.	SPEED rpm	AMBIENT PRESSURE psia
DESIGN POINTS			
0G OR 1G HORIZONTAL	0	24000	55
1G VERTICAL	160	24000	55
OPERATING RANGE	-160 to +160	12000 to 28800	55

40 KW(e)

	LOAD lbs.	SPEED rpm	AMBIENT PRESSURE psia
DESIGN POINTS			
0G OR 1G VERTICAL	0	24000	15
1G HORIZONTAL	160	24000	15
OPERATING RANGE	-160 to +160	12000 to 28800	15

ORBITAL LOAD: 640 lbs. (MAXIMUM)
LUBRICANT: He - Xe MIXTURE, MW = 39.94

* GRAVITY LOAD ONLY. DOES NOT INCLUDE UNBALANCED AERODYNAMIC THRUST LOADS OR ALTERNATOR THRUST LOADS.

d. Orbital Loading

As in the case of the journal bearings, the thrust bearings must support a 4 G load during orbital maneuvers for short durations.

Selection of Bearing Geometry

Figure 137 illustrates, schematically, several of the conventional gas thrust bearing geometries. For the purpose of the TAC application only the first two of these (the helical grooved and the shrouded step bearings) were analyzed. The last three bearing types (the plain-step, the tapered land, and the tilting-pad) all have been shown in previous studies to have substantially lower load capacity. The principal reason for this is that they all lack end sealing lands, so that their side leakage flows are higher and their hydrodynamic pressures (and, consequently, load capacities) are lower than those of the shrouded step bearing.

Figure 138 illustrates the full annular shape of the two, initially selected geometries. As noted in this figure, the helical grooved bearing has been used extensively in prior turbomachinery, including both the turbocompressor simulator and the turboalternator of the NASA's "A" Engine. The NASA's "B" Engine (the BRU) uses a plain step thrust bearing.

The next step in the selection of a pad bearing geometry was made on the basis of comparison of calculated load capacities of the helical grooved and shrouded step bearings for the operating conditions of the TAC. This comparison is illustrated in Figure 139 assuming in both cases an 8" O.D. x 4.25" I.D. bearing size. This figure shows that, at the 55 psia ambient pressure corresponding to the 160 KW(e) power level, the two bearing types have virtually the same

THRUST FACE GEOMETRIES
TAC - PRELIMINARY THRUST BEARING DESIGN

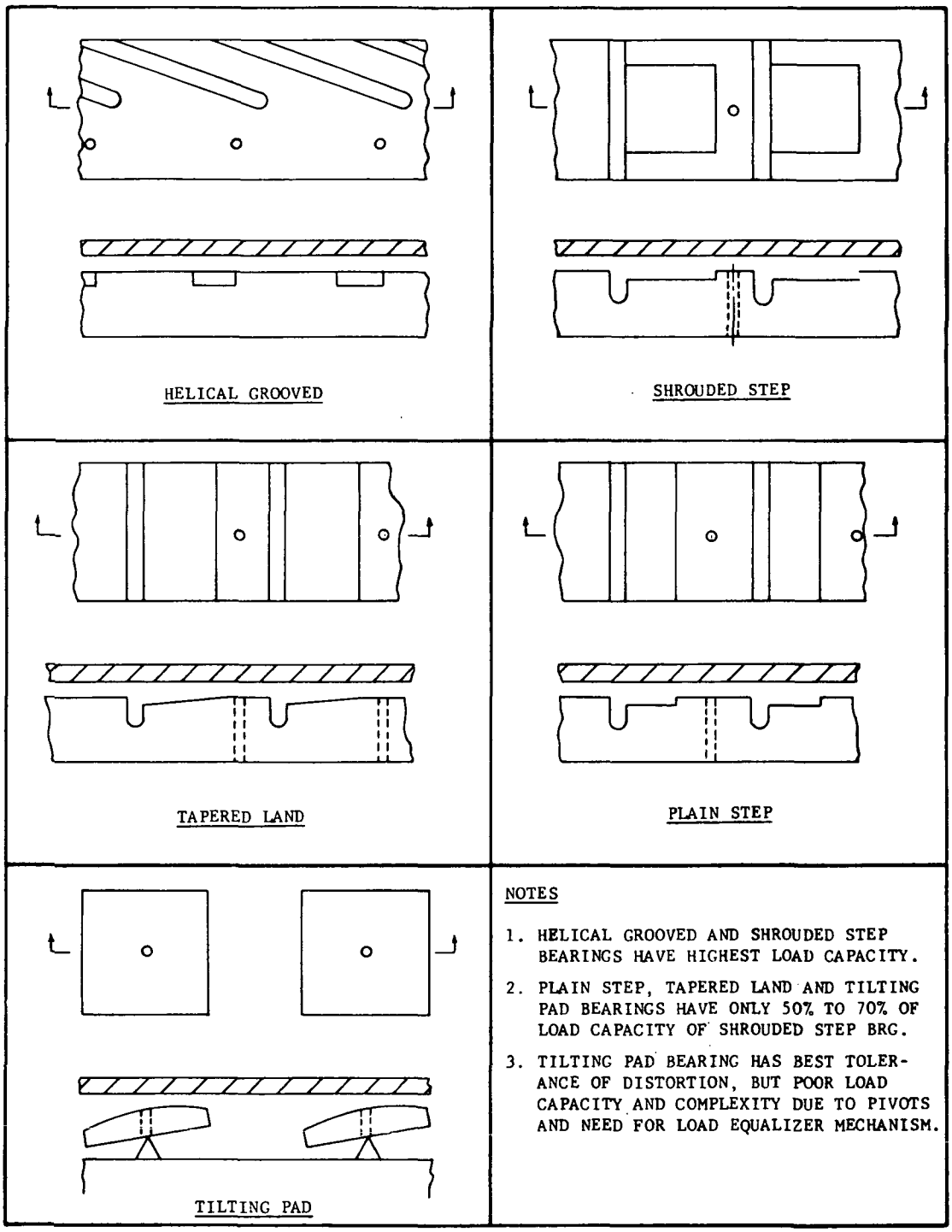

Figure 137

THRUST BEARING TYPES
TAC - PRELIMINARY THRUST BEARING DESIGN

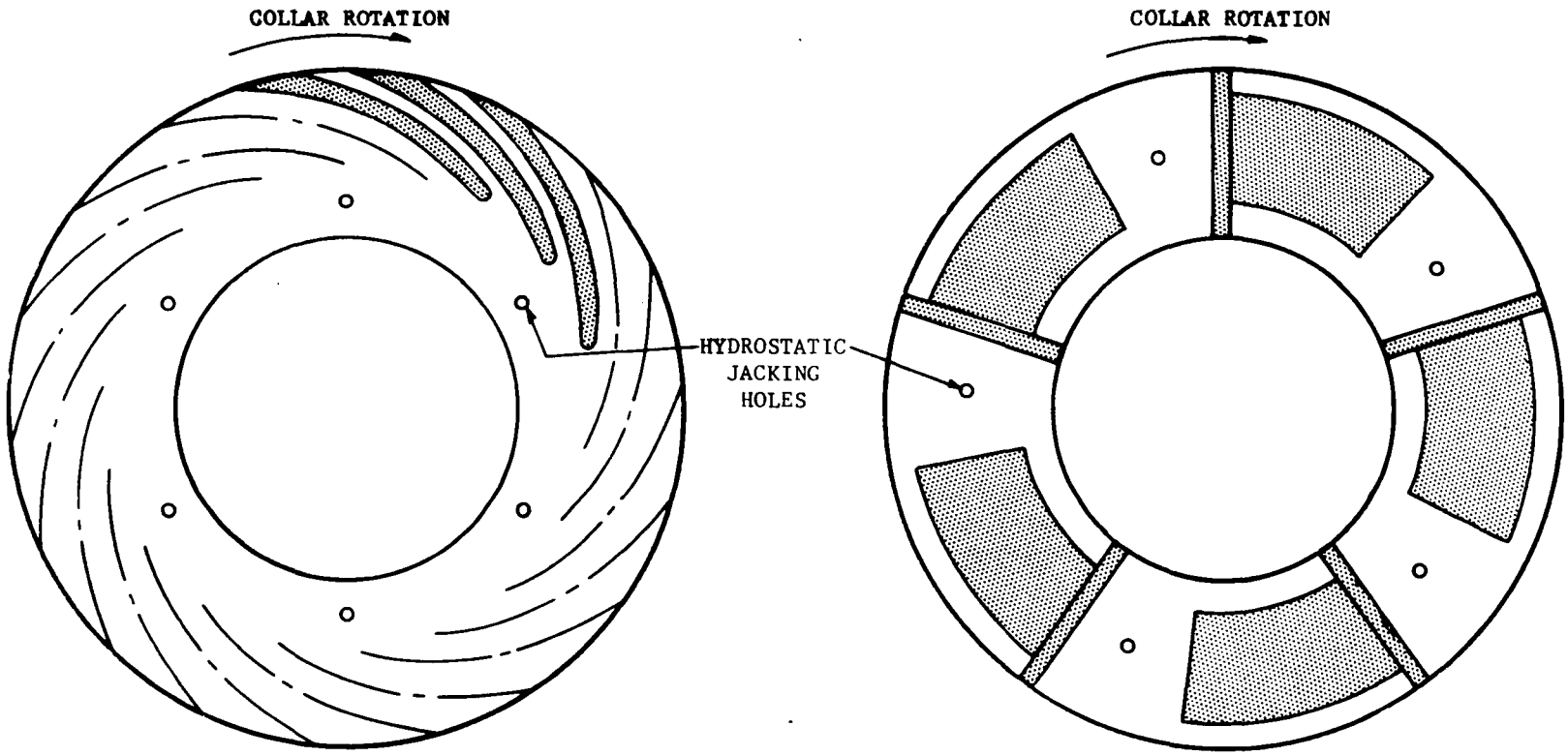

HELICAL GROOVED THRUST BEARING

USED IN: AXIAL FLOW TURBOCOMPRESSOR (3.25" DIA.)
TURBOALTERNATOR (7" DIA.)
N_2 TURBOCOMPRESSOR (7" DIA.)
AND VARIOUS MOTOR DRIVEN GAS BEARING COMPRESSORS FOR NUCLEAR LOOPS (4" TO 7" DIA.)

SHROUDED STEP THRUST BEARING

PLAIN STEP BEARINGS WERE USED IN THE RADIAL FLOW TURBOCOMPRESSOR AND THE BRU (3.5" DIA.)

Figure 138

COMPARISON OF THRUST BEARING TYPES

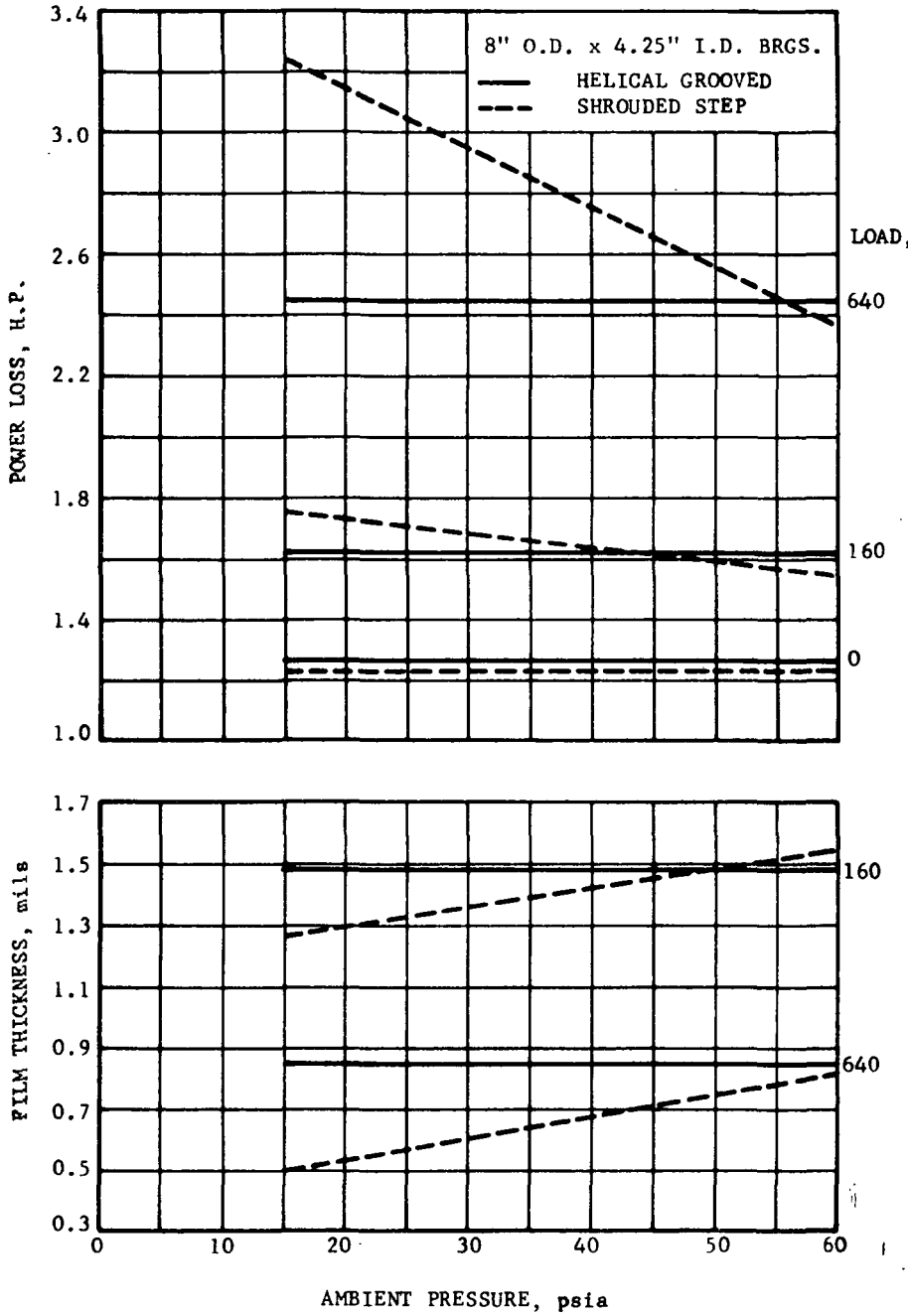

NOTES: 1. AT 55 psia, THE TWO BEARINGS SHOW ABOUT EQUAL PERFORMANCE.

2. THE PERFORMANCE OF THE SHROUDED STEP BEARING DETERIORATES AT LOW AMBIENT PRESSURE AND IS MARGINAL AT 15 psia AND 4G LOAD.

Figure 139

load capacity and very nearly equal power loss over the full range of loads up to 4 G. However, while the helical grooved bearing maintains its load capacity, independently of the ambient pressure down to the value of 15 psia that corresponds to 40 KW(e) power level, the shrouded step bearing suffers a significant loss of load capacity as the ambient pressure level is reduced. In fact, at 15 psia ambient pressure and 4 G load, the film thickness of the shrouded step bearing drops to 0.5 mils which is marginal for an 8" O.D. bearing. The power loss, which in the case of gas bearings is very nearly inversely proportional to film thickness, increases correspondingly in the case of the shrouded step bearing thus magnifying the problem of heat removal.

Since there are no other significant advantages of one bearing type over the other, the helical grooved bearing geometry was selected for TAC application.

Bearing Size and Performance Calculations

Table LX summarizes the design targets selected for the thrust bearing. As in the case of the journal bearings discussed earlier these targets were chosen to provide a factor of safety and to avoid marginally small film thicknesses under any of the specified load conditions, including 4 G loads for short durations.

Figure 140 is a comparison of the calculated film thickness and power loss for double acting, 7" O.D. and 8" O.D. helical-grooved thrust bearings. As shown by this figure and the table at the bottom of the figure, the 7" O.D. bearing would be entirely adequate except at the 4 G load condition where its film thickness reduces to 0.52 mils which is somewhat marginal. The 8" O.D. bearing has calculated film thicknesses in excess of 0.8 mils under all loads up to

TABLE LX

DESIGN TARGETS

1. HIGH LOAD CAPACITY MARGIN OVER THE FULL OPERATING RANGES FOR 40 KW(e) AND 160 KW(e) POWER LEVELS, INCLUDING OFF-DESIGN CONDITIONS UP TO:
   - 4G LOAD AT DESIGN SPEED AND OVERSPEED
   - SPEED RANGE FROM 12,000 TO 28,800 RPM

2. MINIMUM FILM THICKNESS UNDER ALL OPERATING CONDITIONS, INCLUDING 4G LOAD, $> 10^{-4} D_{outer}$.

3. TOLERANCE OF THERMAL DISTORTIONS AND PREVENTION OF "RUNAWAY" THERMAL CONDITION FOR DISTORTIONS UP TO 1 MIL UNDER 4G LOAD.

4. MINIMUM POWER LOSS CONSISTENT WITH ITEMS 1, 2, AND 3 ABOVE.

5. PROVISION OR COOLING PROVISIONS TO SATISFY ITEM 3 ABOVE.

TAC - PRELIMINARY THRUST BEARING DESIGN
EFFECT OF BEARING SIZE

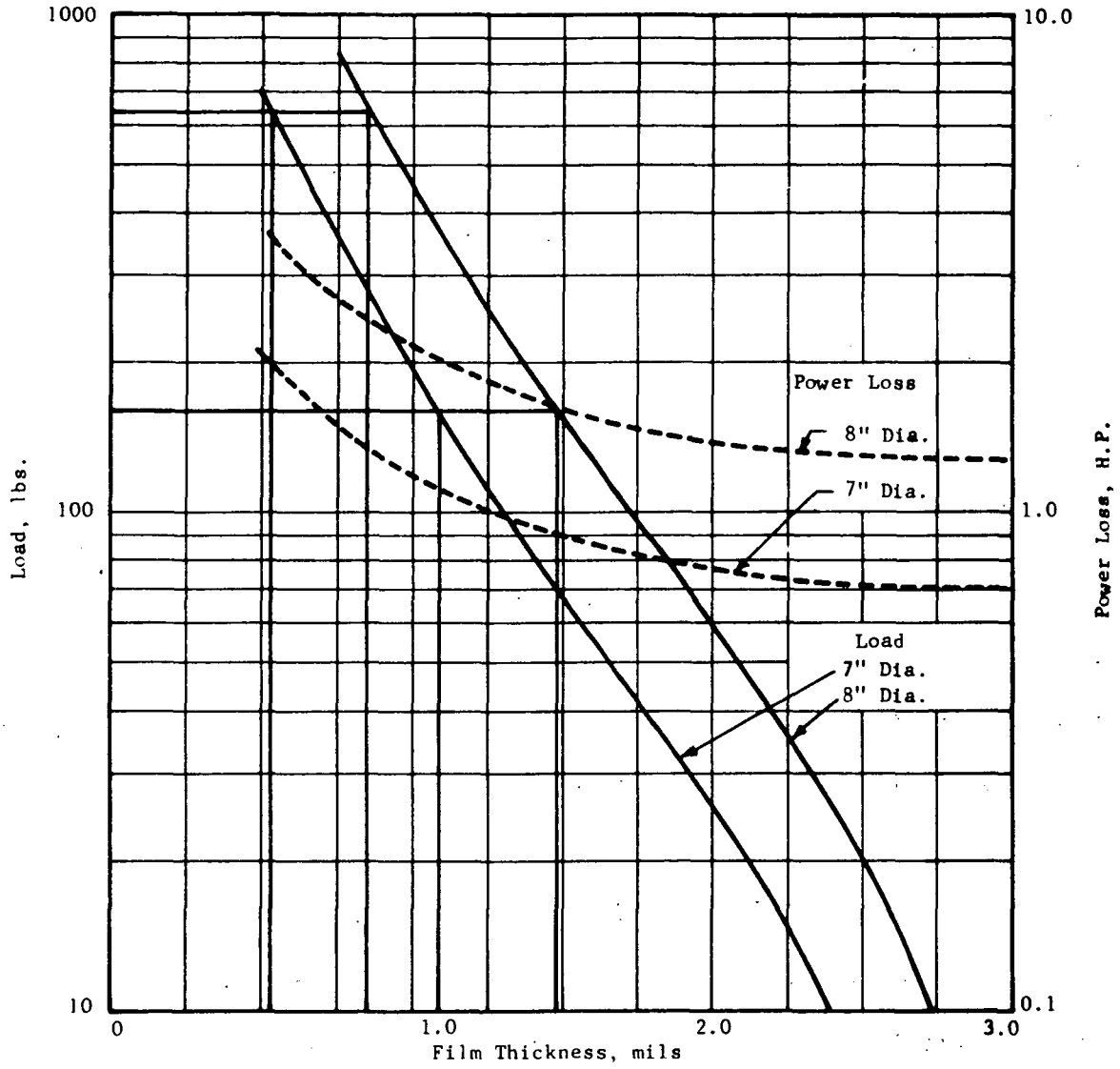

Load lbs.	Diameter inches	Film Thick. mils	Power Loss H.P.
0	8	3	1.26
	7	3	0.71
160	8	1.48	1.62
	7	1.09	1.12
640	8	0.85	2.45
	7	0.52	2.00

Figure 140

and including 4 G and was therefore selected in this preliminary design.

Figure 141 shows the selected geometry for the 8" O.D. thrust bearing. The geometrical parameters such as groove-to-land width ratio, and groove angle arc near the optimum values for this type of bearing (Ref. 45). The groove length selected is a little smaller than optimum to provide adequate radial land lengths on each side of the hydrostatic jacking holes. The groove depth is optimized for thin films (about 0.7 mils), in order to provide additional load capacity margin.

The calculated performance of this bearing over the full speed range (50 percent to 120 percent of the 24,000 rpm design speed) is plotted and tabulated in Figure 142. The data in this figure is for the complete, double-acting bearing with 6 mils axial play. The data shows adequate film thickness over the full, specified range of operation.

Effects of Thermal Distortion

Analysis of gas bearings as well as past experience clearly shows that one of the most critical elements in design of high speed, gas-lubricated thrust bearings is the control of the thermal distortions of bearing and collar surfaces. Since the thermal capacity of the gas flow through a self-acting gas bearing is small, the heat generated has to be removed by conduction. To remove this heat, thermal gradients are set up in the bearing elements and these, in turn, can distort the bearing film resulting in loss of load capacity. In extreme cases, a runaway condition can occur whereby the distortions caused by the thermal gradients result in sufficiently severe loss of load

TAC - PRELIMINARY THRUST BEARING DESIGN

2. BEARING GEOMETRY

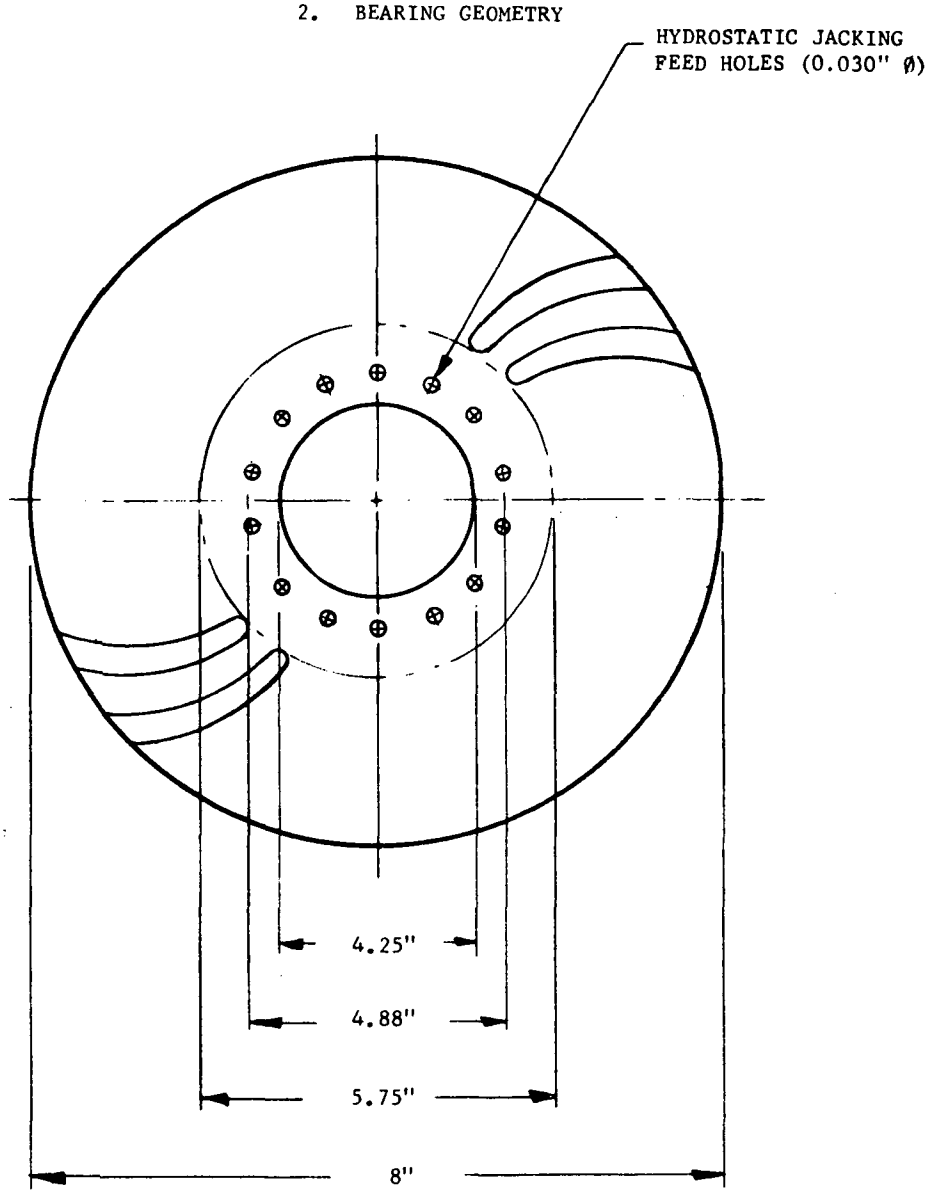

24 GROOVES
GROOVE DEPTH = 0.0022" (I.E. OPTIMUM FOR h = 0.0007")
GROOVE WIDTH/LAND WIDTH = 1.6
GROOVE ANGLE = 71.9°
DOUBLE ACTING BEARING, $h_1 + h_2$ = 0.006"

Figure 141

EFFECT OF SPEED
TAC - PRELIMINARY THRUST BEARING DESIGN

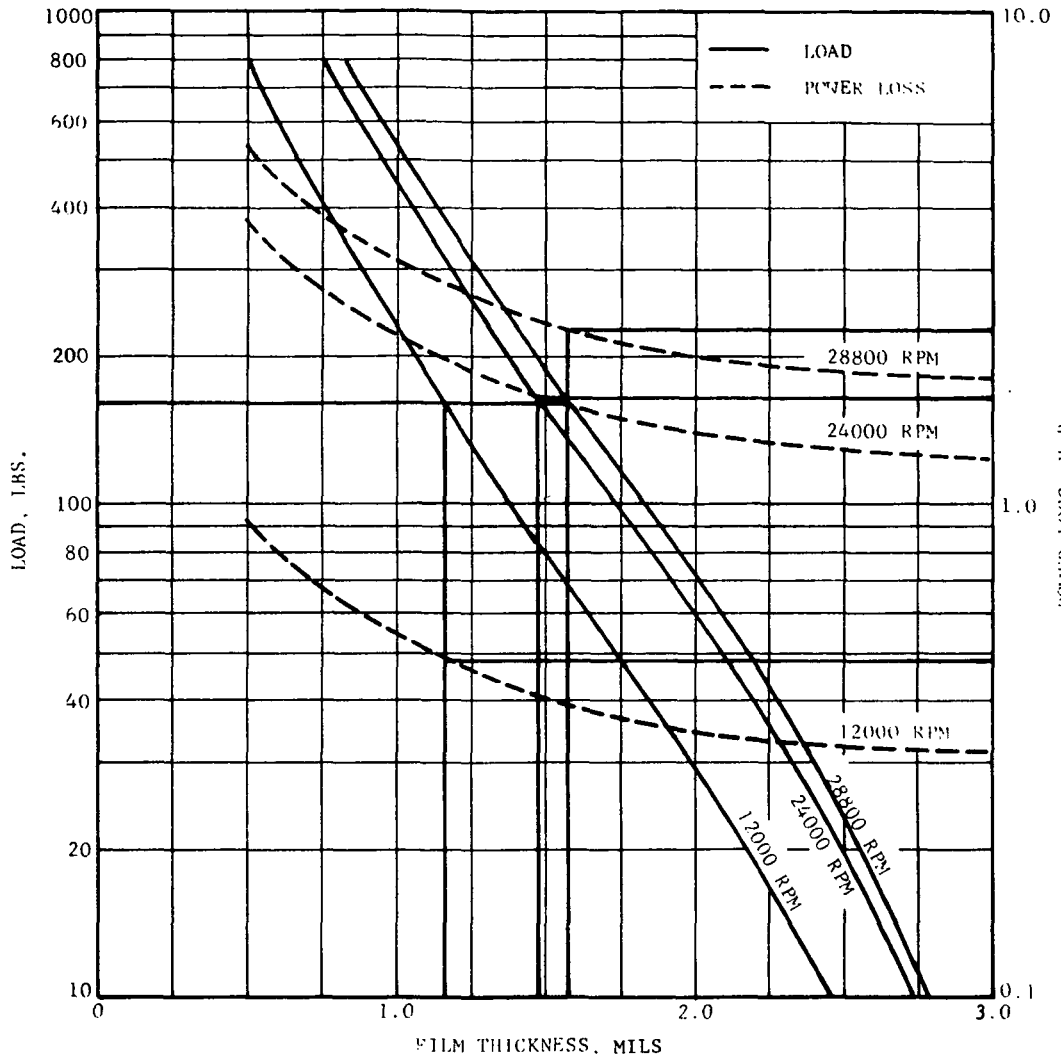

LOAD LBS.	SPEED RPM	FILM THICKNESS MILS	POWER LOSS HP
0	12000	3	0.32
	24000	3	1.26
	28800	3	1.82
160	12000	1.16	0.48
	24000	1.48	1.62
	28800	1.58	2.25
640	24000	0.85	2.45
	28800	0.93	3.30

Figure 142

capacity that the mean film thickness in the bearing is severely reduced. This leads to still larger power loss, thermal gradients, distortions, and ultimately, a failure of the thrust bearing.

Major emphasis was therefore placed on the present preliminary design study on thrust bearing design to minimize thermal distortions. This is separately discussed in this report. Specifically, a liquid cooling scheme for the thrust bearing stator that was successfully used in both the turbocompressor simulator and the turboalternator of the "A" Engine (Refs. 40 and 41) is recommended also for the TAC. This design scheme, by maintaining the rear portion of the thrust housing isothermal, stiffens it and minimizes thermal distortions.

In parallel with the mechanical design study, calculations were made to assess the loss of film thickness and increase in power loss that will accompany distortions of the film shape in an 8" O.D. helical grooved bearing.

The calculation results are given in Figure 143 and show that over a range of distortion up to $\pm$ 0.6 mils, the effect on film thickness is quite moderate. Figure 143 shows that, within this range of distortions, the loss in minimum film thickness is less than 0.6Δ, where Δ is the magnitude of the distortion. The corresponding increase in power loss is very small, less than 0.16 HP throughout, since the mean value of film thickness is little changed by the distortions. These changes in film thickness and power loss are acceptably low and show that the bearing has adequate margin of safety.

TAC - PRELIMINARY THRUST BEARING DESIGN
EFFECT OF DISTORTION

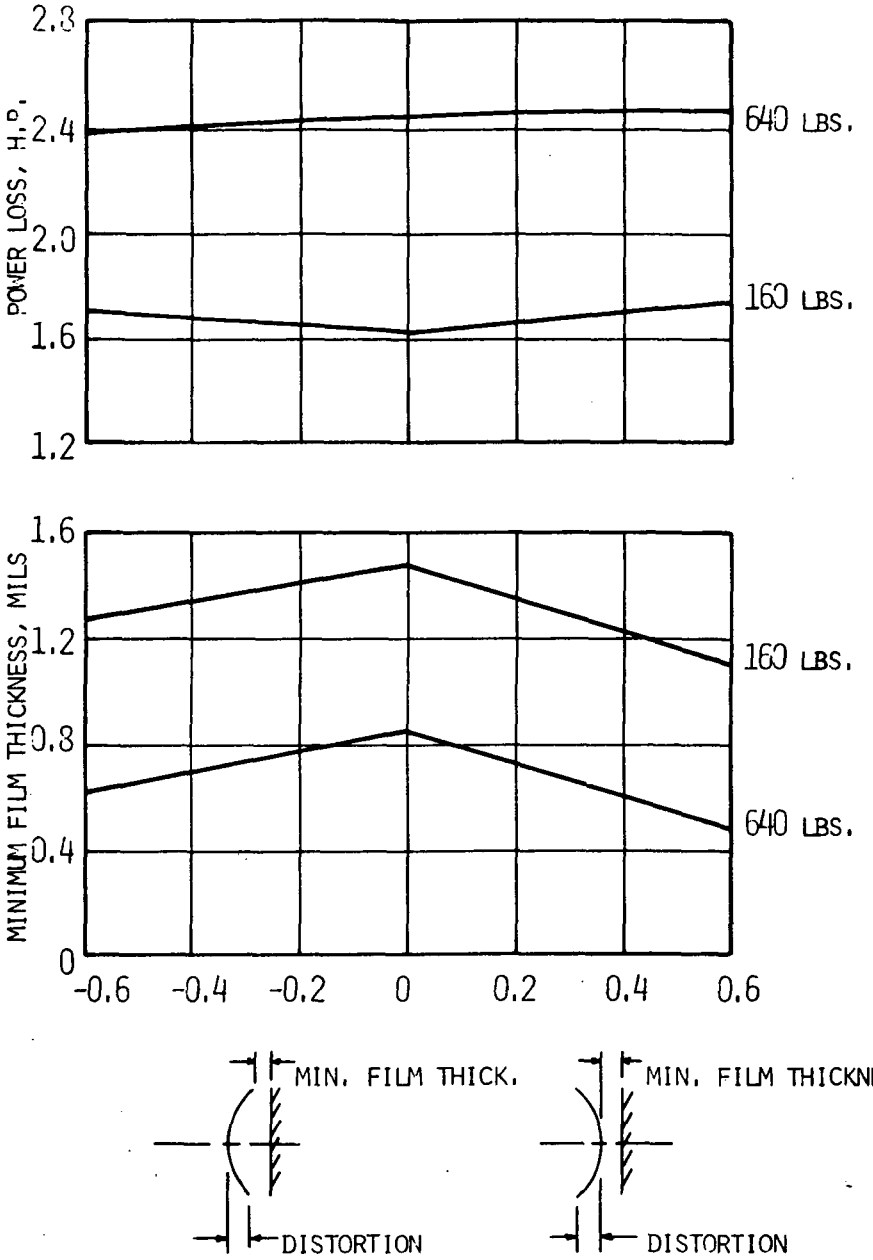

NOTES: OVER THE FULL RANGE OF DISTORTIONS INDICATED:

$$(h_{MIN})_0 - h_{MIN} \leq 0.6\ \Delta$$

$$HP - (HP)_0 \leq 0.15$$

Figure 143

Summary of Conclusions

Table LXI summarizes the conclusions of the preliminary design analysis of the thrust bearings. As in the case of the journal bearings, the analysis and computations indicate that a self-mating, gas-lubricated thrust bearing can be designed to meet the specified operating requirements of the TAC.

With flexure mounting to compensate for static misalignments between the rotor and stator, a potential problem of instability or high amplitude resonance of the combined thrust bearing-flexure mount system may be encountered. This was not analyzed in the present preliminary design study. This problem was not encountered in either the turbocompressor simulator or the turboalternator of the "A" Engine. Nevertheless, a detailed analysis of the stability of the thrust bearing and mount system should be made, using the existing analytical tools, when the design details of the mount are prepared.

TABLE LXI

TAC - PRELIMINARY THRUST BEARING DESIGN SUMMARY

1. HELICAL GROOVED CONFIGURATION IS SELECTED FOR FOLLOWING REASONS:

   (A) HIGH LOAD CAPACITY

   (B) INSENSITIVE TO AMBIENT PRESSURE VARIATIONS IN THE RANGE 55 TO 15 PSIA, CORRESPONDING TO 160 KW(e) AND 40 KW(e) POWER LEVELS. OTHER BEARING TYPES LOOSE LOAD CAPACITY AT THE 15 PSIA CONDITION.

   (C) EXTENSIVE APPLICATION EXPERIENCE IN PRIOR GAS-BEARING TURBOMACHINERY OVER THE SIZE RANGE 3.25" TO 7" O.D.

2. 8" O.D. x 4" I.D. DOUBLE ACTING BEARING IS SELECTED TO PROVIDE LOAD CAPACITY MARGIN UNDER 4G LOAD. CALCULATED FILM THICKNESSES AND POWER LOSSES ARE:

	FILM THICKNESS, MILS		POWER LOSS (BOTH FACES), H.P.	
	8" O.D.	7" O.D.	8" O.D.	7" O.D.
0 G	3	3	1.26	0.71
1 G	1.48	1.09	1.62	1.12
4 G	0.85	0.52	2.45	2.00

   (USE OF 8" O.D. BEARING IN PLACE OF 7" O.D. BEARING PROVIDES DESIRED MARGIN FOR 4G OPERATING CONDITION AT A PENALTY OF APPROXIMATELY 0.5 H.P.)

3. PERFORMANCE CALCULATIONS MADE FOR DISTORTIONS UP TO $\pm$ 0.6 MILS SHOW THAT LOSS OF FILM THICKNESS IS LESS THAN 60% OF THE DISTORTION AND INCREASE IN POWER LOSS IS LESS THAN 0.15 H.P.

4. DISTORTIONS MUCH SMALLER THAN 0.6 MILS ARE READILY ACHIEVABLE BUT REQUIRE LIQUID COOLING DESIGN SIMILAR TO THAT USED IN THE "A" ENGINE TURBOALTERNATOR.

5. THRUST BEARING DESIGN DOES NOT APPEAR TO POSE MAJOR PROBLEM AREAS OR TO REQUIRE MAJOR EXTENSIONS OF THE STATE-OF-THE-ART.

Thrust Bearing Distortion Analysis

As was discussed in the previous section, maintenance of the flatness of the thrust bearing surfaces is extremely important to the successful bearing operation. Both the runner and stator become distorted during operation because of film pressure forces and thermal gradients resulting from dissipation of bearing film generated heat. In addition the runner is subjected to centrifugal distortions. Proper control of thermal distortion is extremely important as a potential for thermal run away always exists. This is a situation where distortions lead to loss of load capacity which results in reduction in film thickness and increased heat generation. To dissipate the additional heat larger thermal gradients result which increases the thermal distortion, etc. For this reason overdesign of the cooling system is required.

The distortions that are of importance to the TAC thrust bearing are pictorially indicated on Figure 144. As can be seen from these sketches, mounting of the stator by its outside diameter and the rotor by its inside diameter results in a tendency for the rotor and stator distortions to compensate for one another in the case of axial thermal gradients and film pressure forces. This is the basic reason for such a mounting scheme in the TAC.

Because of the criticality of the thrust bearing, detailed thermal and distortion analyses were performed on several design iterations until an acceptable solution was obtained. The final model of the thrust bearing is shown on Figure 145, which shows all the pertinent dimensional and other data assumed for the analyses. Analyses were performed utilizing both AISI 4130/4340 and H-11 as these represented the two most likely alternator rotor thus, shaft, material choices during the course of Phase I. It should be noted that the

SUMMARY OF THRUST BEARING DISTORTIONS

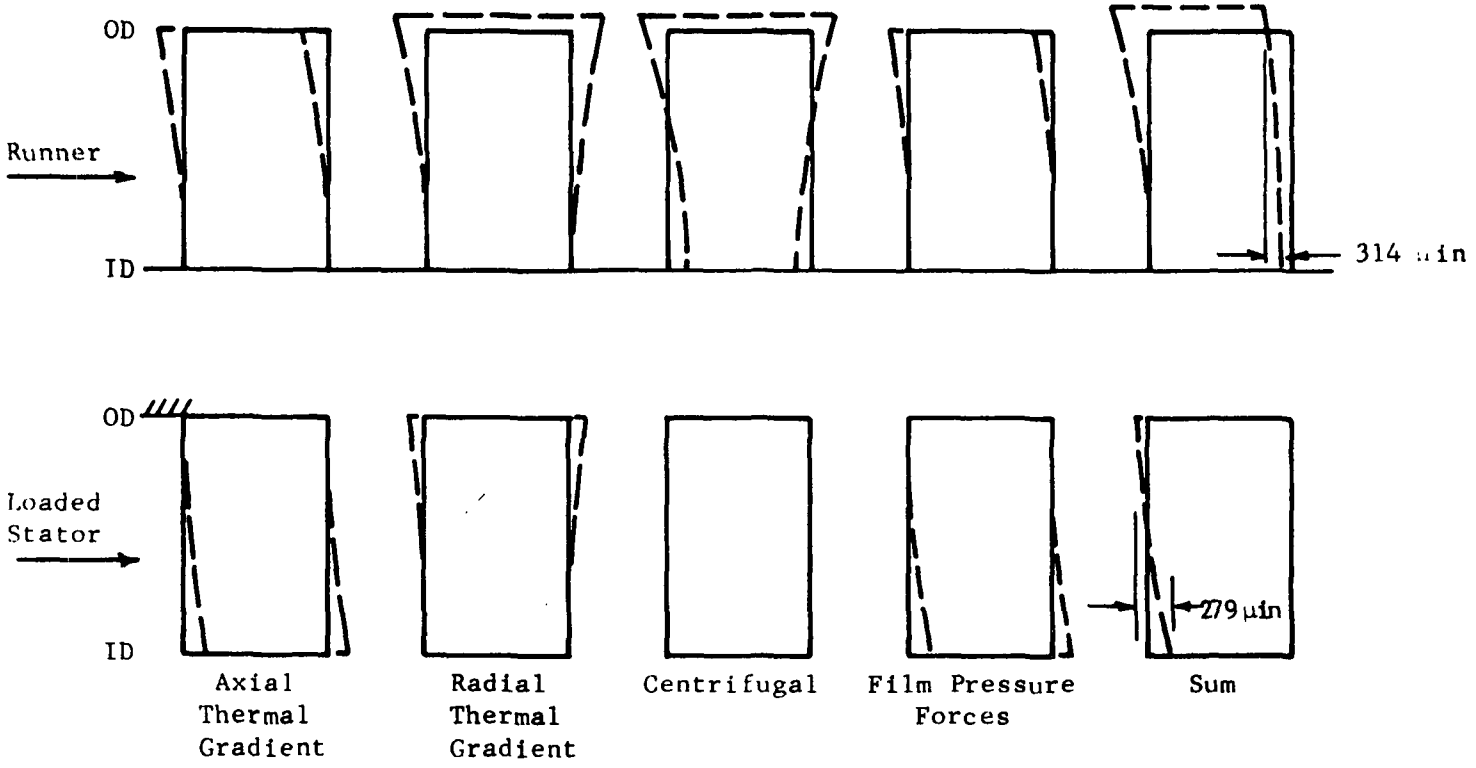

Figure 144

24000 RPM TAC
THRUST BEARING DISTORTION ANALYSIS MODEL

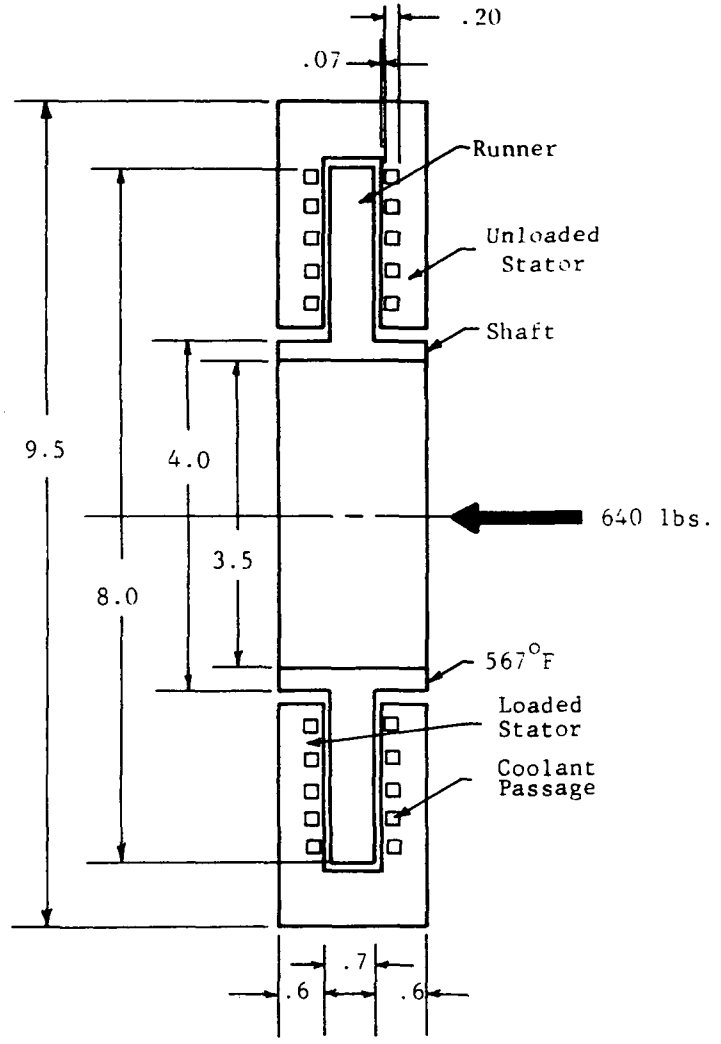

Heat Transfer Coefficients (h = BTU/hr-ft^2-°F)	
Stator Surface	3
Gap at Runner OD	102
Shaft OD	188
Coolant Passages	300
Shaft ID	0
Shaft Ends	0

Temperatures (°F)	
Ambient	575
Coolant (OD to ID)	
Loaded Side	496-506
Unloaded Side	496-501

Heat Input (H.P.)	
Loaded Film	1.58
Unloaded Film	.35
Runner OD	.18

Material	4130/4340	H-11
K (BTU/ft-°F)	21	16.5
α (in/in-°F)	6.85	6.85
ν (lb/in^3)	.284	.284
G (lb/in^2)	10.8 x 10^6	10.8 x 10^6
	.3	.3

Figure 145

heat input assumptions shown on Figure 145 are different from those previously discussed as they were derived from a preliminary design which had no provisions for hydrostatic jacking. During the course of Phase III the analysis was refined to reflect the final bearing load and heat generation parameters.

The thrust bearing stator has internal cooling passages which utilize the same coolant as the alternator (Humble 3152) introduced at 496°F near the OD where the bulk of the heat is generated. The cooling passages are relatively close to the bearing surface while the stator thickness behind the cooling passages is large. The thick portion of the stator is nearly isothermal thus free of thermal distortion and is of course stiff. This portion gives the stator its "backbone" and resists the thermal forces generated by the gradient in the portion between the bearing surface and cooling passages.

The details of the cooling passages (heat exchanger) are shown on Figure 146 along with the pertinent heat transfer, flow and pressure drop data. Since the design analysis of the heat exchanger and the nodal-point thermal gradient analysis of the thrust bearing are accomplished separately there is necessarily a certain amount of iteration between the two until all assumed inputs are matched. The significant parameters resulting from each of the analyses are summarized in Table LXII. As can be seen the significant heat transfer parameters for the two analyses are very close and a good match was obtained.

The total distortions of the stator and runner as a result of the maximum thermal, pressure and centrifugal forces are summarized in Figure 147. These curves show the shape of the distorted bearing film for both alternator rotor materials. The thrust bearing made of H-11 has a greater distorted film

24000 RPM TAC
THRUST BEARING HEAT EXCHANGER

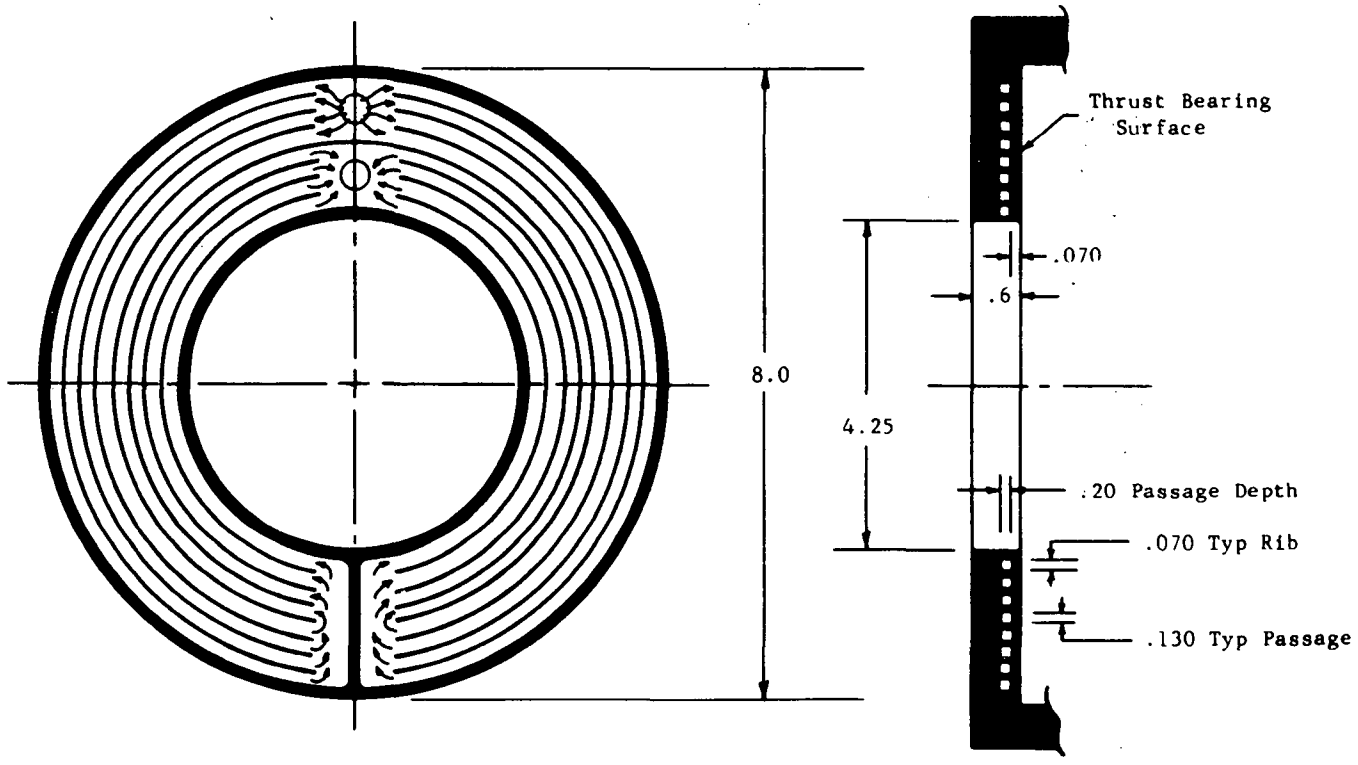

Coolant: Humble No. 3152
h: 312 BTU/hr-ft^2-^{o}F
$\dot{w}$: 567 lb/hr
Δt Cool: 10^{o}F
Vavg: 2.97 ft/sec
ΔP: 2 psi

Eff. H.T. Area: 66 in^2
Δt (metal-fluid): 28^{o}F
Q: 3960 BTU/hr

24000 rpm TAC
Thrust Bearing Heat Exchanger

Figure 146

TABLE LXII

24,000 RPM TAC THRUST BEARING COMPARISON OF THERMAL ANALYSES

	NODAL POINT THERMAL	H.X. DESIGN
Heat to coolant (BTU/hr)	3900	3960
h cooler (BTU/hr-ft^2-^{o}F)	300 (A)	312
T metal - T coolant (^{o}F)	26	28
ΔT coolant (^{o}F)	10 (A)	9.9
Effective area (in^2)	72	66

(A) = Assumed values

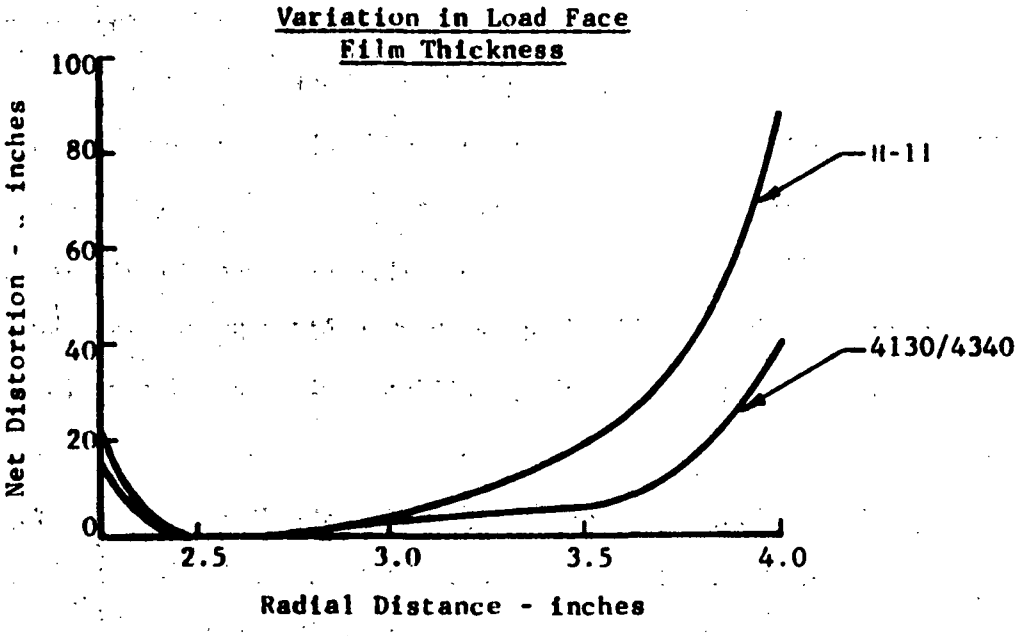
Variation in Load Face
Film Thickness
Net Distortion - .. inches
100
80
60
40
20
0
2.5
3.0
3.5
4.0
Radial Distance - inches
11-11
4130/4340

Figure 147

shape resulting from its lower thermal conductivity. Both, however, have negligible distortions out to a radius of 3.5 inches with the distortion at the O.D. (4.0 radius) still a small portion of the film thickness (more than 800 μ inches).

In conclusion, the thrust bearing design evolved in Phase I has sufficiently large heat transfer coefficients and area to remove the bearing generated heat. The thermal and mechanical distortions within the bearing film region are small when compared to the minimum film thickness and no significant thrust bearing performance degradation is anticipated as a result of distortions.

Alternator Cavity Seals for Gas Bearing TAC

One of the major disadvantages of the 36,000 rpm TAC mounted on gas bearings was the high alternator windage losses occurring because of the high cavity pressure (approximately 120 psia min) and the high rotative speed. With this combination of factors, it was not possible to maintain the maximum windage loss below 9.6 KW.

However, by sealing the alternator cavity from the rest of the interior of the machine which is necessarily at some pressure above compressor inlet (120 psia) and reducing the alternator cavity to some low pressure, it is possible to reduce the alternator windage losses to an acceptable level.

To establish the feasibility of such an approach, a preliminary study was accomplished during Phase I in which both hydrodynamic and hydrostatic/hybrid face type seals were evaluated. Figure 148 shows a conceptual arrangement of an alternator cavity seal adjacent to the compressor end bearing. Conceptually, the seal can be either hydrodynamic or hydrostatic with the major difference being the radial width.

The hydrodynamic type seal schematically shown on Figure 149 is basically a floating spiral groove thrust bearing which acts as a visco pump. The seal is designed in such a manner (by proper relationship of pumping groove geometry and balance of secondary seal diameter) that an equilibrium film thickness — of the order of a mil or less — is achieved at some predetermined pressure differential across the seal face. Under this equilibrium condition there is no net flow across the seal, thus it acts as a high head- zero flow pump.

36 AG TAC
COMPRESSOR END BEARING - SEAL ARRANGEMENT

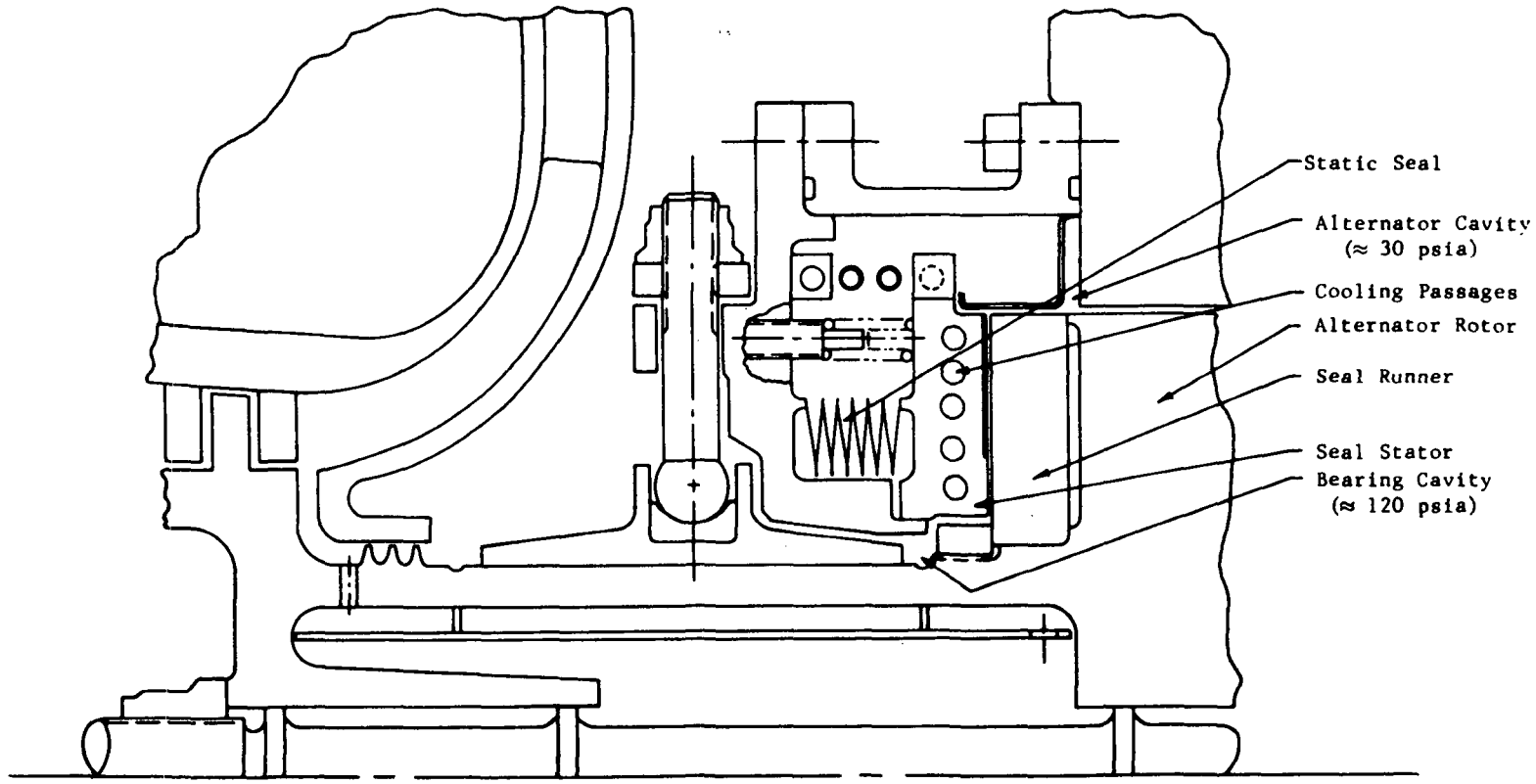

36AG TAC
Compressor End Bearing
Seal Arrangement

2/2/70

Figure 148

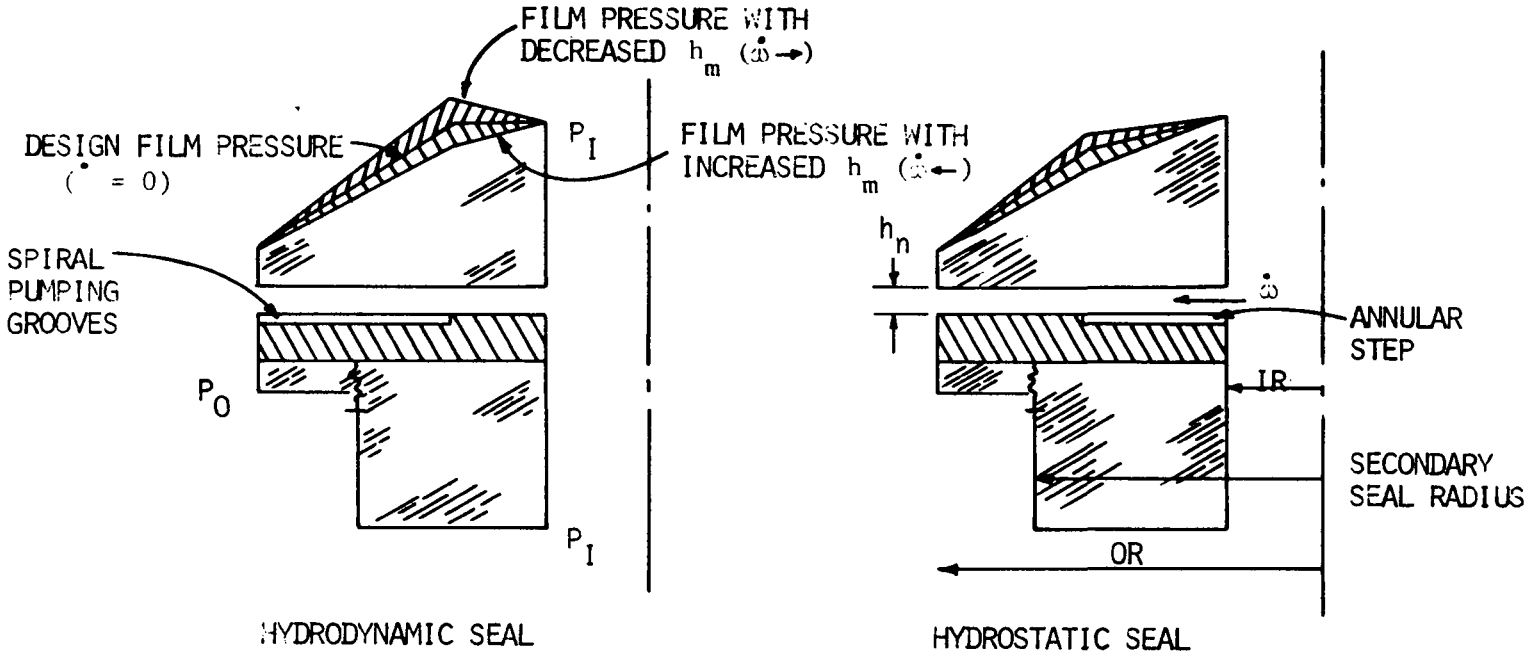

ALTERNATOR CAVITY SEAL CONCEPTS

Figure 149

If the system is perturbed in such a manner as to close the seal gap (reduce film thickness h_m) the seal becomes a more effective pump thus increasing the peak film pressure causing a restoring force to open the seal gap as is shown in Figure 149. If the seal is perturbed in such a manner as to increase the gap, the opposite happens; thus the floating seal has positive stiffness and is stable.

The hydrostatic seal, unlike the hydrodynamic seal, requires an external device to evacuate the cavity and maintain the desired low pressure. The seal in this case does not act as a pump but as an impedence to flow. This impedence is provided by a sealing dam of close clearance (usually a mil or less). Positive stiffness of the floating seal can be achieved by a purely hydrostatic effect as with the annular step shown on Figure 149 or by hydrodynamic grooves or Rayleigh type steps. The latter approach, generally termed a hybrid seal, sometimes provides higher stiffness than the pure hydrostatic seal. The leakage of either approach having the same radial width and clearance is about the same. For the purpose of the preliminary study accomplished in Phase I, the pure hydrostatic was considered since the major factor was leakage.

The significant results of the alternator cavity seal study accomplished during Phase I are summarized in Table LXIII. The basic size of the hydrodynamic seal was initially selected to be 6.0 inches OD to match the alternator OD at that point in the Phase I study and 3.0 inch ID as this was consistent with the stub shaft size. Table LXIII shows calculated performance for two 6.0" OD x 3.0" ID hydrodynamic seals. The calculated performance of the first, with a .00056 film thickness, represents the results of a power loss

TABLE LXIII

36000 RPM GAS BEARING TAC
SUMMARY OF PRELIMINARY ALTERNATOR CAVITY SEAL DESIGNS

SEAL TYPE	OD INCH	ID INCH	h_{min} INCH	P_{ID} PSIA	P_{OD} PSIA	$\dot{\omega}$[1] LB/SEC	SEAL[1] KW	WINDAGE KW	PUMP[2] KW	TOTAL KW
HYDRODYNAMIC	6.0	3.0	.00056	120	5	0	4.05	1.40	0	5.45
HYDRODYNAMIC	6.0	3.0	.00063	120	30	0	3.60	5.90	0	9.50
HYDROSTATIC	5.0	3.4	.001	120	30	.018	.63	5.90	2.86	9.39

1 TOTAL FOR TWO SEALS

2 RESONANT PISTON COMPRESSOR WITH 84% EFFICIENT MOTOR

optimization which considered both seal power and alternator windage loss to achieve minimum combined losses (5.45 kw). Although this operating film thickness resulted in minimum combined power, the resulting cavity pressure (5 psia) was insufficient to provide adequate heat transfer properties to remove rotor pole tip electrical losses. It was determined that a cavity pressure of at least 30 psia was required, thus the second hydrodynamic seal design with the larger film thickness. As can be seen in Table LXIII the increased film thickness reduces the seal loss but the resulting higher cavity pressure causes a significant increase in alternator windage. The combined loss is, however, still within the 6 percent allowable.

The major potential problem with the hydrodynamic seal, like that of the thrust bearing, is distortions and possible thermal runaway. The problem is much more acute with the seal than with the thrust bearing, however, because of the former's thinner film and higher heating density. Such a seal would necessarily require a sophisticated cooling scheme.

The seal distortion problem is considerably simpler with the hydrostatic or hybrid type seal because smaller radial widths and larger film thicknesses can be employed to reduce the heating density and the leakage flow can be utilized as a partial coolant. The hydrostatic seal shown on Table LXIII was sized (5.0" OD x 3.4" ID) smaller than the previously discussed hydrodynamic seal to reflect later iterations of the alternator and stub shaft sizes. The film thickness was set at .001 inch to be consistant with normal bearing practice for the size. The power loss of this seal is extremely small because of its small size and large film thickness and of course the alternator windage is the same as the 30 psia hydrodynamic seal case.

In the hydrostatic seal case, it was assumed that a resonant piston compressor could be used to evacuate the cavity to 30 psia. This is a high head low flow reciprocating pump which is driven by a linear electric motor through a spring in such a manner that the piston mass - spring system is resonant. Thus, no fly wheel or crank bearings are required. Compressors of this design concept have been built for NASA under contracts NAS-8-11660 and NAS-8-20720. The calculated input power required to pump the seal leakage is 2.86 kw which, when added to the seal and windage losses, totals very nearly the power required by the hydrodynamic seal approach.

From the preliminary study accomplished during Phase I it can be concluded that it is feasible to minimize the alternator cavity windage losses by incorporating close clearance cavity seals. The hydrodynamic zero leaking seal offers the advantage of system simplification by eliminating the need for separate pumping components. It represents, however, an advancement in the state-of-the-art and development is necessary in cooling and distortion minimization.

The hydrostatic or hybrid seal represents less of a development problem because of its potential larger film thickness and lower heating density. Development of reliable pumping components, however, is required.

BEARING SURFACE MATERIALS

Compatible surface materials that can sustain both low speed and high speed rubs without surface damage and consequent deterioration of hydrodynamic load-carrying ability are essential for successful operation of high speed turbo-machinery such as the TAC. In particular, the bearings should be capable of sustaining:

1. Unlubricated starts and stops without hydrostatic jacking.
2. Short duration contacts at high speed that can occur from shock loads or a system malfunction.

Previous experimental studies of gas bearing materials have been conducted under NASA Contracts NAS3-6013 and NAS3-9433 and Air Force Contract AF33(615)-3235 (References 40, 46 and 47 respectively). In all these cases the tests were conducted using pivoted bearing pads, 1.5" diameter x 1" long riding on a rotating journal to closely simulate running conditions in an actual bearing. Under Contract NAS3-9433 (Ref. 46), these tests were supplemented by additional ones conducted with a helical grooved thrust bearing. All the tests included both start-stop and high speed impact rubs at speeds of 38,500 rpm (Refs. 46 and 47) and 50,000 rpm (Ref. 40).

A variety of material combinations, both solid and plasma sprayed coating were tested. The test temperatures were:

Room Temperature	(Refs. 40, 46, 47)
500 to 550 F	(Ref. 40)
900 F	(Refs. 46, 47)
1400 F	(Refs. 46,47)

At room temperature and in the 500-550 F temperature range, the combination of chrome oxide vs. chrome oxide proved to be far superior to any of the other combinations tested and it exhibited excellent tolerance of both repeated starts and stops and repeated high speed rubs. At 900 F, however, the wear rate was quite high so that other combinations, notably aluminum oxide vs. nickel chrome bonded chrome carbide, were preferred both at that temperature and at 1400 F.

In view of its excellent performance at temperatures up to 550 F, chrome oxide vs. chrome oxide was used for the bearings of the NASA's "A" Engine turbocompressor simulator and turboalternator. It has also been used successfully and without any incidents in a variety of other gas lubricated rotating machinery. Table LXIV lists the field experience with this material combination.

Under NASA Contract NASw1713 the turbocompressor simulator of the NASA's "A" Engine has been used to experimentally evaluate the dynamic performance of gas bearings under vibration and shock conditions. Table LXV, lists the principal tests that have been conducted to-date. Here again, the material combination is self-mated chrome oxide and it has demomstrated the capability of withstanding repeated high speed contacts without significant wear, surface damage or consequent deterioration of hydrodynamic load capacity.

Presently, in connection with the preliminary design and development of an advanced gas-lubricated, air breathing aircraft engine for the U.S. Army, under Contract DAA 302-69-C-0062, additional material testing under start-stop conditions is in progress using the following material combinations:

TABLE LXIV

TAC - PRELIMINARY BEARING DESIGN

FIELD EXPERIENCE WITH CR_2O_3 COATED GAS LUBRICATED TURBOMACHINERY BEARINGS

APPLICATION	DRIVE	RATED POWER AND SPEED	YEAR DELIVERED	ACCUMULATED OPERATING HOURS	COMMENTS
CIRCULATOR FOR ADVANCED REACTOR EXPERIMENT	MOTOR	18 HP at 19,500 RPM	1966	8000	DRY START
CIRCULATOR FOR CHEMO-NUCLEAR LOOP AT BROOKHAVEN	MOTOR	2 to 10 HP 3000 to 10,000 RPM	1966	200	DRY START
SECONDARY LOOP COMPRESSOR FOR HTGR UNIT NO. 1	MOTOR	18 HP at 25,000 RPM	1968	1200	DRY START
SECONDARY LOOP COMPRESSOR FOR HTGR UNIT NO. 2	MOTOR	18 HP at 26,000 RPM	1970	200	DRY START
"A" ENGINE TURBOALTERNATOR	TURBINE	12 HP at 12,000 RPM (Operated at up to 30 HP)	1967	1400	JACKING PROVIDED
"A" ENGINE TURBO COMPRESSOR SIMULATOR	TURBINE		RETAINED AT MTI FOR TECHNOLOGY PROGRAM TESTS FOR NASA	400	DRY START RADIAL. JACKING PROVIDED FOR THRUST. EXTENSIVE SHOCK & VIBRATION TESTING

TABLE LXV

TAC - PRELIMINARY BEARING DESIGN

SHOCK AND VIBRATION TESTS

TURBOCOMPRESSOR SIMULATOR FOR NASA "A" ENGINE

SPEED - 30000 RPM

LUBRICANT - AMBIENT AIR

ROTOR WEIGHT - 10.5 LBS.

SIMULATOR ATTITUDE	ENVIRONMENTAL FACTOR	REPETITIONS (OR DURATION)	FUNCTIONAL EFFECT
HORIZONTAL	DRY START-UPS	16	NONE
HORIZONTAL & VERTICAL	20G HALF-SINE SHOCK	60	NONE
VERTICAL	60G SHOCKS	21	NONE
HORIZONTAL & VERTICAL	VIBRATION UP TO 15G's	100 HOURS WITH ROTOR RUNNING 27 MIN. WITH ROTOR INERT	NONE
VERTICAL	VIBRATION PRECISELY AT FLEXURE NATURAL FREQUENCY AT 7G's AMP.	SEVERAL MINUTES	FLEXURE FAILURE
VERTICAL & HORIZONTAL	MOISTURE AND DUST IN HYDROSTATIC SUPPLY	> 100 HOURS	NONE (BUT NOTICEABLE DEBRIS ACCUMULATION)
VERTICAL & HORIZONTAL	AGGREGATE OF ABOVE		o JOURNAL BRG. PIVOTS SHOWED WEAR SPOTS 3/4 WAY THRU PROGRAM AND WERE REPLACED. o SURFACES CLEANED THREE TIMES DURING TEST PROGRAM. o FRACTURED FLEXURE REPLACED.

Material Combination	Temperature
Cr_2O_3, Self Mated	80 and 800 F
Cr_3C_2, Self Mated	80 and 800 F
50% Cr_2O_3, 50% C_3C_2, Self Mated	80 and 800 F

Spin tests, using a 2 1/2" diameter shaft coated with the above materials at 90,000 rpm and 1000 F are also in progress.

If these tests show that the temperature capability of chrome oxide extends to 800 F, it would be a good choice for the TAC where the design values of bearing temperature are less than 700 F. Alternately, self-mated chrome oxide, as well as other combinations, notably chrome carbide (either self-mated or versus aluminum oxide), silicon nitride and others, should be tested at the operating temperatures of the TAC before a final materials choice is made.

LIQUID FILM BEARINGS AND SEALS

The use of oil film bearings and seals on the 36,000 rpm TAC offers two significant potential advantages:

1. Extremely low alternator windage losses because the oil can be used as an effective sealing fluid to maintain extremely low alternator cavity pressures — approaching oil vapor pressure.
2. The oil film bearings have an indefinite life and are tolerant of foreign material and short time overloads.

The major problems associated with the oil film bearing approach are the reliable isolation of oil from the alternator and fluid machinery cavities both during operation and shut-down, and the minimization of viscous power losses.

For the purposes of the Phase I Preliminary Study, the major emphasis was on the evaluation of an integrated bearing seal design which would eliminate all non-working wetted surfaces and size minimization to reduce power. The advanced SNAP 8 type spiral groove face seal was adapted to the TAC design as it offers the significant advantage over other pumping type seals of a stable oil-vapor interface, combined shut-down capability, and recirculation which provides internal cooling.

A conceptual drawing of the bearing-seal arrangement is shown on Figure 150. This arrangement consists of a tilting pad journal bearing and two opposed shrouded Rayleigh step thrust bearings in a double acting arrangement. The inactive faces of the thrust runners are utilized as seal runners to eliminate unecessary drag losses. The only significant wetted surface that is inactive is the OD of the thrust runners. The seals are backed up in the vapor or gas regions

36000 RPM OIL LUBRICATED TAC BEARING - SEAL ARRANGEMENT

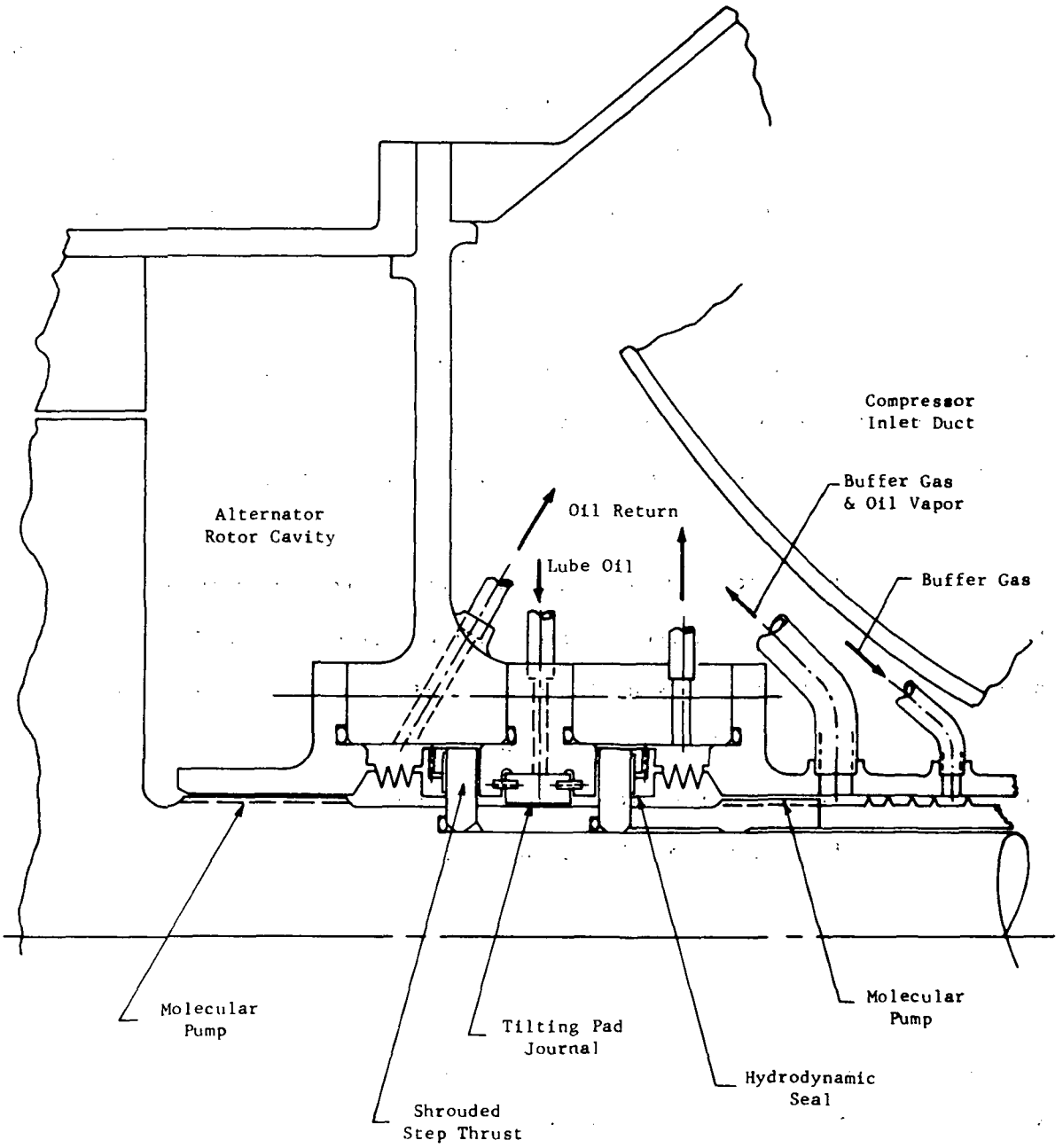

36000 rpm Oil Lubricated TAC
Bearing - Seal Arrangement

Figure 150

by molecular pumps on the shaft to aid in returning oil droplets to the hydrodynamic seal. On the compressor side is a gas buffer seal to insure that no oil vapor enters the cycle system. The buffer gas-oil vapor line would be connected to the separation system which is discussed in Section .

The power consumed by the bearing seal arrangement shown in Figure 150 is shown in Figure 151 as a function of shaft diameter. This is the sum of one journal bearing, two thrust bearings, two seals, and the losses at the runner OD. The journal bearing has a length to diameter ratio of 0.25 and the thrust bearing was sized to carry 600 lbs. ($\approx$ 4 G) at a film thickness of .0005 inches. Since most of the power is consumed by the thrust bearings, particular care was taken to insure that they were made no larger in radial width than was required to support the thrust load. The affect of reduced OD to ID ratio with increasing shaft diameters (ID) has been factored into the power loss calculations.

As can be seen from Figure 151 the losses associated with a single bearing-seal are large and increase very rapidly with diameter. Furthermore, the flow required to be pumped through the system to remove the heat generated is sizable. It should be pointed out that the 25^{o}F Δt used in calculating the Figure 151 flow curve may be excessive when considering lubricant life. If lower maximum lubricant temperatures are required, the flow rate will either have to be increased or a cavity cooler utilizing the lower temperature coolant will have to be incorporated.

Performance calculations were made on one configuration of the SNAP 8 type hydrodynamic face seal to establish its feasibility to the TAC application. This seal is shown schematically on Figure 152. The size shown was the minimum conceivable that could be incorporated into the aft end of the TAC arrange-

36000 RPM OIL LUBRICATED TAC BEARING AND SEAL LOSSES ALTERNATOR DRIVE BEARING CONFIGURATION

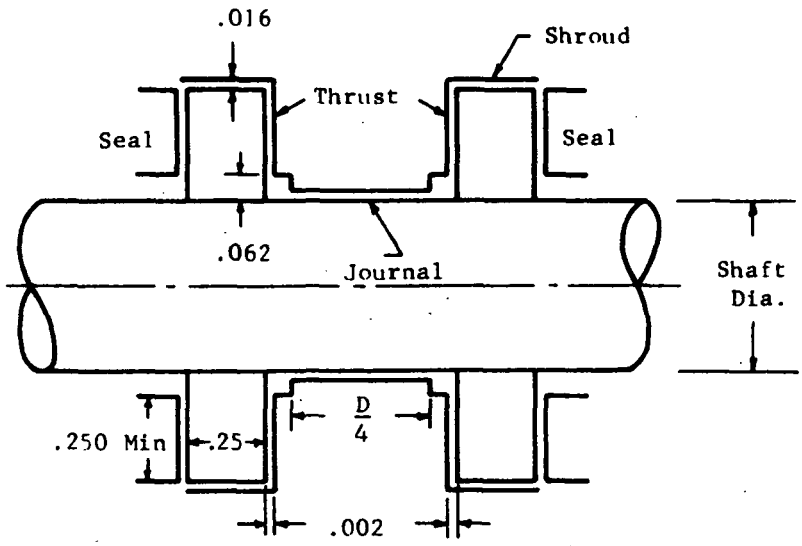

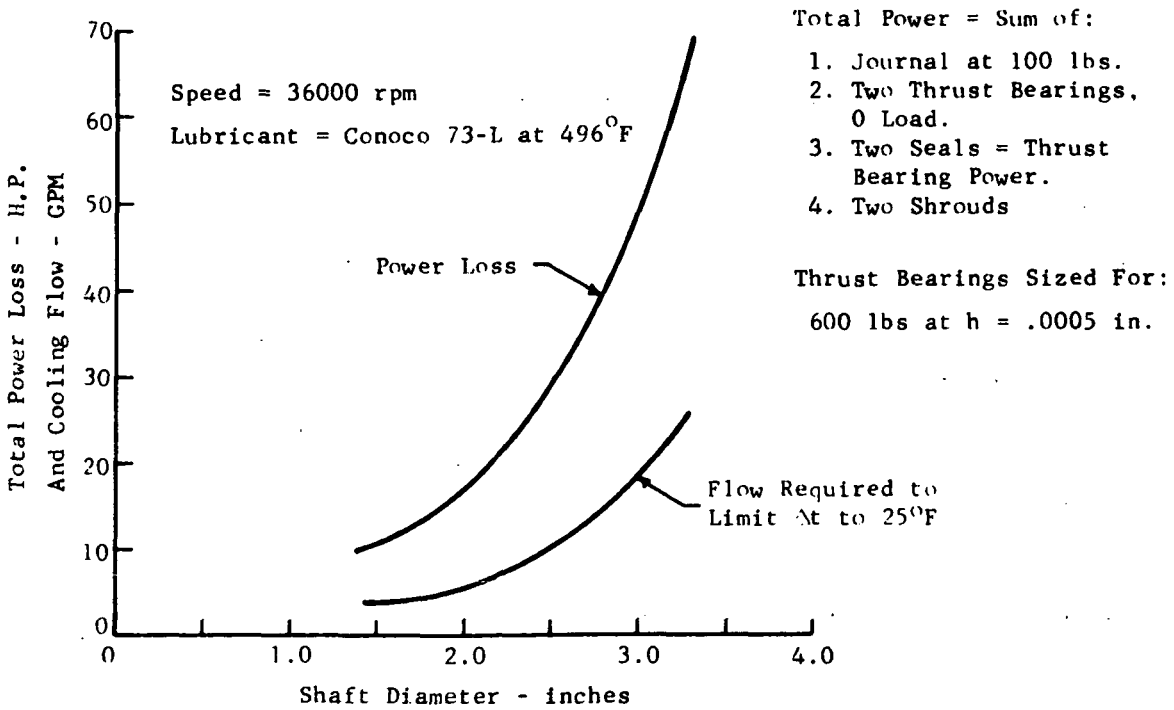

Figure 151

TYPICAL HYDRODYNAMIC OIL SEAL

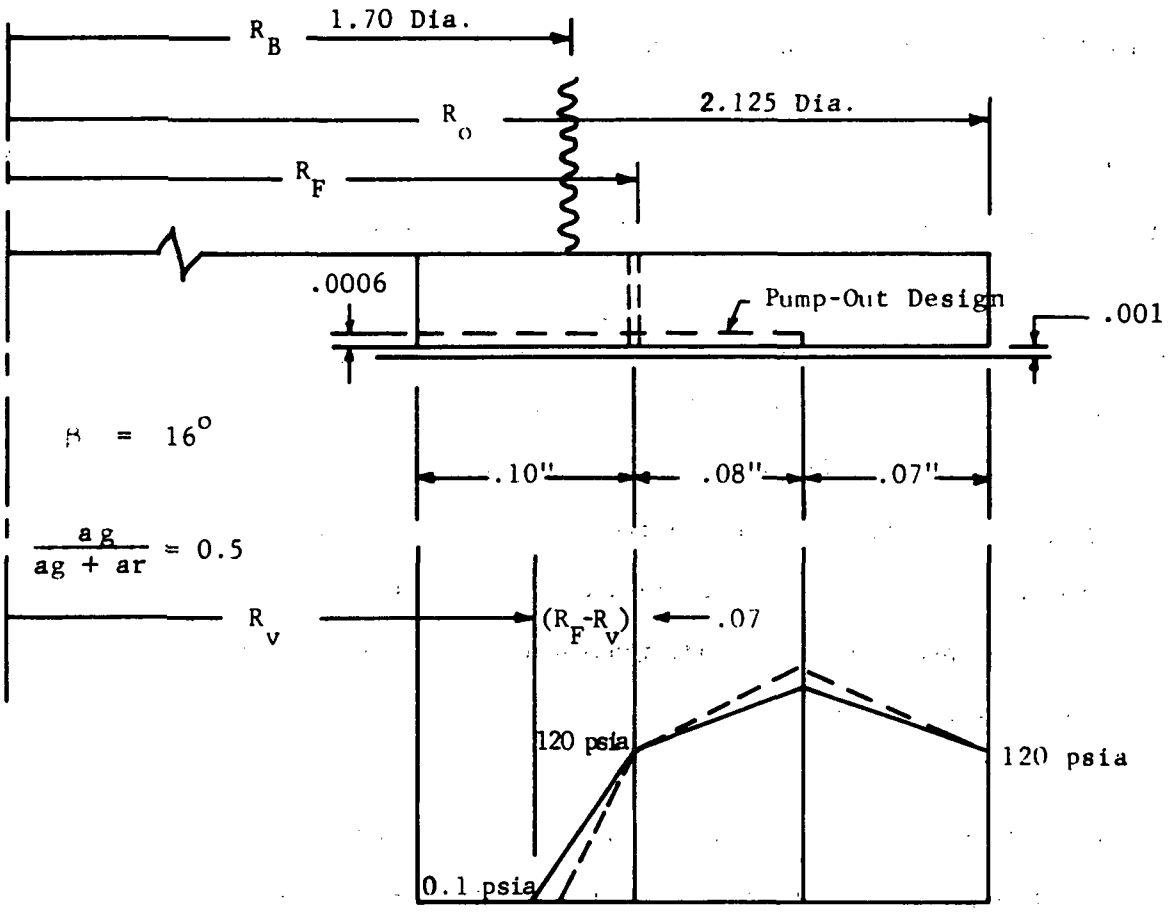

Operating Conditions:

N = 36000 rpm
Lubricant - Conoco 73-L at 496°F
Stiffness - 1.2×10^5 lb/in
Power Loss - ≈ .6 H.P.
Circulating Flow - 26.2 lb/hr
Adiabatic Δt - 84°F

Figure 152

ment shown in Figure 28. The results of the calculations which are also summarized on Figure 152 indicate that a seal as small as 2.125 inch OD can support the required 120 psi ΔP.

Figure 152 shows the seal geometry assumed for the analysis and a schematic of the pressure profile at 36,000 rpm with a 1 mil face gap (minimum film thickness) supporting a 120 psi ΔP. As can be seen from the profile, 0.07 inches of engagement is required inside of the feeding groove to the liquid-vapor interface. The stiffness of the seal fluid film (1.2×10^5 lb/in) is adequate to insure that the floating stator will follow the runner. The flow recirculating from the feeding groove to the OD is 26.2 lb/hr which results in an adiabatic Δt of $84^{\circ}F$. which may be excessive and lead to excessive thermal distortions. A detailed thermal analysis of the entire bearing-seal area will be required in the final design of such an approach and, if the seal fluid temperature rise proves to be a problem, minor modification of the grooving can be made to improve the flow situation.

The SNAP 8 face type seal calculations were made with the aid of existing MTI thrust bearing computer programs. As a check on the validity of the design approach, the same analyses were applied to the seal that was tested under Contract NAS3-11824. The calculated values of film thickness are shown compared with the forementioned test data in Figure 153. The good agreement between theory and test confirms the adequacy of the design approach.

The design analyses on oil bearings and seals conducted during Phase I indicated that the bearings have ample load capacity and are certainly well within the state-of-the-art. The spiral groove face seal presents desirable advantages and is a feasible approach for the application.

COMPARISON OF SNAP-8 SPIRAL GROOVE FACE SEAL THEORY AND TEST

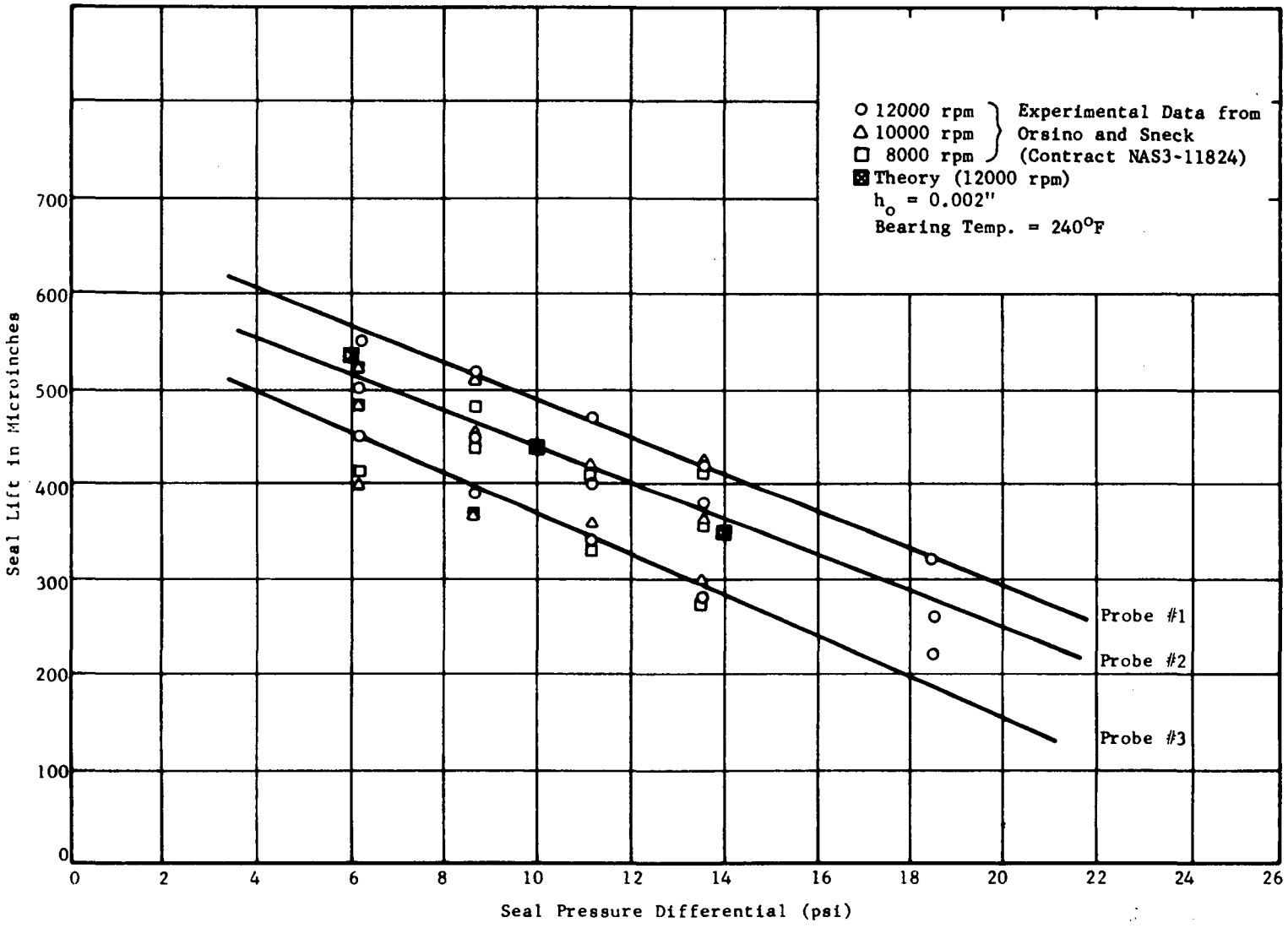

Figure 153

The seal, however, still represents a development item since its performance has not been demonstrated at TAC speed and pressure conditions. Also of significant system importance, the power consumption of the oil film bearings and seals represents a sizable percentage of the TAC output.

ROLLING ELEMENT BEARINGS

There are a number of very good reasons why rolling element bearings should be given full consideration for use in the Brayton TAC system:

Ball bearing technology is well-established by years of analytical and empirical experience. Applications have recently been made in increasingly hostile environments. Bearing material technology advances steadily, allowing significant increases in life. While the required bearings would not likely be standard or easily obtainable, they would probably be relatively minor variations not requiring analytical design studies to the extent required of gas or oil film bearings.

Ball bearings would be smaller in size than gas or oil film bearings supporting the same loads.

Angular contact ball bearings can support thrust loads without the need for the separate thrust bearings which gas or oil film bearings require.

Short interruptions of the lubricant supply can be tolerated by ball bearings without the catastrophic results which would occur in fluid film bearings.

The friction losses in mist lubricated ball bearings are relatively low - comparable to or less than for fluid film bearings, depending upon the conditions being compared.

The starting torque is low because of rolling contact between the ball bearing components instead of the possibly dry sliding contact between fluid film bearing components.

The internal clearances of ball bearings will probably be tighter than those of fluid film bearings, therefore providing better control of blade tip and seal clearances.

These arguments are summarized in Table LXVI.

Approach to Ball Bearing Analysis

The basic analysis tool used was the RECAP computer program, a well-proved code used generally throughout the country. It is based upon the standard AFBMA formulas, with certain improvements such as the addition of centrifugal loading of the outer races by the balls. Bearing

TABLE LXVI

REASONS FOR CONSIDERING BALL BEARINGS FOR TAC

- BALL BEARING TECHNOLOGY WELL ESTABLISHED
- COMPACT SIZE
- NO SEPARATE THRUST BEARING REQUIRED
- TOLERANT OF SHORT LUBRICATION INTERRUPTIONS
- LOW FRICTION LOSSES
- STARTING TORQUE LOW
- BEST CONTROL OF TIP AND SEAL CLEARANCES

B_{10} lives (90% survival) are calculated for the bearings, assuming "bearing quality" 52100 steel.

An increased life factor of 20 was applied, assuming the use of ausformed M-50 steel. This factor is believed to be conservatively realistic, based upon recent tests.[48] The ausforming process does introduce considerable complexity in the fabrication process.

Since the B_{10} life criteria is not considered sufficiently reliable for a space system, it was attempted to find design solutions based upon $B_{0.1}$ life (for two bearings, $0.999^2 = 0.998$ survival) without success for the required five year life. Therefore, the B_1 life criteria ($0.99^2 = 0.980$) was used. The bearing life factor used to calculate time to failure was reduced from 1 to 0.1.[49]

A criteria which was added to the computer results was that of comparing the bearing DN values (bearing bore diameter in mm x operating speed in rpm) for each possible solution with DN values of bearings in service and their survival potential.

Computer calculations were made for several fixed loading conditions to determine the optimum bearing sizes within practical limits to produce maximum life. Also considered were different number of balls, several ball contact angles, and the feasibility of using hollow balls to decrease internal bearing centrifugal loads.

Necessary items of input information for the computer analyses were the bearing equivalent load, composed of rotor weight, dynamic radial load, axial thrust, and bearing preload components. In order to reduce the dynamic radial loads by providing some measure of damping, not provided by the ordinary bearing designs, radially compliant mountings described later were used.

With all input information calculated by hand, the computer analyses were made for several loading conditions, corrected using the material and B_1 life factors, plotted, and the B_1 lives were calculated for the design point.

The same life versus load curves for various bearing configurations were used to estimate B_1 lives for off-design conditions, including maneuver loads greater than normal loads.

The effects of decreased race hardness and oil viscosity at elevated temperatures were estimated.[50,51]

The effects of elastohydrodynamic lubrication parameters on life at different operating conditions were estimated from the same literature.

Assuming the lubricant supply system to be similar to that of a previous NASA study [52], as directed, the lubrication system power losses were estimated.

This approach is summarized in Table LXVII.

Parasitic Power Losses in Lubrication System of TAC on Ball Bearings

The parasitic power losses of the lubrication system required to support the ball bearings were estimated from [52] for a 35 mm bearing operating at 36 krpm. The two compartments are the same except that the forward bearing compartment has a probe disk and a separator which the aft bearing does not have, giving the forward compartment increased losses of 40 watts. The total loss for both compartments is 1.760 kw, as shown by Table LXVIII.

The referenced bearings had lighter effective bearing loads than expected for the present system (about 150 versus 350 pounds), but the increased load will not significantly affect bearing heat generation.

Radially Compliant Support for Ball Bearing

An example of a radially compliant support for a ball bearing which is presently being used successfully in a major aircraft gas turbine is shown by Figure 154. Radial compliance (radial spring rate of about 10,000 lb/in) is provided by a circumferentially slotted cylinder which is fixed on one end and has the bearing mounted in the other. The material left between slots forms a number of axial beams of high axial stiffness which maintain good axial position control. The OD of the end of the slotted cylinder which contains the bearing fits with a clearance of a few mils inside a static ring. Oil is introduced between the ring and the end of the slotted cylinder to provide oil-film squeeze damping. The small radial clearance also acts as a snubber to limit radial motion of the ball bearing and main rotor shaft.

With this system significant improvements in dynamic rotor response were obtained over that of a conventionally stiff-mounted ball bearing,

TABLE LXVII

APPROACH TO BALL BEARING ANALYSIS

- UTILIZE RECAP COMPUTOR PROGRAM TO CALCULATE BEARING B_{10} LIVES
  - 52100 STEEL ASSUMED
- APPLY INCREASED LIFE FACTOR OF 20 FOR AUSFORMED M-50 STEEL
- APPLY DECREASED LIFE FACTOR OF 0.10 FOR B_1 LIVES
  - $B_{0.1}$ LIFE DESIRED BUT NOT POSSIBLE
- COMPARE BEARING DN VALUES WITH EXPERIENCE
- OPTIMIZE BALL SIZE
- CALCULATE BEARING EQUIVALENT LOAD CONSIDERING ROTOR WEIGHT, DYNAMIC RADIAL LOAD, AXIAL THRUST, AND BEARING PRELOAD
  - USE RADIALLY COMPLIANT MOUNTING TO DECREASE DYNAMIC LOAD
- CALCULATE B_1 LIFE AT DESIGN POINT
- ESTIMATE EFFECTS OF LOADS GREATER THAN DESIGN LOAD
- ESTIMATE BEARING LIFE EFFECTS OF DECREASED RACE HARDNESS AND OIL VISCOSITY AT OPERATING TEMPERATURE
- ESTIMATE ELASTODYDRODYNAMIC LUBRICATION EFFECTS ON LIFE
- ESTIMATE LUBRICATION SYSTEM POWER LOSSES BASED ON PREVIOUS NASA WORK

TABLE LXVIII

PARASITIC POWER LOSSES IN LUBRICATION SYSTEM ON TAC ON BALL BEARINGS

	35 MM FWD COMPARTMENT	35 MM AFT COMPARTMENT
BEARING HEAT GENERATION	185 WATTS	185 WATTS
FACE SEAL HEAT GENERATION	605	605
OIL PUMPING POWER	52	52
GAS PUMPING POWER	18	18
PROBE DISK DRAG	18	-
SEPARATOR DRAG	22	-
TOTAL LOSS PER COMPARTMENT	900 WATTS	860 WATTS
TOTAL POWER LOSS	1.760 KW	

EXAMPLE OF RADIALLY COMPLIANT, AXIALLY STIFF, SNUBBED SUPPORT FOR BALL BEARING

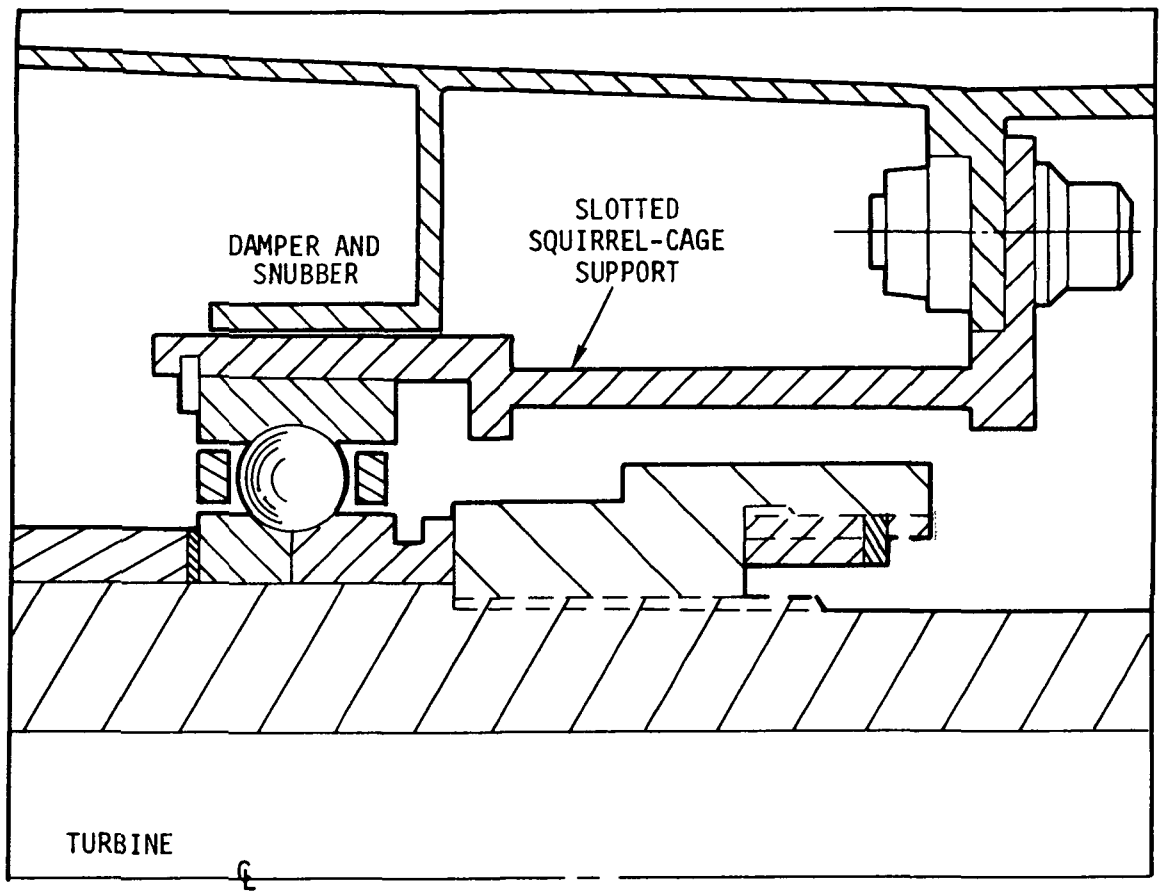

Figure 154.

as reported earlier. The damper provides about 20 lb-sec/in of damping, which reduces the dynamic radial load on per bearing to 105 pounds at 36,000 rpm.

Ball Size Optimization

Computer calculations were made for 35 mm bore angular contact bearings with 18° contact angle and balls of 0.188 - 0.500 in. diameter. The two equivalent loads used covered the range of interest, the 39 pound equivalent load per bearing being overly optimistic and the 512 pound load overly pessimistic. The computer calculations were adjusted for B_1 life and ausformed M-50 steel material.

The 5-year (43,829 hours) life line of Figure 155 shows that the heavier load has no chance to meet the life requirements. Both loading conditions indicate optimum ball sizes in the range of 0.375 in. or slightly greater. For all subsequent calculations particular attention was given to these sizes.

Not shown are the studies made using different bearing sizes, contact angles, numbers of balls, and hollow balls. The latter produce significantly longer lives by decreasing the centrifugal stresses due to the mass of the balls. However, hollow balls cannot be produced by ausforming and therefore are of no value because the favorable gains do not offset the loss in material life factor. Also, hollow balls have reliability problems at the seam where two hollow hemispheres are joined.

The elimination of the 50 mm bearings from consideration appears proper from empirical experience. The 35 mm bearings have a DN value of 1.26×10^6 mm-rpm while the 50 mm bearing DN is 1.80×10^6 mm-rpm. The empirical DN value for reliably achieving long operating lives is about 10^6 mm-rpm.

Calculation of Equivalent Loads

Using the formula: $P = XVF_r + YF_a$ (53)

where F_a = axial load, lb.

F_r = radial load, lb.

P = equivalent load, lb.

V = rotation factor, unity when the inner ring rotates with respect to the load

X = radial factor (tabular function)

B_1 LIVES FOR 35 MM 18° ANGULAR CONTACT BEARINGS AS FUNCTION OF BALL DIAMETER AND EQUIVALENT LOAD

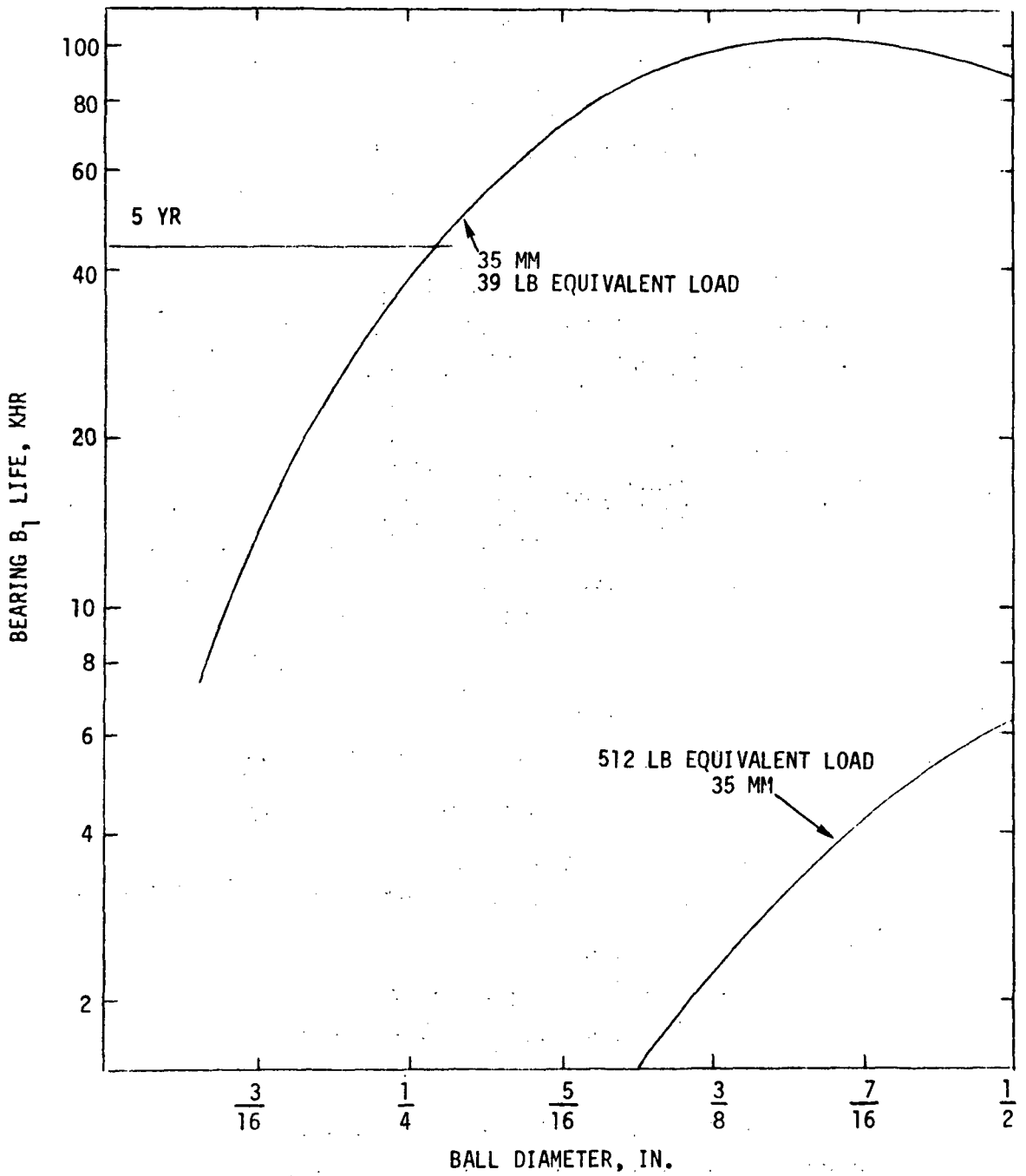

Figure 155.

Y = thrust factor (tabular function)

the equivalent bearing loads may be represented by Figure 156. The crosses identify the various equivalent loads used for the analytical studies. The expected long-term equivalent load of 354 lb. is shown, being composed of the following components:

F_r	F_a
105 lb. dynamic load	150 lb. bearing preload
50 lb. weight load	0 ± 100 lb. aerodynamic thrust
155 lb./bearing	250 lb. maximum/bearing

B_1 Lives of 35 mm 18° Angular Contact Bearings

The relationship between equivalent bearing loads and bearing B_1 lives for 35 mm 18° angular contact bearings with 0.375, 0.438, and 0.500 in. diameter balls are shown in Figure 157. Not shown is similar information for 50 mm bearings, which have significantly lower lives. The expected normal operation load of 354 pounds is identified, which shows that 0.500 in. ball diameter gives the best results. Even these balls give only about a third of the life goal of five years. A similar point which is labelled "Zaretsky" identifies a more optimistic calculation made by NASA using an experimental revision of the RECAP program which is being checked against actual test results. Even this optimistic calculation is about 13 percent below the design life.

Effect of Abnormally Heavy Loads on Bearing Life

Studies of B_1 lives of 35 mm 18° angular contact bearings with ten balls of 0.5 in. diameter loaded 100 percent of the time with an equivalent load of 39 pounds (= 0 percent of the time at 512 pounds), loaded 100 percent of the time at a 512 pound equivalent load, and several intermediate fractions of time loaded with 512 pounds (the rest of the time loaded with 39 pounds) defined Figure 158. The main points to be noted are the very fast decrease in B_1 life as the percentage of time heavily loaded increases. The design life can be met only when the bearings are very lightly loaded almost all the time.

Effect of Bearing Temperature on Material Hardness

To illustrate a major difference between the special M-50 steel

EQUIVALENT BEARING LOAD AS A FUNCTION OF RADIAL AND THRUST LOADS FOR 18° ANGULAR CONTACT BEARINGS

$$P = XF_R + YF_A$$

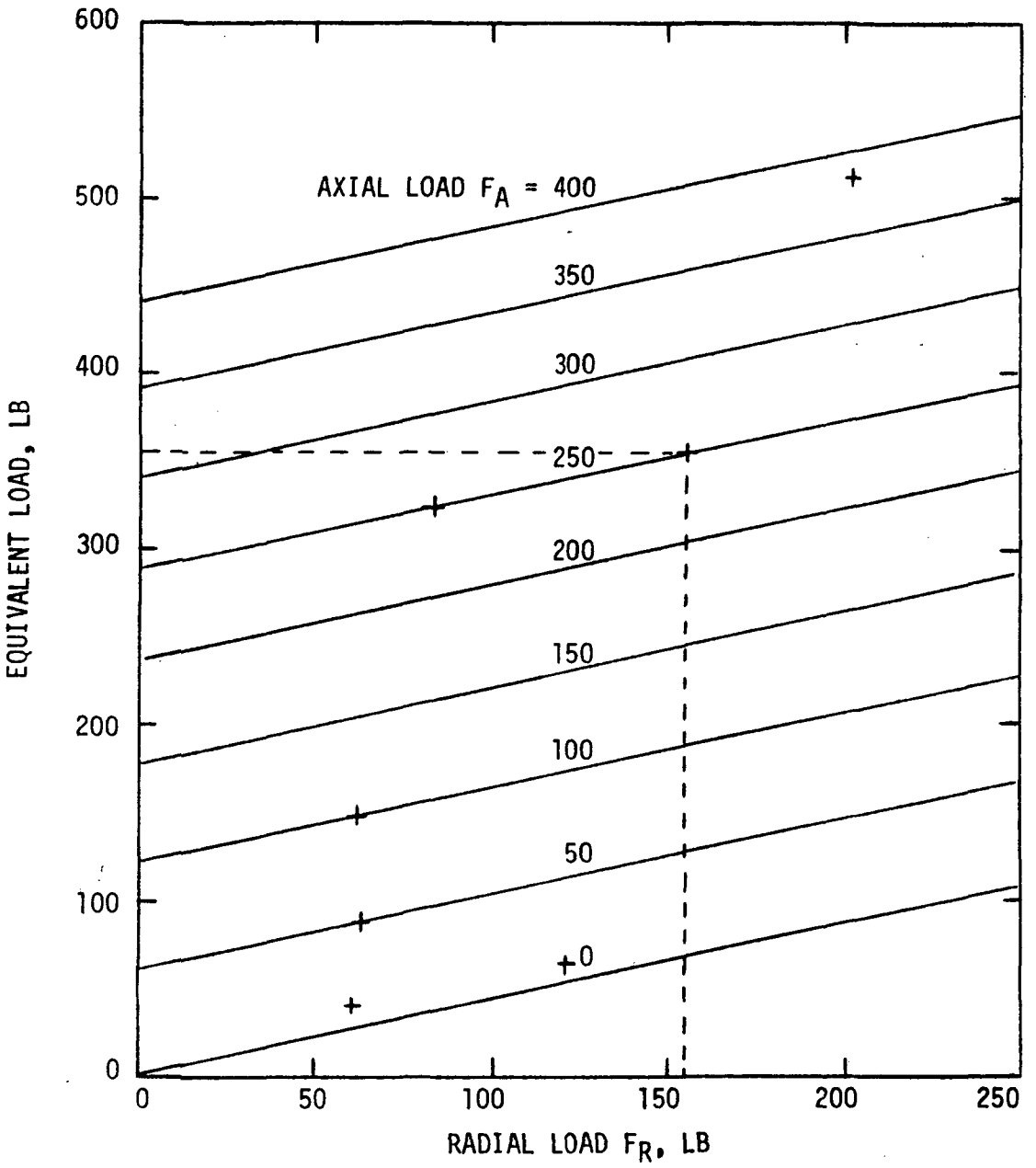

Figure 156.

B_1 LIVES VS. EQUIVALENT LOAD AND BALL DIAMETER FOR 35 MM 18° ANGULAR CONTACT BEARINGS

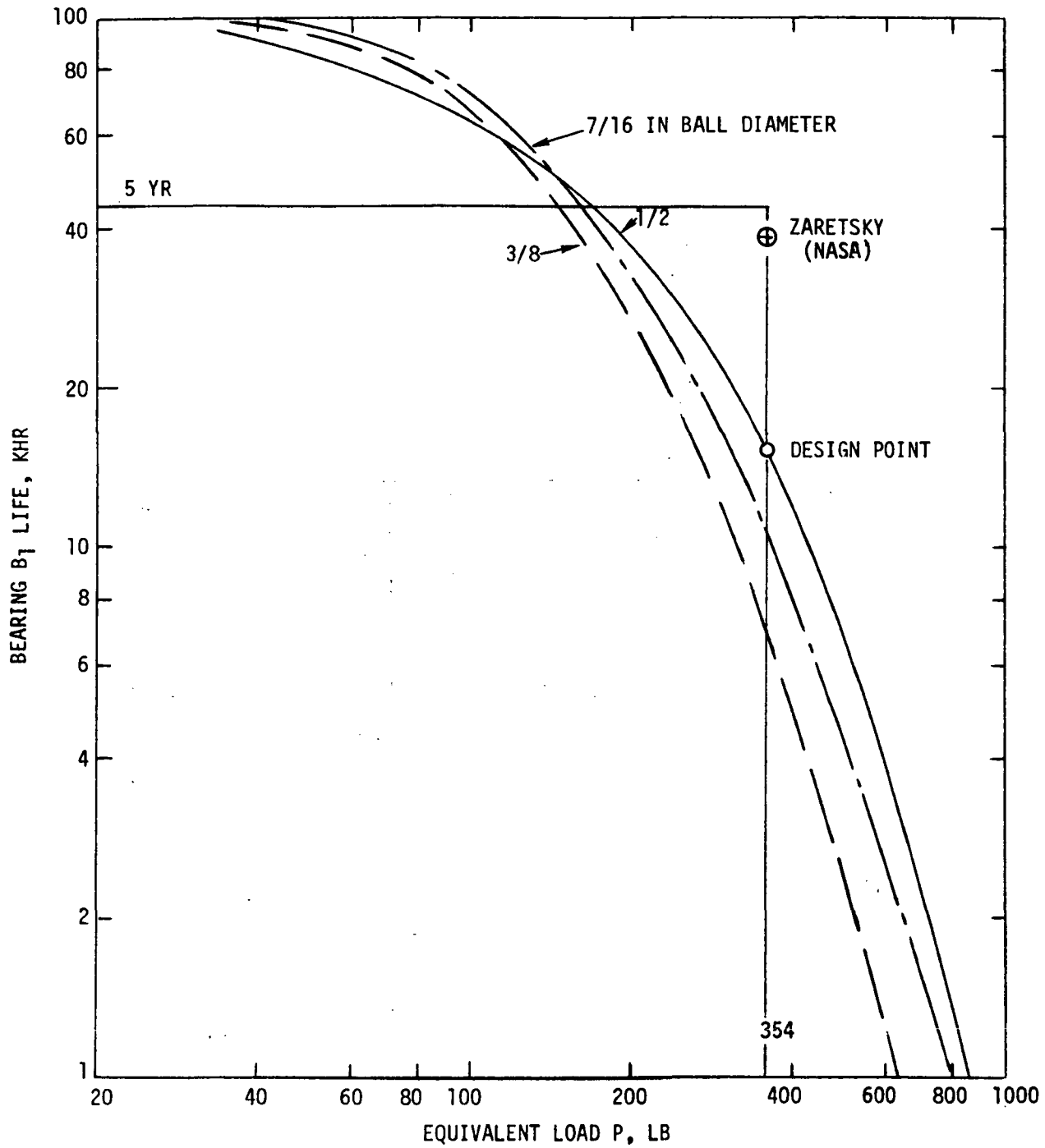

Figure 157.

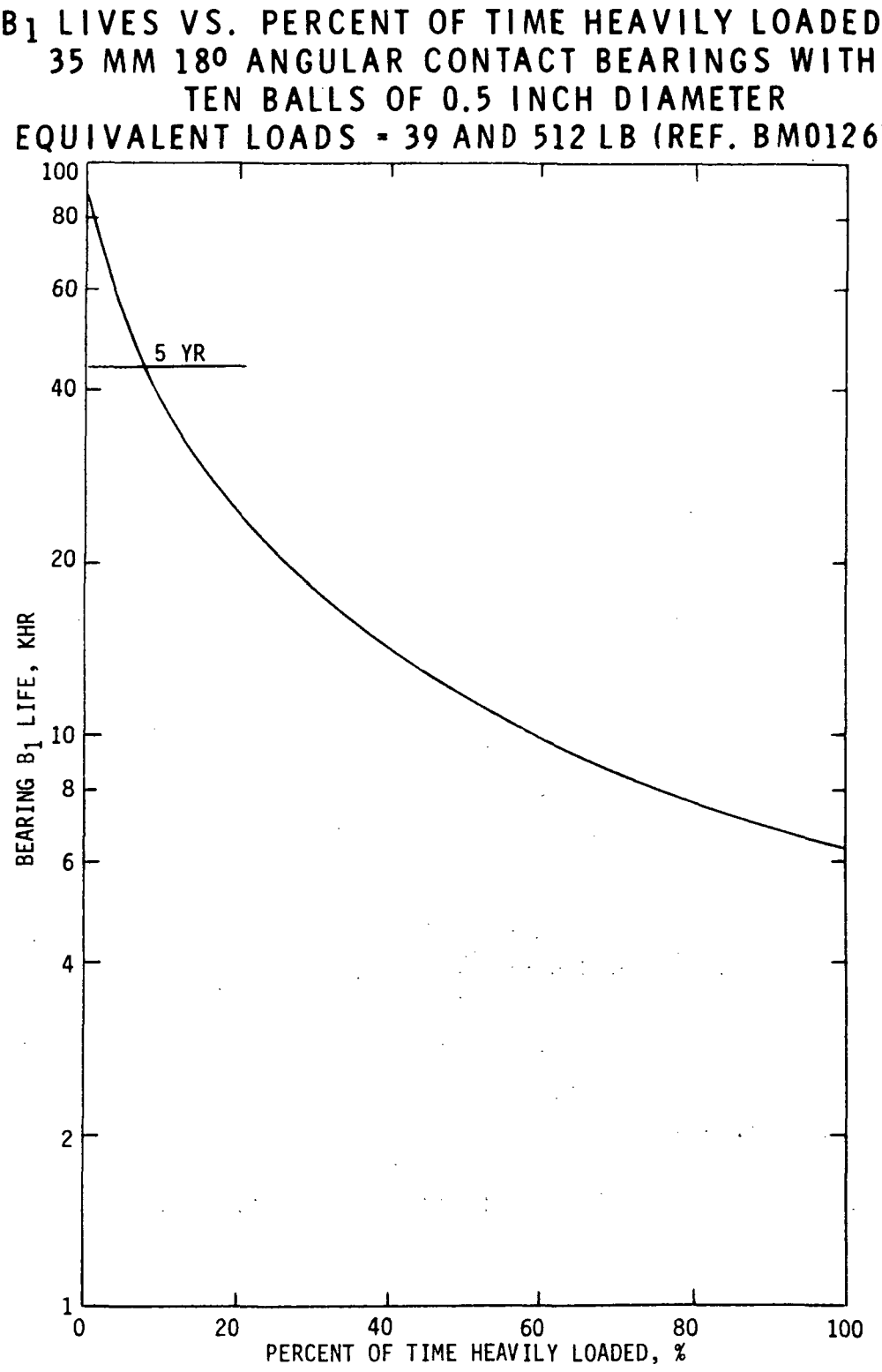
B_1 LIVES VS. PERCENT OF TIME HEAVILY LOADED FOR
35 MM 18° ANGULAR CONTACT BEARINGS WITH
TEN BALLS OF 0.5 INCH DIAMETER
EQUIVALENT LOADS = 39 AND 512 LB (REF. BM012670)
100
80
60
40
20
10
8
6
4
2
1
5 YR
BEARING B_1 LIFE, KHR
0
20
40
60
80
100
PERCENT OF TIME HEAVILY LOADED, %

Figure 158.

proposed for use with the standard 52100 bearing steel, Figure 159 may be used. It shows the superior hardness of M-50 at all operating temperatures. If $58R_c$ hardness is considered the minimum allowable to prevent brinelling and maintain sufficient strength during operation, the M-50 steel can be used at 600°F while 52100 steel cannot be used above 400°F.

Also, at the expected bearing operating temperature of 350°F, the M-50 steel is two R_c points harder. The significance of this is explained later.

The ausformed M-50 steel has a life factor of 20 over the RECAP calculations, while the vacuum remelted consumable electrode 52100 steel has a life factor of 4. The life factor differences are even more important than the hardness differences.

Effect of Bearing Operating Temperature on Bearing Life

The effect of bearing operating temperature on bearing life may be estimated by using the proportionality

$$\text{Life} \propto \nu^{0.25}\, e^{0.1\,(R_{c2}-R_{c1})} \qquad (51)$$

where e = base of natural logarithms, -

R_{c1} = hardness of M-50 steel at operating condition 1, R_c

R_{c2} = hardness of M-50 steel at operating condition 2, R_c

ν = oil kinematic viscosity, centistokes (assumed the same as bearing operating temperature)

A life figure is calculated for 100, 300, 400, 500 and 600°F. The life ratio L_T/L_{Ref} is calculated by dividing the life figures for 300, 400, 500, and 600°F by the life figure for 100°F, giving the lower curve of Figure 160. The remainder of the curves are developed similarly.

The figure shows the drastic decrease in life with each increment of operating temperature and shows that the bearings should operate at as low a temperature as possible to achieve maximum life. The life ratio of 350°F compared to a reference temperature of 100°F is 0.38, for instance, indicating that 62 percent of the 100°F life has been lost. If 350°F is the design temperature, a 100°F increase in that temperature will decrease the life by 20 percent. Thus the lubrication system must be designed to reliability give the lowest possible operating temperature, which is estimated to be 350°F for the present system.

HARDNESS OF 52100 AND M-50 BEARING STEELS AS FUNCTION OF TEMPERATURE

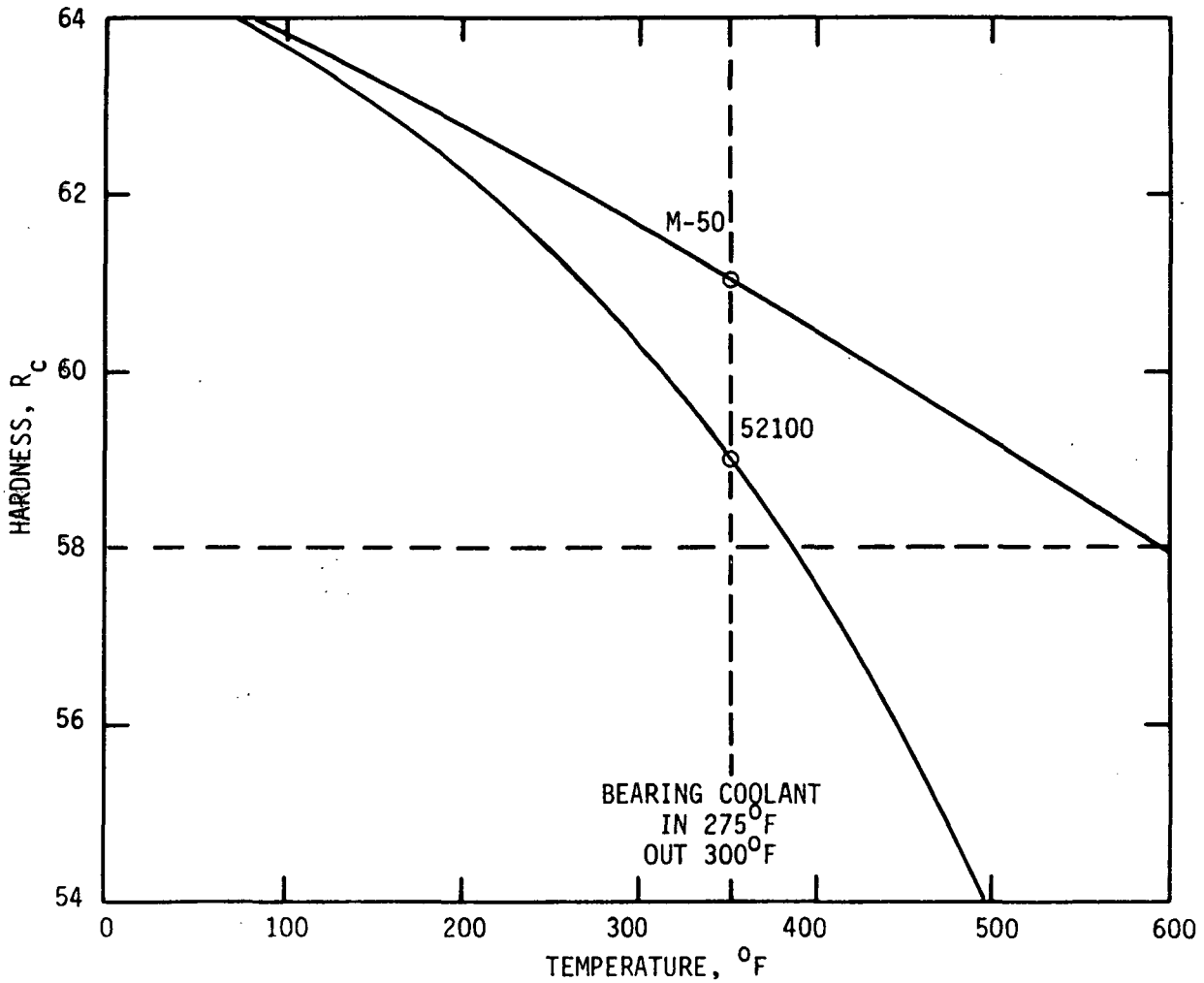

Figure 159.

BEARING LIFE AT TEMPERATURE/BEARING LIFE AT REFERENCE TEMPERATURE AS FUNCTION OF OPERATING TEMPERATURE CONSIDERING EFFECTS OF OIL VISCOSITY AND BEARING HARDNESS

$$\text{LIFE} \propto \nu^{0.25}\, e^{0.1\,(R_{c2}-R_{c1})^*}$$

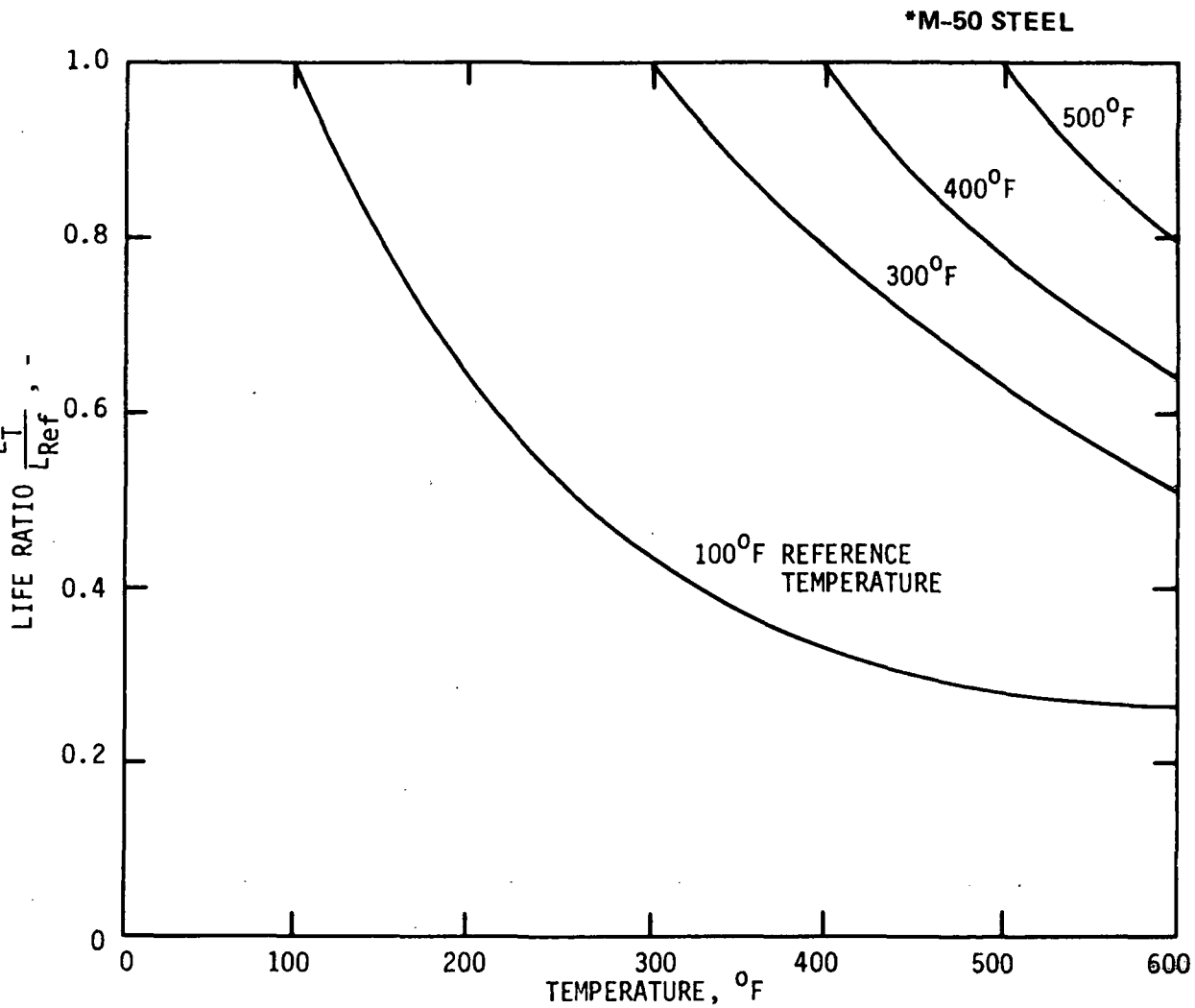

Figure 160.

Elastohydrodynamic Effects on Bearing Life

A ball bearing film parameter Λ may be calculated from the relationship shown in Table LXIX.

$$\Lambda = H\ (\mu o\ \alpha)^{0.7}\ N^{0.7}\ P_o^{-0.09} \qquad (50)$$

where H = factor from reference, which is a function of bearing diameter and series

N = operating speed, rpm

P = bearing equivalent load, lb.

Λ = bearing film parameter -

$\mu_o\alpha$ = viscosity - pressure factor, which is a function of oil kinematic viscosity

The table shows that the light and medium series bearings have film parameters which are so low that lubricant-related surface distress will occur because their elastohydronamic films will not separate the contacting surfaces. Extremely short bearing lives will result. While the heavy series has a thicker elastohydrodynamic film, surface distress can be expected to produce lives lower than the standard expectations. Therefore, the previous life estimations must be revised downward.

Lubricant Loop for TAC on Ball Bearings

A schematic of the lubricant loop for the TAC on ball bearings, similar to that of Reference (52), is shown by Figure 161. Dry cycle gas, cycle gas mixed with oil mist, and liquid oil flow loops are identified with their rates in lb/hr.

Shown on Table LXX are the major parameters of the lubrication system. The parameters are based upon the 10.5 kw power level of Reference (52), but would be maintained as listed in every respect unless the present TAC system required variations. Certainly, adjustments in pressures and temperature would be required because of the different compressor operating conditions, and these changes would require flow rate adjustments. A complete lubrication system analysis would be required in a later phase of the program.

The referenced study had a 6 kw system operating at 36 krpm. The turbine and compressor operated at temperatures similar to the present system, but with compressor inlet gas at 14.2 psia through a 1.9

TABLE LXIX

BALL BEARING FILM PARAMETER Λ

$$\Lambda = H\,(\mu_o \alpha)^{0.7}\, N^{0.7}\, P_o^{-0.09}$$

	35 MM BALL DIAMETER SERIES		
	HEAVY	MEDIUM	LIGHT
EHD CRITERIA H-FACTOR	1.3×10^5	8×10^4	7×10^4
VISCOSITY-PRESSURE FACTOR $(\mu_o \alpha)^{0.7}$ $\nu_o \sim$ SUS AT 300^o-600^oF		1.3×10^{-8}	
SPEED FACTOR $(N^{0.7})$ N = 36,000 RPM		1547	
LOAD FACTOR $(P_o^{-0.09})$ P_o = 354 LB		0.59	
FILM PARAMETER Λ*	1.54	0.95	0.83

*$0 < \Lambda < 1$ WILL PRODUCE LUBRICANT-RELATED SURFACE DISTRESS AND EXTREMELY SHORT BEARING LIFE.

$1 < \Lambda < 1.5$ WILL PRODUCE MARGINAL LUBRICATION AND BEARING LIFE LESS THAN STANDARD EXPECTATIONS, ACCOMPANIED BY SURFACE DISTRESS.

CONCLUSION: ELASTOHYDRODYNAMIC FILM IS INSUFFICIENT TO GUARANTEE ADEQUATE BALL AND RACE SURFACE SEPARATION AND PRODUCE LONG LIFE.

LUBRICANT LOOP FOR TAC ON BALL BEARINGS. FLOW RATES IN LB/HR

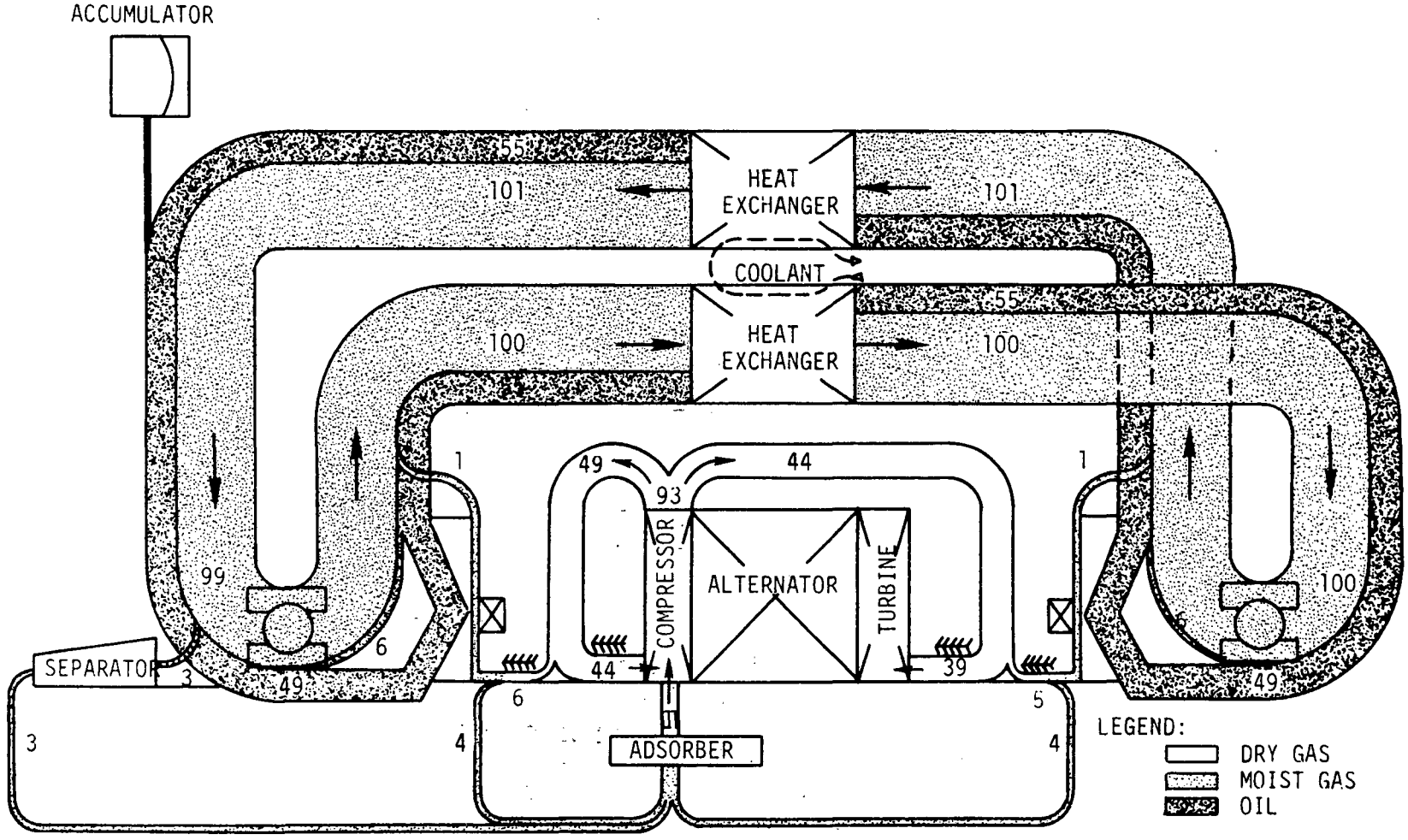

Figure 161.

TABLE LXX

BALL BEARING LUBRICANT LOOP PARAMETERS

Location	Flow Rate, lb/hr. Mist	Liquid	Gas	Temperature °F	Pressure psia
Forward Bearing Inlet	99	55	0	275	24
Exit	99	6	0	386	28
Beneath Forward Bearing	0	49	0	275	24
#1 Heat Exchanger Inlet	100	55	0	386	28
Aft Bearing Inlet	101	55	0	275	25
Exit	100	6	0	275	26
Beneath Forward Bearing	0	49	0	275	25
#2 Heat Exchanger Inlet	101	55	0	327	25
Past Forward Face Seal	1	0	0	-	38
Past Aft Face Seal	1	0	0	-	34
Through Separator	3	0	0	275	24
Through Fwd Bearing Labyrinth to Adsorber	4	0	0	-	38
Through Aft Bearing Labyrinth to Adsorber	4	0	0	-	34
Forward Buffer Flow	0	0	49	-	38
Aft Buffer Flow	0	0	44	-	34
Through Compressor Labyrinth to Compressor Inlet	0	0	44	-	38
Through Turbine Labyrinth to Turbine Exhaust	0	0	39	-	25
Adsorber to Compressor Inlet	0	0	11	-	24

pressure ratio and turbine inlet gas at 25.8 psia through a 1.75 pressure ratio.

The study considered a 20 mm compressor end bearing and 35 mm turbine end bearing, both being extra-light series of M-50 steel with one-piece cages. The bearing lives were controlled by the larger bearing, and a B_1 life of 13,400 hours and B_{10} life of 58,000 hours were predicted for effective loads of approximately 150 pounds.

The face seal life, based upon carbon wear, fell within the same life range. Oil contamination of the power system, with mean seal diameters of 2.0 in. at the compressor end and 1.5 in. at the turbine end, was estimated to be about 0.05 grams in 10,000 hours.

Immediately inboard of each bearing was an impeller machined into the sealplate to act as a scavenge pump for the oil mist passing through the bearing and seal.

Compact tubular heat exchangers outside the TAC cooled the two-phase oil-gas mixture as it was pumped between bearing compartments.

The separator overhung from the compressor end of the shaft was a conical housing assembly containing a woven metallic matrix to condense oil vapor carried in the gas. This gas was used to replace leakage through the two face seals. An external absorber with polyurethane prefilter and glass wool further purified the makeup gas.

An oil inventory control system maintained the oil level in a rotating pool with an immersed stationary scoop connected by piping to an external accumulator.

The lubricant used in the design study was a 5P4E polyphenyl ether oil.

Buffer labyrinth seals were used to prevent the oil mist from entering the compressor inlet or turbine exhaust. Clean compressor gas flowed toward each bearing through an adjacent labyrinth seal, with most of the buffer seal flow directed to the compressor inlet through an adjacent labyrinth and to the turbine exhaust through an adjacent labyrinth.

Summary of Ball Bearing Problems

Ball bearing bore size, series, contact angle, and number and size of

balls were optimized. The latest and best bearing material and processing technology was assumed. Realistic long-term bearing loads were applied. A reliable bearing life computer program was utilized. The latest method of decreasing bearing dynamic radial loads was incorporated. The desired bearing reliability of 0.998 (two bearings at $B_{0.1}$ life) was reduced to 0.980 (two bearings at B_1 life). All of these were considered as being reasonable and prudent approaches, neither overly optimistic nor pessimistic. Even so, the calculated bearing lives were only 36 percent of the desired five year life.

Further consideration of the decreased material hardness and oil viscosity at elevated operating temperatures showed that the elastohydrodynamic film between bearing components would not guarantee their separation, and would lead to bearing lives less than 36 percent of the goal. It also pointed out the necessity of having a support system which would reliably guarantee the lowest possible bearing operating temperatures. This, in turn, requires extensive lubrication system analysis and development.

Since the bearings selected would not meet the life goal under normal operating conditions, they have no overload capacity.

The assumption of ausformed M-50 steel as the bearing material and processing method implies the need for a development program and very expensive bearings with long procurement times.

The lubrication system required has many components, some of complex design. It will require further study and development beyond presently available analyses.

It is expected that the lubrication system will contaminate the cycle fluid more than is allowable, especially during startup, even if extreme care is taken during these periods.

The lubricant is likely to deteriorate in five years under exposure to the high temperature and radiation environments.

These arguments are summarized in Table LXXI.

Supporting the TAC on oil mist lubricated rolling-element ball bearings for five years is not recommended.

TABLE LXXI

SUMMARY OF BALL BEARING PROBLEMS

- BEARING LIFE AT DESIRED RELIABILITY CANNOT BE ACHIEVED
- NO OVERLOAD CAPACITY
- AUSFORMED M-50 STEEL DEVELOPMENT PROBLEM
- COMPLEX LUBRICATION SYSTEM
- OIL CONTAMINATION OF SYSTEM, ESPECIALLY AT START-UP
- PROBABLE DETERIORATION OF LUBRICANT IN FIVE YEARS

IV. PHASE III - CONCEPTUAL DESIGN STUDY

A. SUMMARY

The main effort in the third phase of the subject design study was applied to the feasibility study of the two-pole Lundell alternator and to the completion of the TAC design based upon the revised design conditions.

For the alternator the ANADUR wire insulation was ruled out for the case of five-year life because of the likelihood that it would enter the main gas circuit of the powerplant in the form of abrasive dust. Preferred would be bare wire with mica or alumina in the slots and mechanically separated and plasma-sprayed end turns. As a result the alternator cavity pressure would have to exceed 14 psia for a 240-volt winding and 53 psia for a 480-volt winding to avoid corona effects. Organic insulation would eliminate the corona effect but require a 107°F coolant sink. A 60-slot two-pole Lundell alternator is feasible. However, an 84-slot alternator would result in a smaller-size alternator having better part load efficiency than the six-pole configuration but slightly lower full load efficiency. In order to retain the flexibility of reconnecting the alternator winding to go from 480 to 240 volts and replacing the stock and winding only to go to 120 volts, a third material is recommended to be introduced into the rotor. Several cooling configurations can be designated into the alternator to cool it.

The designs of the journal and thrust bearings have been revised such that they meet all design requirements. The film thicknesses are adequate for design load and both the thrust and journal bearings have adequate overload margins.

The third critical speed is safely (49%) above the 120 percent speed point. The second critical speed (12,000 rpm) which must be damped, can be well controlled if the total unbalance is kept below 0.070 in-oz. Even with the use of a steel compressor impeller rotor response is little affected below 30,000 rpm.

In addition to the decreases in turbomachinery dimensions from the Phase I design, an important change was to eliminate the control hole through the turbine rotor to reduce stress, making all turbine stresses within the allowable values. This necessitated introducing the journal coolant gas at the compressor end of the rotor, a slight complication. The weight of the TAC unit went up 45% from Phase I due mainly to the increased size of the two-pole alternator. The cycle efficiency dropped from 0.284 in Phase I to 0.270 inspite of a higher turbine pressure ratio (lower heat-exchanger and piping relative pressure drops) because of reduced turbomachinery inlet temperatures, decreased alternator efficiency and increased windage. The 84-slot two-pole alternator would slightly increase the cycle efficiency because the windage loss would be less than for the 60-slot configuration.

ALTERNATOR DESIGN

INTRODUCTION AND SUMMARY

The Phase III studies were directed toward determining the feasibility of a 400 Hz, 2-pole Lundell alternator for the TAC configuration and the preparation of a preliminary design. Several conditions were investigated to determine the versatility of the design for various potential applications. Areas of concentrated study included electrical design selection for armature reconnectability from 120 to 480 volts (L-N), thermal analysis for several pressures and temperatures based on HeXe and Argon gases, part load analysis, corona conditions, and the use of substitute organic insulation systems.

Comparison is made between the present design and the 6-pole Lundell alternator design recommended in Phase I. However, the designs are not directly comparable since the 2-pole alternator in Phase III is more conservative than the 6-pole of Phase I. This is because of the conservative assumptions used in the initial design selection in Phase III. Their selection was based upon concern over the ability to adequately cool the 2-pole alternator. Subsequent thermal analyses late in the Phase III revealed that the assumptions were conservative. Due to the limited period of Phase III, there was not sufficient time to go back and re-evaluate the design in line with the Phase I, 6-pole. However, a non-optimized two pole design, having a current loading level close to that of the optimized 6 pole design was identified at the end of the effort. This design, for operations in the $\frac{1}{4}$ to full load range is more attractive than the 60 slot (conservative) 2 pole design.

The results of the studies indicate that the 2-pole, 400 Hz Lundell TAC alternator is both feasible and practical. Although the 2-pole is not as attractive as the Phase I, 6-pole selection in many aspects, the results did not reveal any aspect of its design which would definitely preclude its use. A cooling circuit was devised which would cool the alternator more than adequately; the electromagnetic efficiency was found to be 1.8 points lower than that for the 6-pole at full load and

1.6 points higher at $\frac{1}{4}$ load. For overall efficiency, the spread is 1.5 points at full load to 0 at $\frac{1}{4}$ load. The weight of the 2-pole alternator is 1.67 times that of the 6-pole alternator weight; the 2-pole rotor is about 35 percent heavier than the 6-pole rotor. Optimization of the 84 slot 2 pole design should reduce the weight differences, and could also improve the 2 pole design efficiency, particularly at full load.

The voltage unbalance is within the 9 percent limit (based on an improved analytical method adopted during Phase II studies).

The magnetic and mass unbalance forces were analyzed and appear to have technically feasible design solutions, even though the 2-pole has inherently more difficult problems. One area of concern for both the 2-pole and the 6-pole is the magnetic unbalance in the auxiliary gap; further analyses will be required before solutions can be defined which are compatible with the bearings and alternator. Certainly one solution is to increase the gap to the point that percentage gap variations around the periphery are small.

The pressures at which corona may occur differed little with those presented in Phase I. Unless subsequent development tests prove otherwise, it appears reasonable to ignore the transient (peak) voltages in setting the allowable minimum-pressure/maximum-voltage combinations. This alleviates problems somewhat by permitting lower pressures to be specified for the 240 volt winding, but it still does not eliminate the concern for the potential corona inception. Corona related to the use of the organic insulation is discussed with the text.

The thermal analysis and maps revealed three interesting design aspects. First, the temperatures at the higher pressure (86 psia, 59.3 nt/cm^2) and higher windage loss are as low as those for the lower pressure (70 psia, 48.3 nt/cm^2). This is because, at the higher pressure, there is a greater mass flow of gas in the gas recirculation cooling system which carries off the heat from the higher losses. Secondly, for the stub shafts analyzed, the rotor will absorb or reject negligible heat from or to the 500°F (approximately) bearings (533°K). Thirdly, the hottest gas temperature occurs in the auxiliary gap. The thermal analyses also showed that end bell cooling should be used in the absence of a gas flow through the auxiliary gap.

Comparison between the 2-pole and 6-pole alternators indicates that with the exception of increased weight and lower full load efficiency, there are few critical differences between the two; that is, any differences that could be distinguished as major criteria for selection or rejection.

ELECTRICAL DESIGN CONSIDERATIONS

A. Summary of Requirements

Preliminary design and performance parameters for a 400 Hz, 2-pole, 240 volt L-N Lundell alternator with high temperature insulation were established to determine the design feasibility specifically with regard to the following:

a. Weight and efficiency at design power output.

b. Magnetic and mass unbalanced forces on the rotor.

c. Rotor stresses at 24,000 rpm and 20% over-speed.

d. Windage losses with Helium-Xenon mixture in the rotor cavity at a full-load compressor inlet pressure of 70 and 86 psia (48.3 and 59.3 nt/cm^2) for a coolant temperature of 325°F (436°K) and at 70 psia (48.3 nt/cm^2) for 466°F (514°K) coolant.

e. Temperature distribution for coolant temperatures of 325°F (436°K) and 466°F (514°K) with argon in the gap except that windage losses for the HeXe mixture shall be used to determine the temperature distribution.

f. Voltage limitations due to corona as a function of pressure of a helium gas.

g. Voltage unbalance.

h. Reconnectability between 240 and 480 volts L-N.

Specific electrical specification requirements for the alternator are listed below:

a. The alternator shall have a maximum continuous rating of 160 kwe with a 3-phase output at a 0.75 lagging load power factor and an overload rating of 320 kva at 0.9 lagging load power factor for 5 seconds after temperature equilibrium has been reached.

b. The alternator shall be capable of operating at 120% of design speed without a catastrophic failure under all loads up to and including rated TAC load conditions (160 kwe, 0.75 lagging power factor) for a limited time.

c. The design life criteria for the alternator shall be 5 years operating time under the specified conditions for the TAC assembly.

d. The alternator shall be in accordance with MIL-G-6099A (ASG) in accordance with the latest revision in effect for the following:

   1. Short-Circuit Capacity. Paragraph 4.5.12 for a minimum time of 5 seconds for each occurrence.

   2. Phase Balance. Paragraphs 4.5.10, 4.5.10.1 and 4.5.10.2 except that paragraph 4.5.10.1 is amended to read ". . . the individual phase voltages shall not deviate from the average by more than 2.25, 4.5, and 9 percent,* respectively."

e. The alternator shall be designed to the maximum extent possible so as to reduce to a minimum windage losses. A windage loss less than 6 percent of the rated output for a full-load pressurized rotor cavity shall be considered a design goal.

f. For systems radiator size and weight considerations, it is desired to operate the alternator stator at elevated temperatures. The alternator shall utilize high-temperature magnetic, electrical and insulation materials which include stainless steel or Inconel-clad silver for the conductors, Anadur "S" for the insulation between conductors, and high-purity ceramic, 99.5 percent alumina, for the slot insulators. A maximum of 300°F (167°K) temperature increase shall be permitted between the coolant supply temperature and the alternator hot spots at the 160 kwe power level.

*The individual phase voltages shall be 2.25, 4.5, and 9 percent initially but 1.5, 3 and 6 percent figures shall be a design goal.

g. Specification MIL-G-6099 (A) (ASG).

1. Waveform. Paragraph 4.5.16* - In addition, the total rms harmonic content of the line-to-neutral voltage wave, when the alternator is operating into a purely resistive load, shall be less than 5 percent from 10 percent to 100 percent maximum design load of 160 kwe.

2. Output Voltage Modulation.* Paragraph 4.5.13, except that modulation shall not exceed 0.5 percent.

h. Shock, Vibration, and Acceleration - The alternator shall be in accordance with the environmental specifications NASA Nos. P2241-1 and P2241-2 except paragraph 2.3.3.1 of specification P2241-1 shall be replaced with paragraph 3.5.1.4 from environmental specification No. 417-2, revision C, dated June 1, 1969. Assumed acceleration is 1.5 g's in both directions along mutually perpendicular axis.

i. Radiation Environment - The design radiation environment shall be 10^7 rads, 10^{13} nvt fast neutrons per square centimeter (> 1 Mev) unless otherwise specified.

j. Position Sensitivity - The alternator shall be designed to operate in any position in both zero "G" and one "G" environments.

k. Voltage-Regulator-Exciter and Speed Control - While the VRE, speed control, and power conditioning equipment were not a part of the study, their effects on the alternator were considered in the design study. The speed control for transient load changes shall be of the phase-controlled parasitic load type. Frequency regulation shall be assumed to be within ± 1 percent of design frequency for a change in external load of from 10 percent to full design output power. Some form of system gas pressure modulation is contemplated for long term or scheduled control of power level.

*This shall be a design goal without analytical verification.

l. It is anticipated that the TAC units shall be employed in multiple units, thus they may be required to be electrically paralleled.

m. The alternator stator winding shall permit the direct substitution of organic insulated windings at some future date with a reduced coolant supply temperature of 107°F (315°K).

n. Rated voltage shall be 240 volts L-N, 3 phase, wye connected initially; however, the stator winding design shall permit reconnecting the above coils to produce 480 volts L-N. In addition, the feasibility of bonding a high magnetic permeability pole face material to the rotor (in order to reduce pole face losses) shall be investigated. If the above is deemed feasible, a stator shall be designed which then permits 120, 240, or 480 volts L-N windings.

Configuration Design Selection and Features

During the Phase I studies, a preliminary 2-pole, 400 Hz Lundell alternator design was derived. This design had 48 stator slots, 8 series turns per phase, an 8 inch rotor O.D. (20.4 cm), and used Hiperco 27 for the rotor magnetic material. SAE 4340 alloy was selected for the rotor magnetic material for the Phase III, 2-pole, 400 Hz alternator design and a design analysis using the Phase I selected parameters (i.e., 48 slots, etc.) was performed with the SAE 4340 magnetic alloy in the rotor. This design required a rotor O.D. of 8.4 inches (21.4 cm) and had pole face losses which were approximately 3.4 times as large as the previous design. The higher pole face losses were caused by the lower permeability of the SAE 4340 material as compared to Hiperco 27. A radial gap study was performed to evaluate the effect, on alternator weight and efficiency, of increasing the radial gap to reduce pole face losses. Results of this study are shown in Figure 162 . Indications are that radial gaps in the range of 0.100 to 0.120 inches (0.254 to 0.305 cm) provide optimum results regarding alternator weight and efficiency. As shown in Figure 162, pole face losses decrease and stationary field coil losses increase with increasing radial gap. Increasing the radial gap transfers some of rotor surface losses to the stator field which normally is desirable from heat

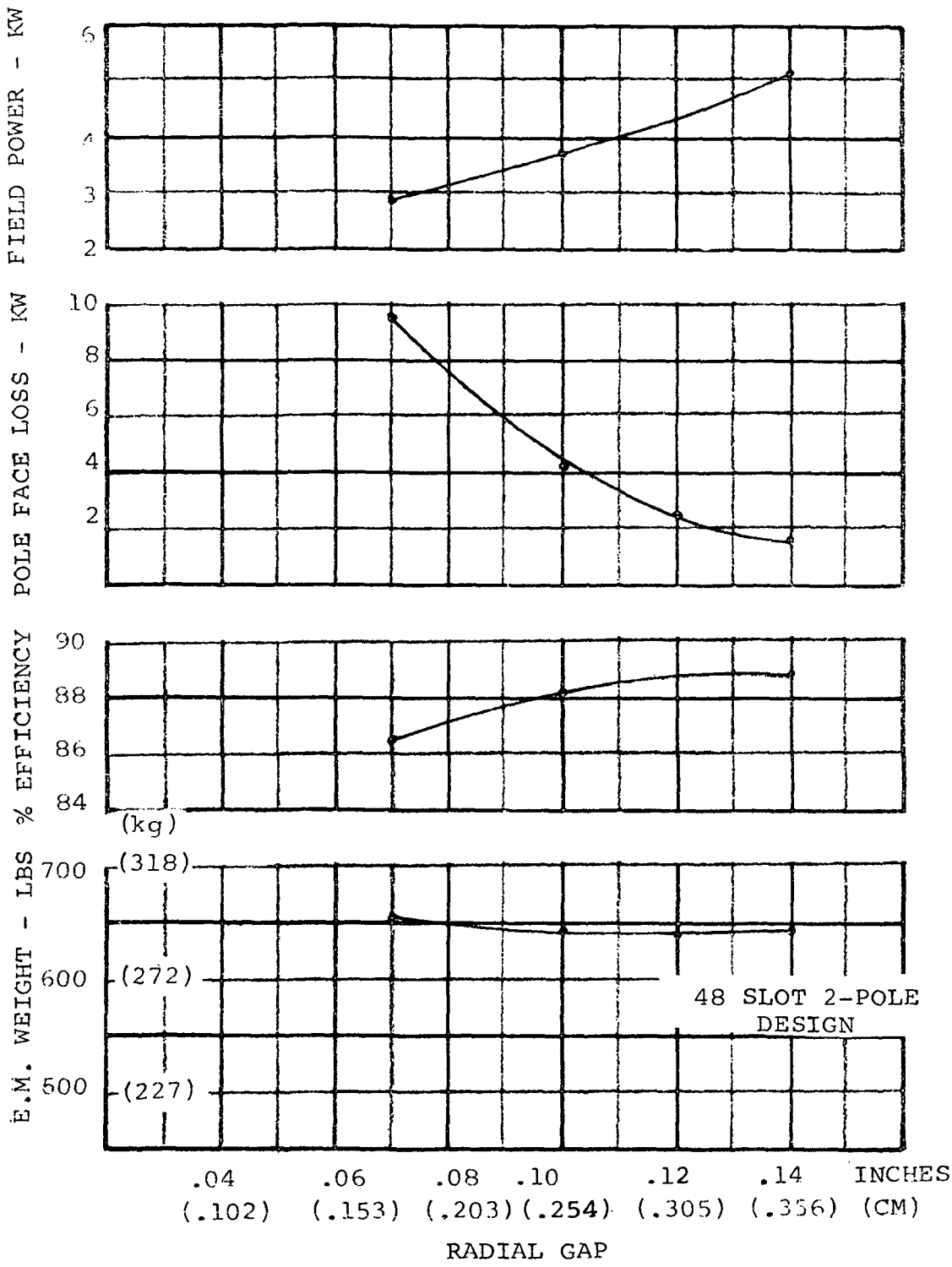
FIELD POWER - KW
6
4
3
2
POLE FACE LOSS - KW
10
8
6
4
2
% EFFICIENCY
90
88
86
84
E.M. WEIGHT - LBS
(kg)
700
(318)
600
(272)
500
(227)
48 SLOT 2-POLE
DESIGN
.04
(.102)
.06
(.153)
.08
(.203)
.10
(.254)
.12
(.305)
.14
(.356)
INCHES
(CM)
RADIAL GAP

Figure 162

transfer considerations. A radial gap of 0.120 inches (0.305 cm) was selected; however, this can be reduced to as low as 0.100 inches (0.254 cm) if this later seems desirable.

Preliminary indications were that the 8.4 inch (21.3 cm) rotor O.D. was too large. The stator slots were increased to 60, thereby increasing the number stator turns from 8 to 10 for the 240 volt L-N case. This configuration resulted in a rotor O.D. of 8.0 inches (20.4 cm), and reduced the total pole face loss. This is because the greater number of slots decreased the tooth ripple (or no-load) component of pole face loss (which was predominant for the 48 slot design). The load harmonic component of pole face loss became predominant for the 60 slot design, and a further increase in the number of stator slots (and turns) would further increase this loss component.

It is most probable that a higher number of stator turns and slots can be tolerated from a pole face loss standpoint if a further reduction in rotor diameter is deemed necessary. This conclusion is confirmed in the 84 slot design summarized in Table LXXII. However, the 60 slot configuration was settled upon because of considerations regarding the gas recirculation scheme utilized for cooling. The pressure for gas circulation is created in the tapered cone section of the rotor. Preliminary indications were that the larger radius and height of the cone section provided by the 8 inch (20.4 cm) rotor O.D. design would be desirable to provide satisfactory pumping head for forced convection cooling, and that rotor stress levels were satisfactory. Later thermal analysis indicated it ensured a conservative design; further optimization may show that a smaller rotor O.D. would still produce adequate forced convection cooling for a 2-pole machine. This is the case with the 84 slot design of Table LXXII .

The 60 slot alternator configuration was designed for 240 volts line to neutral; however, the alternator windings can be reconnected to produce 480 volts L-N. This is accomplished by connecting the two parallel circuits in series. Because the stator is wound for the minimum of two conductors per slot and the maximum number of parallel circuits is two, the 60 slot stator cannot be reconnected or rewound to produce 120 volts L-N. In order to provide a stator that can be reconnected and/or

TABLE LXXII

DESIGN SUMMARY
TAC ALTERNATOR
84 SLOT DESIGN, 2- POLE
COOLANT TEMPERATURE: ; 466°F & 325°F

RATING: 214 kVA at .75 P.F. Lagging

VOLTAGE: 240/416 reconnectable to 480/832

SPEED: 24000 rpm

FREQUENCY: 400 Hz

DIMENSIONS: INCHES	
ROTOR O.D.	7.5
ROTOR LENGTH	12.78
STACK LENGTH (OVERALL)	3.58
STACK O.D.	15.16

ELECTROMAGNETIC WEIGHTS: lbs	
ARMATURE	17.0
FIELD	43.0
FRAME	172.9
STACKS	98.0
ROTOR	135.4
TOTAL	466.3

MATERIALS:	
ac CONDUCTORS	321 SST CLAD SILVER
FIELD CONDUCTORS	CUBE COPPER ALLOY
ARMATURE LAMINATIONS	.004 INCH THICK HYPERCO 27
FRAME	HYPERCO 27 FORGINGS
ROTOR MAGNETIC	SAE 4340 @ Re 33
ROTOR NON-MAGNETIC	INCONEL 718 @ Re 38
INSULATION	
ac WINDING	ANADUR
SLOT LINER	ALUMINA
SLOT SEPARATOR	SYNTHETIC MICA
FIELD WINDING	SYNTHETIC MICA

WINDING DETAILS	
NUMBER OF SLOTS	84
CONDUCTORS PER SLOT	2
SERIES TURNS PER PHASE	14
PARALLEL PATHS (240 V L-N)	2
PARALLEL STRANDS	2
PHASE BELTS	60°
PITCH	2/3
BARE CONDUCTOR DIMENSIONS, INCHES	.081 x .144

TABLE LXXII (Cont.)

ROTOR TIP SPEED (24000 RPM): feet/sec	786
MAIN GAP: INCH	.120
AUXILIARY GAP: INCH	.050
CURRENT DENSITIES: AMPS/IN^2	
ac WINDING	6827
FIELD WINDING	3973
FLUX DENSITIES: KL/IN^2	
BACK IRON	74
TEETH	98
MAIN GAP	42
POLE	94
FRAME	117
AUX. AIR GAP	46
F.L. LOSSES: WATTS (466°F COOLANT TEMP.)	
POLE FACE	1091
BACK IRON	2559
TEETH	376
ARMATURE	5175
FIELD	3929
ELECTROMAGNETIC SUBTOTAL	13060
WINDAGE (70 PSIA)	5670
TOTAL	18730
EFFICIENCY: %	
ELECTROMAGNETIC	92.5
OVERALL	89.5
REACTANCES: P.U.	
XD	2.03
X'D	.436
X"D	.384
Xq	.925
X"q	.085
X_2	.234
X_o	.013
TIME CONSTANTS, HOT SECONDS	
T'DO	.272
T'D	.052
TA	.003
Td"	.005
VOLTAGE UNBALANCE: %	
2/3, SINGLE PHASE CURRENT	7.5

rewound to provide 120, 240, or 480 volts L-N, a 30 slot stator design was made. For the 120 volt configuration, the 30 slot stator is wound with two conductors per slot and two paralleled paths. The two paralleled paths are reconnected in series to provide 240 volts L-N. To obtain 480 volts L-N, the stator must be rewound with four conductors per slot. As a consequence of reducing the stator slots from 60 to 30, the rotor pole face losses increased by a factor of approximately 5.5. This is caused by the larger slot pitch and slot opening of the 30 slot design which increases the amplitude of the rotor surface flux pulsations. The high pole face losses of this configuration can be reduced to approximately one-fourth by bonding a high magnetic permeability pole face material such as SAE 1010 to the rotor.

Because some question existed* regarding the feasibility of pole face bonding and because the higher voltage levels are preferred, the 60 slot design was selected for all performance calculations. The 60 slot alternator configuration and the slot configuration for the various slot designs are shown in Figure 163. There are some small dimensional differences between the 30 slot alternator designed and 60 slot alternator design shown; however, the configuration in Figure 163 is representative of both for all practical purposes. The rotor configuration is shown in Figure 164 . A summary of design details for the different slot designs is given in Tables LXXIII through LXXIV.

The two pole Lundell rotor consists of two magnetic pole sections cantilevered from flux collector rings located at each end of the rotor. The space between the magnetic pole sections is filled with Inconel 718 alloy which is non-magnetic. This material is bonded to the magnetic pole sections to provide a homogeneous structure to reduce rotor stress and provide a smooth rotor surface to minimize windage losses. The flux from a given rotor pole face passes radially through the adjacent radial gap into the stator teeth and then passes circumferentially through the depth behind the slot (DBS) to and through the teeth and radial gap adjacent to the other pole. After entering the pole, the flux passes axially through the pole body to the flux collector ring. The flux then passes through the auxiliary radial gap, into the stator frame

*The addition of bonding a third pole face material appears to present no problems after review by bonding experts; see Appendix A.

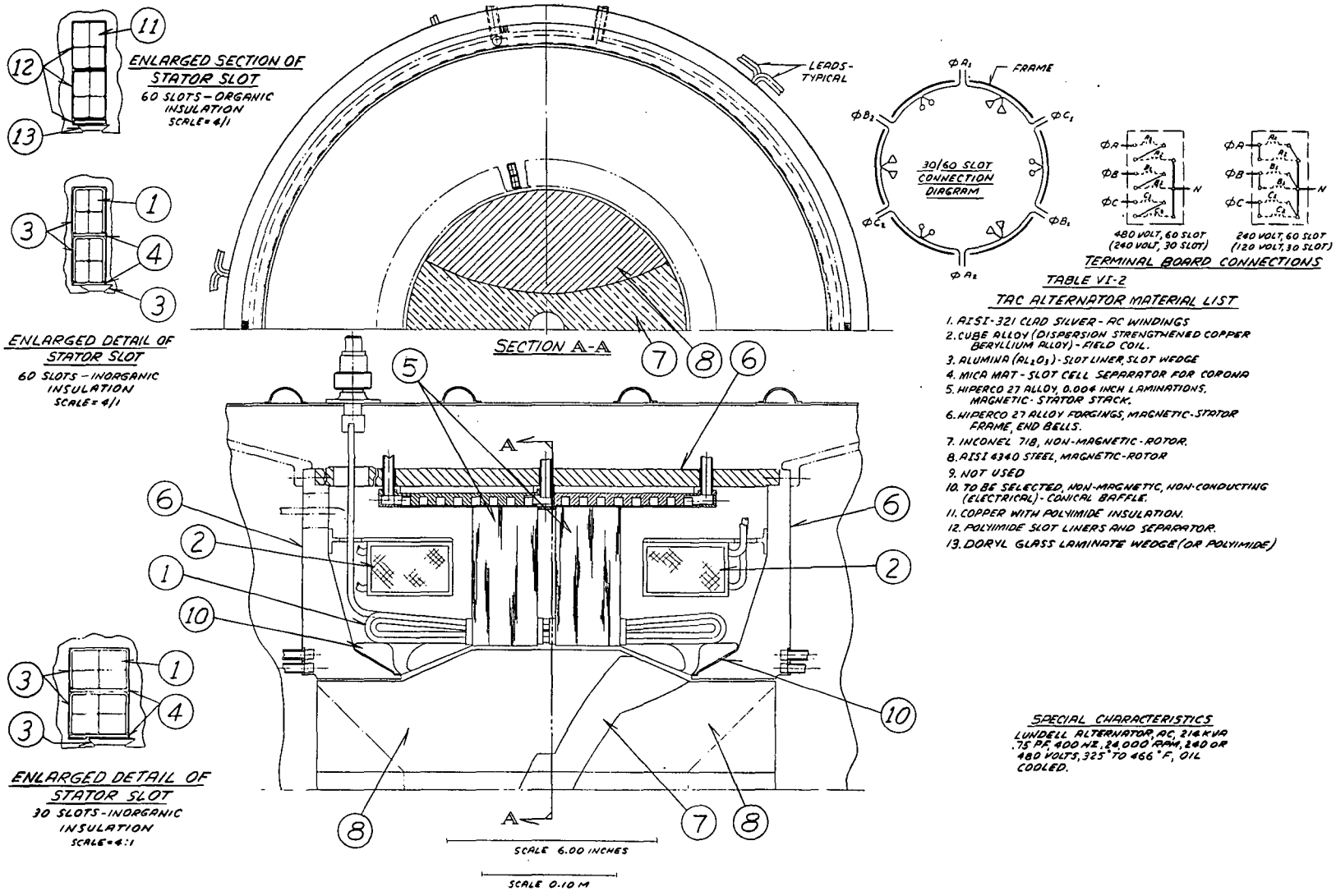

TABLE VI-2

TAC ALTERNATOR MATERIAL LIST

1. AISI-321 CLAD SILVER - AC WINDINGS
2. CUBE ALLOY (DISPERSION STRENGTHENED COPPER BERYLLIUM ALLOY) - FIELD COIL.
3. ALUMINA (AL_2O_3) - SLOT LINER, SLOT WEDGE
4. MICA MAT - SLOT CELL SEPARATOR FOR CORONA
5. HIPERCO 27 ALLOY, 0.004 INCH LAMINATIONS, MAGNETIC - STATOR STACK.
6. HIPERCO 27 ALLOY FORGINGS, MAGNETIC - STATOR FRAME, END BELLS.
7. INCONEL 718, NON-MAGNETIC - ROTOR.
8. AISI 4340 STEEL, MAGNETIC - ROTOR
9. NOT USED
10. TO BE SELECTED, NON-MAGNETIC, NON-CONDUCTING (ELECTRICAL) - CONICAL BAFFLE.
11. COPPER WITH POLYIMIDE INSULATION.
12. POLYIMIDE SLOT LINERS AND SEPARATOR.
13. DORYL GLASS LAMINATE WEDGE (OR POLYIMIDE)

SPECIAL CHARACTERISTICS

LUNDELL ALTERNATOR, AC, 214 KVA .75 PF, 400 HZ, 24,000 RPM, 240 OR 480 VOLTS, 325° TO 466° F, OIL COOLED.

Figure 163

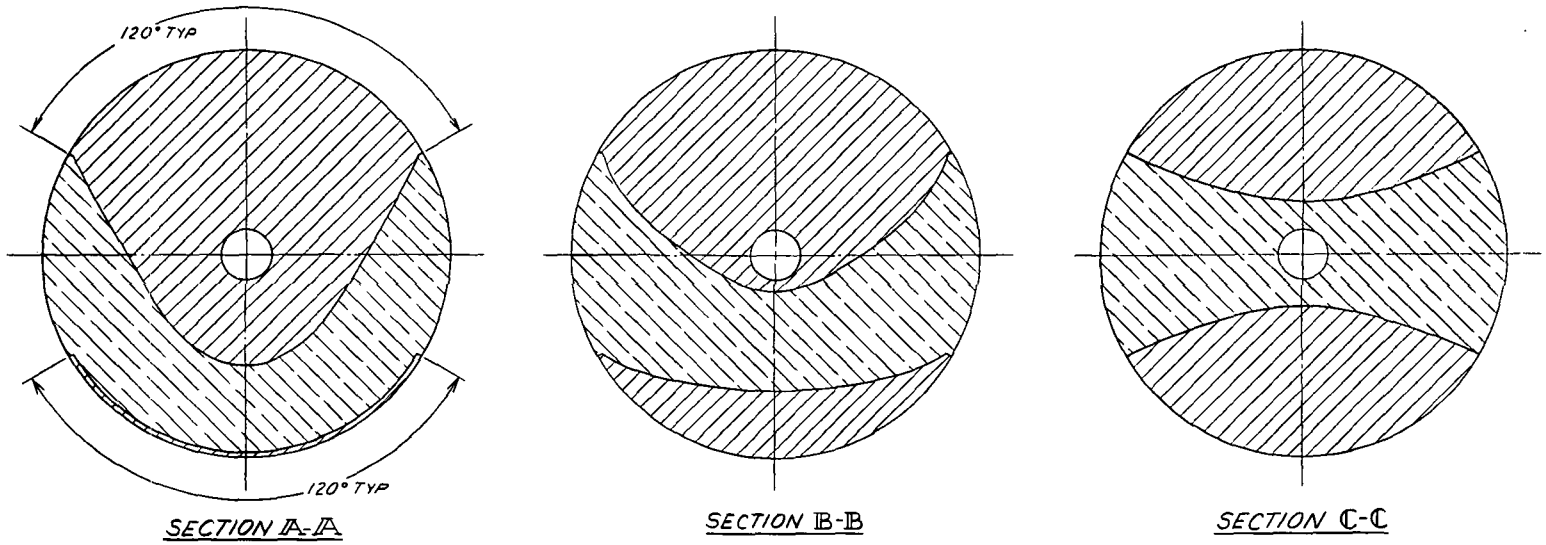
120° TYP
120° TYP
SECTION A-A
SECTION B-B
SECTION C-C

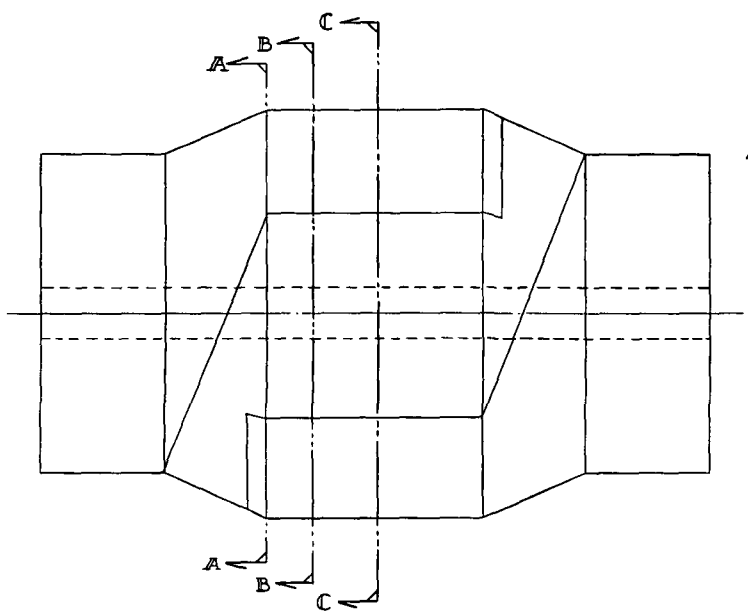
C
B
A
A
B
C

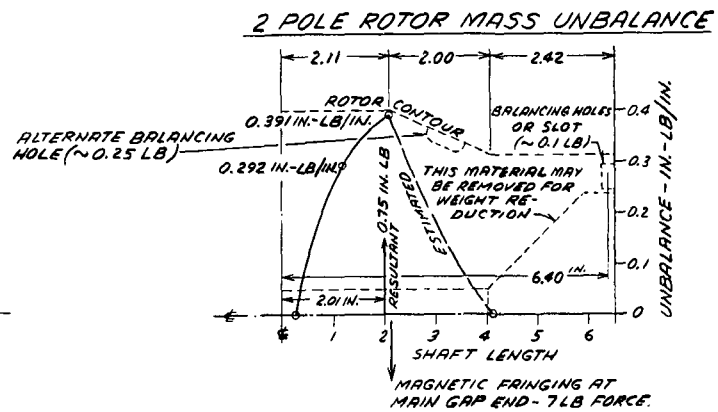
2 POLE ROTOR MASS UNBALANCE
2.11
2.00
2.42
ROTOR CONTOUR
BALANCING HOLES OR SLOT (~0.1 LB)
ALTERNATE BALANCING HOLE (~0.25 LB)
0.391 IN.-LB/IN.
0.292 IN.-LB/IN.²
THIS MATERIAL MAY BE REMOVED FOR WEIGHT REDUCTION
0.75 IN. LB RESULTANT
ESTIMATED
6.40 IN.
2.01 IN.
0.4
0.3
0.2
0.1
0
UNBALANCE - IN.-LB/IN.
0
1
2
3
4
5
6
SHAFT LENGTH
MAGNETIC FRINGING AT MAIN GAP END - 7 LB FORCE.
- NONMAGNETIC STEEL
- MAGNETIC STEEL

Figure 164

TABLE LXXIII

DESIGN SUMMARY
TAC ALTERNATOR
60 SLOT DESIGN, 2-POLE
COOLANT TEMPERATURE: 466°F & 325°F (514 & 436°K)

RATING: 214 kVA at 0.75 P.F. Lagging

VOLTAGE: 240/416 reconnectable to 480/832

SPEED 24000 rpm

FREQUENCY 400 Hz

DIMENSIONS: INCHES		
ROTOR O.D.	8.0	(20.4 cm)
ROTOR LENGTH	13.04	(33.2 cm)
STACK LENGTH (OVERALL)	4.22	(10.7 cm)
STACK O.D.	16.21	(41.2 cm)
OVERALL O.D.	18.5	(0.47 m)
OVERALL LENGTH	13.9	(0.35 m)

ELECTROMAGNETIC WEIGHTS: lbs (kg)		
ARMATURE	26.9	(12.2)
FIELD	43.3	(19.6)
FRAME	211.7	(95.9)
STACKS	135.5	(61.5)
ROTOR	153.1	(69.5)
TOTAL	570.5	(258.7)

MATERIALS:	
ac CONDUCTORS	321 SST CLAD SILVER
FIELD CONDUCTORS	CUBE COPPER ALLOY
ARMATURE LAMINATIONS	0.004 INCH (0.102 mm) THICK HIPERCO 27
FRAME	HIPERCO 27 FORGINGS
ROTOR MAGNETIC	SAE 4340 @ Rc 33
ROTOR NON-MAGNETIC	INCONEL 718 @ Rc 38
INSULATION	
ac WINDING	ANADUR
SLOT LINER	ALUMINA
SLOT SEPARATOR	SYNTHETIC MICA
FIELD WINDING	SYNTHETIC MICA

WINDING DETAILS:	
NUMBER OF SLOTS	60
CONDUCTORS PER SLOT	2

TABLE LXXIII (Continued)

SERIES TURNS PER PHASE (240 V L-N)	10	
PARALLEL PATHS (240 V L-N)	2	
PARALLEL STRANDS	4	
PHASE BELTS	60°	
PITCH	2/3	
BARE CONDUCTOR DIMENSIONS, INCHES	0.081 X 0.144	
(mm)	(2.06 X 3.66)	
ROTOR TIP SPEED (24000 RPM): feet/sec (m/sec)	837	(255)
MAIN GAP: INCH (mm)	0.120	(3.05)
AUXILIARY GAP: INCH (mm)	0.050	(1.27)
CURRENT DENSITIES: AMPS/IN^2 (Amps/cm^2)		
ac WINDING	3425	(530)
FIELD WINDING	3757	(581)
FLUX DENSITIES: KL/IN^2 (Webers/m^2)		
BACK IRON	76	(118)
TEETH	113	(175)
MAIN AIR GAP	46	(71)
POLE	86	(133)
FRAME	98	(152)
AUX. AIR GAP	58	(90)
% HARMONICS:		
THIRD	0	
FIFTH	2.71	
SEVENTH	2.18	

FOR THE TWO TEMPERATURES:	466°F (514°K) COOLANT	325°F (436°K) COOLANT
F.L. LOSSES: WATTS	1166	1258
POLE FACE	3782	4355
BACK IRON	564	650
TEETH	2132	1709
ARMATURE	3513	3513
ELECTROMAGNETIC SUBTOTAL	11158	11484
WINDAGE	8610	9150
@ PSIA (nt/cm^2)	70(48.3)70	
TOTAL	19768	20634
EFFICIENCY: %		
ELECTROMAGNETIC	93.2	93.3

TABLE LXXIII (Continued)

OVERALL	89.0	88.6
REACTANCES: P.U.		
XD	1.21	
X'D	0.277	
X"D	0.244	
Xq	0.55	
X"q	0.148	
X2	0.146	
Xo	0.008	
TIME CONSTANTS, HOT SECONDS		
T'DO	0.291	
T'D	0.059	
TA	0.0052	
Td:	0.0051	
VOLTAGE UNBALANCE: %		
2/3, single phase current	3.0	

TABLE LXXIV

DESIGN SUMMARY
TAC ALTERNATOR
30 SLOT DESIGN, 2-POLE
COOLANT TEMPERATURE: 466°F (514°K)

RATING: 214 kVA at 0.75 P.F. LAGGING

VOLTAGE: 480 VOLTS L-N, reconnectable to 240 V L-N, rewind for 120 Volts L-N

SPEED: 24000 rpm

FREQUENCY: 400 Hz

DIMENSIONS: INCHES

ROTOR O.D.	8.0	(20.4 cm)
ROTOR LENGTH	12.32	(32.6 cm)
STACK LENGTH (RADIAL DUCT NOT INCLUDED)	3.5	(8.9 cm)
STACK O.D.	16.51	(42.0 cm)

ELECTROMAGNETIC WEIGHT: lbs (kg)

ARMATURE	26.2	(11.9)
FIELD	44.4	(20.1)
FRAME	204.3	(92.8)
STACKS	136.3	(61.9)
ROTOR	145.0	(65.7)
TOTAL	556.2	(252.4)

MATERIALS:

ac CONDUCTORS	321 SST CLAD SILVER
FIELD CONDUCTORS	CUBE COPPER ALLOY
ARMATURE LAMINATIONS	0.004 INCH (0.102 mm) THICK HIPERCO 27
FRAME	HIPERCO 27 FORGINGS
ROTOR MAGNETIC	SAE 4340 @ Rc 33
ROTOR NON-MAGNETIC	INCONEL 718 @ Rc 38
INSULATION	
ac WINDING	ANADUR
SLOT LINER	ALUMINA
SLOT SEPERATOR	SYNTHETIC MICA
FIELD WINDING	SYNTHETIC MICA

WINDING DETAILS:

NUMBER OF SLOTS	30
CONDUCTORS PER SLOT	4
SERIES TURNS PER PHASE (480 V L-N)	20
PARALLEL PATHS (480 V L-N)	1
PARALLEL STRANDS	2
PHASE BELTS	60°
PITCH	2/3
BARE CONDUCTOR DIMENSIONS, INCHES	0.182 X 0.128
(mm)	(4.62 X 3.25)

TABLE LXXIV (Cont.)

ROTOR TIP SPEED (24000 rpm): feet/sec (m/sec)	837	(255)
MAIN GAP: INCH (mm)	0.120	(3.05)
AUXILIARY GAP: INCH (mm)	0.050	(1.27)
CURRENT DENSITIES: AMPS/IN^2		
ac WINDING	3304	(513)
FIELD WINDING	3921	(607)
FLUX DENSITIES: KL/IN^2		
BACK IRON	75	(116)
TEETH	103	(160)
MAIN AIR GAP	55	(85)
POLE	85	(132)
FRAME	102	(158)
AUX. AIR GAP	58	(90)
% HARMONICS:		
THIRD	0	
FIFTH	2.71	
SEVENTH	2.33	
F.L. LOSSES: WATTS (Doesn't account for forced convection cooling temperatures)		
POLE FACE (SAE 1010 pole face)	1485	
BACK IRON	3762	
TEETH	468	
ARMATURE	2324	
FIELD	3946	
ELECTROMAGNETIC SUBTOTAL	11985	
WINDAGE (approx.)	8600	
@ PSIA (nt/cm^2)	70	(48.3)
TOTAL	20585	
EFFICIENCY: %		
ELECTROMAGNETIC	93.0	
OVERALL	88.6	
REACTANCES: P.U.		
XD	1.1	
X'D	0.262	
X"D	0.230	
Xq	0.504	
X"q	--	
X2	--	
XO	0.007	
TIME CONSTANTS, HOT SECONDS		
T'Do	0.234	
T'D	0.051	
TA	--	
Td"	0.005	

TABLE LXXV

		0.75 P.F.				0.75 P.F.				0.9 P.F.
COOLANT TEMP: 325°F (436°K)	KWe	40	80	160	240	40	80	160	240	320 KVA
INSULATION: INORGANIC	P. U. LOAD	1/4	1/2	1	1 1/2	1/4	1/2	1	1 1/2	O.L.
FULL LOAD CAVITY PRESSURE: 70 PSIA (48.3 nt/cm^2)										
LOSSES: WATTS										
ARMATURE		99	401	1,709	4,313	55	222	918	2,195	4,311
FIELD		1,199	1,730	3,513	8,151	868	984	1,465	2,342	6,111
POLE FACE		511	659	1,258	2,269	485	565	891	1,443	2,261
TOOTH		624	633	650	667	618	620	625	630	657
BACK IRON		4,184	4,241	4,355	4,471	4,143	4,158	4,188	4,221	4,404
TOTAL ELECTROMAGNETIC		6,616	7,664	11,484	19,872	6,169	6,549	8,087	10,831	17,744
WINDAGE		3,550	5,710	9,150	12,080	3,550	5,710	9,150	12,080	13,640
OVERALL		10,166	13,374	20,634	31,952	9,719	12,259	17,237	22,911	31,384
EFFICIENCIES: %										
ELECTROMAGNETIC		85.81	91.26	93.30	92.35	88.64	92.43	95.19	95.68	94.20
OVERALL		79.73	85.68	88.58	88.25	80.45	86.71	90.27	91.28	90.17
CURRENT DENSITIES: AMPS/ IN^2										
ARMATURE CURRENT		856	1,713	3,425	5,138	640	1,280	2,560	3,840	5,138
FIELD CURRENT		2,187	2,627	3,743	5,702	1,861	1,981	2,418	3,057	4,937
FLUX DENSITIES: KL/IN^2										
BACK IRON		74	75	76	77	74	74	74	74	76
TOOTH		110	111	112	114	109	109	110	110	113
MAIN GAP		44	45	46	46	44	44	44	45	46
POLE		72	77	86	95	69	70	74	80	92
FRAME		78	84	98	112	74	75	81	89	108
AUX. AIR GAP		46	50	58	75	44	45	48	53	64
FIELD AMP TURNS		7,654	9,195	13,101	19,957	6,514	6,933	8,462	10,698	17,280

Amps/in^2 times 0.155 = Amps/cm^2
KL/in^2 times 1.55 = Webers/m^2

TABLE LXXVI

COOLANT TEMP: 325°F (436°K)		0.75 P.F.				1.0 P.F.				0.9 P.F.
INSULATION: INORGANIC	KWe									
FULL LOAD CAVITY PRESSURE: 86 PSIA (59.3 nt/cm^2)	P. U. LOAD	40 1/4	80 1/2	160 1	240 1 1/2	40 1/4	80 1/2	160 1	240 1 1/2	320 KVA O.L.
LOSSES: WATTS										
ARMATURE		99	401	1,709	4,313	55	222	918	2,195	4,311
FIELD		1,199	1,730	3,513	8,151	868	984	1,465	2,342	6,111
POLE FACE		511	659	1,258	2,269	485	565	891	1,443	2,261
TOOTH		624	633	650	667	618	620	625	630	657
BACK IRON		4,184	4,241	4,355	4,471	4,143	4,158	4,188	4,221	4,404
TOTAL ELECTROMAGNETIC		6,617	7,663	11,485	20,872	6,170	6,548	8,088	10,831	17,744
WINDAGE		4,060	6,520	10,440	13,800	4,060	6,520	10,440	13,800	15,580
OVERALL		10,677	14,183	21,925	34,672	10,230	13,068	18,525	24,631	33,324
EFFICIENCIES: %										
ELECTROMAGNETIC		85.81	91.26	93.30	92.00	86.64	92.43	95.19	95.68	94.20
OVERALL		78.93	84.94	87.95	87.38	79.63	85.96	89.62	90.69	89.63
CURRENT DENSITIES: AMPS/IN^2										
ARMATURE CURRENT		856	1,713	3,425	5,318	640	1,280	2,560	3,840	5,138
FIELD CURRENT		2,187	2,637	3,743	5,702	1,861	1,981	2,418	3,057	4,937
FLUX DENSITIES: KL/IN^2										
BACK IRON		74	75	76	77	74	74	74	74	76
TOOTH		110	111	112	114	109	109	110	110	113
MAIN GAP		44	45	46	46	44	44	44	45	46
POLE		72	76	86	95	69	70	74	80	92
FRAME		78	84	98	112	73	75	81	89	107
AUX. AIR GAP		46	50	58	66	44	45	48	53	64
FIELD AMP TURNS		7,654	9,195	13,101	19,957	6,514	6,933	8,462	10,698	17,280

Amps/in^2 times 0.155 = Amps/cm^2

KL/in^2 times 1.55 = Webers/m^2

where it returns axially to the other end of the alternator and to the pole of origin through the other auxiliary gap.

The stationary field coils are located above the end extensions of the ac winding. As shown in Figure 163 , there is an excess of space available for the field coils; as a result, the size of the field coil can be increased in order to reduce the field coil losses and amperes required from the voltage regulator-exciter.

Because the end extensions are long and the depth of the magnetic section behind the slots is large for 2-pole machines, the 2-pole configuration does not lend itself to efficient cooling by conduction of losses to the stator O.D. Because of this, forced convection cooling was adopted to cool the end extensions. The stator stack was divided into two sections to allow room for a 0.5 inch (1.27 cm) passageway for radial gas flow. A detailed description of the forced convection cooling scheme is presented in MECHANICAL DESIGN CONSIDERATIONS.

The configurations of the alternator slots are designed so that the alternators can be rewound using an organic insulation system for the 107°F (315°K) coolant temperature condition. Two different sizes of quadruple layer polyimide insulated rectangular wire are used to obtain a proper fit in the slot. The slot liners are composed of a double layer, polyimide film insulation. The slot liners are overlapped between phases to provide added high voltage protection as shown by the slot detail in Figure 163 . Organic insulations degrade with time and temperature; therefore, if long life is desired, the operating temperature of the insulation must be limited to achieve the desired life. Available data for a selected polyimide insulation system indicated that the winding temperatures must be less than 417°F (487°K) to achieve 5 years thermal life. Average winding temperatures using a coolant temperature of 107°F (315°K) are well below this limit, as indicated by the thermal maps given in MECHANICAL DESIGN CONSIDERATIONS. A summary of the design for the low temperature organic insulated 60 slot TAC alternator is given in Tables LXXVII and LXXVIII.

TABLE LXXVII

COOLANT TEMP: 107°F (315°K) / INSULATION: ORGANIC / FULL LOAD CAVITY PRESSURE: 70 PSIA	0.75 P.F.				1.0 P.F.				0.9 P.F.
KWe	40	80	160	240	40	80	160	240	320 KVA
P. U. LOAD	1/4	1/2	1	1 1/2	1/4	1/2	1	1 1/2	O.L.
LOSSES: WATTS									
ARMATURE	61	250	1,077	2,774	34	138	574	1,369	2,769
FIELD	1,201	1,736	3,539	8,358	869	985	1,471	2,356	6,188
POLE FACE	511	660	1,259	2,271	485	564	890	1,442	2,261
TOOTH	707	717	737	757	699	701	705	710	744
BACK IRON	4,738	4,804	4,940	5,078	4,685	4,699	4,729	4,761	4,988
TOTAL ELECTROMAGNETIC	7,217	8,266	11,552	19,239	6,771	7,087	8,369	10,628	16,950
WINDAGE	3,960	6,360	10,200	13,480	3,960	6,360	11,200	14,800	15,200
OVERALL	11,177	14,626	21,752	32,719	10,731	13,447	19,569	25,428	32,150
EFFICIENCIES: %									
ELECTROMAGNETIC	84.72	90.64	93.27	92.58	85.52	91.86	95.03	95.76	94.44
OVERALL	78.16	84.54	88.03	88.00	78.85	85.61	89.10	90.42	89.96
CURRENT DENSITIES: AMPS/IN^2									
ARMATURE CURRENT	628	1,256	2,512	3,767	469	939	1,877	2,816	3,767
FIELD CURRENT	2,189	2,631	3,757	5,774	1,861	1,982	2,422	3,065	4,968
FLUX DENSITIES: KL/IN^2									
BACK IRON	74	75	76	77	74	74	74	74	76
TOOTH	110	111	113	114	109	109	110	110	113
MAIN GAP	44	45	46	46	44	44	44	44	46
POLE	72	77	86	95	69	70	74	80	92
FRAME	78	84	98	112	74	75	81	90	108
AUX. AIR GAP	46	50	58	66	44	44	48	53	64
FIELD AMP TURNS	7,660	9,210	13,150	20,209	6,515	6,937	8,478	10,729	17,389

Amps/in^2 times 0.155 = Amps/cm^2

KL/in^2 times 1.55 = Webers/m^2

TABLE LXXVIII

		0.75 P.F.				1.0 P.F.				0.9 P.F.
COOLANT TEMP: 107°F (315°K)	KWe	40	80	160	240	40	80	160	240	320 KVA
INSULATION: ORGANIC	P. U. LOAD	1/4	1/2	1	1 1/2	1/4	1/2	1	1 1/2	O.L.
FULL LOAD CAVITY PRESSURE: 86 PSIA										
LOSSES: WATTS										
ARMATURE		61	249	1,069	2,761	34	138	571	1,369	2,710
FIELD		1,201	1,736	3,539	8,358	869	985	1,471	2,356	6,188
POLE FACE		511	660	1,259	2,271	485	564	890	1,442	2,261
TOOTH		707	717	737	757	699	701	705	710	744
BACK IRON		4,738	4,804	4,940	5,078	4,685	4,699	4,729	4,761	4,988
TOTAL ELECTROMAGNETIC		6,818	8,166	11,543	19,181	6,772	7,087	8,366	10,638	16,891
WINDAGE		4,480	7,210	11,550	15,260	4,480	7,210	11,550	15,240	17,210
OVERALL		11,298	15,376	23,093	34,441	11,252	14,297	19,916	25,878	34,101
EFFICIENCIES: %										
ELECTROMAGNETIC		85.44	90.74	93.27	92.60	85.52	91.86	95.03	95.76	94.46
OVERALL		77.98	83.88	87.39	87.45	78.04	84.84	88.93	90.27	89.41
CURRENT DENSITIES: AMPS/IN^2										
ARMATURE CURRENT		628	1,256	2,512	3,767	469	939	1,877	2,816	3,767
FIELD CURRENT		2,189	2,631	3,757	5,774	1,861	1,982	2,422	3,065	4,968
FLUX DENSITIES: KL/IN^2										
BACK IRON		74	75	76	77	74	74	74	74	76
TOOTH		110	111	113	114	109	109	110	110	113
MAIN GAP		44	45	46	46	44	44	44	44	46
POLE		72	77	86	95	69	70	74	80	92
FRAME		78	84	98	112	74	75	81	90	108
AUX. AIR GAP		46	50	58	66	44	44	48	53	64
FIELD AMP TURNS		7,660	9,210	13,150	20,209	6,515	6.937	8,478	10,729	17,389

Amps/in^2 times 0.155 = Amps/cm^2

KL/in^2 times 1.55 = Webers/m^2

Performance Summaries

Alternator electrical performance was determined for loads corresponding to $\frac{1}{4}$, $\frac{1}{2}$, 1 and $1\frac{1}{2}$ times rated kilowatt power output at load power factors of 0.75 lagging and 1.0 respectively. Breakdowns of losses, current densities, flux densities, efficiencies, and field ampere turns are given in Tables LXXII through LXXVIII for coolant temperatures of 325°F (436°K) and 107°F (315°K) and for rotor cavity pressures of 70 psia (48.3 nt/cm^2) and 86 psia (59.3 nt/cm^2) respectively.

Plots of alternator efficiency as a function of per unit kilowatt load are presented in Figures 165 through 169 for the above stated conditions. The electromagnetic efficiency and overall efficiency (includes windage losses) are shown for comparisons. The case of increased stack length is illustrated on Figure 166 to show potential part-load efficiency improvements.

Load and no-load saturation curves are given in Figures 170 and 171 for the high temperature and low temperature alternators respectively. Calculations performed for the overload conditions of 320 kva at 0.9 pf lagging indicate a winding temperature rise of 376°F (290°K) in five seconds assuming the highest coolant temperature of 466°F (514°K). The calculation assumes all of the heat is stored in the ac winding during the 5 second time period and is somewhat pessimistic. The average winding temperature at the end of 5 seconds would be about 944°F (779°K). This temperature is well below the melting point of silver, 1761°F (1234°K) and within the temperature limits of the selected inorganic insulation.

MISCELLANEOUS ELECTRICAL DESIGN CONSIDERATIONS

Corona

The ac winding of the alternator is surrounded with a Helium-Xenon gas mixture. The gas pressure is assumed to vary as a linear function of load ranging from $\frac{1}{4}$ load to $1\frac{1}{2}$ times rated load. It is known from Paschen's characteristic curves for gases that the inception of corona is a function of voltage, gas pressure, and electrode spacing. The

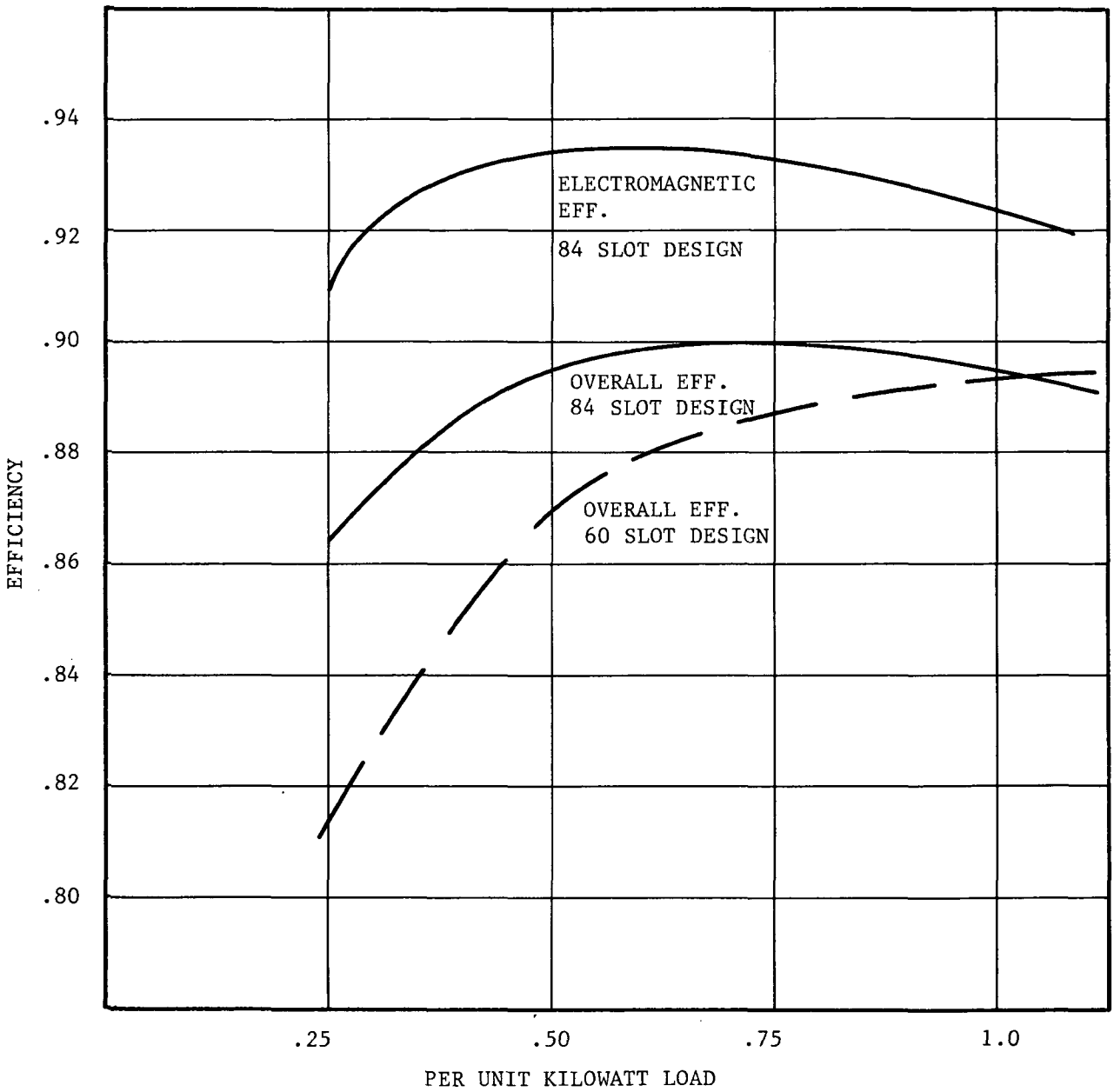
.94
.92
.90
.88
.86
.84
.82
.80
EFFICIENCY
ELECTROMAGNETIC EFF.
84 SLOT DESIGN
OVERALL EFF.
84 SLOT DESIGN
OVERALL EFF.
60 SLOT DESIGN
.25
.50
.75
1.0
PER UNIT KILOWATT LOAD

Figure 165

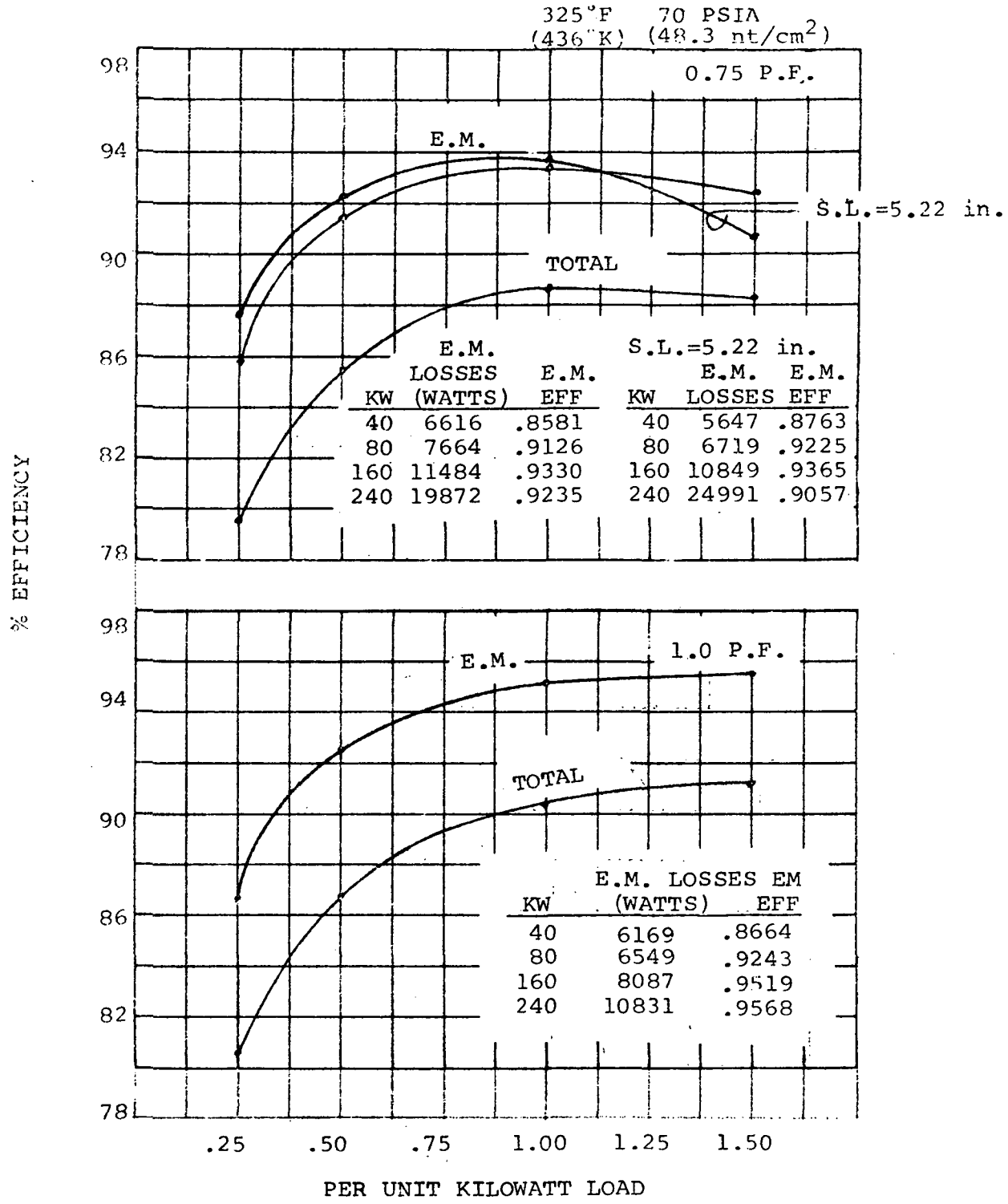

Figure 166 (60 Slots)

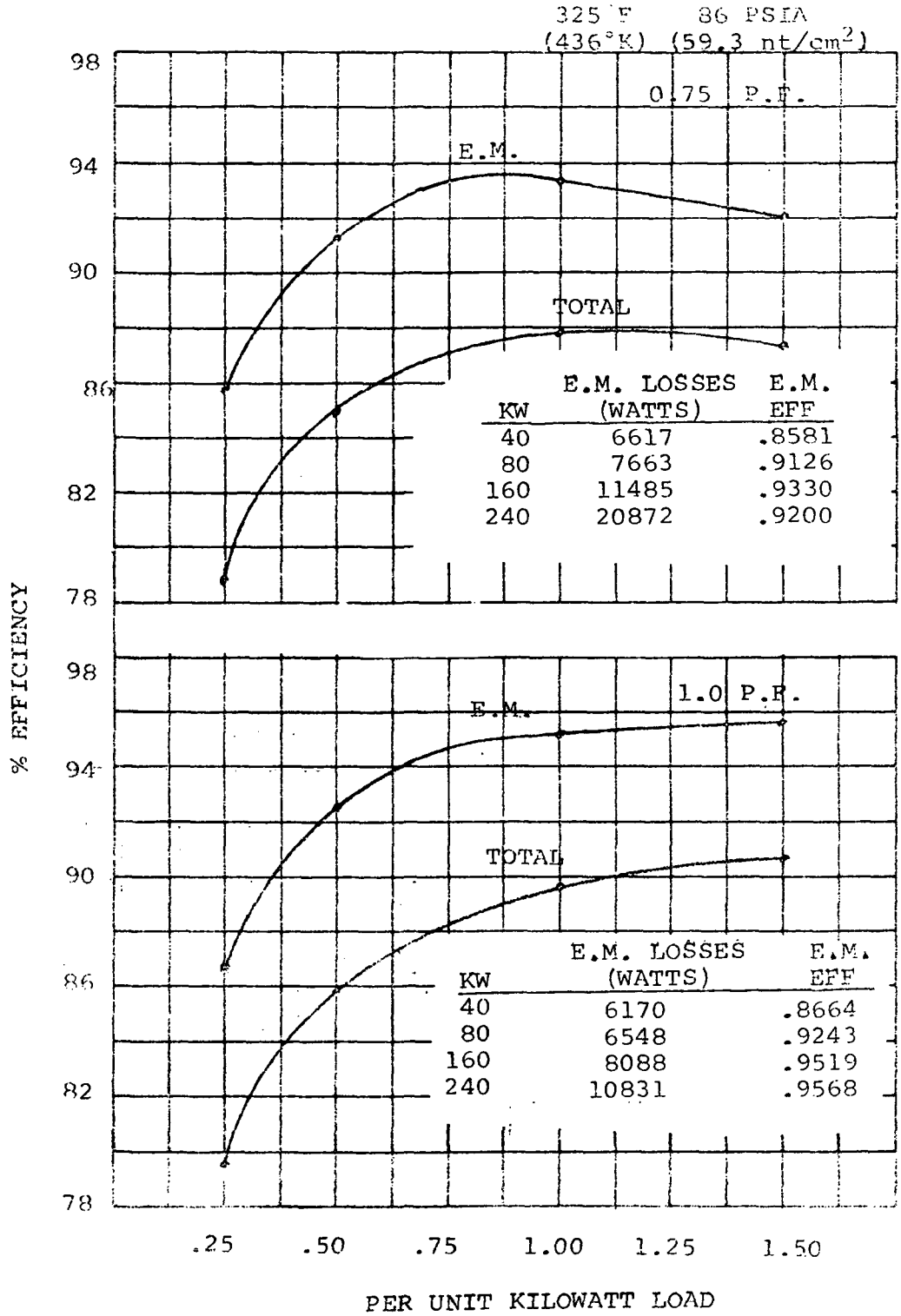

Figure 167 (60 Slots)

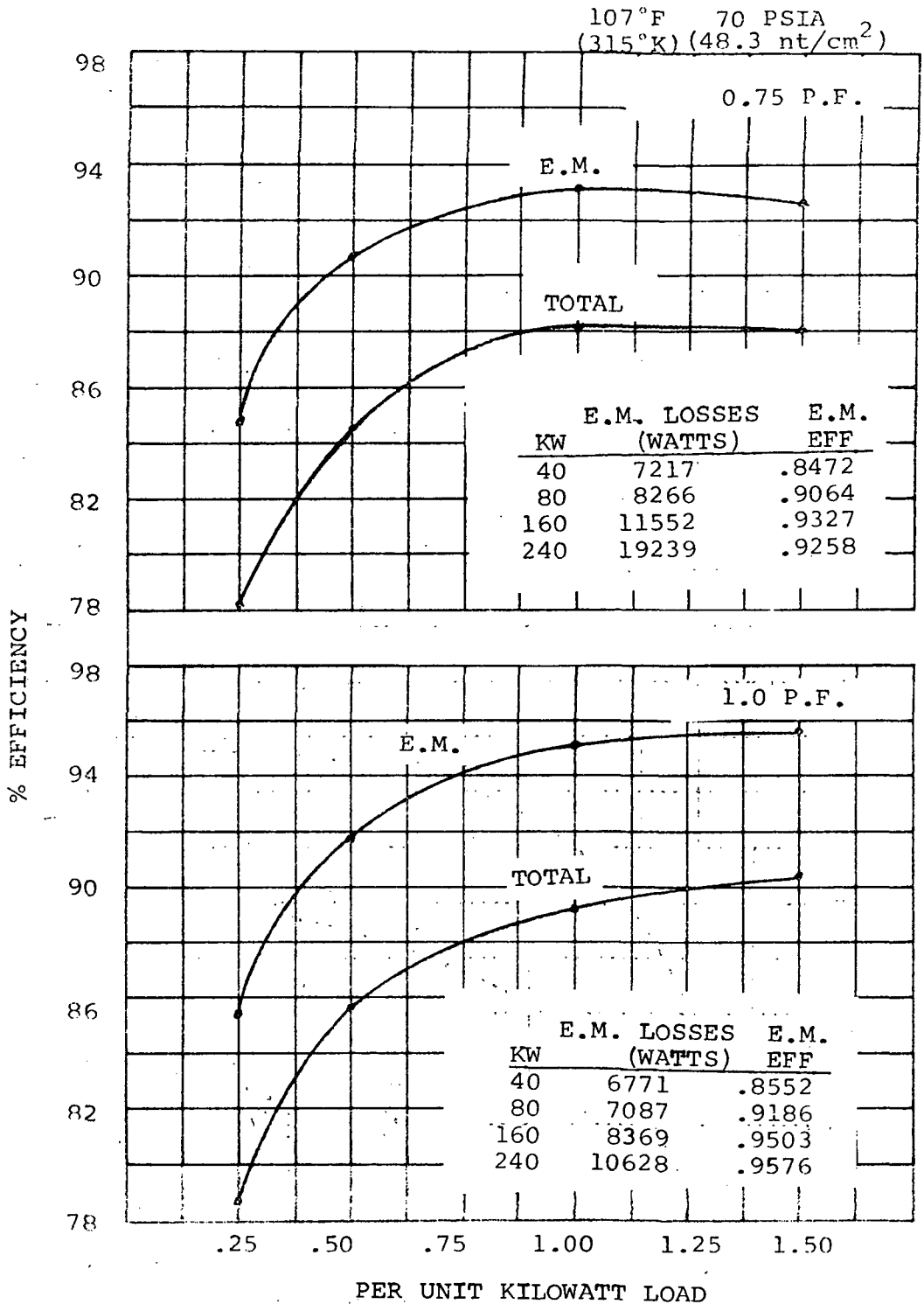

Figure 168 (60 Slots)

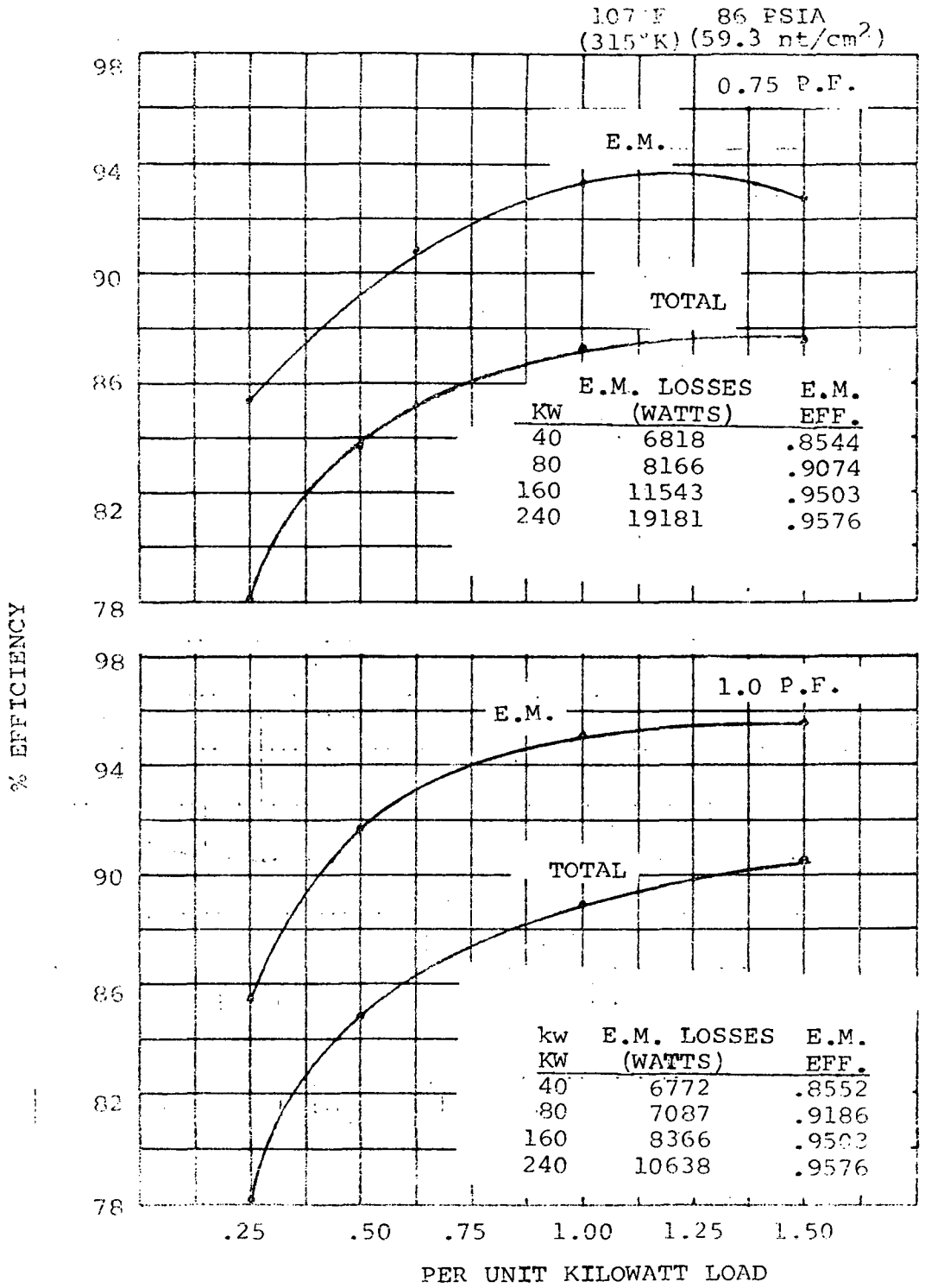

Figure 169 (60 Slots)

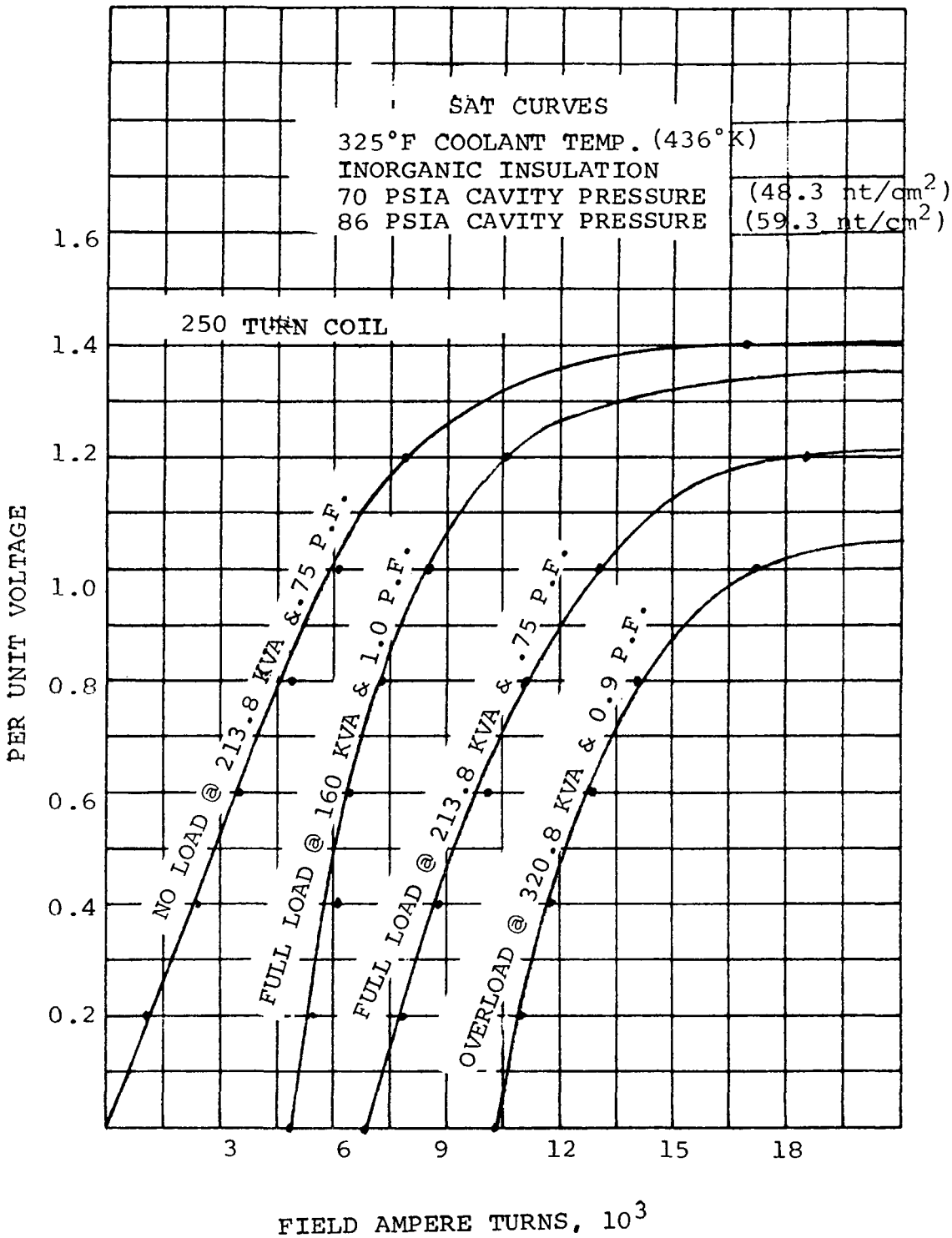

Figure 170 (60 Slots)

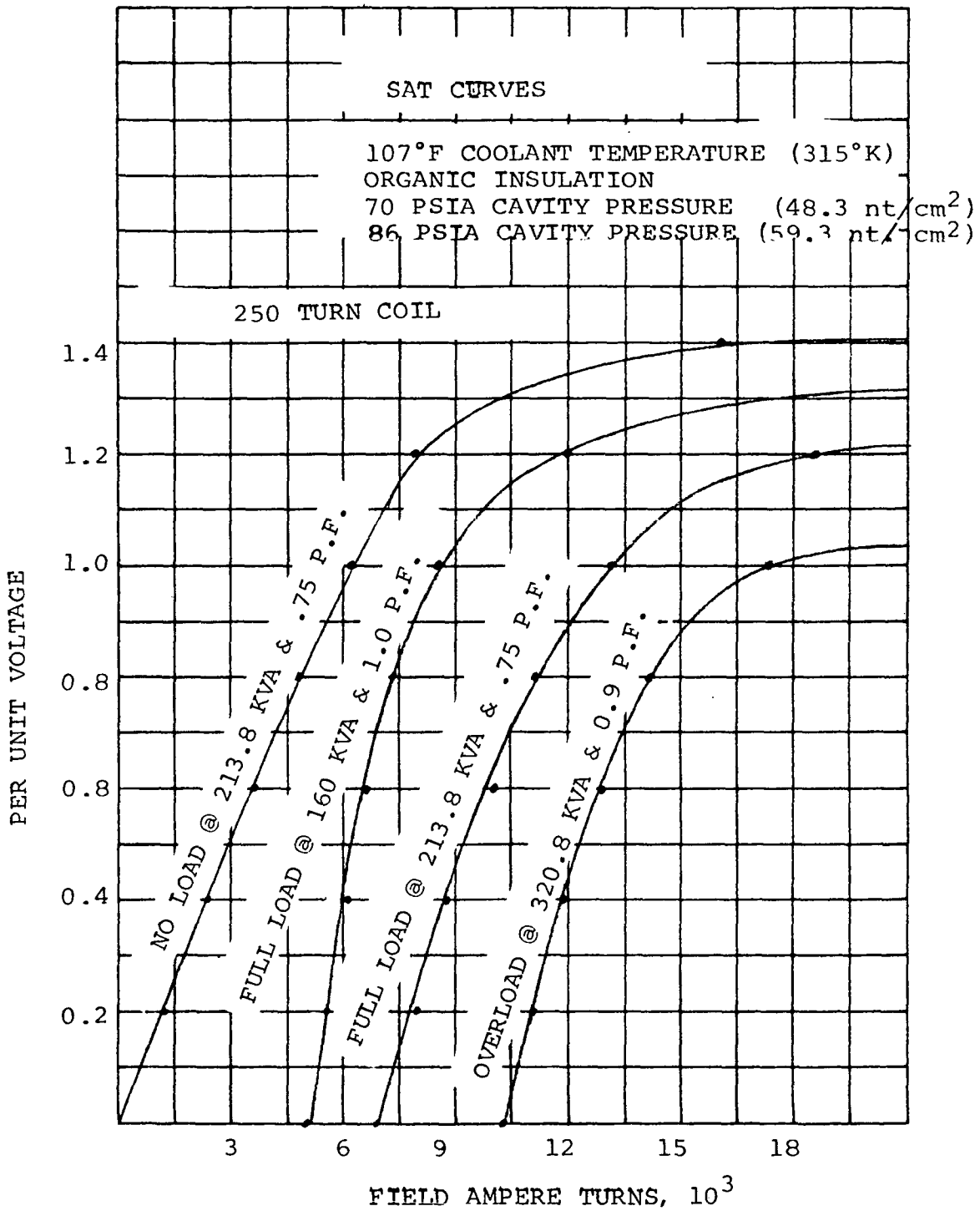

Figure 171 (60 Slots)

voltage gradient through the gas is dependent upon the dielectric constant and thickness of the insulation materials between the electrodes. Because the gas pressure in the stator cavity of the alternator is variable, calculations were made to determine the minimum allowable pressure to prevent ionization (corona) of the gas for the three specified alternator voltages. Results of these calculations are presented in Table LXXIX.

The first three lines in the table present results for the inorganic, high temperature insulation system. In order to portray the effects of increasing the insulation thickness on minimum allowable pressure, calculations were repeated for the case of phase-to-phase voltage in the slot assuming that all insulation thicknesses are doubled. The results indicated in Table LXXIX show that the minimum pressure is reduced to approximately one half of the previous quantities.

Calculations were repeated for the organic, low temperature insulation system assuming that the winding is not impregnated with a varnish. The minimum allowable pressures calculated for this case are approximately the same as for the inorganic insulation system. This seems surprising in view of the lower dielectric constant of the organic insulation; however, the insulation thicknesses selected were less than for the inorganic insulation system. This was done primarily because of higher available dielectric strength and poorer heat transfer properties. Increasing the thickness of the insulation would result in lower minimum allowable pressures as indicated previously for the inorganic insulation system.

The fact that no varnish impregnation was assumed in the organic insulation system calculations is significant. If it is assumed that the winding is completely impregnated with a compatible varnish, then the minimum pressure for corona inception cannot be accurately calculated. Theoretically, a varnished winding is solid and does not contain any gas filled spaces. In reality, however, small bubbles or cavities do occur. The type of gas and the pressure in these cavities cannot be accurately predicted. In general, the use of a varnish impregnation will significantly increase the corona resistance of the winding. The mechanism of failure would be caused by the presence of

TABLE LXXIX

MINIMUM ALLOWABLE PRESSURES

BASED ON CORONA CONSIDERATIONS

ALTERNATOR VOLTAGE (No Transients)	INSULATION	MINIMUM ALLOWABLE PRESSURE TO PREVENT IONIZATION OF GAS, PSIA (nt/cm^2)	
		PHASE TO PHASE IN SLOT	PHASE TO STACK IN SLOT
120/208	Inorganic	No Limit	No Limit
240/416	Inorganic	14 *6 (9.7) (*4.1)	8
480/832	Inorganic	53 *26 (37) (*18)	49 (34)
120/208	Organic, no varnish	No Limit	No Limit
240/416	Organic, no varnish	15 (10)	No Limit
480/832	Organic, no varnish	56 (39)	41 (28)

* For double insulation thicknesses

corona pulses occurring in the entrained cavities in the solidified insulation. The electrons and ions in the gas bombard the insulation on each pulse and erode away the insulation. Harmful chemical reactions can occur. In general, for insulating materials, the time-to-failure at any applied voltage is a measure of corona resistance. Inorganic insulations are much better in this respect than organic insulations. An inorganic insulating material such as alumina may induce corona in a gas at a lower voltage than for an organic material such as polyimide, but it is better able to withstand the effects of the corona pulses. Long life can be achieved for organic insulations by operating the insulation at reduced voltage stress levels.

Voltage Unbalance

The unbalance in the three-phase voltage of the alternator when operating with a single-phase current load equal to 2/3 of the rated current was determined for the alternator designs presented in Phase I and Phase III. The method of calculating one of the reactance values that indirectly effects voltage unbalance was changed during the Phase I to Phase III interim. The quadrature-axis sub-transient reactance ($X''q$) which is used in determining the negative sequence reactance (X_2) was previously determined by neglecting the quadrature axis damping provided by eddy currents flowing in the solid rotor surface. The procedure now used for calculating $X''q$ is based on a modification of procedures outlined in the Westinghouse East Pittsburgh Design Manual for turboalternators which accounts for sub-transient damping effects. A check on the new calculation procedure was made by comparing calculated results and test results for the 1200 Hz alternator of the Brayton Rotating Unit (BRU).[54] The value of voltage unbalance obtained by test is 5.2 percent for a 2/3 rated current, single phase, unity power factor load. The calculated value is 5.85 percent. It was previously calculated to 11.8 percent using the initial methods of Phase I.

MECHANICAL DESIGN CONSIDERATIONS

Thermal Analysis

1. Method of Cooling

Direct conduction of the internal losses to heat sinks on the magnetic frame was not considered for the two-pole alternator since previous studies of the six-pole alternator, which offered more favorable conditions for direct conduction, revealed this mode of cooling was not adequate. A portion of the losses generated within the pole faces, conductors and gas must be transported by forced convection.

Forced convection within the alternator is obtained by recirculating the cavity gas through the conical gap around the rotor whereby the rotor produces a pumping action on the gas. The gas then passes through the main gap between the stator and rotor. A split stack provides a radial passage from the main gap to a heat-exchanger which is located between the stack and the magnetic frame. The heat-exchanger also serves as a non-magnetic separator between the back-iron and the frame. After the gas passes through the heat-exchanger, it flows around the field coil and through the end extensions of the windings. Special baffles are used around the conical sections of the rotor. These baffles are designed to (1) cause the gas to enter the conical gap near the end of the auxiliary radial gap, (2) cause the gas to flow into the main gap with minimum leakage at the ends of the stacks, and (3) cause some of the gas to flow through the ends of the windings.

2. Pumping of the Gas

Pumping of the gas is produced by the action of the conical surfaces upon the gas within the gap. The head developed by this action was estimated from:

$$\Delta P = 1/2K \rho \frac{R_o^2 w^2}{gc} (1 - R_i^2/R_o^2)$$

where

ΔP = pressure head, $Lb_f in^{-2}$

ρ = density of gas, $Lb_m in^{-3}$

w = rotor speed, 800 π radian sec^{-1}

R_o = rotor radius (main gap) = 4.0 in

R_i = rotor radius (auxiliary gap) = 3.25 in

K = 0.5 = average circumferential velocity of gas relative to the circumferential velocity of rotor surface

gc = 386.4 $Lb_m in\ Lb_f^{-1}\ sec^{-2}$

In general, it was assumed that the head developed within the conical gap was equal to the centrifugal head which would be developed by solid body rotation of the gas at one-half of the speed of the rotor.

3. Pressure Drop

The pressure drop within the gas flow circuit was estimated from:

$$\Delta P = 1/2\ \rho\ V_H^2 \left(\frac{fl}{D} + \Sigma\ C_{dh}\right) + 1/2\ \rho\ V_R^2\ \Sigma C_{dR}$$

where

V_H = velocity of gas in the heat-exchanger

V_R = velocity of gas in baffles and gap around the rotor

C_{dh} = loss coefficients for heat-exchanger (entrance, exit, turning, etc.)

C_{dR} = loss coefficient for baffles and gaps

fl/D = friction factor for heat-exchanger

V_H/V_R = constant = 3.0 in/2.75 in = 1.091

With an allowance of one dynamic head of loss for each entrance, turn, and exit plus an adequate allowance for the friction factor, the pressure drop for the flow circuit became:

$$P = 1/2\ \rho\ V_H^2 \quad (9.34)$$

and equating the pump head to the pressure drop gives:

$$V_H \approx 80 \text{ ft sec}^{-1} \ (24.4 \text{ m sec}^{-1})$$

$$V_R \approx 73.2 \text{ ft sec}^{-1} \ (22.3 \text{ m sec}^{-1})$$

In general, the volumetric flow rate through the circuit was considered constant since Reynolds number effects upon the friction and other loss coefficients was neglected.

4. Coolant Flow Rate

The flow rate based upon a velocity of 80 ft sec^{-1} (24.4 m sec^{-1}) in the heat-exchanger is given in Figure 172 as a function of pressure and the average temperature of the gas. These flow rates were used for the heat transport calculations.

5. Heat Transfer Coefficients

The heat-transfer coefficients for argon gas within the heat-exchanger, auxiliary gap, main gap, and on the windings are given in Figures 173 and 174. The surface area on the gas side of the heat-exchanger was considered to be 7.51 ft^2 (0.697m^2, both sides of the split stack). Each side consists of 275 parallel passages (4.38 inches (11.1 cm) long) with a flow area per passage of 0.01 in^2 (0.2 inches x 0.05 inches; 0.508 x 0.127 cm and 0.0645 cm^2).

6. Windage Losses

Windage losses were calculated for HeXe gas since this gas produces a lower Reynolds number (higher drag coefficient) than argon gas at the same conditions. Windage losses as a function of gas temperature are given in Figures 175 , 176 , and 177. Drag coefficients from NASA TMX-52851 were used. A comparison of the windage loss in the main gap obtained by the method used for the Phase I study and by the recent data reported

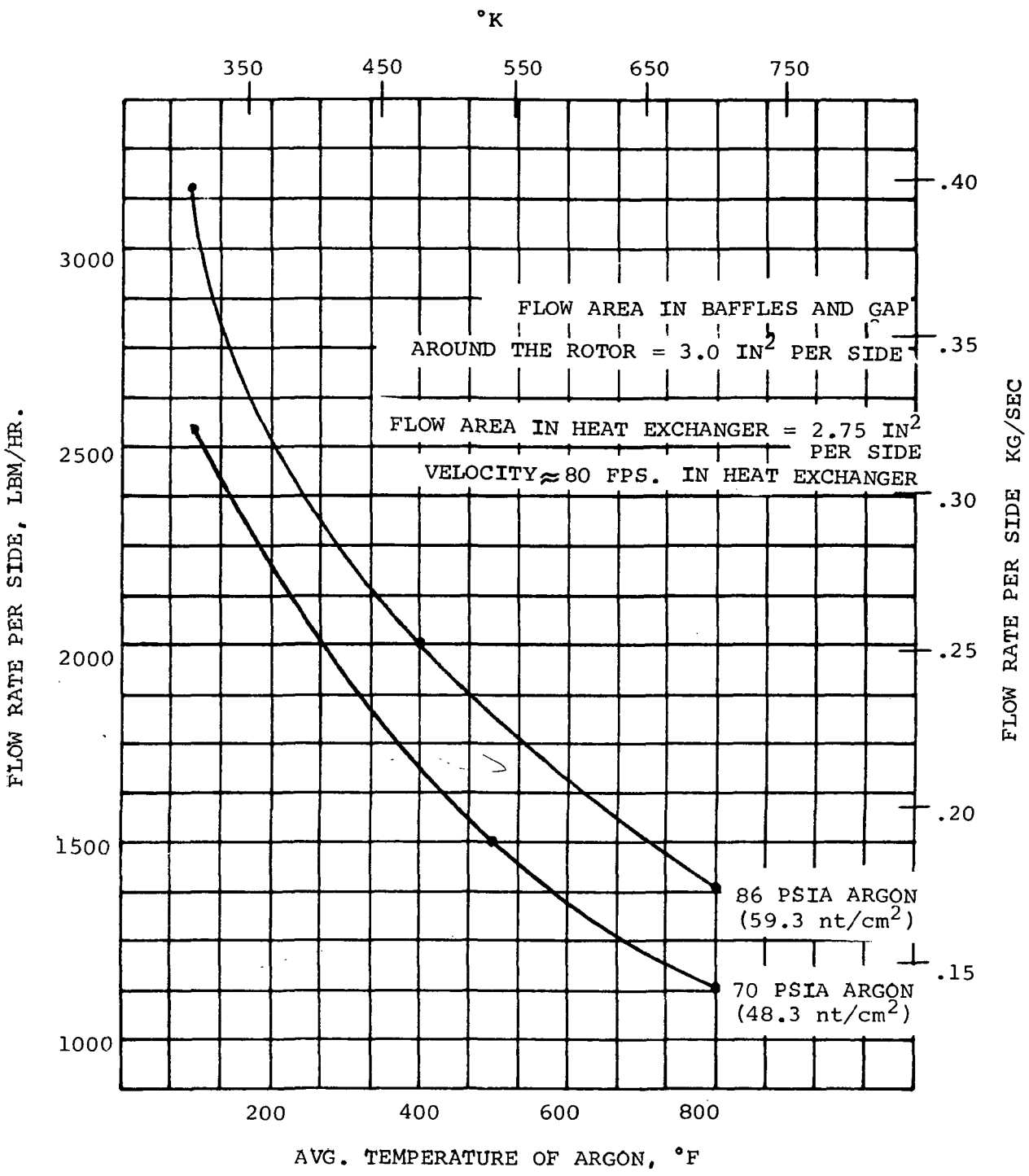
°K
350
450
550
650
750
3000
2500
2000
1500
1000
.40
.35
.30
.25
.20
.15
FLOW AREA IN BAFFLES AND GAP AROUND THE ROTOR = 3.0 IN² PER SIDE
FLOW AREA IN HEAT EXCHANGER = 2.75 IN² PER SIDE
VELOCITY ≈ 80 FPS. IN HEAT EXCHANGER
86 PSIA ARGON (59.3 nt/cm²)
70 PSIA ARGON (48.3 nt/cm²)
FLOW RATE PER SIDE, LBM/HR.
FLOW RATE PER SIDE KG/SEC
200
400
600
800
AVG. TEMPERATURE OF ARGON, °F

Figure 172

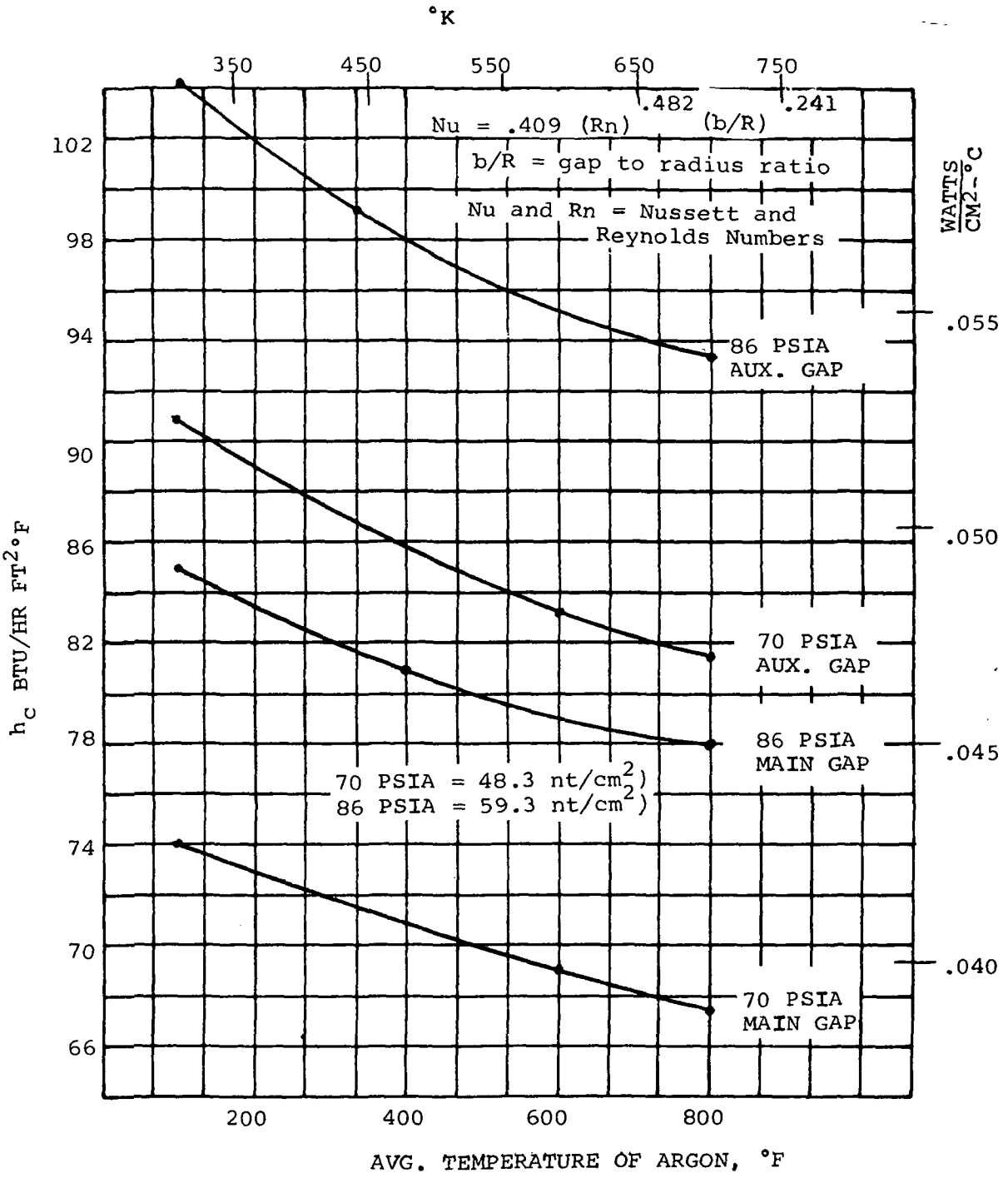
°K
350
450
550
650
750
.482
.241
Nu = .409 (Rn) (b/R)
b/R = gap to radius ratio
Nu and Rn = Nussett and Reynolds Numbers
102
98
94
90
86
82
78
74
70
66
86 PSIA AUX. GAP
70 PSIA AUX. GAP
86 PSIA MAIN GAP
70 PSIA MAIN GAP
70 PSIA = 48.3 nt/cm2)
86 PSIA = 59.3 nt/cm2)
.055
.050
.045
.040
WATTS/CM2-°C
hc BTU/HR FT2°F
200
400
600
800
AVG. TEMPERATURE OF ARGON, °F

Figure 173

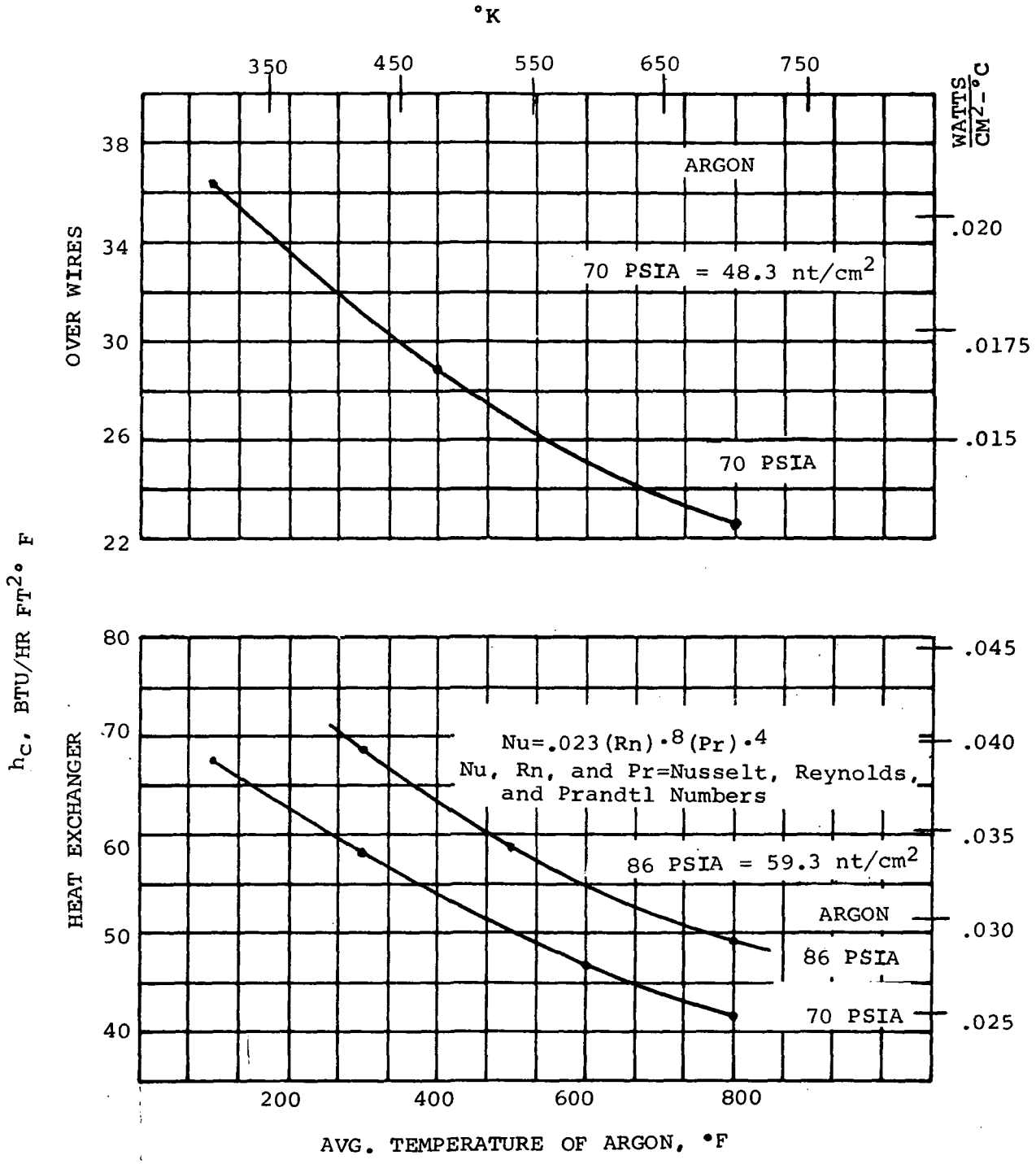
°K
350
450
550
650
750
WATTS/CM2-°C
.020
.0175
.015
38
34
30
26
22
OVER WIRES
ARGON
70 PSIA = 48.3 nt/cm2
70 PSIA
hc, BTU/HR FT2° F
80
70
60
50
40
HEAT EXCHANGER
.045
.040
.035
.030
.025
Nu=.023(Rn)·8(Pr)·4
Nu, Rn, and Pr=Nusselt, Reynolds, and Prandtl Numbers
86 PSIA = 59.3 nt/cm2
ARGON
86 PSIA
70 PSIA
200
400
600
800
AVG. TEMPERATURE OF ARGON, °F

Figure 174

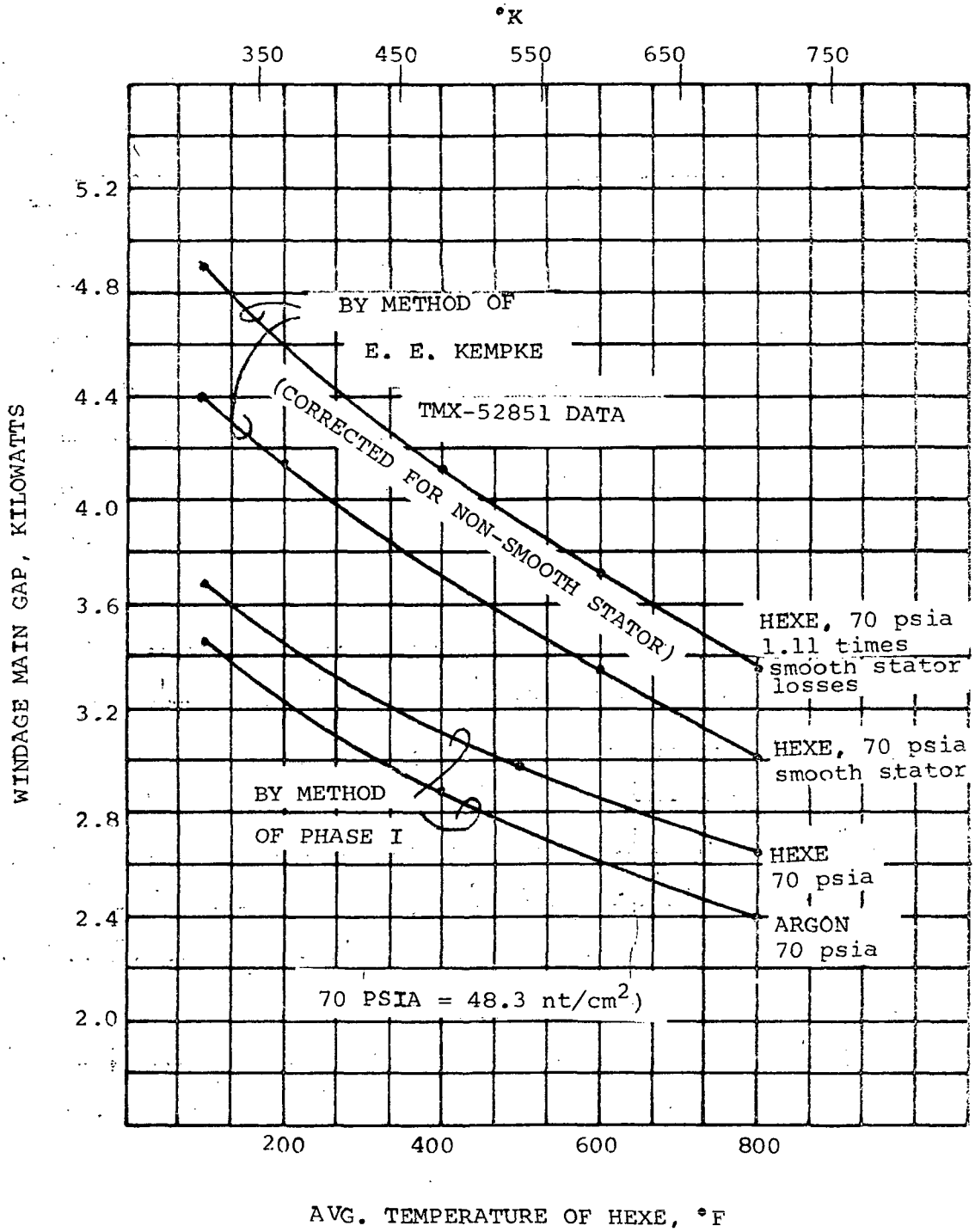
°K
350
450
550
650
750
5.2
4.8
4.4
4.0
3.6
3.2
2.8
2.4
2.0
WINDAGE MAIN GAP, KILOWATTS
BY METHOD OF
E. E. KEMPKE
TMX-52851 DATA
(CORRECTED FOR NON-SMOOTH STATOR)
HEXE, 70 psia
1.11 times
smooth stator
losses
HEXE, 70 psia
smooth stator
BY METHOD
OF PHASE I
HEXE
70 psia
ARGON
70 psia
70 PSIA = 48.3 nt/cm²)
200
400
600
800
AVG. TEMPERATURE OF HEXE, °F

Figure 175

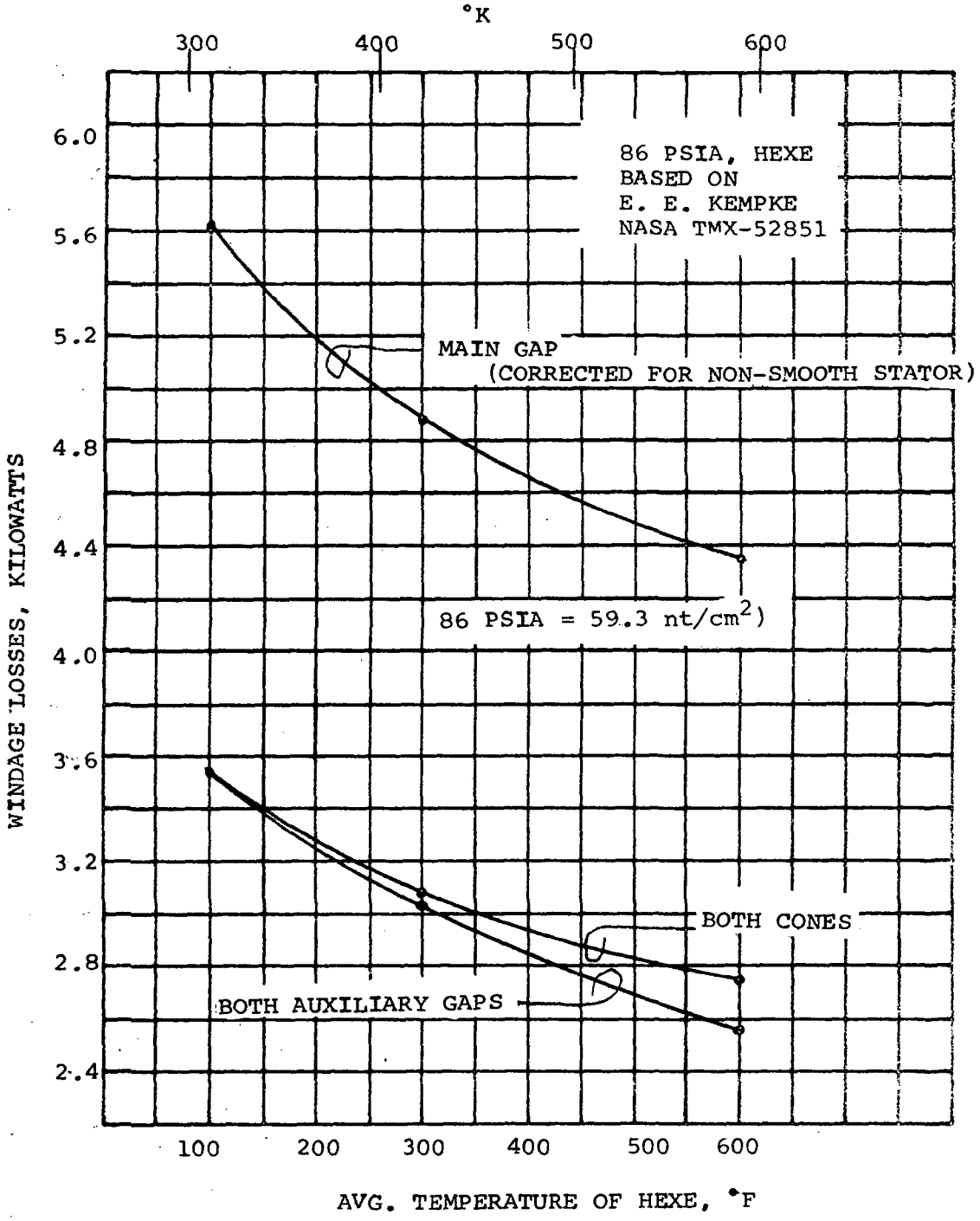
°K
300
400
500
600
6.0
5.6
5.2
4.8
4.4
4.0
3.6
3.2
2.8
2.4
86 PSIA, HEXE
BASED ON
E. E. KEMPKE
NASA TMX-52851
MAIN GAP
(CORRECTED FOR NON-SMOOTH STATOR)
86 PSIA = 59.3 nt/cm²)
BOTH CONES
BOTH AUXILIARY GAPS
WINDAGE LOSSES, KILOWATTS
100
200
300
400
500
600
AVG. TEMPERATURE OF HEXE, °F

Figure 176

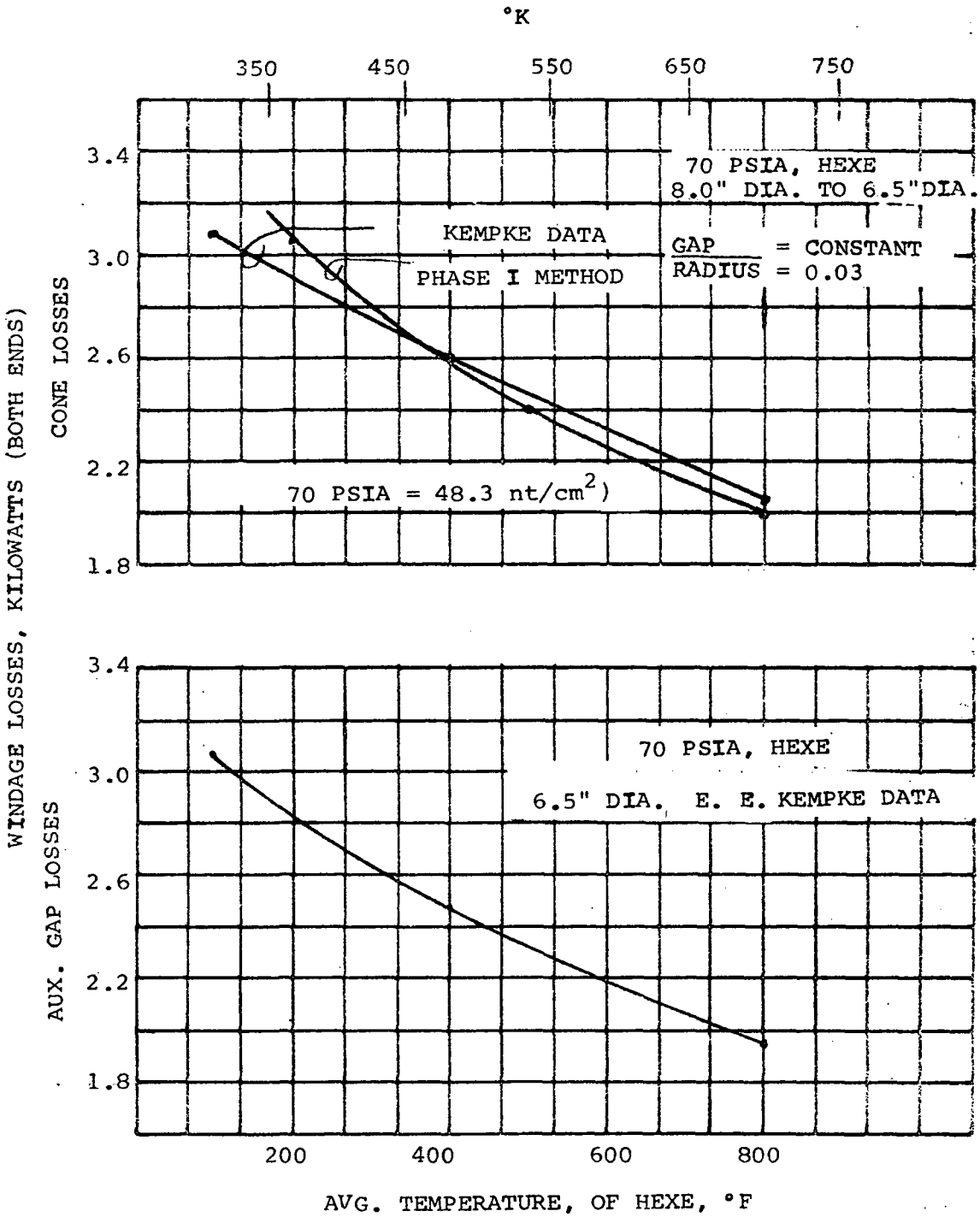
°K
350
450
550
650
750
3.4
3.0
2.6
2.2
1.8
70 PSIA, HEXE
8.0" DIA. TO 6.5"DIA.
KEMPKE DATA
PHASE I METHOD
GAP / RADIUS = CONSTANT
= 0.03
70 PSIA = 48.3 nt/cm²)
CONE LOSSES
70 PSIA, HEXE
6.5" DIA. E. E. KEMPKE DATA
AUX. GAP LOSSES
200
400
600
800
AVG. TEMPERATURE, OF HEXE, °F
WINDAGE LOSSES, KILOWATTS (BOTH ENDS)

Figure 177

in TMX-52851 by E. E. Kempke is given in Figure 175. The new data gives approximately 30 percent higher loss. Therefore, the new data was used for the cooling studies.

7. Thermal Maps

Computer programs were utilized to perform all analyses excepting the temperature rise of the liquid coolant and the maximum and minimum temperature of the gas. A 30°F (17°K) temperature rise of the liquid coolant was used for all calculations. The mean temperature difference between the gas and liquid in the heat-exchanger and the temperature rise of the gas were obtained by iterative calculations. The gas temperatures were treated as boundary temperatures which were improved after each iteration until the temperature rise of the gas correlated with the heat flow into the gas at each point along the flow path. The analysis did not include the alternator field coils since their thermal state is relatively independent of other alternator temperatures. The field coils can be cooled by coolant coils which are an intimate part of the field coil package. The field coils do not represent difficult cooling problems as indicated in the Phase I studies where a more compact field coil design was analyzed.

Thermal maps are presented in Figures 178 through 187 for the conditions and situations listed in Table LXXX.

All of the cooling configurations and conditions which were investigated fullfilled the requirement of the investigation since the hot-spot temperature for all designs was less than 300°F (167°K) above the coolant supply temperature.

Design No. 5 from Table LXXX represents the design with the least merit for a coolant supply temperature of 466°F (514°K) since the temperature at an adiabotic interface between the rotor and bearings is high, 693°F (640°K). Approximately one kilowatt of heat must be conducted through the interface to decrease the interface temperature 100°F (55°K). Addition of coolant within the endbell, as represented by Design No. 3, decreased the temperature of the adiabatic interface from 693° to 623°F (640° to 602°K). Similarly, the addition of a small gas flow through the auxiliary gap without coolant in the

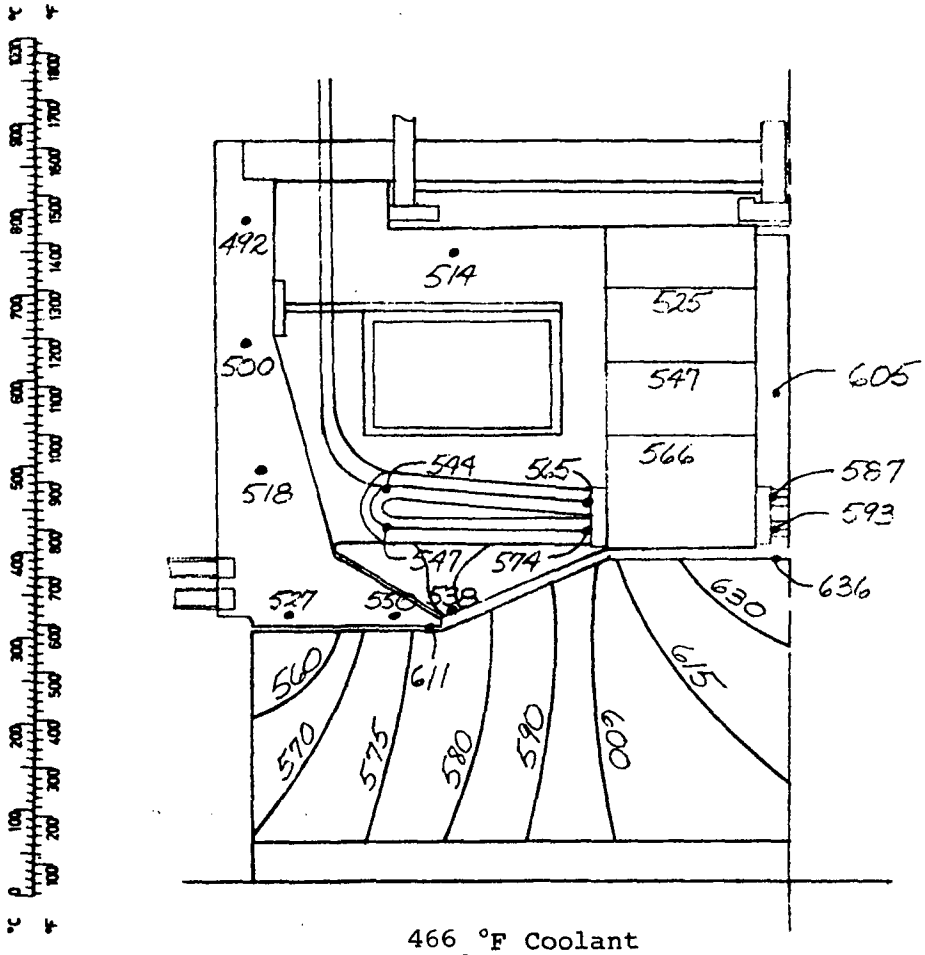

466 °F Coolant
514°K
(48.3 nt/cm^2)70 psia Cavity Pressure

Special Conditions:
Gas Flow in Auxiliary Gap
End Bell w/o coolant

Avg. Pole Face Temp. 626°F (603°K)
Avg. Winding Temp. 567°F (570°K)

Windage	Avg. Gas Temp. °F	Windage Loss Watts (HeXe)
Main Air Gap	583 (560°K)	3,750
Cone Gap	547 (558°K)	2,380
Aux. Air Gap	540 (555°K)	2,240
	Total Windage	8,370

Gas Circulation Rate 1410 lbm/ hr. per side (0.175 kg/sec)
Aux. Gap Gas Flow Rate 191 lbm/ hr. per side (.024 kg/sec)
Aux. Gap Gas Flow Inlet Temp. 400°F (478°K)

Figure 178

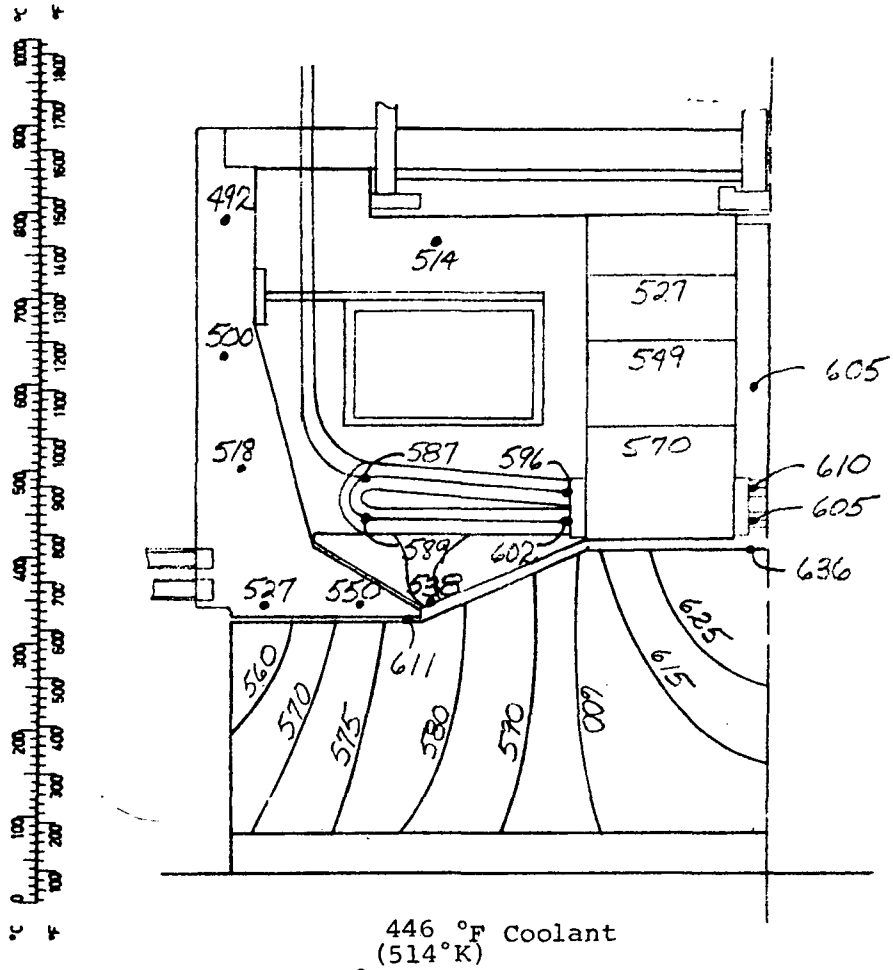

446 °F Coolant
(514°K)

(48.3 nt/cm^2) 70 psia Cavity Pressure

Special Conditions:

Gas Flow in Auxiliary Gap

End Bell w/o Coolant

Partial Gas Flow over End Extensions

Avg. Pole Face Temp. 626°F (603°K)
Avg. Winding Temp. 587°F (582°K)

Windage	Avg. Gas Temp. °F	Windage Loss Watts (HeXe)
Main Air Gap	583 (580°K)	3,750
Cone Gap	547 (558°K)	2,380
Aux. Air Gap	540 (555°K)	2,240
	Total Windage	8,370

Gas Circulation Rate 1410 lbm/hr. per side (0.178 kg/sec)
Aux. Gap Gas Flow Rate 191 lbm/hr. per side (0.024 kg/sec)
Aux. Gap Gas Flow Inlet Temp. 400°F (478°K)

Figure 179

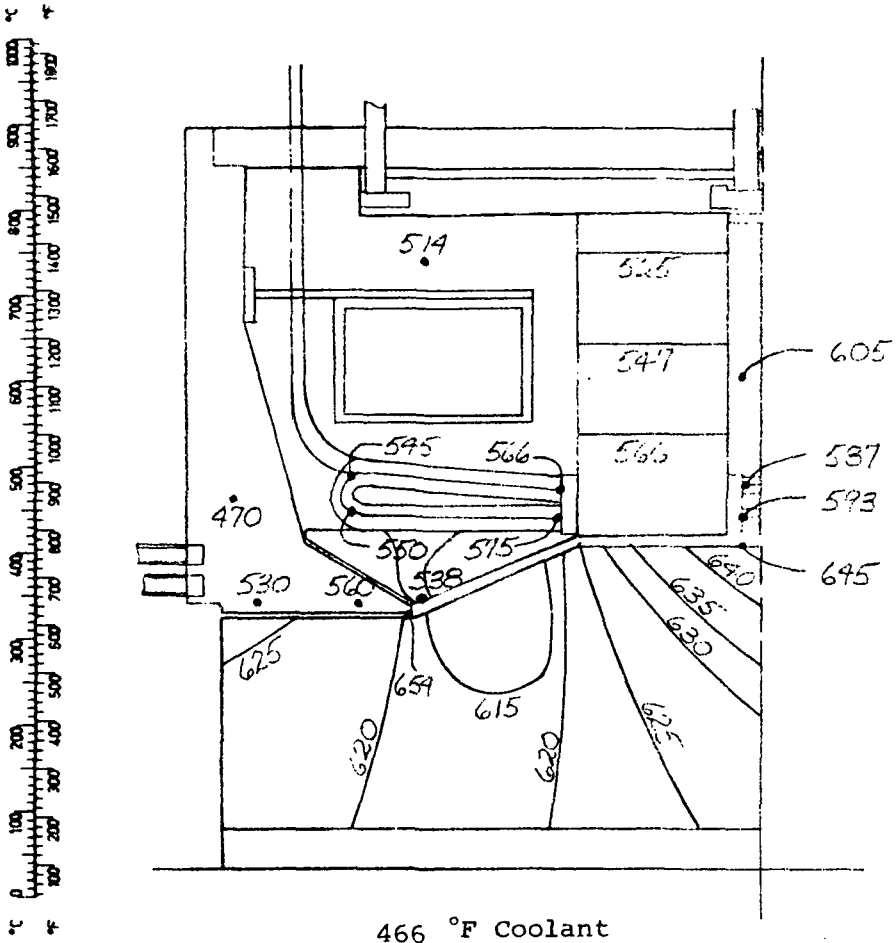

466 °F Coolant
514°K
(48.3 nt/cm^2) 70 psia Cavity Pressure

Special Conditions:

None

Avg. Pole Face Temp. 636°F (608°K)
Avg. Winding Temp. 568°F (571°K)

Windage	Avg. Gas Temp. °F	Windage Loss Watts (HeXe)
Main Air Gap	583 (580°K)	3,750
Cone Gap	547 (558°K)	2,380
Aux. Air Gap	643 (613°K)	2,120
	Total Windage	8,250

Gas Circulation Rate 1410 lbm/hr per side (0.178 kg/sec)
Aux. Gap Gas Flow Rate
Aux. Gap Gas Flow Inlet Temp.

Figure 180

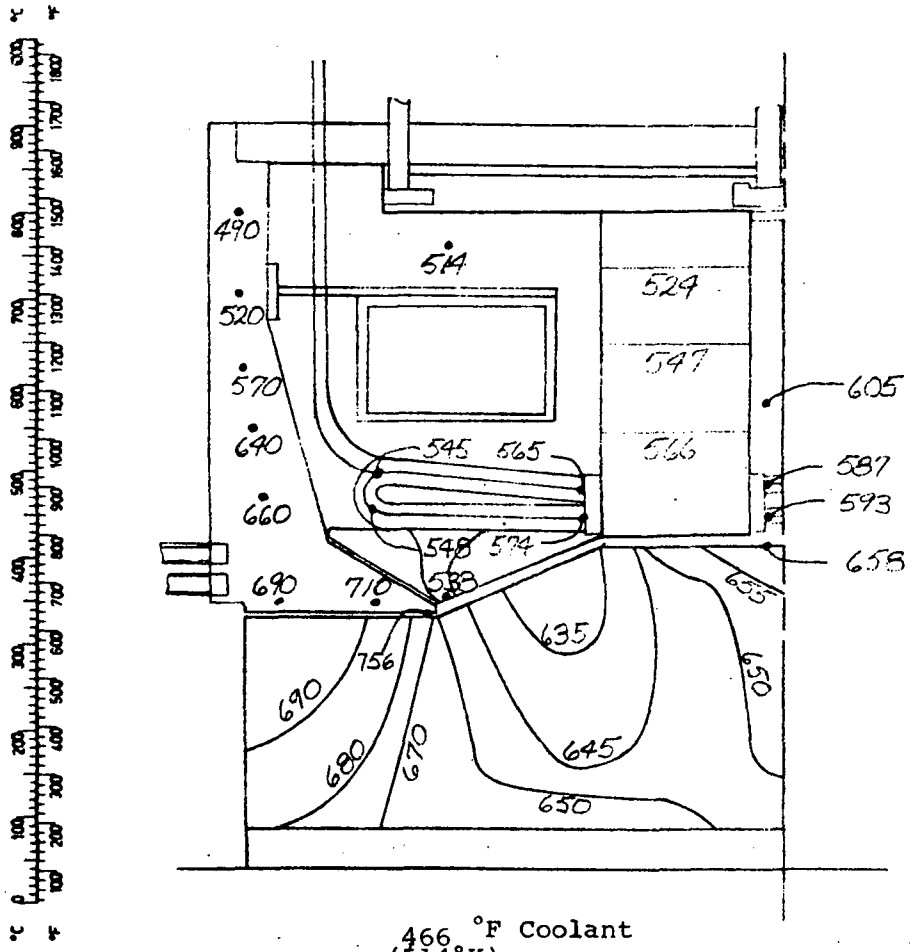

466 °F Coolant
(514°K)
(48.3 nt/cm^2) 70 psia Cavity Pressure

Special Conditions:

End Bell w/o Coolant

Avg. Pole Face Temp. 652°F (637°K)
Avg. Winding Temp. 568°F (570°K)

Windage	Avg. Gas Temp. °F	Windage Loss Watts (HeXe)
Main Air Gap	583 (580°K)	3,750
Cone Gap	548 (559°K)	2,380
Aux. Air Gap	758 (676°K)	2,000
	Total Windage	8,130

Gas Circulation Rate 1410 lbm/hr. per side (0.178 kg/sec)
Aux. Gap Gas Flow Rate
Aux. Gap Gas Flow Inlet Temp.

Figure 181

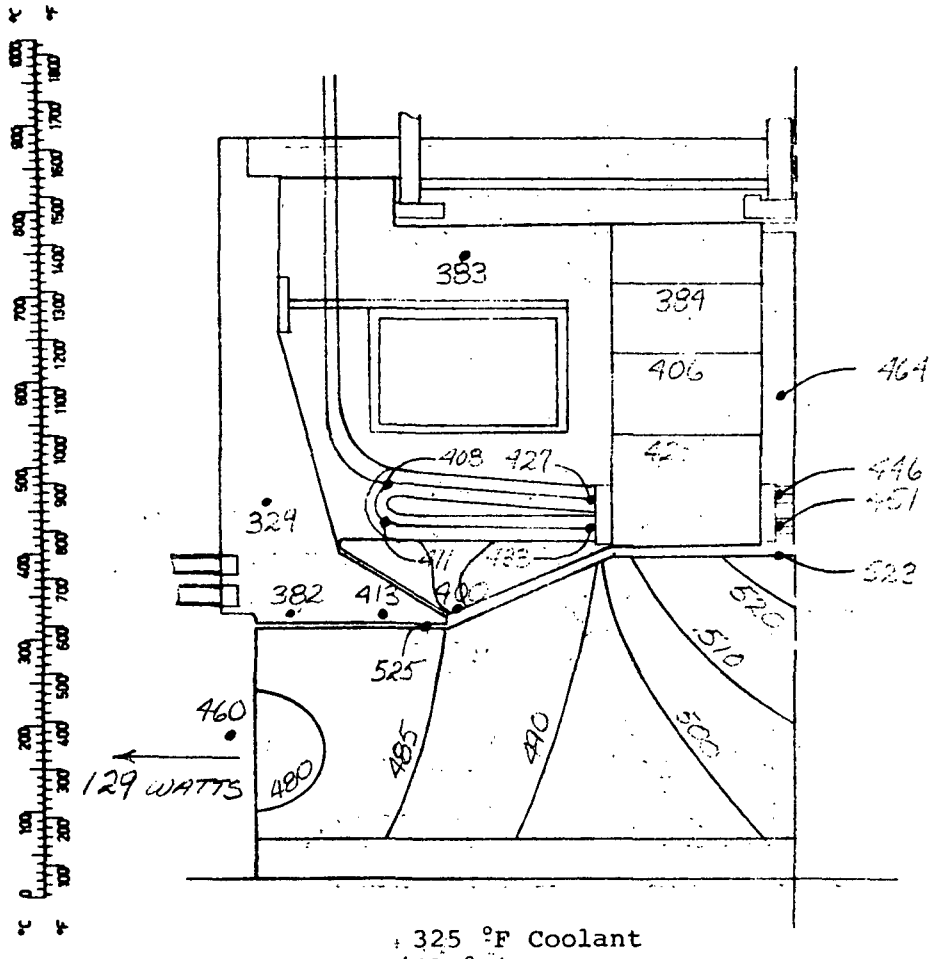

325 °F Coolant
(436°K)
(48.3 nt/cm^2) 70 psia Cavity Pressure

Special Conditions:

Heat Flow out of Rotor

Avg. Pole Face Temp. 516°F (543°K)
Avg. Winding Temp. 429°F (494°K)

Windage	Avg. Gas Temp. °F	Windage Loss Watts (HeXe)
Main Air Gap	444 (503°K)	4,030
Cone Gap	408 (462°K)	2,580
Aux. Air Gap	513 (543°K)	2,270
	Total Windage	8,880

Gas Circulation Rate 1610 lbm/hr. per side (0.203 kg/sec)
Aux. Gap Gas Flow Rate
Aux. Gap Gas Flow Inlet Temp.

Figure 182

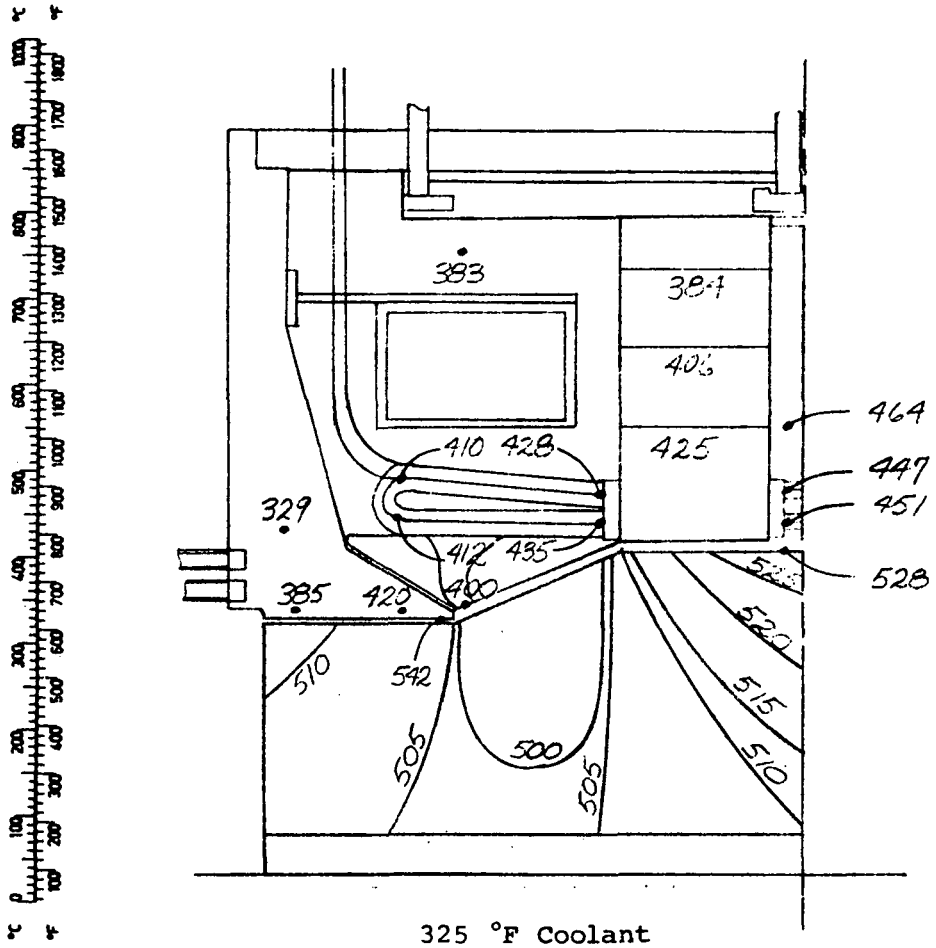

325 °F Coolant
(436°K)
(48.3 nt/cm^2) 70 psia Cavity Pressure

Special Conditions:

None

Avg. Pole Face Temp. 522°F (547°K)
Avg. Winding Temp. 429°F (494°K)

Windage	Avg. Gas Temp. °F	Windage Loss Watts (HeXe)
Main Air Gap	445 (503°K)	4,030
Cone Gap	408 (461°K)	2,580
Aux. Air Gap	531 (551°K)	2,250
	Total Windage	8,860

Gas Circulation Rate 1610 lbm/hr per side (0.203 kg/sec)
Aux. Gap Gas Flow Rate
Aux. Gap Gas Flow Inlet Temp.

Figure 183

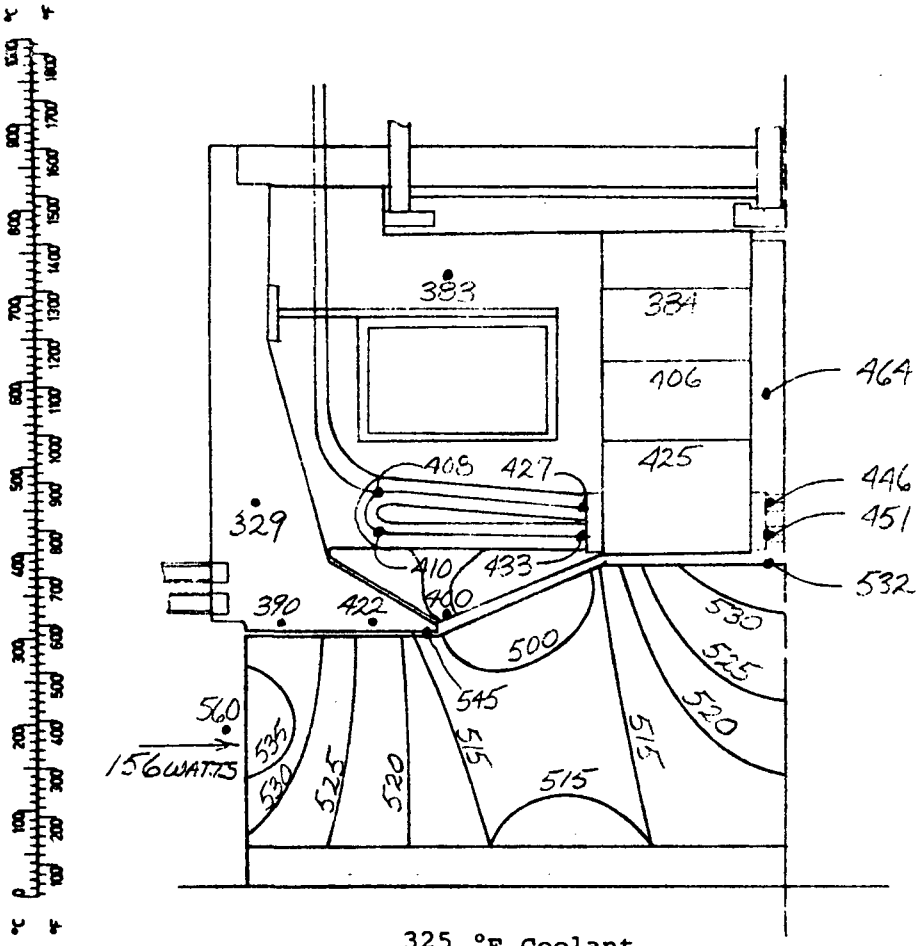

325 °F Coolant
(436°K)

(48.3 nt/cm^2) 70psia Cavity Pressure

Special Conditions:

Heat Flow into Rotor

Avg. Pole Face Temp. 527°F (548°K)
Avg. Winding Temp. 428°F (493°K)

Windage	Avg. Gas Temp. °F	Windage Loss Watts (HeXe)
Main Air Gap	445 (502°K)	4,030
Cone Gap	408 (482°K)	2,580
Aux. Air Gap	537 (553°K)	2,240
	Total Windage	8,850

Gas Circulation Rate 1610 lbm/hr. per side (0.203 kg/sec)
Aux. Gap Gas Flow Rate
Aux. Gap Gas Flow Inlet Temp.

Figure 184

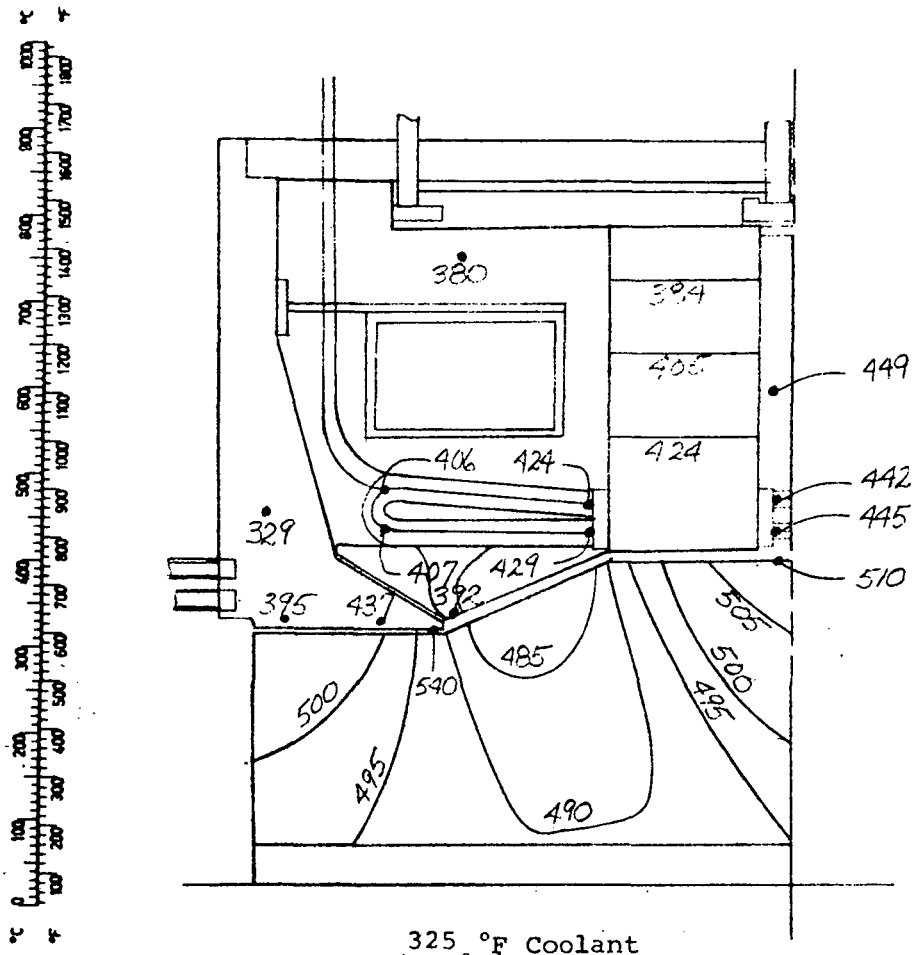

325 °F Coolant
(436°K)

(59.3 nt/cm^2) 86 psia Cavity Pressure

Special Conditions:

None

Avg. Pole Face Temp. 504°F (536°K)
Avg. Winding Temp. 424°F (491°K)

Windage	Avg. Gas Temp. °F	Windage Loss Watts (HeXe)
Main Air Gap	433 (497°K)	4,590
Cone Gap	400 (478°K)	2,940
Aux. Air Gap	526 (548°K)	2,660
	Total Windage	10,190

Gas Circulation Rate 1990 lbm/hr per side (0.25 kg/sec)
Aux. Gap Gas Flow Rate
Aux. Gap Gas Flow Inlet Temp.

Figure 185

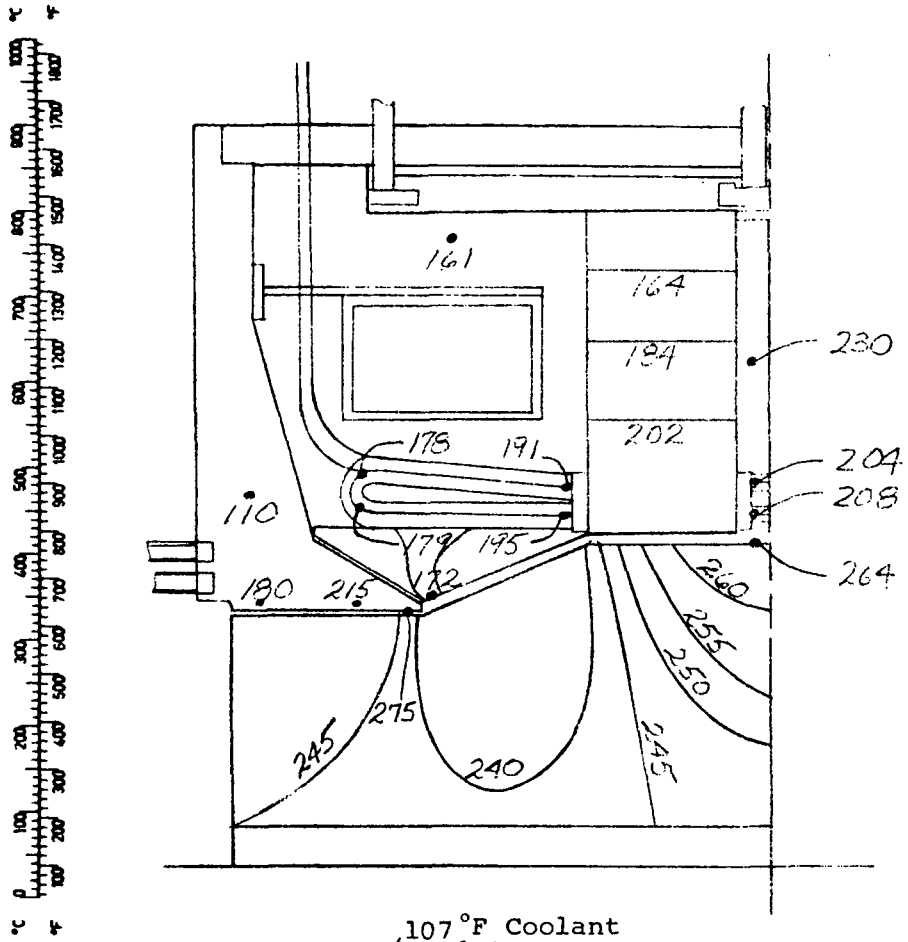

107°F Coolant
(315°K)

(48.3 nt/cm^2) 70 psia Cavity Pressure

Special Conditions:

None

Avg. Pole Face Temp. 257°F (398°K)
Avg. Winding Temp. 192°F (363°K)

Windage	Avg. Gas Temp. °F	Windage Loss Watts (HeXe)
Main Air Gap	218 (377°K)	4,550
Cone Gap	185 (358°K)	2,940
Aux. Air Gap	261 (401°K)	2,710
	Total Windage	10,200

Gas Circulation Rate 2200 lbm/hr. per side (0.277 kg/sec)
Aux. Gap Gas Flow Rate
Aux. Gap Gas Flow Inlet Temp.

Figure 186

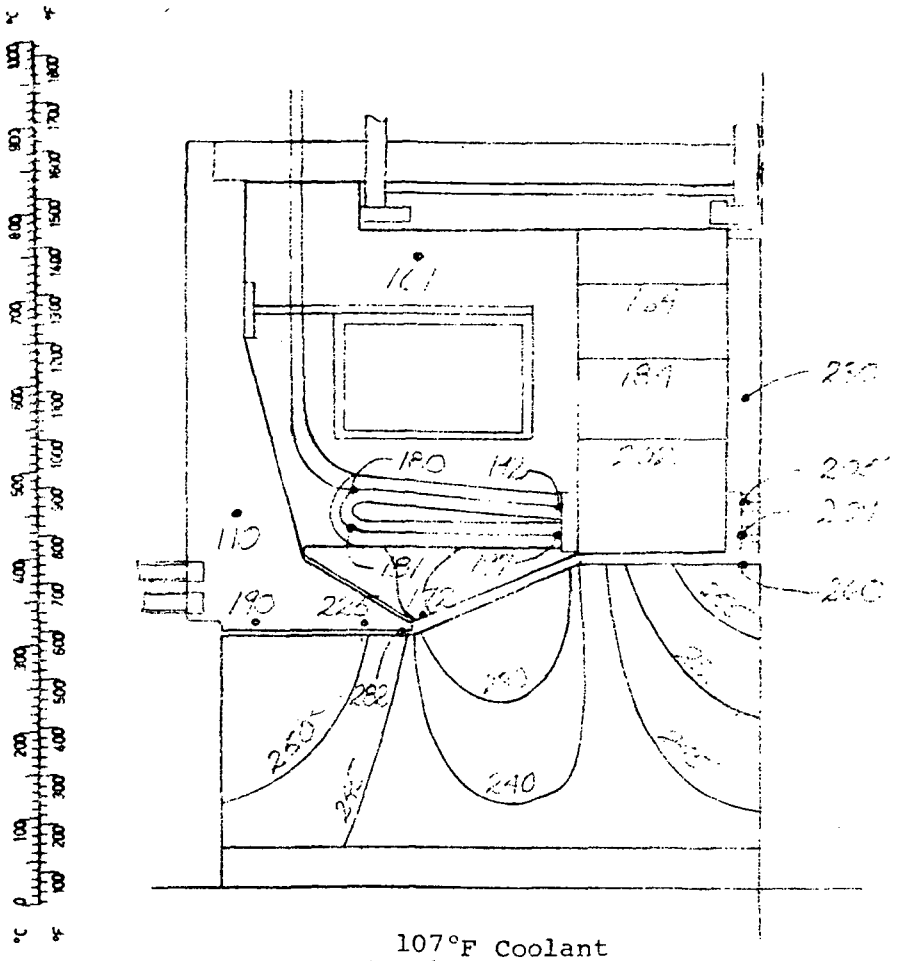

107°F Coolant
(315°K)

(59.3 nt/cm^2) 86 psia Cavity Pressure

Special Conditions:

None

Avg. Pole Face Temp. 253°F (397°K)
Avg. Winding Temp. 194°F (363°K)

Windage	Avg. Gas Temp. °F		Windage Loss Watts (MeXe)
Main Air Gap	219	(377°K)	5,140
Cone Gap	186	(359°K)	3,310
Aux. Air Gap	268	(409°K)	3,100
	Total windage		11,550

Gas Circulation Rate 2710 lbm/hr. per side (0.341 kg/sec)
Aux. Gap Gas Flow Rate
Aux. Gap Gas Flow Inlet Temp.

Figure 187

TABLE LXXX

LISTING OF THERMAL MAPS

DESIGN NO.	COOLANT SUPPLY TEMP. °F (°K)	CAVITY PRESS. PSIA (nt/cm^2)	COOLANT IN END BELL	FLOW THROUGH AUX. GAP	FULL FLOW THROUGH END EXTENSIONS	HEAT FLOW IN OR OUT OF ROTOR	FIGURE NO. THERMAL MAP	MAX. HOT SPOT TEMP. °F (°K)	MAX. POLE FACE TEMP. °F (°K)	MAX. WINDING TEMP. °F (°K)	BEARING STUB SHAFT INTERFACE TEMP. °F (°K)
1	466 (514)	70 (48.3)	NO	YES	YES	NO	III-6	636 (608)	636 (608)	593 (585)	561 (567)
2	466 (514)	70 (48.3)	NO	YES	NO	NO	III-7	636 (608)	636 (608)	610 (593)	561 (567)
3	466 (514)	70 (48.3)	YES	NO	YES	NO	III-8	645 (613)	645 (613)	593 (585)	623 (602)
4	466 (514)	70 (48.3)	NO	NO	YES	NO	III-9	712 (650)	658 (621)	593 (585)	693 (640)
5	325 (436)	70 (48.3)	YES	NO	YES	OUT	III-10	523 (547)	523 (547)	451 (507)	460 (512)
6	325 (436)	70 (48.3)	YES	NO	YES	NO	III-11	528 (548)	528 (548)	451 (507)	505 (537)
7	325 (436)	70 (48.3)	YES	NO	YES	IN	III-12	560 (566)	531 (551)	451 (507)	560 (566)
8	325 (436)	86 (59.3)	YES	NO	YES	NO	III-13	510 (539)	510 (539)	445 (503)	500 (533)
9	107 (315)	70 (48.3)	YES	NO	YES	NO	III-14	264 (402)	264 (402)	208 (371)	247 (383)
10	107 (315)	86 (59.3)	YES	NO	YES	NO	III-15	260 (400)	260 (400)	208 (371)	251 (396)

end bell, as represented by Design No. 1, decreased the temperature of the adiabatic interface from 693° to 561°F (640 to 567°K). In general, it appears that either the addition of coolant in the end bell, the addition of forced circulation through the auxiliary gap, or a combination of both can be used to obtain desired interface temperatures between the rotor and stub shaft.

Design No. 2 of Table LXXX is a slight variation of Design No. 1. For this design, the forced convection mode of heat-transfer from the end extensions to the gas was reduced by decreasing the heat-transfer coefficient by a factor of four. The maximum temperature of the windings increased from 593 to 610°F (585 to 593°K). This means the flow pattern over the conductors will not be critical to the thermal state of the windings. Furthermore, the likelihood of damage to the ANADUR insulation on the conductors when subject to a high velocity gas stream precludes the use of a cooling scheme which requires a high convection mode of heat-transfer from the end extensions.

Design No. 5 through No. 8 of Table LXXX are cases investigated for a coolant supply temperature of 325°F (436°K). Heat flow in and out of the stub shaft interface was considered. Figure 188 gives the heat flow rate across the interface as a function of the interface temperature. An adiabatic solution for the turbine and compressor components gave 503 and 499°F (536 and 533°K) for the turbine and compressor stub shaft, respectively. It can be noted from Figure 188 that little heat will flow into or out of the rotor for this coolant temperature.

A comparison of Design No. 9 with Design No. 7 and a comparison of Design No. 10 with Design No. 11 shows the influence of cavity pressure upon the temperatures. In general, increasing the cavity pressure from 70 to 86 psia (48.3 to 59.3 $\frac{nt}{cm}2$) did not have a significant effect upon the thermal state of the alternator. Windage losses increased, the gas flow rate, and the forced convection mode of heat-transfer increased also. However, the net change in the thermal maps was slight.

With the low temperature windings and coolant supply temperature, there appears to be a significant temperature difference between the rotor and bearing system based upon an adiabatic interface with coolant in the end bells. A cooling scheme without coolant in the end bell

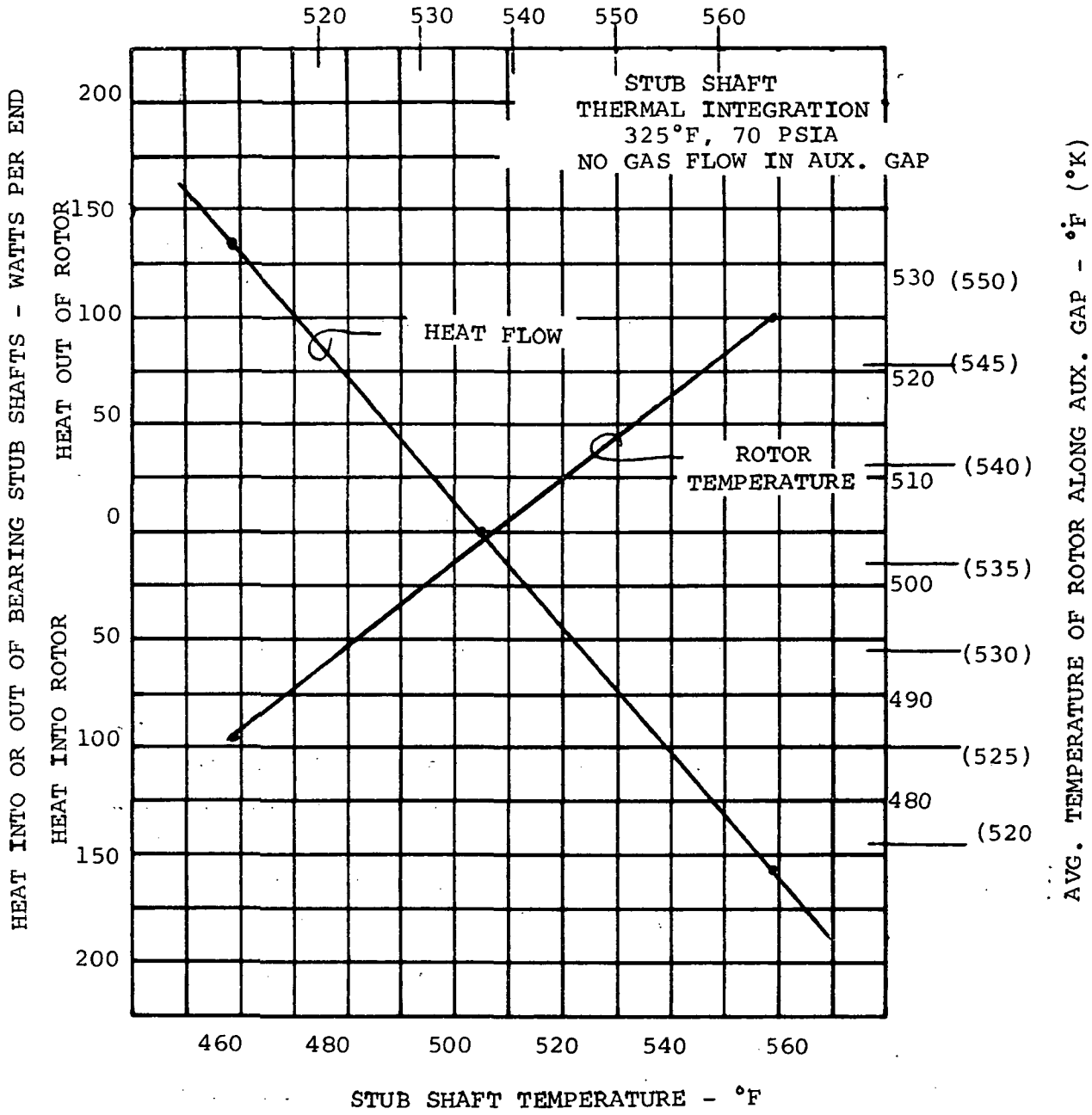
520
530
540
550
560
STUB SHAFT
THERMAL INTEGRATION
325°F, 70 PSIA
NO GAS FLOW IN AUX. GAP
200
150
100
50
0
50
100
150
200
HEAT OUT OF ROTOR
HEAT INTO ROTOR
HEAT FLOW
ROTOR
TEMPERATURE
530 (550)
(545)
520
(540)
510
(535)
500
(530)
490
(525)
480
(520
460
480
500
520
540
560
STUB SHAFT TEMPERATURE - °F
HEAT INTO OR OUT OF BEARING STUB SHAFTS - WATTS PER END
AVG. TEMPERATURE OF ROTOR ALONG AUX. GAP - °F (°K)

Figure 188

would probably offer an advantage over Design No. 9 and 10 of Table LXXX since the adiabatic interface temperature of the rotor would approach that of the possibly hotter stub shaft.

In summary, the thermal analysis of the 2-pole alternator at rated load for 70 and 86 psia (48.3 and 59.3 nt/cm^2) and for coolant supply temperatures of 107, 325 and 466°F (315, 436 & 514°K) indicate the gas recirculation cooling scheme is both feasible and practical. A considerable portion of the internal losses within the generator are transported by the gas to the heat sink within the frame. Typical values for the heat transport mode are:

	Typical	
Cavity Pressure	70 psia (48.3 nt/cm^2)	86 psia (59.3 nt/cm^2)
ΔT of gas	90°F (50°K)	70°F (39°K)
Gas flow rate	2800 Lbm h_r^{-1} (0.353 kg sec^{-1})	4000 Lbm h_r^{-1} (0.505 kg sec^{-1})
Specific heat of gas (Btu Lbm^{-1} $^oF^{-1}$) (Cal gm^{-1} $^oC^{-1}$)	0.1243	0.1243
Heat transport	9.2 kw	10.2 kw

The temperature of the interface between the rotor and stub shaft can be varied to be compatible with the thermal state of the bearing by alterations of the cooling scheme with the auxiliary gaps and within the end bells.

Rotor Stress and Bonding

The maximum stress intensity (92,500 psi, 63,800 nt/cm^2 will occur around the central hole in the 8.0 inch (20.4 cm) cylinder at 20% overspeed. Tensile properties of the rotor materials are:

Material	Hardness	Temperature	0.2% Yield Strength	Tensile Strength
SAE 4340	RC32	700°F (643°K)	110,000 psi (76,000 nt/cm^2)	130,000 psi (89,700 nt/cm^2)
Inconel 718	RC38	700°F (643°K)	125,000 psi (86,300 nt/cm^2)	150,000 psi (103,400 nt/cm^2)

A comparison of the maximum stress and the stress at design speed (24,000 RPM) with the tensile properties of the materials gives:

$$\frac{\text{stress @ 24,000 RPM}}{\text{Y. S. of SAE 4340}} = \frac{64,200}{110,000} = 59.4\%$$

$$\frac{\text{overspeed stress}}{\text{T.S. of SAE 4340}} = \frac{92,500}{130,000} = 71.1\%$$

% creep strain at bore in 5 years $< 0.01\%$.

The strength of the joint between the SAE 4340 and alloy 718 has approached the ultimate tensile strength of the parent materials in past developments. If this characteristic continues when the 4340 is strengthened for the specific requirements of this application, the joints will have adequate strength. The time-temperature-pressure cycle for bonding in an autoclave have been developed for bonding rotors with lesser strength requirements. This cycle will have to be modified to produce the strength required for this application. Experiments are necessary to determine whether the SAE 4340 can be strengthened during the bonding cycle or during a heat-treatment cycle after bonding of the materials. Thus, positive conclusions cannot be made relative to the integrity of the rotors until these experiments have been performed.

A separate and complete discussion of the bonding of the rotor is presented in Appendix A.

Mass Unbalance

The rotor detail, including significant cross-sections to illustrate the non-symetric distribution of magnetic and non-magnetic steels, and a plot of the mass unbalance are shown in Figure 164. The density of the non-magnetic steel (Inconel 718) is 5% greater than the density of the magnetic steel (AISI 4340). This density difference results in the center of mass of sections between the small end of the conical section and the (axial) center of the shaft being shifted toward the predominantly non-magnetic side of the shaft center line. Because the pattern shown for the left end of the rotor is reversed on the right end, a couple will exist. The magnitude of the mass unblance was calculated for sections AA and BB on Figure 164, and then plotted, with the points of zero unbalance, to determine the unbalance (per unit axial length). This plot (shown on Figure 164) was integrated to determine a resultant unbalance of 0.75 inch-pounds (0.864 kg-cm) with a moment arm of 2.01 inches (5.11 cm) from the shaft center for each end of the shaft.

This mass unbalance, which is inherent in the two-pole rotor design, can be balanced by means of holes or weights at the rotor planes at the outboard ends of the auxiliary gaps. Using holes, several 0.5 inch (1.27 cm) diameter holes are required at each plane. These would be located in line with the center of the non-magnetic steel at the corresponding end of the rotor, and would remove about 0.1 pounds (0.0045 kg) of magnetic iron. To prevent a reduction of the auxiliary gap magnetic flux path, and a resultant decrease in alternator capacity, these holes would be located at a diameter of about 5.875 inches (0.1492 m), with a depth of 0.25 inches (0.064 cm). These counterbalancing holes would be part of the basic rotor design and would be drilled prior to final balancing. The same planes would be available for final balancing purposes after manufacture of the rotor.

An alternate balancing produce, also in the unbalance plot of Figure 164, would remove about 0.25 pounds (0.1134 kg) from the non-magnetic steel at, or near, the conical surfaces. This corresponds to about 0.84 cubic inches (13.8 cubic centimeters) of steel.

Either of the above balancing procedures, or a combination of them, may be used for the initial balancing to overcome the severe unbalance of the non-symetrical 2-pole rotor. The "alternate" method may prove desirable to reduce the difference in the moment arms between the removed material and the unbalanced mass plane.

A potential complication to the task arises when the effects of thermal expansion and creep are considered. Specifically, the non-magnetic alloy 718 will expand about 0.03% more than the magnetic AISI 4340 from room temperature to the average estimated operating temperature with 466°F (514°K) coolant. This effect, plus the effects of creep, may result in warpage of the rotor and a consequent unbalanced moment.

Experimental development will be required to obtain an acceptable balancing technique for the unsymmetric 2-pole rotor, and to determine the short and long term effects of thermal expansion and creep.

The 6-pole rotor, with its symetrical magnetic and non-magnetic materials (each cross section is balanced), is inherently balanced. In addition, it should not be subject to warping due to differential thermal expansion or material creep. Thus, little development should be required in this area for the 6-pole alternator.

Magnetic Unbalance

1. Leakage Flux and Main Gap Considerations

A magnetic moment is created by the unequal leakage flux passing from the stack ends to the rotor at each end of a 2-pole Lundell alternator. The magnitude of this force for the TAC alternator was calculated by making flux plots of the leakage flux passing through the conical sections of the rotor at each end to determine the flux density and magnetic force distribution along the conical rotor section. Integration of the force distribution resulted in a radial unbalance force of 58.4 pounds (26.5 kg) acting in opposite directions at each end of the rotor. Although these forces were not considered excessive, the tips of the rotor poles were extended a small distance beyond the armature stack to reduce the forces to 7 pounds (3.2 kg) at each end. The extensions increased rotor leakage flux a small amount. While this unbalanced force will oppose the mass unbalance, the force will vary with excitation and therefore cannot be used as a balancing force.

2. Auxiliary Gap

When the auxiliary gap varies circumferentially, as when the shaft is eccentric to the end bell, a non-uniform flux density occurs and an unbalanced magnetic force acts on the shaft. The magnitude of this force can be estimated by the following method.

The radial gap (g), as a function of angular position, is expressed as:

$$g = c - e \cos \theta$$

where

g = radial gap at θ, inches
c = average radial gap, inches
e = radial eccentricity, inches
θ = angular position on the shaft, $\theta = 0$ at the position where $g = c-e$

The local radial flux density may be expressed as:

$$B = \frac{3.19\ NI}{g} \times 10^{-3} = Bavg\ (1 - \frac{e}{c} \cos \theta)^{-1}$$

where

B = magnetic flux density, kilolines/in^2
Ni = ampere turns across the gap, amperes
Bavg = average magnetic flux density, kilolines/in^2

The force acting upon the shaft in the direction of the radial eccentricity is given by:

$$F_e = \frac{LR}{72.13} \int_0^{2\pi} B^2 \cos \theta \, d\theta$$

where

F_e = force acting on the shaft in the direction of eccentricity, pounds
R = radius of shaft, inches
L = length of air gap, inches

Evaluation of this definite integral gives the force per unit of eccentricity:

$$\frac{F_e}{e} = \frac{2\pi RL}{72.13c} \text{Bavg}^2 \left(1 - \frac{e^2}{c^2}\right)^{-1.5}$$

The average gap (c) around the shaft is large compared with the radial eccentricity (e) of the shaft. Thus, e^2/c^2 is small compared to unity. Therefore, the spring constant due to magnetic attraction becomes:

$$\frac{F}{e} = \frac{\text{(Area of gap)}}{72.13} \times \frac{\text{Bavg}^2}{c}$$

The magnetic spring forces in the auxiliary gap at one end of the 2-pole alternator at standstill with full load excitation is:

$$\frac{F}{e} = \frac{47.5 \times (58)^2}{72.13 \times .05} = 4.43 \times 10^4 \text{ Lb}_f/\text{in}$$
$$(7.75 \times 10^4 \text{ nt/cm}$$

DESIGN COMPARISONS

During the Phase I studies, several frequency, speed, and alternator combinations were screened to establish the relative merits of each from the standpoint of the alternator and the design impact on the system. As a result of those studies, a 6-pole 1200 Hz, 24000 rpm Lundell alternator was recommended. The alternative choice of a 36000 rpm shaft speed or the choice of an inductor alternator were rejected as impractical as was the choice of a 4-pole, 800 Hz, 24000 rpm Lundell. The latter was identified as the most attractive alternator, but the 800 Hz frequency is a very poor system choice.

For the Phase III studies, emphasis was limited to a 2-pole, 400 Hz, 24000 rpm Lundell alternator since the NASA had determined that the system requiring the TAC unit could require a significant amount of 400 Hz power. However, this requirement does not preclude the use of a 1200 Hz alternator with a frequency converter which, under certain conditions, may be a lighter, more efficient (and better performing) power source. Because of this, the potential choice of either a 6-pole, 1200 Hz or a 2-pole, 400 Hz alternator is still possible, and it is appropriate that the two be compared.

Table LXXXI summarizes the items for comparison. Table LXXXII presents the comparison data and discussions.

The comparative data on weight and efficiency are probably the most

TABLE LXXXI

ITEMS FOR COMPARISON

Electromagnetic Weight

Electromagnetic Efficiency

Overall Alternator Efficiency

Part Load Efficiency and Inherent Losses

Cooling

Rotor Machining

Rotor Fabrication

Rotor Bonding Requirements/3rd Material

Stator Stack Fabrication

Armature Coil Fabrication

Armature Assembly

"Development" Requirements

Mass Unbalances

Thermal Distortion of Shaft

Magnetic Unbalances

Overall Size

VRE and Field Power Requirements

TABLE LXXXII

COMPARISON OF 2-POLE AND 6-POLE ALTERNATORS

ITEM	70 PSIA CAVITY (48.3 nt/cm^2) 6-POLE	70 PSIA CAVITY (48.3 nt/cm^2) 2-POLE
ELECTROMAGNETIC WEIGHT	279 lbs	466 lbs
	Further optimization may reduce the 2-pole weight slightly. The rotor for the 2-pole alternator presented is about 35 percent heavier than the 6-pole rotor. This difference, however, can be reduced.	
ELECTROMAGNETIC EFFICIENCY	94.2% @ Full Load 89.3% @ 1/4 Load	92.4% @ Full Load 90.9% @ 1/4 Load
	Part-load efficiency of the 2-pole is 1.6 points higher.	
OVERALL ALTERNATOR EFFICIENCY	91.0% @ Full Load (approx.) 86.3% @ 1/4 Load (approx.)	89.5% @ Full Load 86.4% @ 1/4 Load
	Based on 70 PSIA (48.3 nt/cm^2) cavity and estimate using Ph III windage calculation methods.	Based on 70 PSIA (48.3 nt/cm^2) cavity and Ph III windage calculation methods.
PART LOAD EFFICIENCY & INHERENT LOSSES	Based on a comparison of the 90 slot 6-pole design and the 84 slot 2-pole design, core losses, because of higher frequency, are higher in 6-poles, in spite of the larger core volume of the 2-pole design. Field losses are higher for 2-poles because of higher armature reaction mmf and a larger main gap. 2-pole armature winding losses are higher for 2-poles because of the relatively large amount of wire in the end turns. Because of the effect of the field and armature winding losses, full load efficiency is higher for the 6-pole design. Quarter load efficiency, including windage, is essentially the same for the 2-pole and 6-pole design.	
COOLING CAPABILITIES	Since different conditions and an improved cooling scheme were used on the 2-pole configuration in Phase III, we do not have comparative temperatures between the two for direct tabulation. However, both can be cooled adequately to meet the 300°F (167°K) maximum temperature gradient to the hot spot.	

TABLE LXXXII (Cont.)

	6-POLE	2-POLE
ROTOR MACHINING	The conclusion of electrical discharge machining experts is that the 6-pole rotor pieces will be more difficult to make, but they are only slightly more difficult.	
ROTOR FABRICATION	With proper machining to obtain the proper fit-up, bonding experts see no differences between bonding a 6-pole and a 2-pole rotor. This applies for both brazing and diffusion pressure bonding.	
ROTOR BONDING REQUIREMENTS/ 3RD MATERIAL	Adequate design obtainable with two materials for 120 volt design.	May require a 3rd material on the pole faces for a 120 volt design.
	Pressure diffusion bonding experts state that the addition of the 3rd material to the rotor does not present additional problems with proper development. The possible requirement of a 3rd material for the 2-pole should not be considered detrimental.	
STATOR STACK FABRICATION	e.g.: DBS = 1.25 inches (3.18 cm)	e.g.: DBS = 3.21 inches (8.15 cm)
	The greater height of the depth-behind-slot (DBS) on the 2-pole is of concern since this enhances the possibility of stack flare and folding. While the 6-pole requires special mechanical structure to retain the stack, the 2-pole requires even more. (Structure not shown on layouts presented)	
ARMATURE COIL FABRICATION	e.g.; 40° THROW	e.g., 120° THROW
	Both have five turns per coil set but the 2-pole is pulled over a greater arc. The expanse of this arc makes handling more difficult and enhances the likelihood of handling damage to the wire insulation.	
ARMATURE ASSEMBLY	e.g.; 4.55 inch end-turn length (11.6 cm)	e.g.; 12.23 inch end-turn length (31.1 cm)
	The very large end-turn length of the 2-pole is of concern, especially over the life of the machine as the insulation falls off and/or the coils shift or sag (closing the spacing between phases). Special end-turn supports or potting encapsulation will be required for the 2-pole. Also, the longer span will have a significantly lower natural frequency and greater amplitude which may be of concern for vibration integrity. Standard, 8-pole aircraft alternator end-turn designs have a measured natural frequency of 700 Hz (typical).	

TABLE LXXXII (Cont.)

	6-POLE	2-POLE
"DEVELOPMENT" REQUIREMENTS	Will require special rotor development, etc. common to the 6-pole and 2-pole, but it has no distinctive development requirements particular to the 6-pole alone.	According to the three previous items, will probably require some stator fabrication development on the first unit. Unbalances and nonsymmetrical rotor deformation problems at high temperatures will require experimental development.
MASS UNBALANCES	Symmetrical	Nonsymmetrical from end to end and over the circumference. Requires removal of about a cubic inch of Inconel from each cone section of the rotor.
THERMAL DISTORTION OF SHAFT	Thermal distortion is symmetricl	The rotor has a non-symmetrical distortion pattern due to 2-pole configuration; may cause problems such as warping of the shaft.
MAGNETIC UNBALANCES	Has unbalance in auxiliary gap and in main gap; no unbalanced moments due to pole fringing flux.	Has unbalance in auxiliary gap and a small moment due to unsymmetrical fringing flux about pole ends; no unbalance in main gap.
OVERALL SIZE	9.5 inches long X 13.6 inches dia.	12.8 inches long X 17.5 inches dia. (Non optimized design)
	Volumetric space for the field coil is limited and may dictate restrictions to end bell stator mounting structure.	Ample room for field coil and for changing the end bell configuration to accommodate stator mounting.
	The greater dimensions of the 2-pole adds structural weight to the unit and increases the bearing span. However, more space is available for design innovations as pointed out above.	
VRE AND FIELD POWER REQUIREMENTS	F.L. field power = 1.16 kW	F.L. field power = 3.93 kW
	The 2-pole requires a VRE with about twice the rating; however, because the field coil space is crowded on the 6-pole, the ampere rating of the 6-pole alternator VRE may be 2 to 3 times greater; e.g., 80 to 90 amperes typical, to obtain the necessary ampere turns. The number of turns is limited by the minimum practical wire or strap size which will still yield a design that is capable of being easily cooled. On the 2-pole, because of the extra volume available, the necessary ampere turns can be obtained by a greater number of the same size turns.	

significant; analysis shows there are, with two exceptions, few other comparative items in the list that significantly influence the choice. The two exceptions to this might be: (1) the long length of the armature end-turns on the 2-pole (they are too long for a simple, reliable design), and (2) the rotor related design problems brought on by the unsymmetrical configuration of the two poles themselves.

FAILURE MODE, EFFECT AND CRITICALITY STUDY

The FME&CS is carried out for purposes of identifying and cataloging the various modes and effects of component failures down to and including subassembly levels wherever possible. The components and subassemblies are categorized by a reliability model that consists of:

(1) Rotor,

(2) Stator and stator coolant,

(3) Windings and insulation.

The bearings and seals are not considered as part of the TAC alternator reliability model.

The FME&CS is undertaken at a joint meeting of the engineers most experienced in the design philosophies. At this meeting, all known possible failure modes are identified, discussed, and tabulated. The failure modes identified are correlated according to immediate or long term effects on the system.

For the study, it is assumed the alternator was in an operating condition and successful operation constitutes the ability to produce useful power. The "power system" is defined as the TAC and its ability to produce power. The effect of the failure on the power system is evaluated from the standpoint of life, power output, overload, shorts, vibration, unbalance, overspeed capability, etc. The guiding philosophy in cataloging the failure modes is "How does the power system respond to the various failure modes." The probable causes of the failure are listed to explain how a particular failure might occur.

The tabulation of the FME&CS is presented in Table LXXXIII. In all, twenty-six failure modes are catalogued in the table.

TABLE LXXXIII

NASA/TAC ALTERNATOR
FAILURE MODE, EFFECT & CRITICALITY ANALYSIS

Mode of Failure	Probable Causes of Failure	Immediate Effect on Operation	Long Range Effect on Operation	Effect on Power System
		ROTOR		
Non-uniform creep rate or yield	Due to non-uniform properties	Increases vibration	Potential bearing failure	Loss of System
Shaft rubs	Due to loss of concentricity	Increased vibration, seizure	Wear or seizure	Loss of System
Fatigue	Abnormal bearing whirl	----	Rotor disintegrates	Loss of System
Crack propagation in rotor bore	Due to embrittling and high stress	Increases strain	Rotor disintegrates	Loss of System
Major loss of concentricity	Due to loss of bearing	Rub and/or loss of rotation	----	Loss of System

TABLE LXXXIII (Cont.)

NASA/TAC ALTERNATOR
FAILURE MODE, EFFECT & CRITICALITY ANALYSIS

Mode of Failure	Probable Causes of Failure	Immediate Effect on Operation	Long Range Effect on Operation	Effect on Power System
		ROTOR (Continued)		
Material property change	Embrittlement creep, resistivity permeability	Minor change in power output	Excessive creep or yield	Shorten Life
Excessive gas temperature	Due to system malfunction	Yield or rupture of bond	Excessive creep or yield	Loss of system or shorten life.
Excessive stub shaft temperature	Loss of heat barrier between alternator and turbine	Possible yield or rupture of bond	Excessive creep or yield	Shorten life
Loss of cavity control pressure	Due to seal failure or vent plugging	Increased cavity pressure & windage	Excessive rotor creep rate	Shorten Life

TABLE LXXXIII (Cont.)

NASA/TAC ALTERNATOR
FAILURE MODE, EFFECT & CRITICALITY ANALYSIS

Mode of Failure	Probably Causes of Failure	Immediate Effect on Operation	Long Range Effect on Operation	Effect on Power System
		STATOR & STATOR COOLANT		
Leak in cooling duct	Due to fatigue stress	Oil in gas system	Accumulative carbon on windings	Loss of output or system
Gas or oil flow decreased or stopped	Due to solids accumulation or system malfunction	Excessive temperatures and losses, rotor overheat	Accelerate deterioration	Shorten life or loss of system
Heat exchanger separating from frame or stack	Due to bond or contact pressure loss	Excessive temperatures and losses	Accelerate deterioration	Shorten life
Stack clamps fatigue	Due to mechanical or electrical fatigue	Separation of stack, loss of power	Fretting wear on stator	Noise, loss of system.
Excessive coolant temperature	Due to system malfunction	Excessive losses, loosen stack fits	Accelerated deterioration or increased vibration	Shorten life

TABLE LXXXIII (Cont.)

NASA/TAC ALTERNATOR
FAILURE MODE, EFFECT & CRITICALITY ANALYSIS

Mode of Failure	Probable Causes of Failure	Immediate Effect on Operation	Long Range Effect on Operation	Effect on Power System
		STATOR & STATOR COOLANT (Continued)		
Fatigue of laminations	Due to mechanical or electrical vibration	Breaks off, flux unbalance	Decrease output, wears into rotor	Shorten life or loss of system
Mounting point loosens	Due to vibration, excessive temperatures	Increased vibration loss of concentricity	Accelerated fatigue and breakage	Shorten life or loss of system
		WINDINGS & INSULATION		
Extended short circuit operation	System malfunction, long end turns touching	Armature conductors open	----	Loss of output
Slot cell insulation fatigue	Due to mechanical and electrical vibration	Loss of slot liner or wedges	Stator shorts	Shorten life or loss of output
Cladding breaks	Due to handling abuse, electrical stress, poor manufacturing	Silver migrates out of wire	Shorts insulation or opens wire	Reduced or loss of output

TABLE LXXXIII (Cont.)

NASA/TAC ALTERNATOR
FAILURE MODE, EFFECT & CRITICALITY ANALYSIS

Mode of Failure	Probably Causes of Failure	Immediate Effect on Operation	Long Range Effect on Operation	Effect on Power System
		WINDINGS & INSULATION (Continued)		
Anadur frets away	Due to mechanical and electrical vibration	Loosening of windings, plug heat exchanger	Accelerated deterioration	Shorten life
Armature conductor opens	Due to mechanical or electrical failure	Reduction in output, phase unbalance	----	Reduced or loss of output
Field conductor opens	Due to mechanical or electrical failure	Loss or output, over speeds	----	Loss of output or system
Field turns short	Insulation wear	Increase excitation to maintain voltage	Accelerated deterioration	Reduced output
Excessive coolant temperatures	Due to system malfunction	Increased losses, wires sag	Accelerated deterioration, possible short	Shorten life or loss of output
Lead fatigue	Due to mechanical and electrical vibration	Open circuits	----	Reduced output or los or output
Electrical shorts	Due to vibration	Excessive temperatures and losses, reduced output	Accelerates deterioration	Shorten life, reduced output

CONCLUSIONS

Pertinent conclusions associated with the Phase III studies are as follows:

(1) The likelihood of the high-temperature ANADUR wire insulation eventually entering the gas circuit as an abrasive dust may preclude the use of ANADUR in the TAC alternator. A possible high temperature alternative is a bare wire with mica and alumina in the slots and with the end turns either (1) uninsulated and physically supported (separated) or (2) insulated with plasma sprayed alumina. Alternately a ceramic-eze insulation could be applied to the wire. This will require materials development to reduce laboratory techniques to practical hardware. The other alternative is the organic insulation system.

(2) It appears it is technically feasible to cope with the unbalances and non-uniform deformations of the 2-pole rotor. However, these introduce problems which are unique to the unsymmetrical 2-pole configuration. The severity of these new problems must be clarified by experiments before one can conclude that the performance of the TAC over its five- to potential ten-year life will not be plagued with problems which could have been obviated with a symmetrical 6-pole alternator.

(3) The present 60-slot design having the 8-inch (20.4 cm) rotor OD is conservative. Future designs such as an optimized version of the 84-slot design will result in a smaller diameter, typically 7.5 inches (19.1 cm). This will also reduce the weight to less than twice the 6-pole alternator weight.

(4) At part load, the 84-slot 2-pole design equals or exceeds the 6-pole design efficiency.

(5) Reconnectability from 240 to 480 volts is physically possible. In addition, if corona precludes the use of even 240 volts, it will be possible to obtain a 120-volt design by substituting a different stack and winding into the same frame and rotor configuration. The use of the same rotor is based upon adaptation of a third material into the pole faces per conclusion (7) below.

(6) Corona considerations limit the minimum cavity pressure to 14 psia (9.7 nt/cm^2) at 240 volts (possibly half that is absolutely required).

At 480 volts, the limiting pressure is 53 psia (37 nt/cm^2). Substitution of an organic insulation for a 107°F (315°K) coolant system is entirely feasible and would possibly permit the use of output voltages up to 480 volts depending on the quality of the impregnation.

(7) Addition of a third material to the rotor pole faces apparently does not increase the complexity of gas pressure bonding the rotor, and is therefore recommended. Its use also significantly enhances the likelihood of achieving a 7.5 inch (19.1 cm) rotor OD and of achieving a single, basic alternator configuration capable of being built with outputs of either 120, 240, or 480 volts.

(8) Several cooling configurations can be designed into the alternator to adequately cool it. Any one of the acceptable configurations can handle the multitude of different pressures, temperatures, gases and boundary conditions anticipated. The latter includes relatively widely divergent rotor stub shaft boundary conditions.

APPENDIX A

ROTOR FABRICATION

The rotor design was reviewed to determine if design requirements could be satisfied in an Inconel 718-4340 Lundell rotor fabricated by hot isostatic pressure welding (high temperature gas pressure diffusion bonding). Analysis shows that this technique will be suitable for this application with minimum development. Feasibility of this approach is currently being demonstrated at the Westinghouse Astronuclear Laboratory under Contract NAS 3-11837, "Development of a Gas Pressure Bonded Four-Pole Alternator Rotor." Current results in this program have indicated joint strengths of 55,000 psi are readily achieved using non-optimized welding schedules. Actual joint strengths of 136,000 psi (bending) have been achieved. Welding schedules for the 81,400 psi joint strength at 700°F required for 20% overspeed appear entirely realistic.

Similarly, 92,500 psi yield strength at 700°F is achievable in both base metals since the metallurgical heat treatment and welding thermal cycles are compatible. Strength will be achieved in the 718 by selecting welding temperatures and times compatible with solution annealing and/or aging temperatures. The 4340 strength will then be developed, as the assembly cools in the autoclave, through transformation of the austenitic structure to a mixture of martensite, ferrite and bainite. With controlled autoclave cooling, this structure has given a hardness of R_C30. Slightly higher cooling rates can provide higher hardness.

In addition, this process for fabrication of the rotor can be utilized to attach pole inserts of improved magnetic properties to reduce pole face losses. Typically, these would be a mild steel such as AISI 1010. Rotor fabrication would still be accomplished in one operation by welding the 718, 4340, and 1010 in one autoclave run.

Metallurgical Considerations

Satisfactory joints between 718 and 4340 have been obtained by holding for four hours at 1650°F and 30,000 psi. These joints, in fact, appear to be overdeveloped and it is anticipated that shorter times at temperature or lower temperatures will give higher strength joints.

The ideal bonding temperature from the standpoint of metallurgical structure will be in the range of 1325°F to 1400°F since this is the first aging temperature of 718 and will be above the Ae3 temperature of 4340. If this temperature range proves suitable for rotor fabrication by hot isostatic pressure welding, then the 718 can be aged to the required strength during rotor welding. Similarly, this temperature will austenitize the 4340 permitting transformation on cooling to achieve the desired strength level. Interestingly, the deep hardening characteristics of 4340 are sufficient to achieve $R_C 30$ at a controlled furnace cooling rate of 240°F/hour. Since this rate can be increased, even higher strengths may be realized. In this process 718 would not have to be double aged. The second aging treatment at 1200°F would result in a higher strength of 718 than desired while causing simultaneous transformation of the 4340 to an undesirable low strength spheroidized carbide structure.

The hot isostatic pressure welding process provides increased flexibility if alternate approaches are required to develop adequate joint strength simultaneous with the required base metal structure. An as example, joining could be accomplished by holding for a short time at 1750°F. This provides solution annealing of the 718. The 718 can then be strengthened by aging at 1350°F while strengthening of the 4340 is again achieved upon cooling to room temperature at a controlled rate. In this approach, however, the aging reaction in 718 will be less effective as a result of slow cooling from the solution annealing temperature (400°F/minute is usually specified). This problem is typical of large section sizes in 718 and would require special definition should a higher bonding temperature be required.

Thermal Strain

The ability of a fabricated rotor to withstand the thermal strains associated with the austenite transformationis not entirely resolved at this time. Current results appear encouraging in this respect and a full clarification will be available with the conclusions of Contract NAS 3-11837. The primary concern is that the joint strength must be sufficient to permit accommodation of the expansion of 4340 due to austenite transformation during cooldown of the rotor assembly. A net strain across the interface as high as 1.4% may have to be accommodated. Accommodation will occur by straining of the 4340 since it is the weaker of the two

alloys. It should be emphasized that this problem is common to all the alternate rotor fabrication techniques, all of which require heating above the Ae3 temperature during rotor fabrication.

As cooldown from the rotor joining temperature progresses, straining will increase as the austenite transformation proceeds. At the higher temperatures, above 900°F, the transformation strain will be accommodated at relatively low stress by creep of the 4340. At this point, the 4340 is weakest both because of high temperature and because the transformation product contributes little strength. As the temperature decreases further, and transformation continues, the 4340 strength will eventually increase to such an extent that thermal stresses of the order of the yield strength are required for accommodation of the thermal strain (by plastic deformation). Typically, locked in residual stressed will be near the final yield strength of the 4340. These stresses will probably be highest precisely at the joint interface. Further, straining can be considerably magnified in the vicinity of joint defects.

Although this problem is not fully defined at this time, hot isostatic pressure welding has two distinct advantages individually or in combination over other assembly processes. These are: First, the strain is more readily accommodated by high temperature transformation achieved by cooling at a minimum rate consistent with final strength requirements; and second, compressive loading can be maintained during cooling in an autoclave. In the practice of metal forming compressive loading is frequently beneficial in minimizing failures during deformation.

Rotor Fabrication Development

As described above, two primary objectives must be satisfied by the rotor fabrication process:

- A metallurgical structure of satisfactory strength must be developed in both alloys.
- Stresses associated with the austenite transformation strain must be carried by the bimetal joint to permit accommodation of the strain by plastic deformation, primarily in the 4340 steel.

These objectives are common to all the potential processes and seem most amenable to accommodation in the hot isostatic pressure welding process.

A minimum developmental program will be required since assembly parameters will be deduced from current work in this area. Existing autoclave facilities will accommodate this rotor. An initial proof run will be required to confirm fabrication parameters both in terms of autoclave performance, joint integrity, and joint strength. Sample specimens joined in this run should be recycled in a conventional furnace to the austenitizing (joining) temperature and then cooled at various (increasing) rates to ascertain the criticality of cooling rates on joint integrity. This is necessary to assure that "minimum risk" selection in cooling rate is made for subsequent rotor fabrication runs. Additionally, two rotor runs would be recommended. Both runs would include qualification assemblies deemed suitable for destructive test and hence confirmation of the bonding run. The first rotor would be subjected to performance tests. Initially, there would be overspeed spin tests. However, additional tests which subject joint areas to higher stresses in particular may be desirable. Thermal stresses imposed on the spin test by heating the outside of the rotor would be one approach. Multiple cycling may then be desirable and finally destructive testing of the rotor itself would prove extremely valuable. The second rotor would then be proof tested using procedures evolved from evaluating the first rotor. The second rotor would then be committed to hardware.

APPENDIX B

COMPARISON OF 84 SLOT AND 60 SLOT ALTERNATOR DESIGNS

This appendix presents pertinent design information for a 84 slot, 2-pole alternator design. This design has a substantially higher current loading and ac winding current density than the 60 slot design described in the previous text. Information relative to the 84 slot design is given in Table LXXXIV. The average ac winding temperature was estimated to be 590°F (583°K) from results obtained from the thermal studies performed for the previous design at a coolant temperature of 466°F (315°K). The ac winding temperature of the previous 60 slot design which has a current density of 1/2 that of the 84 slot design was 568°F (568°K). The small difference in average winding temperature for the two designs points out the effectiveness of the forced convection gas cooling scheme.

It is estimated that the half inch smaller rotor diameter of this design (7.5 inch vs. 8.0 inch) (19.1 cm vs. 20.3 cm) will reduce the cooling gas flow rate by about 12-1/2%. Although the reduced flow rate was not factored into the winding temperature estimate, it is not expected to produce any significant effects.

The 84 slot design has a higher overall efficiency for loads less than full rated load, whereas the 60 slot design produces higher overall efficiencies for loads greater than rated load as shown in Figure 189. A breakdown of performance values is given in Table LXXXIV.

The rotor O.D. of the 60 slot design can be reduced to 7.5 inches without exceeding the rotor flux density of the 84 slot design. For this case, the efficiency curves of the two designs would compare more favorably because of lower windage losses at the lower diameter. However, the shape of the efficiency curves would still be described previously, that is, the 84 slot design efficiency would be higher at the partial loads.

Although the 84 slot design, in its present unoptimized form, actually meets all specified requirements, it is marginal in ability to generate rated voltage at the 320 KVA .9 P.F. overload condition, excessive field power being required for this. If this capability becomes important (more so than efficiency at part load), another design, such as a 72 slot design, should be investigated.

TABLE LXXXIV
DESIGN SUMMARY
TAC ALTERNATOR
84 SLOT DESIGN, 2-POLE
COOLANT TEMPERATURE: 466°F (315°K)

RATING: 214 kVA at 0.75 P.F. Lagging

VOLTAGE: 240/416 reconnectable to 480/832

SPEED: 24000rpm

FREQUENCY: 400 Hz

DIMENSIONS: INCHES (cm)

Rotor O.D.	7.50	(19.1)
Rotor LENGTH	12.78	(32.4)
STACK LENGTH (OVERALL)	3.58	(9.1)
STACK O.D.	15.16	(38.5)

ELECTROMAGNETIC WEIGHTS: LBS. (kg)

ARMATURE	17.0	(7.7)
FIELD	43.0	(19.5)
FRAME	172.9	(78.5
STACKS	98.0	(44.5)
ROTOR	135.4	(61.5)
TOTAL	466.3	(212.)

MATERIALS:

ac CONDUCTORS	321 SST CLAD SILVER
FIELD CONDUCTORS	CUBE COPPER ALLOY
ARMATURE LAMINATIONS	0.004 INCH (0.102 mm) THICK HIPERCO 27
FRAME	HIPERCO 27
ROTOR MAGNETIC	SAE 4340 @ Rc33
ROTOR NON-MAGNETIC	INCONEL 718 @ Rc38
INSULATION	
ac WINDING	ANADUR
SLOT LINER	ALUMINA
SLOT SEPERATOR	SYNTHETIC MICA
FIELD WINDING	SYNTHETIC MICA

WINDING DETAILS:

NUMBER OF SLOTS	84
CONDUCTORS PER SLOT	2
SERIES TURNS PER PHASE (240 V L-N)	14
PARALLEL PATHS (240 V L-N)	2
PARALLEL STRANDS	2
PHASE BELTS	60°
PITCH	43
BARE CONDUCTOR DIMENSIONS, INCHES	.081 X .144

TABLE LXXXIV (Cont.)

ROTOR TIP SPEED (24000 rpm): feet/sec (m/sec)	786	(240)
MAIN GAP: INCH (mm)	0.120	(3.05)
AUXILIARY GAP: INCH (mm)	0.050	(1.27)
CURRENT DENSITIES: AMPS/IN^2 (Amps/cm^2)		
ac WINDING	6827	(1060)
FIELD WINDING	3973	(615)
FLUX DENSITIES: KL/IN^2 (Webers/m^2)		
BACK IRON	74	(115)
TEETH	98	(152)
MAIN AIR GAP	42	(65)
POLE	94	(146)
FRAME	117	(181)
AUX. AIR GAP	46	(71)
F. L. LOSSES: WATTS		
POLE FACE	1091	
BACK IRON	2559	
TEETH	376	
ARMATURE	5105	
FIELD	3929	
ELECTROMAGNETIC SUBTOTAL	13060	
WINDAGE	5670	
@ PSIA (nt/cm^2)	70	(48.3)
TOTAL	18730	
EFFICIENCY:%		
ELECTROMAGNETIC	92.5	
OVERALL	89.5	
REACTANCES: P.U.		
XD	2.03	
X'D	0.436	
X"D	0.384	
Xq	0.925	
X"q	0.085	
X2	0.234	
XO	0.013	
TIME CONSTANTS, HOT: SECONDS		
T'DO	0.272	
T'D	0.052	
TA	0.003	
Td"	0.005	
VOLTAGE UNBALANCE: %		
2/3 SINGLE PHASE CURRENT	7.5	

TABLE LXXXIV (Cont.)

COOLANT TEMP.: 466°F (514°K) INSULATION: INORGANIC FULL LOAD CAVITY PRESSURE: 70 PSIA (48.3 nt/cm^2) 84 SLOT DESIGN	KWe P.U. LOAD	40 1/4	80 1/2	160 1	240 1 1/2	0.9 P.F. 320 KVA O.L.
LOSSES: WATTS						
ARMATURE		279	1146	5105	14194	14101
FIELD		814	1413	3929	249078	40891
POLE FACE		174	352	1091	2347	2344
TOOTH		350	358	376	3[illegible]1	386
BACK IRON		2380	2439	2559	2683	2630
TOTAL ELECTROMAGNETIC		3997	5708	13060	268[illegible]6	60442
WINDAGE		2270	3580	5670	74[illegible]0	8450
OVERALL		6267	9288	18730	276176	68892
EFFICIENCIES: %						
ELECTROMAGNETIC		90.9	93.4	92.4	46.5	82.7
OVERALL		86.4	89.6	89.5	47.2	80.7
CURRENT DINSITIES: AMPS/IN^2						
ARMATURE CURRENT DENSITY		1714	3425	6827	10275	10275
FIELD CURRENT DENSITY		1809	2382	3973	31633	12817
FLUX DENSITIES: KL/IN^2						
BACK IRON		70	71	74	76	75
TOOTH		75	95	98	101	100
MAIN GAP		40	41	42	43	43
POLE		68	76	94	112	108
FRAME		77	89	117	164	149
AUX. AIR GAP		31	41	46	56	54
FIELD AMP TURNS						
AMPS/IN^2 times 0.155 = Amps/cm^2		6989	9206	15352	122231	49525
KL/IN^2 times 1.55 = Webers/M^2						

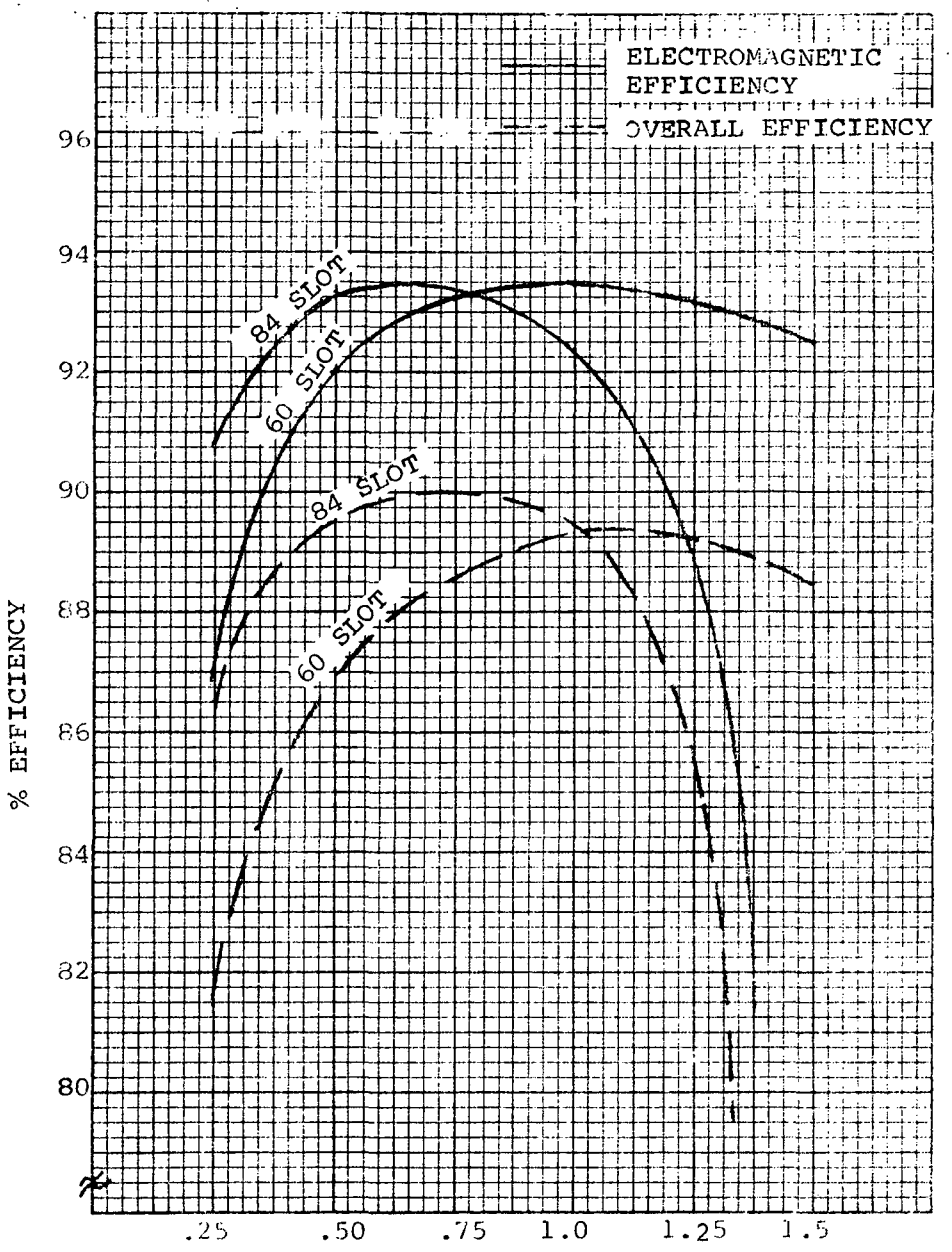

EFFICIENCY TRENDS

Figure 189

The efficiency trends established for the two designs provide useful information regarding available design tradeoffs relative to application requirements.

C. BEARING DESIGN

During the course of Phase III the TAC journal and thrust bearings established for the Phase I 24RG machine were re-evaluated in light of the revised cycle state points and alternator configuration. The significant differences in the Phase I and Phase III design requirements that affect bearing design are summarized below.

Condition	Phase I	Phase III
Working Fluid	He-Xe	He-Xe and Argon
Gas Temperature at Brg.	600°F	350°F
Viscosity	6.5×10^{-9} reyn	5.2×10^{-9} & 4.5×10^{-9}
Pressure Level	15 and 55 psia	17.5 and 70 psia
Alt. Gap Force Gradient	0	40×10^{3} lb/in
Max. Operating Speed Acceleration	4.0 G	1.5 G

The effect of the reduction in design value viscosity from the high temperature He-Xe mixture to that of lower temperature Argon was, in the case of the thrust bearing, off-set by the reduction in maneuver acceleration loads. However in the case of the journals, the addition of the 2 pole alternator magnetic force gradient negated the load reduction achieved by the acceleration reduction.

New bearing sizes were established which have adequate load capacity at 12,000 rpm with minimum gas lubricant viscosity and density conditions (Argon at 350°F and 17.5 psia). The loads assumed for Phase III design purposes are summarized on Table LXXXV.

The principle radial forces that must be taken by the journal bearings arise from the gravity and acceleration loads; and the magnetic force gradient at the alternator auxiliary gap resulting from rotor-stator radial displacement. For design purposes, it was initially assumed that the maximum shaft radial displacement within the bearing would be .003 inches and that the bearing would be concentric with the auxiliary gap within .0015 inches (TIR). This results in a maximum auxiliary gap rotor-stator radial displacement of .00375 inches and a radial force of 150 lbs. (It should be noted that the results of subsequent bearing calculations showed that the maximum bearing radial displacement is .0032

TABLE LXXXV

SUMMARY OF BEARING LOADS

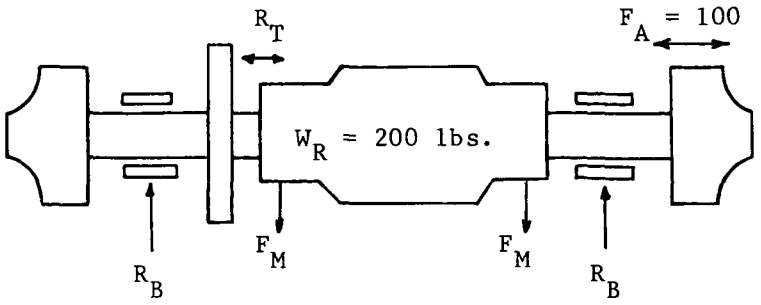

F_M = 40,000 LB/IN x ΔR

ΔR = RADIAL DISPLACEMENT OF ROTOR IN AUXILIARY MAGNETIC GAP

= .003 INCHES WITH BEARING UNDER MAXIMUM LOAD

PLUS

= .00075 INCHES (.0015 TIR) TOLERANCE STACK-UP BETWEEN ALTERNATOR ℄ AND BEARING ℄

= .00375 INCHES

$F_M = 40 \times 10^3 \times 3.75 \times 10^{-3} = 150$ LBS.

TOTAL DESIGN LOAD:

R_B (at 12,000 RPM) = $\frac{W_R}{2} + F_M$ = 250 LBS.

R_B (at 24,000 RPM) = $1.5 \frac{W_R}{2} + F_M$ = 300 LBS.

R_T (at 12,000 RPM) = $W_R + F_A$ = 300 LBS.

R_T (at 24,000 RPM) = $1.5\ W_R + F_A$ = 400 LBS.

inches at 12,000 rpm and .002 inches at 24,000 rpm). One G (horizontal ground operation) at 12,000 rpm and 1.5 G at 24,000 rpm was used as design values resulting in the 250 and 300 lb. total bearing loads.

In the axial direction the alternator magnetic forces are negligible but tolerance to aerodynamic thrust as a result of unbalanced turbine and compressor wheel pressure distributions must be considered. One hundred pounds was used for design purposes. Also the same acceleration criteria as the journals was used for the thrust bearing resulting in design loads of 300 lbs. and 400 lbs. at 12,000 rpm and 24,000 rpm respectively.

JOURNAL BEARINGS

As in Phase I, the journal bearing is a four pad tilting pad on flexures with a stiffness of 15,000 lb/in. These flexures accommodate the shaft centrifugal growth and the radial thermal gradients between shaft and housing. The significant journal bearing design parameters are summarized on Table LXXXVI. The pivot radial clearance (.0013 inches) and the preload (1 - pivot clear./bearing clear.) was set to insure stable operation at the reference operating condition (24,000 rpm vertical operation). The radial thermal growth (.00104 inch) shown in Table LXXXVI results from the 80°F Δt between shaft and housing determined in Phase I. As noted above the pad flexures accommodate both the thermal and centrifugal growths (each of which are of the same magnitude as the clearance) and, as shown in Phase I, will accommodate large deviations from the 80°F Δt without undue bearing performance degradation.

The performance of the journal bearings without changing clearance or other geometric properties was examined using both He-Xe and Argon each at 17.5 and 70 psia over a speed range of 6,000 rpm to 36,000 rpm and a load range of 0 to 300 lbs. Under no condition was the film thickness less than .00026 inches (12,000 rpm - 300 lb. load case). Furthermore the pad natural frequencies were always greater than 150% of the operating speed. Thus, no pad resonance problems are anticipated.

The journal bearing minimum film thickness as a function of load at 12,000 rpm and 24,000 rpm for the pressure extremes using both He-Xe and Argon are shown in Figures 190 and 191. Here it can be seen that the minimum film thickness at the design load conditions of 250 lbs. at 12,000 rpm and 300 lbs. at 24,000 rpm are in no case less than $.3 \times 10^{-3}$ inches.

TABLE LXXXVI

JOURNAL BEARING SUMMARY

TYPE : 4 PAD TILTING PAD

SIZE : 4" DIA. x 4" LG.

MOUNT CONFIGURATION: LOWER TWO PADS HARD MOUNT (K = 1,000,000 LB/IN)
UPPER TWO PADS SOFT MOUNT (K = 15,000 LB/IN)

AT REFERENCE OPERATING CONDITION OF:

24,000 RPM

17.5 PSIA

ARGON AT 350°F ($\mu = 4.5 \times 10^{-8}$ REYNS)

ZERO LOAD

PIVOT RADIAL CLEARANCE	$= 1.3 \times 10^{-3}$ INCHES
BEARING RADIAL CLEARANCE	$= 4.0 \times 10^{-3}$ INCHES
SHAFT RADIAL CENTRIFUGAL GROWTH	$= 1.060 \times 10^{-3}$ INCHES
SHAFT RELATIVE RADIAL THERMAL GROWTH	$= 1.040 \times 10^{-3}$ INCHES

UNDER ALL CONDITIONS EXAMINED

W = 0 LBS.; 6,000 - 36,000 RPM
W = 300 LBS.; 12,000 - 24,000 RPM

} { ARGON AND He-Xe
17.5 PSIA AND 70 PSIA

PIVOT FILM THICKNESS ALWAYS > $.26 \times 10^{-3}$ INCHES

PAD NATURAL FREQUENCIES (PITCH, ROLL, RADIAL) > 1.5 N

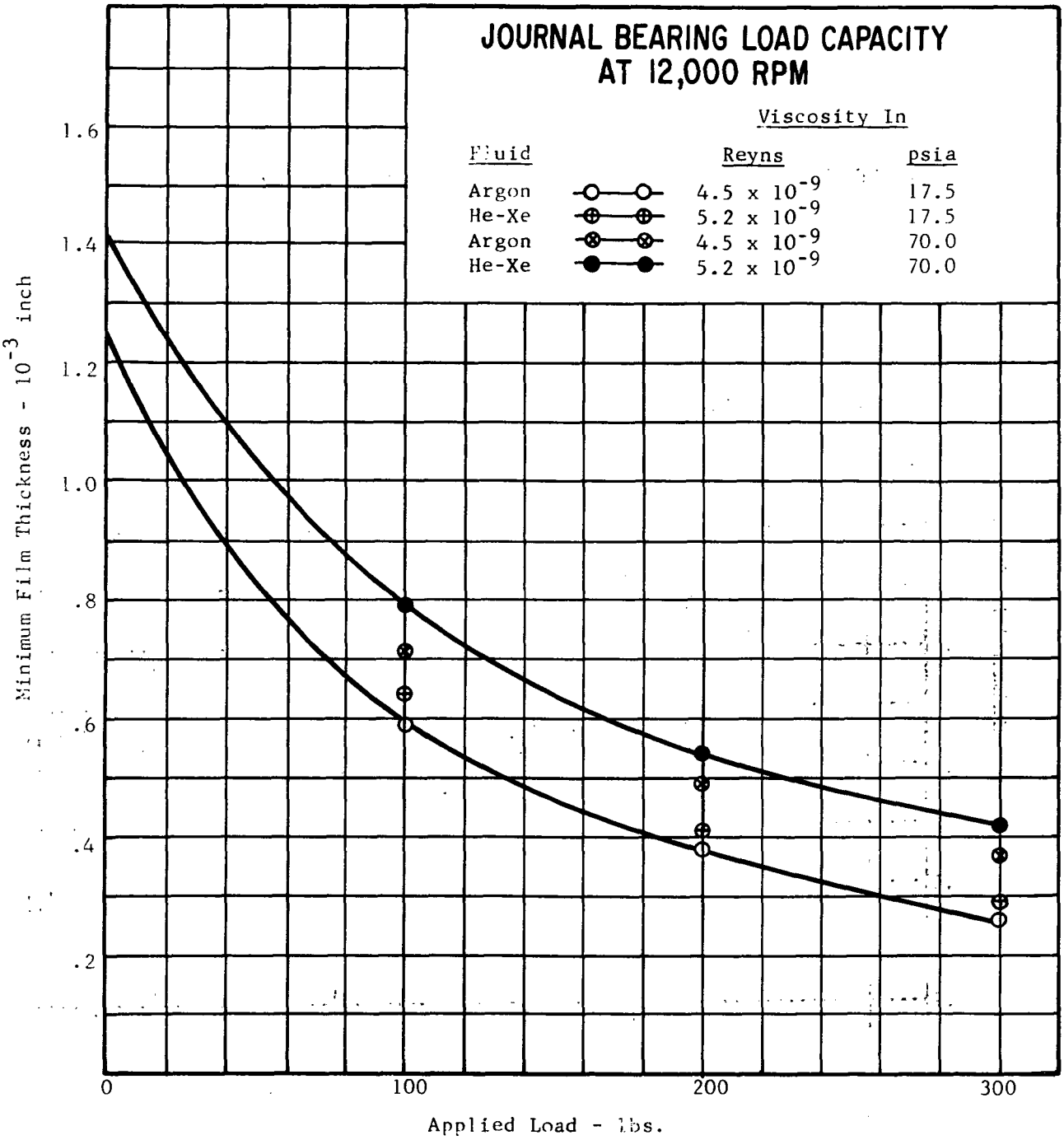
JOURNAL BEARING LOAD CAPACITY
AT 12,000 RPM
Viscosity In
Fluid
Reyns
psia
Argon
4.5 x 10-9
17.5
He-Xe
5.2 x 10-9
17.5
Argon
4.5 x 10-9
70.0
He-Xe
5.2 x 10-9
70.0
Minimum Film Thickness - 10-3 inch
1.6
1.4
1.2
1.0
.8
.6
.4
.2
0
100
200
300
Applied Load - lbs.

Figure 190

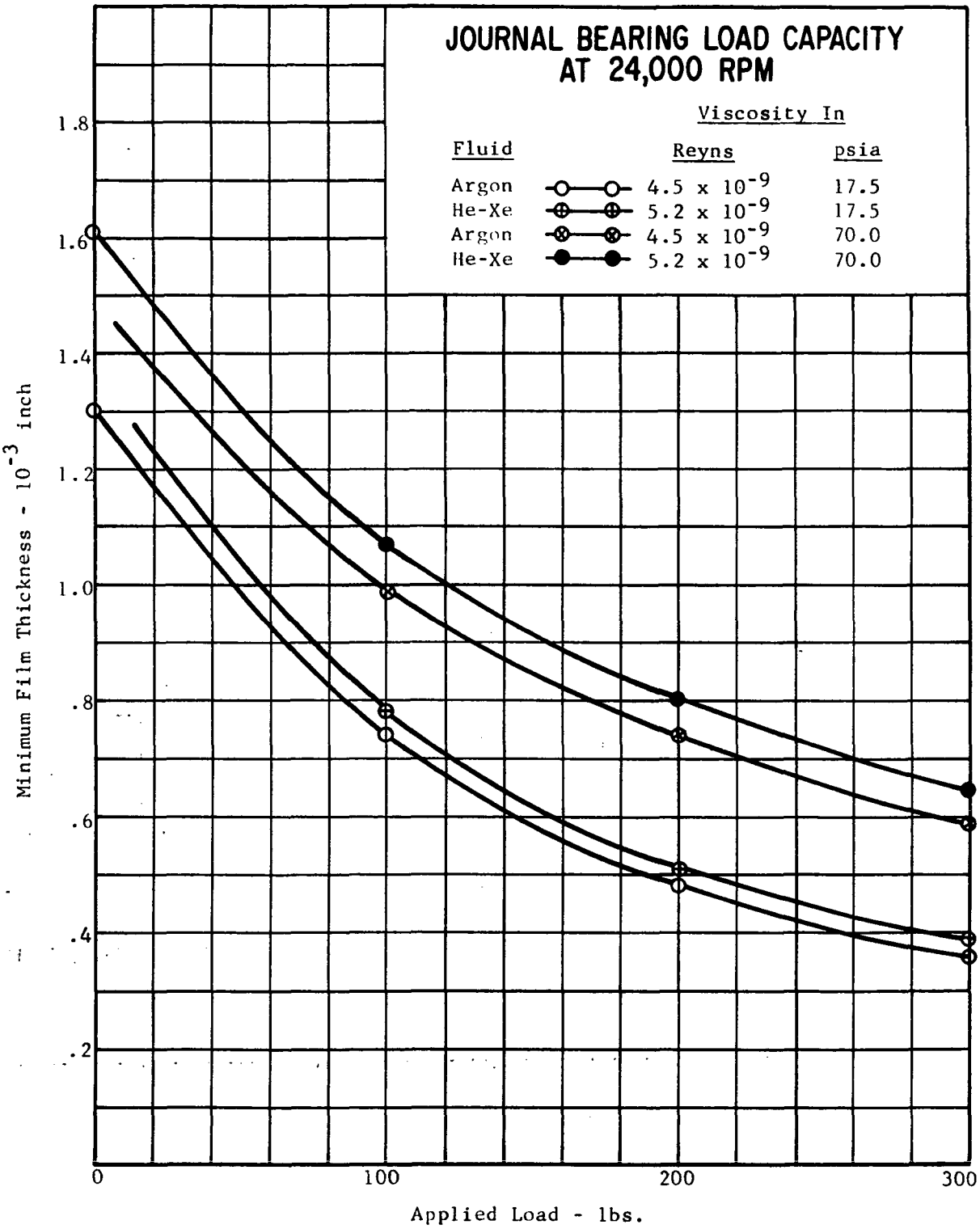
JOURNAL BEARING LOAD CAPACITY
AT 24,000 RPM
Viscosity In
Fluid
Reyns
psia
Argon 4.5 x 10-9 17.5
He-Xe 5.2 x 10-9 17.5
Argon 4.5 x 10-9 70.0
He-Xe 5.2 x 10-9 70.0
Minimum Film Thickness - 10-3 inch
1.8
1.6
1.4
1.2
1.0
.8
.6
.4
.2
0
100
200
300
Applied Load - lbs.

Figure 191

Actually the film thickness will be larger than the $.3 \times 10^{-3}$ inches as the magnetic loads assumed for design purposes are unrealistically high. As was noted above the calculated radial bearing displacement is .002 inches at 24,000 rpm instead of the assumed .003 inches resulting in a 40 lb. reduction in load or a total load of 260 lbs. at 24,000 rpm. The minimum film thickness under this condition is $.4 \times 10^{-3}$ inches.

Furthermore, this is only a short time load occuring under the 1.5 G maneuver condition. At 12,000 rpm, the calculated bearing displacement under load equalled the assumed .003 inches, but the 40,000 lb/in force gradient occurs only at full alternator field excitation - an unrealistic condition at one half speed. Thus the calculated bearing film thickness at 12,000 rpm is also quite conservative.

Figure 192 shows the journal bearing power loss as a function of speed for the extremes of load and working fluid state points. The bearing stiffness and damping coefficients as functions of speed under conditions of vertical and horizontal operation (0 and 100 lbs) for each of the working fluids and state point extremes are shown on Figures 193 and 194. The two extremes of these curves were used for the dynamic response calculations discussed elsewhere in this report.

THRUST BEARING

The thrust bearing designed for the Phase III conditions is, as in Phase I, a pump-in spiral groove type with provision included for incorporation of hydrostatic jacking on the inner seal area. The diameter has been reduced from 8.0 to 7.75 inches as a result of the lower acceleration requirements. As was indicated previously, the reduction in viscosity from the high temperature He-Xe to low temperature Argon conditions results in a corresponding reduction in load capacity. Thus, the change in bearing size was not large.

The thrust bearing load capacity as a function of film thickness for He-Xe at 70 psia and Argon at 17.5 psia (the extreme cases) at 24,000 rpm and the minimum load capacity at 12,000 rpm are shown on Figure 195. Also shown on Figure 195 is the geometry definition and the 24,000 rpm power loss.

JOURNAL BEARING POWER LOSS RANGE

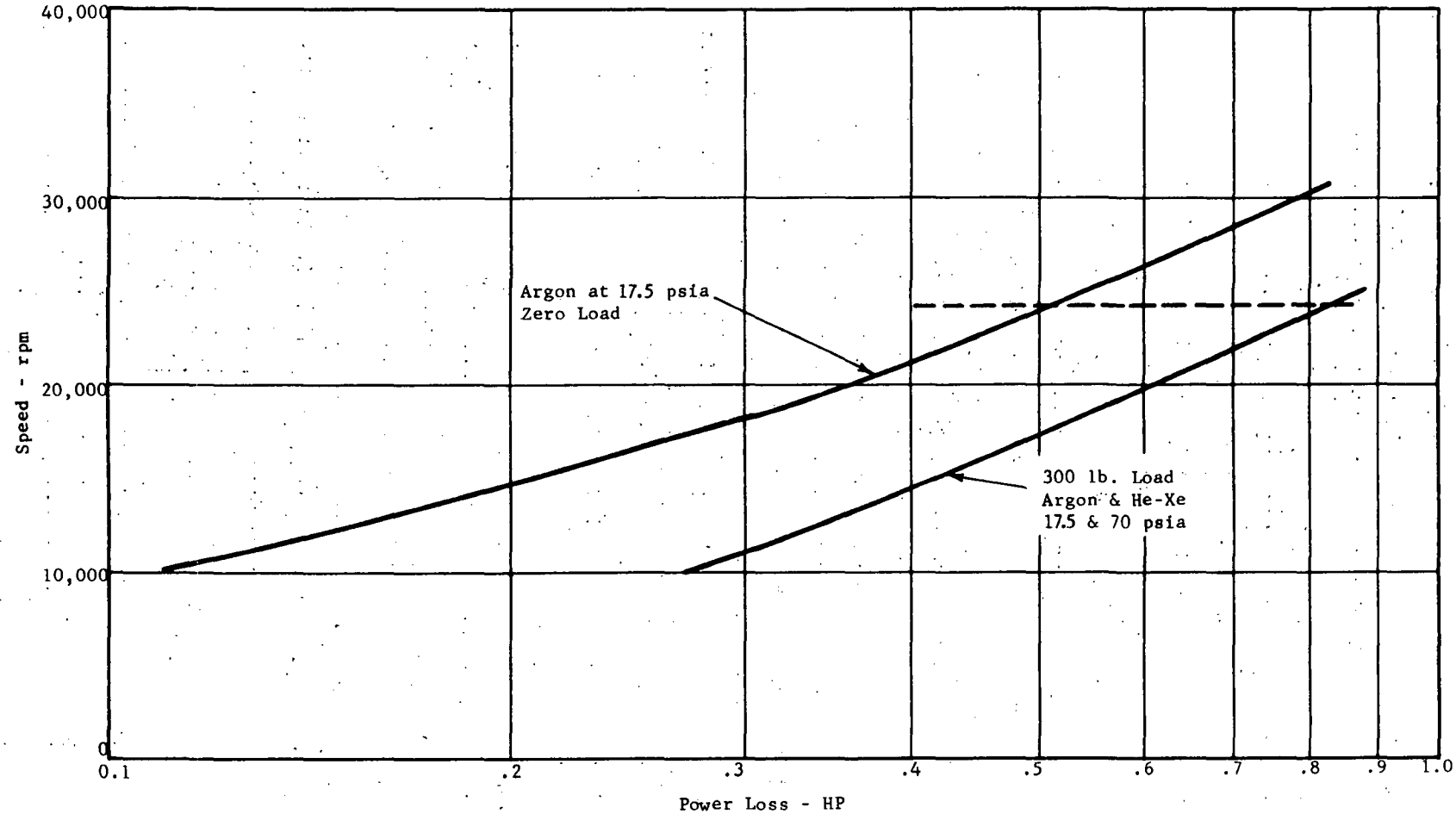

Figure 192

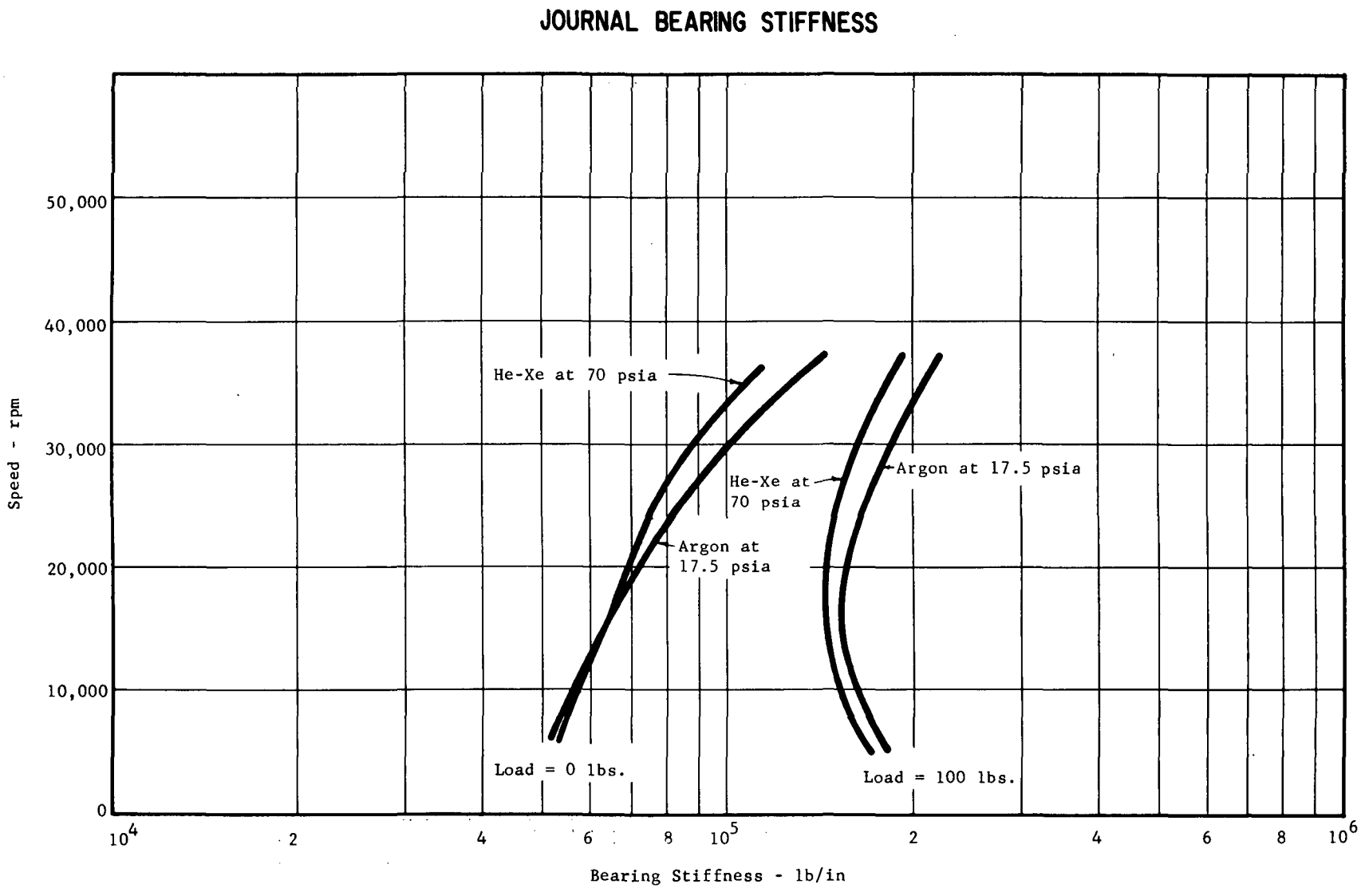
JOURNAL BEARING STIFFNESS
Speed - rpm
50,000
40,000
30,000
20,000
10,000
0
He-Xe at 70 psia
He-Xe at
70 psia
Argon at
17.5 psia
Argon at 17.5 psia
Load = 0 lbs.
Load = 100 lbs.
10^4
2
4
6
8
10^5
2
4
6
8
10^6
Bearing Stiffness - lb/in

Figure 193

JOURNAL BEARING DAMPING

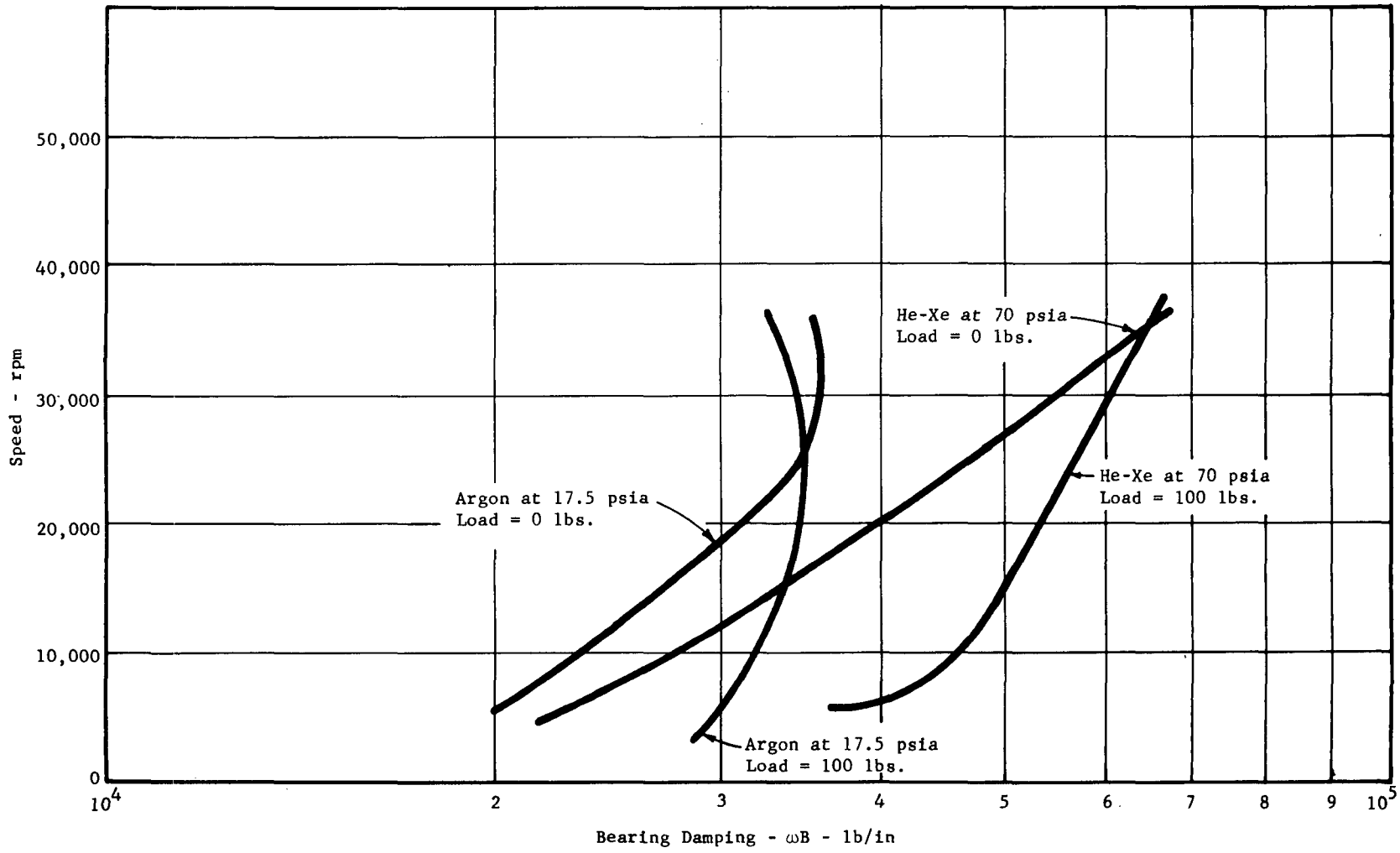

Figure 194

THRUST BEARING PERFORMANCE

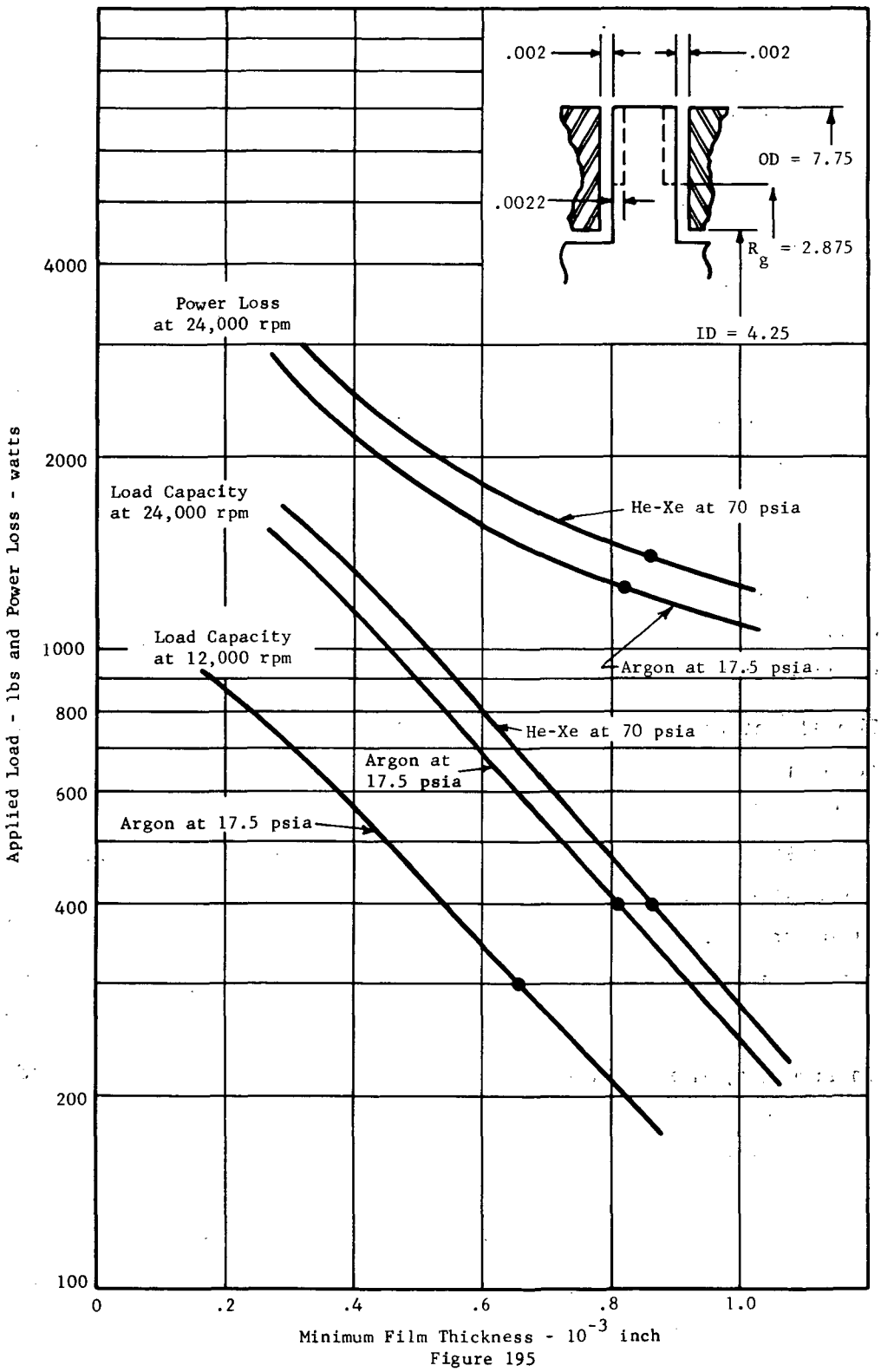

Figure 195

The film thickness under design load conditions (400 lbs.) at 24,000 rpm is in excess of .8 mils and as can be seen from Figure 195, considerable short time overload capacity is available. For short time overload conditions, a minimum film thickness of .4 mils should be readily achievable - limited only by the effect of thermal and mechanical distortions. At 12,000 rpm the minimum design load (300 lbs.) film thickness is .65 mils - somewhat smaller than the 24,000 rpm design. However, the power loss is only 1/4 (speed squared effect) thus the thermal distortions will be negligible and again very small (approaching .4 mils) film thickness should be available.

The maximum thrust bearing power loss at design conditions is 1400 watts which corresponds to a required cooling rate of 42 watts/in^2. The heat exchanger designed during Phase I was sized for 40 watts/in^2 (total face power equal 1440 watts). As these two heat fluxes are nearly equal it can be concluded that, with a similar cooling scheme and heat exchanger geometry, the thermal distortions will be near equal to those predicted in Phase I. Mechanical distortions should, however, be smaller in magnitude because of the lower design load and smaller diameter.

The effect of thermal distortion on thrust bearing performance was checked over a range to 150 μ inches and the results are shown on Figure 196. It should be noted that the maximum film distortion calculated in Phase I was somewhat less than 100 μ inches. The results on Figure 196 show a maximum reduction in film thickness of just over .1 mils with practically no change in power loss (or heat flux). Thus, no thermal runaway is anticipated and again pushing to smaller film thickness for overload conditions should prove to be practical.

In summary, the minor design revisions made to the journal and thrust bearings have made them entirely suitable for the Phase III design conditions. Over the range of viscosity for the two different working fluids and the pressure extremes resulting from power level changes the bearings maintain adequate film thicknesses for the design load conditions. The thrust bearing has good margin for overload conditions and the journals have an inherent margin as a result of the conservative design load values assumed.

EFFECT OF THRUST BEARING DISTORTION AT 24,000 RPM

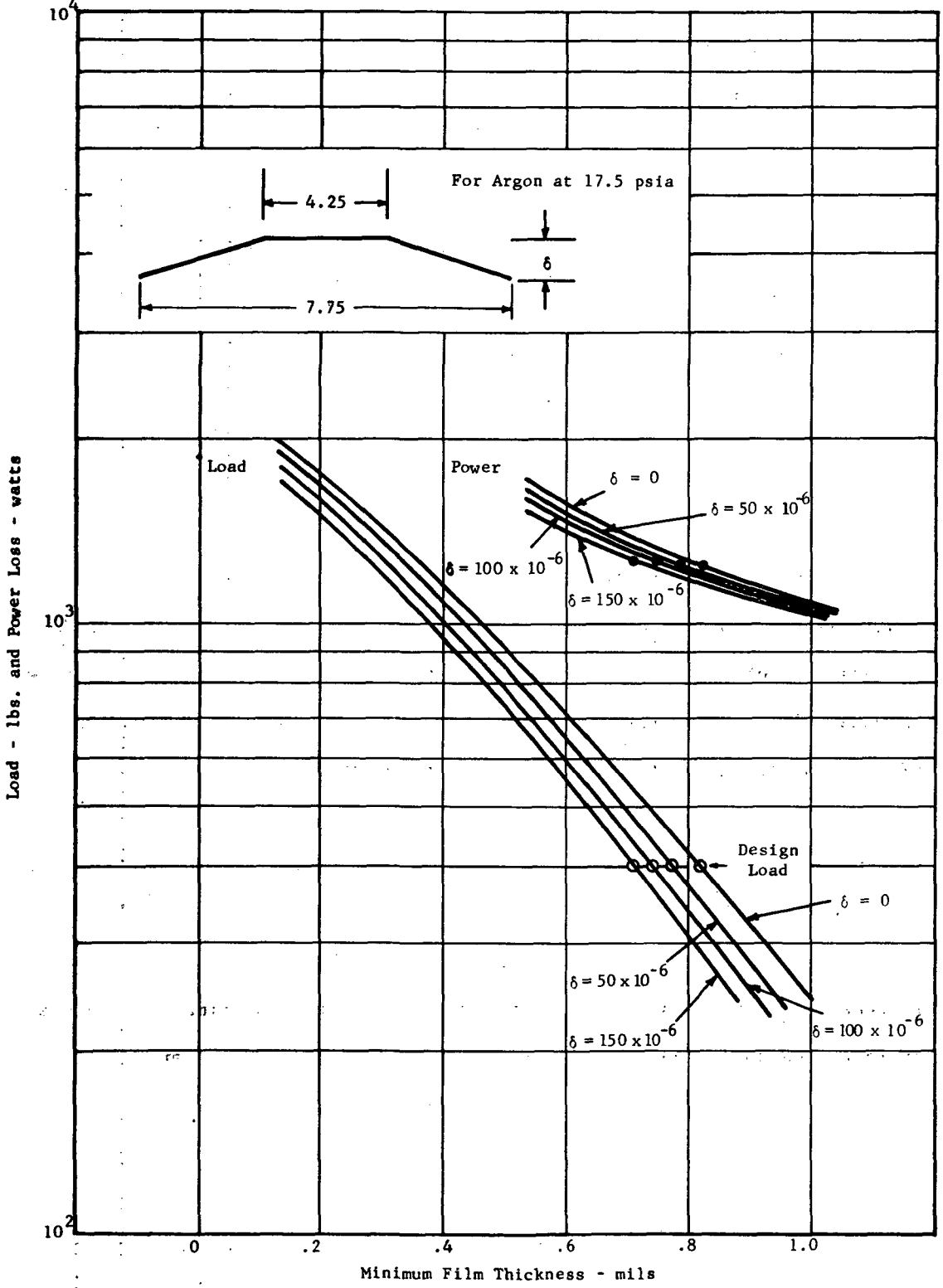

Figure 196

D. DYNAMIC ANALYSIS

BEARING-ROTOR DYNAMICS

The basic 24RG TAC design was subjected to additional rotor dynamic analysis during Phase III to establish the effects of the revised Phase III design conditions on the dynamic response of the TAC rotor. The significant design differences between Phase I and III affecting the rotor vibrational behavior and investigated during Phase III were:

Increased size of the two pole alternator

Alternator auxiliary gap magnetic force gradient of 40,000 lb/in

Bearing dynamic coefficients resulting from size and fluid property differences.

The configuration of the Phase I and III 24RG TAC's are shown schematically on Table LXXXVII along with a comparison of critical speeds. The total rotor weights are not significantly different, primarily because very early large diameter alternator rotor designs were used for the Phase I study which offsets the effect of the Phase III alternator length increase.

As would be expected the first criticals are not significantly different between the Phase I and III configurations because of the weight similarity. The second critical is higher for the Phase III configuration as a result of increased bearing span and the third critical is reduced primarily because of increased total length. The third critical is still, however, 49% above the overspeed condition which is in excess of the minimum 30% margin customarily used for design purposes.

The undamped critical speed map for the Phase III TAC is shown on Figure 197 along with the mode shapes for bearing stiffness equal to 10^5 lb/in. The

TABLE LXXXVII

PHASE I AND PHASE III GAS BEARING TAC WITH RADIAL COMPRESSOR

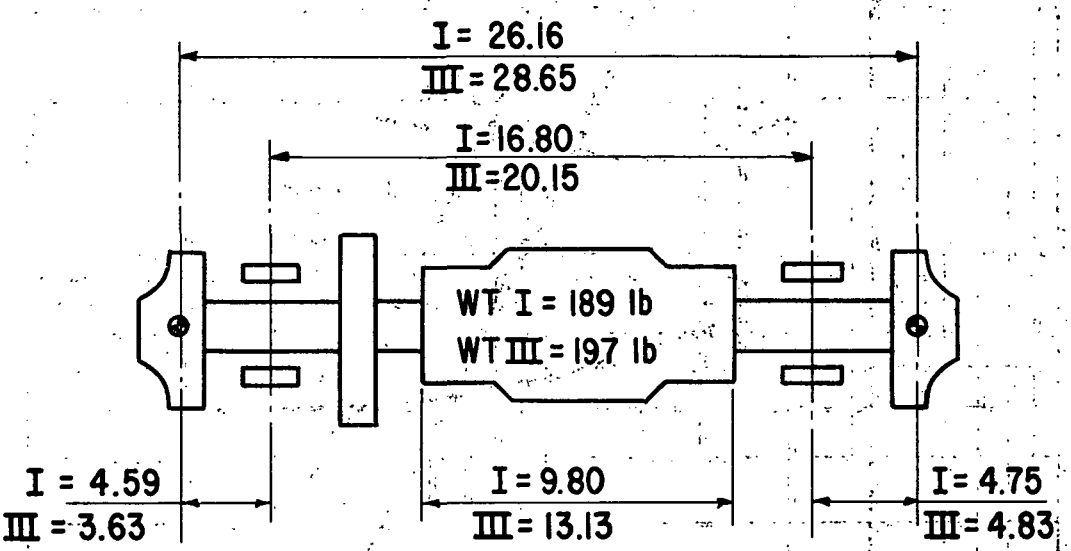

CRITICAL SPEEDS AT $K_{BRG} = 10^5$ LB/IN

	PHASE I	PHASE III
FIRST	5900	5800
SECOND	7600	9000
THIRD	49000	43000
3RD $N_{CR}/28,800$	1.68	1.49

TAC UNDAMPED CRITICAL SPEED
(WITH TITANIUM COMPRESSOR)

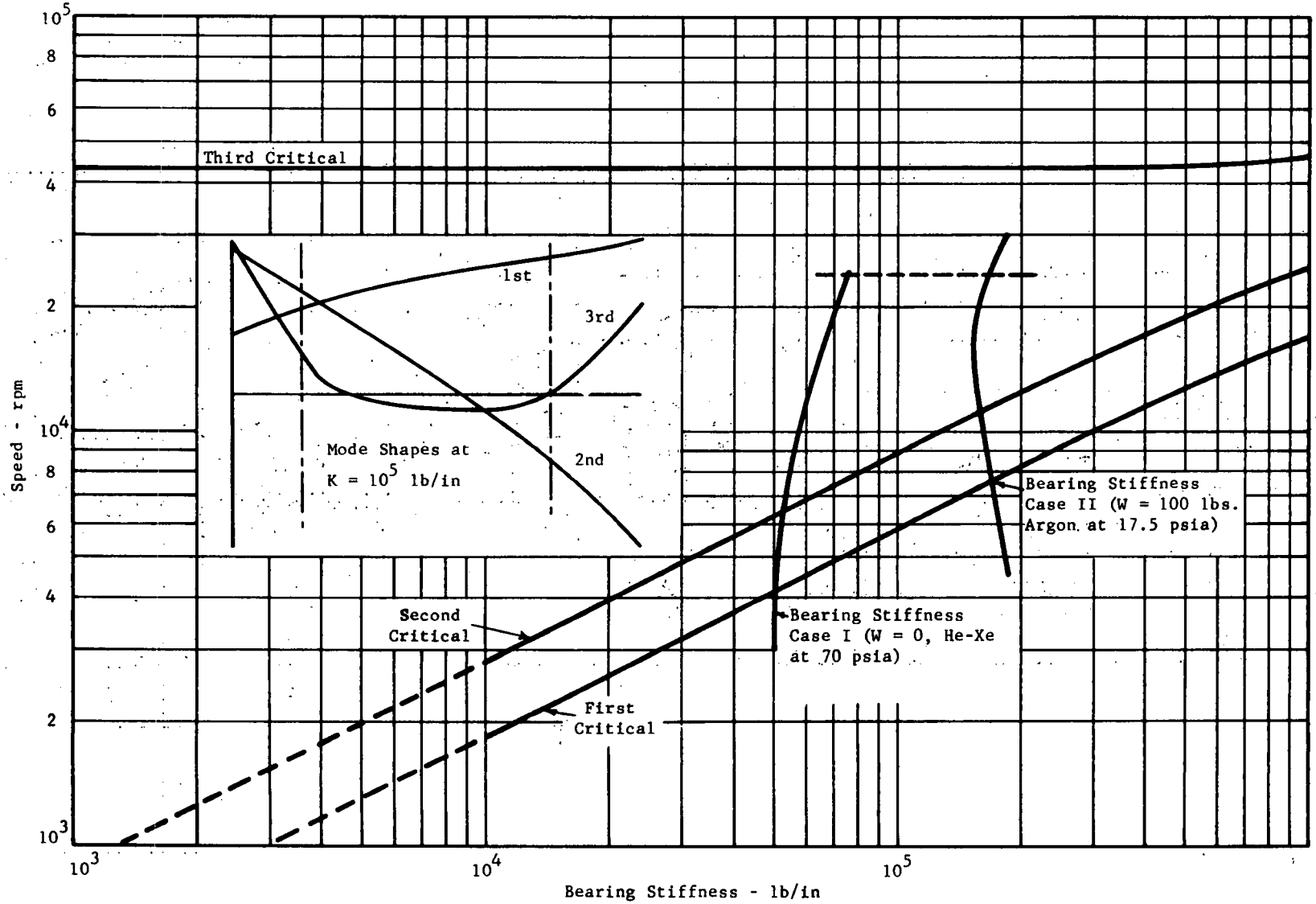

Figure 197

first two criticals are relatively rigid and display the typical characteristics of a symmetrical rotor, i.e. essentially pure translatory and conical first and second modes. The third displays a significant amount of bending in the alternator stub shafts with one mode very near the bearing. Obviously the third is to be avoided.

Also shown on Figure 197 are the extreme cases of bearing stiffness over the range of working fluid choice and state point; and zero bearing load (vertical operation) and 100 lbs. bearing load (horizontal ground operation). These values of bearing stiffness along with the corresponding damping values are shown in Figure 194 of the journal bearing section were used to calculate the dynamic response of the rotor discussed below.

The response of the rotor to mechanical unbalance was calculated assuming a total unbalance equivalent to a 100 μ inch shift of the rotor C.G. with respect to the $\mathbb{C}$ defined by the journal surfaces. This unbalance was equally divided between the turbine and compressor backfaces both in-phase and out-of-phase with each other. This location of unbalance is a worst case situation as it accentuates both the criticals closest to the operating speed (the second with out-of-phase unbalance and the third with in-phase unbalance). The calculations were made for both of the stiffness vs. speed cases shown on Figure 197 and the forementioned corresponding damping-speed relationships which cover the extremes of the assumed cycle and environmental conditions.

The results of the dynamic response calculations are shown on Figures 198 and 199 for bearing stiffness cases I and II respectively. Plotted on each curve is the bearing amplitude as function of speed and that part of the rotor that has

TAC DYNAMIC RESPONSE
BEARING STIFFNESS CASE I

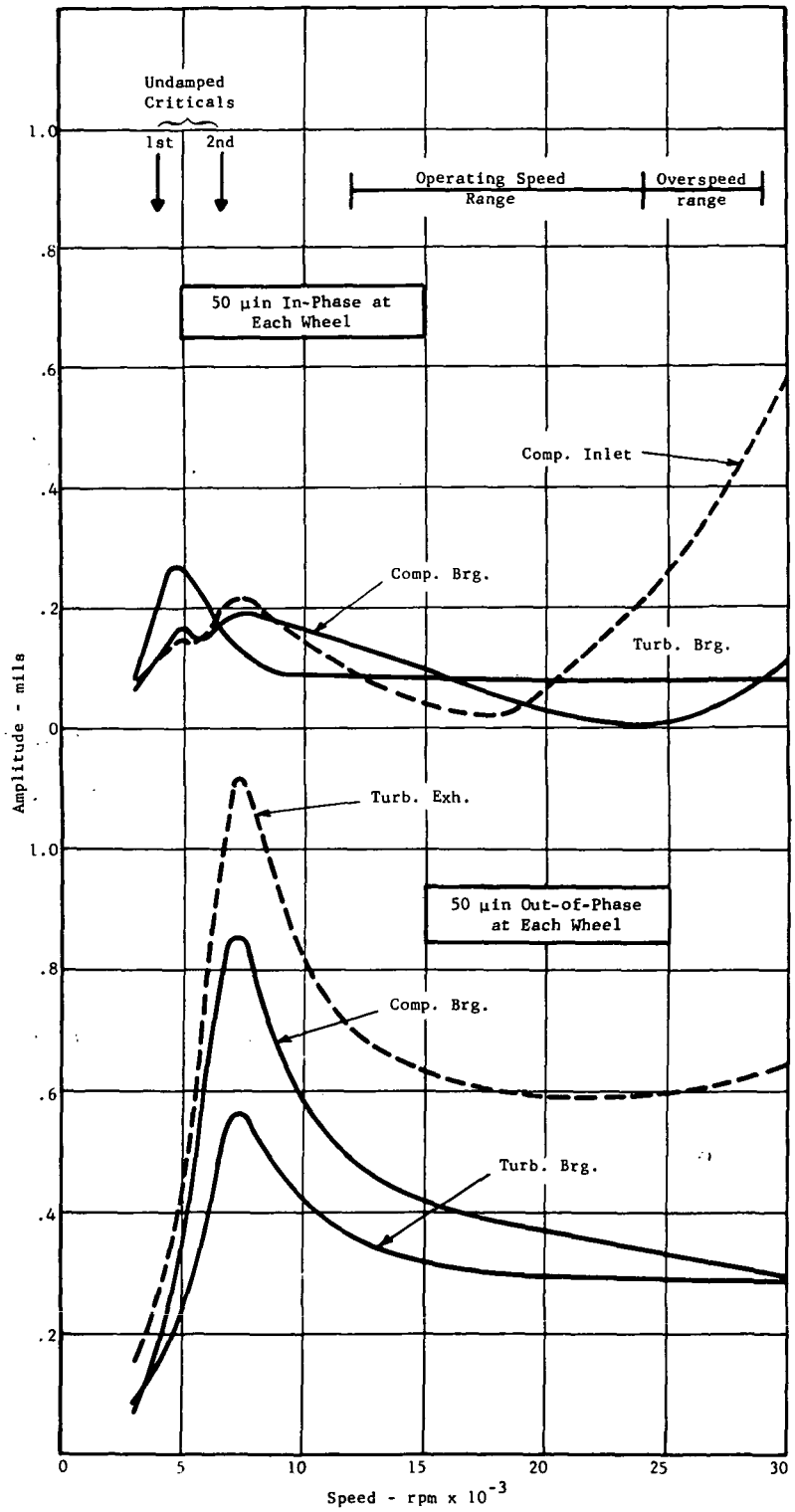

Figure 198

TAC DYNAMIC RESPONSE
BEARING STIFFNESS CASE II

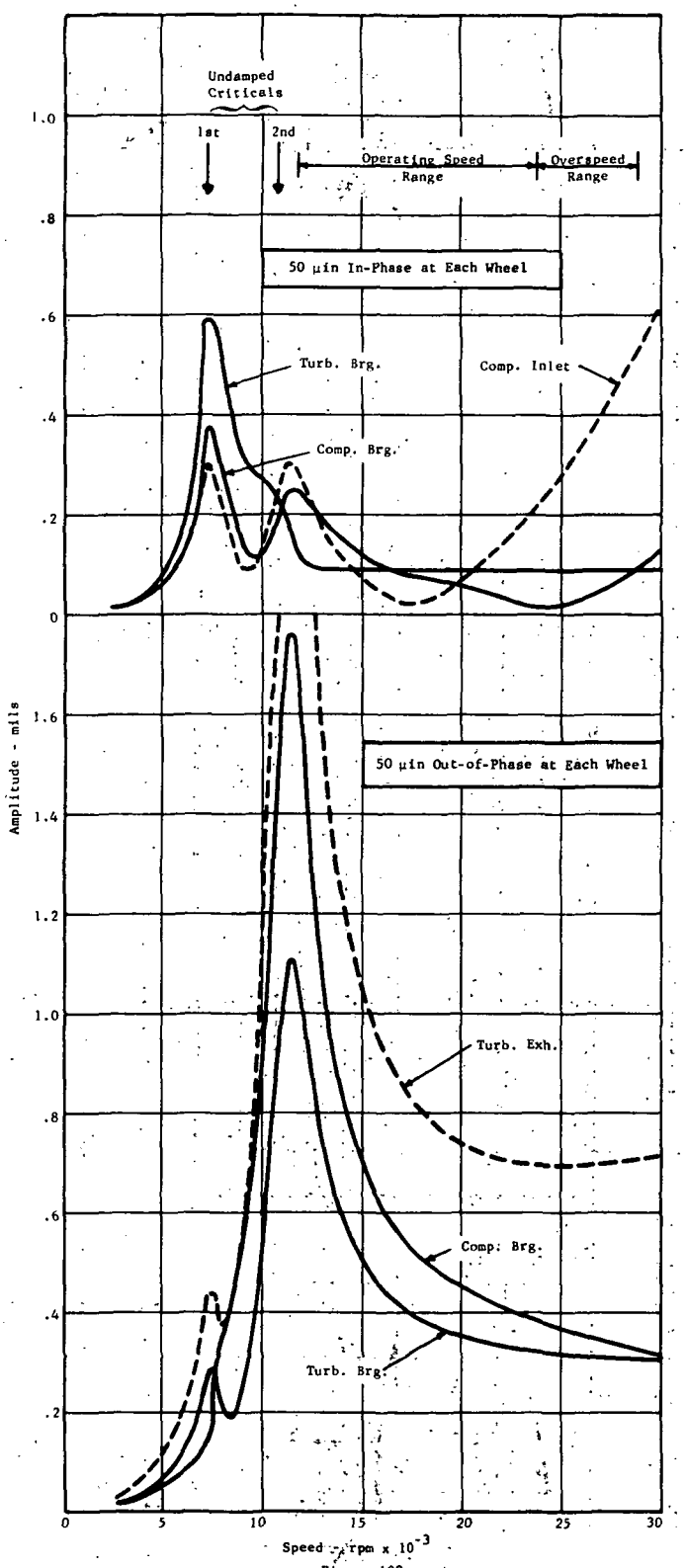

Figure 199

maximum amplitude at 24,000 rpm. It should be noted that the part of the rotor displaying maximum amplitude at 24,000 rpm is not always the same part displaying maximum amplitude at resonance.

In both bearing stiffness cases I and II, the predominant resonance mode is as expected, that is the first critical is predominant and effects of the third at higher speeds are seen with in-phase unbalance and the second is predominant with out-of-phase unbalance. For the lower bearing stiffness case I the resonances (1st and 2nd criticals) are well controlled and display the characteristics of a reasonably well damped system. In the case of high stiffness corresponding to horizontal operation the criticals are poorly damped and large in amplitude as a result of the higher critical speed (because of higher stiffness) and the poorer damping to critical damping ratio. This poorer damping ratio results from two factors.

1. Under highly loaded conditions the ratio of bearing stiffness (which controls critical damping) to bearing damping inherently increases.
2. Under high bearing stiffness conditions, much of the rotor to housing relative motion takes place within the pad flexure which has, for all practical purposes, no damping; thus the inherent bearing damping is less effective.

The amplitudes of vibration at 24,000 rpm at the bearings for both bearing stiffness cases with out-of-phase unbalance are between .3 and .4 mils. The bearing minimum film thickness with a 100 lbs. applied load is close to .8 mils (see Figure 191). Thus the shaft orbit uses about half the available bearing clearance which is considered an acceptable upper limit.

However at 12,000 rpm where the amplitudes are greatest (Figure 199, out-of-phase), the turbine bearing amplitude approaches 1.8 mils as compared to a 100 lbs. load operating film thickness of only .6 mils (see Figure 190). For safe start-up and shut-down conditions the orbit at resonance should be limited to about 75% of the available clearance or about .4 mils at 12,000 rpm.

This simply means that the maximum residual unbalance will have to be limited to a total of 22 μin. (11 at each plane). This value, equivalent to .070 in-oz, is well within the capabilities of current balancing state-of-the-art. With this reduced unbalance, the design speed amplitudes will be correspondingly reduced, thus greater tolerance to balance degradation with time will be realized.

Also calculated was the response of the rotor assuming, in addition to the bearing case I and II characteristics, a negative force gradient equivalent to 40,000 lb/in at each alternator auxiliary gap rotor location. The results of these calculations are shown on Figures 200 and 201 where it can be seen that the negative force gradient has little significant effect on the rotor vibrational behavior. The major differences are:

1. The resonant peaks are very slightly shifted to a lower speed.
2. The vibration amplitudes are slightly higher below the first resonance and slightly attenuated above the first predominant resonance.

These trends are as would be expected as a result of lowering the effective support stiffness of the rotor. The lower effective stiffness results in lowered values of critical speed and larger vibration amplitudes above the first critical for a given driving force. Also, by lowering the effective support stiffness and maintaining the same absolute value of bearing damping,

TAC DYNAMIC RESPONSE (WITH 40,000 LB/IN FORCE GRADIENT AT EACH ALTERNATOR AUXILIARY GAP)

BEARING STIFFNESS CASE I

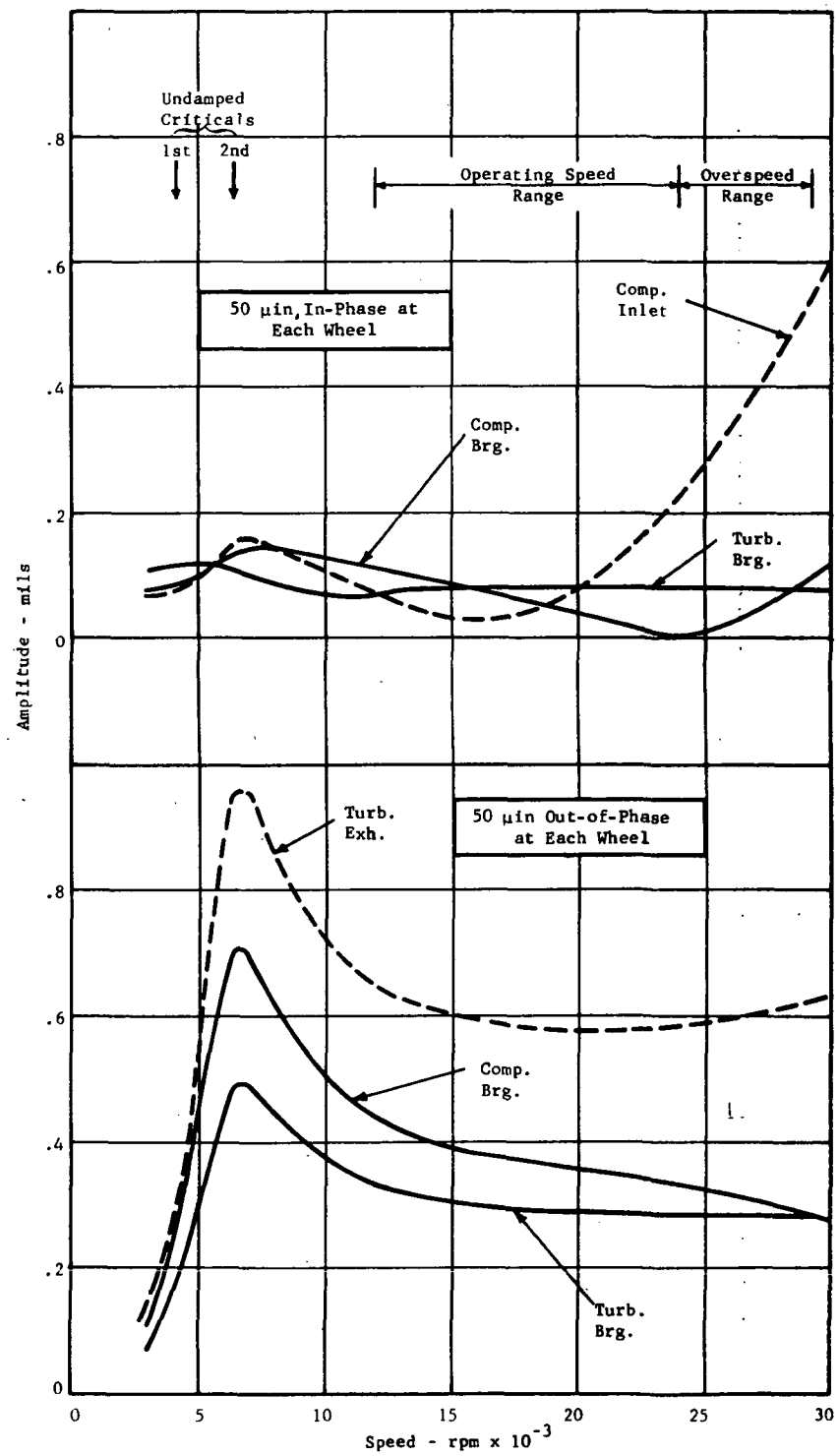

Figure 200

TAC DYNAMIC RESPONSE (WITH 40,000 LB/IN FORCE GRADIENT AT EACH ALTERNATOR AUXILIARY GAP)

BEARING STIFFNESS CASE II

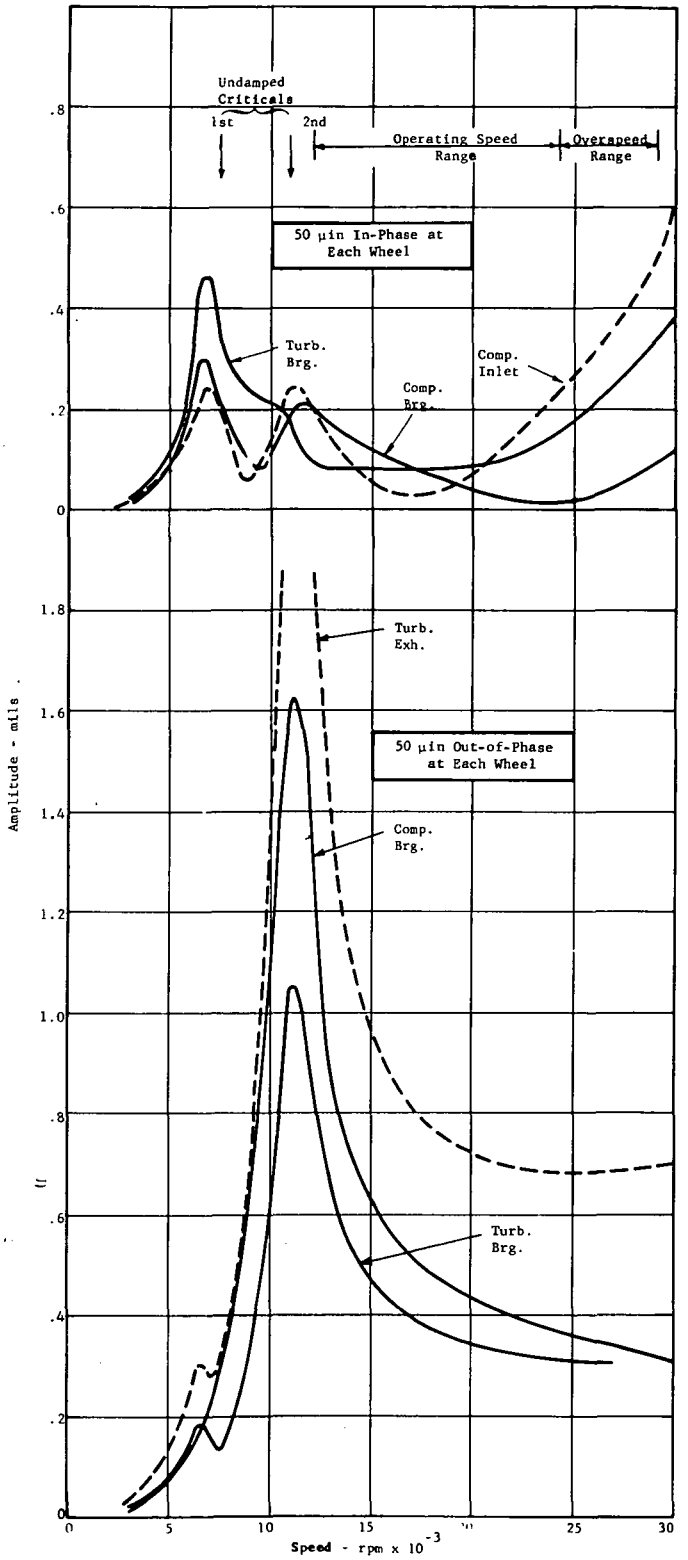

Figure 201

the critical damping ratio is increased. This has the effect of attenuating the critical and amplitudes above the critical.

The amplitudes shown on Figures 200 and 201, as noted above, are not markedly different from those on Figures 198 and 199, thus the same observation regarding unbalance hold when considering the effect of magnetic force gradient.

The effect of substituting a steel compressor wheel for a titanium wheel on rotor critical speeds and response amplitudes was also checked. The critical speeds in Table LXXXVIII reflect the unexpected trends. The difference in rotor weight is small (steel wheel is approximately 6 lbs. heavier) thus the first critical is virtually unaffected. The total difference in weight being concentrated at one end, however, lowers both the second the third criticals. The third critical is 33% above the required overspeed condition. Greater margin may be desirable and is achievable by a slight increase in compressor end bearing diameter.

The response to 50 μin of unbalance out-of-phase at each wheel for bearing case II (which was the worst amplitude case) was also calculated and is summarized in Table LXXXIX. The amplitudes of vibration were not significantly different between the steel and titanium compressor cases with the major difference being a slight lowering of the predominant resonance (second critical).

In summary, the third critical speed of the Phase III TAC rotor is acceptably far removed from the overspeed condition — by a factor of 1.49. The rotor response calculations did not show any significant effect of the third critical to 30,000 rpm. The predominant resonance was the second critical speed

TABLE LXXXVIII

COMPARISON OF TAC CRITICAL SPEEDS WITH TITANIUM AND STEEL COMPRESSOR WHEELS

CRITICAL SPEEDS (RPM) AT $K_{BRG} = 10^5$ LB/IN

	TITANIUM	STEEL
FIRST	5800	5800
SECOND	9000	8500
THIRD	43000	38500
3RD $N_{CR}/28,800$	1.49	1.33

TABLE LXXXIX

COMPARISON OF TAC ROTOR-BEARING RESPONSE WITH TITANIUM AND STEEL COMPRESSOR WHEELS

COMPRESSOR BEARING AMPLITUDES — BEARING CASE II

50 μIN OUT-OF-PHASE AT EACH WHEEL

SPEED (RPM)	TITANIUM (MILS)	STEEL (MILS)
8,000	.35	.37
10,000	.9	1.2
12,000	1.5	1.0
18,000	.51	.41
24,000	.38	.33
30,000	.30	.29

522

occurring at about 12,000 rpm. This poorly damped critical can, however, be well controlled by limiting the total residual unbalance to .070 in-oz. Furthermore, this residual unbalance results in negligible rotor amplitudes at design speed.

The 40,000 lb/in negative force gradient at the alternator magnetic gap has negligible influence upon the rotor dynamic behavior. Also, the use of steel instead of titanium for the compressor wheel has little influence upon the rotor dynamic behavior over the speed range to 30,000 rpm.

E. TAC UNIT DESIGN

Shown in Figure 202 is the drawing of the Phase III TAC. Because of the decreased inlet temperatures to the compressor and turbine from the values of the Phase I 24RG configuration, the tip speeds have been reduced in keeping with the same aerodynamic loading. Since the rotative speed is the same as in Phase I, tip diameters of the compressor and turbine had to be reduced 9% and 11.5%, respectively. A comparison of design data for the Phase I and Phase III 24RG configuration is shown in Table XC. The requirement for operating the turbine at 1600°F for extended time was retained, however, in Phase III. The compressor inlet pressure was increased in Phase III consistent with about the same specific speeds as in Phase I. In order to have the convenience of using existing 400 Hz equipment without a frequency converter, a Lundell alternator was selected with two poles. This requires an increase in the diameters of the alternator rotor and stator about 10% and 28%, respectively. In order to reduce the stress in the turbine hub, the bore was removed. This necessitated introducing the cooling at the compressor end of the rotor. This cooling gas is used to limit the axial temperature gradient along the journals. The removal of the turbine bore reduced hub stress 38% and, based upon 1600°F operation, made the stresses in the rotor blades become the critical stresses, with a unity factor of safety. Due to a change in specified maneuver loads between Phases I and III, the thrust-bearing outer diameter was reduced slightly. The liquid cooling of the thrust-bearing stator has the same configuration as in Phase I.

The radial-inflow turbine has a symmetrically placed inlet scroll to minimize casing stresses due to internal pressure and thermal gradients. The exit-diffuser configuration used in Phase I was retained.

Provisions are made for the working gas to be pumped toward the center of the alternator stack by the conical portions of the alternator rotor. The gas is later cooled in a heat exchanger and returned to the alternator stator-rotor gap.

The weights of the Phase I and Phase III 24RG machines are synopsized in Table XCI. The Phase III alternator rotor is 38 percent heavier than that of the Phase I alternator. The Phase III alternator stator is 83

PHASE 3 BRAYTON CYCLE
TURBO-ALTERNATOR-COMPRESSOR
24RG-5a

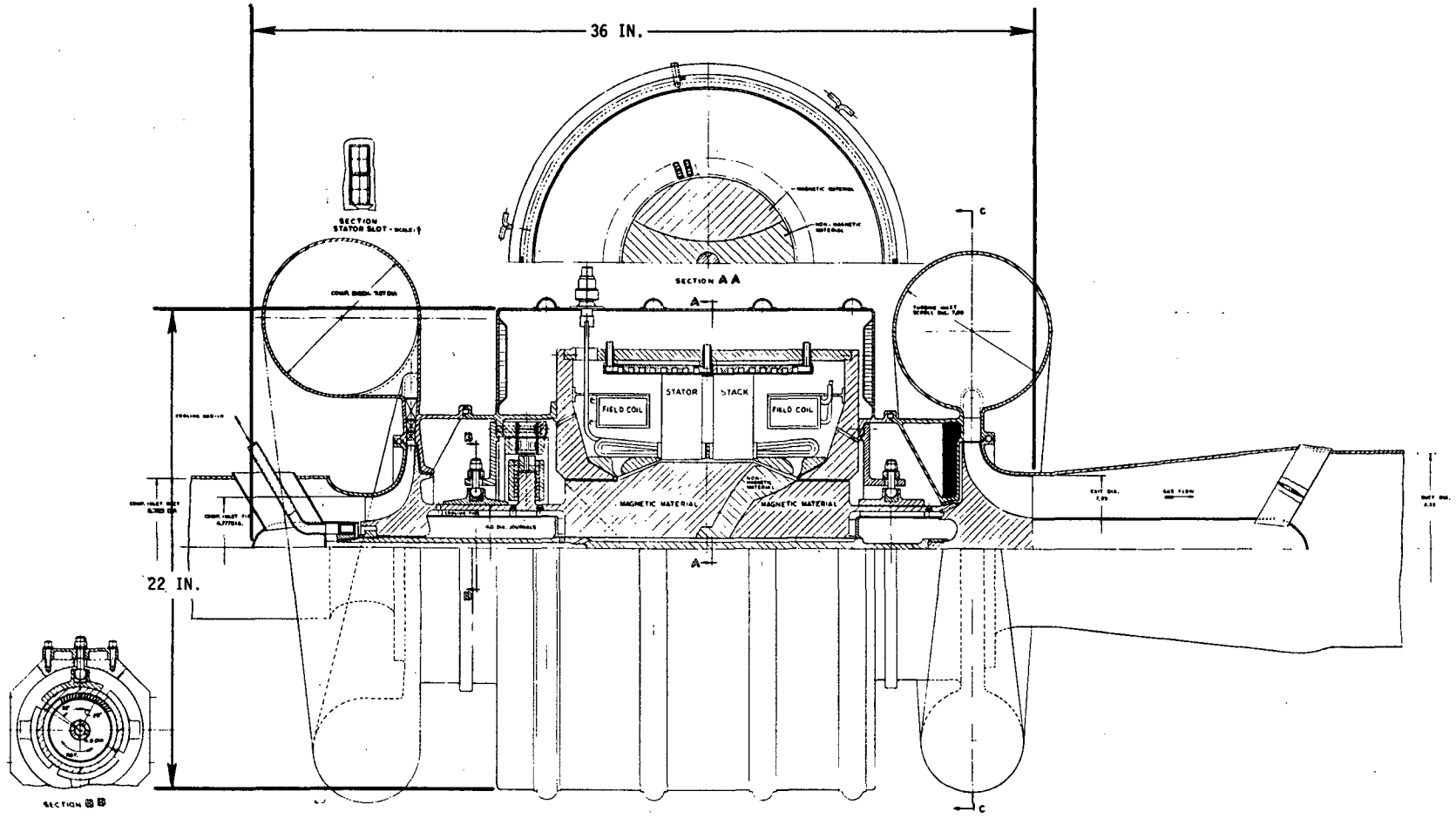

Figure 202

TABLE XC

COMPARISON OF PHASE I AND PHASE III
24RG BRAYTON TAC DESIGN PARAMETERS

	Phase I	Phase III
Power Fluid Inlet Temperature, °F	240	120
Inlet Pressure, psia	55	70
Flow Rate, lb/sec	11.1	13.7
Compressor Exit Temperature, °F	475	315
Exit Pressure, psia	105	133
Tip Diameter, in.	10.4	9.4
Scroll Diameter, in.	7.5	7.1
Peak Effective Stress, ksi	27	23
Turbine Scroll Inlet Temperature, °F	1600	1150
Inlet Pressure, psia	101	130
Diameter, in.	7.6	7.0
Turbine Blade Inlet Temperature, °F	1450	1033
Inlet Pressure, psia	77	99
Exhaust Temperature, °F	1203	831
Exhaust Pressure, psia	57	72
Tip Diameter, in.	11.1	9.9
Blade Peak Effective Stress, ksi	25	25
Hub Peak Effective Stress, ksi	40	25
Lundell Alternator Stator Dia., in.	14.4	18.4
Rotor Length, in.	11.8	13.1
Frequency, Hz	1200	400
System Outer Can Diameter, in.	15	22
Rotor Length, in.	32	36
Rotor Weight, lb.	152	187
Stator Weight, lb.	446	682
Total Weight, lb.	598	869
Thrust Bearing Dia., in.	8	7.8

TABLE XCI

24RG TAC WEIGHT SUMMARY (POUNDS)

	PHASE I	PHASE II
COMPRESSOR	10	8
ALTERNATOR-ROTOR	98	135
TURBINE	25	22
STUBSHAFTS/TIEBOLT	19	22
TOTAL ROTOR	152	187
ALTERNATOR-STATOR	181	331
CASING	265	351
TOTAL STATOR	446	682
TOTAL WEIGHT	598	869

percent heavier than that of the Phase I alternator. The Phase III casing weighs 32 percent more than the Phase I casing. The Phase III 24RG total weight is 271 pounds, or 45 percent more than its Phase I counterpart.

F. PERFORMANCE ANALYSES

For Phase III the TAC operating conditions were changed as shown in Table XCII. The temperatures were reduced to the SNAP-8 conditions, and flow rate and pressure level were increased to achieve 160 KWe output. The turbine pressure ratio was increased which means that there is less pressure drop in the heat exchanger and the ducting.

The specific speed of the compressor is 91.5 for Phase III compared with 88.5 for Phase I. The corresponding specific speeds for the turbine are 79.1 and 76.7. Because these values are only about 3% different, the turbomachinery for Phase III was scaled from the 24 RG Phase I designs. For dynamic similarity of two machines, which have the same pressure ratio and polytropic exponent, the value of U^2/RT should be a constant, where U is the wheel speed, R is the gas constant and T is the inlet temperature. An alternate form of this criterion is $ND/\sqrt{RT}$ where N is rotative speed and D is the wheel diameter. This relationship was used to scale the Phase I compressor and turbine diameters to the Phase III conditions. The scale factors are $\sqrt{580/700}$ or 0.91 for the compressor and $\sqrt{1610/2060}$ or 0.884 for the turbine. The flow areas of the Phase I designs were scaled to maintain a constant value of the flow function $\frac{W\sqrt{T}}{P\ A}$, and the area scale factors were 0.884 for the compressor and 0.853 for the turbine. A comparison of the dimensions is shown in Table XCIII.

Cycle calculations were made to determine the performance of the Phase III design for the 6-pole and 2-pole alternators. The effect of the lower temperatures was to lower the cycle efficiency from 0.284 to 0.257. Increasing the turbine pressure ratio raised the cycle efficiency to 0.275 as seen for the 6-pole alternator in Table XCIV. Reducing the alternator efficiency to 0.93 and increasing the windage loss to 5.5 KW for the 2-pole alternator reduced the cycle efficiency to 0.27.

TABLE XCII

TAC OPERATING CONDITIONS

	Phase I	Phase III
Turbine Inlet Temperature, ^{o}R	2060	1610
Compressor Inlet Temperature, ^{o}R	700	580
Flow Rate, lb/sec	11.1	13.73
Compressor Inlet Pressure, psia	55	70
Compressor Pressure Ratio	1.9	1.9
Compressor Efficiency	.859	.859
Turbine Efficiency	.91	.91
Rotative Speed, rpm	24,000	24,000
Turbine Inlet Pressure, psia	101.4	130.
Turbine Pressure Ratio	1.786	1.824

TABLE XCIII

TURBOMACHINERY DIMENSIONS

Compressor	Phase I	Phase III
Impeller Inlet Hub Radius, in.	1.3125	1.142
Impeller Inlet Tip Radius, in.	2.625	2.424
Impeller Exit Tip Radius, in.	5.182	4.718
Impeller Exit Passage Width, in.	.420	.408
Vaned Diffuser Inlet Radius, in.	5.493	5.00
Vaned Diffuser Exit Radius, in.	7.55	6.87
Vaned Diffuser Exit Width, in.	.57	.554
Inlet Pipe Radius, in.	3.50	3.29
Exit Scroll Radius, in.	3.76	3.54
Radius to Scroll Outlet, in.	11.37	10.35
Turbine		
Inlet Scroll Radius, in.	3.776	3.49
Nozzle Inlet Radius, in.	6.791	6.00
Nozzle Exit Radius, in.	5.83	5.16
Impeller Inlet Radius, in.	5.553	4.91
Impeller Exit Tip Radius, in.	3.879	3.524
Impeller Exit Hub Radius, in.	1.562	1.286
Diffuser Exit Radius, in.	4.963	4.585
Exit Pipe Radius, in.	4.71	4.35

TABLE XCIV

TAC PERFORMANCE COMPARISON

	Phase I	Phase II	Phase III	
		Low Temp.		
	6 Pole	6 Pole	6 Pole	2 Pole
Losses, KW	7.36	7.36	7.36	8.61
Leakage, % Flow	3.23	3.23	3.23	3.23
Compressor Efficiency	.859	.859	.859	.859
Turbine Pressure Ratio	1.786	1.786	1.824	1.824
Turbine Efficiency	.91	.91	.91	.91
Alternator Efficiency	.942	.942	.942	.93
Cycle Efficiency	.284	.257	.275	.27
Flow Rate, lb/sec	9.85	14.07	12.81	13.06

V. REFERENCES

1. Rothbart, H. A., Mechanical Design and Systems Handbook, McGraw-Hill Book Co., N.Y., 1964, pp. 6-56.
2. Joice, L. J., and La Banc, E. J., "GE 12 Redesigned Compressor Blade and Vane Laboratory Test," General Electric Company Report No. TM 69AEG1071, September 10, 1969.
3. Kourokevas, G. D., "T-58-8 Stall Checker Kit Vibration Survey," General Electric Company Report, TM 68AEG1269, 1968.
4. Jennings, B. H., and Rogers, W. L., Gas Turbine Analysis and Practice, McGraw-Hill Book Company, N.Y., 1953, pp. 426-434.
5. Kemp, R. H., Hirschberg, M. H., and Morgan, W. C., "Theoretical and Experimental Analysis of the Reduction of Rotor Blade Vibration in Turbomachinery Through the Use of Modified Stator Vane Spacing," NACA TN 4373, September 1958.
6. Renner, L. R., Johnston, J. T., and Kline, S. J., "Performance and Design of Straight Two-Dimensional Diffusers," Thermo-Science Division, Department of Mechanical Engineering, Stanford University, No. P.D.-8, September 1964.
7. Sprenger, H., "Experimental Investigation of Straight and Curved Diffusers" (British Translation, May 1962) ASTIA AD 277113.
8. Tsyl, E. R., et al., "Overall Performance in Argon of a 6-inch Radial-Bladed Centrifugal Compressor," NASA TM X-1622, August 1968.
9. Perrone, G. L., Milligan, H. H., "Brayton Cycle 3.2-inch Radial Compressor Performance Evaluation," NASA CR-54968, May 1966.
10. Blair, L. W., "Aerodynamic Performance of the GE 2.2 lb/sec Centrifugal Stage Component Tests - B/U 1 to B/U 12," G.E. TM 70AEG1487, April 1970.
11. Balje, O. E., "A Study on Design Criteria and Matching of Turbomachines," ASME 60WA-231, 1960.
12. Stanitz, J. D., "One Dimensional Flow in Vaneless Diffusers of Radial- and Mixed-Flow Centrifugal Compressors, Including Effects of Friction, Heat Transfer, and Area Change," NACA TN 2610, January 1952.
13. Goldstein, S., Modern Developments in Fluid Dynamics, Oxford Press (1938).
14. Faulders, C. R., "Experimental and Theoretical Study of Vaneless Diffuser Flow with Supersonic Entry," M.I.T. Gas Turbine Laboratory, Cambridge, Mass., June 1952.
15. Dean, R. C., Senoo, Y., "Rotating Wakes in Vaneless Diffusers," ASME Journal of Basic Engineering, September 1960.
16. Brown, W. B., "Friction Coefficients in a Vaneless Diffuser," NACA TN 1311, May 1947.
17. Eckert, B., Axialkompressoren und Radialkompressoren, Springer-Verlag, Berlin (1953).

18. Sovran, G. and Klomp, E. D., "Experimentally Determined Optimum Geometries for Rectilinear Diffusers with Rectangular, Conical, or Annular Cross Section," Fluid Mechanics of Internal Flow, Elsevier Co., Amsterdam (1967).

19. Runstadler, P. W. and Dean, R. C., "Straight Channel Diffuser Performance at High Inlet Mach Numbers," ASME Trans., September 1969.

20. Rohlik, H. E., "Analytical Determination of Radial Inflow Turbine Design Geometry for Maximum Efficiency," NASA TN D-4384, February 1968.

21. Steward, W. L., Whitney, W. J., and Wong, R. Y., "A Study of Boundary-Layer Characteristics of Turbomachine Blade Rows and Their Relation to Over-all Blade Loss," J. Basic Eng. Vol. 82, No. 3, September 1960, pp. 588-592.

22. Shepherd, D. G., "Principles of Turbomachinery," MacMillan Co., 1956.

23. Henry, J. R., Wood, C. C., and Wilbur, S. W., "Summary of Subsonic Diffuser Data," NACA RM L56F05, October 1956.

24. Nusbaum, W. J. and Kofskey, M. G., "Cold Performance Evaluation of 4.97-inch Radial - Inflow Turbine Designed for Single-Shaft Brayton Cycle Space-Power System," NASA TN D-5090, March 1969.

25. Futral, S. M., Jr., and Holeski, D. E., "Experimental Results of Varying the Blade-Shroud Clearance in a 6.02-inch Radial - Inflow Turbine," NASA TN D-5513, January 1970.

26. Nusbaum, W. J. and Wasserbauer, C. A., "Experimental Performance Evaluation of a 4.59-inch Radial-Inflow Turbine over a Range of Reynolds Number," NASA TN D-3835, February 1967.

27. Northern Research and Engineering Corporation, "The Design and Performance Analysis of Radial-Inflow Turbines," Cambridge, Mass., 1964.

28. Eckert, B., "Axial Kompressoren und Radial Kompressoren," Springer-Verlag, Berlin, Germany, 1953.

29. Katsanis, T., "Use of Arbitrary Quasi-Orthogonals for Calculating Flow Distribution on a Blade-to-Blade Surface in a Turbomachine," NASA TN D-2809, May 1965.

30. Jamieson, A. W. H., "The Radial Turbine Gas Turbine Principles and Practice," Sir Harold Roxbee Cox, ed., D. Van Nostrand Co., Inc., 1955.

31. Cocanower, A. B., Kline, S. J., and Johnston, J. P., "A Unified Method for Predicting the Performance of Subsonic Diffusers of Several Geometries," Stanford University Mechanical Eng. Dept. Report PD-10, May 1965.

32. Hoerner, S. F., "Aerodynamic Drag," Otterbein Press, Dayton, Ohio, 1951.

33. Tysl, E. R., Ball, C. L., Weigel, C., and Heidelberg, L. J., "Overall Performance in Argon of a 6 Inch Radial-Bladed Centrifugal Compressor," NASA TM X-1622, August 1968.

34. Nusbaum, W. J., and Kofskey, M. G., "Cold Performance Evaluation of 4.97 Inch Radial-Inflow Turbine Designed for Single-Shaft Brayton Cycle Space-Power System," NASA TND-5090, March 1969.

35. Belt, R. N., "Silent Electrical Power Generators for Tactical Applications," Appendix E, U. S. Army MERDC, Report No. 1954, June 1969.

36. Schnetzer, E., "Potassium Turboalternator Preliminary Design Study, Final Report Phase I," prepared for NASA, Nuclear Systems Programs, Space Systems, General Electric Co., GESP-296, 1969.

37. Bagwell, D., "TOSS, An IBM 7090 Code for Computing Transient or Steady State Temperature Distributions," Union Carbide Nuclear Co., Oak Ridge Gaseous Diffusion Plant, AEC R&D Report No. K-1494, 1963.

38. Becker, K. M. and Kaye, J., "Measurements of Diabatic Flow in an Annulus with an Inner Rotating Cylinder," Trans. ASME, Series C, Vol. 82, 1962, pp. 97-105.

39. Bjorklund, I. S. and Kays, W. M., "Heat Transfer Between Concentric Rotating Cylinders," Trans. ASME, Series C, Vol. 81, 1951, pp. 175-186.

40. Curwen, P. W., "Research and Development of High Performance, Axial-Flow Turbomachinery," NASA CR-801, May 1968.

41. Frost, A., Lund, J., and Curwen, P. W., "High Performance Turboalternator and Associated Hardware," NASA CR-1291, March 1969.

42. Cheng, H., Wilson, D., Arwas, E., and Castelli, V., "Research and Development of High Temperature Gas Bearings, I - Analysis and Design of Three Gas Bearings for High Temperature Operation," NASA CR-1476, November 1969.

43. Licht, L., and Eshel, A., "Study, Fabrication, and Testing of a Foil Bearing Rotor Support System," Ampex Report RR 68-2, NASA CR-1157, November 1968.

44. Peterson, M. B., et al., "Analytical and Experimental Investigation of Gas Bearing, Tilting Pad Pivots," MTI Report 69TR39, NASA CR-72609, September 1969.

45. "Design of Gas Bearings," MTI/RPI Course Notes, Vol. 2, Chapter 6.3 - "Fixed Thrust Bearings" - (First Edition 1967, Second Edition 1968).

46. Murray, S. F., "Research and Development of High Temperature Gas Bearings, II - Selection and Evaluation of Gas Bearing Materials in Argon at 900°F and 1400°F," NASA CR-1477, December 1969.

47. Wilson, D., and Murray, S. F., "Gas Lubrication Research for 1900°F, Non-Isothermal Operation," Air Force Technical Report AFAPL-TR-67-57, Part III, August 1969.

48. Bamberger, E. N., "Manufacture of Jet Engine Thrust Bearings by Ausforming - Interim Report No. 9," General Electric Report R69AEG446, January 1, 1970.

49. Bisson, E. E., and Anderson, W. J., Advanced Bearing Technology, NASA SP-38, p. 377, 1964.

50. Anderson, W. J., and Zaretsky, E. V., Machine Design "Bearings Reference Issue," June 13, 1968, p. 33.

51. Zaretsky, E. V., Anderson, W. J., and Bamberger, E. N., "Rolling-Element Bearing Life from 400° to 600°F," NASA TN D-5002, January 1969.

52. Cohen, R. and Clausi, J., "Design of Brayton Rotating Unit on Rolling-Element Bearings," PWA-3549, November 1968.

53. AFBMA Standards, "Method of Evaluating Load Ratings for Ball Bearings," Section 9, Rev. 4, October 1960.

54. Dunn, J. H., "The 1200-HZ Brayton Electrical Research Components," NASA CR-72564, March 19, 1969.

NASA-Langley, 1971 – 22
Coml., Birmingham, Ala.

"The aeronautical and space activities of the United States shall be conducted so as to contribute . . . to the expansion of human knowledge of phenomena in the atmosphere and space. The Administration shall provide for the widest practicable and appropriate dissemination of information concerning its activities and the results thereof."

— NATIONAL AERONAUTICS AND SPACE ACT OF 1958

NASA SCIENTIFIC AND TECHNICAL PUBLICATIONS

TECHNICAL REPORTS: Scientific and technical information considered important, complete, and a lasting contribution to existing knowledge.

TECHNICAL NOTES: Information less broad in scope but nevertheless of importance as a contribution to existing knowledge.

TECHNICAL MEMORANDUMS: Information receiving limited distribution because of preliminary data, security classification, or other reasons.

CONTRACTOR REPORTS: Scientific and technical information generated under a NASA contract or grant and considered an important contribution to existing knowledge.

TECHNICAL TRANSLATIONS: Information published in a foreign language considered to merit NASA distribution in English.

SPECIAL PUBLICATIONS: Information derived from or of value to NASA activities. Publications include conference proceedings, monographs, data compilations, handbooks, sourcebooks, and special bibliographies.

TECHNOLOGY UTILIZATION PUBLICATIONS: Information on technology used by NASA that may be of particular interest in commercial and other non-aerospace applications. Publications include Tech Briefs, Technology Utilization Reports and Technology Surveys.

Details on the availability of these publications may be obtained from:

SCIENTIFIC AND TECHNICAL INFORMATION OFFICE

NATIONAL AERONAUTICS AND SPACE ADMINISTRATION

Washington, D.C. 20546